Influence of organic liquid on microwave-assisted pyrolysis of biomass

Mohammed Ziaul Hossen Chowdhury **CChem MRSC**

PhD

University of York

Chemistry

June 2019

Abstract

Development of thermal methods of biomass utilisation is vital for the establishment of bio-refinery technologies. Of such technologies, microwave-assisted pyrolysis is one of the most promising approaches to activate lignocellulose. However, the role of extractives contained within lignocellulose biomass during microwave activation remains unknown. This study investigated how the nature of extractives controls the mechanism of the microwave interaction with lignocellulosic structural components. A general introduction of present and future biorefinery approaches is discussed in Chapter 1. In Chapter 2, the literature review of forest waste extractive, NIR based forest waste characterisation and solvent effect on microwave-assisted cellulose pyrolysis will be discussed. In Chapter 4, the influence of extractive on microwave-assisted pyrolysis of biomass was investigated. The work of Chapter-5 & 6 was focused on the identification of physical-chemical parameters of organic liquid additives. In Chapter 7, the development of a new resonant cavity perturbation (RCP) instrument was discussed. The influence of microwave on Menschutkin-type reaction is highlighted in Chapter-8.

Based on obtained experimental results, two novel, fast and inexpensive methods - simultaneous thermogravimetric analysis and near-infrared spectroscopy were shown to be applicable for the identification of the aforementioned lignocellulosic extractives. The multi parameters of complex cellulose-additives interactions in the presence of microwave irradiation were successfully investigated via chemometric methods for the first time.

It was established that additives play significant and complex roles in the MW pyrolysis process. The degree of microwave pyrolysis was found to be dependent on the critical size of the molecular volume rather than the molecular functional group. Hydrophobic wax and wax-esters reduce the biooil yield of microwave pyrolysis while a specific molecular shape improves the rate of pyrolysis through a sustained microwave-interaction at high temperature.

The developed understanding of the microwave-biomass interaction mechanism will potentially facilitate the development and industrialisation of future microwave-based biorefineries.

Contents

List of Tables

List of Figures

Dedication

To my parents

Nurul Hossen Chowdhury and mother Fatema Begum

who taught me how not to abandon the dream of life!

Acknowledgement

I would like to thank my supervisor Professor James H Clark for giving me the opportunity to pursue a PhD in the first place. If he would not have considered my personal circumstances with kindness and compassion, it would be possible to see the end of this program. My other supervisor Dr Vitaly Budarin guided me regularly with much patience during this research journey, and his support and assurance helped me to become an independent researcher. I am very thankful to my supervisor Dr Andrew J Hunt for his kind guidance in numerous difficult times.

I am very thankful to The Swedish Research Council FORMAS to fund this PhD work. I am also thankful to Professor Paul Geladi of Sveriges Lantbruks Universitet of Sweden to teach me multivariate data analysis and its practical application.

I am very thankful to the Electromagnetic Communication Group, Department of Electronics for support in various way especially to allow me to develop automated complex dielectric measuring instrumental using their facility. During the resonant cavity perturbation (RCP) instrumental development, Dr Martin Robinson, Dr Iain Will, Charan Panesar of Electronics Department, Abigail Mortimer, Mark Roper, Stuart Murray and Timothy Ayres of Department of Chemistry of the University of York directly contributed in the form of technical work and advice. I am thanks to all of them. Some of the funding of the RCP work was provided by Dr Alice Fan and Professor James H Clark. I am very grateful to them. I am also thankful to Dr Miguel D Ruiz-Cabello of Electromagnetismo y Física de la Materia, Universidad de Granada, to help me to develop a python-based program to run RCP device. Many thanks to all technical staff of the Green Chemistry Centre of Excellence (GCCE) for their kind word and support.

I am also thankful to Andrew Maneffa, Tom Giles and Alisa Doroshenko for being so kind in some of my difficult time and in good time also!

Of course, no need to mention that my family has passed some very difficult to stay beside me to support what I always wanted to become, a scientist! So thank you all, not abandoning me!

Declaration

I declare that this thesis is a presentation of original work and I am the sole author.

This work has not previously been presented for an award at this, or any other University.

All sources are acknowledged as References.

1 INTRODUCTION

1.1 Pathway to Sustainable Bioeconomy

1.1.1 Sustainability

The World Commission of environment described sustainable development as "*development that meets the needs of the present generation without compromising the ability of future generations to meet their own needs*".[1] The definition of sustainability could be interpreted in many ways. It describes human well-being in terms of economic growth by using natural resources without depletion in long term.[2] Both resource utilisation and waste generation rates are the indicators of sustainability. Sustainability conception could adhere to the weak or strong paradigm. The weak sustainability paradigm only concerns neoclassical economics, in which human well-being is justified by ensuring non-declining resources over time. Strong sustainability also covers the ecological economics along with human well-being, and non-marketable values and attributes are evaluated.[2] The basis of sustainability underlies the philosophy of the restrained use of resources to ensure future generation's needs are met. Economic development should not impact on environmental and social equity. The balancing of the economic, ecological and social impact is referred to as the three pillars of sustainability. The balance of priority on people, planet and profit is coined as three Ps.

1.1.2 Circular economy

The Circular Economy (CE) concept incorporates both environmental and ecological economics into weak sustainability (Figure 1).[3] Circular economy is defined as "*An economy which is restorative and regenerative by design and aims to keep products, components, and materials at their highest utility and value at all times, distinguishing between technical and biological cycles*".[4] The long-lasting design of product with excellent maintenance, repair, reuse, refurbishing, recycling and remanufacturing ensure the achievement of circular economy. The circular economy is often expressed by the three R's as Reduction, Reuse and Recycle.[5] CE is restorative and regenerative by design. The overall goal of the circular economy is to decouple the resource consumption from economic growth in addition to promoting close-loop pattern economy.[3] To achieve the goal of CE, the input resource is needed to sit within the loop of energy and materials in such a way that the leakage of emissions, energy and generated wasted become minimal.[5] The circular economy has emerged from the infusion of several schools of thought such as *Biomimicry, Performance economy and Cradle-2-Cradle* within the last few decades.[6]

A circular economy ensures sustainability by the balancing of business, environment and society. CE suggest improving environmental benefit through improving air, soil and water quality, reducing greenhouse gas (GHG), lowering energy and water demand and regenerating ecosystem.[7] CE stresses to the restorative and regenerative activity of economy to create the resource value as oppose to depleting and extractive away of it.

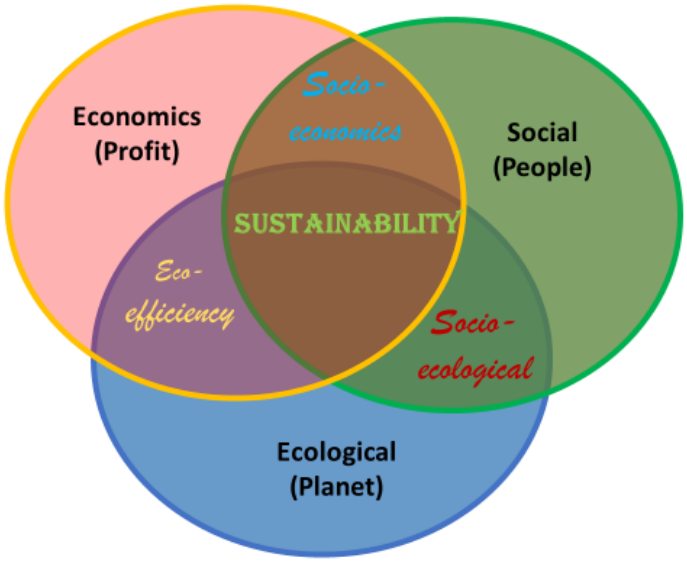

Figure 1 Relation of sustainability and circular economy.

1.1.3 Green Chemistry

It was widely released in the late 1980s that from an environmental point of view waste prevention, is better than pollution control and waste remediation. Prevention of waste at the source reduces the cost of treatment and more efficient use of raw material strength the economy. At the beginning of the 1990s, the US Environmental Protection Agency (EPA) introduced the term green chemistry to shift from waste treatment to waste prevention. In 1998, Anastas and Warner published the green chemistry principles which are:

The **twelve principles of green chemistry** are:

1. **Prevention**: Prevention of waste is more environmental friendly than treating the waste as it is created.
2. **Atom Economy:** All the atoms of a molecule should be needed to convert into useful material the end of the process.
3. **Less hazardous chemical syntheses**: In any chemical process the use or generation of toxic environmental material needed to be avoided.
4. **Designing safer chemicals:** Product design should be such that it should be as non-toxic as possible while performing its desired function.

5. **Safer Solvents and auxiliaries**: If auxiliary substances using is unavoidable, it should be as less hazardous as possible.
6. **Design for energy efficiency**: Energy requirement of a process should be minimum and at ambient pressure and temperature if possible.
7. **Use of renewable feedstock**: Whenever feasible, non-renewable feedstock should be replaced with renewable ones.
8. **Reduce derivatives**: To avoid additional waste generation whenever possible generation of derivative such as the use of protecting group should be avoided.
9. **Catalysis**: To avoid stoichiometric reagents, small quantities of catalytic reagents should be preferred.
10. **Design for degradation**: The design of the chemical product should be such that after the end of the product life, they should be non-harmful and degradable.
11. **Real-time analysis for pollution prevention**: To prevent hazardous substance to form, the real-time in-process analytical method needs to develop.
12. **Inherently safer chemistry for accident prevention**: The process of producing the substance and the substance itself should be produced in such a way that the hazard of explosions, accidental releases and fire should be minimum.[8]

1.1.4 Green Chemistry, Sustainability and Circular Economy

The first green chemistry metrics, prevention of waste is expressed with the E factor (kgs waste/kg product) while second metrics atom economy is expressed with mol weight of product/sum of mol weight of starting materials.[9] E factor was first published at 1992.[10] Before the publication of the E factor, chemical and pharmaceutical industries preferred to determine process efficiency in terms of product yield. The concept of the E factor and atom economy rather suggests the resource efficiency and elimination of waste is the determining factor of chemical process efficiency. Since then, pharmaceutical industries made a substantial improvement in their research development and industrial process to integrate green chemistry principle. The E factor has played the central role to propel the implementation of green chemistry in academia and industry. The continuous progressing of catalytic alternative development and replacement of toxic and hazardous solvent by cleaner substitute certainly driving to the road of sustainability. Yet, two more important milestones to achieve the goal of sustainability. Firstly, existing fossil-based commodity chemicals needed to be replaced with renewable biobased source and also design new biodegradable and biocompatible material. Secondly the transition from an unsustainable linear economy to the circular economy which

conserves the resource and eliminates waste. By achieving this target, a truly green economy can be established. To evaluate the manufacturing processes environmental impact, implementation of mass-based green metrics tools with life cycle assessment (LCA) is required.[10]

1.1.5 Circular Chemistry Concept

However, it is recognised that in the green chemistry concept, there is no economic component. To make green chemistry more holistic and fully compatible with the circular economy, recently J. Chris Slootweg *et al.* has introduced the Circular Chemistry concept.[11] Their proposed twelve principles of circular chemistry (CC) are:

1. Collect and use waste: Waste should be transformed into marketable value-added products.

2. Maximise atom circulation: All the atoms of the existing molecule should be aiming to utilise.

3. Optimise resource efficiency: Resource conservation should be ensured by reuse and preserving finite feedstock.

4. Strive for energy persistence: Energy should be efficiently used to maximise its value.

5. Enhance process efficiency: To enhance the post-process, reuse and recycling, innovation should continually improve.

6. No out-of-plant toxicity: Chemical processes should ensure no toxic compounds is released into the environment.

7. Target optimal design: Product design should such that ensuring a maximum life, the recycling steps such as separation, purification and degradation becomes easy.

8. Assess sustainability: To identify inefficiency in the chemical process, environmental assessment such as LCA should be performed.

9. Apply ladder of circularity: At every ladder of circularity, the end of life option of the product should strive for maximum utilisation.

10. Sell service, not product: Chemical producer should consider service-based business.

11. Reject lock-in: To implement innovation, the business and regulatory environment needed to be flexible.

12. Unify industry and provide a coherent policy framework: To enable circularity in the chemical process, the industry and policymakers should work hand in hand.

1.1.6 Biorefinery Concept

In petroleum refining process crude oil is fractionated and processed into various useful products such as petrol, diesel, kerosene, liquefied petroleum gas (LPG), jet fuel for energy

generation purpose and some fractions are used for raw material for petrochemical industry.[12] [13] For example, Naphtha, a raw material of petroleum is used as building block chemical for ethylene, propylene, butadiene toluene, ethylbenzene or xylene.[13] In the late 1990s, the biorefinery concept arises as the analogues of the petroleum refinery to refer that from the renewable feedstock of biomass such as building block chemical or platform molecule could be gained.[14] The US Department of Energy (DOE) states "*A biorefinery is an overall concept of a processing plant where biomass feedstocks are converted and extracted into a spectrum of valuable products*".[14]

An example of Petro-refinery product valeric esters substitution from biomass lignocellulose is shown in Figure 2.[15]

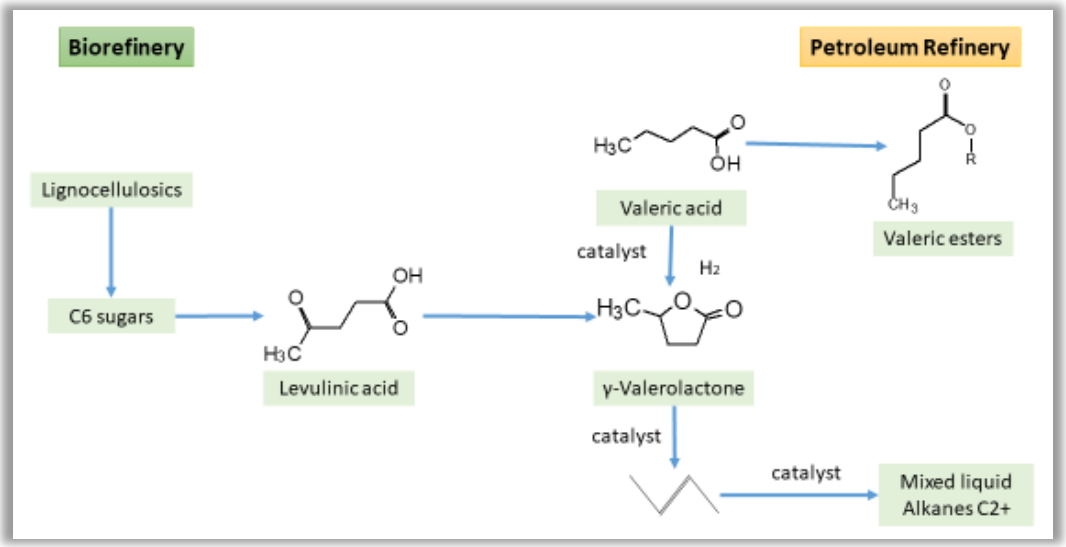

Figure 2 Biomass lignocellulose transformation into a substitute product of Petro-refinery

In Section 1.5 an overview of biorefinery in the aspects feedstocks, products and process will be more elaborated.

1.1.7 Biorefinery, Circular Economy and Bioeconomy

The definition of bioeconomy (BE) is evolving as time has progressed, and it is described and understood differently among different sectors.[3] Bioeconomy can be defined as "*an economy based on the sustainable production and conversion of renewable biomass into a range of bio-based products, chemicals and energy*".[16] The Nova Institute, EU has interpreted BE and circular economy in the relation of biorefinery as graphics in Figure 3

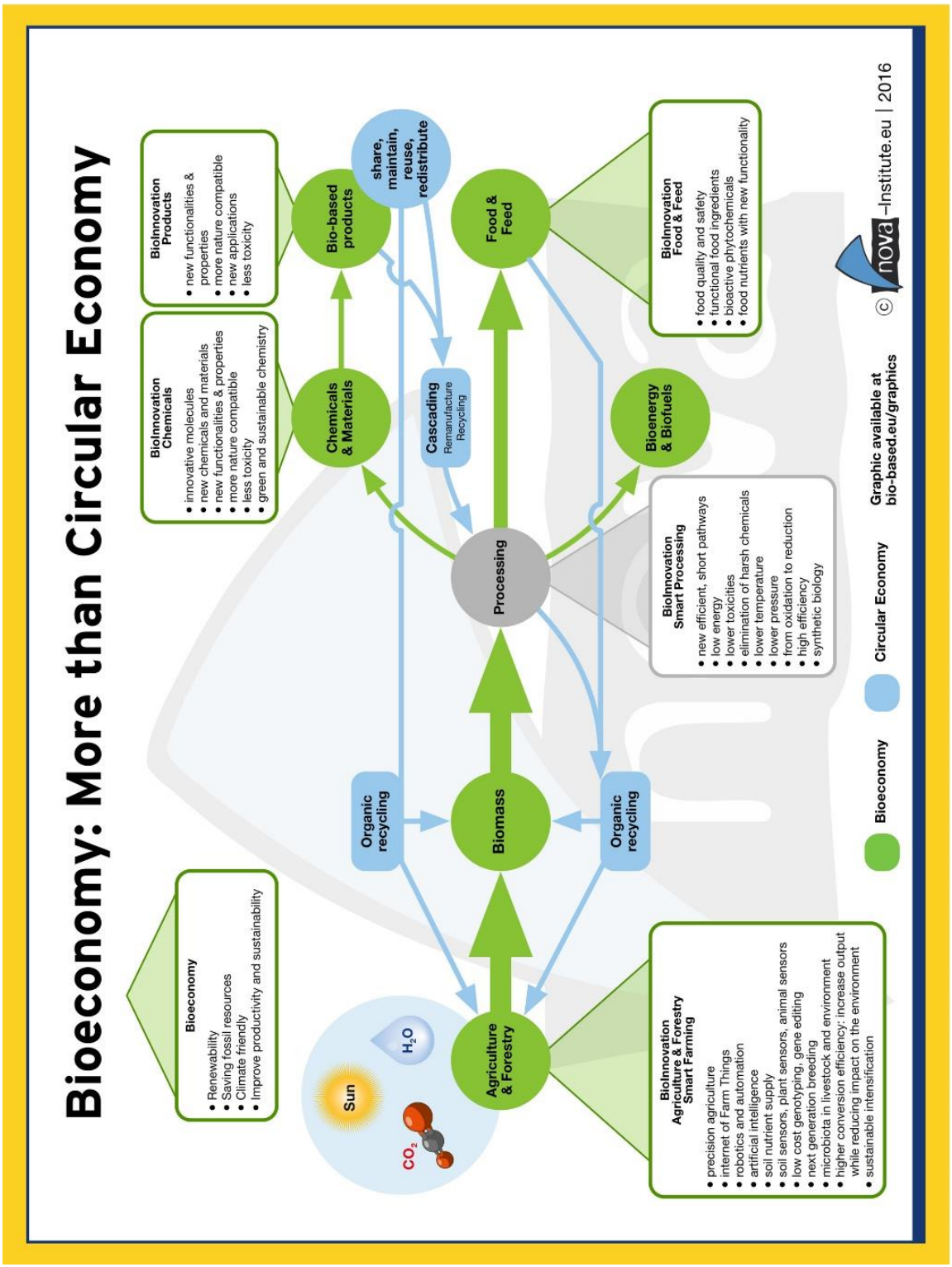

Figure 3 Bioeconomy and circular economy relationship. Reprinted with permission from NOVA.

The Global Bioeconomy Summit of 2015 has highlighted that bio-based economy may support at least eleven of UN sustainability development goals which are (SDG 2: End hunger, SDG 3: Ensure healthy lives, water and sanitation for all, SDG 7: Energy for all, SDG 8 & 9:

Sustainable economic growth and sustainable industrialization, SDG 11: Sustainable cities, SDG 12: Sustainable consumption, SDG 13: Combat climate change, SDG 14: Ocean, seas and marine resources) of the 17 Sustainable Development Goals.[17] It is clearly understood that the BE concept is more optimistic to attain sustainability. But to meet the multiple objectives of sustainability, the competency of BE is uncertain. The main concern of uncertainty of BE arises from socio-economic and environmental impact when bio-based activities will increase. Soil erosion, water pollution and loss of biodiversity, biosecurity, and greenhouse gas performance among the concern when the economic aspect of transition is priority.[18, 19] Although the bio-based economy is expected to bring socio-economic benefit through rural development and employment opportunities, the redirection of resources could affect labour, capital and investment from other sectors.[2] The relationship between agricultural commodity price and biofuel product is also under debate. To evaluate the right balance of those issues more indicators needed along with LCA and carbon footprint.[20 21] To achieve the overall goal of bioeconomy, public and private researches need to collaborate closely at national and international level by sharing resources and knowledge. An interdisciplinary strategic approach is required for system thinking, understanding technologies, local species and for evaluating the social and economic performance of bioeconomy.[17 22] A holistic approach to bioeconomy transition will deliver economic growth, rural development, geopolitical stability and boost the global competitiveness of markets.[22]

1.1.8 Bioeconomy in Europe: An Overview

According to the EC, European bioeconomy currently enjoys 2 trillion Euros of market share and 22 million jobs across varied sectors, including food, chemicals, bioenergy, agriculture and forestry.[23] It is hoped that BE will bring benefits and opportunities in Europe while associated risk and trade-offs are also concerned.[23] To overcome the associated risks and to ensure smart and green growth, intelligent design and implementation of bioeconomy are needed. Particularly the commitment from government, stakeholders and public support is required to implement the agenda of bioeconomy. To succeed on this goal, a coherent and integrated effort is needed to increase by increasing research, technological development and policy formulation.

1.2 Renewable Resources

An increasing world population that demands a higher standard of living is leading to a significant environmental impact; however, the earth's capacity to take on such a burden is limited. Although technological development may lead to the use of fewer resources per

activity however solving the issue of recycling and reuse of waste material is important but cannot alone solve the anthropogenic footprint on the earth's environment. About 90% of organic chemicals and more than eighty percent of the energy is derived from fossil fuel in the world. Nuclear energy, hydro-electric and solar energy contribute less than 10% in the global energy source.[24] Energy can be gained from various alternatives such as wind, sun and water. However, sustainable materials and chemical mainly achievable from substance and economy of substances mostly depend on plant biomass.

While fossil fuel's regeneration cycle is hundreds of millions of years, the forest biomass can be regenerated in less than eighty years when left untouched or if controlled by humans.[25] The regeneration cycle of shrubs and grasses are even within a few years, as shown in Figure 4. Among all three sources, the density of biomass on a mass per unit surface area is highest for woody biomass.

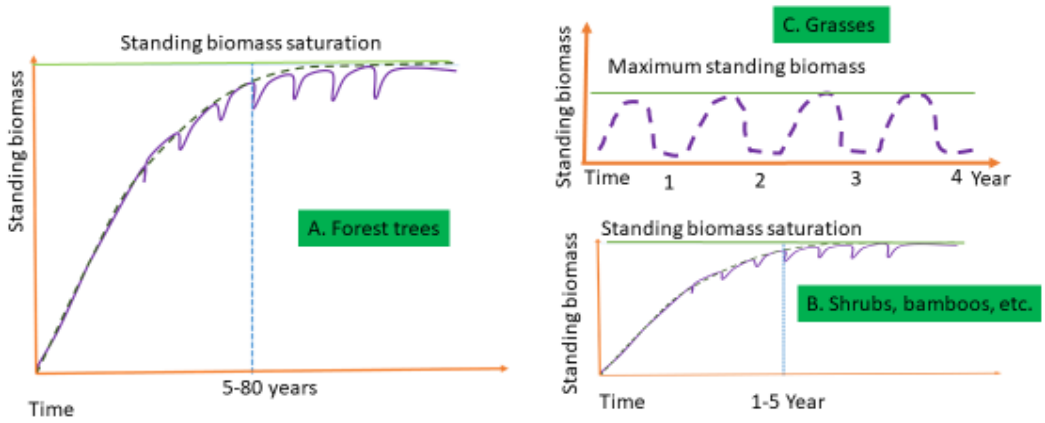

Figure 4 The dotted line of the scheme shows standing biomass accumulation as a function of time. The dip in the solid line represents minor periodic disturbances due to drought, fire or insect attacks.

Biomass has tremendous potential not only to reduce the gap of using renewable resources for energy but also for organic chemical and polymeric materials. To avoid the threshold limit of the environmental burden on the earth, utilisation of renewable feedstocks could be the way forward and to develop a sustainable natural environment. The development of renewable alternative energy, chemicals and materials are the key drivers to switching away from fossil fuel-based economy.[26]

1.2.1 Natural Biomass Resources

Globally 170×10^9 t of biomass is produced yearly through photosynthesis.[27] Only a very small portion (3%) of this resource is served in the non-food areas, such as for chemicals.[14] The European Union has agreed in the Renewable Energy Directive II (RED II) that the target of renewable energy consumption by 2030 is 32% of the total energy used. It is also agreed in RED-ll that 14% of consumed energy in road and transport should come from a renewable source. Biomass R&D Technical Advisory Committee (2002b) in the roadmap of "The Biomass Technology in the United States" published the target Share of chemicals from biobased as 25% by 2030. It is also understood that tropical deforestation needed to be avoided to grow biofuel crops such as soybean and palm oil.[28] To bridge the gap between the need of renewable biomass supply and non-competitive alternative resource, utilisation of forest waste in biorefinery concept will fulfil not only the demand of energy and material but also the demand of biobased chemicals.

1.2.2 Waste Biomass as a Renewable Resource

Biomass waste, such as manure, crops, agricultural and agro-industrial waste, food waste, forestry residues can be converted into fuels, energy, chemicals, and other value-added materials.[29] Between 1300-1600 million tons of food is wasted every year either in the food production chain or during distribution supply chain or after the final stage of human consumption.[30] It is published that 45-55% of total municipal waste is food waste.[31]

The losses of food mean a loss of energy and resources that were deployed during the production and supply chain. Food waste is a promising feedstock for a variety of product and intermediate of industrial application. Chemicals such as organic acids and furans, polyhydroxyalkanoates or chitin and products like bio-lubricants, biosurfactants or nanoparticles can be produced from food waste.[32] Another renewable resource is agricultural waste. Major agricultural wastes include rice straw, wheat straw, whereas corn straw and bagasse.[33] Globally 600-900 million tons of rice straw are produced per year of most of which is burned.[34] Only a small amount of this rice straw is utilised as animal feed. Globally only 5% of corn straw is used for bedding and feed. At the industrial process, less than 1% of corn straw is utilised. In the USA, more than 90% of corn straw is left in the fields.[33] All of those abandoned organic waste may cause large-scale pollution of soil, water and air. One metric ton of organic solid waste decomposition is accounted for 90-140 m^3 of methane and 50−110 m^3 of carbon dioxide released into the atmosphere.[35] If all of those agricultural waste could be integrated into the circular waste management system, then the high value of compounds could

be extracted profitably.[35] The value-added extraction compounds do not only contribute to the economic profit but also partially detoxify the waste for further biological post-treatments.[36]

1.3 Forest Resources

About 30% of the total land area of the earth is covered with forest.[37] About 37 % of the area of Europe is forested and thus making around 27% of the world forest.[37] Finland and Sweden is covered by 72% and 66% forestland respectively.[37] For timber production most commercial tree specifies in the Nordic area are Norway spruce (Picea abies) and Scots pine (Pinus sylvestris). According to the Swedish National Survey 2010, 40.5% of Swedish forest is covered by Norway spruce, and 38.9% forest area is contributed by Scots pine.[38] Lodgepole pine, birch and some broadleaf trees are also grown in the Swedish forests. Swedish forest agency reports in 2011 that about 2.9 billion cubic meters standing volume of trees are available on productive forest.[38]

According to the Food and Agricultural agency of the United Nations global forest resources assessment 2015, 1,836 million (M) cubic meter (m^3) of round wood is harvested for industrial timber purpose globally.[37] Almost the same amount of wood (1,863 M m^3) is used for fuel purpose worldwide.[37] For timber purpose, 1026.6 million m^3 coniferous round wood is used globally and about 438.7 M m^3 of sawn wood is produced from that source.[37] The chips and particles produced from swan process treated as waste and mainly used for fuel purpose.[37] In 2014, 241.5 million m^3 of Chips and particle of the wood residue was produced globally.[37] Only about 26.4 million m^3 wood residue is converted as fuel pellet from that residue.[37] Paper and board industry uses 12% of harvested wood.[37] According to the suggestion of the British Bark Industry, out of all soft roundwood consumed by various industry in the UK, about 7% if it was bark.[39] From this estimation, about 260 million cubic meters of bark enters into industry excluding any wood bark left in forest floor and during the process of entering the round wood into the industry. Moreover, all the roundwood statistics enter into FAO Forest Products Yearbook, excluding bark portion (FAO-STAT Forestry). For this reason, the actual figure of bark generated from the forest could be higher than 7%.[40, 41]

1.3.1 Forest Waste

More than 30% of wood parts such as tops, branches, roots and stumps (see Figure 5) are left behind in the forest during the harvesting of merchantable wood.[42, 43]

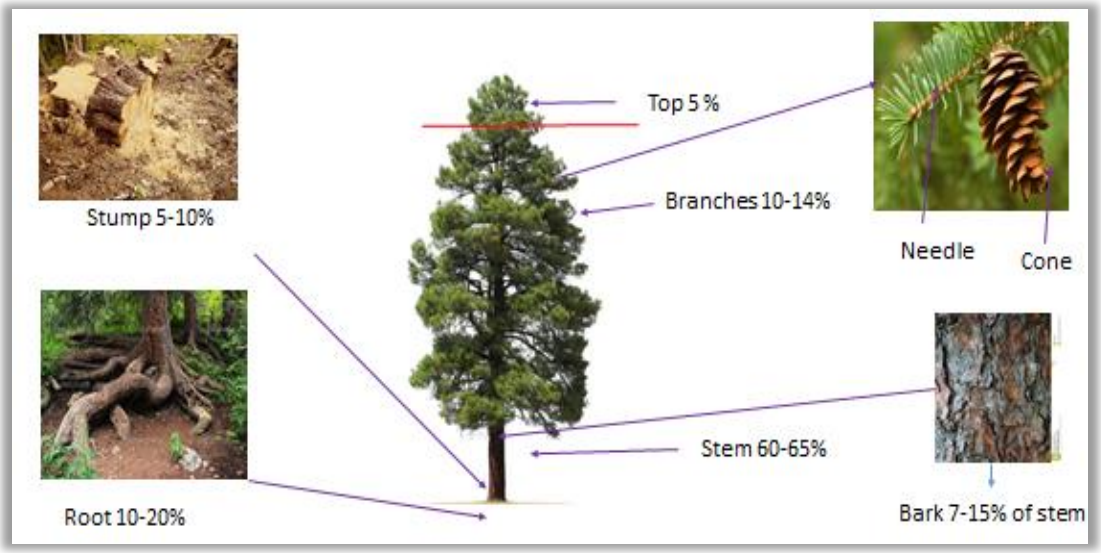

Figure 5 Tree parts proportion according to timber harvesting.[42, 43]

Imperfect commercial trees and other non-commercial trees are also generated in forest floor during commercial thinning and final felling. Deadwood, dying trees, and small trees are also cleared from logging forest during pre-commercial thinning. All of these biomasses are collectively regarded as forest residue or waste category. In Europe, 82% of the raw material of forest industry comes from the sustainably managed forest.[39] Of a sustainable forest, up to 30% of the residue is left on the forest floor for ecological benefits of the materials are mainly collected either to burn for fuel to generate energy and power, or it may have ended up in the landfill. Globally, 50-55% of wood is burnt for fuel supply.[44]

1.3.2 European Forest Products and Waste

Around 215 million hectares (ha) of European land-mass is forest, and additional 36 M ha (5.5%) covers the wooded land.[37] Northern Europe is most extensively forested (53%).[37] Finland's three quarter land-mass is forested, and Sweden is placed at the second position (68%) (Figure 6).[37, 45] Europe's total stem volume is currently 35 billion m^3 and 84% of it available for wood supply.[37] Except for the South American region, European forest growing stock (133 m^3/ha) is higher than the world average. More than half (57%) of these European stock is coniferous.[37] Most of these coniferous are occupied in Finland (75%) and Sweden (72%) (Figure 6).[37] Europe's net annual increment of wood (839.7 M m^3) is higher than felling

(582.3 M m^3).[37] Out of a total reported 407 M m^3 round wood removal in Europe, the highest removal was in Sweden (70 M m^3).[37] Round wood removal value in Europe is 18,237 million Euro.[37] In Europe, average wood energy consumption is 0.68 (m^3/capita).[37] According to Forestry Research Institute, Sweden 11 TWh of power comes from forest residue.

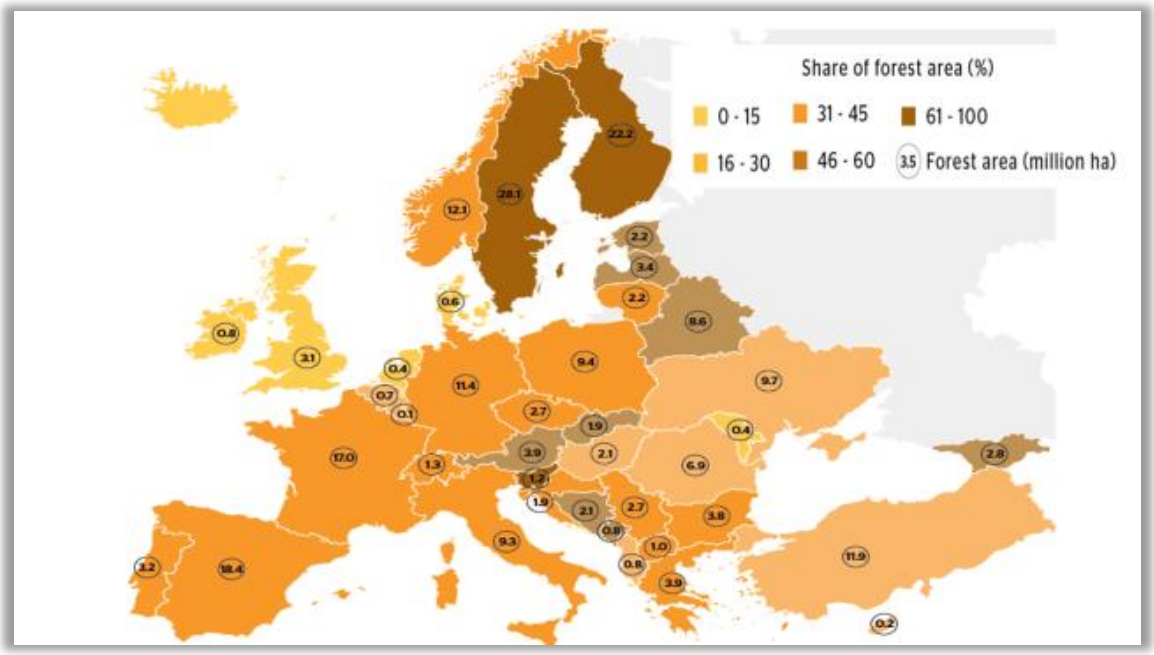

Figure 6 Forest area (million hectares) and share (percentage) of land area by country, 2015.[46](Reprinted with permission from Forest Europe)

1.4 Structure of Lignocellulosic Biomass

For the utilisation of forest waste in the biorefinery concept, the knowledge about lignocellulose components is essential. The major components of wood biomass are cellulose, hemicellulose, lignin and extractives (see Figure 7). Dependent from sources of plant material may contain (40-50%) of cellulose, (20-35%) of hemicellulose and (15-30%) of lignin.[47] To get the maximum value of woody biomass in a biorefinery, pre-treatment and careful separation of its components such as extractives, cellulose, lignin and hemicellulose is needed.[48] In subsections below, the wood components, properties and current and potential uses are discussed. Commercial wood can be categorised as softwood and hardwood. Coniferous woods fall into the softwood category, although all kind of softwood is not soft and vice versa is true for the hardness of hardwood. But the chemical composition, especially extractives, differs in softwood from hardwood. Hemicellulose and lignin chemical composition also differ in softwood and hardwood. The wood components do not also contain uniformly at all the parts such as branches, leaves or heartwood of any tree.

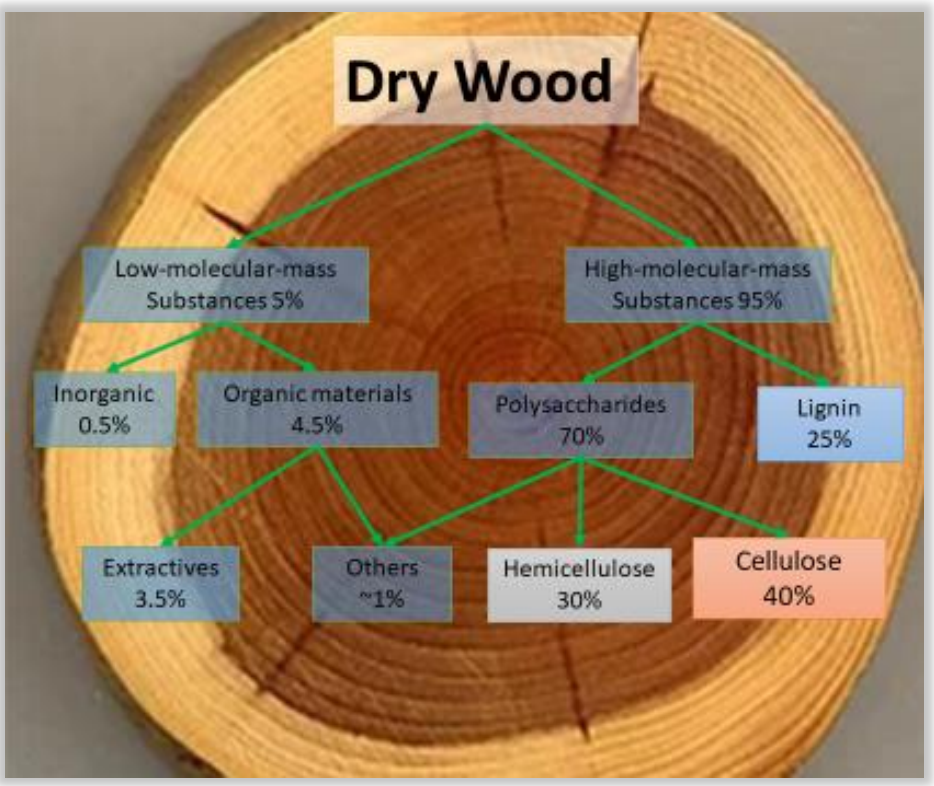

Figure 7 General category of wood components.[49]

The components of wood are more elaborately discussed in following sub-sections.

1.4.1 Overview of Cellulose Properties and Applications

Cellulose is made up by linking to the anhydro-β-glucopyranose unit to form a linear macromolecule or cellular nano strip (Figure *8*).[84] The degree of polymerisation (DP) may vary from 100 DP to 8000-10,000 monomeric unit long.[85, 86] The hydroxyl groups of cellulose monomeric units are highly hydrophilic.[87] Theses long string of cellulose align on top of each other by the bond of these hydroxyl groups and form cellular microfibrils and possesses a degree of crystalline structure.[84] The high degree of crystallinity of cellulose gives it a high degree of thermal resistance than other polysaccharides of lignocellulosic biomass.[88] The microfibrils of cellulose again bunched up with other microfibrils with hydrogen bond and form nanofiber.[48] The nanofibers again bundled together to form cellulose fibre structure.[48] The cellulose fibre forms the main structural part of cell-wall by combining with hemicellulose and lignin.[84]

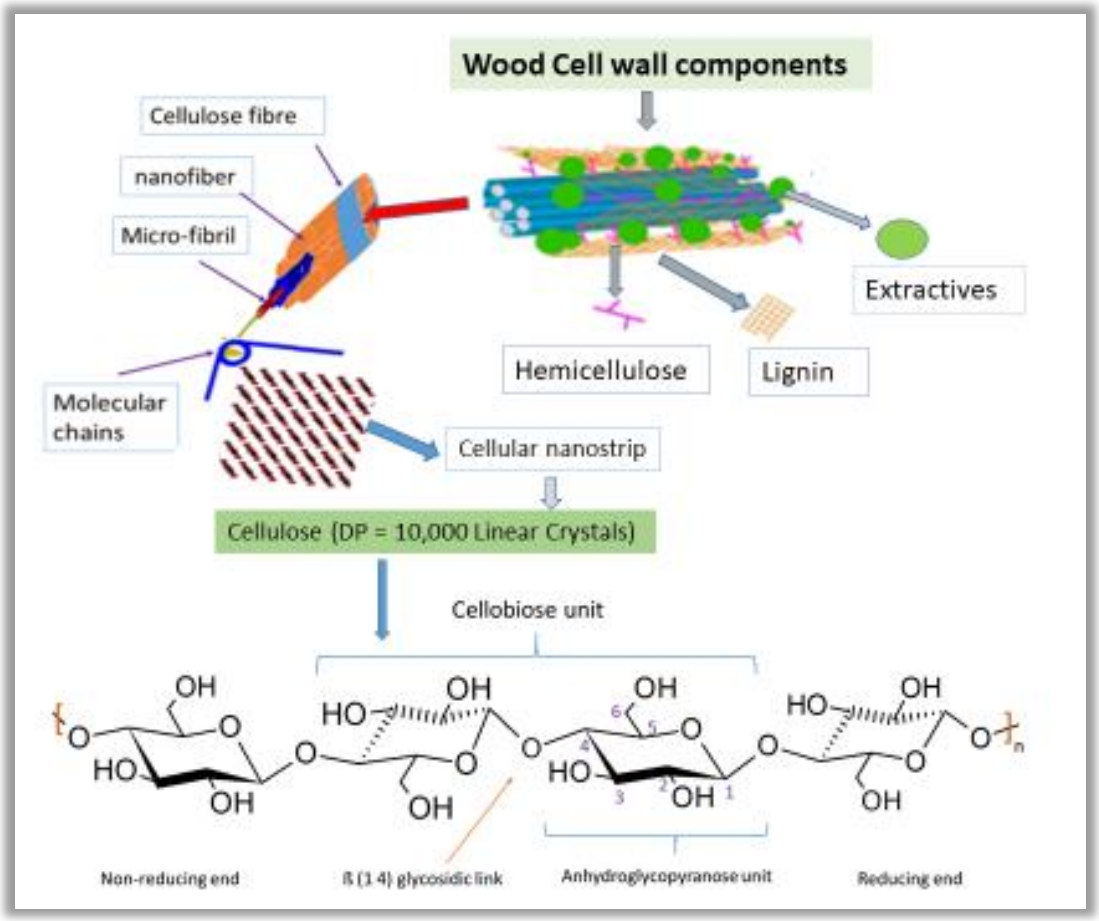

Figure 8 Major Wood components and structure of cellulose.

The complex fashioned extended intra and intermolecular network of hydrogen bonds of a single anhydroglucopyranose unit (AGU), is the basis of physical and chemical properties of this complex material. The chain stiffness of cellulose is enabled by intramolecular hydrogen bonds and the sheet-like structure of the linear polymer that arises from intermolecular hydrogen bonds (Figure 9).[89 50]

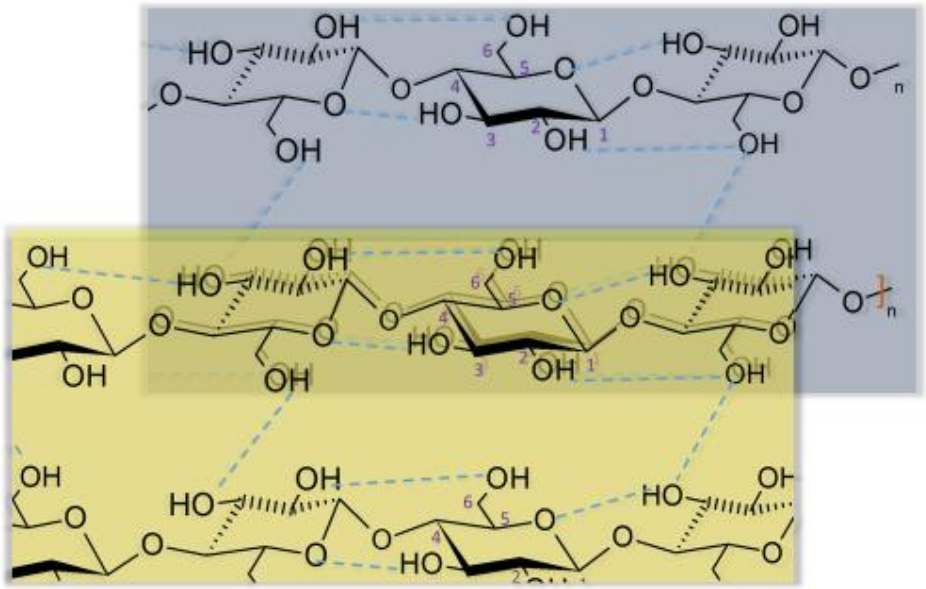

Figure 9 Intermolecular and intramolecular hydrogen bonds in multi-layered cellulose.[50]

This amphiphilic nature of cellulose is highlighted in recent literature[90-92] and by their qualitative hypothesis is concluded that all the three hydroxyl groups of equatorial glucopyranoside are hydrophilic while the axially directed hydrogens of the rings are hydrophobic.[51] The differences in polarity at the sides of flat ribbons and structural anisotropy also fit with this theory.[93-95]

Although in a recent quantitative statistical thermodynamic approach proposed a different view by studying cellobiose, that hypothesis yet needs to be proven for cellulose at various conditions.[96] About 95% of cellulose gained through the wood pulping process is used in the paper industry.[26] The second most commercial application of cellulose is in the textile fibre industry. One such application is cellulose xanthate (Viscose). The coating material, film and cigarette filter are produced from cellulose acetate. Cellulose was found in the application of slowly released steroid drug matrix, filtration membrane, in moulding frame.[26] The Food and pharmaceutical industry widely use cellulose derivatives of cellulose ether, cellulose esters such as methyl, ethyl and propyl cellulose, used in the detergent product and drilling aid purpose at the mining industry. The pharmaceutical and cosmetic industry also uses cellulose as coating and adhesive.[52]

1.4.2 Hemicellulose

The chain of polyoses is shorter than the cellulose chain. The chain is branched and formed by the combination of 150-200 unit of pentose, hexose, deoxyhexose sugar monomers and hexuronic acid (Figure 10).[53] Because of this reason hemicellulose is less crystalline than cellulose.[54]About 25-30% of wood tissue is made up of Hemicellulose. The polymeric chain

of hemicellulose formed by the combination of more than one monomeric sugar unit as opposed to cellulose.[54]

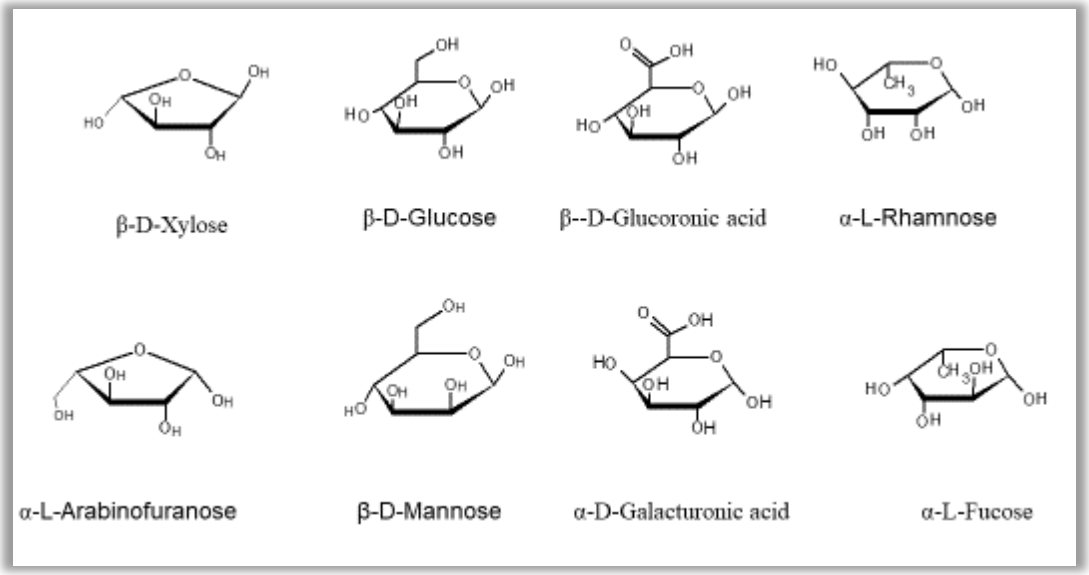

Figure 10 some sugar components of polyoses

Unlike cellulose, the bonding of six-membered rings may either bond α- or β-forms. Glucose, mannose, galactose, rhamnose, arabinose are such sugars contained in hemicellulose. The main chain of polyose consists of the only homopolymer such as xylan (Figure 11). Among pentose, xylose is abundantly found in hemicellulose. L-arabinose is another pentose found in hemicellulose.

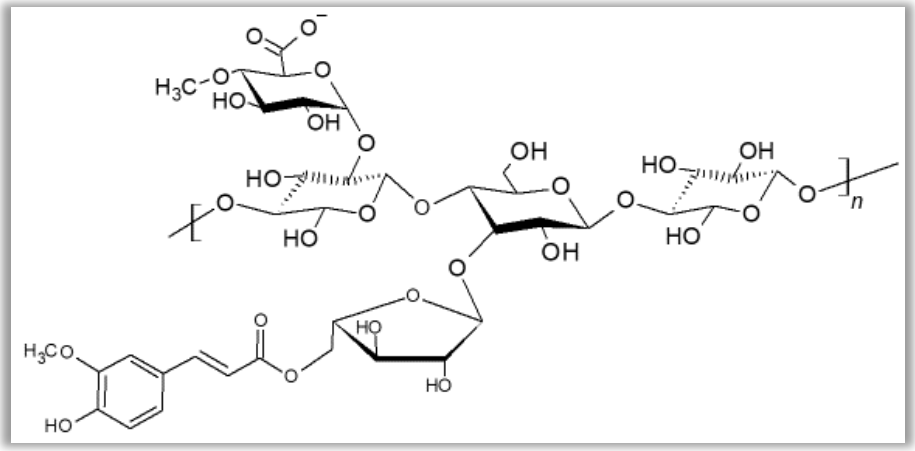

Figure 11 Xylan: A hemicellulose polymer of wood.

The sugar component of hemicellulose can be used as the feedstock of fermentation for the production of ethanol or other alcohols such as glycol, xylitol and butanol and arabitol.[52] Acetic acid and acetone can also be derived in the fermentation process along with methane and

hydrogen. Pentose could be converted in another important platform compound furfural which has wide use in resin, wax production as a solvent.

1.4.3 Lignin

The third most abundant component of the plant cell wall is Lignin and main non-carbohydrate polymeric source of a plant.[26] Cellulose and hemicellulose are bound together by lignin to protect the cell wall of the plant from enzymatic and chemical degradation. The plants mechanical strength and to stand upright on earth is down to lignin's incorporation into the plant cell wall. The distribution of lignin in various plant varies widely (20-40%).[55] The lignin content of branches, stem and bark also differs in plant and also at younger and older trees.
Lignin is insoluble in their native state, and therefore isolation and structural determination in the native state is still not achieved.[54] In lignin, a large number of phenylpropane units are combined in a non-linear fashion and form a three-dimensional molecular structure without any certain combination.[53] Three main precursors of this highly complex aromatic rich components are p-cumaryl alcohol, coniferyl alcohol and synapyl alcohol (Figure 12).[55]

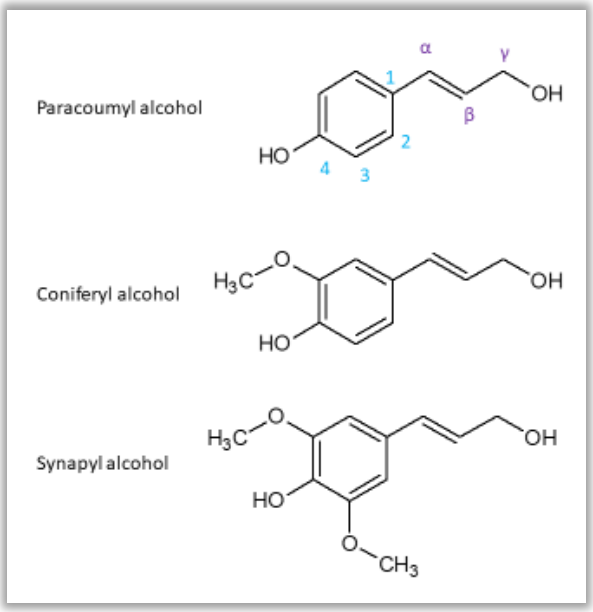

Figure 12 Major Lignin component

The syringyl unit of lignin is found to be more abundant in hardwood than softwood.[55] Due to its structural heterogeneity, the structure of lignin is the most difficult natural polymer to study. For this reason, the lignin structure is normally presented as a model. A model of spruce lignin structure with 16 polypropylene until is drawn below following the scheme of Alder (Figure 13).[55]

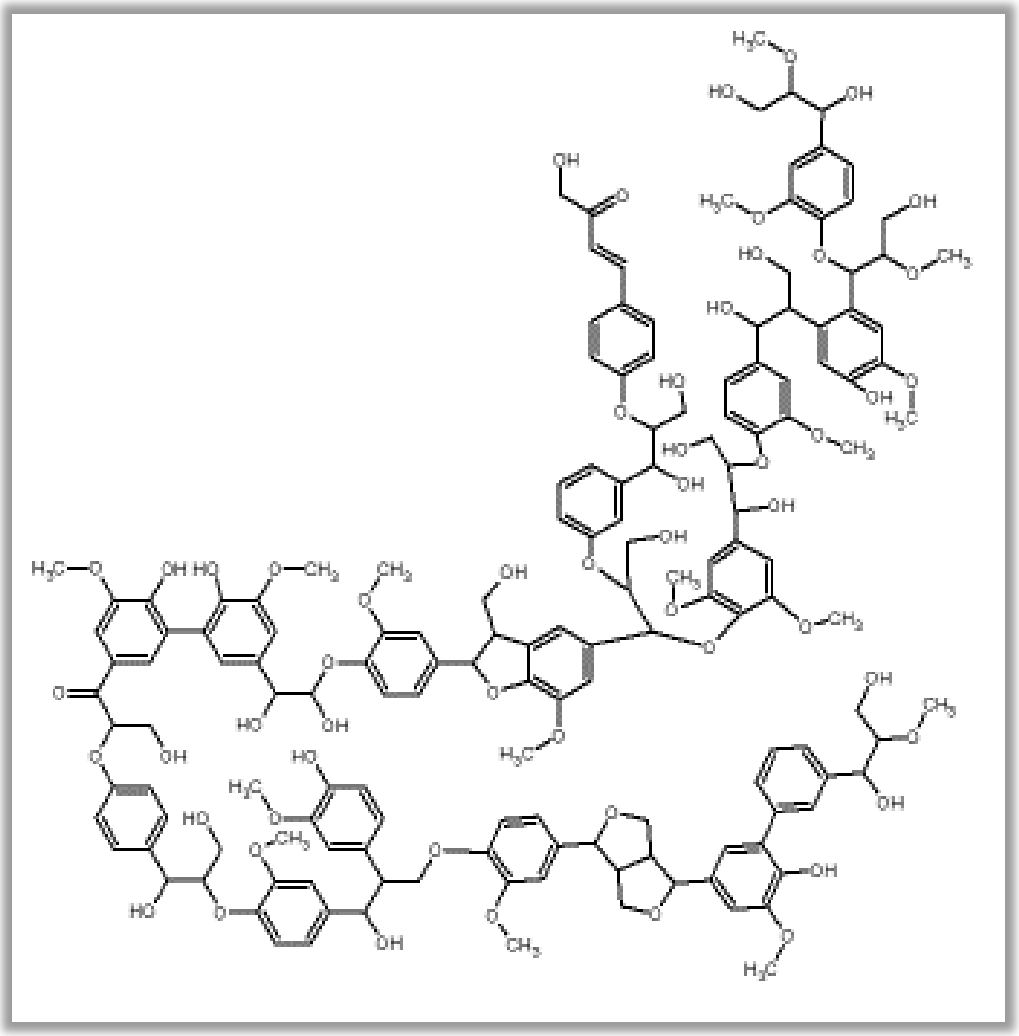

Figure 13 Structural Scheme of Spruce Lignin. [55, 56]

From unsulfonated lignin, vanillin is produced. Plywood industry uses unsulfonated lignin as resin. Sulfonated lignin can be used as emulsions, dispersants in paint, dyes, in cleaning agent and pesticides.[52] Lignin also used in animal feed pellets as binder.[52]

1.4.4 Inorganics and Water

Biomass may contain 1-1.5 % of inorganics. Along with chlorine and heavy metals and trace amounts of other minerals, Calcium and Potassium are most abundant in the biomass.[57] Moisture content in biomass greatly varies due to various factors. The water molecule may present in free or bound form with lignin, hemicellulose and cellulose.[58, 59]

1.4.5 Extractives

Apart from the wood component above-mentioned, there is also a range of small to appreciable quantities of extraneous components which are termed as extractives due to extractable with solvents. Based on the chemical structure, extractives are classified into various groups. These

chemicals components consist of terpenes and its derivatives, fatty acids, carbohydrates, polyhydric alcohols and aromatic compounds.[54] The building block of terpenes is isoprene unit. Monoterpenes are consists of two isoprene units, and sesquiterpenes form with three isoprene units (Figure 14).

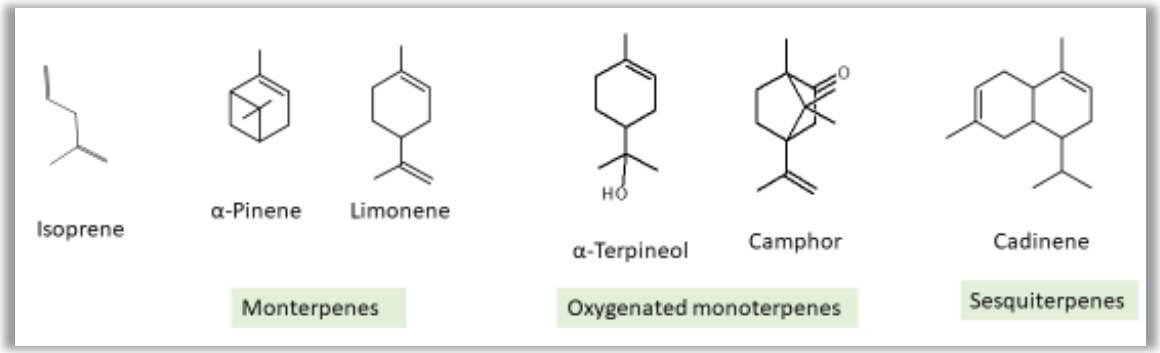

Figure 14 Basic structure of the various terpenes

Terpenes are pure hydrocarbons, and most of them linked intermolecularly.[60] Functional groups such as OH, C=O, COOH etc. with terpenes forms the structure of terpenoids. While in hardwood wood only monoterpenes are present, in softwood all classes of terpenes present. Monoterpenes can be acyclic, monocyclic or bicyclic. Monoterpenes are volatile and could be extracted with steam distillation. Turpentine, the volatile wood oil, is mainly monoterpene. All softwood contains α- pinene and β-pinene along with limonene. Camphene, myrcene, β-phellendrene and Δ-carene are also common terpenes of softwood and a rate of mixed composition of those terpenes gives a characteristic of softwood.[60] Along with heredity, environmental factors also contribute to the characteristic composition of extractives of a plant.[60] Sesquiterpenes also present in volatile terpene oils. Diterpenes and diterpenoidic acid is part of softwood oleoresins.[60] Pimaradiene, thunbergene, manoyloxide, pimarinol, Levopimaral, pimaric acid and abietic acids are examples of neutral diterpenes and its derivatives (Figure 15).

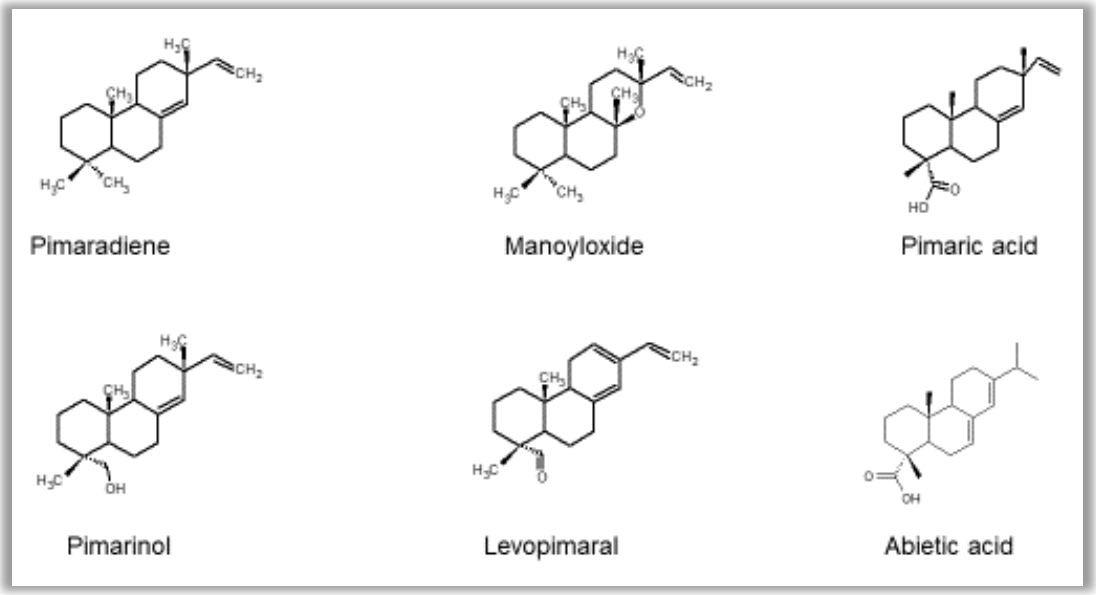

Figure 15 various forms of diterpenes.

Some softwood may also contain triterpenes. Those structures are assigned into sterane type steroids structure. The precursors of those compounds are acyclic squalene and are found in conifers. ß-sytesterol (Figure 16) is the main steroid group of softwood. About 0.3-0.4 % fats and 0.08-0.09% waxes are found in Scots pine.[60] Free alcohols and saturated or unsaturated fatty acids with 16-22 carbon atoms are also found in extractives (Figure 16). In softwood, more than twenty fatty acids exist. The fatty acids normally esterified with glycerol as triglycerides. [60]

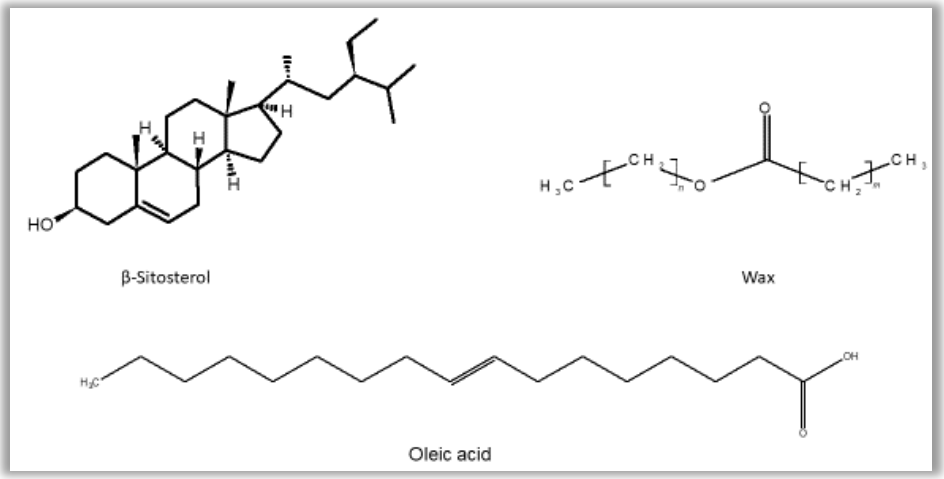

Figure 16 Sterols, fats and waxes

Various phenolic compounds are also found in wood extractives. Vanilin, coniferyl aldehyde, p-hydroxybenzaldehyde, p-ethylphenol, guaiacylglycerol, syringyl and coniferin are some

simple phenolic compounds of softwood (Figure 17).[60] In lignan two phenylpropane units are linked together. The dimeric structure of some of the lignan is present in lignin. Pinoresinol, conidendrin, leariciresinol and matairesinol are some examples of lignan (Figure 17).

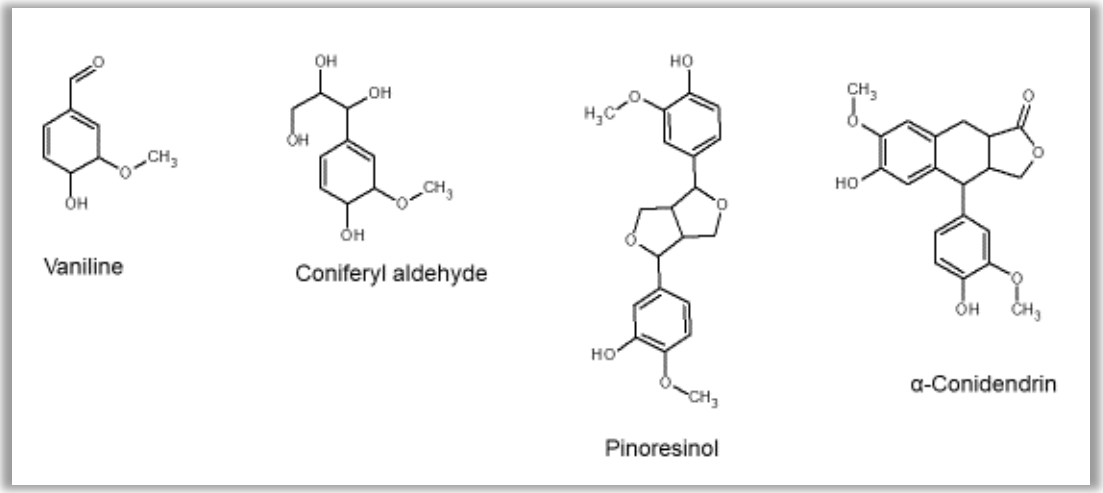

Figure 17 Phenols and lignans

The aromatic compounds stilbene, such as 4-hydroxylstilbenes, 4-methoxystilbene, pinosylvin, pinosylvin dimethyl ether and piceid acid are found in the heartwood of softwood (Figure 18).[60] The darkening of wood during light exposure is caused by those stilbene compounds.

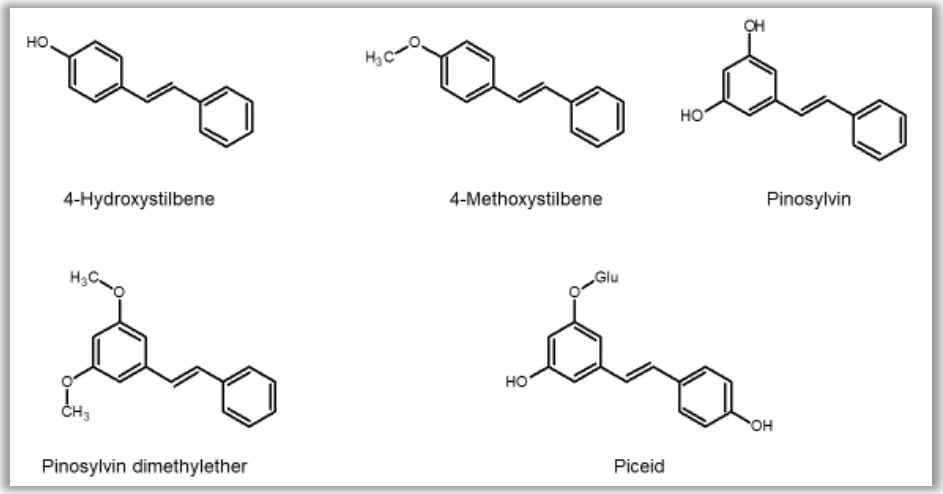

Figure 18 Derivatives of stilbenes found in softwood

Floavoniods are another extractive class of compounds and it can be sub-classed as flavanes, flovones, flavonoids and isoflavones. Chrysin, taxifolin, pinocembrin, pinostrabin, catechin and pinobanksin are some softwood flavonoids (Figure 19). Catechin forms the structure of condensed tannin or phlobaphenes.

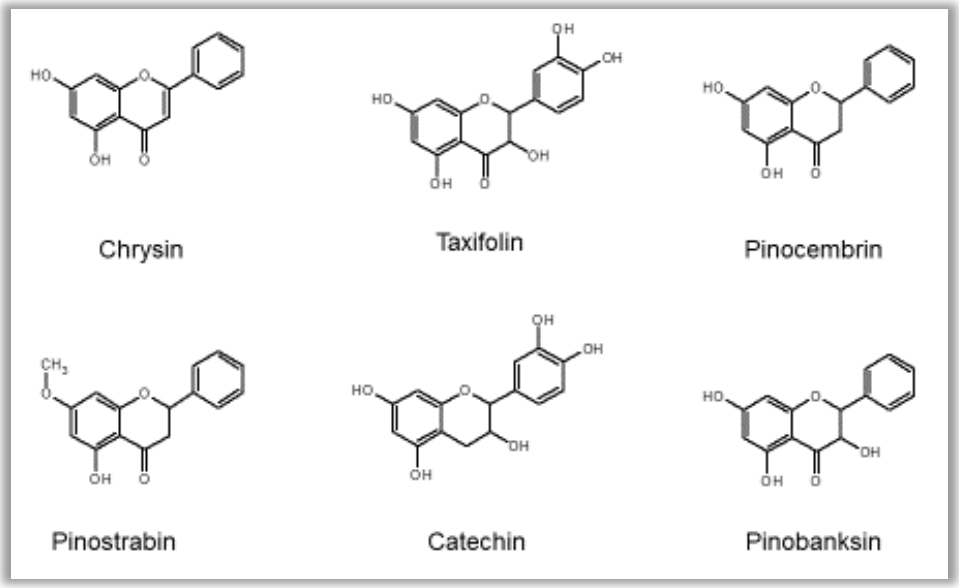

Figure 19 some softwood flavonoids.

Apart from those mentioned extractive class and subclasses, n-alkanes are also found in extractives. Sugars such as glucose, sucrose and fructose are also found in water-soluble extractives. Polyoses are also present in extractives. In tropical hardwood, along with protein, nitrogen-containing alkaloids such as berberine, quinine, lindenine also occur in specific species (Figure 20) and as many as 67 different alkaloids are reported.

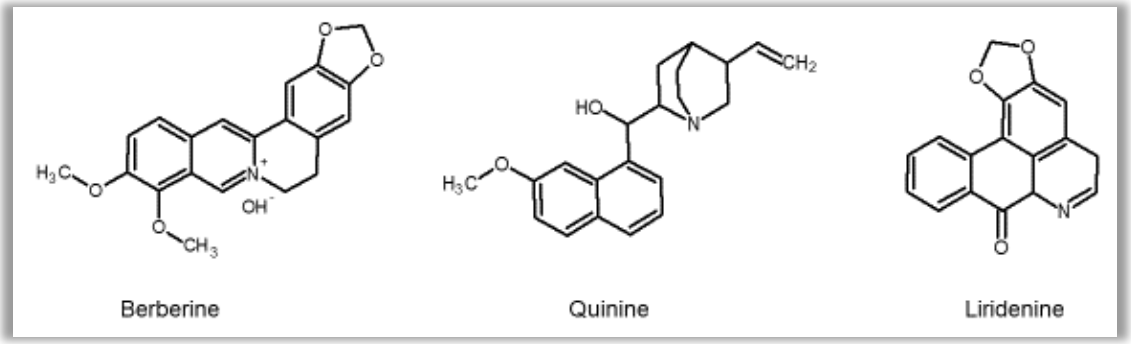

Figure 20 Alkaloids from hardwoods

In the case of Scots pine, the extractives are reported from 2.5 to 4.5% on a dry mass wood basis.[61] Percentage of wood extractive as dry mass for Scots pine is reported at 4.5%.[61] It is understood that all components of wood need to be optimally utilised for the commercial success of forest waste biorefinery.[13, 26] Structures of all components are different and could be potentially separated. Unfortunately, there is less emphasis on integrating extractives to the biorefinery process. It is also known that some specific extractive compounds may be found other than from xylem of wood. For example, the needles of conifers may contain specific resin

acids such as imbricataloic acid, pinofolic acid. Some cyclic acid (quinic acid and shikimic acid) and cyclitols (myoinositol and pinitol) are found in the needle (Figure 21).

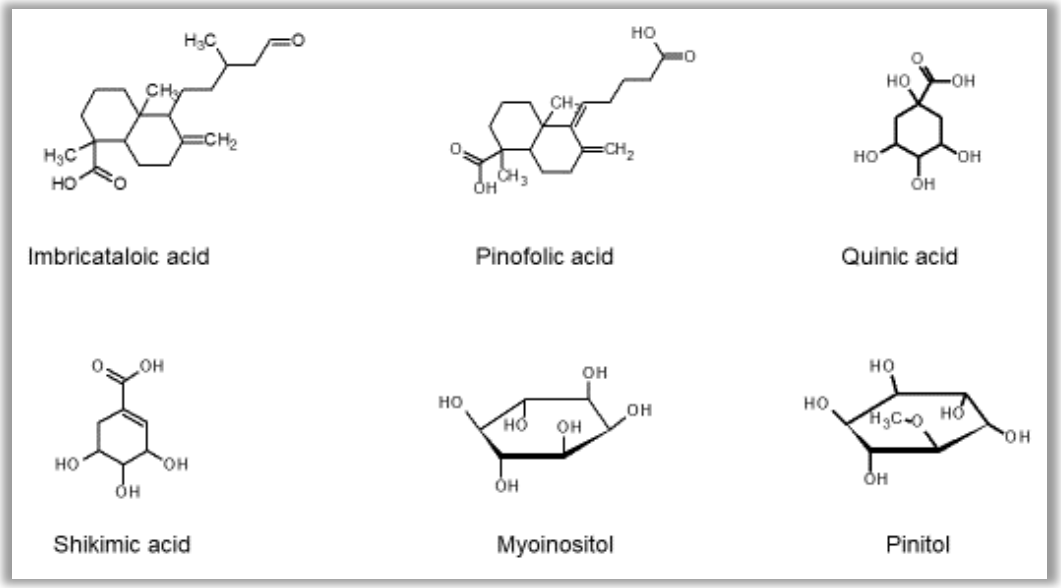

Figure 21 Extractives found in needles

1.5 Biorefinery Processes for Platform Molecules

The diverse component of lignocellulose biomass has the potential to convert sufficient platform molecules to replace petro-refinery chemicals. The feedstock of biorefinery platform molecule could be from polysaccharides (starch, cellulose, hemicellulose, inulin, chitin etc.), protein, lignin and extractive (terpenes, triglycerides, pigments, waxes, etc.) of lignocellulosic biomass. The monomeric hydrolysis sugars of polysaccharides such as glucose, fructose and xylose and mono and disaccharides of edible carbohydrates can be converted into platform molecule as is shown in Figure 22 (e.g. ethanol, itaconic acid).[62] By enigmatic hydrolysis of starch, glucose is already being in the product at industrial scale from potato, corn, wheat and tapioca for platform molecule.[63]

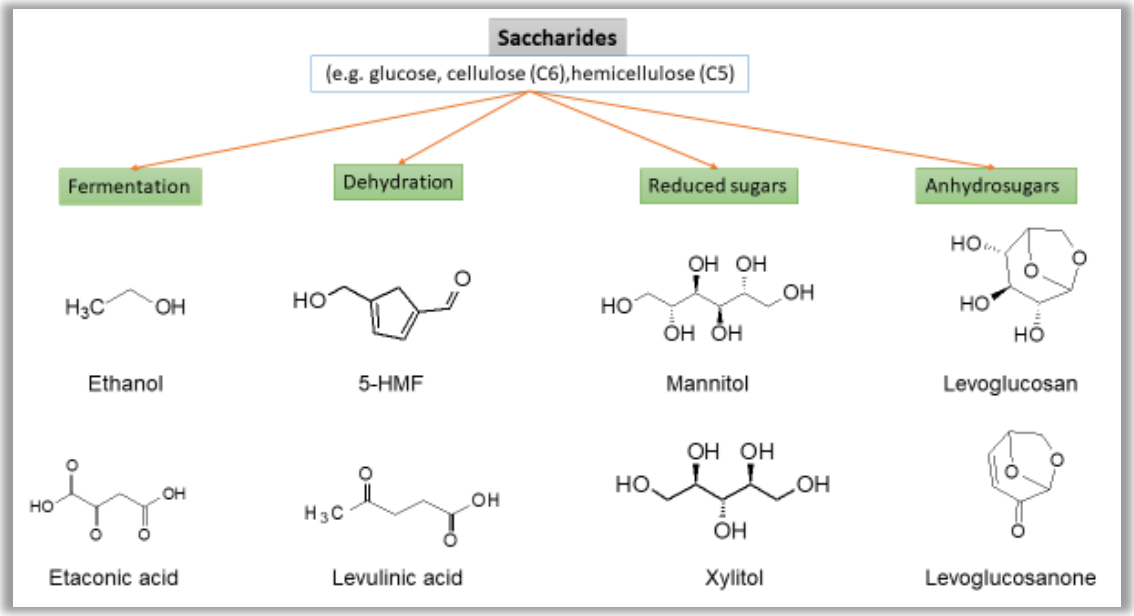

Figure 22 Example of saccharides derived platform molecules.

Using the biorefinery method, from cellulose two valuable platform chemical isosorbide and 5-hydroxymethylfurfural could be commercially gained.[64] Through liquefaction of cellulose, other platform chemicals such as sorbitol, fructose, mannitol, furfural, levulinic acid, malic acid, erythrose, lactic acid, hydroxyacetone, glyceraldehyde etc. could be gained.[64] Lignin is the potential source of biobased aromatics. As lignin is very complex and difficult to separate into its simpler components, still there is no industrial success although research is ongoing. Due to this limitation of separation, presently pyrolysis (>500 °C) and hydrothermal hydrolysis (<400 °C) and hydrogenolysis conversion of lignin is a popular route to get platform molecules from lignin (Figure 23).[65] In hydrogenolysis conversion, steam is replaced with hydrogen often accompanied by a catalyst. As hydrolysis and hydrogenolysis condition is milder than pyrolysis, conversion of lignin into platform molecules is more favoured towards hydrolysis and hydrogenolysis.[62] In Figure 23, it is showing some lignin-derived platform chemicals such as guaiacol, eugenol, vanillin, vanillic acid, syringol, catechol and their route to obtain.[66]

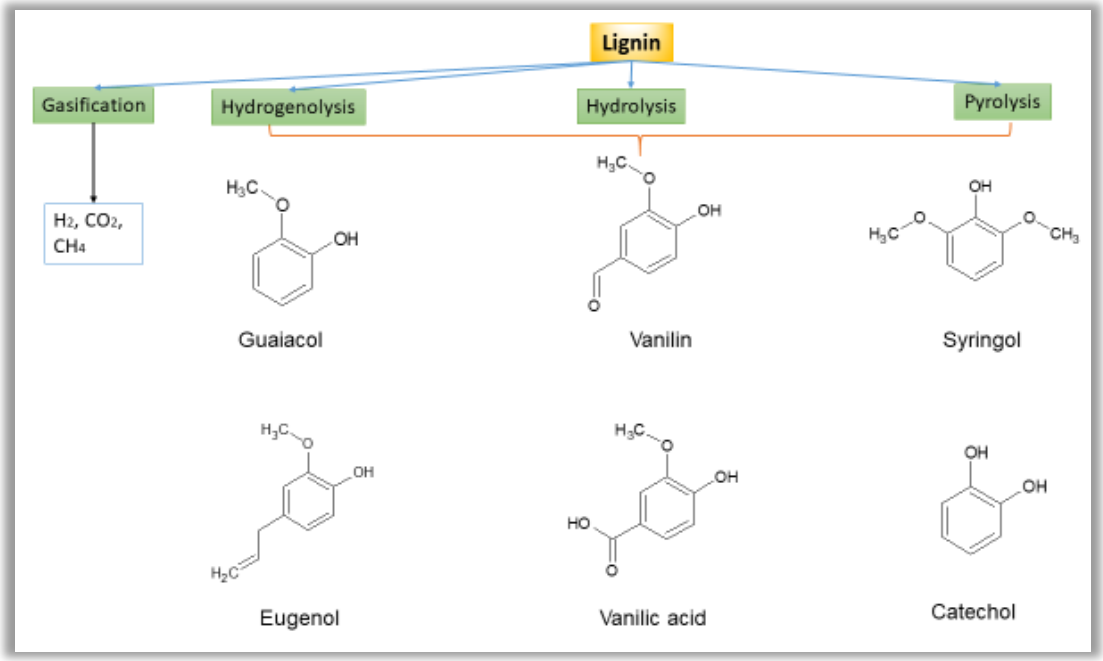

Figure 23 Examples of lignin-derived platform molecule.

Extractives are a great source of platform molecules. Extractives are comparatively simpler (such as extraction with a solvent or just pressing of seeds) to obtain than main wood components such as lignin and cellulose derived platform chemicals. Secondary metabolites such as terpenes, phenolics, triglycerides, tannins, sterols and flavonoids are examples of extractive. A short description of extractives was provided in section 1.4.5 previously. The largest volumes of available extractives are triglycerides. Some example of extractive utilisation is in the production of soap, lubricants, resins, stabiliser, plasticiser or bio-diesel.[62] The amount and character of extractive dependents on plant species and environment. For example, palm oil has over forty percent of saturated palmitic acid.[67] In linseed oil, it consists of more than fifty percent is linolenic acid while in corn and soybean predominant compound is linoleic acid. In castor oil, ricinoleic acid is dominant. [68] Platform molecule glycerol could be derived from free fatty acid and fatty acid esters.[69] Terpene such as α-pinene and turpentine oil can be used as a platform molecule through isomerisation, oxidation, reduction or hydration. Citrus peel extracted limonene is also another example of a potential platform molecule source. Terpene itself already being in the use of flavour and fragrance or as solvent.[70]

The US Department of Energy published top ten carbohydrate-based platform chemicals which are ethanol, furans, glycerol and derivatives, biohydrocarbons, lactic acids, succinic acids, hydroxypropionic acid/aldehyde, levulinic acid, sorbitol and xylitol. The present

challenge is to direct and selectively covert of those products in commercial-scale through sustainable technology.

1.6 Biorefinery: Past Present and Future

1.6.1 Types of Biorefinery

As it was mentioned in 1.1.6 of introduction, a biorefinery facility is an integrated operation to convert biomass into various chemicals, biomaterials and energy to maximise the value of biomass and to reduce waste. If feasible, food and feed product may also be incorporated into the process. The Joint European Biorefinery vision for 2030 targeted to meet 30% of the chemical will be sourced from biomass (the proportion of high-value-added chemicals and polymers target even above 50%). Thirty percent of the heat and power energy of EU will be sourced from biomass by 2030.[71] Biorefinery as it developed historically, can be described with three different phases: Phase-1, Phase-2 and Phase-3 biorefinery.[27, 72]

1.6.1.1 Phase-1 Biorefinery

Only one type of feedstock is used in a single process. The major product is also one only in this type of biorefinery. This simple biorefinery is already commercially in operation and economically stable. Many of those biorefinery types produce biodiesel in the EU. In Figure 24, a biodiesel production scheme is shown, which uses the transesterification process to produce biodiesel and glycerine in a single step.[73] Pulp and paper industries also fall into this category. As this type of facility is fixed, the recovery of investment and operational cost are not flexible to through conversion of the facility when the feedstock is not in constant supply or market demand changes.

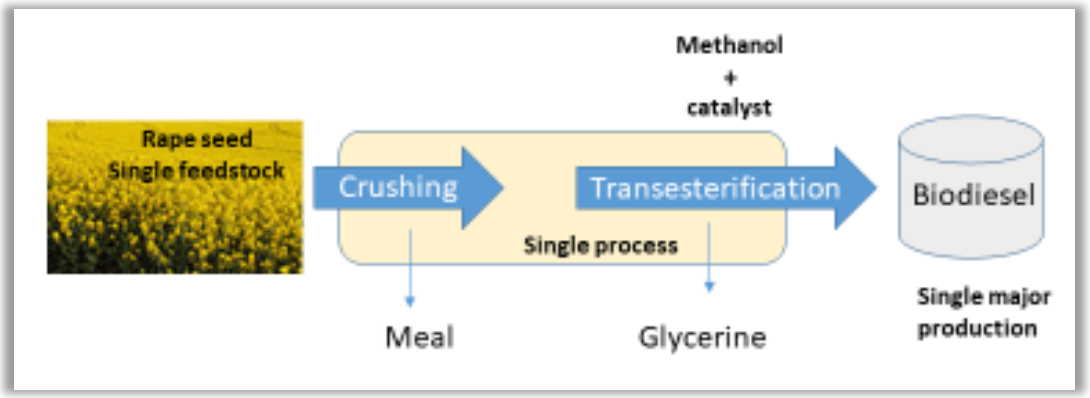

Figure 24 Phase-1 biorefinery for biodiesel production

1.6.1.2 Phase-2 Biorefinery

Although Phase-2 biorefinery only processes one feedstock, it can deliver more than one product. Energy, materials and chemicals are produced in this type of facility and can cope with market demand and supply. A study of Wageningen University has shown that the product cost of biofuel could be reduced up to 30% to produce biodiesel if the phase-2 type of biorefinery is used instead of single type product biorefinery.[71] Figure 25, shows an example of phase-2 biorefinery, which is operated at Roquette site of Lestrem in France. This plant produces polyols, cyclodextrins, organic acids, resins, native and modified starches, proteins and more than 600 carbohydrate derivatives.

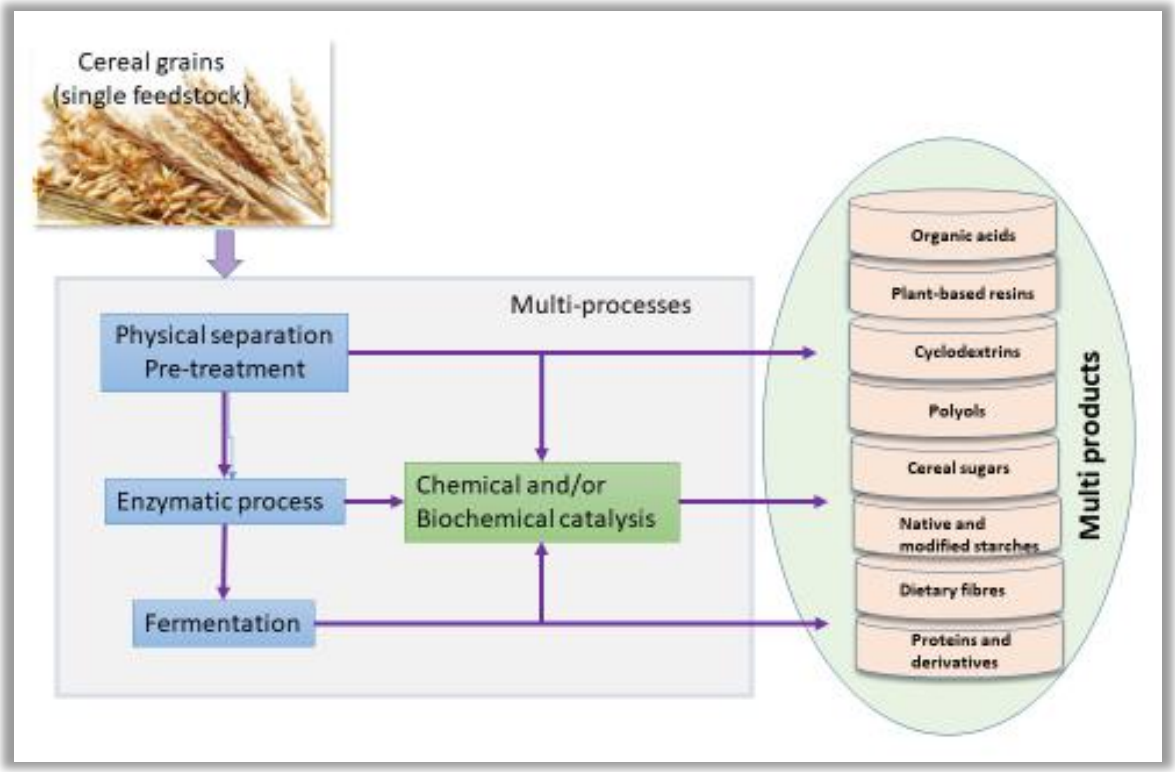

Figure 25 An example of phase-2 biorefinery

1.6.1.3 Phase-3 Biorefinery

Phase-3 biorefinery is the most advanced type of biorefinery. It can not only produce multiple products in multiple processes but can also handle different types of feedstock. Although this type of biorefinery does not yet commercially exists, major works are in progress in the EU and the US to develop these modern types of biorefinery.[71] Due to the high flexibility of feedstock, the changing market demand can be coped with this phase-3 type biorefinery successfully. Five different phase-3 biorefinery system, based on feedstock, is currently in the research and development phase. Those phase-3 biorefineries are:

1. Lignocellulosic feedstock biorefinery
2. Whole-crop biorefinery
3. Green biorefinery
4. Two-platform biorefinery and
5. Marine biorefinery

1.6.1.3.1 Lignocellulosic Feedstock Biorefinery

The lignocellulosic biorefinery feedstock biorefinery will use wood, corn, straw or any other types of lignocellulosic materials as feedstock to produce food and feed, energy, materials, chemicals (Figure 26).[71]

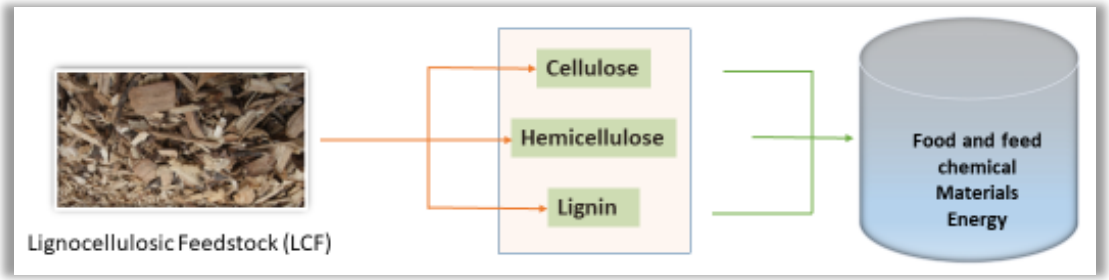

Figure 26 Lignocellulosic feedstock biorefinery in a simplified diagram

The US-based ZeaChem has built a demonstration phase-3 lignocellulose based integrated biorefinery plant at the Port of Morrow in Boardman, Oregon. In this plant, they use nearby grown biomass to produce C2 chemical (acetic acid, ethyl acetate, ethanol and ethylene) and C3 chemicals (propionic acid, propylene acetate, propanol and propylene) using microbial and thermochemical process (Figure 27) (http://zea2llc.com/solution/technology/).

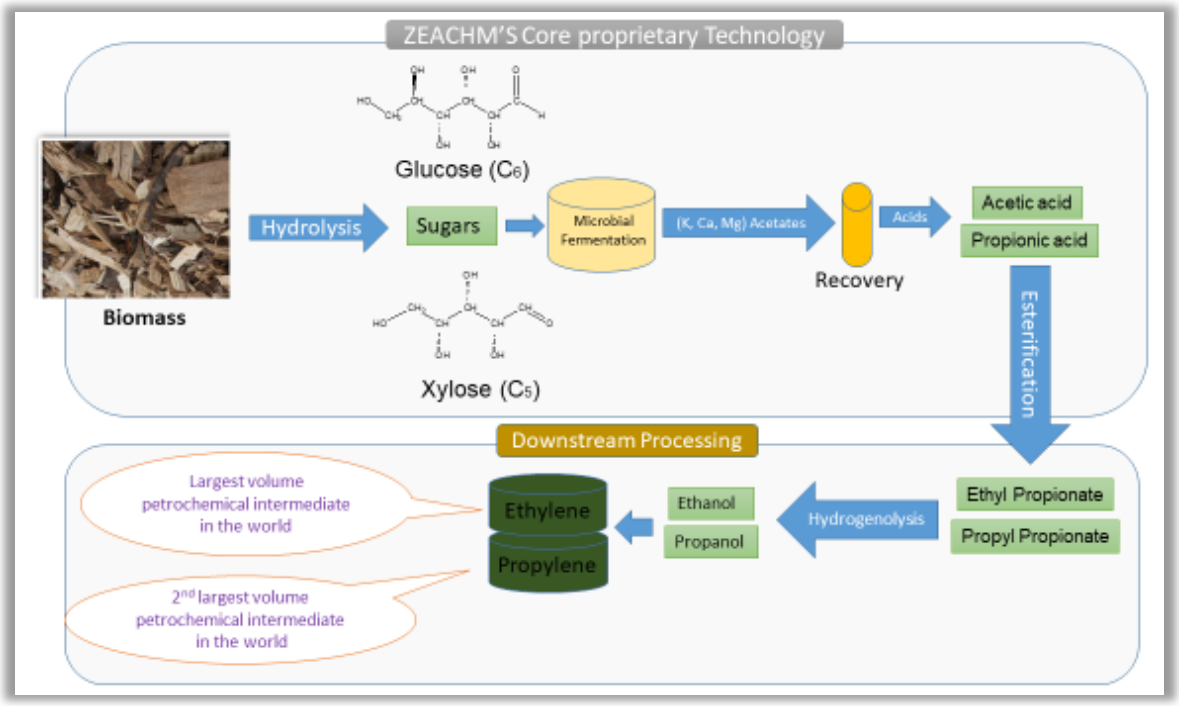

Figure 27 ZeaChem's Phase-3 lignocellulosic demonstration plant's production scheme

Another modern example of phase-3 biorefinery is the SP Processium AB of Sweden.[http 11] It is formed with the collaboration of RISE Research Institute of Sweden and association of some industries which formed based on industrial symbiosis. Those industries use ones forest Lignocellulosic waste by-products as raw material for another industry.[74] Along with some other service providing companies, Sveaskog Förvaltnings AB (timber, pulpwood and biofuel), Umeå Energi AB (energy), Bio Energy Development North AB (conversion and refinement of biomass raw material), Metsä Board Husum (high quality coated and uncoated fine paper and pulp), Mondi Dynäs AB (kraft paper), Ragn-Sells AB (recycle waste product), SCA Packaging Obbola AB (unbleached kraft liner), Domsjö Fabriker AB (speciality cellulose for the textile material viscose, lignin and bioethanol), AkzoNobel Functional Chemicals AB (cellulosic specialities and speciality chemicals) and SEKAB (green chemicals and biofuels) uses one's waste or by-product to generate biomass energy, materials and chemicals (Figure 28).

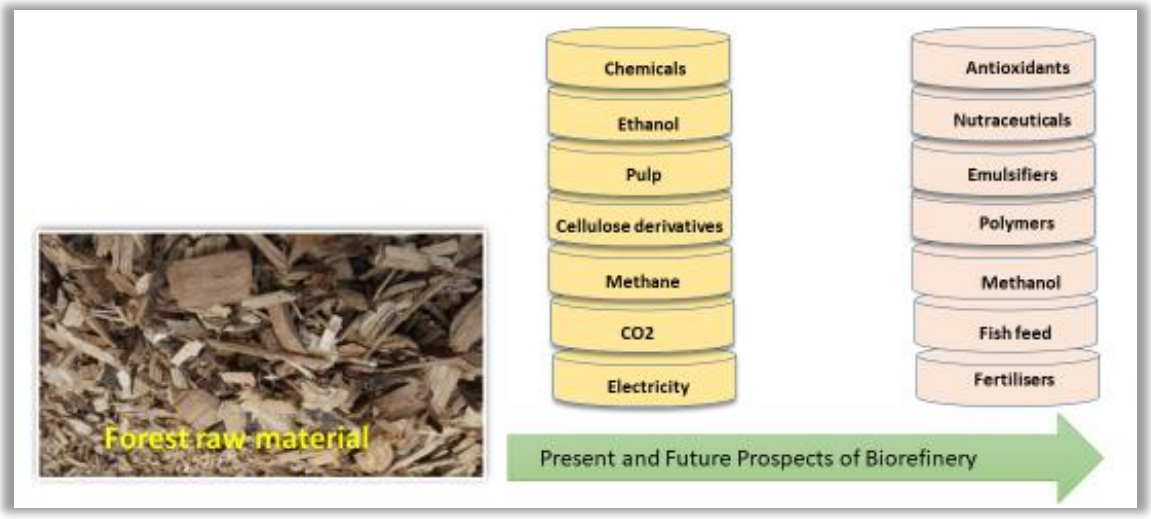

Figure 28 Lignocellulosic biorefinery diagram of SP Processium AB

1.6.1.3.2 Whole-Crop Biorefinery

The whole crop biorefinery, as it says by its name, will use the whole crop as feedstock (Figure 29). The crop and straw are then separated. The seeds are processed to produce starch and other valuable products such as ethanol and bioplastics. The straw is processed as feedstock like it was mentioned in Phase-2 biorefinery.

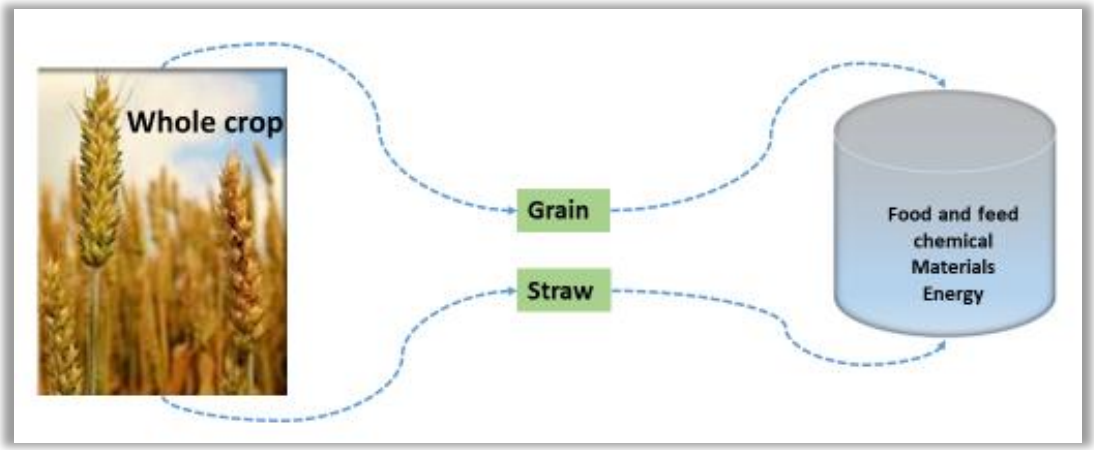

Figure 29 Simplified diagram of whole-crop biorefinery

1.6.1.3.3 Green Biorefinery

Green biorefinery uses green biomass such as green grass, cereals or clover as feedstock in phase-3 biorefinery to produce material and chemicals.[75-77] Green biorefinery is being studied in Germany, Austria and Denmark for last 20 years.[78, 79] Water-rich green biomass is pressed into cakes and nutrition-rich juices (Figure 30). Organic acid, amino acid and dyes are extracted from juices. The press cake is utilised to produce energy, biocomposites, insulation materials

and construction panel etc. A demonstration plant in Brandenburg shown to produce lactic acid, proteins and fodder from wild mix grass and Alfalfa.

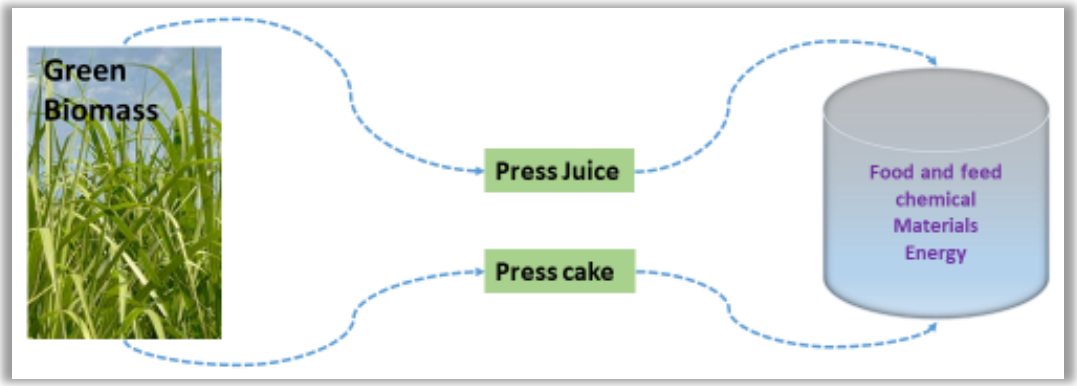

Figure 30 Green biorefinery diagram

1.6.1.3.4 Two-Platform Biorefinery

In this phase-3 biorefinery type, the feedstock is separated into two platforms such as sugar platform (biochemical) and syngas platform (thermochemical). Both platforms can then be utilised to convert value-added chemicals, material, energy, food and feed. Although no biorefinery of this type currently exist in the EU, wheat grain to ethanol fermentation and Lind'e Carbo-V® gasification approach exist independently.[71]

1.6.1.3.5 Marine Biorefinery

There is a huge interest to convert micro and macroalgae to use as the feedstock of phase-3 biorefinery to produce value-added chemicals, material and energy.[80-83] But unlike terrestrial biorefinery development, the marine biorefinery is still in infancy.

1.6.2 Pretreatment in Biorefinery

To utilise lignocellulosic biomass for value-added materials and chemicals, separation of hemicellulose, the delignification of the cell wall, the breakdown of chain length and crystallinity of cellulose, the recalcitration of biomass is needed.[84] According to Mosier *et al*, an ideal pretreatment should reduce no or little biomass size reduction, effective and feasible high solid loading, produce highly digestible feedstock in case of subsequent fermentation process without forming inhibitors, preserve solubilised carbohydrates, cost-effective with low energy consumption.[85] The pretreatment of biomass helps to reduce a significant step into the biorefinery process. For microbial biorefinery process, reducing lignin content help microorganism and to digest cellulose more effective than original biomass due to the less inhibitory effect of lignin on the microorganism.[86] Besides facilitating the more favourable process by pretreatment, it also reduces environmental pollution by releasing the less harmful

chemical into the environment and economically more feasible by reducing waste and controlling cost.[86] In Figure 31, some common and emerging biomass pretreatment process is shown. Among all of those process, the appropriate pretreatment or combination of some of those depends on the types of biomass and biorefinery and targeted chemical, energy and products.[87] For this reason, there is no single "ideal" approach.[88]

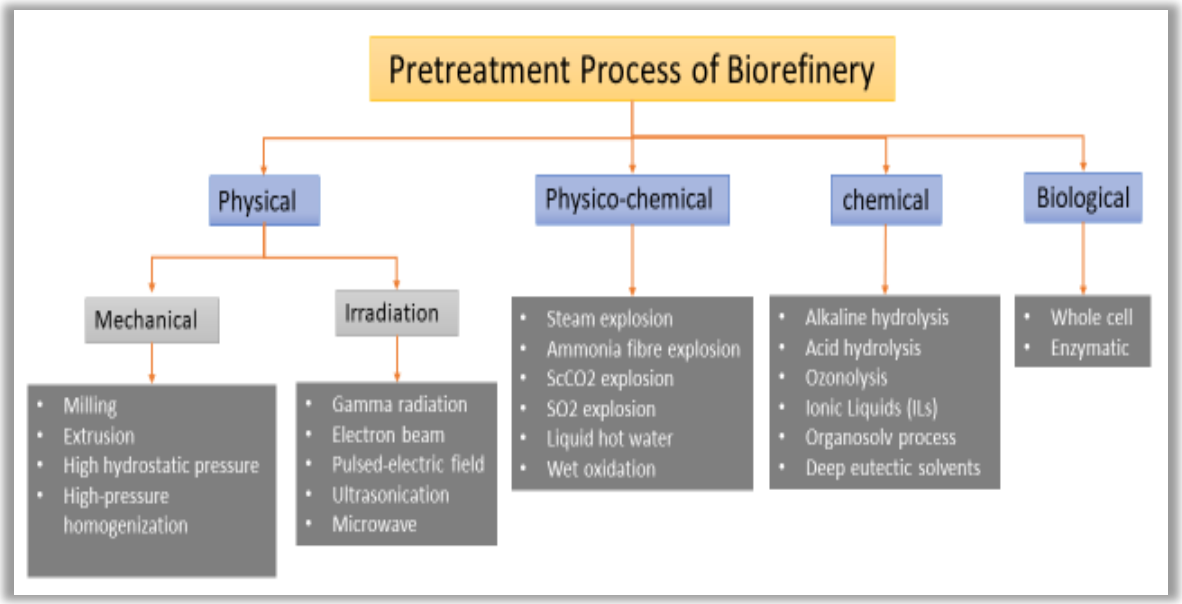

Figure 31 some common and emerging pretreatment process of biorefinery

The major pretreatment process is discussed below:

1.6.2.1 Mechanical Pretreatment

Physical pretreatment can be divided into traditional mechanical size-reducing steps such as milling, extrusion, high hydrostatic pressure or high-pressure homogenisation. Other emerging physical pretreatment processes are gamma radiation, electron beam, pulse-electric field, ultrasonication and microwave irradiation. Using chipping, grinding and milling the size of biomass can be reduced as small as 0.2 mm.[89] The particle size depends on the type of biomass, time of milling and type milling method.[90] The extrusion is another common physical pretreatment method. One or two screws tight together and spin around in the sample feeding path. The extrusion process is combined with high temperature (>300 °C). The combination is two forces causes the lignocellulose biomass to shear.[90] The size and arrangement of screw setting, barrel temperature and screw speed determine the final effect on biomass size reduction.[91] In the ultrasonic method, cavitation inside biomass is created and the shear forces breakdown complex network of biomass structure and facilitate the removal of its components.[92] The use of solvent and its nature can also influence the effect of ultrasonic

pretreatment.[93] Ultrasound frequency, duration of sonication, power and pretreatment temperature also factors of ultrasonic influence.[94] It was reported that use of ultrasonication can reduce hydrolysis time of biomass as high as 80%.[95] The High hydrostatic pressure (HHP) technique produces pressure as high as 600 Mpa, and it is long been used in the food industry as a non-thermal process for Pasteurization.[95] HPP can create pressure on all parts of biomass irrespective of biomass size and shape. The created pressure also reduces the volume, the thermodynamic effect enhance structural reaction and enzyme-catalysed reactions.[95] The High-pressure homogenization (HPH) homogenises the size of suspended biomass particulate by passing through a specific valve in equal volume by creating high pressure.[95]

1.6.2.2 Biological Pretreatment

Biological pretreatment is known as low cost, less energy-consuming and eco-friendly.[95] Lignocellulosic biomass can be pre-treated with lignin-degrading bacteria or fungi as whole-cell or enzymes. Lignin peroxidase, laccases, versatile peroxidase and manganese peroxidase enzymes are used to degrade lignin. Fungi can be used for cellulose, lignin and hemicellulose degradation as a pretreatment step.[95] Soft-rod, white-rot, brown-rot and fungi are used for hemicellulose and lignin degradation.[96] Some white rod fungi can selectively degrade lignin while other white rod fungi can degrade polysaccharides and lignin and as such can remove all carbohydrates from biomass.[97] Hydrolytic and lignolytic extracellular enzymatic systems are present in microorganisms.[97]

1.6.2.3 Physico-chemical Pretreatment

Steam explosion is one of the most common pretreatment methods of lignocellulose pretreatment methods.[95] In high pressure (0.69-4.83 MPa) and temperature (160-260℃), saturated steam is applied on biomass. In this condition, water molecule penetrates inside the biomass structure and then pressure is suddenly removed. In reduced pressure water molecule forcefully escape from biomass like an explosion. The cycle is continued until biomass fibres split. This steam explosion forces cleavages hemicellulose-lignin bonds. It also cleavage glycosidic bonds of cellulose.[98] Hemicellulose further hydrolysed into glucose and xylose monomers which degrade into acetic acid. The produced acetic acid then further hydrolyse hemicellulose and the cycle continues. For this reason, the steam explosion is also called autohydrolysis.[99] The working principle of the SO_2 explosion is similar to the steam explosion.[86] In ammonia Fibre explosion (AFEX) method, liquid ammonia at 1:1 ratio and at around 60-100 ℃ is applied on biomass in a closed vessel.[100] In this condition, the biomass is swelled. When the pressure is released on a sudden, the fibre structure of biomass disrupt, and

cellulose crystallinity reduces. By adjusting the temperature, blowdown pressure, the ratio of water and ammonia the biomass pretreatment is optimised. It also partly release hemicellulose and lignin from biomass. In supercritical CO_2 pretreatment of lignocellulosic biomass, CO_2 diffuses into biomass as a gas at high pressure. Due to its liquid-like solvating power, it can easily form carbonic acid with water molecule inside the biomass cell. When the pressurised $ScCO_2$ released in a low pressure, it shattered the structure of hemicellulose and lignin. The formed carbonic acid act as a catalyst for hemicellulose hydrolysis. In this way, the cellulose fibre becomes more accessible.[101] The liquid hot water (LHW) pretreatment method employs high temperature (170-230 ℃) and at up to 5MPa. Although LHW employs similar condition as steam expulsion, it uses hot water instead of steam. LWH process hydrolyses hemicellulose and releases acetyl groups, and in this way, lignin is also liberated.[102] LHW pretreatment is carried out in the pH range of 4 to 7 to avoid sugar degradation and formation of inhibitor.[103] In wet oxidation (WO) process, lignocellulose biomass is placed in a closed reactor, and high temperature (140-210 ℃) and pressure (20.0 MPa) is applied in the presence of air or oxygen for certain time (5-120 minutes).[104, 105] During wet oxidation process hemicellulose is solubilised, and lignin is decomposed into water, carbon dioxide, phenol and carboxylic acid. The degradation of lignin and solubilisation of hemicellulose facilitate to rupture of the cell wall and open up cellulose crystal.[106]

1.6.2.4 Chemical Pretreatment

Among chemical pretreatment process, alkali pretreatment most widely used method. Alkali reagents such as calcium, potassium, sodium or ammonium hydroxide are used to solubilise lignin of lignocellulosic biomass.[95] Among all of those alkaline reagents, NaOH is found to be the most effective agent for this purpose.[107] The saponification reaction of alkali reagent breakdown the ester linkage between lignin and hemicellulose. In this way, cellulose becomes available to further downstream process such as enzyme reaction.[108] The carbohydrates also become available to enzymatic hydrolysis when uronic acid and acetyl group of hemicellulose are removed during the alkali process.[109] Alkali also causes cellulose to swell and degrade the crystal structure and chain length.[110] The acid pretreatment works on the glycosidic bond of cellulose and hemicellulose.[95] The acid catalytic hydronium ion breakdown the chain length of cellulose and hemicellulose and produce sugar monomer.[111] Both organic acid and inorganic acid are used for the pretreatment purpose. Among organic acids formic acid[112], oxalic acid[113] and maleic acid[114] and inorganic acid are found to be used in acid pretreatment. Nitric acid[115], sulphuric acid[116] and hydrochloric acid[117] are the examples of inorganic acids used for

pretreatment of lignocellulose. When lignocellulose biomass is treated with ozone gas in a confined reactor, it is called ozonolysis of biomass. The exposure of ozone degrades lignin and partially breaks the bond of hemicellulose of biomass by selective oxidation.[89] Ionic liquids (ILs) are a class of solvents which melts <100 ℃ and consists of organic cations and organic or inorganic anions. Organic cations can be pyridinium, imidazolium, alkylated phosphonium, sulfonium or aliphatic ammonium ion.[118] Among all of those types ILs, imidazolium salts are the most common.[119] Both cation and anions of ILs facilitate to breakdown intra and intermolecular hydrogen bond of cellulose by binding with those intra and intermolecular hydrogen and hydroxyl groups by ionic liquid themselves.[95] After the breakdown of biomass, ILs is possible to recover. Deep Eutectic solvents (DES) are comprised of two to three components of ionic fluids interlinked with hydrogen bond and form a eutectic mixture and normally liquid above 100 ℃.[95] DES is similar to ILs in terms of physicochemical properties, but they are biodegradable.[120] DES can form acidic hydrogen donor bond and facilitate to remove lignin and hemicellulose more effectively than ILs.[121]

1.6.2.5 Organosolv Pretreatment

Various solvents such as acetone, methanol, ethanol, organic acid, ethylene glycol are among the solvents that have been used organosolv for biorefinery purpose. Water and catalyst were also mixed in various ratios to optimise the effectiveness of organosolv pretreatment of biomass.[122] To optimise the product yield, the pretreatment temperature, time, concentration of solvent also varied depending on biomass and product type. Solvent works on biomass in three different ways. Firstly, the organic solvent passes inside the biomass, swell through osmosis[86] and increase surface area & pore volume of cellulose.[123], For this reason, enzymatic hydrolysis of hemicellulose and saccharification increase.[123] Secondly, solvent also effect on the aryl ether bond of lignin and cleavage the bond.[124] Thirdly, depending on the pre-treatment condition, glycosidic bonds of major hemicellulose decompose, and a fraction of cellulose also disintegrate into oligosaccharides and monosaccharides. The oligosaccharides and monosaccharides of hexose are converted into HMF and pentose convert into furfural.[125]

High-boiling-point solvents such as ethylene glycol and glycerol also used for this purpose. High boiling point solvent is advantageous over low-boiling-point solvents in terms of low operating pressure, less flammable, low requirement of energy and less toxic.[126, 127] In biodiesel production, the use of glycerol is readily available as large quantity is readily available as a by-product of the oleochemical industry.[128, 129] Use of ethylene glycol as a solvent to remove lignin and hemicellulose from palm oil empty fruit bunches is reported.[130] Although there is no known

commercial-scale use of any solvent in biorefinery, in pilot-scale application use of solvents has proven to be effective. Leaf Resources Limited at Darra in Queensland of Australia already using organosolv in the industrial-scale biorefinery.

1.6.2.6 Irradiation

Gamma radiation can penetrate the structure of lignocellulose.[131] It can degrade the crystalline and amorphous region of cellulose of lignocellulosic of biomass. The gamma radiation also modifies lignin.[132] The gamma radiation also alter the linkage between carbohydrate and lignin in biomass and such decrease the particle size, distribution range, thermal stability and increase specific surface area.[133] Linear accelerator generates Electron beam (EB). When accelerated EB exposed to biomass, it penetrated the cell wall, create free radical and disrupt the structure of lignin, cellulose and hemicellulose.[131] The chain scission and decrystallization of the lignocellulose component makes the biorefinery process effective. Plant biomass is placed in pulsed-electric field (PEF) of two electrodes of voltage pulses with an electrical field strength of 0.1–80 kV/cm for a very short time (10−4 and 10−2 s).[131] The PEF disrupt the biological membrane and changes the local structure.[134] The created pore of cell membrane facilitates hydrolytic enzymes penetration inside the cell wall in the biorefinery process.[90, 135-137] PEF also causes delignification of lignocellulosic biomass.[136] [135] Ultrasound was used for biomass pretreatment by some researchers, and it was shown that the surface structure of the biomass was changed and oxidising radical was produced during ultrasound pretreatment.[138] After ultrasonication on biomass, bubble forms inside and grow up to a critical size and then violently collapse. The ultrasonication process can create pressures up to 1800 atmospheres pressure and 2000–5000 K temperature in the microscopic environment of biomass.[139] The formation of small cavitation bubble and radical chemically alters the structural polysaccharide and disrupt α-O-4 and β-O-4 linkages of lignin.[90, 100] In this way, hemicellulose become accessible and extractable.[139]

1.6.2.7 Microwave Heating Pretreatment

Microwave heating pretreatment (MHP) has recently attracted much attention due to its green credential such as no or less use of solvent.[140] In MHP generation waste or smoke can be avoided and processing time also reduced by tenfold by fasted volumetric heat transfer.[141] It was suggested by Fan *et al.* that the cellulose of lignocellulosic materials depolymerisation is believed to in the amorphous region of the cellulose crystal at a temperature above 180 °C.[142] In the amorphous cellulose region, the hydroxyl group of glucose ring C_6 carbon interact with MW, generate hotspot and transform thermochemically. DC electron transport through the hydrogen chain of the cellulose crystalline region is also possible.[143] Another hypothesis is that

the O-H group of the biopolymer can efficiently absorb MW to cause acceleration of the heat and thus create internal pressure.[144] The created pressure cause changes in the material structure through fast expansion.[145] As many factors influence MW interactions with material including design of reactor vessel, various single-mode and multimode reactors made of glass, teflon or stainless steel are available commercially to optimise material-specific pretreatment process.[146, 147] For atmospheric pressure reactor, MHP medium can be high boiling point solvent such as glycerol, 1-4 butanediol. Ionic liquid, alkali or salt. Closed vessel reactor is used for high-pressure MHP and catalyst, acid or alkali could be used as a medium.[88] For sequential pretreatment strategy, MHP is performed with extrusion, steam explosion, ball milling, ozone or hot water.[88] In Table 1, some example of MHP of lignocellulosic biomass with a combination of other pretreatment and MHP condition were presented.

Table 1 some example of integrated MHP that were performed in lignocellulosic biomass

Feedstock	**Medium**	**MHP condition**	**Reference**
Rice straw	1% aqueous NaOH	700W for 30 min	[148]
Garden biomass	5% sulfuric acid	700W, 200℃ for 5min	[149]
Rice straw	25% acetic acid in 1:15 solid: liquid	230W for 5 min	[150]
Softwood	10% glycerol/water solution in 17:1 liquid-solid ration with 0.1% HCl as catalyst	180 ℃ for 6 min	[147]
Beachwood	1mM ammonium molybdate, 0.88 M H_2O_2	400W for 6min at 140 ℃	[151]
Corn stover	Autohydrolysis, 5% solid	75W for 20 min at 180℃	[152]
Corn stover	Steam explosion, 1.25MPa pressure	540W for 5min at 200 ℃	[153]
Corn stover	10% solid immersed in $CaCl_2$	800 W for 5 min at 200 ℃	[152]

1.6.3 Advantages and Disadvantages of Pretreatment Methods

Pre-treatment		Advantages	Challenges	Way forward
Mechanical	Milling	Reducing the size of biomass improves the efficiency of mass and heat transfer and hydrolysis.[154] Can be used for pretreatment of a wide variety of feedstock.	Operation is a highly energy-intensive and inefficient process.	Cost and efficiency balance needs to improve. Equipment selection for particular size reduction may reduce the overall process economy.
	Extrusion	The sheer stress of extruder disintegrate cellulose fibre, enhanced porosity and increase contact surface for enzymes. Less hazardous and can be operated at moderate temperature.[155]	Consume high energy. Without the use of chemical agents, the effect is insignificant. Generate inhibitory compounds. Hemicellulose degrades partially. Lignin carbohydrate matrix destruction is also incomplete.[101]	Effective on herbaceous type biomass pretreatment.[156] Adaptable in a different process.
	High hydrolytic pressure (HPP)	Pressure distributes equally on all parts of biomass, whatever the shape and size. By decreasing volume, the pressure accelerates all of the structural reactions. Additionally, pressure selectively effects on hydrogen bonds only, Pressure can direct changes in	Operating cost of HPP is expensive for enzymatic reactions and not always practical.	HPP is a promising choice, not only for biomass pretreatment, but also for inducing hydrolytic enzymes stability and activation.[158]

		enzyme structure and thus can changes reaction mechanism.[157]		
	High-pressure homogenisation (HPH)	HPH pretreatment is an eco-friendly method for biogas production. It can destroy the microstructure lignocellulose and enhance enzymatic attack.[159]	Expensive to operate.	HPH is an environment-friendly process and needs no addition of chemicals.
Irradiation	Gamma radiation	Enzymatic hydrolysis rate increases.	Products like glucose may be reduced due to excess radiation.	Combination with another method such as acid treatment may reduce overall operation cost.
	Electron Beam	At the commercial scale, it is proven effective.	Penetration depth is limited and required high-energy.[160]	For profitable industrial use, more research is needed.
	Pulse-electric filed (PFE)	The cell wall structure of lignocellulosic may be effected a various degree depending on the PEF parameters. PEF helps to delignification of lignocellulosic biomass.[161]	Expensive to operate.	PEF is a promising tool for lignocellulosic biomass pretreatment for biofuel production.[135] More research is needed to understand the interaction of lignocellulose and pulsed electric fields.[135]

	Ultrasonic energy	Able to disrupt different form of lignocellulosic matter. Accelerate reaction time and effective over a range of particle sizes.[162] it can reduce hydrolysis time of biomass up to 80%.[138]	At the same ultrasonic conditions different lignocellulose responses differently and hence for specific biomass optimisation adjustment needed.[163]	Combined pretreatment operation proved cost-effective. Pretreatment with ionic liquids and organic solvents shows potential.[162]
	Microwave	Highly energy efficient with increased reaction rate in a short time. The process operation is easy, formed minimum inhibitory product.[164] .	Uncontrolled application of energy may degrade primary products to unwanted secondary products.	Mechanistic understanding of the MW-biomass or interaction of any relevant MW absorbing material in the system is essential to control the overall process.
Physico-chemical	Steam explosion	Environmental friendly, no need for recycling. The energy requirement is low as residence time is short.[165]	Soluble lignin condensation and precipitation cause the biomass less digestible for fermentation. Hemicellulose xylan is also destructed in the process. Soluble sugar is also washed away during hydrolysate wash.[166]	Although SE is less effective for softwoods pretreatment, it is more effective for hardwoods and agricultural residues processing.[166]

	Ammonia fibre	The process needs short residence time, moderate temperature and pH. As it is a dry-to-dry process, no toxic chemicals are generated in downstream processes.[167] The production of inhibitory degradation compound is low in fermentation.[168] [169, 170] [171]	Due to hazardous and corrosive properties, the AFEX process needed highly controlled and expensive corrosion resistance equipment set up and maintenance.[172, 173]	In the AFEX process, cellulose and hemicellulose degrade very little for a long period. Hence high loading of feedstock is possible in the enzymatic fermentation process. AFEX pretreatment is possible at biomass distribution sites for densification to save transportation cost.[174]
	Supercritical Fluid	Carbon dioxide is inert, non-toxic, non-flammable, easily available and inexpensive.[175] The SCF facility can be operated in low temperature and high solid loadings.	Capital cost for SFC pressurised equipment is high. The effectiveness of pre-treatment is low.	Although initial industrial set up cost is high, in a third-generation biorefinery, its full potential could be exploited.
	Liquid hot water	Water is a green solvent and the issue of corrosion is limited. Due to the low-temperature operation, energy consumption is less. LHW also limits the formation of degradation products.[176]	Down-stream processing is energy demanding as the concentration of the product is low in LHW.	As environmental-friendly technologies, no need for expensive recovery cost.

	Wet	Inexpensive agents, such as oxygen and air, are readily available.	In Wet oxidation, high temperature & pressurised reactor is needed and costly to maintain.	Combined pre-treatment methods proven effective for higher product yield.[106, 177-179] Combined use with alkali pretreatment proved effective against inhibition of product formation of fermentation or hydrolysis.[180]
Chemical	Alkaline extraction	The alkaline reagent is comparatively safe and cheap. Alkali treatment swells the biomass and increases the internal surface area.[110] Alkali can easily remove xylan and lignin side chains and increase enzymatic hydrolysis efficiency.[181 109]	Alkaline extraction residence time is long, and neutralisation steps are difficult.	Biomass can be fractionated with mild alkaline treatment for flexible utilisation in biorefinery.[107]
	Acid hydrolysis	Dilute acid pretreatment helps to accelerate hemicellulose and cellulose hydrolysis.	Degrading products of sugars inhibit microbial fermentation. Due to the corrosive nature of the acid, the construction and maintenance of process facility are expensive.	The process solubilises hemicellulose and converts into fermentable sugars without the use of hemicellulosic enzyme. Formation of inhibitory sugar degradation products can be avoided at

				low operating temperature. Dilute acid pretreatment proven more effective for harbecious mater pretreatment than alkali pretreatment of woody biomass.[182]
	Ozonolysis	Ozonolysis can degrade lignin efficiently. The process does not produce toxic compounds in a mild condition of reaction.[183]	The ozonolysis process is costly.[184]	For sugar generation ozonolysis process was proven effective.
	(ILs)	ILs vapour pressure is negligible, non-volatile and its cation & anion is adjustable with need.[86] The ILs are immiscibility with many organic solvents and hence reusable. At low operating temperature, ILs less degrades and become available for recycle.[185]	Ionic Liquids are expensive. It is toxic to microorganism and enzymes.[186]	Production and use of less expensive protic instead of traditional dialkyl imidazolium-based ILs may reduce pretreatment cost.
	Organo-solvent	Size reduction steps of feedstock are less important, saves energy to the pretreatment of woody biomass. Using organosolv pretreatment, it is possible to maintain a mild condition of temperature, pressure and pH	To safely maintain low boiling point high pressurised explosion & fire hazardous organosolv pretreatment, the processing system	Low boiling point organic solvents are easy to recover by distillation. Integrated utilisation of biomass components through biorefinery, the

		which helps to prevent the undesirable product of the process. It is easy to recover the low boiling point organic solvents.[166] The pretreatment of high lignin containing softwood is effective with organosolv.[166]	becomes costly to operate.[105, 122]	overall pretreatment costs may be cut down.
	Deep Eutectic Solvents (DES)	Due to the low-cost synthetic route and biodegradability, it is more suitable than ILs where applicable.[120] DES exhibit selectivity to solubilise biomass fractions. Removal of lignin and hemicellulose is more effective with DES than ILs.[121] In combination with the low-risk HBDs like urea, glycerol, choline chloride (ChCl) is a potential DES.[120]	DES is highly viscous and difficult to use. Under higher pretreatment condition the DES is not stabile enough.[187]	For broader industrial application and scale-up, low viscous DES is needded to develop.
Biological		Low energy demand and eco-friendly.[181, 188, 189 156] Effluent is not produced during the processa and toxic compounds are not released to the environment.[189] Fermentation inhibitors are not produced during the process.[189]	Relatively high time consuming (several weeks) process.[109]	Further research is needed to determine the kinetics steps to reduce the processing time. Need to identify efficient lignin hydrolysing microbes.[95]

1.7 Current Biorefinery Processes

Industrial process of transformation of biomass into value-added products, biofuel, and energy through biochemical, thermochemical and chemical method is already demonstrated as depicted in Figure 32.[190, 191] By using standalone or combining methods (as described in section 1.5) lignocellulosic biomass including oil crops components such as cellulose, hemicellulose, lignin, lipid and starch can be converted into products or energy. The combining use of the above-mentioned process as well as the use of catalyst, microwave energy or appropriate solvent could improve the overall potential of the biorefinery process.[190, 192-194] The biorefinery processes, as shown in Figure 32 is elaborated at the following subsections:

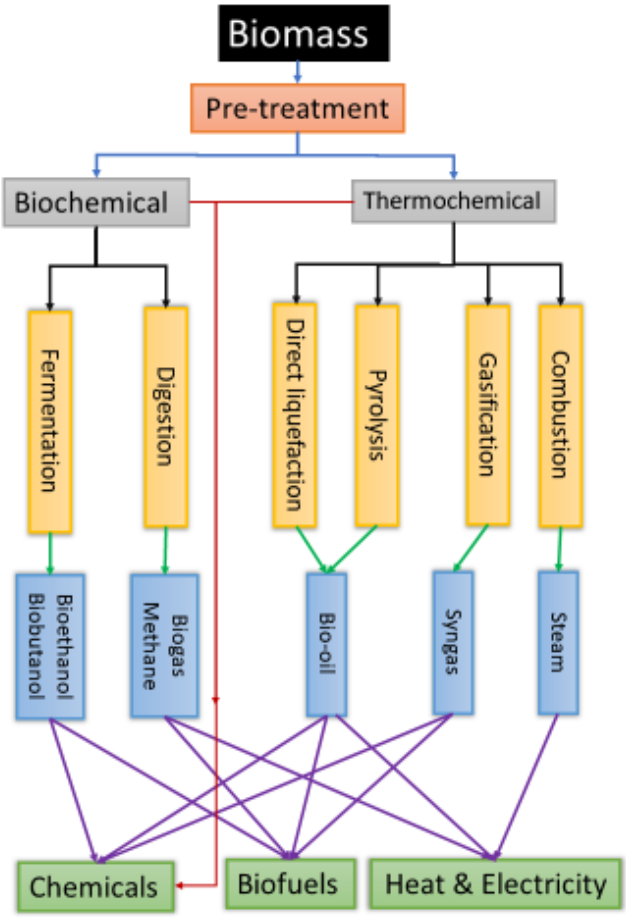

Figure 32 Main pathways of Biomass conversion, key products and main uses.

1.7.1 Biochemical Process

Biological processes are fermentation and anaerobic digestion. A brief overview of the steps are described below:

1.7.1.1 Fermentation

In the fermentation process bacteria and fungi convert biomass sugar into products such as biofuels, bio-chemicals or biomaterials. Based on the nature and chemical compositions of biomass the different type pretreatment methods are normally selected by considering the degree of recovery of carbohydrates and cost involved. To make glucose available for fermentation, in the case of lignocellulose biomass feedstock, lignin and hemicellulose removal pre-process is taken place at first step.[89] Typically acid/alkali hydrolysis is used in the pretreatment step. The hydrolysis and fermentation processes reactor design exist in different configurations such as SHF (Separate Hydrolysis and Fermentation), SSF (Simultaneous Saccharification and Fermentation), SSCF (Simultaneous Saccharification and Co-fermentation) and CBP (Consolidated Bio-Processing (CBP).[195, 196] In the case of separate hydrolysis and fermentation process, the hydrolysate from preprocessed biomass is fermented by yeast or bacteria. The benefit of SHF is the optimisation of saccharification and fermentation in the separated process. The products are either ethanol or butanols and are called Acetone-Butanol-Ethanol fermentation or fermentation ABE.[197 198 199 200, 201] On the other hand, SSF helps to save the time of hydrolysis and fermentation. The sugar and starchy biomass containing only hexose sugars and fermented to only ethanol but lignocellulose hydrolysate contains both hexose sugars (glucose, mannose and galactose) and pentose (xylose and arabinose) sugars. But only a few strains of yeast species such as *Candida shehatae*, *Pichia stipitis* and *Pachysolen tannophilus* are available to ferment pentose sugar.[202] To reduce the complexity of lignocellulose processing, hexose and pentose sugars usually conferment in a single reactor.[203] The fermentation of C6 and C5 sugars are possible to ferment simultaneously as SSCF process (analogous to SSF) to yield high biofuel. In the CBP process the production of cellulases enzyme, hydrolysis of pretreated biomass and fermentation is possible in a single stage which reduces overall process complexity. Due to comparative slow fermentation of pentose sugars than to hexose sugars, high sensitivity to inhibitors and low product tolerance the implication of SSF, SSCF and SSCF process are yet to commercialise .[202] Effective utilization of pentose sugars may be possible by genetically modified the pentose fermenting strain.[204]

The major products of fermentation are chemicals, biofuels and biopolymers. While fermentation is advantageous for low energy requirement and conversion into a wide range of chemicals, but it is labour intensive and takes long conversion time.

1.7.1.2 Anaerobic digestion

In anaerobic digestion (AD), a mixture of bacteria (syntrophic, fermentative, acetogenic and methanogenic) is used to degrade biomass into biogas (methane and hydrogen). The biomass is submitted to bacterial decomposition in the absence of oxygen at 30-65 °C. The anaerobic digestion process can be divided into hydrolysis, acidogenesis, acetogenesis, and methanogenesis stages. A consortium of bacteria breakdown insoluble biomass into water-soluble monomer at the hydrolysis stage. In the acidogenesis stage, the hydrolysate products are then converted into organic acid, alcohol, aldehyde and carbon dioxide. At the next stage, the acetogenesis bacteria further converted the short-chain compounds into. The driven acetates, carbon dioxide, and hydrogen are then finally converted into methane by methanogenic bacteria. Acetic acid is the main source of methane while about 30% of methane is sourced from carbon dioxide at the methanogenesis stage.

Anaerobic digestion process requires low energy and combusted biogas can be used for energy generation. AD can also process a wide range of biomass. The conversion rate of biomass into methane depends on the types of biomass feedstock. Impurities such as hydrogen sulphide, water, carbon dioxide, ammonia and particulates are needed to remove from methane before sending it into combined heat and power generator.

1.7.2 Thermo-chemical Process

Lignocellulose biomass can also be thermo-chemically processed through directly liquefaction, combustion, gasification and fast or slow pyrolysis.[205] In this one phase process cellulose directly transformed into liquid, gas or aqueous-phase.[204] The thermochemical conversion is superior over biological conversion in the sense that, the chemical conversion is fast and less pre-treatment is needed.[206]

1.7.2.1 Direct Liquefaction

In the direct liquefaction process, biomass is subjected to high temperature (up to 500°C) and high pressure (up to 250 bars) in a solvent to convert hydrocarbon oil. In this extreme condition, biomass is depolymerised into monomers to quickly transform into a broad range of polymeric hydrocarbon in oxygen-depleted condition.[205] The benefit of this process is that the process can use wet biomass with high (up to 78%) moisture content.[207] The residence time, selection of solvent, catalyst, temperature and pressure all are critical for optimum yield in the direct liquefaction process.[208] The hot and pressurised liquid product is then cooled, depressurised and separated into hydrocarbon oil and water.

Direct liquefaction is effective for wide ranges of biomass with high product flexibility. External heat and power supply are needed for direct liquefaction.

The main issue of direct liquefaction for various applications such as for transportation fuel is the high oxygen level of the bio-oil.[209] More research is needed to overcome the current issue of upgrading produced hydrocarbon oil.

1.7.2.2 Pyrolysis

In pyrolysis thermal process, biomass (forest residue or agricultural waste) is treated in the absence of air or oxygen to prevent combustion into carbon dioxide.[210] The biomass is submitted to intermediate temperatures (300-600 °C) in the absence of oxygen to obtain liquid pyrolytic oil (i.e., bio-oil), charcoal and light gases. Depending on the heating rate, pyrolysis is divided into first and slow pyrolysis. In fast pyrolysis heating rate could be as high as 1000 to 10,000°Cs^{-1}. In this first pyrolysis process, up to 70% of biomass may be converted into bio-oil. On the other hand, biomass residence time at slow pyrolysis is higher and at a comparatively low temperature. Slow pyrolysis facilitates to carbonise the biomass into primary product bio-char through longer residence time. The bio-oil produced by pyrolysis can be used as fuel for the boiler or turbine to generate heat or electricity. But due to high impurity, low heating value, high viscosity, incomplete volatility and unstable nature of the chemical composition,[211] it is not directly used in engine oil. It can also be further converted into chemicals.[89] The produced bio-char is used for soil remediation.

Although the pyrolysis process is advantageous for shorter conversion time and capability of converting various products, pyrolysis process itself is energy-intensive.

1.7.2.3 Gasification

This technique consists of the thermal decomposition of biomass at high temperature (>700 °C) with limited O_2 levels to generate syngas (i.e., H_2, CO, CO_2 and CH_4). The recommended moisture content of the biomass is less than 10% for better gasification.[212] The syngas can be used for heat, power production and chemicals such as dimethyl ether, alcohol, methanol, organic acid and polyesters.[208, 213]

Gasification process is compatible with various types of biomass including agricultural residue, forest waste, food waste and municipal solid organic wastes.[213] Gasification also a flexible process to produce various products. But the syngas contains impurities of tar, char, alkali, nitrogen and sulfur compounds. So, to remove the impurities before using as syngas at downstream processing a number of steps such as barrier filtering, hot gas cleaning and wet

scrubbing are needed. Gasification also requires external heat and power supply. The most significant barrier of commercialisation of syngas is to the removal of tar and polyaromatic hydrocarbons.

1.7.2.4 Combustion

Thermal conversion of biomass in the presence of an oxidant (normally O_2) to produce CO_2 and H_2O. In the direct combustion process, the biomass is burned in the presence of excess oxygen. The chemical reaction process of direct combustion is very complicated. The produced exothermic energy is converted into electric power. Direct combustion is advantageous for shorter conversion time but requires high energy supply.

1.7.3 Prospects of various biorefinery process

The thermochemical conversion of the above-mentioned process faces a number of issues. The quality of fuels from the thermochemical conversion is far lower than fossil fuel. The mild fermentation process is slow and takes days to get the final product. Although above mentioned conventional process shown potential to convert biomass into platform chemicals, those also suffer significant limitations to be the effective routes for profitable in industrial-scale utilisation. In the conventional pyrolytic process, as the conversion is conducted at high temperature and often accompanied by strong acids/base. Product stability and removal become difficult in such strong condition along with the handling of waste. Process efficiency is also affected by heat transfer limitation. It is understood that a better clean, efficient biomass conversion technology is needed which is economically and environmentally more acceptable. Microwave (MW) assisted biomass conversion has the potential to achieve the goal of a future green, efficient and controllable biorefinery process.

1.8 Introduction and Application of Microwave Heating Process

1.8.1 The concept of Microwave Heating

Microwave energy is a non-ionizing radiation scales from 300MHz to 300GHz. In air or vacuum, the wavelength of MW is one mm to one meter. In electromagnetic spectra, microwaves radiation situated in-between radio waves and infrared. The range of microwave frequency is between 300 MHz to 300 GHz (see Figure 33).[214] The international convention for industrial and scientific microwave heating and drying are 915 ± 25 MHz, 2450 ± 13 MHz, 5800 ± 75 MHz and 22125 ± 125 MHz. For microwave chemistry, the frequency of 2450 MHz is widely used.[215]

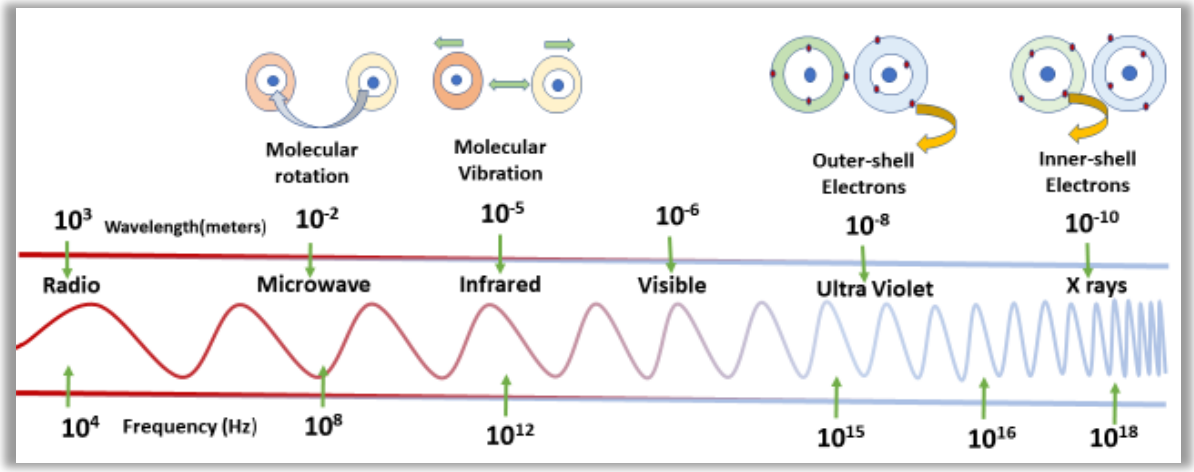

Figure 33 Electromagnetic spectrum, adapted from M. Letellier and H. Budzinski.

As it is depicted in Figure 33, X-ray excites atomic electron of inner-shell, ultraviolet radiation excites electron of atoms outer-shell and infrared vibrate bonding of atoms of the molecule. The MW frequency energy is about 0.23 cal/mol which can only cause the molecular rotation.[216] When MW frequency of industrially available range is applied to a sample, the inter-atomic bonded dielectric parts of an organic compound interact with microwave and start rotating. At an appropriate environment, the rotating bond resonates with applied MW frequency. When the frequency of microwave increase, the dipoles of the sample component are unable to fully restore their original position due to microwave field reversal. When the MW frequency increases further and further, at some point the dielectric reorientation polarisation fails to follow the applied microwave field. The energy of microwave in such way dissipated as frictional heat at the molecular level into the sample. As the rotational dipole collides with another dipole or with the neighbouring rigid molecular part of the biomass component at approximately 2.45 billion times per second the collisional heat builds up very rapidly.

Microwave generator of a microwave device produces electromagnetic waves at microwave frequency (*Figure 34*).

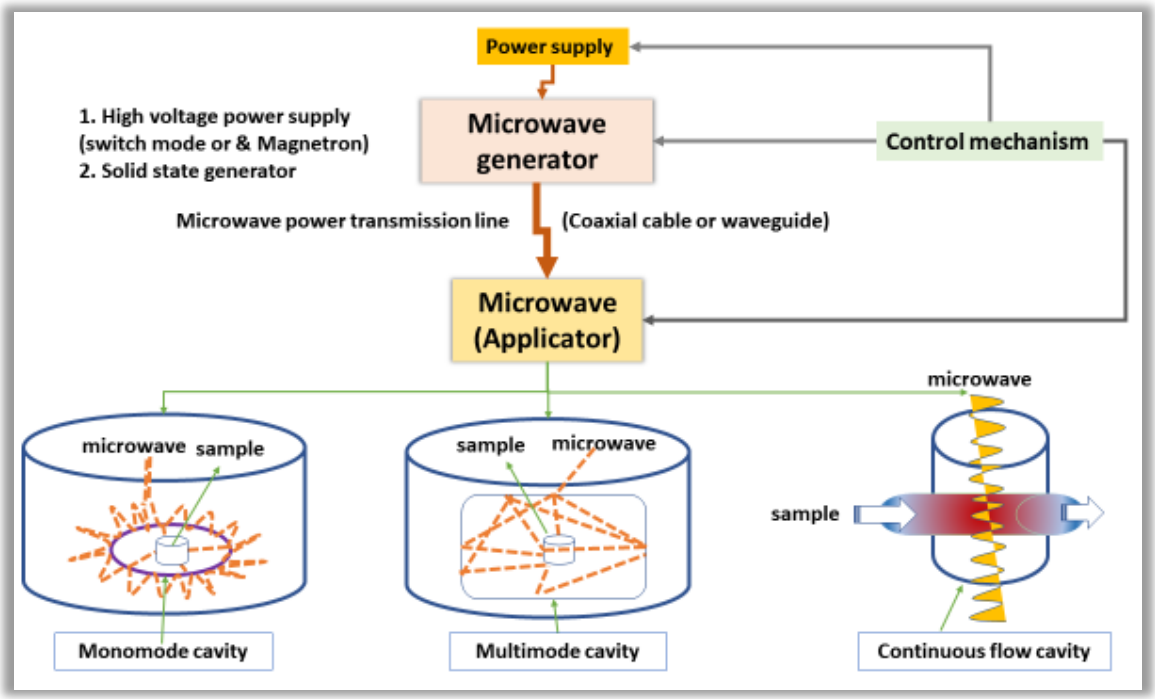

Figure 34 A schematic diagram of a microwave heating system.

The power supply to microwave generator could be switch mode, conventional/inductive power supply, pulse power supply or solid-state RF generator.[217] The advantage of conventional AC power supply system is its robust built quality and comparatively lower cost than other types of MW generators. The switch-mode converts an AC input voltage into DC current for a stable, low current ripple, high quality and narrow bandwidth output electromagnetic wave. The pulse power supply, on the other hand, operates the magnetron in the pulse mode to achieve higher peak output within a specific time period.[217, 218] Solid-state RG generator is made of a solid compact material. In solid-state material electrons and other charge carriers are confined to the material and carry out a particular electronic function.[219, 220] Solid-state RF generator for heating has the advantage of precise control of frequency, power and RF phase. After producing MW, it is then transmitted through a rectangular or circular waveguide or with a coaxial cable inside the microwave cavity where a sample is placed at the maximized energy point.[221] To ensure optimum energy transfer, the shape and size of the waveguide are designed carefully.

Depending on purpose microwave cavity can be designed in many ways. Mono-mode, multimode and continuous flow cavity is depicted in *Figure 34*.[222] The cavity of mono-mode microwave ovens is small and compact. In the mono-mode cavity, through a waveguide/coaxial cable the microwave is passed to the cavity. The cavity is designed in such a way that the MW

is reflected on the cavity wall and form a standing wave. In the focus of the wave standing wave the sample is placed for maximum effect and rapid heating.[223]

On the other hand, multimode microwave ovens cavities are larger. In the multimode cavity, the microwave reflected on the cavity walls in a chaotic manner and thus produce multiple modes of electromagnetic waves are created. Therefore, the energy density of multiple-mode microwave systems is lower than single-mode in per unit area.[224] Although most of the commercial single-mode cavities are only 300 W. Domestic food cooking microwave is an example of multimode MW heating cavity. For industrial heating process, continuous flow cavity is an ideal solution for MW cavity design. The sample can be passed through the MW path either at 90-degree angle of MW path as shown in *Figure 34* or along the MW path. The exact orientation and sample-MW interaction length depend on the specific heating needs.

1.8.2 Comparison of Conventional and Microwave Heating Process

In conventional heating heat transfer through radiation, conduction and convection from the source of heat to the towards the object core. In such a way temperature rise inside the sample. Like, in chemical synthesis oil bath or heating mantles are normally used. The heat in this way transferred though a conductive mechanism through the reaction vessel wall, then to the solvent and reactant. The mode of heat transfer depends on the conductivity of the reaction vessel. In industrial heating, energy can be transferred as conduction or convection through steam and hot-air, dependant on the application. The temperature drop between the outer surface and the inner surface of the reaction vessel can differ hugely spatially and temporally. As such equivalence of thermal source and the inside sample is time-consuming and inefficient. The control of reaction temperature and as such control of by-product formation becomes difficult. In *Figure 35*, on the left-hand side, the conventional heating mechanism is depicted.

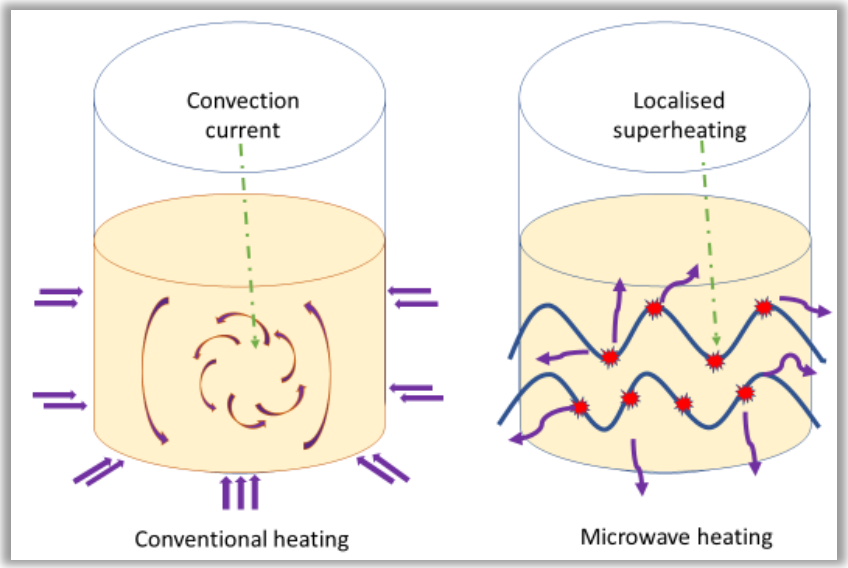

Figure 35 Comparison of the heating mechanism of conventional and microwave heating.

It is simple to understand that conventional heating is inherently non-selective towards solvents, reactants, catalyst, support walls and products. The heating is indifferent to chemically active and inactive elements of the reactor. Due to the above reasons, at industrial scale chemical engineering, the control of tailored and selective heating is a major challenge.

In contrast, microwave reaction vessel materials are made with microwave transparent material. Microwave passes the reaction vessel and directly couple with the dipolar molecule and thus generate heat inside the vessel. The rate of heat generation depends on the ability of microwave and the interacting dipolar molecules. The interaction of MW and polar molecule inside the reaction vessel as such generate instantaneous heat at the exact opposite direction of conventional heating (*Figure 35*, right-hand side). The rate of heating is very fast. Due to instantaneous volumetric heating process, microwave heating is highly attractive compared to conventional heating to ensure higher efficiency.

Many organic reactions under microwave can be started and progressed very fast. Microwave can also increase product yield, reduce process time and improve or modify reaction selectivity and initiate some reaction in the presence of microwave radiation only.[225-238] The associated advantage of MW heating power is exploited in many fields of chemistry such as polymer synthesis,[239] organic/medicinal chemistry,[240-243] solid-phase peptide[244], material sciences,[245-247] drug discovery,[248] nanomaterials research[249] and biochemical processes.[250]

1.9 Microwave-assisted Conversion of Biomass

As MW directly initiate the heating process at the core of the volume, instead of conduction and convection from the surface, biomass heating is much more effective than conventional heating.[251] For the above-mentioned reason, during MW heating, biomass get heated much more quickly than the traditional heating process.[252] During the last few decades, the MW heating was successfully applied for various types of biomass activation,[26, 253] Microwave heating offers several advantages over conventional heating of biomass, as it is often more specific (reducing the amount of secondary products), controllable,[254 255] energy (non-contact energy transfer, volumetric energy absorption and dissipation)[256] as well as cost-efficient[257] (due to shorter the reaction time) and therefore in many cases, MW may be very promising tool of green technology. Furthermore, Microwave processing is effective at both pilot and industrial scale.[258] Microwave technology could be used as a hydrothermal or pyrolytic way. The MW pyrolytic process is performed under an inert atmosphere with a limited presence of water. The hydrothermal process is performed in the presence of excess water and often accompanied by a catalyst.

1.9.1 Microwave-assisted Liquefaction of Biomass

In conventional conduction/convection heating process, liquefaction of lignocellulose biomass requires long reaction time and liquefaction rate is not also satisfactory. Use of a large amount of solvent such as phenol to facilitate liquefaction in the conventional process also causes various environmental and sustainability concern.[208, 259-262] Contrary, microwave liquefaction not only fast and energy effective, but it also influences liquefied products properties and reduces products average molecular weight than conventional liquefaction.[263, 264] The First published work of biomass liquefaction using MW energy was demonstrated by Krzan *et al.* [265, 266] Since then various types of biomass such as agricultural residues (rice straw, bagasse, corn stover, corncobs wheat straw, and cotton stalk) [267], Ulva prolifera[268], microalgae[269], sugar beet pulp[270], oil palm empty fruit bunch cellulose[271], Sargassum polycystum C. Agardh[272], coconut fiber[273], grapefruit[274], peony oil palm empty fruit bunch fiber[275], Chinese fir, bamboo, hemp xyloid stem[276], mixed softwood pellets[277], wheat straw alkali lignin[278], banana pseudostem[279], sweetgum sawdust[259] and organosolv lignin of olive tree prunings[280] have been investigated for the production biobased materials and platform chemicals. As the chemical composition and physical structure of various types of lignocellulose differ widely, the dipolar interaction of those components with the microwave also differs and thus varies the liquefaction yield of different biomass.[262, 281-283] A study on

crop residues at the same microwave-assisted liquefaction conditions was shown that corncobs, corn stover, and wheat straw produces significantly higher rate of liquefaction than that of rice straw.[267] The variation of liquefaction rate of different woody biomass of under same MW condition was also found out.[276] Biomass particle size[270, 284] and moisture content also influence on MW liquefaction rate.[285]

1.9.1.1 *Effect of Solvent on MW-assisted Liquefaction*

The condition of hydrothermal liquefaction, residence time and temperature influence the aqueous products.[286] Liu *et al* have demonstrated that in HTL, 5 minutes residence time significantly increases desirable products (levoglucosan, glucose, xylose, fructose and acetic acid) from rice straw comparing 30 minutes residence time.[287] Use of solvents besides water shows potential to derived platform molecule in mild condition for liquefaction of wood.[259] Fan *et al* recently showed that using acetic acid simultaneous production of lignin and oligosaccharides is possible using acetic acid catalyst at a temperature range of 150 °C - 210 °C from rapeseed meal.[288] In a study, it was observed that the microwave-assisted liquefaction ability of poplar sawdust in the presence of simple glycols such as ethylene glycol and propylene glycol is higher than higher analogues such as diethylene glycol, polyethylene glycol and dipropylene glycol.[266] The reason associated with liquefaction rate may relate with the interaction of solvents dielectric property and viscosity. The same phenomenon as above was observed at liquefaction of wheat straw alkali lignin in alcohols.[278] Another study demonstrated that higher boiling point alcohols are more effective than low boiling point alcohols at lower than 120°C MW-assisted liquefaction condition.[289] Although, the liquefaction efficiency of the feedstocks could enhance by methanol, it could also prevent further decomposition of the sugar derivatives into 5-hydroxymethylfurfural and levulinic acid.[290] Although it is known that the higher ratio of solvent to solid increase liquefaction yield in conventional and MW-assisted liquefaction, the overall solvent to solid ratio requirement is lower at microwave liquefaction system than that in conventional liquefaction.[291] It was discovered that MW-assisted liquefaction of coconut fibre was achieved 89% yield at 5: 1 solvent: biomass ratio and no further increment of yield was gained after increasing solvent ratio.[273]

1.9.1.2 *Effect of Catalyst on MW-assisted Liquefaction*

Catalyst is has been widely used conventional liquefaction process and the effectiveness of catalyst in MW-assisted liquefaction of biomass is also recognised.[292-295] An acid-based catalyst such as phosphoric acid, hydrochloric acid, and formic acid sulphuric acid was used for MW-

assisted liquefaction of biomass. Sulphuric acid is proven to be a preferred solvent for liquefaction of lignin.[295, 296] For the production of nonphenolic compounds, the use of sulphuric acid shown to be more effective than the FeS binary catalyst and zeolite.[297] Catalytically ability of sulphuric acid for microwave liquefaction of cellulosic materials was proven far better than levulinic acid, sodium hydroxide, acid monohydrate and p-toluene sulfonic.[298] S. Tabasso *et al* have demonstrated levulinic acid production from a post-harvested tomato plant with MW irradiation at 225 °C, and for 2 min in presence of HCl.[299] Feng *et al* have selectively produced methyl levulinate production from lignocellulosic waste using directional microwave-assisted liquefaction.[300] Carnaroglio *et al.* have used dilute $Pb(NO_3)$ catalyst solution at 220 °C to produce lactic acid and glycolic acid from lignocellulosic biomass in 3MPa pressurised MW system.[301] Microwave-assisted liquefaction system also seems to be affected by the catalyst concentration in the feedstock. It is found out that increasing adobe an optimum level of catalyst in the system decreases the rate of liquefaction.[273, 302] It was also recognised that optimum level of catalyst concentration is lower than that of conventional catalysis.[268, 303]

1.9.1.3 Temperature and Time

In the microwave heating process, temperature and time also the key influencing factors of liquefaction parameter. The temperature was determined to be the most influential factor of rice straw liquefaction.[282] In the case of other lignocellulosic biomass liquefaction with microwave, the temperature was found to the paramount influencing factor.[281, 293, 304] The depolymerisation of bamboo using ethanol as solvent at low power, it demonstrated that time was less influential than temperature.[305] The most notable feature of temperature in MW liquefaction of biomass is that the bulk temperature of biomass is significantly lower than the conventional method. The cellulose of oil palm empty fruit bunch fibre was liquefied at under 175°C.[271] Coconut fibre was also optimally shown to be liquefied at 160°C in another research.[273]

It is important to note here that, in the common commercially available single-mode microwave reactors, a calibrated external infrared (IR) sensor is used to detect the reaction temperature.[306] The sensor is integrated into the MW cavity to detect the Pyrex reaction vessels surface temperature from a specific distance. The IR sensor is generally robust and reliable to measure temperature in a wide range of temperature. As IR sensor cannot be used to directly determine the actual reaction mixture contained inside the reaction vessel, there is always a difference inside the reaction vessel temperature and outside temperature determined by the IR sensor. Therefore, without simultaneously recording of internal temperature, it is difficult to know the

exact reaction temperature at a specific time. An aid of thermo-vision camera might help to detect the actual temperature inside the reaction vessel.[307] By using so-called ‘‘simultaneous cooling’’ technique[308], the reaction vessel can be cooled from the outside by compressed air while being irradiated by microwaves. Using the “simultaneous cooling’’ technique, it was found out that while external IR sensor temperature was 180 °C than the internal temperate was 210 °C (measured by internal FO temperature probes), a difference of 30°C.

It can be concluded from the above discussion that in MW assisted liquefaction of biomass, solvent, types & size of raw material, solvent or catalytic reagent have a recognisable effect on the rate of product yield and quality. It was also shown in some studies that use of MW power, temperature and time of liquefaction process can be used to optimise the production and quality.

1.9.2 Microwave-assisted Pyrolysis of Biomass

The effectiveness of MW pyrolysis of biomass over conventional methods is already established.[309, 310, 311] A number of study on microwave pyrolysis of biomass was performed already. The feedstock includes corn stalk bale [311], coffee hulls [312], rice straw [313, 314], corn stover [315, 316], wheat straw [317], algae [318], peanut shell and maize stalk [319]. Several microwave pyrolysis studies were also performed on woody lignocellulose biomass such as pinewood sawdust [320], Douglas fir pellets [321], fir sawdust [322], oil palm biomass [323, 324], wood [251] and oil palm empty fruit bunches [325, 326]. It was realised that the microwave pyrolysis of biomass is considerably distinguished from conventional techniques.[311, 327]

The feedstock character of different lignocellulose biomass, especially amount water content and dielectric properties of biomass component can significantly influence the microwave heating process. [328] Both liquid and gas yield of MW-assisted pyrolysis can vary depending on water content and presence dipolar molecules in the biomass. J. Robinson *et al.* studied dielectric loss factors of dry and wet wood samples at different temperatures. [328] They concluded that at above 500°C temperature, the loss factor (Ɛ``) of both dry and wet samples dielectric loss factor increased significantly due to formation of char which act as microwave-absorber. They also observed that a 6.3% water containing sample produce 13% liquid yield and 19% of gas yield. But when the water content was increased to 22%, both the liquid yield was decreased to 3.5% and gas yields to 4.5% respectively. From their study, it can be concluded that the moisture content of biomass in MW-assisted biomass pyrolysis is an import biomass pyrolysis rate determining factor.

The biomass input size also can affect the rate of pyrolysis.[329] Miura *et al* have rapidly MW pyrolysed large and small pieces of larch wood sample at different MW oven.[329] They have revealed that to pyrolysed large woodblock sample needs comparatively less power for per unit of wood pyrolysis.

To study the effect of microwave power level on biomass pyrolysis, Hu *et al*. performed an experiment using a 2.45 GHz and 3750 W microwave oven.[330] A Chlorella vulgaris (a wild type of algae) was used as a sample. The sample was placed on a three-neck quartz reactor of 500 ml inside the MW oven and used N_2 gas as the carrier. When they increased MW power from 750 W to 2250 W, they noticed that gas product yield was improved but the solid fraction yield was decreased. At 1500 W, the bio-oil yield was maximum (35.83 wt.%), whereas, at 2250 W power, the gas yield was maximum. The conclusion was that increasing power maximise gas production and but not effective for solid residue production.

To study the catalytic effect on MW pyrolysis of biomass, Wan *et al*. used various catalysts (KAc, K_2Cr_2O7, Al_2O_3, H_3BO_3, Na_2HPO_4, $AlCl_3$, $CoCl_2$, $MgCl_2$, and $ZnCl_2$) on aspen wood pellets and dry corn stover.[315] From the experiment they revealed that some of the catalyst increase bio-oil yield and reduce char and gas fraction. Their conclusion was that catalysts may act as microwave-absorber through participating in a reaction known as *"in-situ upgrading"*. The absorber like the behaviour of catalyst boost feedstock heating and thus accelerate the thermal decomposition of biomass.[315]

1.10 Potential and Challenges to Utilising the Microwave for Biomass Activation

1.10.1 Potential

As microwave power supply can be cut off instantaneously, microwave pyrolysis of biomass is a much safer option than conventional pyrolysis reactor. Due to the self-limiting endothermic type of property of the microwavable sample, a dangerous level runway of reaction temperatures could be avoided.[331] Due to selective heating, the efficiency of MW heating is incomparable with conventional heating. Selective heating could help to reduce waste volume and treat waste in situ.

Microwave pyrolysis generates more syngas than conventional pyrolysis reactor. [332, 333] Moreover, MW is environmental friendly as it produces less hazardous compounds such as polycyclic aromatic hydrocarbons (PAHs). The excellent advantage of microwave heating mechanism compared to conventional heating is the internal volumetric heating.[329] As the rise

of temperature is very quick though microwave heating, reaction time is much shorter than conventional heating time.

MW interact with internal cell component of biomass, and as such disrupts the physical structure of biomass at the molecular level.[334] The unique phenomena MW causes new chemical profile than conventional thermal conversion. As MW heating is caused by the interaction of dipolar and ionic component of biomass, at higher glass transition temperature biomass become more interactive due to increasing chain end mobility.[335] As it was mentioned previously, in the amorphous cellulose region, the hydroxyl group of $–CH_2O_{(6)}H$ group become more interactive with MW in glass transition temperature. Those groups act as "molecular radiator" and transfer MW energy into the chemical structure.[142] This unique behaviour, promoting hydrolysis and different pyrolytic mechanism of biomass with MW, lowers pyrolysis temperature of the bulk medium of biomass than conventional pyrolysis.[89] Although there is continuing debate accuracy of measurement temperature.[306]

1.10.2 Challenge

Both single-mode and multimode microwave reactors when formed standing waves and from localised microwave field strength at certain spot/positions inside the sample placed in the MW cavity.[324] The hot spot may cause excessive heat in a specific spot of biomass and may cause thermal runaway. Such process influences the quality and yield of MW-assisted process.[299] In control environment the hot spot of single-mode microwave oven may not cause a major issue but in a multimode microwave oven, a hot spot may form large temperature gradients inside the sample and may interrupt the intended reaction pathway. To ensure the uniformity of microwave flux density and thermal distribution in a multimode cavity, several techniques such as employing magnetic stirrers, turntable inside the microwave oven, a fan or increasing the microwave frequency may be useful.

After a certain temperature, the increase of heating energy inside the sample under microwave will cause to reduce the dielectric loss factor of the sample. As a result, the ability of the sample to interact with a microwave will also reduce and after a specific temperature, the sample becomes microwave transparent. This self-limiting heating is a disadvantage and may hinder the decomposition of the material at a higher temperature. To overcome the issue, more power input may require as such a process become energy-intensive.[336] Once again, the self-limiting heating could also be advantageous if limiting excess heating could prevent certain high-value product degradation through further heating. This unique phenomenon could be exploited through further research for practical application.

Due to ineffective measurement of reactor temperature of under a microwave condition erroneous temperature measurement might mislead the actual impact of MW efficiency.[306]

Continued efforts to develop larger-scale continuous systems will help to drive the field forward, as will studies aimed at a detailed description of the mechanisms of activation and interaction of microwaves with biomass. One of the key difficulties is how to compare research done on different instruments and under different operating conditions, as many variables are at play, and understanding how these will affect comparison of the pyrolysis of biomass (itself variable geographically and seasonally) and the analysis of the products (very complex and occasionally incorrect) is a significant challenge. Studies aimed at converting biomass to useful platform molecules (for synthetic purposes rather than for fuel) are also ongoing, and appear to be close to producing useful contributions.

1.11 The Aim, Objective and Novelties of This PhD Work

It was also found out that during MW activated conversion, in the presence of an appropriate organic solvent, the product selectivity, stability and yield may increase.[337-339] The reasons for this improvement are not completely understood. But it is commonly accepted that the improvement is a result of specific dielectric properties of reagents, products and solvents [340, 341] Therefore, to maximise the product selectivity, stability and yield without compromising optimum energy output and heating efficiency the careful selection of solvent is vital depending on specific organic reaction or material (such as biomass) conversion. However, there is still a lack of systematic investigation to establish the hidden reason for a successful application of the solvent effect. Only a limited amount of dielectric information of solvent is available in the literature except dielectric data of water.[342] Moreover, the published data are not in the same frequencies, patchy, inconsistent and are not traceable due to lack of international standardisation.[342, 343] But the successful implication of microwave reactors for any MW assisted conversion stage, the readily available solvent-MW thermal interaction data is vital for a synthetic or process chemist. As most of the commercial MW reactors generate MW radiations at 2.45GHz, it is vital that at this frequency, the thermal behaviour of the polar solvent under MW radiation is known to the researcher in full temperature range. It is also equally important that the selection of solvent is not compromised the greener aspect while possible. To serve this purpose, we need to have a list of green solvents dielectric loss factor (ε``) and loss tangent (δ) database at an appropriate temperature range.

Most of the work in MW liquefaction and pyrolysis is performed in lab scale, lab to scale up for industrial bioenergy application much more research is needed to meet all the obstacles on the way. The main obstacles are a better and comprehensive understanding of the interaction and relationship among microwave, biomass and heating medium. Identify high-efficient microwave absorbing solvents-system for biomass transformation into value-added products at optimum way and also easily separate the product from the solvent. Scaling-up of microwave reactors to meet large scale production of value-added products in a cost-effective and green chemical way. To advance the research for industrial application, all the above-mentioned challenge needed to be addressed. It is strongly suggested here that the research work in this PhD would pave the way for the future direction of microwave-based biorefinery.

1.12 Thesis Layout

This PhD was part of a broader research project entitled **C**ost-**E**ffective **T**ailored **Ex**traction of high-value chemicals from low-cost conifer biomaterials (**CETEX**) and was funded by the Swedish Research Council *FORMAS*. One of the project partners was the Department of Forest Biomaterial Technology at Sveriges Lantbruks Universitet or SLU in Umea, Sweden. For the **CETEX** project, three specific cheap and quick growing conifers of Swedish forest; Scots pine (*Pinus sylvestris*), Norway spruce (*Picea abies*) and Lodgepole pine (*Pinus contorta*) waste assortment were selected for systematic analysis and to evaluate the potential of gaining high-value chemicals, materials and energy by implementing biorefinery concept. The work packages were distributed among the project partners and investigators. In this specific research PhD research, the influence of organic liquid on microwave-assisted pyrolysis of some of the selected biomass will be evaluated. The PhD thesis works consist of the following chapters:

1. Chapter 1 presents the research introduction with a brief description of Sustainable bioeconomy, renewable resources, forest resources, the structure of lignocellulosic biomass, types of biorefinery pretreatment, biorefinery process and discussion about microwave biorefinery process with its advance, disadvantage and future prospect.
2. Chapter 2 is focussed on literature review:
    a. An assessment of Swedish forestry waste will also be discussed. The role of extractive compounds on microwave pyrolysis of assorted forestry waste will be also be highlighted.

b. A brief introduction of near-infrared analysis (NIR) and the application of NIR for forest waste characterisation will be discussed. Overview of multivariate data analysis in the context of NIR spectroscopy will be briefed.

c. The influence of organic liquids physicochemical property on cellulose microwave-assisted will be also be discussed.

d. A literature overview of solvent-microwave interaction, the interaction of solvent with cellulose and solvent product will also be discussed.

e. Then the basic concept of dielectric loss factor and measurement technique will be briefly discussed.

f. The relation of Menschutkin reaction with Arrhenius type reaction activation will be discussed at this stage.

3. In Chapter 3 the experiment section of subsequent chapters will be described.
4. In Chapter 4 the influence of extractive component on forest waste and cellulose pyrolysis will be presented.
5. Chapter 5 discusses some organic additives physicochemical property on the rate of cellulose pyrolysis.
6. Chapter 6 demonstrates the influence of microwave irradiation on the solvent-cellulose interaction
7. Chapter 7 describes the development of a new resonant cavity perturbation instrument and its successful application towards the study of temperature-dependent dielectric property of solvents.
8. Chapter 8 gives an experimental result discussion of how dielectric property of solvent could influence on Menschutkin type reaction.

Chapter 9 discuss the conclusion of the research and suggestions for future work

1.12.1 Connectivity of thesis chapters

The connectivity of all of the thesis chapters is shown in Figure 36 below:

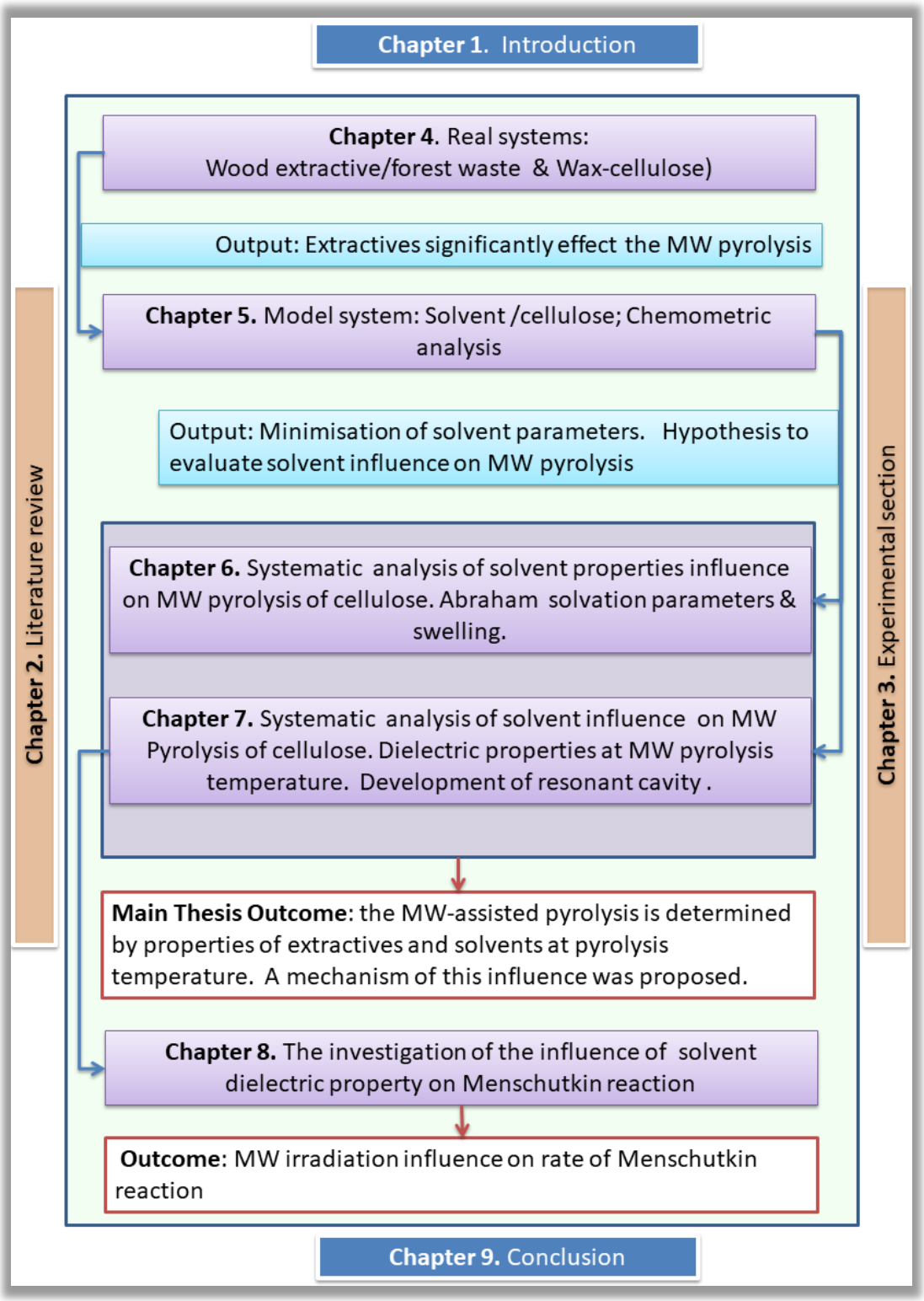

Figure 36 Connectivity of these chapters

2 Literature Review

At section 1.11 of the introduction, the motivation, aim and objective of this PhD research work were highlighted. As it was mentioned in the thesis layout (section 1.12), in this chapter the literary work of highlighted topics will be discussed as depicted in the following diagram (*Figure 37*).

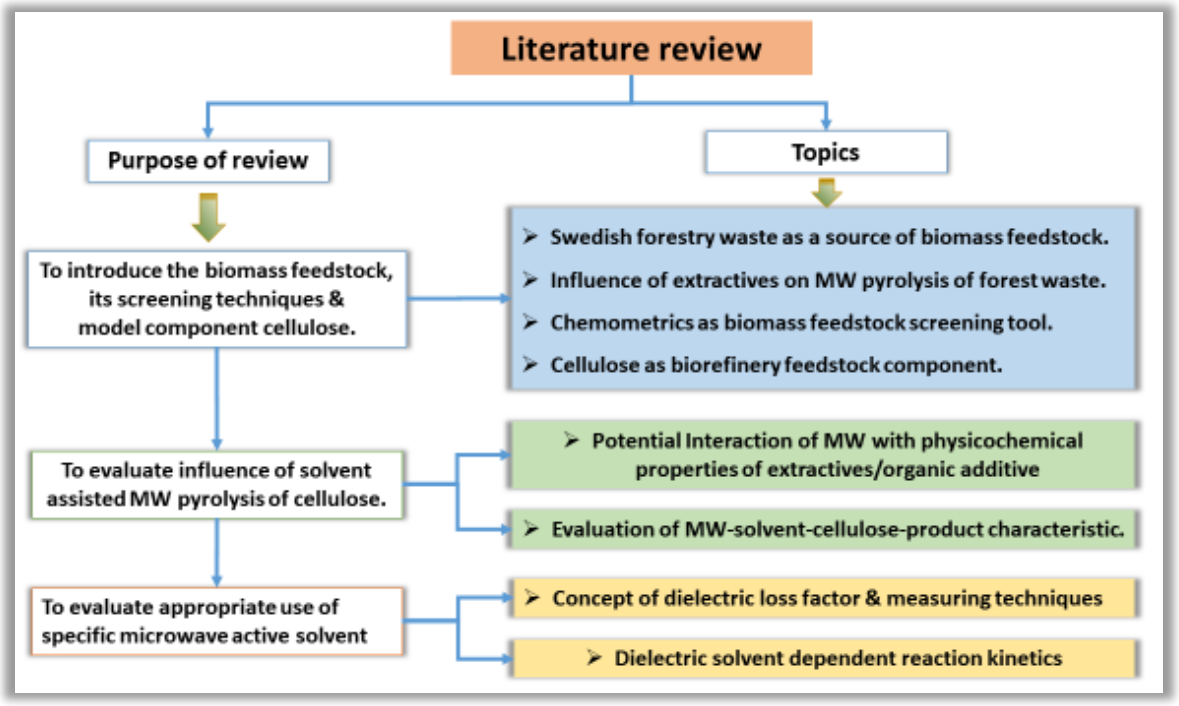

Figure 37 Schematic diagram of literature discussion flow.

It was also mentioned in the thesis layout that the feedstock was chosen as Swedish forest waste according to CETEX research project proposal which was funded by Swedish Forest Research Council FORMAS. The subtopics of relevant literature will be discussed under appropriate topics.

2.1 An assessment of Swedish Forestry Waste as a Biorefinery Feedstock

It is possible to convert forest waste into a source of energy, biomaterials, chemicals such as nutraceuticals, antioxidants and cosmetics ingredients using the biorefinery concept.[26, 253] Backlund *et al*. have surveyed the relevant Swedish industries on the potential of bio-refinery products, energy price and wood assortments.[344] It was found out in a study by Backlund *et al.* that only the parts of the wood which could be transported are suitable for commercialisation. The majority of present-day industries focusing on the utilisation of cellulose and hemicellulose. Therefore, the demand for tree parts is for stem-wood 32%, branches 19%, bark 16%, roots 10%, knots 10%, needle 6% and no specific 8% (Figure 38).

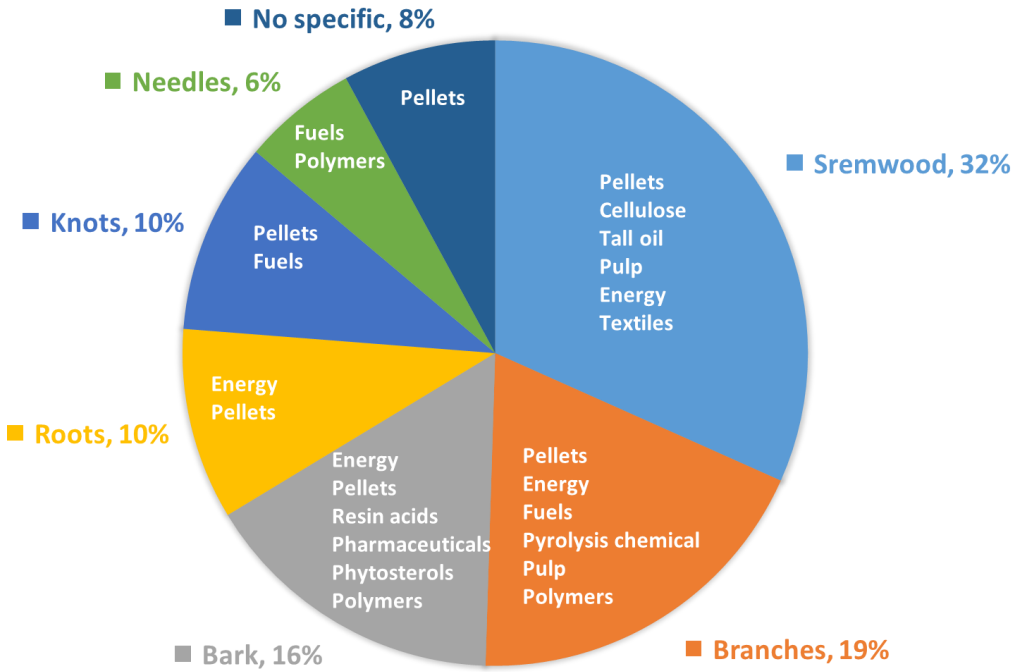

Figure 38 Major areas of industrial applications of forest waste parts (Source Backlund et al., 2014)

The Backlund *et.al.* survey information highlights the fact that there is currently a lack of commercial routes to obtain specific chemicals from different parts of the wood. However, such technologies have to be flexible given that different species and parts of forest plants are widely varied in terms of chemical composition, as shown in *Table 2*.

Table 2 Chemical composition of Scots pine parts.

Assortment type	Cellulose%	Hemicellulose%	Lignin%	Extractives%	References
Stem wood	40.7 (1.2) *	26.9 (0.6)	27	5.0 (1.0) *	37, 43, 44, 345-350
Bark	22.2 (3.2)	8.1 (0.4)	13.1 (5.4)	25.2 (5.2)	348-353
Branches	32.0	32.0	21.5 (5.9)	16.6 (7.1)	347-350, 354
Needle	29.1	24.9	6.9 (0.8)	39.6 (1.3)	348-350, 355
Stump	36.4	28.2	19.5	18.7	349
Roots	28.6	18.9	29.8	13.3	349

* Bracketed numbers represent the error from the mean percentage of values as reported in the relevant literature.

From the above table data, it is seen that changes of extractives in wood parts varied in almost eight times from 5 wt% in stemwood to 40 wt% (needle). The amount of the wood main

structural components is also significantly diverged (from 22 to 40 wt % for cellulose, from 8.1 to 32 wt% hemicellulose and from 6.9 to 29.8 wt% for lignin).

Such variation in the composition of different parts of the plant highlights the fact that the development of a forest-based biorefinery will require a fast, simple and compatible method of wood assortments selection. It is proposed here that Near-infrared (NIR) spectroscopy could be a cheap, simple, reliable and non-invasive method to detect the chemical components of biomass. For the verification of NIR analysis, thermogravimetric analysis (TGA) will also be employed in this work.

From the above discussion, it is understood that the extractive of wood could play a significant role in the development of a forest-based biorefinery. In the following literature survey, the role of extractive during a various form of biomass conversion is discussed.

2.2 Influence of Extractive Components on Biomass Processing

The chemicals components of extractives are mainly terpenes and its derivatives, fatty acids, carbohydrates, polyhydric alcohols and aromatic compounds.[54] A brief description of those extractive components is discussed at section 1.4.5 in the introduction. While crystalline cellulose is strongly resistant to thermal, chemical, and biological attack, extractives are the least resistant to thermal and chemical degradation.[356] As a rule of thumb, the higher extractives containing biomass means lower recalcitrant biomass due to lower cellulose content in nature.[357] Depending on the origin and age of lignocellulosic species, the extractive composition and percentage of content widely varied.[358, 359] The variation of extractive content interns may dictate many physical and chemical properties of biomass processing applications. But unfortunately, a very little investigation was carried out on this crucial subject matter. In the literature survey, only a few research works were found in the whole subject matter and those work were limited to pulp mill sludge processing,[360] lignin acidolysis,[361] enigmatic hydrolyses,[362, 363] palletisation process,[364] biochar formation,[365] caloric value,[366] biomass pyrolysis process,[367] and bio-oil production yield. [368]

2.2.1 Influence on Pulp mill Sludge Processing

It is known that softwood pulp mills are enriched with high levels of wood extractives.[369, 370] The lipophilic extractives compounds such as sterols, sterol esters, triglycerides, resin acids, monoterpenes, fatty acids and phenolics that are released from wood at the pulp processing stages. The pulp sludge treating anaerobic digestion condition is not suitable to degrade the extractive compounds. But for biological growth is proven to be inhibited by the presence of

underrated extractives.[371] Sierra-Alvarez *et. al* has demonstrated that 20–330 mg/l concentrated resin acids are responsible for 50% inhibition of methanogenesis of forest industry wastewater.[372] S. Baroutian et al. have shown in a study that wet oxidation (at 220 °C and 20 bar) before anaerobic digestion can effectively degrade extractive components and hence improve anaerobic digestion of extractives.[360] But thermal hydrolysis at the same operating condition is not effective to degrade extractives.

2.2.2 Influence on Enigmatic Hydrolysis

Zimu Li *et al.* pretreated corn stover with liquid hot-water (LHT) for fermentation.[363] They have found that removal of extractives during LHT hydrolysis improves the enzymatic process. At the same pretreatment condition, extractive free corn stover presented higher cellulose digestibility (87%) than ordinary corn stover (71%). They have assumed that during LHW pretreatment process some water-soluble extractive may reduce xylan by acting as a buffer of H^+ from water and acetic acid. It might also possible that some extractive could condense on stover after LHW pretreatment and as such hinders cellulose hydrolysis.

H. Horhammer *et al.* also have shown that if non-structural components including extractives are removed from poplar whole-tree chips then extractive free wood enhances hydrolysis pre-processing and as thus improve performance of fermentation.[362] Their economic modelling indicates that a pre-processing unit of poplar whole-tree chips extractives could bring significant economic benefits in a proposed biorefinery.

2.2.3 Influence on Lignin Acidolysis

It is well known that wood contains biogenic natural formaldehyde (CH_2O). Heating of wood generates much higher levels of formaldehyde which vary according to tissue type, moisture content and tree species.[373, 374] Lignin is the major source of biogenic formaldehyde and it generates through lignin acidolysis.[375] Guigui Wan *et al.* wanted to have a mechanistic understanding of biogenic formaldehyde formation so that the knowledge could be used to manipulate for some beneficial purpose. They have found that in lignin thermochemistry, the selectivity of lignin acidolysis or thioacidolysis pathways could be dominated by the presence or absence of extractive content different types of wood.[361]

2.2.4 Influence on Palletisation Process

Nielsen *et al.* have studied the effect of extractives and storage on the pelletizing process of sawdust.[364] They have shown that if extractives are removed from biomass, the pellet strength is increased significantly. The energy requirements of the pelletizing process are also reduced

if the extractive content of the biomass is lowered. It is thought that the energy requirements in the pelletizing process are reduced due to extractives role as plasticizers and lubricants. Another reason for the improvement of pellet strength if extractives are removed is because extractives free biomass component binds better. Their work shows that differences in energy consumption for different wood species palletisation depend on extractive contents of those biomasses.

2.2.5 Influence on Char Formation

Agnieszka Korus et al. prepared biochars from raw and acetone extracted pine wood and it was concluded that char quality s greatly influenced by extractive content in pine char. The removal of extractives increases char microporosity and acidity. They have discovered that the longer pyrolysis residence time of extractive containing wood enhances char formation at the expense of liquid products. It was suggested by them that the extractives removal effect was strongly related to the pyrolysis heating rate and subsequent char activation time. Furthermore, studies are needed to establish this correlation. It can be concluded that the magnitude of the effect of the extractives can be altered with thermochemical treatment conditions for a specific purpose.

2.2.6 Influence on Caloric Value

Ro´ger Moya *et al.* studied ten fast-growing wood species of Costa Rica for fuelwood characteristics and its relation with chemical properties and extractives.[366] Although it was believed many that the fuel capacity of biomass in the presence of extractives increase but the authors have found little evidence in its favour.[376] They concluded that the caloric value of biofuel depends on the nature of the extractive components and the presence of relative quantities. If extractives contain a higher amount of terpenoid hydrocarbons and lipids the caloric value of biofuel may increase while the presence of higher oxygen-containing compound may decrease the caloric value of biofuel.

2.2.7 Influence on Biomass Pyrolysis Mechanism

The influence of extractives on the mechanism of biomass pyrolysis was studied by Guo *et al*.[367] Guo *et al* selected Mongolian pine (Pinus sylvestris var. mongolica) and Manchurian ash (Fraxinus mandschurica) to remove extractive by using ethanol.[367] They studied the extractives effect on biomass pyrolysis using thermogravimetric analyser coupled with Fourier transform infrared spectroscopy (TG-FTIR). The spectra of original biomass, extractives, and extracted residues were analysed to draw mechanism of biomass pyrolysis. In a previous investigation, Ranzi *et al* have proposed a competitive route for levoglucosan and acetic acid during pyrolysis

of cellulose.[377] According to them, through chain-end depolymerization reaction, cellulose degrades to levoglucosan. But Guo has findings proposed that the presence of extractives in biomass enhance the formation of acetic acid and inhibit the formation of levoglucosan. They also concluded that extractives need less energy to decompose than original biomass and extracted residues. The weight loss of extractives also happens in a wider temperature range. They also concluded that at low temperature, extractives generate water, CO, and CO2. But at high temperature, secondary cracking products of methanol and methane is produced from extractives. The presence of extractives catalyses acid formation while its absence enhances water and CO2 formation.

2.2.8 Influence of Extractives on Biooil Yield

Yanpeng Wang *et al.* has performed deoxy-liquefaction of three kinds of biomass (corn stalk, A. ordosica, and wheat straw) to investigate the influence of extractives on alkane production and biooil yield.[368] Their study concludes that most of the alkanes in the oil mainly derive from the decomposition of hydrocarbon and triglyceride which existed in the extractives of biomass. The extractives of the biomass inhibit the formation of gas & char and enhance the oil yield according to their conclusion during deoxy-liquefaction.

2.2.9 Evaluation of Extractives Influence on Microwave-assisted Pyrolysis of Biomass

The effectiveness of the MW pyrolysis of biomass compared to conventional thermal methods such as pyrolysis and torrefaction is already established.[309, 310, 311] These research focused on MW treatment of whole biomass without removal of any extractive components. As the extractives content within biomass could be as high as 40% (e.g. in the needle), they may significantly contribute to the overall MW pyrolysis processing of assorted wood. The only study that was found to be engaged in this line of thinking, was performed by Behdad Moghtaderi *et al.*.[378] At atmospheric pressure and ambient temperature, they used 9.47 GHz MW frequency to investigate the dielectric properties of Slash pine and Spotted gumwood based on Von Hippel's transmission line method and found that the effect of extractives and mineral content may change the dielectric properties of woody biomass.[378] However, their research was limited only to wood pre-treatment for furniture production.

It is well known that a significant part of the biomass is cellulose.[379-382] As biomass is very complex, to understand the role of extractives on biomass pyrolysis, cellulose was considered as a simple model component to study the interaction of extractive and cellulose in this thesis.

2.3 Chemometrics as Biomass Feedstock Screening Tool

For an economically feasible biorefinery, biomass raw material characterisation is needed to be cheap and quick that suit in a biorefinery process. At present, the most lignocellulosic materials analysis method is derived from contemporary plant-based animal feed digestibility assessment.[383] But rather than contemporary absolute compositional analyses biomass, raw feedstock screening is more appropriate for lignocellulosic based biorefinery.[384] Raman scattering, NIR and mid-infrared (MIR) absorption spectroscopy are potential inexpensive tools for biomass screening purpose.[383] However, the main difficulties in choosing these tools are convolute the spectra and interpret the data for chemicals of interest. The mathematical algorithms to extract useful information from those complex data using, often using specially developed software is termed as Chemometrics. For example, to determine phenolic hydroxyl groups from milled wood lignin, Principal Components Regression (PCR) and Partial Least Squares (PLS) could be used.[385] In a review, Tsuchikawa discussed that use of chemometrics aided Near-infrared (NIR) spectroscopy could improve monitoring and analysis of the pulp and paper industry process and for making the industry more cost-effective.[386] In the same way, for the screening of various biomass populations, Principal Component Analysis (PCA) can be used as a useful tool for high throughput compositional screening.[387, 388] The NIR data could also be analysed using exploratory data analysis without having any supervised preliminary chemical information.[389, 390]

The theory of one chemometric method, PCA PCR, Multilinear regression (MLR) will be discussed in next subsections as those tools will be used for some of the experiments in this thesis. Those tools will be used for extractives and moisture content of selected Swedish forest waste residue using NIR, organic liquids influence on microwave pyrolysis of cellulose, solvent-cellulose interaction and solvent-cellulose pyrolysis product interaction determination in this thesis.

2.3.1 Principal Component Analysis (PCA)

Principal component analysis (PCA) forms the core of multivariate data analysis.[391] The samples and the value of its parameters form a matrix. The matrix data is distributed along the X, Y and Z axes according to its values and variables. A plane or line is then searched in the three-dimensional direction in the least square fashion to cover the most variation in the data with a minimum residual value of the data, as shown in *Figure 39*. After finding the best fit of the data in the new three dimensions, the most explained variation of the data is directed as the principal component (PC) one. The next explained variety of the data sits on orthogonally of

PCA-1 in a new plane by the best possible fitting of the data with minimum residue. The unexplained part of the data is then best to fit into to PC-3 at the orthogonal of PC-1 and PC2 plane. The remainder of the unexplained variation is tried to fit in PC-4, PC-5, and so on in the multidimensional space until the hundred percent variation of the data is explained. As PC-1 and PC-2 explain most of the variations of the data, if any real correlation among the variable exists, then it would have been shown in these two new vectors. The position of the samples along a PC is called Scores, and the angular cosine of the variables of PC is called Loadings. The samples with similar explained information stay close to each other in the new space. The samples in the centre provide little information as they do not explain any variations of the data.[392-394]

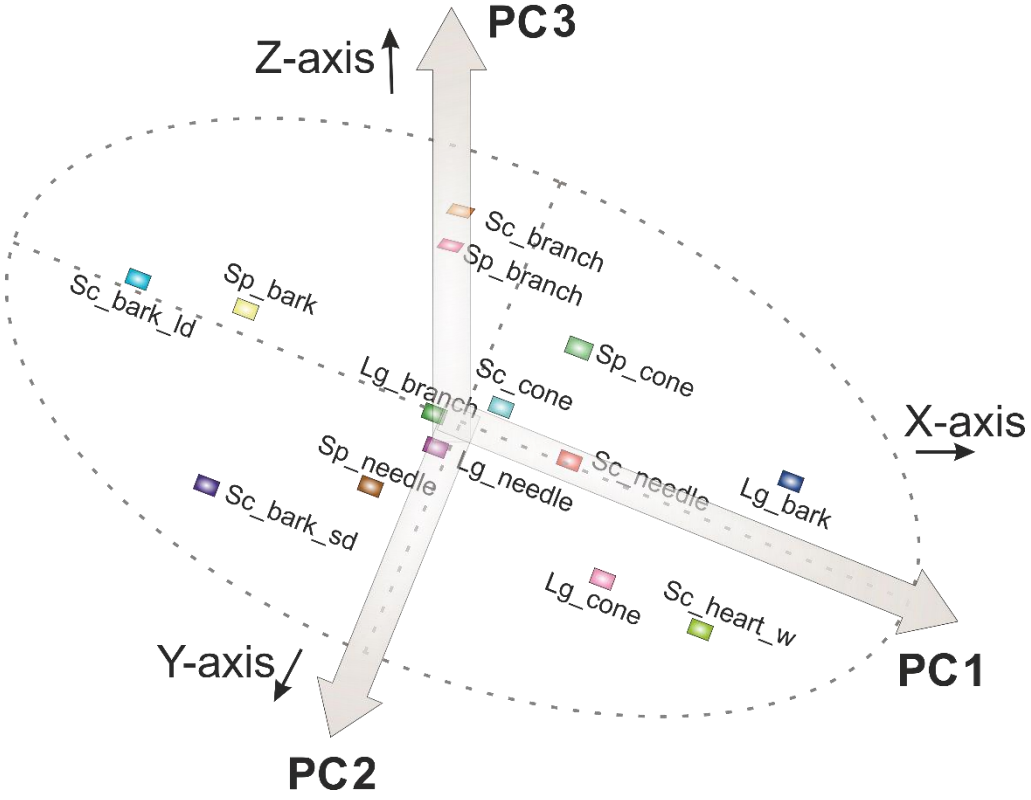

Figure 39 Scores and loading plot of PCA.

2.3.2 Principal Component Regression (PCR)

Principal regression analysis (PCR) is a regression analysis technique which regresses the outcome of principal components rather than original exploratory variables. PCR is a two-step procedure of converting the PCA data matrix. In the first step, a PCA is performed on X-matrix to decompose the data which is then fitted to a multilinear model using the PCs score instead of original X-variables. The new linear vector Y is projected onto a new plane (*Figure 40*), directed by the solution of equations.

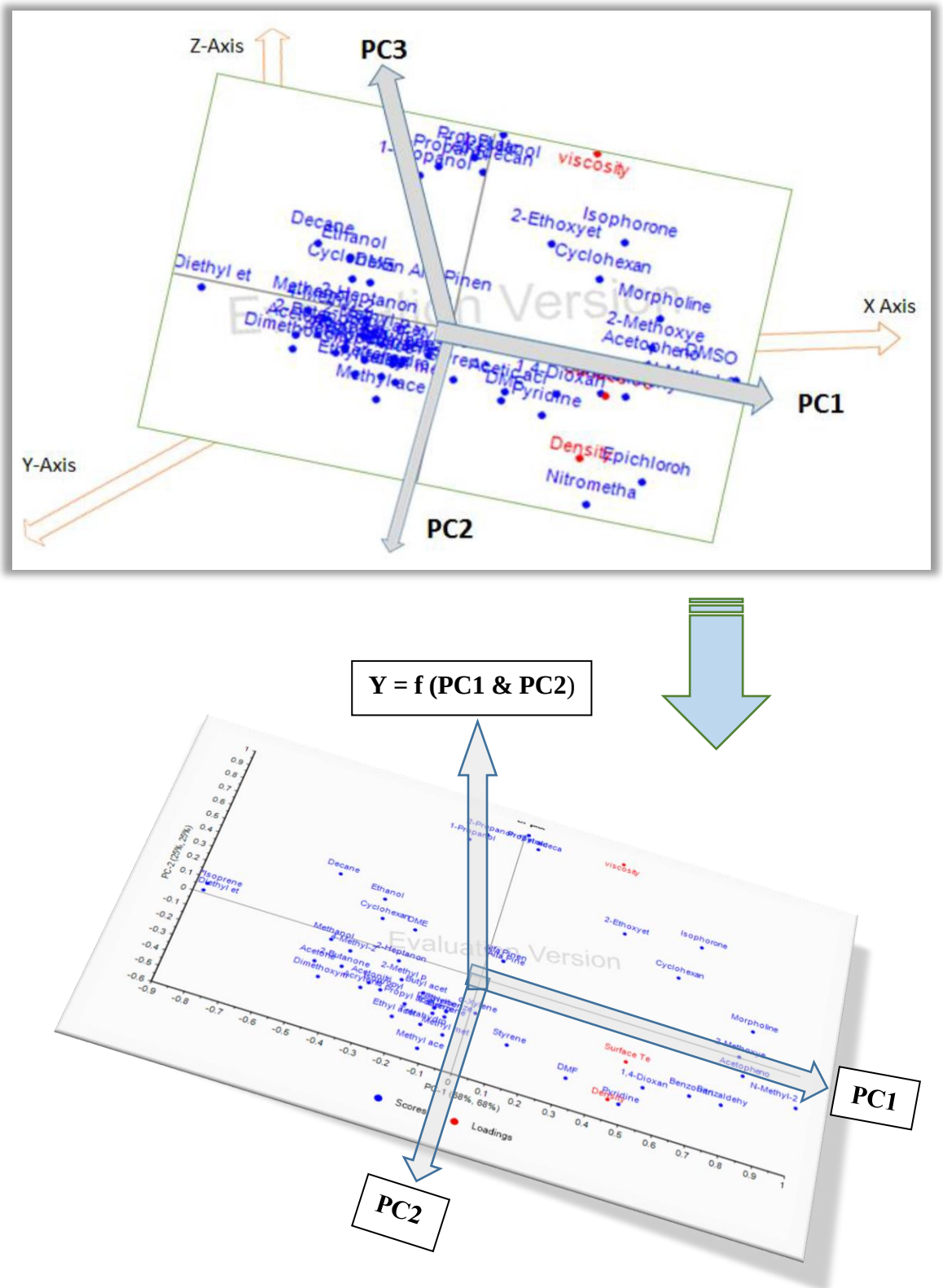

Figure 40 New linear vector projection from the original PCA to show PCR procedure

2.3.2.1 *Residuals and Influence of PCA*

In the application of multivariate analysis for the detection of a residual and influential outlier, Hotelling T^2 statistics are used to find the most influential sample for a variable in the data matrix, and F-test is used to find the sample of high residual value of any variance. The higher influential sample in any PC direction is shown by Hotelling T^2 statistics (named after Harold Hotelling who formulated PCA theory in 1933) to describe the distance from the centre of the model. In *Figure 41*, it can be seen that DMSO is not well described by PC4 of the model. On the other hand, component four was highly influenced by Carbon tetrachloride, and this compound might distort the model. For an ideal model to describe any future sample matrix, those residual and influential values should be removed.

In the experimental design of the current investigation, some very high influential organic solvent/liquid of a specific property would be selected and would be coated on cellulose for MW pyrolysis. The percentage of yield of above MW pyrolysed additive-cellulose would help to understand the influence of a specific additives property.

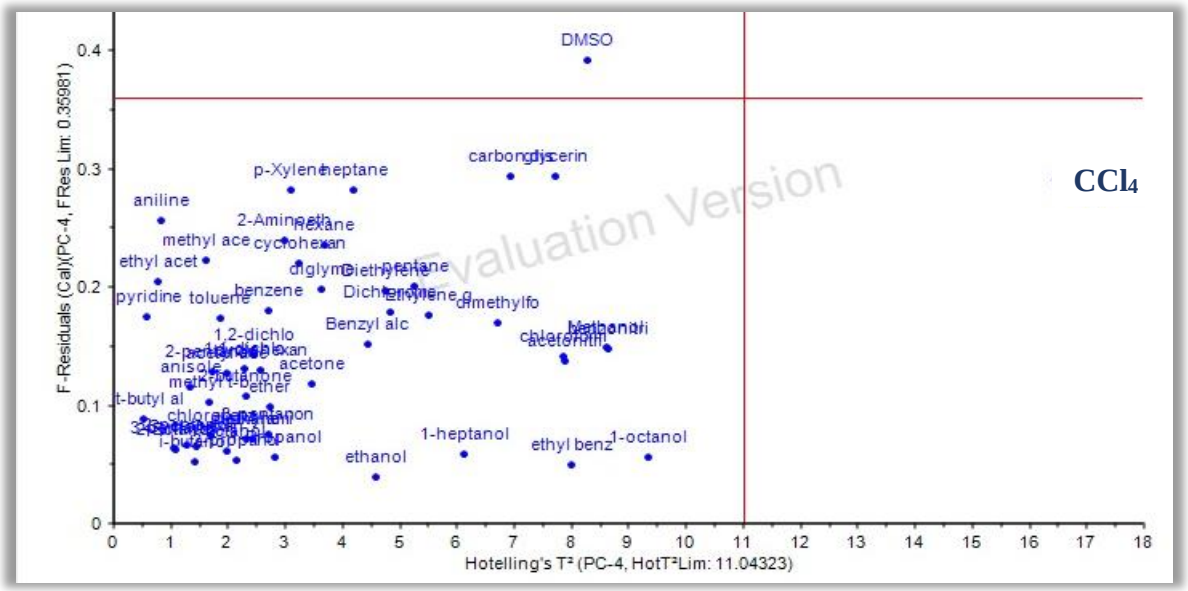

Figure 41 Influential plot

2.3.3 Multiple linear regression (MLR)

The multiple linear regression (MLR) model was used for analysing solvent-cellulose interaction in this work. If it is thought to be a response y is related to multiple independent variables (x_1, x_2,..), those variables could be expressed with a multivariable equation as expressed in *Equation 1* with unknown parameters (β_1, $\beta_{1,...}$) attached with each variable. The

MLR investigate how a dependent variable or response ($\hat{y}$) could be related to two or more independent variables (x_1, x_2,..) or predictors by estimating new parameters (b_1, b_1…) for those independent variables. The least-square method is used on sample data to get the values of the estimated parameters and to minimise the sum of squared residuals, or deviation, between the observed values and estimated ones (*Equation 3*).

$$y = \beta_0 + \beta_1 x_1 + \beta_2 x_2 + \beta_3 x_3 + \ldots\ldots + \beta_p x_p + \mathcal{E}$$

Equation 1

$$\hat{y} = b_0 + b_1 x_1 + b_2 x_2 + b_3 x_3 + \ldots\ldots + b_p x_p + \mathcal{E}$$

Equation 2

$$min \sum (y_1 - \hat{y}_1)^2$$

Equation 3

The MLR solution works well for less than ten variables provided that no strong collinearity is allowed between two parameters. The number variable also needs to smaller than the number of samples. The MLR solution was thought to be an ideal way forward to investigate solvent-cellulose interaction issues in this thesis.

2.4 Principle of Near-Infrared (NIR) Analysis

The theoretical and practical aspects of NIR analysis and its scope of use in the context of the waste material evaluation was also investigated to gain objective of optimisation of forest waste pre-treatment procedure to increase feedstock quality in terms of transport, storage, energy efficiency and value-added products from extractives. Among the different vibrational spectroscopic techniques, NIR is fundamentally different from others such as Raman and Mid Infrared Red (MIR) spectroscopy in terms of theoretical principles and practical applications.[395, 396] Whereas the polarizability of homonuclear and polar molecular functional groups is the basis of Raman spectroscopy and dipole moment is the basis of MIR spectroscopy, the anharmonicity of X-H groups such as CH/OH/NH functionalities creates absorption and diffusive reflection spectroscopic bands within the near-infrared region of the electromagnetic spectrum.[397] This anharmonicity causes overtone and combinational vibrations of X-H groups which are weak and complex but also very rich in information if an accurate interpretation can be formulated.[389, 390, 397-399] There are various commercially available NIR instruments based on the distinct character of NIR instrumentation such as optical configurations, scan rates, detector types, sample averaging technique, dust proofing,

waterproofing, and vibration tolerance. The instrument can also be designed to optimise Near-infrared transmittance, reflectance (Figure 42) or a combination of both.[396, 397, 400]

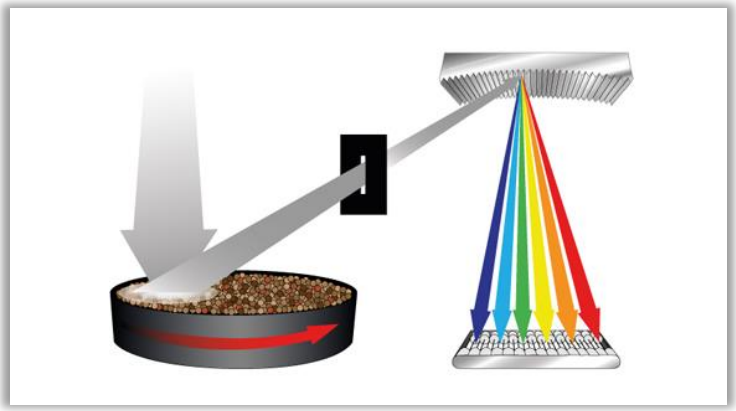

Figure 42 Scanning reflective NIR Technique.

2.5 Application of NIR in the Preprocessing of Forest Waste

Solid and liquid forestry wastes have highly variable extractive contents which can often change as a result of chemical reactions such as; micro-organism degradation of carbohydrates, auto-oxidation of fatty acids *etc*. during storage and transport.[401-403] Furthermore, volatile organic compounds such as aldehydes and ketones may be released during the auto-oxidation of unsaturated fatty acids, and further autodegradation of lower molecular weight aldehydes and carboxylic acids may occur during the process.[404] For these reasons, quick identification and extraction of value-added chemicals, especially compounds with short carbon chains from degradable waste materials, are required by industry. The NIR technique is an appropriate candidate for this purpose as the important chemical bonds (C-O, C=O, C-H, N-H, O-H) in proteins, fats, carbohydrates and water all absorb radiation in the region of 900-2500 nm.[405-408] As such, NIR could be employed in forest waste pre-process industry to capture the information regarding the functional groups contained within material under investigation. This analysis will be fast, non-destructive, good penetration depth and needs little or no preparation. Because of the high speed of the measurement, NIR can be used for online characterisation across the whole chain of the forest-waste biorefinery including original feedstock, intermediate products and final compounds. The NIR method can also be applied for the separation of mixed forestry wastes such as needles, stump, branches and barks. The quality assessment of these separated individual parts can also be conducted using NIR analysis by employing a Supervised multivariate computational data analysis model.[409] Currently, this type of model has yet not been developed for a biorefinery application, and its usage requires a systematic investigation of the NIR properties of the forestry waste under investigation.

2.6 Microwave-assisted Activation of Cellulose

Using the bio-refinery concept, biomass waste could be converted into a source of energy, biomaterials, and high-value chemicals.[26, 253] It is well known that a significant part of the biomass is cellulose.[379-382] Moreover, cellulose is the precursor of levoglucosenone (LGO)[410-422] and 5-hydroxymethylfurfural (HMF), which are important chemicals as a platform molecule.[417, 423-435] Pyrolysis was recognised as an effective way to convert lignocellulose as liquid chemicals.[436] Although the cellulose chemical structure is simple, the mechanism of its pyrolysis is not fully understood and requires significant investigation. Currently, the biggest challenge of pyrolysis is to increase the yield of liquids products which could be easily separated. However, the products selectivity through pyrolysis is usually low due to primary products polymerisation (char formation) and their decomposition to gases.[393]

It has been recently reported that inhibition of the polymerisation reaction can be achieved by pyrolysis of biomass in a polar solvent by dilution and stabilisation of the low-molecular-weight products.[437] Solvent-assisted pyrolysis leads to enhanced yield by inhibiting the polymerisation of levoglucosan (LGA) and LGO.[418] Aromatic solvents are known to be able to stabilise levoglucosan (1,6-anhydro-β-D-glucopyranose), the major pyrolysis intermediate of cellulose, against thermal degradation including char formation.[340, 341] However, the efficient production of LG is not easy, because thermal polymerisation and dehydration reactions of LG occur at>250 °C[438], which is much lower than the temperature required for the formation of LG from cellulose (around 350 °C).[340, 439]

LG and other glycosides are known to be stabilised in aromatic[438] and polyether[440] solvents up to the temperature around 350 °C. Hosoya *et al.*[441] reported that the stabilisation efficiency increased in direct correlation with the π-electron density of aromatic solvents. The phenomenon mentioned above is rationalised as π electrons of aromatic solvents [438] and ether oxygens of polyethers[440] act as hydrogen bond acceptors for hydroxyl groups of these glycosides, inhibiting proton donation to the carbohydrate molecules. Based on this stabilisation mechanism, complete solvation of carbohydrate molecules would be critical to maximising this stabilisation effect, so insoluble cellulose is expected to behave very differently to soluble compounds.[340] Cellulose pyrolysis starts with a decrease of the degree of polymerisation (DP) to around 200°C,[442-444] corresponding to the length of cellulose crystallites,[445-448] and subsequent thermal decomposition occurs from the crystallite surface.[341, 449-451] According to that idea, the formation of primary pyrolysis products and their secondary reactions, including char formation, occur inside the cell wall.

Thus, the aromatic solvent must be able to penetrate the cell wall to control the pyrolysis reactions. Shoji *et al*. [341] reported that cellulose was completely converted into volatile products by fast pyrolysis of cellulose–aromatic solvent mixtures by complete inhibition of char formation. They also claimed that polar aromatic substitutes are necessary to realise this behaviour. Such substituents may help the aromatic compound to penetrate inside the space between crystallites. Nevertheless, the action of aromatic solvents on the cell wall remains unclear. There is also some significant success on achieving value added-chemicals such as levoglucosenone (LGO), 5-hydroxymethylfurfural (HMF), levulinic acid, from cellulose by using ionic-liquids (IL)[411, 423, 452-458] such as ([EMIM]$CH_3C_6H_4SO_3$) and polar aprotic solvents such as tetrahydrofuran (THF), ɣ-valerolactone (GVL) and sulfolane during pyrolysis [418, 425, 435, 437, 450, 459]. But there is still a lack of systematic investigation to establish the hidden reason for a successful application of the solvent effect on cellulose activation or not being able to do so successfully in a particular investigation. To understand the general solvent-effect on cellulose, a systematic approach to the solvent effect on cellulose is needed to be established. The interaction of cellulose with a wider range of solvents that contains various functional groups may help to evaluate the current molecular-level understanding of solvent cellulose dissolution mechanism.

Alternative methods of biomass pyrolysis improvement have been reported by application of microwave (MW) to activate biomass. It is widely accepted [309, 310, 311] that the efficiency of cellulose conversion to bio-oil in the presence of MW- irradiation increase. The improvement of efficiency is due to the mild and controllable conditions of this process.[252, 334, 460] As it was mentioned earlier, microwave irradiation disrupts the hydrogen bonding within cellulose, promoting the breakdown into its monomeric units.[461] At cellulose softening temperature, at 180°C or above, MW causes rotation of the polar CH_2OH groups in the cellulose network and results from the cleavage of polysaccharide chain.[142] Moreover, MW pyrolysis method is preferred as it is fast, selective, effective and controllable.[462] Some significant MW assisted work was performed on lignocellulose materials in the last two decades using various forms of catalytic agents and solvents,[88, 193, 463-466] but the systematic study of cellulose itself were very few.[339, 413, 467] Even among those few works, most of those workers were rather focused on amorphous cellulose than microcrystalline cellulose.[468, 469 252]

2.7 Influence of Additives Physicochemical Properties on Microwave-asssited Pyrolysis of Cellulose

Various physicochemical factors of an added chemical species (i.e. additive) may influence both the initiation and yield of MW pyrolysis of biomass and its component such as cellulose. To understand which properties of biomass extractive components and organic solvent or additive could influence cellulose pyrolysis, it needs further research. For experimental design and formulate a hypothesis, it is taken an attempt here to screen some important physicochemical properties of on organic liquids which may influence on interaction of the organic liquid with microwave irradiation. At the initial stage, a list of organic liquid parameters which could explain the influence of organic additives on cellulose pyrolysis was discussed at the next subsection and to refine the proposed list of solvent parameters. It was presumed that this list has to cover dielectric properties of the compounds (to explain MW interaction with additives), their thermodynamic properties (to explain the additives heating mechanism during pyrolysis), the macroscopic molecular-relaxation time (τ) of the additives and some chemical characteristics such as polarity, acidity and molecular weight.

2.7.1 The interrelation of Physicochemical Properties

After an extensive literature search, following relationship among additives physicochemical factors are found. Those relations of organic liquids physicochemical properties are hypothesised to relate organic liquids interaction with the microwave. Hence those properties of organic liquid might influence pyrolysis of cellulose under microwave irradiation.

2.7.1.1 Dielectric Constant and Dipole moment

Surendra G. Sudrik *et al.* synthesised a variety of α-diazo ketones under microwave irradiation and conventional heating method.[470] Due to the dipolar nature of the diazo carbonyl functional group, α-diazo ketones possess high dipole moments. It was demonstrated that in microwave irradiation and at the presence of a dielectric solvent, the high dipolar products changes it conformation into Z-configuration.

2.7.1.2 Microwave Heating and pKa

In a given media, although the acidity of a compound is influenced by both the solvent effect of the medium and the electronic effects of the substituents. But it is very difficult to assess which element contributes to the acidity at what extent. It is also not easy to determine small differences of acidity between similar molecules. Emre Mentese *et al.* synthesised some benzylidenamino compounds in a microwave at solvent-free condition through auto pyrolysis

and determined their pKa with a potentiometric method.[471] They have shown that the extent of the autopyrolysis reaction performed in MW depends both on the intrinsic basicity and intrinsic acidity of the solvent.

2.7.1.3 Polarity and Enthalpy

M. Rodriguez *et al.* have investigated the influence of activation energy and polarity in microwave-assisted organic synthesis and in a conventional way.[472] For that purpose, they have computationally studied six types of reactions under microwave irradiation. Those reaction types are exothermic reactions with low activation energy (E_a <20 kcalmol^{-1}), endothermic reactions with low activation energy (E_a <20 kcalmol^{-1}), exothermic reactions with high activation energy (E_a = 20-30 kcalmol^{-1}), endothermic reactions with high activation energy (E_a = 20-30 kcalmol^{-1}), exothermic reactions with activation energy (E_a <30 kcalmol^{-1}) and endothermic reactions with activation energy (E_a <30 kcalmol^{-1}). They have concluded that endothermic reaction that needed higher activation energy than 30 kcalmol^{-1} do not take place either in conventional or in MW condition. In the presence of polar media (reagent, solvent and catalyst), exothermal and endothermic reactions can be improved with medium activation energy (E_a = 20-30 kcalmol^{-1}) and enthalpy of formation. The polarity of the media needed to be in the 7D to 20D.

2.7.1.4 Surface Tension and Solubility

Y. M. Tang *et al.* synthesised 1-Vinyl-3-alkyl/ esterimidazolium halide ionic liquid using microwave energy and investigated surface properties and solubility by using density functional methods.[473] Density functional theory (DFT) is a quantum mechanical modelling method to investigate the electronic structure of many-body systems, such as atoms, molecules, and condensed phases. They have found out a relation of surface tension with solubility parameters of the ionic liquid. They have also established that the solubility of the title ionic liquids decreased as the dielectric constant of the solvent decreased.

2.7.1.5 Dielectric Media and Polarizability

When a weak external electric field is applied to an electronic system, molecular dipole polarizability (α) describes the deformability of the charge distribution of the system. This property describes the π-electron delocalization of conjugated molecules. Ysaias J. Alvarado *et al.* have experimentally and theoretically determined static and dynamic electronic mean polarizability and the dispersion of the polarizability of 2- and 3-methylthiophene compounds in solution, by using refractometric techniques.[474] As a solvent of those molecules they have

used CCl4 and CH3CN and studied the effect of solvents on those molecules polarizability. When polarizability is measured experimentally at the applied field, it is called dynamic polarizability, whereas as the extrapolating value of dynamic polarizability at zero frequency is called static polarizability. Ysaias J. et al. has found that for both 2 - and 3-methylthiophene the dispersion of the electronic polarizability strongly depends on the dielectric nature of the media.

2.7.1.6 Microwave Field and Relative Polarity

Surasak Hemwimon *et al.* performed extraction of anthraquinones from roots of Morinda citrifolia.[475] They have used ethanol, acetone, acetonitrile, and methanol as a solvent for this microwave-assisted extraction purpose. They have found the percent of anthraquinones recovery highly dependent on the type of solvents used. It was also remarkable that the amount of water present in the extraction solvent changes the rate of anthraquinones recovery. They concluded that water increase swelling of plant tissue matrix and as such increase relative polarity of it.

2.7.1.7 Density, Viscosity and Conductivity

H. Huang *et al.* proposed a green recovery of phenolics from rice bran using glycerol based on viscosity, conductivity and density.[476] They have noticed that the changing of glycerol solution density significantly changes the recovery capacity of phenolic compounds.

2.7.1.8 Viscosity and Dielectric Relaxation Time

S. Messieh *et al.* studied the relation of solvent viscosity with the dielectric relaxation of some acetophenone derivatives (ortho-methyl acetophenone and para-methyl acetophenone).[477] They have used a various mixer of paraffin oil and carbon tetrachloride to prepare a different ratio of viscous solvent to dissolve the acetophenone derivatives. They have then studied dielectric properties of those acetophenone derivatives over 0.2GHz to 18 GHz frequency range. The applied frequency and dielectric loss factor (Ɛ``) absorption curve were plotted to establish a relationship between those two parameters. As the viscosity of the solvents increases, the relaxation time associated with the orientation of the molecules also increases. It was realised by them that the established relation of viscosity (η) and relaxation time (*τ)* as $\tau = A.\eta^{\alpha}$ cannot explain their inter-relation.

2.7.1.9 Viscosity and Surface Tension

Another interesting relation among physicochemical parameters is the relation between viscosity and surface tension. Numerous attempts were taken in the past to illustrate the general relationship of surface tension and viscosity, but the only equation worth mentioning here is:

$$\ln \sigma = \ln A + \frac{B}{\eta}$$

Equation 4

In *Equation 4*, σ is the surface tension, and η is the viscosity, A and B are arbitrary constants. The relation was proposed by Pelofsky in 1966 to describe surface tension and viscosity of pure or mixed components of n-alkanes and some functional groups compounds of their class.[478-480] The wood extractive mixtures, a complex natural substance, and often consist of many compounds which contain a variety of different functional groups not only alkanes. It is likely that extractives may not follow this simple rule of surface tension and viscosity.

2.7.1.10 Vapour Pressure and Enthalpy of Vaporisation

The enthalpy of vaporisation ΔH_{vap} is related to vapour pressure P, according to Clausius-Clapeyron equation (*Equation 5*) in which, the value of R is 8.3145 J mol^{-1} K^{-1}, the symbol A is a constant and T is the temperature at Kelvin.[481]

$$P = A \exp(-\Delta H_{vap}/RT)$$

Equation 5

2.7.1.11 Dielectric Constant, Dipole Moment and Polarisability

Debye-Langevin equation (*Equation 6*) establishes correlations between dielectric constant with dipole moment and polarizability.[482]

$$\frac{\varepsilon_r - 1}{\varepsilon_r + 2}\frac{M}{\rho} = \frac{N_A}{3\varepsilon_0}\left(\alpha + \frac{\mu^2}{3Tk_B}\right)$$

Equation 6

Here in this equation, ε_r is the dielectric permittivity, α is the polarisability and μ is the electric dipole moment of the substance. M is the molar mass, ρ is the density of the substance, N_A is the Avogadro's number 6.0221413×10^{23} mol^{-1}, ε_0 is the vacuum permittivity ($8.85418782 \times 10^{-12}$ $C^2 \cdot N^{-1} \cdot m^{-2}$), k_B is the Boltzmann constant (1.38065×10^{-23} J/K), and T is the temperature in Kelvin.

There were no other established relations was found in the literature in terms of being able to describe the relationships among or in-between the proposed physicochemical parameters. Based on the above literature discussion, fourteen characteristics of the organic additives were chosen to describe the influence of additive on MW pyrolysis of cellulose. Those properties

are boiling point, molecular weight, dipole moment, polarisability, dielectric constant, relative polarity, pK_a, viscosity, surface tension, density, enthalpy of evaporation, vapour pressure, thermal conductivity, and specific heat capacity of additive in a liquid state only. The classes of additive that were selected for this experiment are short-chained and long-chained alkane, terpenes, fatty acids, plant wax, aliphatic alcohol and water. The relation of those parameters will be investigated using principal component analysis (PCA) and principal component regression (PCR) to examine if any clear pattern of relationship exists between microwave pyrolysis of cellulose and any of those solvent properties.

2.8 Interaction of Organic Liquid with Cellulose during Microwave-asssited Pyrolysis

2.8.1 Interaction of Solvation Parameters with Microwave Irradiation

On the previous discussion, it was discussed independent solvent/organic liquids individual physicochemical parameters such as boiling point, vapour pressure or molecular weight. But in a complex solvent-solute system, or binary/multiple solvent systems the interaction of Vander Waals forces, hydrogen bond donor/acceptor, electron-pair donor/acceptor or solvophobic interaction may take place. [483] For this reason, the solubility parameters are important factors for understanding microwave heating mechanism of cellulose in the presence of solvent/organic liquid. Along with dielectric parameters, other solvation parameters, such as partial excess thermodynamic parameters may also be needed to define for bulk solution interaction behaviour with the microwave.[484]

The thermodynamic parameters, such as vapour pressure,[485] glass-transition temperature,[486] excess Gibbs free energy, enthalpy, and entropy were already evaluated for a binary solution of alcohol and nonpolar solvent.[487-489] The complexity behaviour between the molecular structure of the binary solution and microwave heating behaviour is recently studied by Takuya Sumi *et al.*.[489] In their experiment, they have used semiconductor microwave generator to produce 2.45 GHz microwave on a single-mode applicator where have placed a various mixture of ethanol and nonpolar solvent. The dielectric properties of the sample were investigated at various temperatures at up to 60 °C. They have demonstrated that the dielectric characters of solution were caused by the molecules cluster structure in the liquid. By microwave activation, those clusters can be broken and dielectric relaxation & reorientation of the solution mixture will be changed.

The work of Sumi *et al.* is supported by Onsager claim of polarization and the dielectric behaviour of liquid molecules in presence surrounding molecules.[490] Onsager-Kirkwood-

Fröhrich (OKF) latter refined Onsager theory and made a generalised theory of interaction between a molecule and the surrounding molecules as the following equation:

$$\varepsilon_s - \varepsilon_\infty = \left(\frac{\varepsilon_s + 2}{3}\right)^2 \left(\frac{3\varepsilon_s}{2\varepsilon_s + \varepsilon_\infty}\right)\left(\frac{Ng\rho\mu^2}{3\varepsilon_0 kTM}\right)$$

Equation 7

Here k is the Boltzmann constant; ε_0 is the permittivity of the vacuum; ε_S and ε_∞ are the relative dielectric constants at small and infinite angular frequencies; T is the temperature; M and ρ are the molecular weight and the density of the substance, and μ describes the dipole moment of the molecule. The parameter is termed as Kirkwood correlation factor. During microwave interaction, Kirkwood correlation factor (g) of a molecule with its neighbour molecules may change in renewed alignment. The new magnitude of g is termed as g^{eff} factor and can also be written as g = Zcosɵ. In this new relation, ɵ is the angle between the dipole moment of a molecule and its neighbours and Z is the number of neighbour molecules of the surrounded molecule. Unfortunately by using the above theory, it is not easy to calculate microwave heating value for even a very simple liquid system by measuring accurate cluster formation of liquid molecules. For this reason, practical measurement of microwave heating is needed for a complex system such as cellulose-solvent interaction in changing the temperature during MW pyrolysis. It is worth noting here that changes of bulk dielectric parameters of the solution with temperature may not wholly correlate with actual microwave heating in real-time.[489]

2.8.2 Evaluation of Solvation Parameters for MW Pyrolysis of Cellulose

There is evidence of the effective use of MW radiation to produce value-added chemicals from cellulose by using different catalysts such as water, acid, zeolite or ionic liquid media.[298, 339, 465, 491, 492] However, there was never a combined use of solvent and MW-pyrolysis of cellulose. There is a small amount of research work recently published in which combined use of solvent and catalyst for biomass microwave pyrolysis were reported.[493, 494] Because of the complex approach on the reported work, the rule of solvent in MW irradiated cellulose liquefaction was not focused, and the mechanism is not addressed. In this project, a systematic approach is developed to investigate the influence of the nature of the different solvents on the mechanism of MW-assisted cellulose pyrolysis. As it is seen in *Figure 43*, three main types of solvents impact on the MW assisted pyrolysis system was identified.

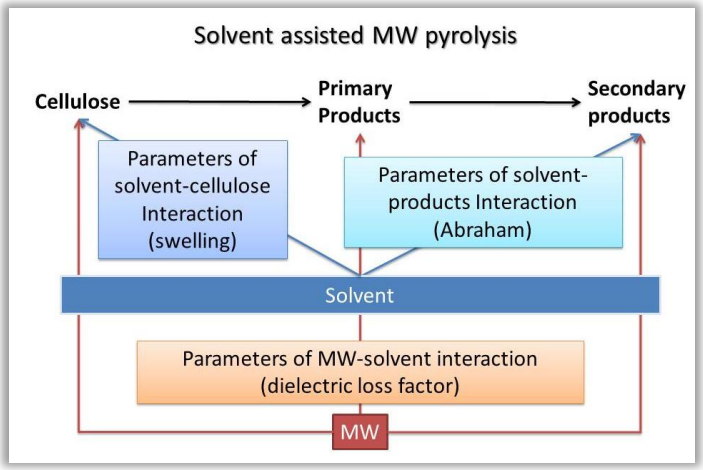

Figure 43 Investigation steps of suggested Solvent assistance MW pyrolysis process.

Firstly, the pyrolysis process could be influenced by the solvent on cellulose. Secondary, solubilisation could stabilise/activate primary and secondary pyrolysis products. Besides, solvents might transfer electromagnetic energy of MW irradiation to the system as heat. It was necessary to identify a group of parameters as it is drawn in *Figure 44*, which could describe all the types of interactions to address the inter-relation as mentioned above.

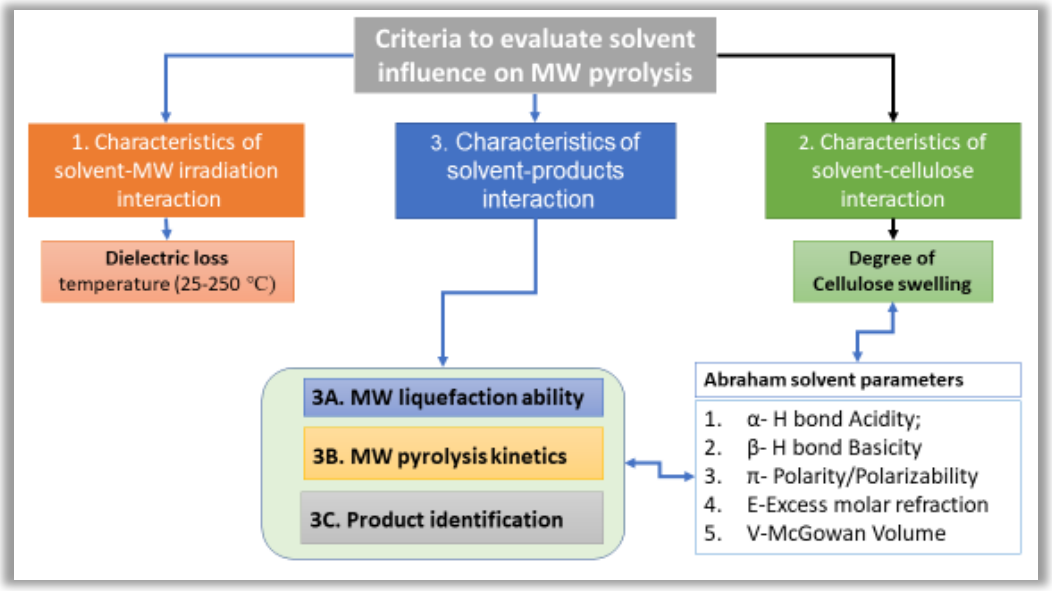

Figure 44 Scheme of MW-solvent-cellulose interactions

2.8.2.1 Characteristics of solvent-cellulose interaction

Because of alternative crystalline/amorphous structure, cellulose could be accepted as a lightly cross-linked polymer.[94] This concept makes it enable to apply the Flory-Rehner theory,[495] which shows that a swelling degree can be used as a quantitative parameter for cross-linked polymer-solvent interaction. Indeed, during the majority of cases involving cellulose dissolution, the first step is cellulose swelling due to the penetration of solvent inside the

amorphous region while the main crystalline structure remains unaltered.[496] It describes the equilibrium swelling of a lightly cross-linked polymer in terms of crosslink density and the quality of the solvent. Therefore, one of the methods available for studying the solvation power of liquids for a given polymer and for determining the polymer-solvent interaction parameter is measuring equilibrium swelling of the cross-linked polymer.[497] Following the presented overview, it is suggested in this work to use the degree of cellulose swelling as a parameter describing cellulose-solvent interaction. The correlation of solvent reactivity phenomena of cellulose with its degree of swelling was studied on various occasions in the past, but a general association was never established.[123] Nonetheless, swelling remains an important step of various processes such as mercerisation of cellulose and polymer chemistry.[498-500] It was also decided here to measure the impact of solvent on cellulose by the degree of swelling of cellulose as a breakdown step for observing the overall influence of organic liquids on MW pyrolysis process. The degree of cellulose swelling was measured using various scales in the past. Microcrystalline cellulose was measured shown by a weight changed,[501] by the number of molar weight,[502] using synchrotron radiation wide-angle X-ray diffraction (WAXRD),[503] wet electrospinning apparatus,[504] or by spectrophotometrically,[505] for specific applications in some research work before. In this work, the measurement of swelling was performed by the scale of height of samples before and after swelling.

2.8.2.2 Characteristics of solvent-products interaction

Solvent solute interactions could be classified as Vander Waals, the ion/dipole forces, hydrogen-bond donor/acceptor, electron-pair donor/electron-pair acceptor and solvophobic interactions.[483] By choosing a particular solute to quantify multi-parameters, the concept of linear solvation energy relationships (LSER) was introduced.[506] The renowned Kamlet-Taft,[507, 508] and the Abraham parameters are based on this concept.[509] But to work on the LSER concept, experimental data are needed which are not always available and to search for greener replacement solvent, the need for the theoretical descriptor is raised. Based on quantum chemistry theory and computational modelling, the theoretical COnductor-like Screening Model (COSMO) was developed by Klamt to fill the need mentioned above.[510] Later, the model was adjusted for real solvent and termed as the COnductor-like Screening Method for Real Solvent (COSMO-RS).[511] According to the COSMO-RS concept, the solute molecule is considered to be embedded in a cavity, and it is surrounded by a virtual conductor ($\varepsilon=\infty$) as the reference state for molecules in solution. The calculation from the model provides the screening charges density σ, the only significant variable of local pair-wise surface interaction.[512] From

the COSMO-RS framework, a σ-potential histogram and the chemical potential $\mu_s(\sigma)$ of a molecule can be generated. From the mentioned chemical potential curve, 61 discrete values of $\mu_s(\sigma)$ can be created. PCA can then reduce the set of 61 descriptors to three descriptors and be clustered in 3D space using k-means clustering. On the three new axes, 85% of the data variance is still retained for the physicochemical interpretation of the descriptor. The most informative axis interprets the hydrogen bond donor ability of the solvent (HBD). The second axis is highly correlated with the electron pair donor ability of the solvent (EPD). The third axis, perpendicular to the plane of the first two axes, correspond to the lipophobicity and the dipolarity. The solvents are clustered mainly ten subgroups in 3-D space through Classification and Clustering as mentioned above. The selection of the organic liquids that will be tested in this project is based on these ten-sub classes.[513] Where possible the organic liquids were chosen from a list of greener solvents which were sub-classed according to the COSMO-RS model.[514] Whenever possible, the choice of liquid was high-boiling point liquid at around 200 °C or above and as 'green' as possible. The target of MW pyrolysis of cellulose was to perform in the liquid that does not boil at cellulose softening and pyrolysis temperature in MW, which is at around 180 °C.[309] The dielectric loss factors of those selected solvents will be measured by using a custom-made dielectric perturbation resonant cavity at elevated temperature (250 °C). The interdependency of elevated temperature with dielectric loss factor, swelling of cellulose, solvation parameters of organic liquids, evolved pyrolysis liquid and residue from pyrolysis will be systematically evaluated to select a short list of solvents. The short-listed solvent-cellulose interaction products will then be characterised to identify the potential of value-added chemicals.

2.8.2.3 Characteristics of solvent-MW irradiation interaction

The rate of heating of a sample within a microwave cavity depends on the instrument design and the nature of permittivity of the sample within the MW-condition as depicted in *Figure 45*, and the efficiency of that complex interaction can be generally described through the dielectric loss factor (ε''). The instrumental parameter except electric field strength could be determined for industrial MW setting.

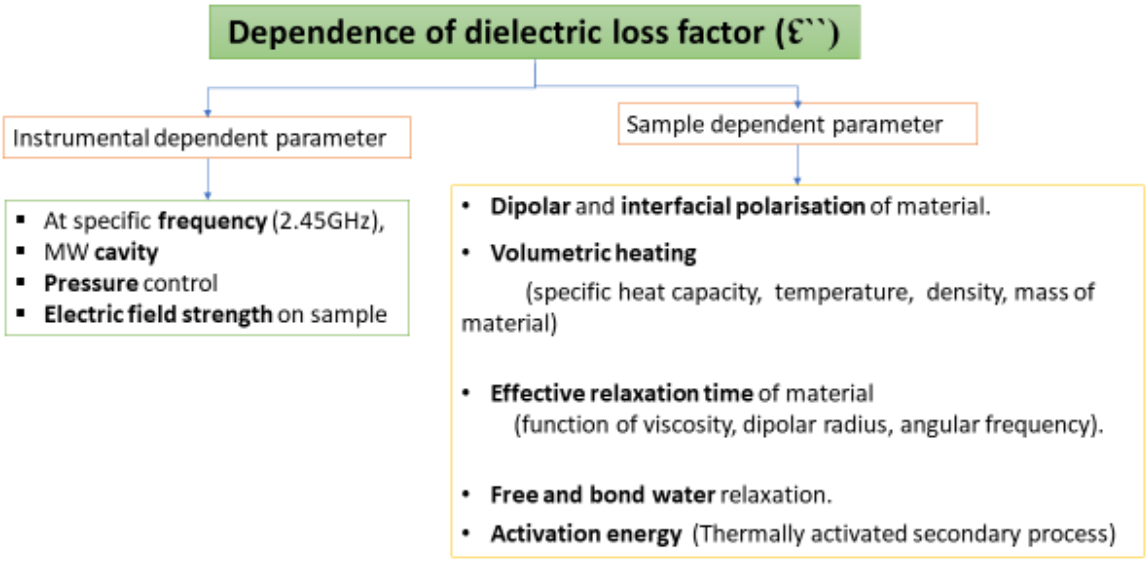

Figure 45 Dielectric loss tangent dependence criteria of material.

As the industrial microwaves are operated in the narrow frequency range, and most of the biomass contains moisture, the loss factor of biomass is mainly dipolar in nature and relied on d.c. conductivity, Maxwell-Wegner effect, bound and free water relaxation as shown in *Figure 46* .[515]

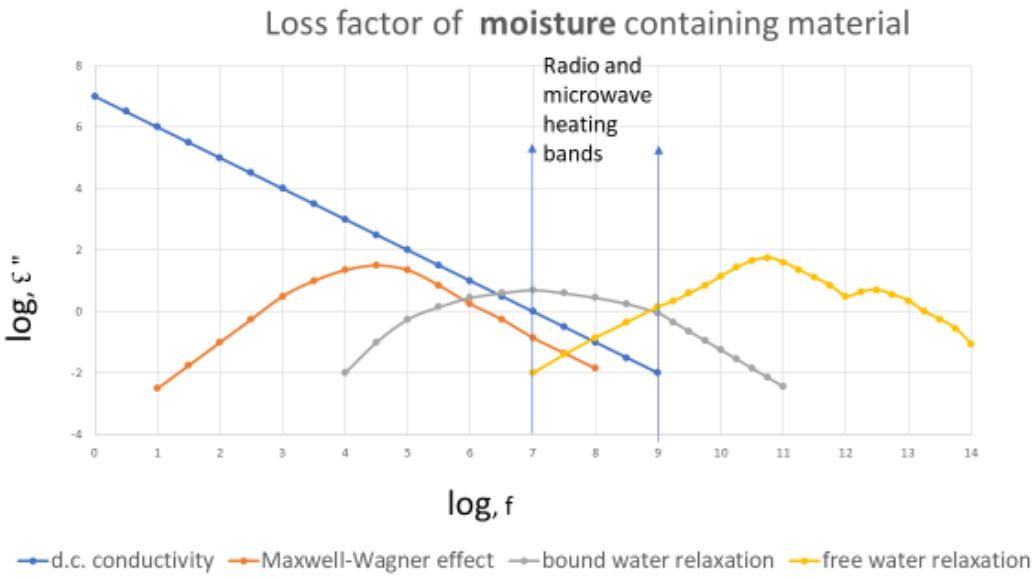

Figure 46 Frequency dependence loss mechanism

The volumetric heating rate in an MW system could also be derived from the function of permittivity (ε), specific heat capacity C_ρ, the electrical field strength (E) and sample density according to equation (1) below.[516]

$$\frac{dT}{dt} = \frac{2\pi j \varepsilon E^2}{C_p}(b + a\rho)$$

Equation 8

Here in *Equation 8*, a & b are constant. So, the heating rate could also be used for the estimation of MW-solvent interaction. But the approach of *Equation 8* involves a higher degree of complexity, including the prediction of solvent density and calorific value. However, it is very important to note that dielectric properties are a function of temperature and should be estimated at the temperatures appropriate to biomass pyrolysis (180 ℃ for cellulose). It is decided here to use the dielectric loss factor as a parameter to investigate MW-assisted pyrolysis of cellulose in the presence of a solvent, considering all the factors mentioned above.

The suggested approach requires an instrumental set-up creation for the measurements of the dielectric loss factor of organic liquid/material at high temperature.

2.9 The Basic Concept of Dielectric Loss Factor and Measuring Techniques

In a vacuum, on an arbitrarily closed surface dS, if an electric field **E** is applied, then the total charge closed by the surface **Q**, at the direction of (Dn) can be written as *Equation 9* to express as an electric flux (ψ) (*Figure 47*).[517] The constant $\boldsymbol{\varepsilon_o}$ is called permittivity of free space.

$$\varepsilon_o \int_{\text{Closed surface}} Dn \, dS = Q$$

Equation 9

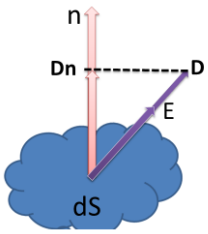

Figure 47 Electric flux

If the medium is changed, say for in an organic solvent, the above equation can be written as *Equation 10*, and the added constant ε_r is the specific property of that solvent and defined as relative dielectric constant ε_r. The dielectric constant also sometimes written as ε`.

$$\varepsilon_o \varepsilon_r \int_{\text{Closed surface}} Dn\, dS = Q$$

Equation 10

The product of $\boldsymbol{\varepsilon_o}$ and $\boldsymbol{\varepsilon_r}$ is simply called dielectric constant and written as $\boldsymbol{\varepsilon}$. Another variable, dielectric displacement (***D)***, is a density vector or electric flux and is expressed for a total charge of the enclosed system and written as *Equation 11*.[518]

$$\boldsymbol{D} = \varepsilon_o \varepsilon_r \mathbf{E}$$

Equation 11

Now, if the medium is a polar liquid and is placed in an alternating electric field at the appropriate frequency (***f)***, in this case at 2.45 GHz, then the dielectric polarisation arises either due to physical rotations of a molecular dipole or the distortion of electron cloud distribution at the molecular level (*Figure 48*).[519] If the average dipole moment (**μ**) of a solvent dipole in MW field is termed as (qx_i) then the displaced dipole can be written as *Equation 12*, where q is the charge and x_i is the charge separation (*Figure 49*).

$$\mu = qx_i$$

Equation 12

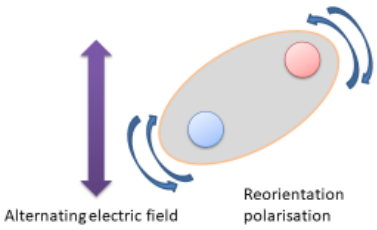

Figure 48 Reorientation polarization

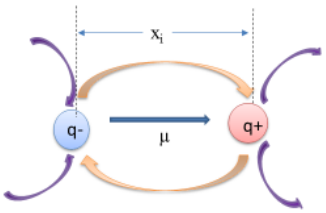

Figure 49 Polarization of charge

The polarization field, ***P***, is the summation of all the charges in a small volume containing *N* dipoles, expressed as the charge density (*Equation 13*).

$$P = \frac{\sum_{i=1}^{N} qx_i}{\delta v}$$

Equation 13

The difference between the charge density vector ***D*** and the polarization vector ***P*** can be written as *Equation 14* to calculate the remaining free charges. The ratio between the bound and free charges is called electric susceptibility.[518]

$$\boldsymbol{D} - \boldsymbol{P} = \boldsymbol{\varepsilon_o E}$$

Equation 14

Now, as we know, an alternating current-carrying conductor also exhibits a magnetic field to its surrounding, the induced magnetic field ($\mathbf{B_n}$), on an arbitrary surface (s) near it, would create a magnetic flux (Φ) as *Equation 15*.

$$\int_s Bn \, dS = \Phi$$

Equation 15

Similarly, as *Equation 11*, the magnetic flux can be written as *Equation 16*, where μ_o is the permeability in free space and μ_r is relative permeability.

$$\mathbf{B} = \mu\mathbf{H} = \boldsymbol{\mu_o \mu_r H}$$

Equation 16

Concluding from *Equation 10* and *Equation 16* (the basis of Maxwell's first and second law) changing the electric field leading to a magnetic field, and then changing the magnetic field to electric filed creates a propagated electromagnetic energy in the waveform as in *Figure 50*.

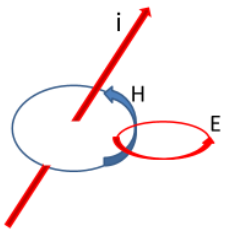

Figure 50 propagative continuous waveform

The field vector **E** and **H** in a dielectric medium, for a time-harmonic three-dimensional Helmholtz waveform, can be derived as,

$$\nabla^2 E = - \omega^2 \mu_o \varepsilon_o \varepsilon` E$$

Equation 17

$$\nabla^2 H = - \omega^2 \mu_o \varepsilon_o \varepsilon` H$$

Equation 18

Here ω is the angular frequency. If it is considered a rectangular coordinate system and a plane of a sinusoidal waveform of electric field vector as $\mathbf{E_x}$ and magnetic field vector as $\mathbf{H_y}$ in the coordinate, then the wave would propagate in z-direction in free space at the speed of light (*Figure 51*).[520]

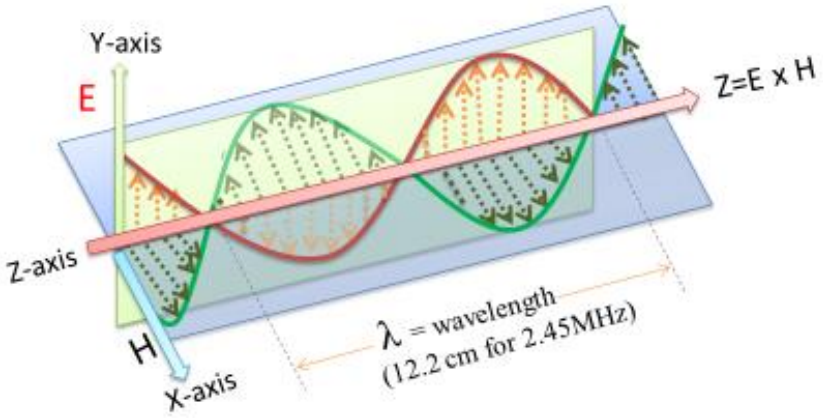

Figure 51 Wave propagation in free space

In an unbound medium with no reflection, the time-harmonic solution of *Equation 17* is a forward wave, as stated in *Equation 19*, where at (z = 0) $E_x=E_0$ and γ represents the propagation constant.

$$E_x = E_o e^{(jwt-\gamma z)}$$

Equation 19

The propagation constant γ can be rewritten as *Equation 20*. The symbol α is the attenuation constant and β is the phase constant.[520]

$$\gamma = \alpha + j\,\beta$$

Equation 20

The rate of change of total electric flux causes conduction current density on a surface (*Figure 50*) due to conduction effect and can be expressed as following function.[518]

$$\boldsymbol{J_c} = \sigma \boldsymbol{E}$$

Equation 21

Where the term σ is the conductivity of the medium. At the high-frequency heating, the total current density is,

$$\nabla x\, \boldsymbol{H} = \boldsymbol{J} = \sigma \boldsymbol{E} + j\omega\varepsilon_o\, \varepsilon` \boldsymbol{E}$$

Equation 22

So far only the loss mechanism discussed here is the conduction effect considering dielectric constant as real, which only contributes to the stored energy of the system. Now *Equation 22* can be rearranged as *Equation 23*.

$$\boldsymbol{J} = j\omega\varepsilon_o\, (\varepsilon` - j\sigma/\omega\varepsilon_o)\, \boldsymbol{E}$$

Equation 23

But in the free space, where the conductivity of the medium is zero (σ=0),

$$\boldsymbol{J} = j\omega\varepsilon_o\, \varepsilon` \boldsymbol{E}$$

Equation 24

Both *Equation 23* and *Equation 24* could be expressed in a single form as *Equation 25*

$$\boldsymbol{J} = j\omega\varepsilon_o\, \varepsilon_c{}^* \boldsymbol{E}$$

Equation 25

by defining $\varepsilon_c{}^*$ for complex dielectric constant as of *Equation 26* where the conduction effect dominates.

$$\varepsilon_c{}^* = \varepsilon' - j\sigma/\omega\varepsilon_o = \varepsilon' - j\varepsilon_c''$$

Equation 26

In the same way, in the high-frequency MW region, as in the case of 2.45 GHz, where reorientation polarisation dominates, *Equation 26* could be written as *Equation 27*. The subscription d refers to the dipolar or polarisation mechanism.

$$\varepsilon_d{}^* = \varepsilon' - j\varepsilon_d''$$

Equation 27

To consider all form of losses such as Maxwell-Wagner, dc conductivity, atomic and electronic polarisation along with dipolar polarisation, complex dielectric constant (ε*) is generally expressed as *Equation 28*. The symbol ε_{eff}'' represent effective loss factor, the loss accountable for

all possible mechanism in high-frequency heating and the real part (ε') expressed for stored energy at any stage of the heating process.

$$\varepsilon^* = \varepsilon' - j\varepsilon_{eff}''$$

Equation 28

Since most of the dielectric measuring techniques are not able to provide all losses separately, *Equation 28* is widely used for the real and imaginary and complex dielectric constant. The ration of the real and imaginary part is called effective loss tangent (tan δ_{eff}) or energy dissipation factor (*Equation 29*). The loss tangent is a helpful parameter to compare the heating rate of two or multiple organic solvents of similar physical and chemical properties.[519]

$$\tan \delta_{eff} = \varepsilon_{eff}''/\varepsilon'$$

Equation 29

For the purpose of simplicity, the term ε_{eff}'' will be written as ε" and tan δ_{eff} as tanδ for time to time in this document. The loss tangent term (tan δ) is a single expression to represent an organic solvents unique ability to convert the thermal energy of MW radiation inside the solution or in the MW reactor cavity. The loss tangent is an important parameter to consider to pick up an appropriate solvent for a specific purpose to compare the heating rate between two or among multiple organic solvents of similar physical and chemical property.[29]

But it also needs to be kept in mind that as the loss tangent (tan δ) is only a ratio of energy conversion rate but not the magnitude of actual energy dissipation capacity. Two solvents with the same ratio of loss tangent with the very different dielectric scale of loss factor (ε``) and relative dielectric constant (ε`) magnitude cannot be meaningfully expressed with tan δ. Say, for example, at 2.5 GHz and 50ºC, the loss tangent of MeOH is 0.38 while at the same condition, the loss tangent of propanol is 0.86.[521] From the above comparison, it should not be assumed that the total thermal energy gained from MW energy would be higher in propanol than in MeOH at the same condition. The total thermal conversion for both solvents would also be relied upon the dielectric loss dissipation factor, as the Ɛ" of MeOH is 9.00 and Ɛ" of propanol is 5.4 at the same condition. So, here, although tan δ of propanol is more than two times higher than tan δ of MeOH, the dielectric loss factor (ε") of MeOH is almost double than that of propanol. So, realistically, if both solvents would have a significantly close magnitude of dielectric constant (ε`), but comparable different dielectric loss factor (ε"), then the ratio of loss tangent (tan δ) would have represented the meaningful difference of MW-solvent interaction

process. The above statement can be illustrated with another example here: the solvent 1, 3-propanol and 2, 3-butanol is examined at 2.45 GHz at 50 ºC in this work for all three parameters. The relative dielectric constants (ε`) of 1, 3-propanol and 2, 3-butanol are 11.16 and 8.24 accordingly, and the loss factors are 10.9 and 4.4 for 1, 3-propanol and 2, 3-butanol respectively. So, the loss tangents are 0.98 for 1, 3-propanol and 0.53 for 2, 3-butanol. As, the real part of complex dielectric constants of these two solvents are comparably close and the imaginary parts are significantly apart, so the loss tangent difference (0.98-0.53=0.43) of these two solvents is meaningful for MW-solvent interaction comparison. So, from this discussion, it can be further stressed the fact that all of the three parameters (ε`, ε" and tan δ) are needed at a specific temperature and frequency to understand the MW-solvent interaction of various solvents. A very reliable measuring system of both parameters (ε`, ε") is needed at full temperature interaction range to get those dielectric parameters.

Instead of directly measuring effective loss factor (ε_{eff}"), it could also be derived by measuring the rate of the rising temperature of the mass of a material by using specific power as of *Equation 30*. In *Equation 30*, Q_h is the quantity of heat, C_p is the specific heat of a mass of material M_a with the (ρ) density and rise of the temperature from T_0 °C to T °C using average power $P_{av.}$ P_{av} is also expressed as of *Equation 31* where E_{rms} is denoted for root-mean-square electric field strength.

$$P_{av} = Q_h/t = M_aC_p\,(T-T_0)/t$$

Equation 30

$$\text{Where } P_{av} = \omega\varepsilon_0\varepsilon_{eff}"E^2_{rms}V$$

Equation 31

Here V is the volume of material. The field strength E is expressed in E^2_{rms} form because the field strength is not a constant quantity but varies in the space within the cavity of a specific microwave instrument. *Equation 31* can be rewritten into *Equation 34* by rearranging as of *Equation 32* and *Equation 33*.

$$(T-T_0)/t = P_{av}/\,M_aC_p = \omega\varepsilon_0\varepsilon_{eff}"E^2_{rms}V/\,M_aC_p$$

Equation 32

$$(T-T_0)/t = \omega\varepsilon_0\varepsilon_{eff}"E^2_{rms}/\rho C_p$$

Equation 33

$$\varepsilon_{eff}" = (T-T_0)\rho C_p/E^2_{rms}/t\;\omega\varepsilon_0$$

Equation 34

So, the rate of heating and the electric field strength on a sample within a microwave cavity depends on the instrumental design and material is being used. It is complicated to predict the magnitude of the electric field developed within the material since the field strength changes after it is calibrated in the empty MW cavity. The Perturbation technique could be used by placing a tiny amount of sample inside a cavity by ensuring only small perturbation of the MW signal. But the precise measurement is rarely possible to achieve by a chemist using MW instrument available at a commercial laboratory.

2.10 Methods of Measuring Dielectric Loss Factor

The instrumental measuring systems that are commercially available could be divided into three categories. One of those methods is the reflectometric method, which is based on measuring the complex reflection coefficient of the permittivity of the material. By using the coaxial line and waveguide reflectometric technique, Vector Network Analysers (VNAs) are generally employed to measure the complex reflection coefficient. Another technique, transmission method, is a similar technique but rather than reflecting the wave is passed through the material. But the problem of using any of these two methods is that the electric and magnetic fields fall off rapidly with distance. For this reason, skin depth dominates over the accuracy of the measurement.[522] The third technique, resonant cavity perturbation (RCP) method, applies a different principle than the other two methods. The RCP is the more accurate technique for high precision measurement to distinguish small differences of dielectric loss reliably. A short description of this method is mentioned in the next paragraph to understand why it is crucial to make a purpose-built RCP device for this PhD work.

2.11 The Development of Resonant Cavity Perturbation (RCP) Device

In this technique, a small amount of polar liquid is placed in a cavity which is at least hundred-fold larger than the sample volumetrically. Then a specific frequency of a wave is passed through the cavity. The cavity is designed in such a way that the signal resonates inside the cavity. By placing a small sample in a specifically positioned hole of the cavity, a little perturbation of the signal is created. Using VNA, the complex frequency shift $\Delta\Omega$ is measured by calculating $\Delta(1/Q)$ and Δf as stated in *Equation 35*.

$$\Delta\Omega = \frac{\Delta f}{f_0} + \frac{1}{2} j\Delta \left(\frac{1}{Q}\right)$$

Equation 35

The quality factor, Q, is the function of dissipated energy per cycle of total stored energy and Δf is the measurement of frequency change due to the perturbation caused by the lossy sample. Using complex frequency shift $\Delta\Omega$, from *Equation 36*, the complex dielectric loss factor ε* is measured.[484, 522]

$$\mathcal{E}^{*}=1-\frac{\Delta\Omega}{A\Delta\Omega+K}$$

Equation 36

In equation *Equation 36*, the sensitivity factor k is derived from the ratio of sample volume and the cavity size. The depolarization factor (A) of the equation depends on the shape and orientation of the sample.

Using the above formula an in-house RCP instrumental device will be built, calibrated with standard, the selected organic liquids dielectric constant and loss factor will be measured at room temperature. The RCP device will then be placed in an appropriate temperature controllable oven for measuring dielectric constant and loss factor of the organic liquids at a wide range of temperature. The experimental data will then be evaluated to develop any potential mathematical formula for use as a function for dielectric loss factor prediction at any suit temperature without practical experiment in acceptable confidence limit. It will be also a target to make the RCP instrument completely automated using software interface for user-friendly experimentation purpose.

Along with answering all of the research question laid out in this Literature review, it is also the aim of thesis work to examine microwave influence on solvent dependent reaction kinetics or non-thermal effect. The purpose of this last research question in this thesis is to highlight the fact that the dielectric property knowledge of solvents and reagents is crucial to take advantage of MW power for exploiting a specific reaction process.

2.12 Influence of Microwave on Solvent Dependent Reaction Kinetics

The development of electrolyte chemistry is crucially dependent on a systematic investigation of dielectric properties of solvents.[523, 524] Proper understanding of the solvent dielectric properties allows the estimation of solvation energy and entropy as well as solubility for the majority of organic and inorganic salts.[525] Furthermore, the dielectric constant has a significant impact on the constant of equilibrium involving ions and has a crucial effect on the rate of the reactions accompanied by charge distribution rearrangement.[526, 527 528] The Menshutkin reaction, in which two uncharged reactants form an ionic product, is the most investigated

example of the dielectric properties influence on the reaction progression mechanism.[529-531] However, the understanding of the actual mechanism, of solvent interaction around the transition state complex formation and the diffusion process of the product is not well established.[529, 532] The temperature and frequency-dependent nature of dielectric properties make it even more complicated to understand reaction mechanism and kinetics in changing temperature.[342, 533, 534] There are a lot of data about the dielectric constants of various solvents at room temperature.[535] However, there is only a limited number of the solvent such as water, and some common laboratory solvents of which dielectric constants were measured in all temperature range from melting to boiling point.[521] The majority of this common solvent has a low boiling point with high vapour pressure. Due to too short temperature range, low boiling point solvent is not suitable to examine the separation of dielectric constant impact from the main part of energy activation. For example, a recent investigation of Menschutkin reaction mechanism applied temperature range from 20 to 80°C.[536] At this temperature range, those solvents dielectric properties was changed no more than 20%. It is challenging to decide on the mechanism of dielectric properties influence based on such short variation in key parameter. To investigate such impact, the choice of the solvent has to be as such that with changing temperature dielectric constant changes strongly in both directions as increasing and decreasing.

During the last few decades, microwave-assisted chemistry brings new attention to the dielectric properties of solvents.[533, 537-539] One of the major focus of MW chemistry is the investigation of the so-called “microwave” effect or “non-thermal” effect.[235, 540-542] Currently, there are two explanations of the differences in the reaction rates observed between conventional and microwave conditions. Some researchers believe that this difference is the result of a lack of correct temperature monitoring systems under MW reaction condition. Another explanation of the MW influence on the reaction rate is based on the hypothesis of "molecular radiator".[543] This hypothesis based on the assumption that MW heating could create micro-heterogeneous temperature patch due to volumetric interacting of MW with individual molecules within a system. As the microscopic relaxation time of molecules differs depending on the surrounding environment, the heating rate also differs, resulting in microheterogeneity of temperature. The energy of activations of a reaction in conventional and MW conditions have to be compared to test these hypotheses. It is well-known that dielectric constant influences reaction mechanisms.[536, 544] The approach of this work is to investigate the temperature dependence of the solvent dielectric properties in specific MW frequency.[533]

It is expected that in the normal liquid state, the kinetics of the reaction should follow Arrhenius type equation (*Equation 37*):

$$k = Ae^{-Ea/RT}$$

Equation 37

where *k* is the rate constant, *T* is the temperature in Kelvin scale, *A* is the pre-exponential factor and constant for each chemical reaction, R is the universal gas constant, and E_a is the reaction activation energy. This equation indicates that the rate of reaction constant depends on the frequency of those molecules which have enough energy to overcome an activation barrier ($e^{-Ea/RT}$) for transition state (TS) and on the pre-exponential factors A, which depends on the vibration kinetic frequency of the collisions of those molecules which have appropriate orientation in the transitional state. Here we have investigated a Menschutkin type reaction in which 1-bromohexane and trihexylamine are used as the reactant (*Equation 38*):

$$[CH_3(CH_2)_5]_3N + CH_3(CH_2)_5Br \rightarrow [CH_3(CH_2)_5]_4N^+Br^-$$

Equation 38

In this study, propylene carbonate was chosen as a solvent. The objective of this experiment was to understand how the effect of solvents dielectric property on Menschutkin reaction progression rate changes when the liquid system is subjected to MW radiation. The advantage of using microwave power for the activation and progression of organic reaction is already established due to the fact that the microwave heating is volumetric, rapid and controllable.

At present, the majority of research groups are very sceptical about the MW effect.[306, 484, 545] The energy of a microwave photon for 2.45 MHz is around 1 x 10-5 eV (1.602176565e-24 J). This value is significantly lower than any covalent (~5 eV) or even hydrogen bond ((~0.2 eV) energy and therefore it was stated in a number of publications that there is no possibility for MW influence on reaction energy activation. Currently, there are two explanations of the difference in reaction rates observed between conventional and microwave conditions. Some researchers believe that this difference is the result of a lack of correct temperature monitoring systems under MW reaction condition. Another explanation of the MW influence on reaction rate is based on the hypothesis of "molecular radiator".[241, 546] This hypothesis based on the assumption that MW heating could create micro-heterogeneous temperature distribution due to this heating is volumetrically interacting with individual molecules within a system. As the microscopic relaxation time of Molecules differs depending on the surrounding environment, the heating rate also differs resulting in temperature micro-heterogeneity.

3 Experimental

The sample selection, processing of the sample for experiment, experimental design, instrumental analytical tools and data analysis method of this PhD research work was performed according to the diagram shown in *Figure 52*.

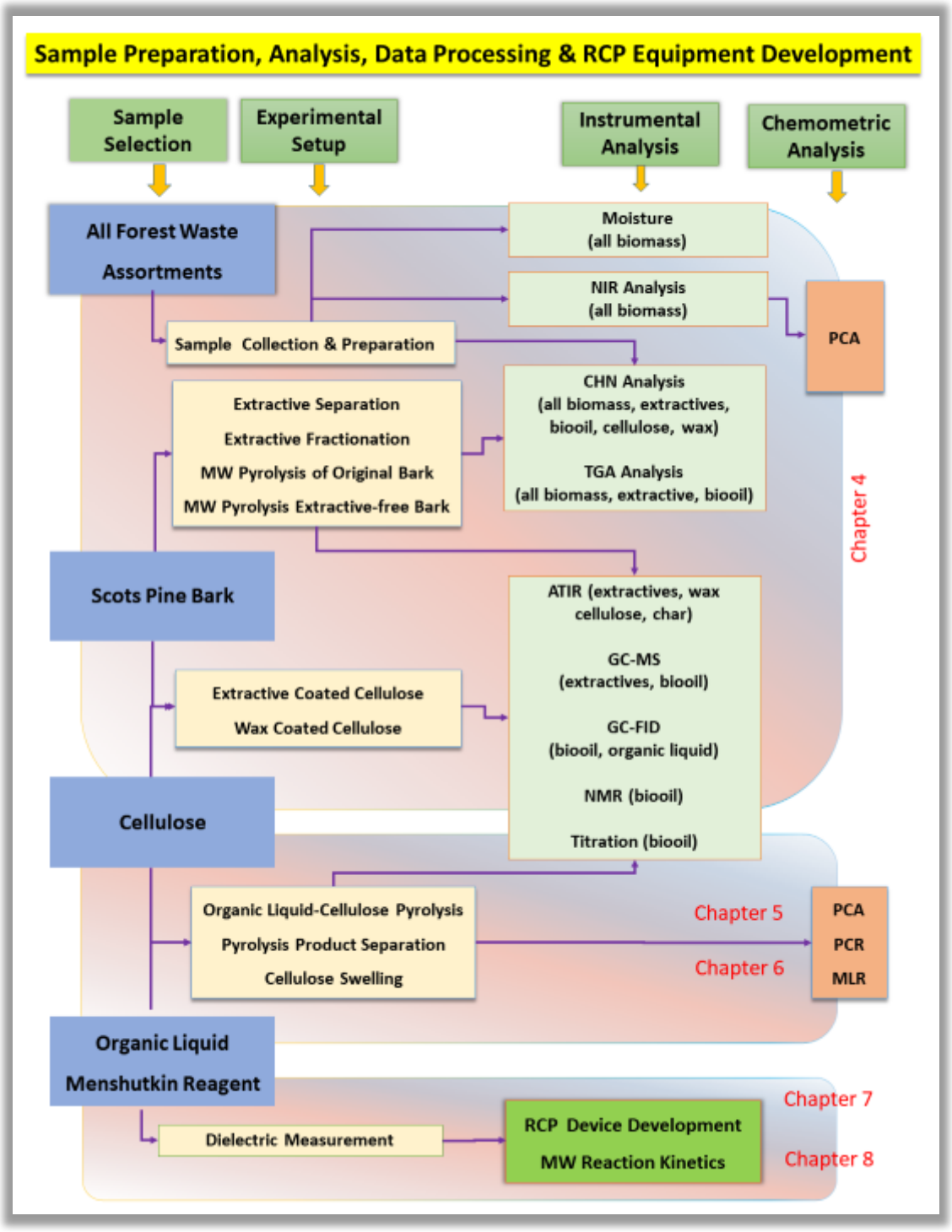

Figure 52 Sample preparation, Experimental design, Analysis methods and data processing tools used in the thesis.

As it is shown on the top of the flow diagram of *Figure 52*, there are four headings with a green coloured background. Under those heading the selection of samples for this thesis, the experimental procedures, the instrument typically used for analysing of samples and data analytical tools used for data processing is mentioned. The left-most headings present sample types under its row with a blue background. Those sample types are All forest waste assortment, Scots pine bark, Cellulose and organic liquids. Under the experimental setup section, all types' experimental work that was selected for this PhD is covered. Here it was also described what types of sample were selected for which purpose and how the sample was made ready for instrumental analysis. At the rightmost header, under the Chemometric analysis column, it was shown which analytical data will be processed due to the multivariate nature of the produced data. As it can be seen in the diagram, the forest waste samples will be screened with the near-infrared spectroscopic instrument and then the generated data will further proceed with PCA. It can also be seen that the whole diagram was divided into three shades at the background which is indicative of at which chapters the result of the experiment will be analysed and discussed. The analytical result of all biomass samples, Scots pine bark & its extractives and cellulose will be discussed in chapter 4 as indicated at thesis layout (section 1.12). In chapter 5 & 6, the microcrystalline cellulose and some organic liquid will be used as samples for experimentation and some of the data will be analysed with multivariate statistics such as Principle Component Analysis (PCA), Principal Component Regression (PCR) and Multi Linear Regression (MLR). In chapter-7, the same selected organic liquids that were used for chapter 5 & 6 will be examined for dielectric loss factor (Ɛ") analysis by using a custom made RCP device. Finally, the examination of Menshutkin reaction for dielectric reaction kinetics under microwave will be discussed at chapter-8.

This experimental chapter will be discussed in four sections below, according to the above title heading of sample selection, experimental setup, instrumental analysis and chemometric data analysis.

3.1 The source and Preparation of Forest Waste Assortment

As it was mentioned at thesis layout (section 1.1.2) that in this research work three specific cheap and quick growing conifers; Scots pine (*Pinus sylvestris*), Norway spruce (*Picea abies*) and Lodgepole pine (*Pinus contorta*) waste assortment were selected for systematic analysis. The steps for sample selection were as follow:

- Selection of sample location: Nearby Vindeln, 64^0 09′ N 19^0 40′ E, Sweden.

- Specification (age and stem diameter) of the samples (*Table 3*).
- Plant aged and growing conditions (One even aged stand/ tree species and one stand for heartwood stump).
- Selection of tree species (in the CETEX project it was limited to bark, needles and branches).
- For the Scots pine stump heartwood: only stumps above the ground level on a five-year-old clear-cut area were selected.

Table 3 Sample specification

Tree species	Tree age (annual rings at stump level)	Stem diameter (h=1.3 m)
Scots pine	147	269
Norway spruce	128	241
Lodgepole pine	31	128

The list of samples is shown in Table 4.

Table 4 Forest waste samples prepared for study in this PhD project.

Scots pine	Norway spruce	Lodgepole pine
Cone	Cone	Cone
Branches	Branches	Branches
Needle	Needle	Needle
Scots pine bark large diameter (LD*)	Bark	Bark
Scots pine bark small diameter (SD**)		
Scots pine stump		

*Scots pine wood was selected from large diameter wood log which was taken from 1.3 meters above the ground (25 years old tree). **The Scots pine small diameter bark was collected from same height but smaller diameter log (10 years old tree).

The sample collection and preparation was performed at the Biofuel Technology Centre (BTC) in Umea during my industrial placement (April-May 2015) at Sveriges Lantbruks Universitet (SLU), Sweden. The BDC is a research pilot plant for refining solid biomass and to serve as an educational resource. Dr Daniel Eriksson was my guide and trainer for the sample collection

and preparation. Sample preparation such fractionating, chipping and sieving using various chopper and grinder. At *Figure 53*, a chopper and grinder are shown which I have used to prepare the biomass assortments into 1 mm size. At Figure 54, it is shown some chopped Scots pine stems heartwood chips, Scots pine branches chips along with 1 mm sized Scots pine stump heartwood, Norway spruce bark, Scots pine branches and Scots pine needles into separate airtight bags.

Figure 53 some tools of biomass densifier. (From left Chopper and grinder).

Figure 54 Prepared Scots pine stump heartwood, Norway spruce bark, Scots pine branches and Scots pine needles (left to right).

3.2 Experimental Set UP

3.2.1 Separation of Extractives and Preparation of Extractive-free Scots Pine Bark

To remove extractive and to collect extractive free large-diameter Scots pine bark, a large scale experiment was performed. In a two-litre volumetric flask, 100 gram of sample was placed. Then one litter of MeOH (Fisher Scientific brand, analytical grade) is added into the flask. The

flask is then placed on to a hot plate with a cold water condenser fitted on the top. Then the hot plate temperature adjusted at MeOH boiling point while stirred the mixer with a magnetic stirring bar. After one hour, the heating was stopped and further cooled down for 30 minutes, then the liquid extractive containing mixer was decanted onto a sintered glass filter funnel (Fisher brand, pore size 3) using an air vacuum. The collected MeOH extractives solution was then rota-evaporated at 40 ℃ water bath to concentrate into about 75 ml solution. The recovered methanol is transferred into a 250 ml volumetric and kept in room temperature. On the remaining methanol-wetted residue, again one litter of MeOH is added and the previous cycle was performed to collect the extractive. After performing the third time extraction, all the extractive is combined and used further fractionation. The residue is then dried at 80 ℃ in an oven for two hours before store. The extractives of all three cycles of extraction are combined and used for the next experiment mention in the next section. The extractive-free reside were further used for microwave pyrolysis experiment.

The whole extraction experiment process was performed three times on another two other sets of 100 g large-diameter Scots pine bark. A mass balance analysis on extractive-free Scots pine bark residue was performed by averaging of the three separate sets of experiments.

3.2.2 Fractionation of Scots Pine Bark Extractive

The extractives of large-diameter Scots pine bark that were obtained in methanol following the procedure of the previous section, were settled in room temperature one hour. Then the solution was kept in the fridge for two days for separating out the extractive parts that were insoluble in methanol at low temperature. This kind of separation process is known as winterification process. Through decanting, the soluble part is further centrifuged to remove any insoluble extractive compounds. The MeOH soluble part is further concentrated via rota evaporation at about 40 ml by removing excess MeOH. Then the above-mentioned process of cooling down in the fridge for two days, centrifuge and separation is performed. The final remaining MeOH soluble extractive part is then subjected to rota evaporation to remove the solvent completely. This methanol soluble compounds of extractives are termed as FR-1 for the future experiment.

The collected methanol insoluble extractive compounds through decantation are then subjected to 40 ml of cyclohexane. Then kept into the fridge for two days. The cyclohexane soluble part is then centrifuged for 5 minutes before removing the cyclohexane soluble part through decantation. The cyclohexane part is then rota evaporated to remove all cyclohexane from the solution. The cyclohexene free extractive part is now termed as FR-2.

The final remaining, cyclohexene insoluble part after centrifuge is collected in the same way after rota evaporation is any existing cyclohexane solvent. This part of extractive is termed as FR-3. The whole separation process is shown in a schematic way in *Figure 55*.

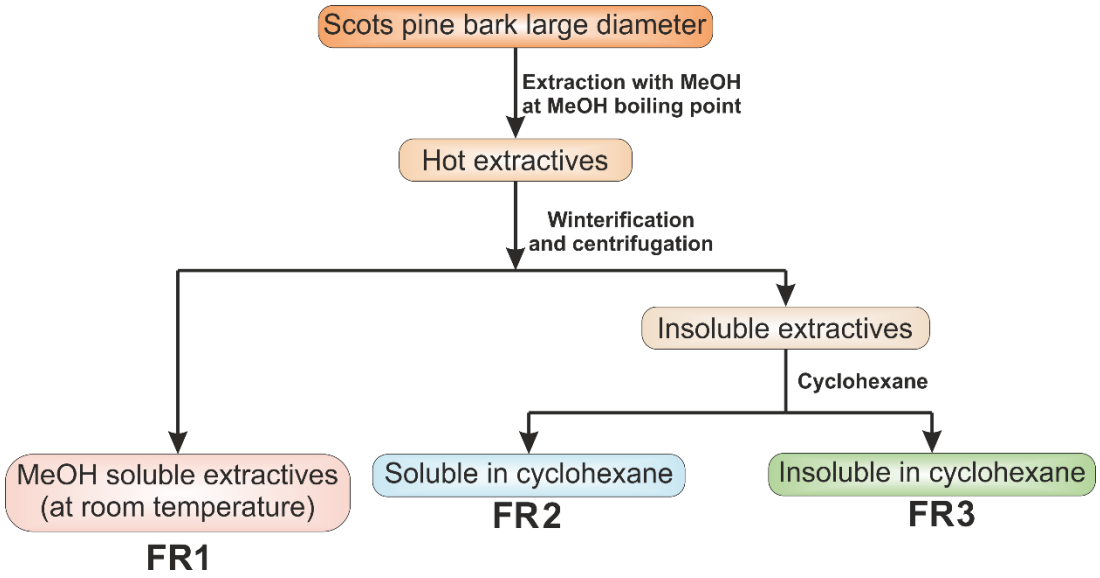

Figure 55 Scheme outlining the methodology used for the separation of Scots pine bark extractives.

To ensure complete removal of solvents from fractionated extractives compounds, all three FR1, FR2 and FR3 fractions were tested using ATR-IR, STA and GC-FID. The polarity based separated FR1, FR2 and FR3 compounds were then weighted for the record of mass balance and then kept in the freezer for storage before further experimental use (*Figure 56*).

Figure 56 MeOH extractive (FR1 (left), FR-2 (middle) and FR-3 (right).

3.2.2.1 Mass Balance of Extractives Yield

To compare the masses of FR1, FR2 and FR3 fractions separated in the way of section 3.2.2, another 10 gram of Sots pine large-diameter bark is subjected to soxhlet extraction method using the same MeOH solvent. It was found that in both ways collected total extractives are almost the same. For simplicity of mass balance calculation, the rest of the Scots pine assortments were also evaluated with mentioned soxhlet extraction method using MeOH as a

solvent. The percentage of extractive gained from large diameter scots pine bark was 14% calculated by using the following formula:

$$\text{Yield} = \frac{Mass\ of\ recovered\ bioil\ (g) - Mass\ of\ raw\ material(g)}{Mass\ of\ original\ large\ diameter\ Scots\ pine\ bark} \times 100\%$$

3.2.3 Microwave-assisted Pyrolysis of Original and Extractive-free Scots Pine Bark

A Microwave-assisted pyrolysis experiment was set up in two stages (see Figure 57) to compare optimum energy requirement for biooil yield from the original Scots pine bark and from extractive-free Scots pine bark residue (obtained in the way as described in section 3.21) using CEM discovery synthesizer. In the first stage, the bark sample was straightway used for MW pyrolysis without any treatment. In another set of experiments, the extractive-free bark residue was microwave-assisted pyrolysis in the same way as before. The original sample is referred to as Sample-A (and was used according to 'method-A') and residue of MeOH extraction is termed as Sample-B (used according to 'method-B').

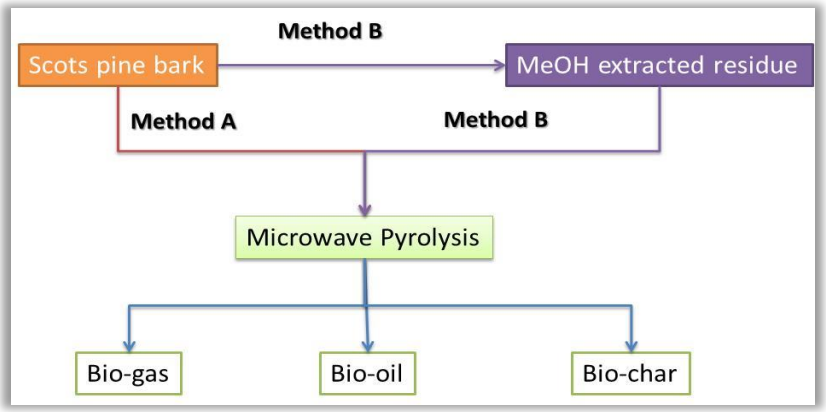

Figure 57 Scheme of MW experiments.

The experiment was set up in a fixed power mode of CEM discovery MW Synthesizer. Four different power conditions (150W, 200W, 250W and 300W) were applied to three grams of Scots pine bark (LD) samples. The sample size was selected as three-gram. The reaction vessel was a 35 ml Pyrex tube sealed with a cap of 300 bar pressure controlled mechanisms. After pyrolysis, the biooil was transferred into a small beaker and stirred at elevated temperature of around 30°C for about 4 minutes and then filtered through a sintered flask with ample of MeOH wash. The char and bio-oil were collected. Bio-oil was rota-evaporated and yield is measured. The char fraction was oven-dried for at least two hours at 75°C, weighted and kept for further analysis. The temperature kinetics, biooil, char and gas production yield was compared both method-A and method-B samples pyrolysis.

3.2.4 Microwave-assisted Pyrolysis of Extractive Fractions Coated Cellulose

In four, 10 ml microwave reaction vessels, one gram of microcrystalline cotton cellulose was mixed homogeneously with fifty milligrams of FR-1, FR-2, FR-3, All-FR (extractives that were not fractionated) along with one equally treated blank cellulose sample. The MW conditions were set up as 200W power, 180^{o}C temperature and a hold time of 1 minute following attainment of the maximum temperature. ATIR-FTIR spectra were recorded before and after MW pyrolysis and also following the removal of bio-oils. All sets of IR data were baseline corrected and normalized in the same way.

3.2.5 Microwave-assisted Pyrolysis of Wheat Straw Wax Coated Cellulose

3.2.5.1 Wheat straw wax

As an available and representative epicuticle plant wax, wheat straw was selected to coat the cellulose sample to carry on the MW pyrolysis process. The major components of the wheat straw wax and its physical properties were determined previously at the Green Chemistry Centre of Excellence in York and elsewhere.[547, 548]

3.2.5.2 Sample preparation for MW pyrolysis of cellulose

About four-gram of wheat straw wax was solubilized with 300 ml of EtOH in a 100 ml volumetric flask and was heated on a hot plate until the wax was dissolved completely. Then 100 gram of cotton microcrystalline cellulose (Sigma Aldrich) was added to the solution. The mixture was stirred and waited to mix until the solvent started boiling. Then the mixture was rota-evaporated and vacuum oven-dried overnight to remove the solvent completely. Another batch of 100 g of cellulose was treated as the same condition before but this time without adding any wax in it. For preparing the samples into 10 ml of MW reaction vessels, 1g of dry powdered cellulose or wax-coated cellulose sample were packed at the same density and volume by tapping the powder for squeezing into the same height by measuring with a scale (*Figure 58*).

Figure 58 measuring the height of wax-coated cellulose sample prepared for microwave-assisted pyrolysis.

3.2.5.3 Treatment of wheat straw wax in microwave power

A small chunk of solid wheat straw wax was MW pyrolysed (closed vessel, 150W power, maximum temperature 300 °C and total hold time of 3 minutes). The physical appearance was noted (*Figure 59*). The mass balance was also performed to evaluate the mass loss of the wax in the MW experimental condition.

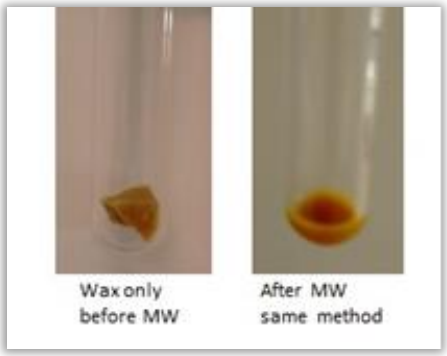

Figure 59 MW pyrolysis of pure wheat straw wax.

Only 0.1% of the mass was reduced after pyrolysis, as shown in *Table 5*.

Table 5: Mass balance calculation of MW pyrolysed wheat straw wax.

Mass before pyrolysis	Mass after pyrolysis	Loss of weight	% of weight lost	Mean	STD deviation
0.969	0.969	0	0.00		
1.104	1.105	-0.001	-0.09	0.0906	0.24
0.276	0.275	0.001	0.36		

The mass balance information indicates virtually no physicochemical changes happen to wax at experimental MW condition. This information will be used for the mass balance calculation of wax-coated cellulose pyrolysis at the same experimental limit.

3.2.6 Selection of Organic Liquid for Additive Coated Cellulose

3.2.6.1 Experimental design

As it was discussed in section 2.7 of the literature review (Chapter-2), fourteen physicochemical properties of organic liquids were chosen for investigating any direct influence of those properties on microwave-assisted pyrolysis of cellulose. Those selected fourteen physicochemical properties of organic liquids are boiling point, molecular weight, dipole moment, polarisability, dielectric constant, relative polarity, pK_a, viscosity, surface tension, density, enthalpy of evaporation, vapour pressure, thermal conductivity and specific heat capacity. The logic behind the selection of those physicochemical properties was grossly based on the fact that dielectric properties (dielectric constant and dielectric loss factor) of organic liquid is an established characteristic of microwave-induced heating factor. During the discussion in section 2.7 of the literature review, it was highlighted that some physicochemical properties such as dipole moment and polarizability are related to dielectric properties. Hence, those properties of organic liquid might influence the interaction of microwave with cellulose during its pyrolysis. In the same way, polarity and pKa may influence dipole moment or polarizability of organic liquid, which could, in turn, relate with dielectric constant. Using the same approach, a wave of relation could be established among density and dipole moment & polarisability or density and polarity and pKa as depicted in *Figure 60*. All of those properties may subsequently contribute to the dielectric constant and hence with microwave heating. Viscosity and surface tension also relates to density. The Boiling point and vapour pressure are also related to density. By using similar logic, some more physicochemical properties were thought to interconnect as shown in *Figure 60*. Now, at this stage an experiment deign is needed with which a minimum number of microwave-assisted additive-coated cellulose pyrolysis work could be perfumed to evaluate whether any or some of the relationship or all of the relationship in the network of *Figure 60* are proven to be true.

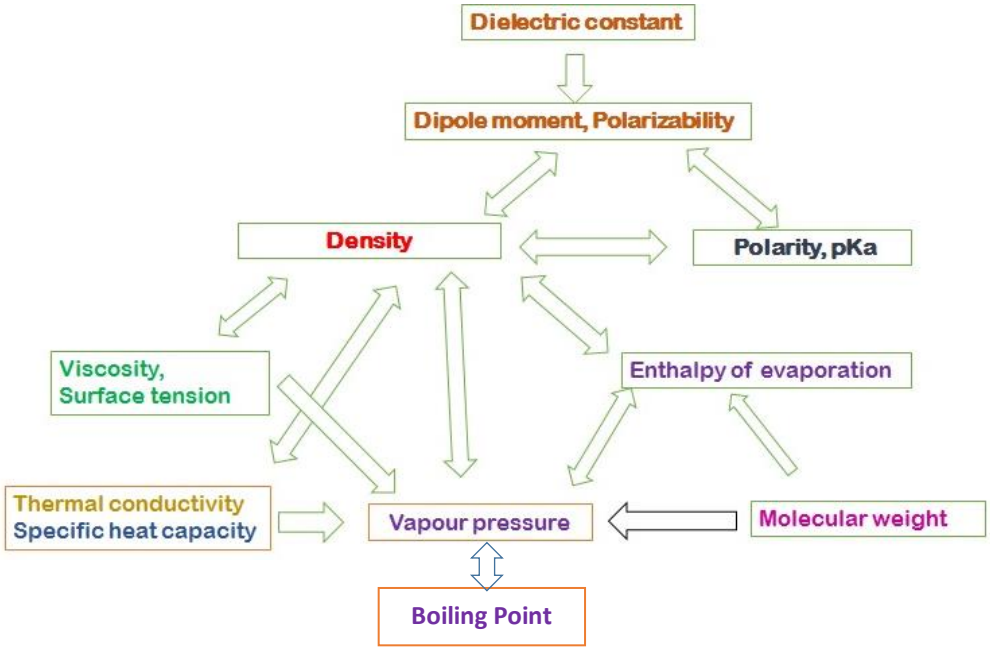

Figure 60 Interactive nature of chemical parameters based on MW influence.

The classes of additive that were selected for this experimental purpose were short-chained and long-chained alkane, terpenes, fatty acids, plant wax, aliphatic alcohol and water. The reason for choosing of those types of chemicals was purely based on some specific high or low physicochemical properties of chemicals than other class such as long-chained alkane are non-polar but has got high molecular weight and very low boiling point. If increasing the chain length of a nonpolar additive compound could enhance cellulose pyrolysis, it could then arrive into the decision that those boiling point, molecular weight are the influential factors for microwave-assisted cellulose pyrolysis. If the microwave-assisted pyrolysis of long-chained alkane coated cellulose on the other hand reduced, then those properties could be thought as the negative influential factor. Terpenes such as isoprene are highly volatile or high vapour pressure creating compound. If microwave-assisted pyrolysis of isoprene coated cellulose is enhanced or reduced then using previous logic positive or negative influential factors of vapour pressure or boiling point could be decided. Fatty acids can represent pKa or polarity. The surface tension and specific heat capacity of water are considerably high, so testing influence water can indicate an influence of those properties on microwave-assisted pyrolysis. Plant wax is highly viscous containing high molecular weight or less thermally conductive. The polarizability, relative polarity or dipole moment of aliphatic alcohol could be changed by the chain length of any alcohol class. At *Table 6* some organic compounds and water were chosen according to the mentioned additive class. All of the compounds could be found in various types of biomass extractive. A water-free oven-dried microcrystalline cellulose (48h on 135°C)

will be used as a blank standard for the list of additive. So the additives selected in *Table 6*, is thought to be an ideal minimum compound for the experimental design for testing actives influence on cellulose pyrolysis.

Table 6 A list of organic liquid was chosen as 10% additive of cellulose for microwave-assisted pyrolysis.

10% additive	
Abietic acids	No additive
Tetradecane	Docosane
Water	Pinene
Linolieic acid	Hentriacontane
Isoprene	Glycerol
Wheat straw wax	1,3-propanediol

Two empirical pieces of evidence were used to calculate the MW pyrolysis process of cellulose in the presence of solvent: the first one is solid residue yield, and another is biooil composition. In this experimental part of the job, attention was also paid to compare the MW and classical (STA) pyrolysis of those additive coated cellulose.

After completing the experiment and analysis of the result, then another set of experiments would be performed. At the second stage of the experiment, by using the experimental evidence of solid residual yield, the chosen additive parameters influence on MW pyrolysis will be evaluated with Chemometric methods such as PCA and PCR. The applied chemometric approach will also be compared with any relevant existing information. The list of the parameters which influence the MW pyrolysis will be generated. The experimental condition and additive parameter selection will be discussed in section 3.4 of this experimental chapter.

3.2.6.2 Sample preparation for MW pyrolysis of cellulose

About one gram of cotton microcrystalline cellulose (Sigma-Aldrich) was prepared by oven-dried at 48h on 135℃. About 4.5 % of the water was removed. The oven-dried cellulose samples were used for all MW experiments. About one gram of dried samples was packed inside of the 10 ml MW reaction vessel in the same way as the experimental section of 3.2.5.2 of this chapter. Then the pipetted 10% liquid additive was straightway injected into the cellulose power inside the reaction vessel and mixed before MW pyrolysis. If the additive is solid then, the cellulose and additive were mixed homogeneously outside of the reaction vessel. No solvent was used to mix the additives. The pyrolysis of the samples was performed in a closed vessel at CEM discovery. The pyrolysis condition was: 150W fixed power, 3 minutes

hold time in a closed vessel. After MW pyrolysis, the samples were washed with EtOH to collect the biooil. The biooil were then concentrated by rota-evaporation and then diluted with EtOH to reach at 15 ml in a 400 ml glass vial to make the equal volume for all of the cases of pyrolysed biooil samples before GCFID, GCMS analysis.

3.2.7 Selected Solvent Criteria for Determining the Influence on Cellulose Pyrolysis

It was highlighted in the literature review (section 2.8 of Chapter-2) that solvation parameters are the important controlling factor of final dielectric constant and loss factor value during microwave irradiation on the macroscopic bulk solution. To evaluate the potential solvation parameters that could contribute to any quantifiable influence on cellulose pyrolysis in the presence of organic liquids, the following solvent selection criteria for experimental setup was decided.

The selection of organic liquid was based on ten subclasses of COSMO-RS model. The initial target is to experiment using five liquids from each of COSMO-RS subgroup, but five solvents were not appropriate (group one and group six) due to health & safety reasons, or else enough compound was not available in the collection. In some cases, it was also not possible to find a solvent in a subclass that has a high enough boiling point (e.g., water in group 10). The total number of liquids in this initial screening was 33. The samples' boiling point and the experimental identification numbers are presented below for each subclass, along with the corresponding chemical structure.

1	**Strong electron pair donor base** (tri-substituted aliphatic amines)

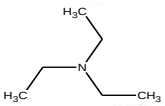

Triethylamine

Compound identity 1A, boiling point 89.5°C

2	**Weak electron pair donor base** (pyridines, primary and secondary amines)

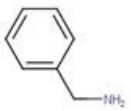

Benzylamine
2A, 185 °C

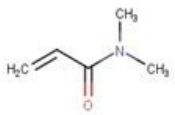

N,N-Dimethylacrylamide
2B, 202 °C

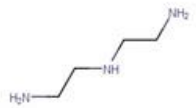

Diethylenetriamine
2C, 200 °C

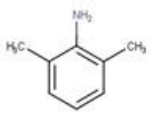

2,6-dimethylaniline
2D, 216 °C

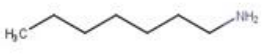

n-Helptylamine
2E, 154 °C

3	**Aprotic dipolar** (most of ethers, esters, ketones and nitriles. It gathers the aprotic polar solvents, ranging from moderate to weak HBA. Possess an oxygen or nitrogen atom, exhibiting a lone pair of electron less available compared to the nitrogen's of Clusters I and II but still determinant.)

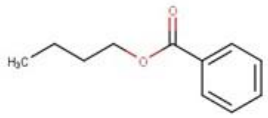

Butyl benzoate
3A, 250 °C

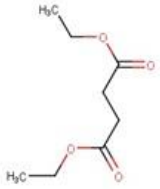

Diethyl succinate
3B, 217 °C

Cinnamyl acetate
3C,265 °C

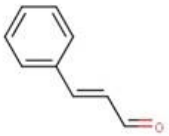

Cinnamaldehyde
3D, 248 °C

Tetraethylene glycol dimethyl ether
3E, 275 °C

4	**Aprotic highly dipolar** (differ from the solvents of cluster III by a smaller hydrocarbon part and their dipolar character is more pronounced compared to similar solvents with longer hydrocarbon chain)

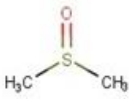

dimethyl sulfoxide
4A, 189 °C

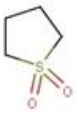

Sulfolane
4B, 285 °C

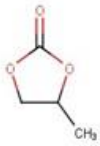

propylene carbonate
4C, °C

5	**Apolar** (such as carbon disulfide, the aliphatic and aromatic hydrocarbons and some halogenated hydrocarbons (chlorobenzene, and m-dichlorobenzene). Their σ profiles, centred close to 0 are typical of that of apolar solvents.

Cyclohexane
5A 80.7 °C

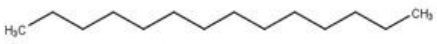

Tetradecane
5B, 252 °C

6	**Asymmetric halogenated hydrocarbons** This group contains aromatic halogenated hydrocarbons (bromobenzene and fluorobenzene) and polyhalogenated aliphatic hydrocarbons.

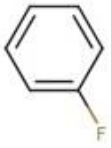

Fluorobenzene
6A, 84 °C

7	**Amphiprotic** This cluster contains essentially aliphatic alcohols.

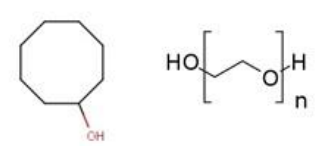

Cyclooctanol
7A, 244.2 °C

PEG 400
7B

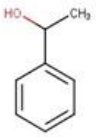

1-phenylethanol
7C, 204 °C

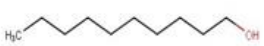

1-Decanol
7D, 230 °C

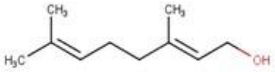

Geraniol
7E, 259.2 °C

8	**Polar protic** This group contains some small alcohols (such as methanol), polyols and N-mono-substituted amides.

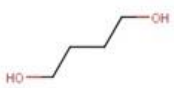

1,4-Butanediol
8A, 228 °C

1,3-Propanediol
8B,214 °C

9	**Organic acidic compounds** (highly hydrogen bond donor solvents, such as aromatic and fluorinated alcohols and acids, are found in group)

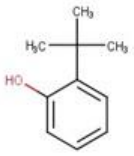

2-tert-Butylphenol
9A, 223 °C

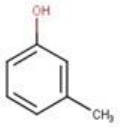

m-cresol
9B, 202.8 °C

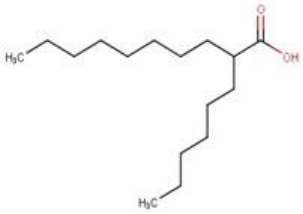

2-Hexyldecanoic acid
9C, 268 °C

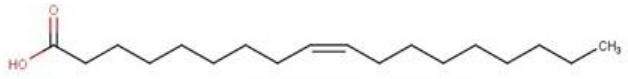

Oleic acid (9D, 360 °C)

10	**Polar structured** (this cluster contains highly structured solvents such as ethylene glycol, formamide or water)

Acetic acid
10A, 117 °C

Water
10B, 100 °C

Ethylene glycol
10C, 196 °C

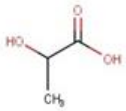

Lactic acid
10D, 122 °C

3.2.7.1 Sample preparation for MW pyrolysis of cellulose

About one gram of cotton microcrystalline cellulose (Sigma-Aldrich) was prepared by oven-drying at 48h on 135°C. About 4.5 % water was removed. The oven-dried cellulose samples were used for all MW experiments. About one gram of dried samples was mixed with 3 ml of solvent packed inside a 10 ml MW reaction vessel before MW pyrolysis. The MW pyrolysis was performed with CEM Discovery with 250 psi pressure in a closed vessel with fixed power of 275W. After pyrolysis, the biooil was removed with acetone, and the remaining residue was dried overnight at an oven set at 85 °C. The mass balance was then performed.

3.2.7.2 Pyrolysed bio-oil Separation

The MW pyrolysed biooil was transferred into a small beaker and stir at elevated temperature of around 30C for 4 minutes and filtered through sintered flask with ample of MeOH wash. The char and bio-oil were collected. Bio-oil was rota-evaporated and yield is measured. The char fraction was oven-dried for at least two hours at 75C, weighted and kept for further analysis.

3.2.8 Cellulose Swelling Measuring Procedure

In 40 ml of vials, 1 gram of microcrystalline cellulose was mixed with 10 ml of organic liquid. The mixture is then shaken for 40 hours and allowed for 16 hours to settle. After settling, the height of cellulose in the liquid was measured using a measuring scale and camera. The camera image was later zoomed in to determine the measurement as accurately as possible. The accuracy was half of a millimetre. Then those were shaken for 40 hours and then settled for 40 hours. Those were then centrifuged for 20 minutes at 2000 rpm. The measurement was taken again at this stage. The difference was converted into a percentage scale by taking the initial height of 1-phenyl ethanol containing cellulose height as the original height of all samples (*Figure 61*). At *Figure 62*, the scaling of measuring the height and volume of the sample is shown. It was done by measuring the volume of water in the bottle converted from the height.

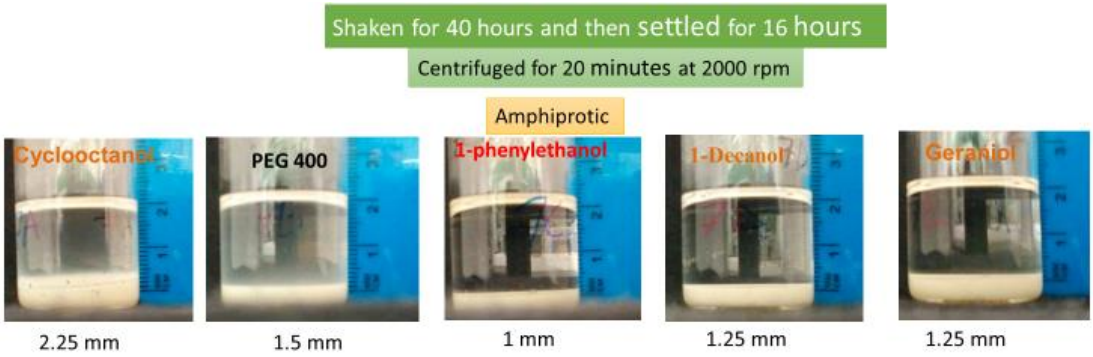

Figure 61 swelled cellulose -solvent for Amphiprotic solvent

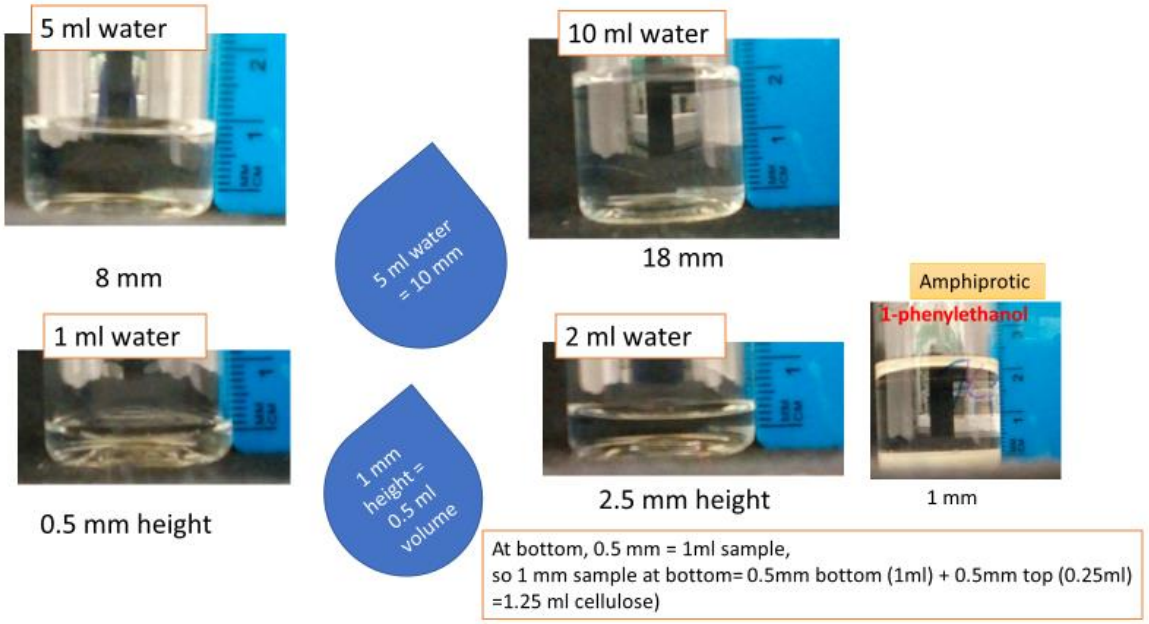

Figure 62 The measurement approach of the volume of swelling by calibrating with water height in the bottle.

3.2.9 Dielectric Constant and Loss Factor Measurement

As for determining dielectric constant and loss factor of organic liquids, new instrument setting was performed, rather than using any standard analytical instrument, a detailed instrumental setup, sample selection, calibration work and automation process will be discussed separately at Chapter 7. The development of an automated complex dielectric measuring instrument was developed at the Department of Electronics Engineering, University of York. Dr Martin Robinson and Dr Iain Will of Electromagnetic Communication Group of York actively supported of this PhD project in terms of technical work and advice on the development of resonant cavity perturbation device. Mr Charan Panesar of Electronics Department, Abigail Mortimer, Mark Roper, Stuart Murray and Timothy Ayres of Department of Chemistry of the University of York directly contributed in the form of technical work and advice. Dr Alice Fan has contributed one thousand pounds of financial support on this project. Dr Miguel D Ruiz-Cabello of Electromagnetismo y Física de la Materia, Universidad de Granada helped to develop a python-based program to run RCP device.

3.2.10 MW Reaction Kinetics (Experimental Method of Menshutkin reaction)

Chemicals: Propylene Carbonate, 99.50%, 1-Bromohexane 98%, Trihexyl amine 96%, Tetrahexylammonium bromide 99%. Propylene Carbonate is obtained from Sigma Aldrich as a 2.5L bottle, and the rest of the chemicals are sourced from Across Organics. All the chemicals are used as received.

Instruments: Conductivity was measured with a Jenway 4510 conductivity meter. Microwave synthesis was performed in CEM Discovery in a 35ml reactor. The instrumental setting is performed as shown in (Figure 63).

Figure 63 Experimental setup.

Reaction mixture: 0.1N of 1-Bromohexane and 0.1N of Trihexylamine was made into 10ml volume separately in a 45ml vial and heated up in a heating block at the relevant temperature until the temperature is stable. Then both reactants mixed and stirred for conventional synthesis.

Calibration of conductivity: a set of a calibration standard with tetrahexylammonium bromide salt in propylene carbonate was made. The conductance of that standard was made at various temperatures. The concentration versus conductance in μS/cm shows that the slope of the conductance at a different temperature is almost the same (Figure 64).

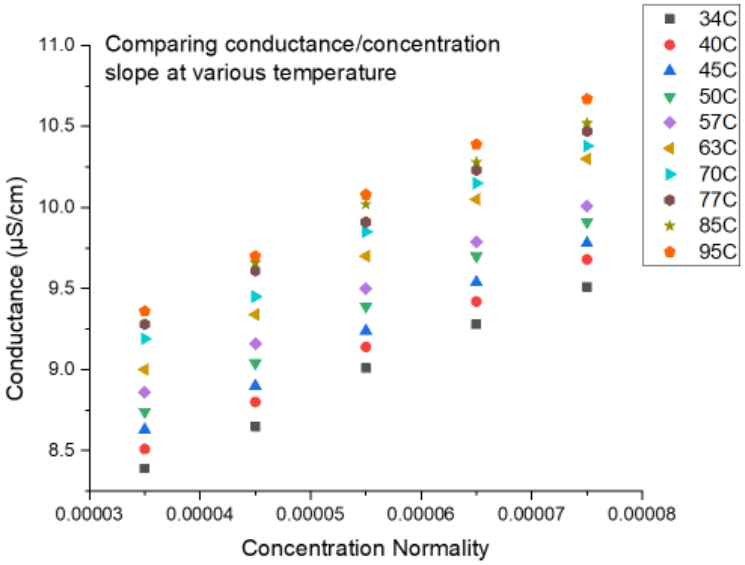

Figure 64 Comparison of conductance vs concentration slope at various temperature.

As, the conductance/concentration in all temperature is the same, for monitoring the reaction rate of all the experiments was used with the calibration of Concentration/Conductance at 12 °C (Figure 65).

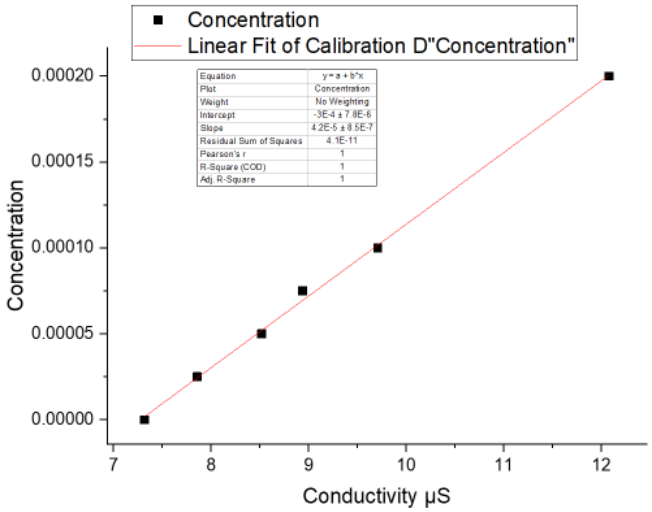

Figure 65 Calibration of Tetrahexylammonium bromide salt at 12°C

3.3 Instrumental Analysis

3.3.1 Moisture Content

Around ten grams of all biomass samples were oven-dried for 48 hours at 30 ℃ in an oven at 10% fan speed in the drying suit at SLU, Sweden. For another set of experiment, the same amount of biomass samples were oven-dried at105 ℃ for 18 hours. All sample mass loss measurements were conducted in triplicate. The calculated results are shown in Chapter 4.

3.3.2 NIR Analysis of Biomass

At the Umea University of Sweden, I was trained to use Foss 6500 by Dr Daniel Ericson of SLU, Sweden. The instrument specifications are fibre optic probe 400-2500 nm, tungsten halogen lamp and rotating measuring cell for reflection/transflection 400-2500 nm. About 3 to 4 gram of original biomass samples were placed in the sample cup without any pre-processing. Then raw NIR data spectral data of all assorted forestry waste were recorded in FOSS NIRS Spectroscopic instrument (Figure 67).

Figure 66 FOSS NIR Spectrometer 6500. The Spectra range is 400-2500 nm.

At *Figure 67* the raw recorded data of all forest waste assortment is shown.

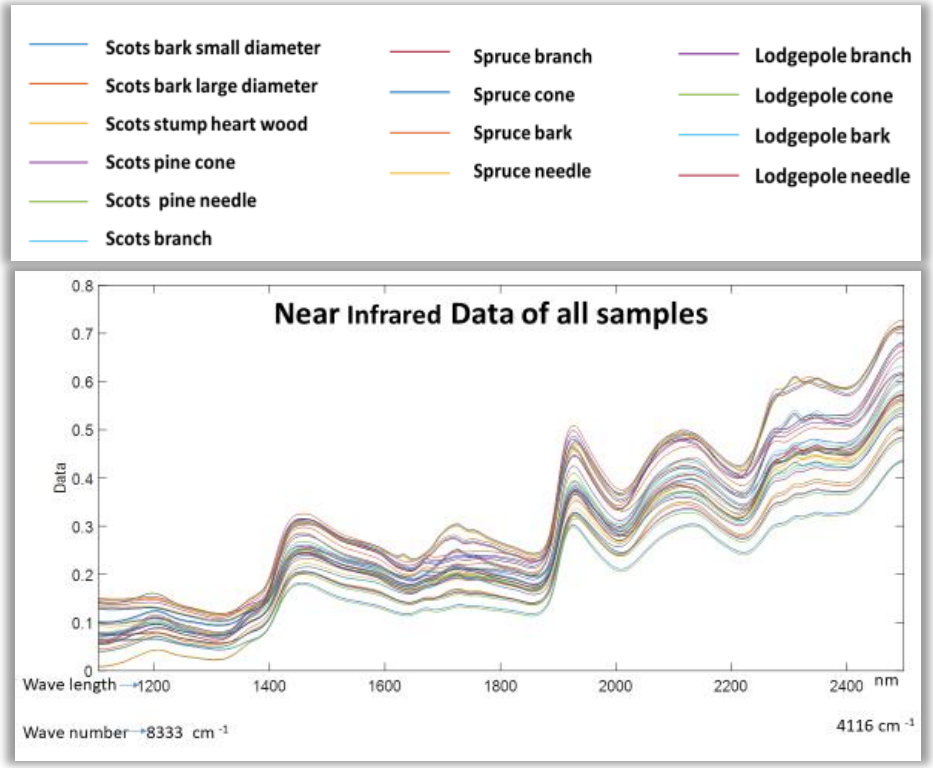

Figure 67 NIR data of all wood assortments.

A post-graduate multivariate data analysis course completed at SLU, Sweden conducted by Professor Paul Giladi. Professor Paul Giladi and Dr Daniel Ericson trained me on associated software and data processing technique that was appropriate for this purpose. The data were analysed with Umetrics and the PLS toolbox of Matlab. The after pre-processing the data, A PCA was performed for further analysis. The work is further discussed at chemometric analysis section.

3.3.3 Elemental microanalysis (CHN)

The Carbon, Hydrogen & Nitrogen (CHN) content of all original biomass samples were determined using an Exeter Analytical Inc. CE-440 analyser. The samples were run by Dr Graeme McAllister of the chemistry department. The oxygen contents of all original biomass were calculated by difference according to the following equation:

$$\text{Percentage of oxygen} = 100\ \% - (\text{C}\ (\%) + H\ (\%) + N\ (\%))$$

CHN analysis of all original biomass, some selected extractives, biooil and cellulose were performed. Ash content data was taken from an earlier report of Stanley E. Corder.[549] Oxygen content was calculated as (100-(CHN+ash).

3.3.4 Thermogravimetric Analysis (TGA)

Thermogravimetric analysis (TGA) of all original biomass, some selected extractives, biooil, cellulose and waxes were performed on Netzsch STA 409 instrument. The scan rate was 10 °C min-1. The sample mass was around 10-12 mg. Nitrogen gas flow was used at a rate of 100 mL min^{-1} and subsequently air at 100 mL min^{-1}.

TGA analysis was performed on all original forest waste biomass samples, on some extractives and biooil. The details associated analysis was described in Chapter-4.

3.3.5 ATIR Analysis

A Bruker Vertex 70 FT-IR/ATR was used to measure attenuated total reflection infrared (ATR-IR) of extractive, cellulose, biooil and char residue. The background and sample were scanned for 64 times for an average reading.

The extractives, microcrystalline cellulose, wheat straw wax, conventionally pyrolysed of cellulose char, microwave-assisted pyrolysed wax-coated cellulose char and additive coated cellulose pyrolysis char were analysed for ATIR.

3.3.6 GCMS Analysis

Perkin Elmer Clarus 500 GC was used for GCMS analysis. The mass detector was a Clarus 500 quadrupole mass spectrometer with electron ionisation mode (EI) at 70 eV. The column was DB5HT capillary column (30 m x 250 µm x 0.25 µm nominal). The column pressure was 22.35 psi with a helium carrier gas. The rest of the parameter was adjusted to have the same eluent time as GC-FID. The mass data were analysed with TurboMass (Ver5.4.2) chemical software and accompanied the NIST library (v.2.2). The internal standards were used for dominant peak identification.

GCMS analysis was performed for large-diameter Scots pine extractives, all additives and biooil obtained from additive coated cellulose pyrolysis. Samples were prepared at a concentration of 10-20 mg/mL in the appropriate solvent. All GC-MS analysis results were discussed in chapter-4.

3.3.7 GC-FID

An Agilent Technologies 6890N Network GC system was used to analyse the GC-FID of extractives and biooil samples. The column used for the purpose was a ZB-5HT capillary column with a dimension of 30m x 250 µm x 0.25 µm. The samples were injected by automated injection (1 µl injection volume) with a split ratio of 30:1 with 81.5 ml/min sample speed. The pressure was

25psi with 86.3 ml/min helium gas flow. The heater temperature was 300℃. The column gas setting was 25 psi with a flow of 2.7ml/minute. The oven ramp was such: The initial oven setpoint 50℃, hold time zero minute, The temperature ramp was 30℃/minute, until 300 ℃. Then hold time for 5 minutes. Total run time was 13.33 minutes. The flame ionisation (FID) heater setpoint was 340 ℃ with H_2 gas flow of 35ml/minute and airflow of 350 ml/minute. Standard of Levoglucosan, levoglucosenone, HMF was run. Qualitative detection of wax was performed with an internal standard. Palmitic acid stearyl ester, stigmasterol, octadecanoic acid, linoleic acid, and hentriacontane were used as standards. Samples were prepared at a concentration of 10-20 mg/mL in the appropriate solvent.

GC-FID analysis was performed on for extractives and biooil obtained from additive coated cellulose pyrolysis, on all additives. All GC-FID analysis results were discussed in chapter-4.

3.3.8 NMR

Proton NMR data were obtained on a JNM-ECS 400 departmental NMR instrument. It was operated at 100 MHz and 25 ℃ in deuterated chloroform ($CDCl_3$).

NMR operation was performed on biooil obtained from scots pine large-diameter bark samples. The discussion of analysis will be found on chapter-4.

3.3.9 Karl Fisher titration

1.1.1 Karl Fisher titration of biooil was conducted using a 907 Titrando unit (Metrohm) with Hydranal Composite 5K and Hydranal KetoSolver as the titrant and working medium respectively. All experiments involved a polarising current of 50 μA, stop voltage of 250 mV and a drift end-point criterion (20 μL min^{-1}) (*Figure 68*). The water content of biooil obtained from microcrystalline cellulose pyrolysis was determined by Karl-Fisher method in chapter-4 at the section of MW pyrolysis of cellulose under the influence of selected additives.

Figure 68 Karl Fisher titration unit of Metrohm

3.4 Chemometric Analysis: PCA, PCR and MLR

The PCA, PCR and MLR were performed using commercial software Unscrambler X 10.5.1 software. The raw sample matrix set was first transformed via mean cantered and scaling with standard deviation. Then it was selected to identify any outlier in the data. Then a data matrix was cross-validated with small data set from the sample matrix itself. The algorithm used for PCA analysis was the single value decomposition (SVD). Then finally a PCA, PCR and MLR over can be plotted to understand any underlying relation among variables. A details explanation of the practical working principle of PCA, PCR and PLS will be discussed in respective result and discussion chapters.

The PCA was performed on NIR data. On additive coated cellulose pyrolysis data both PCA and PCR operation was performed. To discuss solvent cellulose interaction, MLR regression was conducted between the swelling value of cellulose in solvents and the solvents Abraham solvation descriptors. PCA, MLR and cluster analysis was performed on microwave-induced cellulose pyrolysis in the presence of solvents and Abraham solvation descriptors.

4 INFLUENCE OF EXTRACTIVE COMPOUNDS ON MICROWAVE PYROLYSIS OF ASSORTED FORESTRY WASTE AND CELLULOSE

4.1 Characterisation of Extractives

4.1.1 Determination of Moisture Content

The moisture content of the selected biomass was determined by calculating the mass loss upon drying of the biomass under different conditions (varying temperature and time). In the standard way (A5TM D 2974-87), it is preferred to dry any materials at 105℃ in a certain period to remove any water content.[550] However, to avoid extractive losses from biomass, chemist prefers to measure moisture content by drying at 30℃ for longer period of time (48h is used in this case).[551]

In brief, around ten grams of all biomass samples were oven-dried for 48 hours at 30 ℃ and 105 ℃ for 18 hours. All sample mass loss measurements were conducted in triplicate. The calculated results are shown in Table 7. It can be clearly seen that the 105 ℃ oven-dried samples lost almost twice the mass when compared to drying at the milder 35 ℃ for 48h.

Table 7 *Mass loss obtained in two different temperatures and periods of forest waste assortments.*

Wood parts	Species	105°C, 18h	30°C, 48h
Cones	Scots pine	4.18	1.31
	Norway spruce	5.42	2.10
	Lodgepole pine	4.30	1.42
Branches	Scots pine	3.49	1.55
	Norway spruce	4.42	2.93
	Lodgepole pine	3.81	1.66
Needles	Scots pine	3.75	1.41
	Norway spruce	3.72	1.68
	Lodgepole pine	3.52	1.69
Bark	Scots pine large diameter	4.13	1.89
	Scots pine small diameter	4.01	1.36
	Norway spruce	4.65	1.67
	Lodgepole pine	6.26	2.18
Heartwood stump	Scots pine	4.49	3.45

As it is seen in the above table, the two separate methods the loss of mass is substantially different. The 105 ℃ method provides two-time mass loss than the 30 ℃ methods of moisture analysis. The problem of getting two different mass of moisture is understandable, because at high temperature, along with water the low volatile extractive also evaporate. Even at the low-temperature method such as 30 ℃ cannot be entirely reliable due to evaporation of extractive when exposed outside at more extended periods above room temperature.

4.1.2 CHN Analysis

The Carbon, Hydrogen & Nitrogen (CHN) content of all original biomass samples were determined using an Exeter Analytical Inc. CE-440 analyser. The results are given in *Table 8*.

Table 8 CHN measurement of all forest waste assortments.

Sample ID	Element (wt%)		
	C	H	N
Scots cone	**47.0**	**6.2**	**0.2**
Spruce cone	**48.3**	**6.0**	**0.2**
Lodgepole cone	**47.4**	**5.8**	**0.1**
Scots branch	**49.4**	**6.4**	**0.4**
Spruce branch	**49.0**	**6.0**	**0.3**
Lodgepole branch	**48.5**	**6.3**	**0.1**
Scots pine Needle	**50.9**	**6.8**	**1.1**
Spruce needle	**48.8**	**6.1**	**1.0**
Lodgepole needle	**49.7**	**6.3**	**1.0**
Scots bark LD	**50.3**	**5.8**	**0.1**
Scots bark SD	**47.1**	**6.1**	**0.5**
Spruce bark	**47.7**	**5.7**	**0.2**
Lodgepole bark	**51.7**	**6.7**	**0.3**
Scots Stump	**50.6**	**6.4**	**0.0**

The CHN data analysis highlights that carbon and hydrogen contents are independent of the nature of the wood assortments. The carbon content changes from 47 (cone) to 51.7 (bark) wt%. The hydrogen content changes from 5.7 (Spruce bark) to 6.8wt% (Scots pine Needle). Nitrogen content is found to be varied. According to the literature, the nitrogen content is linked

to the presence of free amino acids, chlorophyll and proteins.[55] Therefore, a high concentration of nitrogen in needles could be associated with chlorophyll.

4.1.3 Extractive Content of Scots Pine Assortment

The Soxhlet method was employed to calculate the extractive content of all Scots pine assortment with methanol being used as a solvent. The relevant results are displayed in Table 9 and highlight the fact that Scots pine needle contains very high amounts of extractives while Scots pine cone contains the least amount of extractives.

Table 9 Extractive content of Scots pine assortments.

Scots pine assortment	Experimental extractives content
Scots pine needle	36.5%
Scots pine stump	17.3%
Scots pine bark SD	18.6%
Scots branches	18.7%
Scots cone	9.7%
Scots pine bark LD	16.6%

4.2 Development of a Thermogravimetric Method to Determine Extractive and Moisture Content of Lignocellulose

As lignocellulosic biorefinery feedstock contains many low volatile extractives such as terpenes and pinenes with boiling points close to 100 °C, an efficient and simple methodology has to be applied to effectively separate the water and extractives that are naturally present in the biomass mentioned above. Therefore, during this PhD project work, two independent methods of the extractives estimation based on (i) TGA and (ii) NIR were developed.

Using a Netzsch STA 409 Simultaneous Thermal Analyser, samples were subjected to thermogravimetric analysis (TGA) conducted in a flow of gaseous nitrogen at up to 600 °C. The differential of mass change over time (mass%/minutes) is then plotted against temperature using OriginPro 2018 software.

In all of the available literature regarding lignocellulosic biomass characterisation, for virtually all cases, the TGA/temperature curve area was deconvoluted only into three major wood components (cellulose, hemicellulose and lignin).[83, 374, 552-562] This simplistic treatment results in does not recognise the impact of extractives on such experiments. But as it was shown in

previous experimental data (section 2.2.4) and literature review, extractive content of wood assortment could be as high as 40% (Scots pine needle extractives).[563-565] For this reason, the literature based on thermogravimetric analysis of wood components could be substantially incorrect. In light of this, a new lignocellulosic biomass DTA/temperature curve analysis was developed in order to improve the existing deficiencies concerning the thermogravimetric analysis of lignocellulose.

This novel method will be illustrated using the example of TGA of the large diameter Scots pine bark. The bark was extracted using boiled methanol and the resulting extracts subsequently analysed with DTG (Figure 69). The DTG/temp of extractives has three major peaks around 90 ℃, 250 ℃ and 420 ℃ (peak 1, 2 & 3).

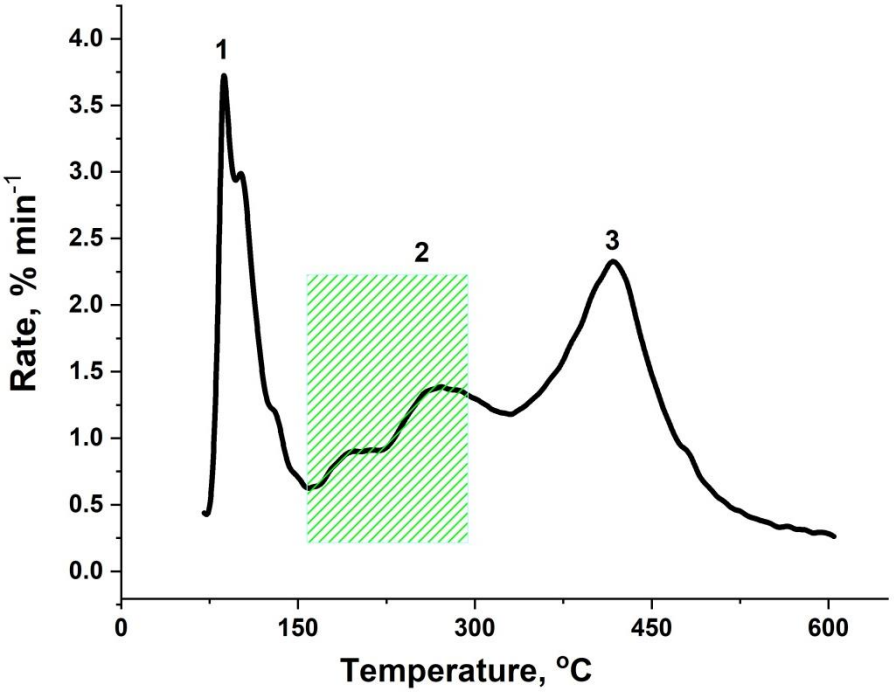

Figure 69 DTG/temp peak deconvolution of Scots pine large-diameter barks methanol extracts.

An example of DTG/temp peak deconvolution for Scott pine bark is shown in Figure 70. The comparison of these peaks with the DTG peaks of the extractives shows that two peaks Figure 70B & Figure 71. As you can see from these figures the peaks of extractive components may co-evolved with the peaks of water (100 ℃), hemicellulose (270 ℃) and lignin (250-450 ℃) and therefore, the contribution of extractives has to be taken into account during the TG analysis of biomass for optimum prediction of major wood components and water content.

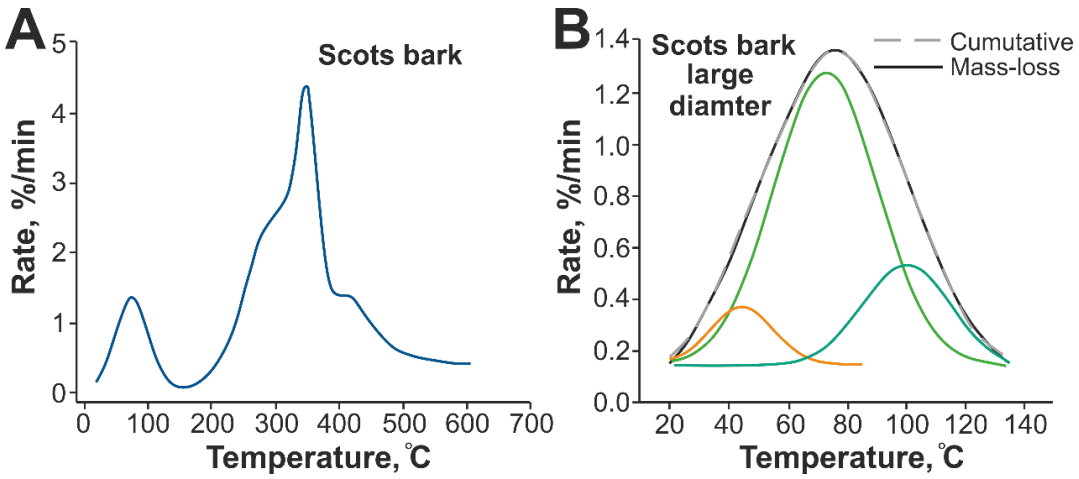

Figure 70 A. DTG/temp (0℃ -600℃), B. DTG/temp from room temp to the first maximum in the DTG curve

Using the STA data of extractives, the improved analysis of STA of the Scots pine bark (LD) was carried out. The low-temperature DTG/temp area is modelled to deconvolute into three peaks taking the maximum water content at 100 C, and two other peaks Figure 70 B at 50 ℃ and 80 ℃ are related to the extractives. The DTG/temp curve after *ca*. 200 ℃ was deconvoluted into seven individual peaks. The peaks around 260 ℃, 367 ℃ and 410 ℃ are assigned explicitly to hemicellulose, microcrystalline cellulose and lignin respectively (peak 2, 5 & 6 in Figure 71). The leftmost (peak-1) and rightmost (peak-7) peaks are assigned as extractives to enable comparison with the major extractive peaks highlighted in Figure 71)

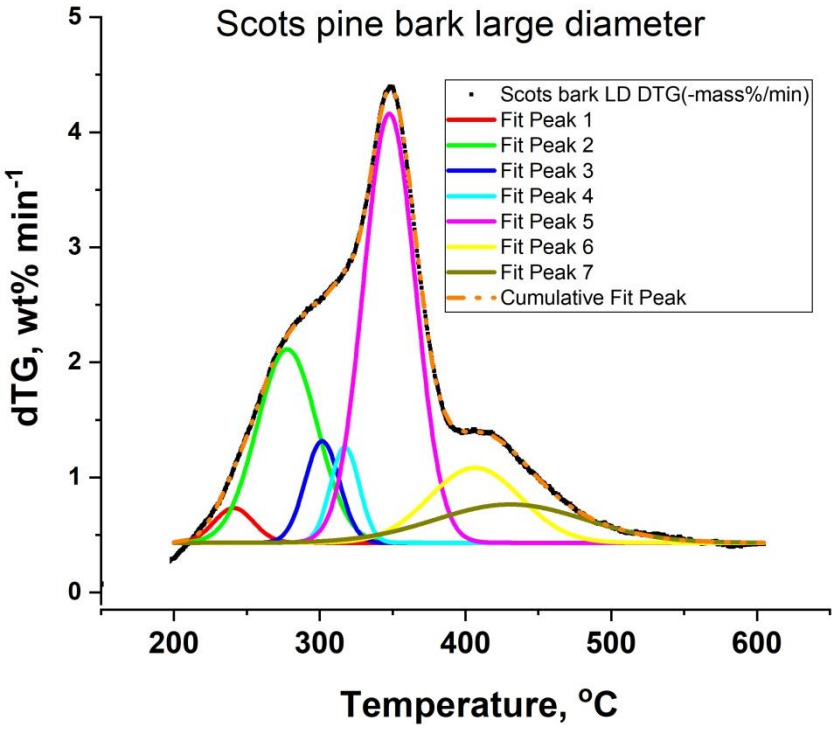

Figure 71 DTG/temp from the first minimum DTG curve valley temperature to 600 ℃.

The developed method of DTG/Temp peaks deconvolution was applied for all pine assortments (see *Table 10*). The DTG/Temp peaks deconvolution of all forest waste assortment is placed on Appendix from Figure 185 to Figure 195.

Table 10 Comparative contribution of all wood components in the deconvoluted DTG/temp peak of pine assortments.

Temperature °C	53 °C	74 °C	100 °C	129 °C	232 °C	280 °C	316 °C	344 °C	367 °C	408 °C	411 °C
Wood assortment	Extractives %		Moisture %	Extractives %		Hemi., lignin, cellulose %			Cellulose %	Lignin %	Extractives %
Scots pine cone	1.0		4.8	1.7	1.8	29.0	10.4	2.7	30.8	11.5	6.3
Norway spruce cone	0.9		5.0	5.1	1.6	17.6	32.7	12.7	9.5	9.3	5.7
Lodgepole pine cone	1.0	4.6	2.0		12.5	6.9	24.2	10.9	22.4	8.6	7.0
Scots pine branches	0.7	4.6	1.3		9.5	11.0	29.6	11.0	16.2	8.5	7.5
Norway spruce branches	1.1	6.3	1.4		9.5	23.5	18.6	11.6	9.6	6.1	12.2
Lodgepole pine branches	1.0	4.5	1.3		3.0	19.9	33.4	15.0	7.3	13.2	1.4
Scots pine needle	0.7	4.4	0.7		10.5	16.5	9.9	4.8	24.7	9.1	18.7
Lodgepole pine needle	2.0	5.2	1.5		1.0	9.8	18.1	24.3	13.3	6.2	18.6
Norway spruce needle	0.6	5.5	1.3		9.5	8.7	14.1	14.8	22.5	5.2	17.7
Scots pine bark LD	1.5	7.7	1.2		2.2	19.3	5.8	4.6	36.8	11.3	9.5
Scots pine bark SD	0.3	6.9	1.9		0.8	18.8	20.9	2.9	25.6	12.3	9.7
Norway spruce bark	0.9	5.9	3.3		1.1	6.0	16.0	25.9	24.1	8.2	8.6
Scots pine heartwood	1.1	4.2	2.8		6.2		26.5	24.5	13.4	13.2	8.1

The above-calculated DTG/temp original Scots pine extractive composition was compared with the extractive results of methanol-based Soxhlet extraction using methanol from original biomass (see Table 8). Both the Soxhlet experimental and STA deconvoluted extractive data are in excellent agreement (Table 11).

Table 11 Comparison of experimental and STA DTG/temp deconvoluted extractives composition percentage.

Scots pine assortment	Experimental extractives content	Extractive calculated using STA DTG Peak deconvolution
Scots pine needle	36.5%	34.2 %
Scots pine stump	17.3%	19.6 %
Scots pine bark SD	18.6%	17.7 %
Scots branches	18.7%	22.3 %
Scots cone	9.7%	10.8 %
Scots pine bark LD	16.6%	21.0%

4.3 Evaluation of NIR for the Determination of Extractive and Moisture Content of a Forest Biorefinery Feedstock

NIR spectra of all assorted forestry waste were recorded with a FOSS NIRS Spectroscopic instrument at SLU in Sweden (Figure 67). The data were further analysed with Umetrics and the PLS toolbox of Matlab. A PCA-1 and PCA-2 data plot of wood assortments NIR spectra are drawn in Figure 72. More than 90% of the sample is located in PCA-1, whereas only around 5% of data remain in the axis of PCA-2 and the remaining 3 % of the data points distributed in PCA-3 and beyond.

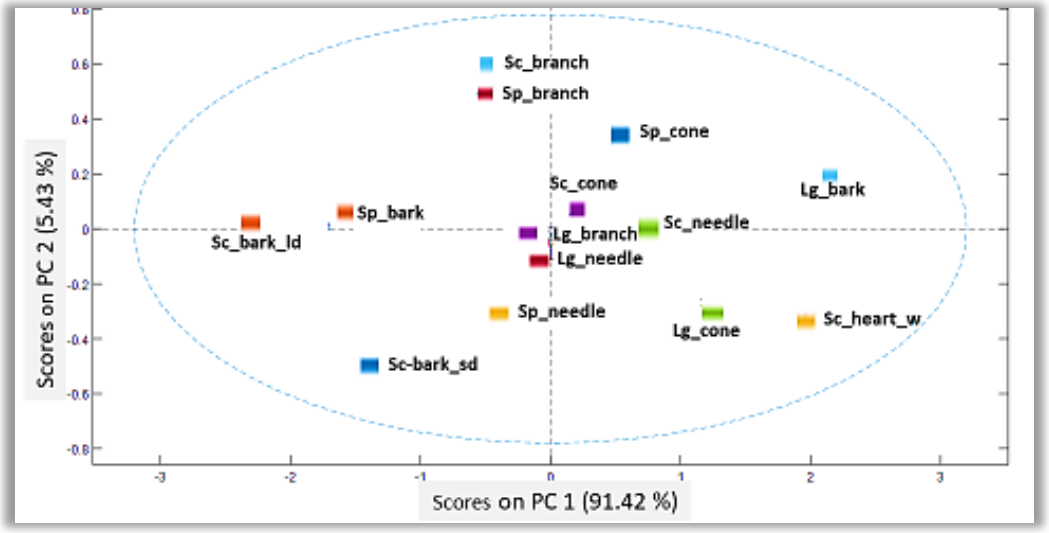

Figure 72 PCA 1 and PCA 2 score plot of all wood assortments.

By analysing the total PCA-1 and PCA-2 plot, it is clearly shown that Lodgepole pine bark, Scots pine bark small diameter and Scots pine heartwood stump contain comparatively different chemical composition with respect to the rest of the samples. These variations of data point distribution in the PCA-1 and PCA-2 score plot may arise from other wood components other than cellulose, as cellulose consists of only one kind of molecular unit, glucopyranose. The best candidates for such components could be lignin or extractives because they demonstrate the biggest variation in quantity and quality among the biomass assortments (see *Table 2*). To further evaluate the source of variations for samples in the PCA score plots, a second-order derivative of all the NIR spectra were computed (Figure 73). The peak assignment of all wood components was performed with literature reference assignments.[386, 394, 398, 399, 406, 407, 566-571]

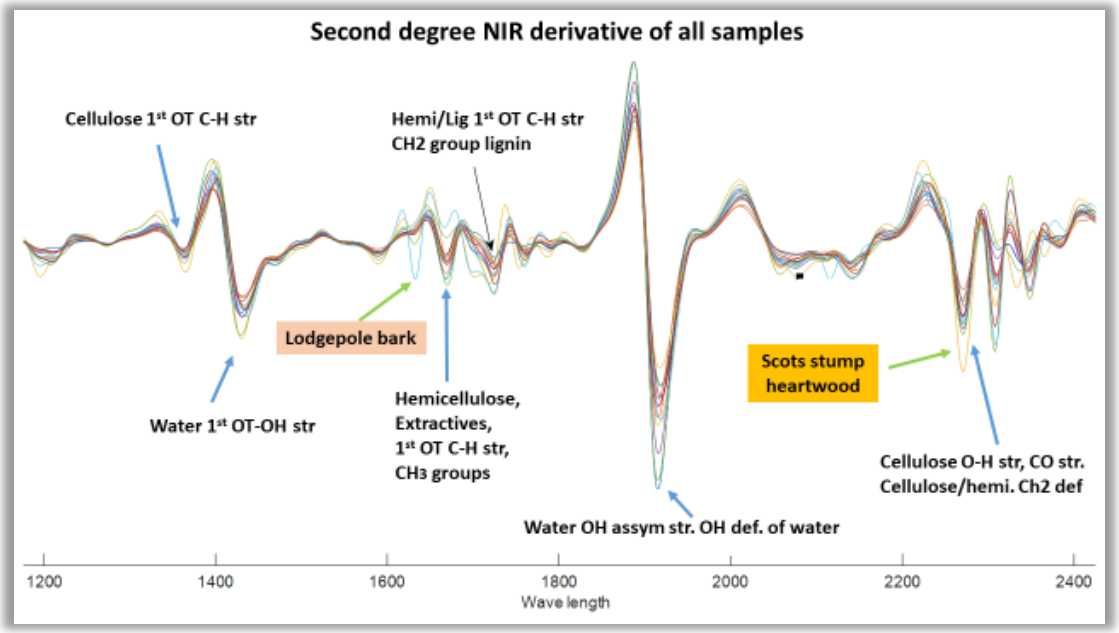

Figure 73 Second degree NIR derivatives of all wood assortments.

The peak at 2277 nm is attributed to the cellulose due to O-H stretching and C-C stretching along with C-H stretching and C-H deformation within the cellulose microcrystal. The peak at 1668 nm is due to the 1st overtone of aromatic C-H stretching. The negative peak at 2134 nm also could be assigned to lignin or extractives because of aromatic C-H stretching and C-C stretching.[568] The peaks at 1616 nm are 1st overtone of C-H stretching of >C=CH_2 group.[406]

The Lodgepole pine bark is in good agreement with the score plot (see Figure 72) which has a distinct peak at 1616 nm, with no other biomass sample containing any peak in that region. According to the literature, this peak can be assigned to an extractive or lignin.[568] Furthermore, barks from other plants have the same peak around 1616 nm. However, their intensities are significantly lower than that of the Lodgepole pine bark peak (Figure 74). This distinct difference may come from variation and/or quantification of extractive compounds. The chemical characterisation of Lodgepole pine bark was indeed shown to have the highest content of extractives among all other parts of Lodgepole pine, and the most abundant extractive of Lodgepole bark is Pimaral (Androst-5-en-7-one).[401] The above example clearly demonstrates that the fast and inexpensive NIR method of analysis can be efficiently used for identifying specific chemicals within different biomass feedstock.

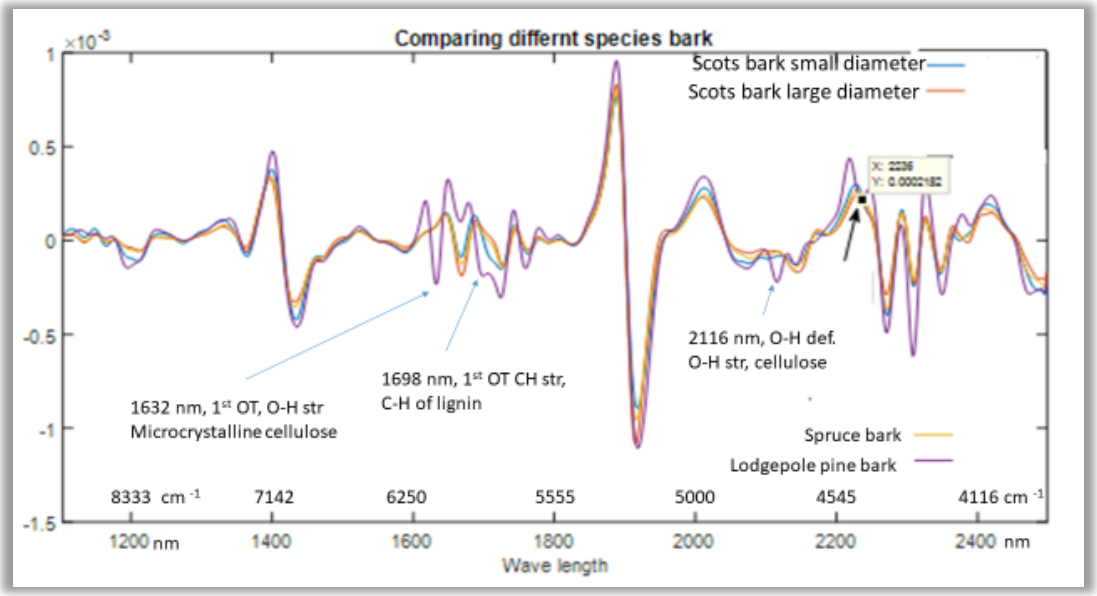

Figure 74 Comparison of second-order NIR spectra of all four bark types.

Similarly, the distinguishable position of Scots pine stump heartwood in the PC-1 vs PC-2 plot could be a result of a higher cellulose content when compared to other assortments of the same species which is supported by both the literature and the STA analysis (Table 10) of Scots pine stump heartwood.[349] The NIR analysis has also demonstrated that the Scots pine stump has a significantly higher intensity of the distinctive cellulose peak at 2277 nm than any other assortments peaks (Figure 73 & Figure 75).

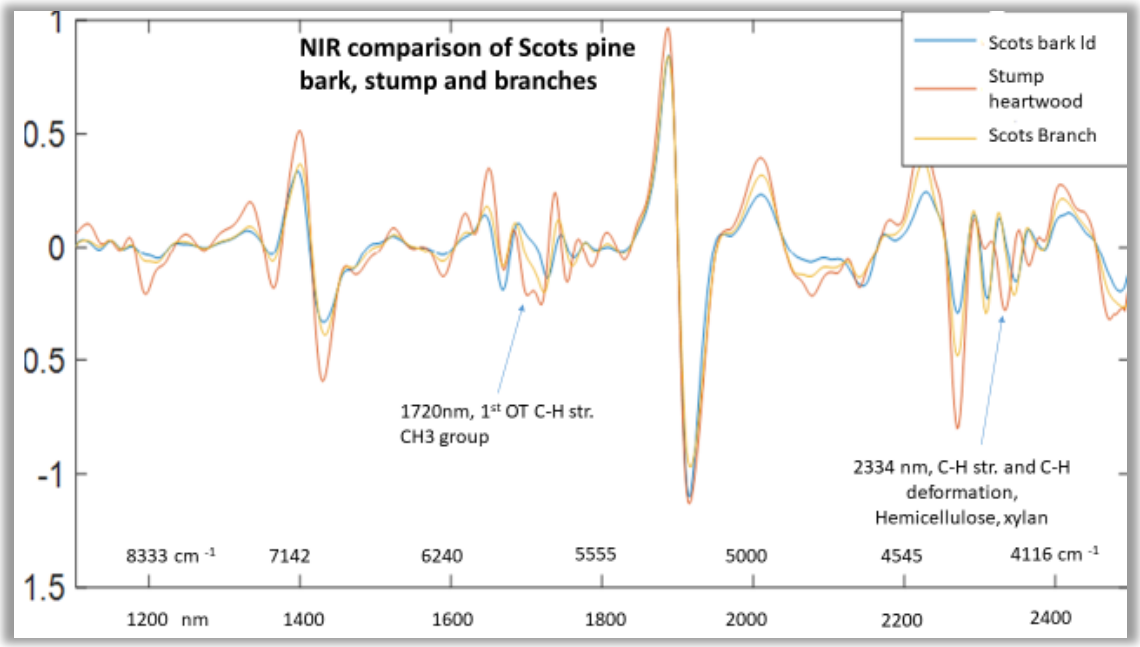

Figure 75 Second-order NIR spectra of Scots pine bark, stump and branches

The NIR analysis can be also applied for moisture content determination. In the second order derivatives of NIR spectra in Figure 73, the strong band at around 1916-1942 nm is assigned to water on account of contributions from O-H asymmetric stretching and O-H deformation of H_2O.[568] An arbitrary scale of water content is made for all wood assortment, using the magnitude of the strong second-order NIR band at 1916-1942 nm. The results of NIR moisture content analysis is then compared with the oven-dried method and STA data (Table 10) of the same biomass sample. The higher magnitude of water content peak of NIR is assigned as "A", and lowest magnitude is assigned as "E". It can now be easily established that moisture content obtained from dTG/ peaks shows a good correlation with the moisture content obtained from oven-dried methods. However, the STA methods give a lower moisture content. The STA data seems more reliable because the interpretation of the STA method involves removing extractives contribution from the water peak based on the mathematical model. Importantly, the NIR water band is in agreement with STA moisture content results.

Table 12 Comparison of biomass moisture contents obtained by different methods.

Wood parts	Species	Size	Oven		STA	NIR
			105°C, 18h	30°C, 48h		(at 1915 nm)
Cones	Norway spruce	Grind	5.42	2.1	5	A
	Lodgepole pine	Grind	4.3	1.42	2	A
	Scots pine	Grind	4.18	1.31	4.8	A
Heartwood stump	Scots pine	Grind	4.49	3.45	2.8	B
Bark	Scots pine small diameter	Grind	4.01	1.36	1.9	C
	Scots pine large diameter	Grind	4.13	1.89	1.2	C
	Norway spruce	Grind	4.65	1.67	3.3	C
Branches	Norway spruce	Grind	4.42	2.93	1.4	D
	Lodgepole pine	Grind	3.81	1.66	1.3	D
	Scots pine	Grind	3.49	1.55	1.3	D
Needles	Lodgepole pine	Grind	3.52	1.69	1.5	E
	Scots pine	Grind	3.75	1.41	0.7	E
	Norway spruce	Grind	3.72	1.68	1.3	E

The developed independent ways of analysis of forest-waste biomass allow for investigation of the influence of extractives on the MW-assisted pyrolysis of the targeted forestry biomass.

4.4 Influence of Extractive Components on MW Pyrolysis of Forest Waste

The effectiveness of the MW pyrolysis of biomass compared to conventional thermal methods such as pyrolysis and torrefaction is already established.[309, 310, 311] These research focused on

MW treatment of whole biomass *without* removal of any extractive components. As the extractives content within biomass could be as high as 40% (e.g. in the needle), they may significantly contribute to the overall MW pyrolysis processing of assorted wood. The only study that was found to engage in this line of thinking was performed by Behdad Moghtaderi *et al.*.[378] At atmospheric pressure and ambient temperature, they used 9.47 GHz MW frequency to investigate the dielectric properties of Slash pine and Spotted gumwood based on Von Hippel's transmission line method and found that the effect of extractives and mineral content may change the dielectric properties of woody biomass.[378] However, their research was limited only to wood pre-treatment for furniture production. To better understand the role of extractives on MW pyrolysis of homogeneous particulate woody biomass and the major wood structural component such as cellulose, a series of systematic experiments was conducted (and is subsequently described) in this report. The next investigation aimed to develop the most effective MW based bio-refinery methods to economically and sustainably produce fine and bulk chemicals from forest waste.

4.4.1 Fractionation of Scots Pine Bark Extractives

Because Scots pine bark has a significant amount of extractives, and it was under-evaluated commercially, Scots pine bark was chosen as a preferred sample for the fractionation study. The extractives of Scots pine bark were separated based on their solubilities in MeOH and cyclohexane. The separation procedure was performed according to the scheme outlined in Section 3.22 at Experimental Chapter.

The MeOH (room temperature) soluble, cyclohexane soluble and cyclohexane insoluble fractions are referred to herein as FR-1, Fr-2 and FR-3, respectively (Figure 55).

4.4.2 GC-MS Analysis of Scots Pine Bark Extractives

GC-MS data analysis and peak assignment were performed based on a literature survey using the NIST 2011 library (http://nistmassspeclibrary.com/) and MS fragmentation pattern analysis. Based on this knowledge, a typical pattern of compound distributions of Scots pine bark extractives before fractionation are shown in Figure 76.

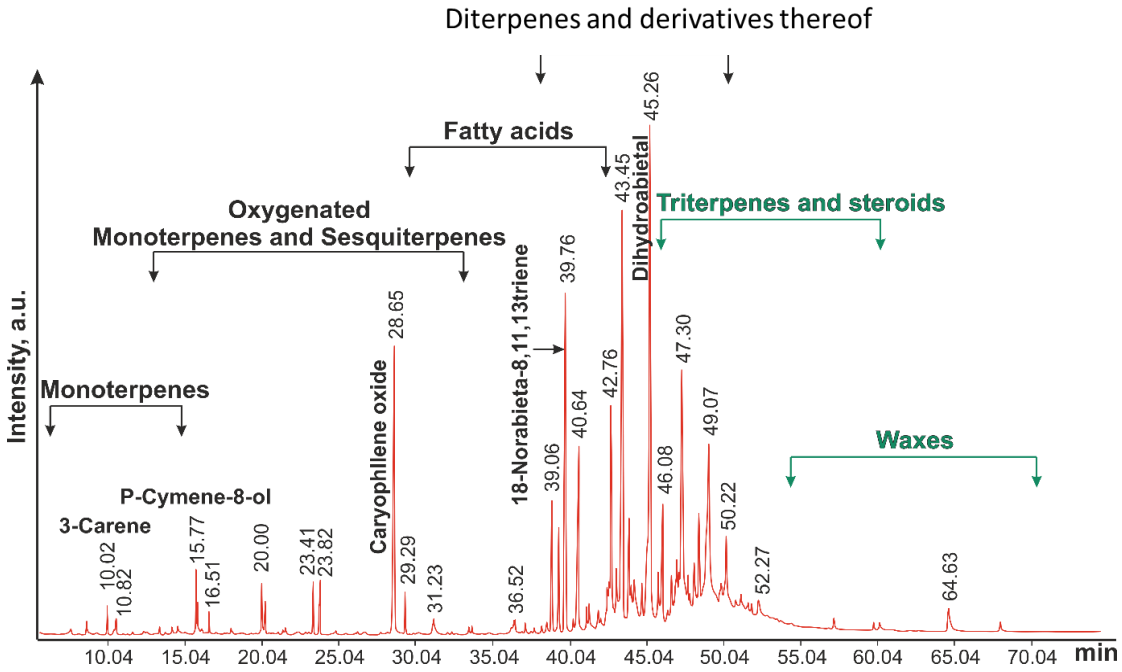

Figure 76 GC-MS functional group profile of all extractive fractions (before fractionation).

The distribution ratio of all the eluted compounds in the GCMS chromatograph of all three fractions (FR1, FR-2 and FR3) is shown in *Figure 77*.

Figure *77* that MeOH-insoluble fractions (FR-2 and FR-3) contain high molecular weight compounds in more substantial quantities, which elute from 27 minutes onwards. From the Scots pine bark's extractives functional group distribution pattern in the GC-MS of Figure 76, it is apparent that di-terpenes (and derivatives thereof), triterpenes, steroids, wax and wax-esters may be present in higher proportions within the MeOH-insoluble fractions (FR-2 and FR-3).

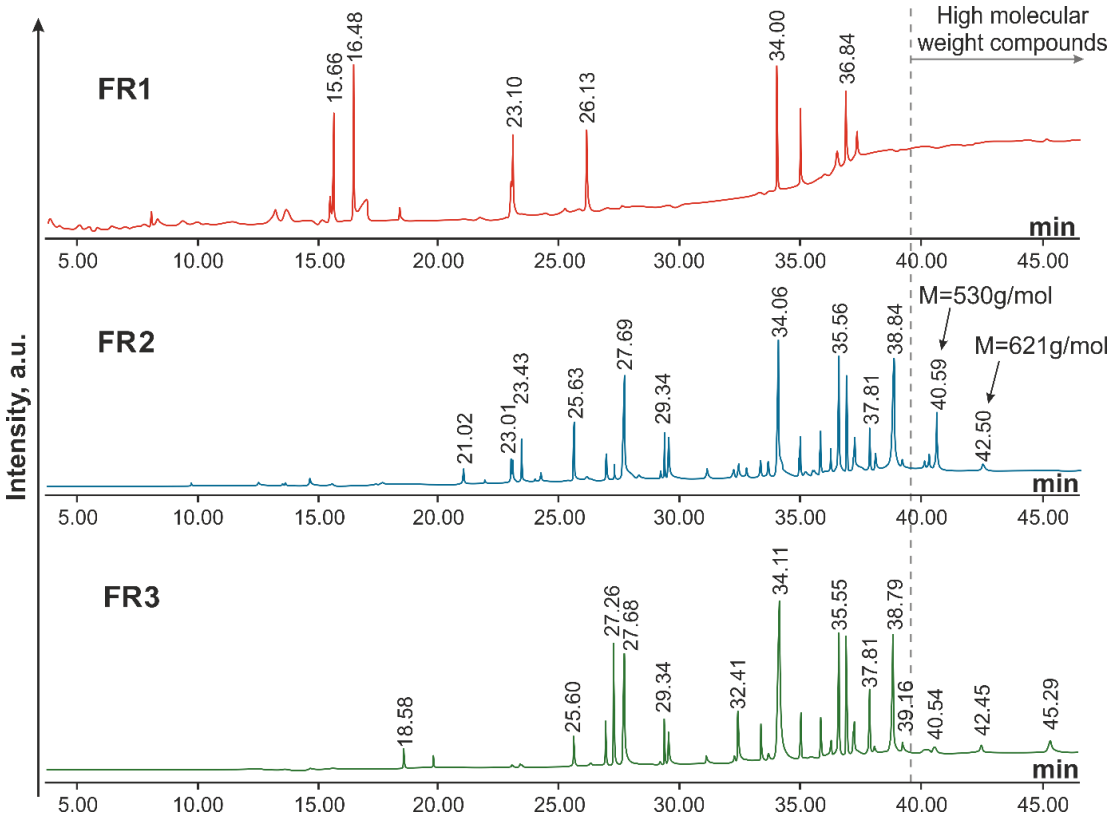

Figure 77 Molecular weight distribution in GC-MS chromatographs of all three fractions of bark.

The distribution ratio of wax and wax-esters in all of the fractions can also be seen in Figure 77. The total elution time for the samples shown in Figure 77 was chosen to be shorter than the method used in the generation of Figure 76. In the chromatograph presented in Figure 77, it can be seen that, from 40 to 45 minutes of elution time, the highest amount of heavy molecular weight compounds were distributed in FR-2, whereas FR-1 contains almost no such compounds. From the fragmentation patterns of the compounds that were present in the FR-2 and FR-3 chromatograms, the peak which was eluted at the 45.29 minutes is illustrated in Figure 78. In Figure 78, the M+. ion of the mass spectrum is 649. The isotopic abundance of this molecular ion is carefully evaluated from M+1, M+2 and M+3 pattern. From the percentage abundance of the M+2 and M+3 ions, it is hypothesised that the molecule has an oxygen-containing ion and that the number of oxygen atoms could be more than one.

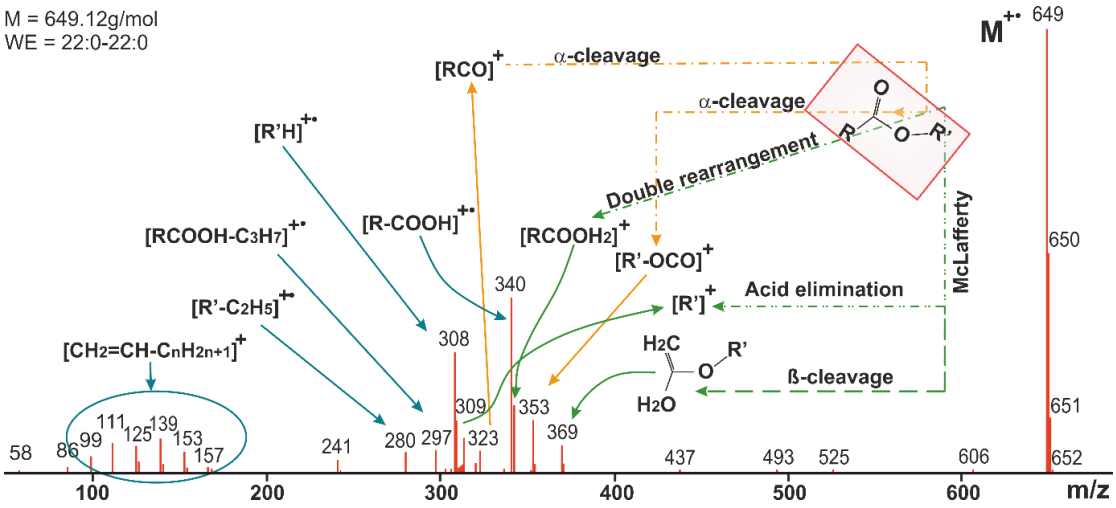

Figure 78 Mass spectrum of the compound eluted at 45.29 minutes.

Suspecting two oxygen atoms in the molecule and no nitrogen, sulphur or halide atoms, a theoretical isotopic distribution of the $M^{+\cdot}$ the peak is calculated in Table 13, according to Sparkman *et al.*.[572] The value of the right-hand column in Table 13 is very close to the molecular ion peak of Figure 78 mass spectrum. From the judgement of the theoretical calculation of the spectral molecular ion, it can be established that the molecular mass of the compound at an elution time of 45.29 minutes is $C_{44}H_{88}O_2$.

Table 13 Isotopic abundance of M+ ion of $C_{44}H_{88}O_2$

Element	% Abundance			% of abundance for C44H88O2			Total contribution to isotopic peak
	Carbon	Oxygen	Hydrogen	Carbon	Oxygen	Hydrogen	
M	100	100	100	100	100	100	100
M+1	1.1	0.04	0.015	48.4	0.08	1.2	49.68
M+2	0.006*n*n	0.2	0	11.62	0.4	0	12.02

To further clarify the molecular formula, the empirical formula of $C_{44}H_{88}O_2$ is run using the isotopic distribution calculator provided by Scientific Instrument Services (http://www.sisweb.com/mstools/isotope.htm, n.d.). The output data and the isotopic plot are shown in Figure 79.

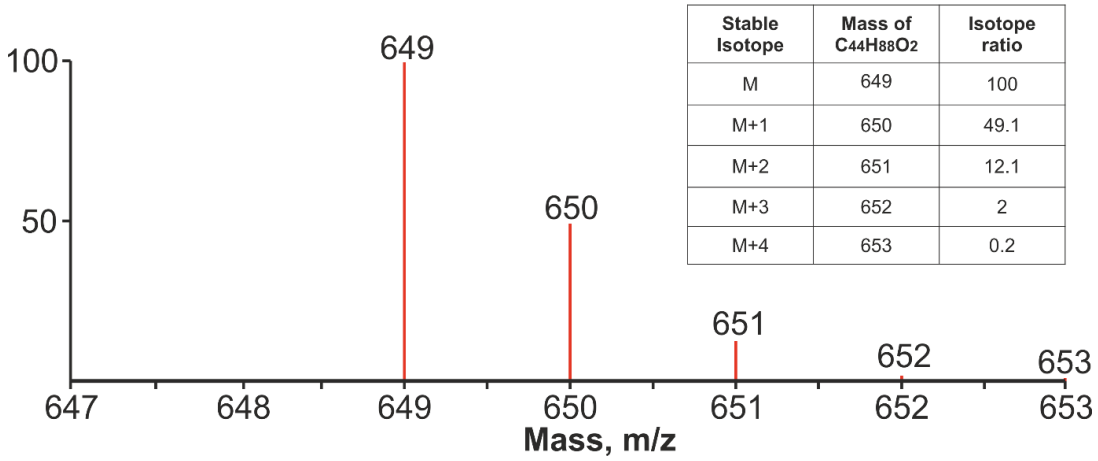

Stable Isotope	Mass of $C_{44}H_{88}O_2$	Isotope ratio
M	649	100
M+1	650	49.1
M+2	651	12.1
M+3	652	2
M+4	653	0.2

Figure 79 Isotopic distribution of a compound with a molecular mass of $C_{44}H_{88}O_2$.

The simulated isotopic plot further verifies the molecular formula. The wax ester, Behenyl behenate displays a nominal mass of 648 and an exact mass of 649.12 which satisfy this molecular ion peak. An annotated fragmentation pattern of this molecule is presented on the top right corner of Figure 79. The base peak here is also the molecular ion peak. The second most abundant peak at *m/z* 340 is generated from a double McLafferty rearrangement of the alkyl ester by removing a cyclic radical through β-cleavage of the acyl group. By removing a neutral acid from the ester through McLafferty β-cleavage, the ion peak of *m/z* $309^{\cdot +}$ is produced. From α cleavage of both ends of the acyl group two distinct peaks [RCO] and [R`-OCO] were generated at *m/z* 323 and at *m/z* 353. McLafferty β-cleavage of acyl group from the opposite end of the alcoholic jointly create *m/z* 369. The other significant ions at *m/z* 280, 297 and 328 resulted from further fragmentation of the major fragments as shown in Figure 79. The major [CH_2=CH-$C_nH_{2n+1}^+$] *m/z* peaks were also shown in Figure 79. From all this evidence, it is clear that the compound in the spectrum presented in Figure 78 is the wax ester docosyl docosanoate (WE 22:0-22:0). This analysis is also supported by Klára Urbanová *et al*, Liang-xiao Zhang *et al* and in textbooks.[573 574 575]

By a similar mass spectral fragmentation analysis, it can be shown that the previous peak at 42.50 minutes belongs to Behenyl arachidate (MW 620; WE 22:0-20:0). Behenyl arachidate only has two carbon units less in its alcoholic part. The strong peak at 40.59 minutes in FR-2 is an unsaturated wax-ester, although the position of double bond was not positively identified.

After GC-MS characterisation of different extractives fractions, a few conclusions can be made. First of all, the FR-1 fraction contains a negligible amount of high molecular weight compounds, while fraction FR-2 has the highest amount of these chemicals.

4.4.3 Thermogravimetric Analysis of Scots Pine Bark Extractives

To get more insight into the bio-oil compounds, thermogravimetric analysis of bio-oil fractions were performed. Using an STA-625, the simultaneous thermogravimetric analysis of the three extractive fractions discussed in section 2.5.1 was performed. The experiments were carried out in the absence of oxygen, over a temperature range of 20°C to 625°C. Differential thermogravimetric analysis (DTG/temperature) was conducted, and the resulting spectra were deconvoluted to enable a more detailed analysis of the DTG/temperature profiles. Deconvoluted peaks for all extractives are shown in Figure 80 below.

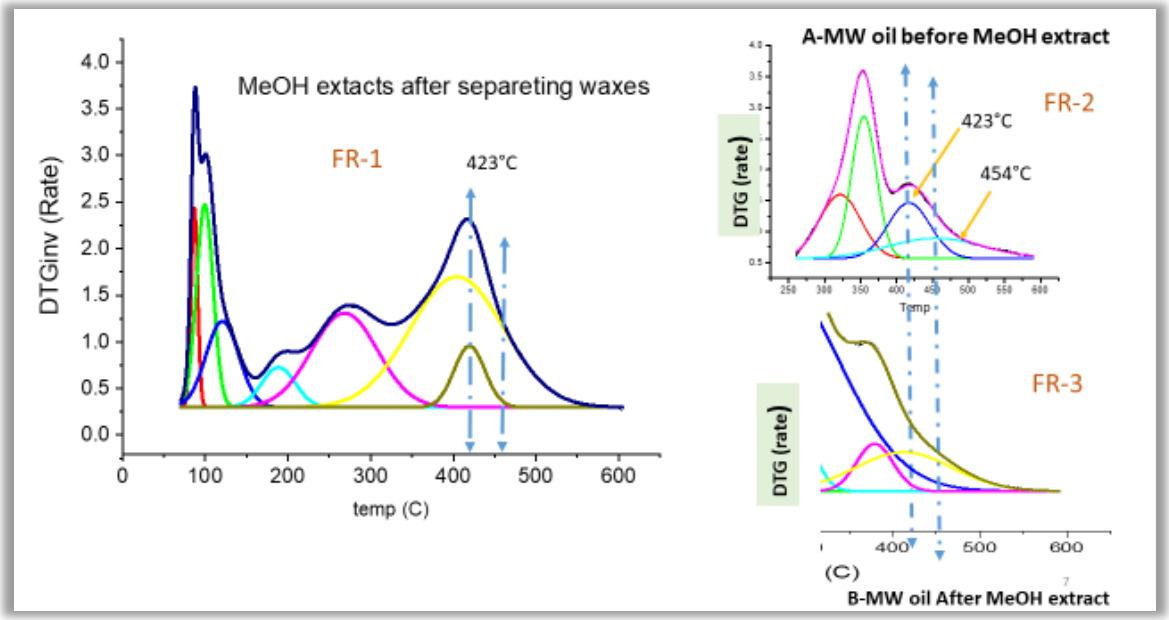

Figure 80 STA DTG/T peak deconvolution of three extractive fractions.

There is a distinctive peak at 400°C in all extractive fractions. In contrast to the FR-3, the FR-1 and FR-2 fractions have a common peak at 423°C, but the peak intensity in FR-1 is almost half that in FR-2. FR-2 stands out from all other fractions with a clear peak at 462°C. Therefore, FR-2 contains the highest amount of high boiling compounds. As FR-2 fractions are soluble in cyclohexane, it is likely to be that this fraction is rich in various long-chain hydrocarbon wax and wax esters. The finding above is in good agreement with the results of GC-MS analysis, as mentioned in the previous section.

4.4.4 Comparison of MW Pyrolysis Yield of Scots Pine Bark with or without Extractives

The experiment is set up in a fixed power mode of CEM discovery MW Synthesizer. Four different power conditions (150W, 200W, 250W and 300W) were applied to three grams of Scots pine bark (LD) samples. The temperature traces of both types of method-A and method-B samples are shown in *Figure 81*.

Optimisation of MW-power for Scots pine bark (with and without extractive)

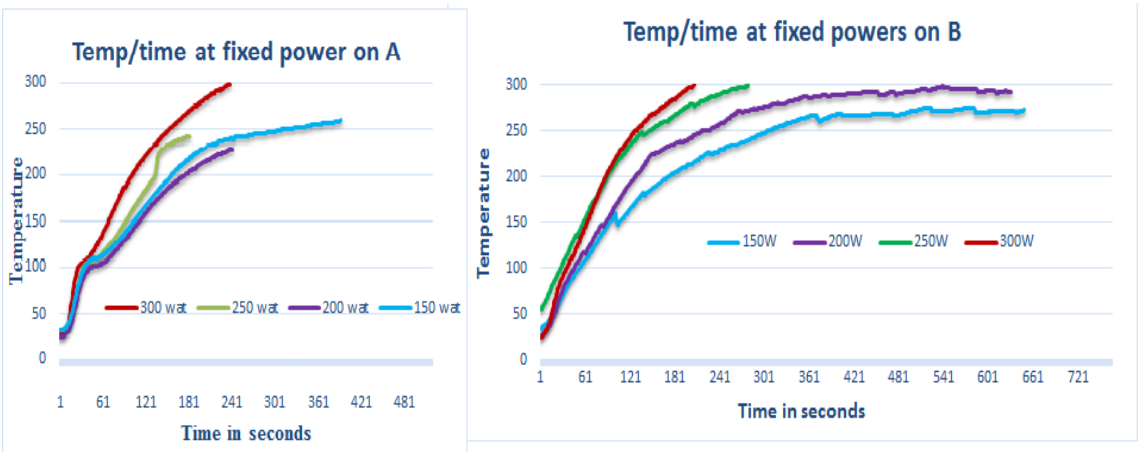

Figure 81 Comparison of temperature change in sample A and B at Fixed power mode.

In both cases, the rate of temperature increase is higher for 300W and 250W than for 200W and 150W of applied power. In samples A, at 100 ℃, there is a sudden discontinuity in the temperature increase which can be attributed to water evaporation. Such a change was not noticeable in the case of sample B, as this sample was dried overnight at 75 ℃ after MeOH extraction. The temperature changes that occurred during the MW treatment of samples produced using both method-A and method-B samples using various power settings are summarised in Figure 82.

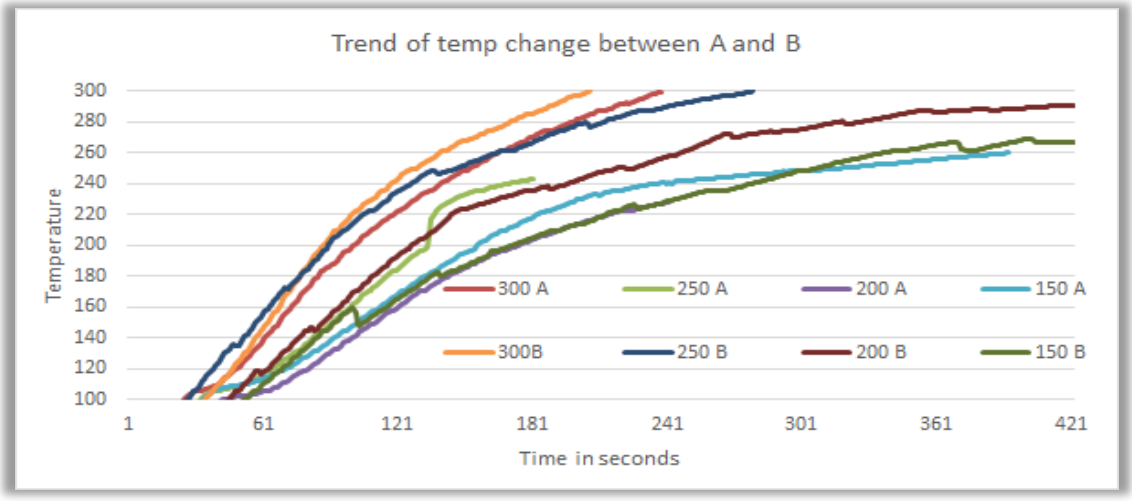

Figure 82 Comparison of the temperature profiles at various fixed powers (150-300 W) of samples produced via method-A and B.

It is noticeable that the rate of temperature increase is higher in the case of sample-B than that of sample-A. At 150W, the MW pyrolysis behaviour of sample-A is complex in nature,

demonstrating discontinuation at around the second minute. This phenomenon could be relevant to the temperature measurement problem.

The difference in the chemical composition of samples A and B may explain the higher temperature rate in the case of sample-B. In the case of the sample-A, up to 100 ℃, the rate of temperature increase is higher than sample-B due to "microwave dielectric heating effect" on the water molecule.[254, 576] However, water is boiled out at around 100℃ significantly reduces the sample heating rate. Moreover, the DTG of the extractive (see Figure 80) showing that extractive chemical compounds are evaporated during all temperature range of experiment taking MW energy away from the sample and reducing the heating rate. The thermal conductivity and energy transfer rate of sample-B also significantly increased due to an increase in the sample density and the absence of low heat transferable extractives. Therefore, it can be concluded that having water in sample-A does not offer a significant advantage over sample-B MW heating process above 100℃.

The mass balance of the products obtained by treating both method-A and method-B samples; bio-oil, biochar and other gases are presented in Figure 83 and Figure 84. The comparison shows that the yield of biochar produced at lower power (below 300W) from sample-A, is higher compared to that of sample-B. Interestingly, the finding is in good agreement with the literature; the char yields are inversely changed with the samples heating rates (see Figure 81).[577] However, bio-oil were produced at higher yield from sample-A compared to sample-B. On average, the bio-oil yield using the sample produced via method-A is only 4% higher than produced via method- B.

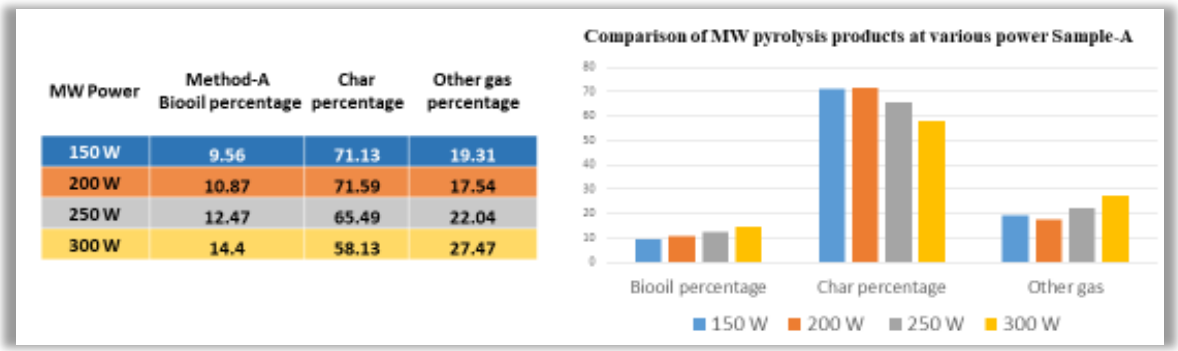

Figure 83 Comparison of the bio-oil, char and other gas produced from sample-A during MW treatment at different power.

MW Power	Method-B Biooil percentage	Char percentage	Other gas percentage
150 W	7.73	65	27.27
200 W	7.93	64.44	27.63
250 W	8.74	64.16	27.1
300 W	11.2	61.92	26.88

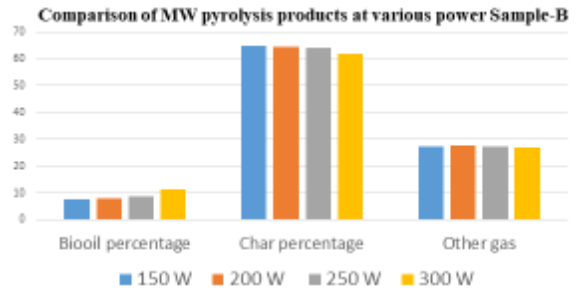

Figure 84 Comparison of the bio-oil, char and other gas produced from sample-B during MW treatment at different power.

Such a contradiction can be solved if the total extractives and bio-oil recovery are combined. It can be seen that the total liquid production in sample-B is about 10% higher as a percentage of dry bark biomass and about 75% higher in terms of like for like recovery of total bio-oil.

The comparison of the influence of power on sample-A and sample-B (Figure 83 and Figure 84) shows that at power below 200W, sample-B produces more gases than sample-A. The increasing power above 200W significantly reduces the char yields and therefore increases the gas yield. At a power of 300W, the char yields for both samples become similar (around 80%). These data demonstrate that a significant amount of energy in the case of the sample-A might be wasted on the heating/thermal transformations of the extractives.

As in the literature review, it was discussed in section 2.2 that it was already indicated by some research in conventional biomass pyrolysis and in processing extractive may dictate the rate of biooil production and quality of char. The extractive indicates to influence pulp mill sludge processing,[360] lignin acidolysis,[361] enigmatic hydrolyses,[362, 363] palletisation process,[364] biochar formation,[365] caloric value,[366] biomass pyrolysis process,[367] and bio-oil production yield. [368] In this work it is now also shown that removal of extractive also reduces the energy requirement in microwave-assisted pyrolysis.

4.4.5 Analysis of Obtained Biooil from Scots Pine Bark Sample

4.4.5.1 Mass spectrometric analysis of biooil

Bio-oils generated from the MW pyrolysis of sample-A was analysed via GC-MS (Figure 85). The NIST 2011 MS database was used for peak assignment of the biooil spectrum.

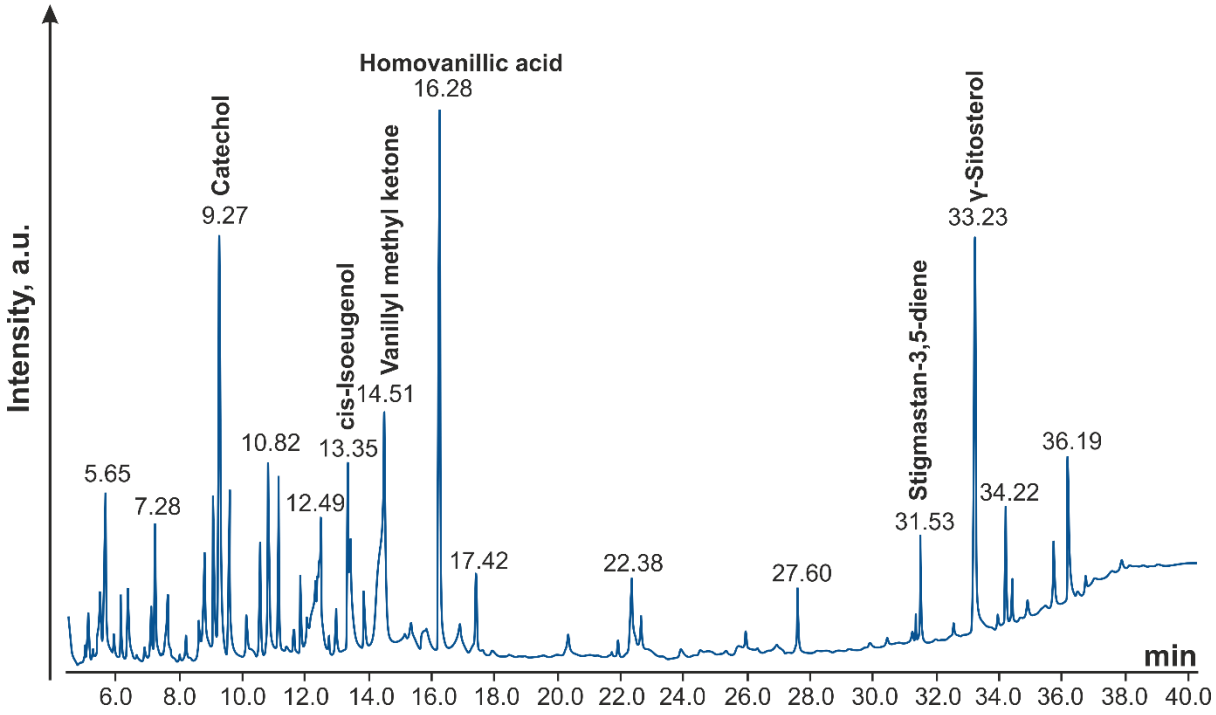

Figure 85 GC-MS analysis of sample-A biooil.

As Figure 85 indicates, lignin-derived compounds such as catechol and vanillic acids are dominant in the spectrum. Along with defragmented lignocellulosic secondary products, high molecular weight sterols, such as γ-Sitosterol are also present in the biooil.

4.4.5.2 NMR analysis of biooil

The NMR sample was prepared in $CDCl_3$ for proton NMR. The NMR data of the bio-oil obtained from Sample-A was also indicative of a strong presence of saturated alkane (0.2 ppm to 1.8ppm) which may come from extractive parts of biomass without any chemical changes during MW pyrolysis process.[467, 578]

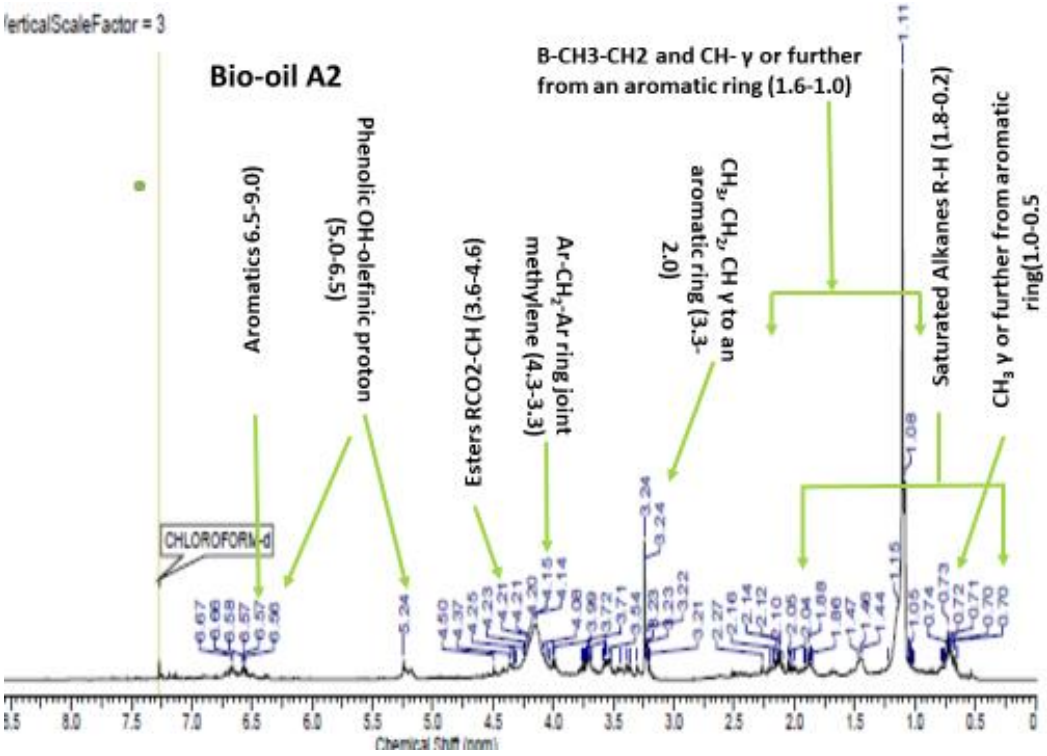

Figure 86 NMR analysis of biooil A2 fraction

4.4.6 STA analysis of large diameter Scots pine bark biooil

Using an STA-625 simultaneous thermogravimetric analyser, in the absence of oxygen, the Samples-A and -B were analysed in the temperature range from 20℃ to 625 ℃. The DTG peaks were deconvoluted to analyse the thermal pattern of biooil. Deconvoluted peaks for bio-oil from method-A and method-B are shown in Figure 87.

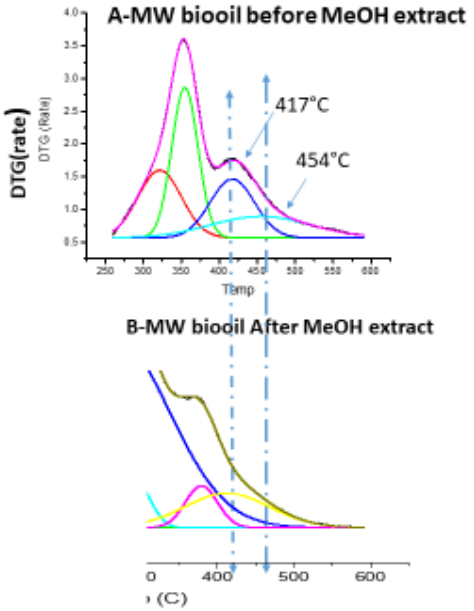

Figure 87 DGT/T peak deconvolution of bio-oil produced from samples obtained using method-A and method-B.

It clearly shows that the DTG of sample-A biooil has a peak at around 454°C, but this biooil peak is absent in DTG of sample-B biooil. As shown in section 2.5, the peaks in this region belong to the extractives (wax or steroids). The peak around 460°C is also observed in the FR-2 DTG (Figure 80) demonstrating that wax and steroids are concentrated in the cyclohexane soluble part of extractives.

4.4.7 Final Remark of Extractive Influence on MW Pyrolysis of Forest Waste

It can now be established that wax and wax-esters can indeed remain unaltered during MW pyrolysis and that the hypothesis of wax and wax-esters acting as inhibitors during MW pyrolysis is more plausible. To further verify the above suggestion, a series of control experiments were performed with better-known substrates - microcrystalline cellulose and straw wax (see the following sections). It was observed from a fixed power MW experiment that, after MeOH extraction, the same power could produce more heat energy when compared to the same amount of bark that had not undergone MeOH extraction. As a result, the time required for MW pyrolysis of extractive-free bark is less than bark containing extractives when operating under the same MW condition. The reduction of power in the case of extractive-free bark is almost half of the required power of bark with extractives. The reduction of power requirement after MeOH extraction may be due to more favourable MW condition such as sample densification and greater energy penetration after extractive removal from the original bark sample.

It was concluded that microwave activated pyrolysis alone without initial solvent extraction may not be ideal for maximum bio-oil extraction from original forest biomass, especially for this specific bark sample. But after appropriate solvent extraction, the total bio-oil recovery improves significantly.

4.5 Influence of Extractive Components on Microwave-assisted Pyrolysis of Cellulose

It was decided to investigate MW pyrolysis behaviour of cellulose-extractives systems to get a better mechanistic understanding of the influence of extractives on the MW pyrolysis of biomass

4.5.1 ATR-IR Analysis of Crystalline Cellulose

A small amount of crystalline cellulose was subjected to attenuated total reflection infrared (ATR-IR). In ATR technique instead of transmitting the infrared light, the wave is reflected on the surface of the material with very small penetration depth (between 0.5 and 2 micrometres).[579] By using this method, the problem of strong attenuation of IR signal with

highly absorbing media can be avoided. The well-studied cotton crystalline cellulose was used as the model wood component for MW pyrolysis investigation in this research work.[580, 581] The chemical structural unit of cellulose and its characteristics ATIR spectrum (including individual peak assignments) are shown in Figure 88.

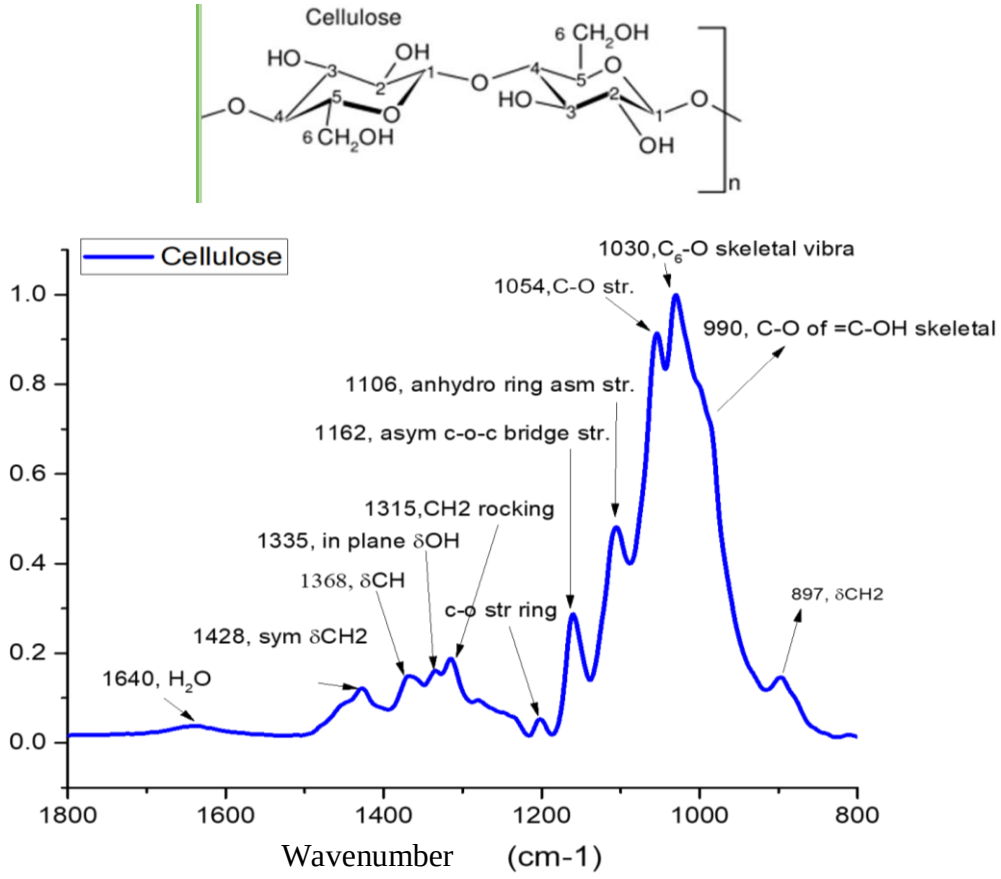

Figure 88 ATIR spectrum of crystalline cotton cellulose and cellulose structural unit (top).

IR spectroscopy of cellulose was investigated and identified in numerous publications, and the assignment of the major peaks are well established.[582-587] The broader band in the 3600-3100 cm^{-1} region represents OH-stretching of hydrogen bond and the peak at 2900 cm^{-1} is C-H stretching vibration.[588] The presence of water and its absorption peak would have appeared at 1641 cm^{-1}.[586] The band At 1430 cm^{-1} is known as the "crystallinity band" and is assigned to a CH_2 stretching vibration.[588] The pyranose ring C-O stretching is at 1200 cm^{-1}, and antisymmetric C-O stretching is at 1170 cm^{-1}.[584] The dominant peak which is used to normalize the spectrum displayed in Figure 88 ATIR spectrum is at 1030 cm^{-1} and corresponds to a C-6 skeletal C-O vibration peak.[584] The peak at 897 cm^{-1} is assigned to an "amorphous" absorption band as in amorphous cellulose the β-(1→4)-glycosidic linkages C-O stretching intensity increases when crystalline cellulose becomes amorphous.[588]

4.5.2 Comparison of Cellulose Chars after Conventional Pyrolysis via ATIR

Cellulose was thermos-gravimetrically pyrolysed in a nitrogen gas flow until a series of specific temperatures were attained - these temperatures were: 286 ℃, 296 ℃, 324 ℃ and 376 ℃. This particular range of temperatures was selected as it is within the range that is commonly reported for cellulose pyrolysis (315 - 400 ℃).[587] The ATR-IR spectra of the char obtained at the temperature mentioned above, in addition to that of pure cellulose are summarised in Wavenumber cm-1

Figure 89.

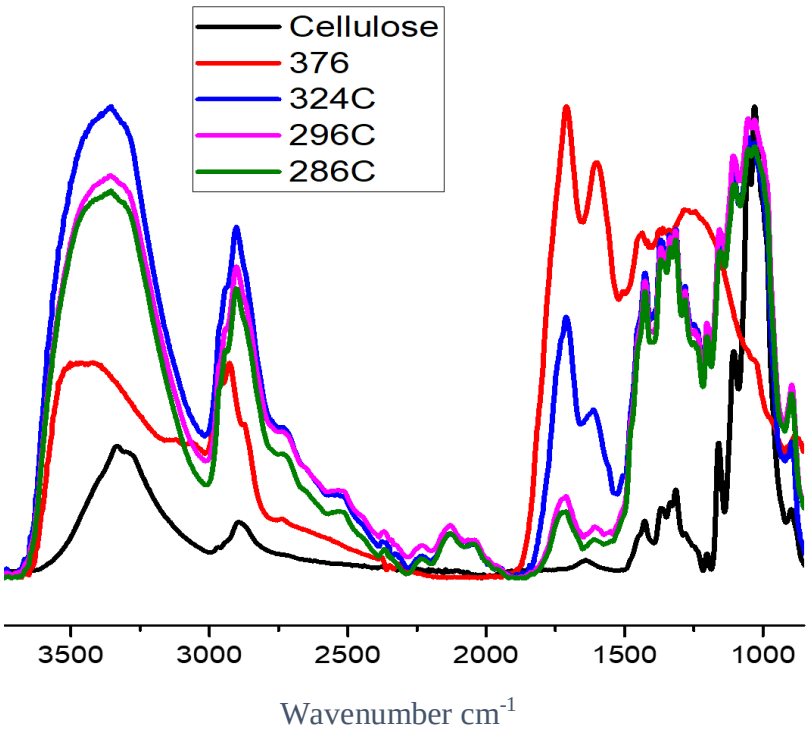

Figure 89 Comparison of cellulose ATR with STA pyrolysed cellulose char produced at various temperatures (286℃ - 376℃).

Although the cellulose ATIR (black line) and STA pyrolysed cellulose char at different temperature shows the varying intensity of several common peaks (Wavenumber cm-1

Figure 89), the major change in the peak intensity with the increase of temperature for all of the samples is most notable in the 1500- 1800 cm^{-1} region. For this reason, the peaks occurring at 1500- 1800 cm^{-1} are generally used to determine the ratio of pyrolysis of lignocellulosic materials.[585-587, 589, 590] The peaks at 1710 cm^{-1} and 1600 cm^{-1} represent characteristics FTIR bands for pyrolysis products of char.[587] The C=O stretching peak of aldehydes, ketones, which might be produced from cellulose pyrolysis, could occur in the range of 1730 - 1700 cm^{-1}. The

aromatic products resulting from pyrolysis display -C=C- stretching, which is typically found in the range of 1631-1600 cm^{-1}.[582, 584, 587] Comparing the peak area and height of 1710 cm^{-1} and 1600 cm^{-1} of Wavenumber cm-1

Figure 89, it is understood that the pyrolysis of cellulose accelerates as the STA temperature increases. In STA pyrolysis, the degradation of cellulose was lowest at 286 ℃ among all of the four selected temperature steps (286 to 376) ℃. The conversion of cellulose became highest at 376 ℃. From the above discussion, it is established that in an MW pyrolysis experiment, the ATIR region of the 1500-1800 cm^{-1} of a char sample could be used to determine the ratio of MW degraded cellulosic biomaterial.

4.5.3 Extractive Fractions Coated Cellulose MW Pyrolysis

In four, 10ml microwave reaction vessels, one gram of microcrystalline cotton cellulose was mixed homogeneously with fifty milligrams of FR-1, FR-2, FR-3, All-FR (extractives that were not fractionated) along with one equally treated blank cellulose sample. The MW conditions were set up as 200W power, 180^{o}C temperature and a hold time of 1minute following attainment of the maximum temperature. ATIR-FTIR spectra were recorded before and after MW pyrolysis and also following the removal of bio-oils. All sets of IR data were baseline corrected and normalised in the same way. The combined IR spectra are shown in Figure 90. The interesting region of the spectra is zoomed-in in Figure 91. The peaks were normalised at 1030 cm^{-1}. In Figure 91, the two sets spectra, before MW pyrolysis and after MW are shown together. The bottom five ATIR spectra are of the material before MW pyrolysis, and the top five are ATIR spectra of the samples after MW pyrolysis. The peak at 1702.4 cm^{-1} is non-conjugated carbonyl C=O stretching.[591] There was no visible peak at this region before MW pyrolysis of the samples. But after MW pyrolysis, the microcrystalline cellulose (green line) peak at 1702.4 cm^{-1} was significantly pronounced.

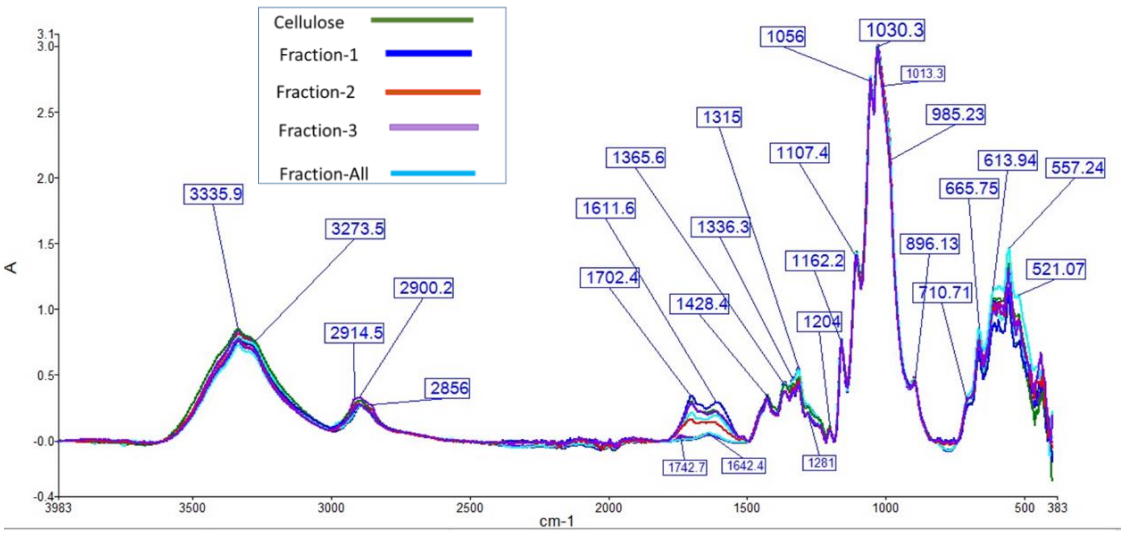

Figure 90 Normalized ATIR spectra of all samples before and after MW pyrolysis

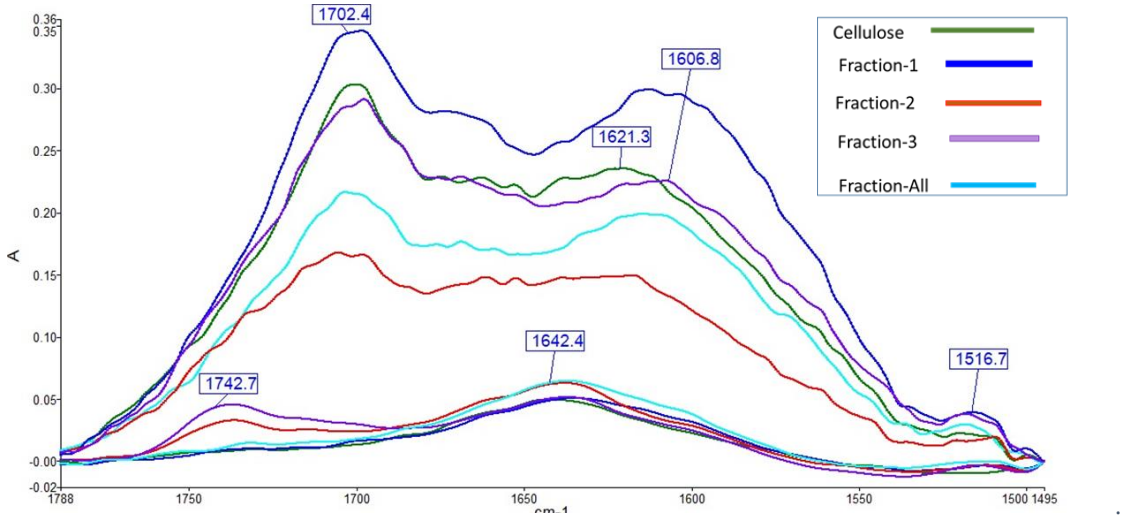

Figure 91 Zoomed in IR spectra of figure 11 at 1700 region

The appearance of the peak at 1702.4 cm^{-1} means that cellulose crystals were broken down drastically and pyrolysed. The pyrolysis of cellulose converted into C=O functional group-containing compounds. The most significant information here is that FR-2 (orange colour) containing cellulose sample underwent minimal conversion when compared to the other samples. The level of change in the FR-2 spectra is only slightly lower than the cellulose spectra. The FR-1 extractive containing cellulose demonstrated the highest 1702.4 cm^{-1} peaks. The great intensity of the carbonyl group might have come from MW pyrolytic decomposition of raisin acid. The blue line of FR-All may represent the most probable overall effect from all of the fractions in the natural state of cellulosic biomass.

Finally, to further verify whether similar results could be obtained using other wax sources (in addition to the Scots pine bark wax that was used above), another set of tests were conducted using wheat straw wax-coated cellulose.

4.6 Influence of Wax on Microwave-assisted Pyrolysis of Cellulose

4.6.1 ATIR of MW Pyrolysed Wheat Straw Wax

The comparison of ATIR spectra of wheat straw wax and MW-exposed wheat straw wax is shown in Figure 92. The intense narrow peaks at around 2915 cm^{-1} and 2850 cm^{-1} are assigned to the anti-symmetric and symmetric stretching bands of $>CH_2$ respectively.[592] The peak at around 1378 cm^{-1} could be due to the C-H bond bend adjacent to a carbonyl group.[593] There are peaks at around 1160 cm^{-1} and 1059 cm^{-1} which could be due to the C-O stretch from any phenolic and sugar molecules that were extracted.[594, 595] The 1738 cm^{-1} peak is C=O stretching of esters[596, 597] and the peak at 1711 cm^{-1} may also be attributed to the ketone and carboxylic acids[597, 598] of wheat straw wax.[548]

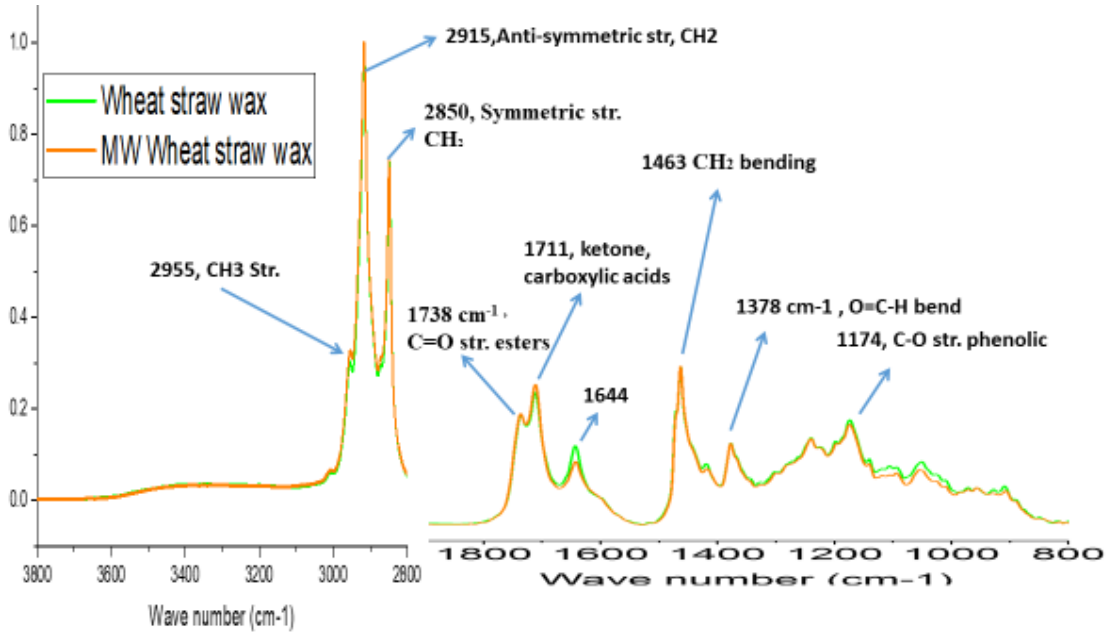

Figure 92 Comparison of ATIR spectra of wheat straw wax and MW-exposed wheat straw wax.

4.6.2 MW Pyrolysis of Wheat Straw Wax Coated Cellulose

A batch of wheat straw wax was solubilised in EtOH and mixed with cotton microcrystalline cellulose (4% mass of wax with respect to cellulose) and dried then dried to remove solvent traces. Another batch of cellulose was also treated using the same condition but without wax. The samples were then transferred into 10 ml of microwave reaction vessels. The method

conditions used for MW pyrolysis (CEM discovery microwave) were as follows: closed vessel, 150W power (fixed), maximum temperature 300 °C and total hold time of 3 minutes. Three replicates of every experiment were used. In Figure 93, two sets of samples are shown after MW pyrolysis. The top set of images shows samples derived from the original cellulose and bottom set is the 4% wax-cellulose samples. It is noticeable that the pure cellulose samples were better pyrolysed. MW pyrolysis kinetic traces of temperature/time (T/t) (left) and pressure/time (P/t) (right) are shown in Figure 94. The mean of all cellulose samples is represented as a black line (the broken grey lines represents error) with the waxed-cellulose samples corresponding to the red trace. The rise of temperature in terms of time was almost similar in both cellulose and wax-coated cellulose samples, although the wax-coated cellulose samples reached slightly higher temperature plateau than cellulose samples on the T/t plot. However, the pressure trend of wax-coated samples was comparatively lower.

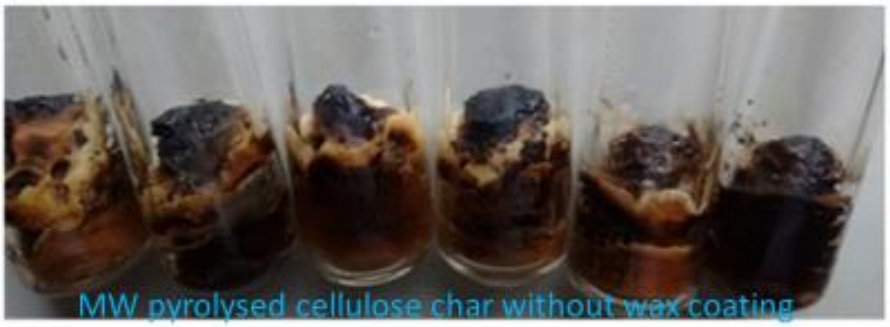

Figure 93 The physical appearance after pyrolysis of cellulose and wax-4% cellulose.

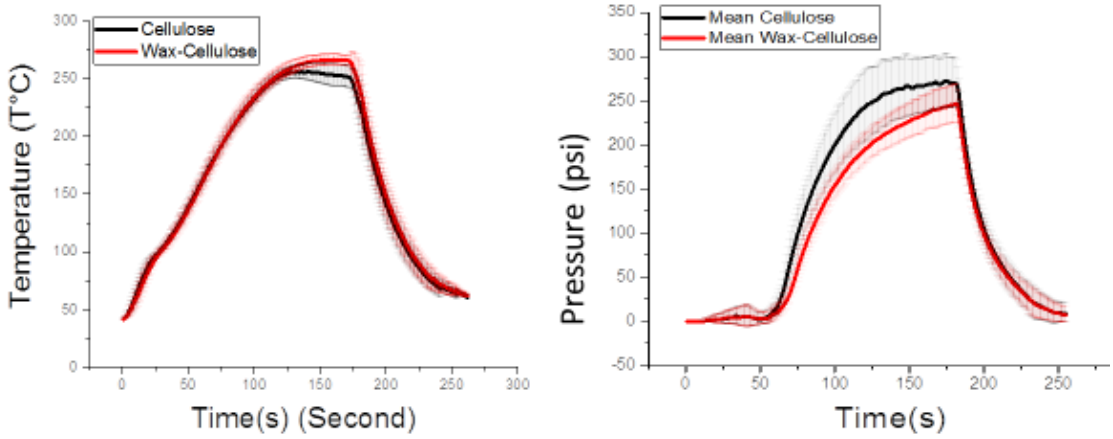

Figure 94 Comparison of cellulose and waxed-cellulose MW pyrolysis kinetics as T-t (left) and P-t (right).

The volatile compound production rate was used as an indicator to compare the influence of wax on MW pyrolysis of cellulose. The pressure vs temperature trends for cellulose and waxed-cellulose samples are presented on the left-hand side of Figure 95 for comparison. The P/T indicates an increasing pressure trend which was suppressed when cellulose was coated with wax, demonstrating that wax inhibits the pyrolysis process, hence the production of gas. The mean of dT/dt of cellulose samples and wax-cellulose samples are plotted against temperature (T) on the right-hand side of Figure 95 to visualise the comparative slope of temperature acceleration. Two distinct peak maxima appeared on (dT/dt)/T trend of both sample types. The first peak at around 70 °C was due to the presence of water. The temperature acceleration at around 70 °C was due to heating up of dipolar water molecules.[599] At about 160 °C to 180 °C range, the second peak of (dT/dt)/T appeared on both sample types, indicating the start of cellulose pyrolysis (Figure 95). The waxed and non-waxed cellulose sample's temperature acceleration trend is very similar after 110 °C, although the rate of temperature deceleration of waxed-cellulose sample is slower as the natural heat-capacity of wax makes the waxed cellulose sample temperature deceleration more time-consuming.

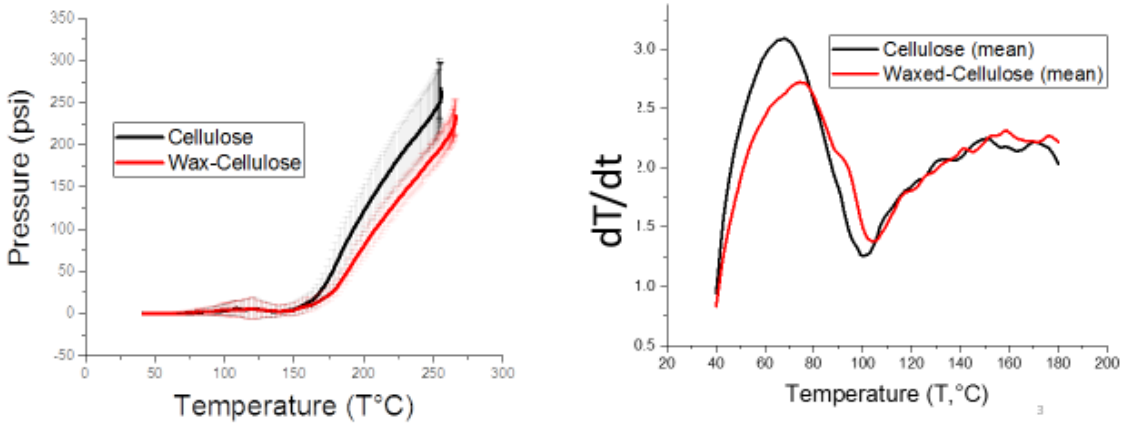

Figure 95 Comparison of cellulose and waxed-cellulose pyrolysis kinetics as P-T (left) and (DT/t)-T (right).

The dP/dt versus temperature is plotted in stack form for both cellulose and waxed-cellulose sample sets to observe the acceleration rate of volatile products during MW pyrolysis reaction progression (Figure 96). A mean comparison of (dP/dt)/T of all of the cellulose samples and cellulose–waxed samples is also constructed in Figure 97. By observing both of the stacks and mean data sets in Figure 96 and Figure 97, it was revealed that the rate of volatile production (measured as dP/dt) from cellulose was higher and occurred at a comparatively lower

temperature range (173°C peak maxima) than wax-coated cellulose samples where the dP/dt maxima were at 185°C. The kinetic trends of both sets of data in Figure 97 indicate that the rate of volatile compound production could be reduced by protecting the material with bio-derived wax and wax esters.

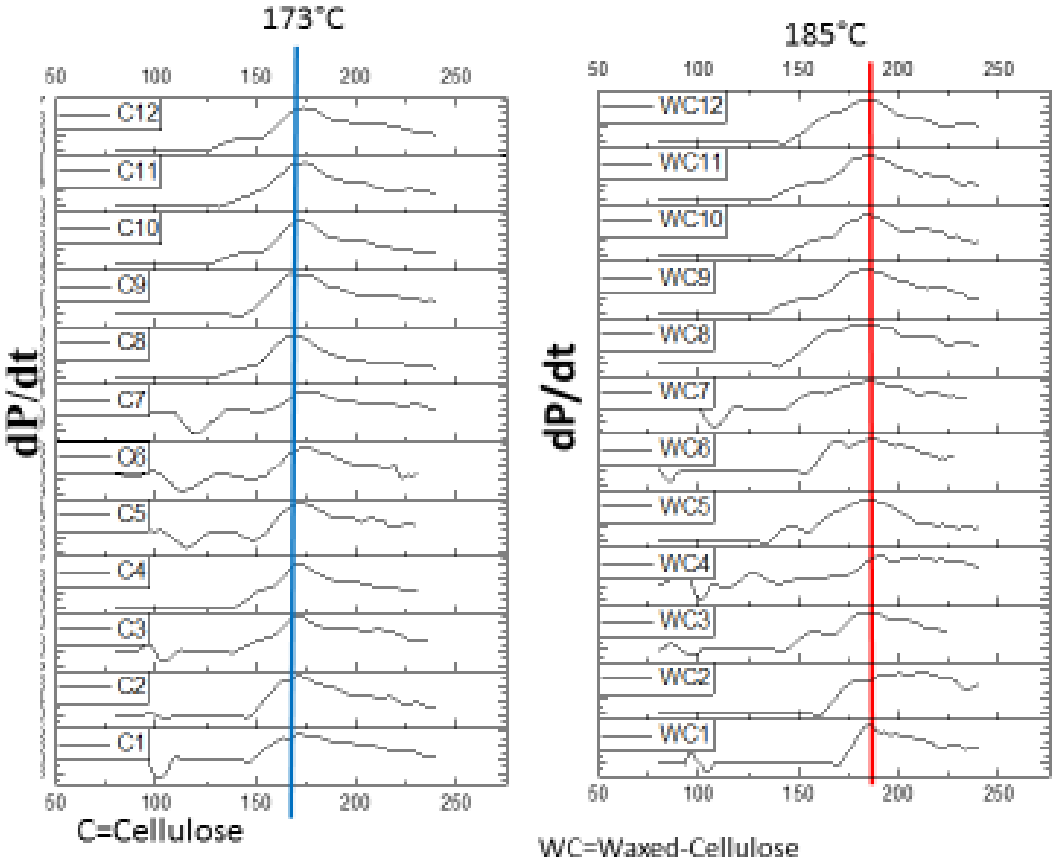

Figure 96 Comparison of MW Pyrolysis kinetics as (dP/dt)-T of cellulose (left) and waxed cellulose (right).

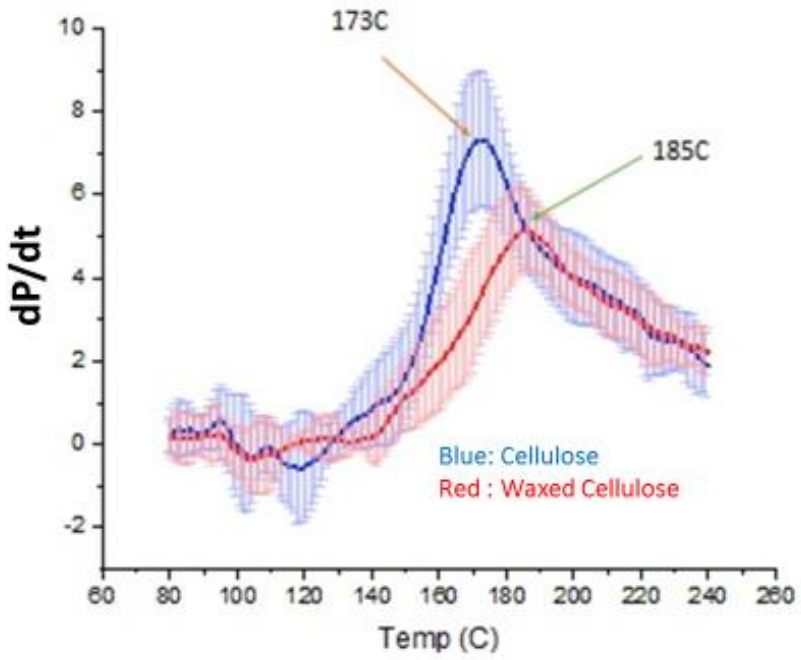

Figure 97 DP/T comparison of Cellulose and Wax samples as a mean of all samples.

All of this evidence supports the hypothesis that lipid interferes MW pyrolysis process of polysaccharides components of wood. From the systematic analysis of kinetic traces, mass balances data, it is strongly suggested that a small portion of extractive could significantly influence on microwave-inductive behaviour of forest waste. It has been proved that wax and wax ester protects biomass by reducing the rate of pyrolysis. This observation opens a new venue to control MW assisted pyrolysis of forest waste by removing or adding extractive components. So far, there is no published article has been found on this interesting MW protecting feature of wax. But in a recent paper, it was suggested that CH_2OH group of amorphous region of microcrystalline cellulose preferentially interact with MW to transfer activation energy from surrounding water molecule to depolymerize cellulose.[600] As those CH_2OH groups are enclosed in cellulose cavity, it can be hypothesised that the availability of water molecule may be repellent by the wax layer of Scots pine bark's outer cell wall.

4.6.3 Mass Balance of MW Pyrolysis Products at 173°C

Another test was performed on cellulose and wax-coated cellulose samples to capture the differences of kinetic trends in a more pronounced way. In this set of MW experimental conditions (fixed power, closed vessel, 150W power, maximum temperature 300 °C and total hold time of 3 minutes) the pyrolysis process was stopped deliberately when the temperature reached 173 °C. The bio-oils were then removed from char using acetone and dried in vacuo, with the spent char being oven-dried overnight at 80 °C. Confirmation of wax and bio-oils removal from char was established by ATIR analysis of wax, char and bio-oils. The result of the experiment was summarised in Table 14.

Table 14 Comparing mass balance of MW pyrolysed cellulose and waxed-cellulose.

System	Wax Yield (%)	Bio-Char Yield (%)	Bio-oil Yield (%)	Bio-gas Yield %
Original cellulose	0	73.7	10.6	15.7
Wax-coated cellulose	4.0	79.6	13.0	7.4
Difference	-	5.9	2.4	-8.3

From the mass calculation, it was found that the production of char from cellulose was 73.7% while the waxed-cellulose char conversion rate was 79.6%. As a result, MW pyrolysis conversion rate of cellulose was reduced by 5.9% when 4% of wax was coated onto cellulose. The cellulose pyrolysis bio-oil production from cellulose pyrolysis was 10.54% and oil from waxed coated cellulose pyrolysis was 13%. However, the yield of oil from waxed coated cellulose pyrolysis is likely to contain the 4% wax that was added at the start of the experiment. By subtracting wax content from the bio-oil (13% - 4%), the cellulose wax samples actual bio-oil yield decreased by 1.5%. The loss of gas from cellulose during MW pyrolysis was 15.8%, and in wax-cellulose samples, it was only 7.4%. The production of volatile gases was reduced by 50% when cellulose was coated by wax.

All of those three MW pyrolysis products yields support the evidence that wax interferes significantly with the MW pyrolysis process of cellulose.

4.6.4 ATIR Comparison of Cellulose and MW-Cellulose Char at 173°C

The chars that were obtained after MW exposure at 173 °C, were analysed by ATIR. In Figure 98, the ATIR peaks of MW cellulose char (red line, Figure 98) and MW waxed cellulose char (blue line, Figure 98), pure cellulose (black line) and wheat straw wax's (green line) are all shown in Figure 98. As it can be seen in Figure 98, there are several interesting pyrolysis products peaks in the 1500-1800 cm-1 region.

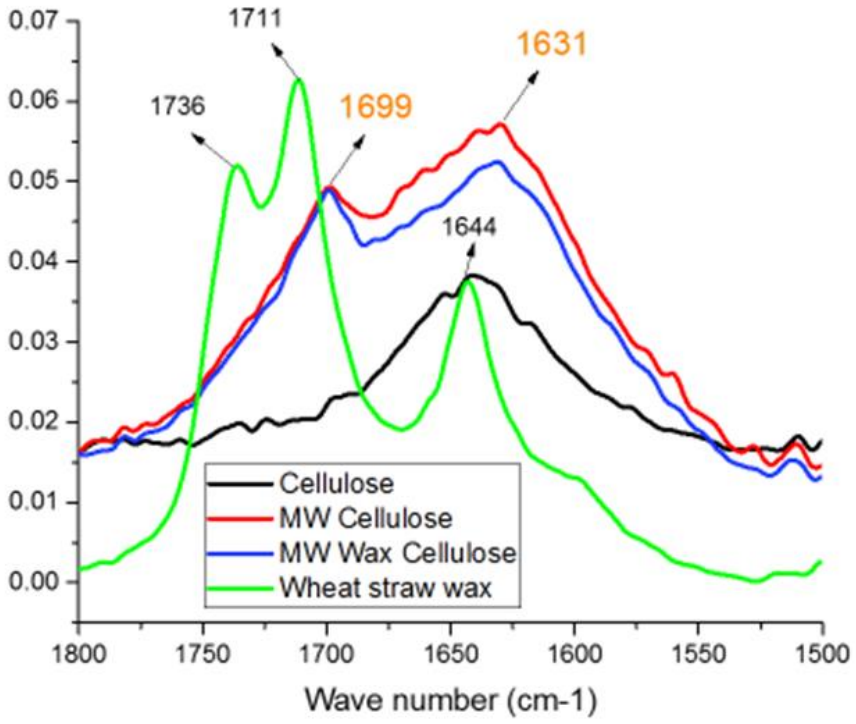

Figure 98 Comparison of ATIR of wheat straw wax, cellulose and MW cellulose char samples The peaks are in the region of 1500-1800 cm$^{-1.}$

The peaks around 1700 cm^{-1} and 1630 cm^{-1} represents characteristics of FTIR bands for pyrolysis products of char.[587] The MW pyrolysis product peak at 1699 cm^{-1} is attributed to C=O stretching of ß–unsaturated aldehydes, ketones and 1631 cm^{-1} is -C=C- stretching of aromatics.[582, 584, 587] Here it is shown that at around 1644 cm^{-1} there is a characteristic peak (attributed to water) in both cellulose and wheat straw wax, but this peak is absent in any MW pyrolysis products. The wheat straw wax also has two more peaks at 1738 cm^{-1} and 1711 cm^{-1}, both of which are absent in MW pyrolysis products of char. The absence of any wax peaks (in Figure 98) in the same region (1738 cm^{-1} and 1711 cm^{-1}) after MW pyrolysis of cellulose, indicates that the char of cellulose and waxed-cellulose are free from wheat straw wax.

4.6.5 Determining the Degree of MW Pyrolysis of Cellulose by ATIR

The degree of structural and chemical conversion of cellulose by MW pyrolysis was calculated as a ratio of the intensities of ATR-IR peaks at 1705 and 1025 cm^{-1}. The deconvoluted peak in the region of 1100-900 cm^{-1} reveals more than two peaks (Figure 99). Pure cellulose has a peak at around 1030 cm^{-1} (pink colour) but does not contain carbonyl peak at 1705 cm^{-1}. After MW pyrolysis, both MW pyrolysed cellulose and waxed cellulose show the distinct carbonyl peak due to the chemical conversion of cellulose (Figure 100). Therefore, this peak was chosen as a characteristic peak of biochar.

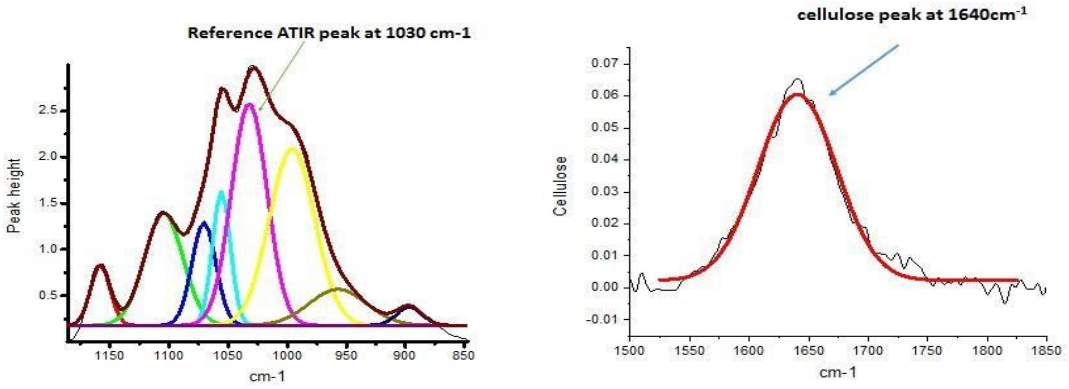

Figure 99 ATIR reference peak deconvolution (left) and cellulose peak at 1640 cm- (right)[1].

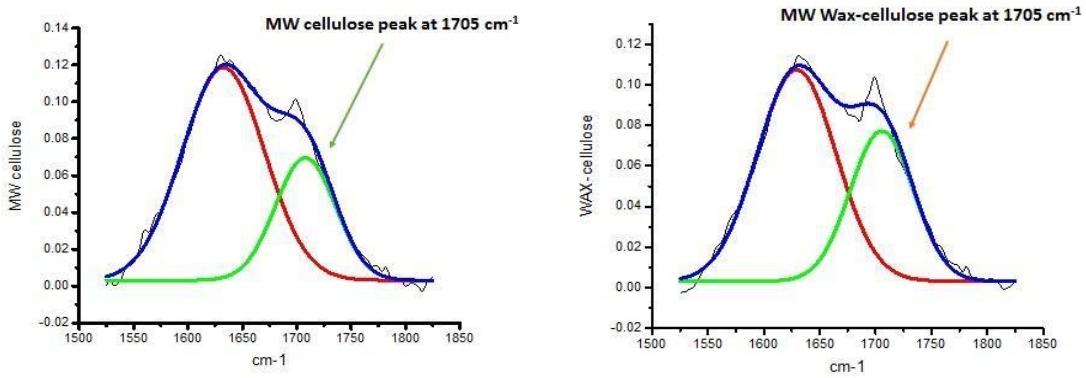

Figure 100 Deconvoluted peak of MW cellulose (left) and MW Wax-cellulose peak (right) at 1705 cm-1.

By dividing the intensity of this non-conjugated carbonyl group with the peak intensity at 1025 cm^{-1}, a scale that can practically measure and compare the degree of conversion of cellulose by pyrolysis is generated. By implementing this scale, it is shown in Table 2 that at 173°C, the presence of wax helped to reduce cellulose conversion significantly.

Table 15 Determination of cellulose conversion rate.

Sample	Peak A 1025 cm^{-1}	Peak B 1 707-1709 cm^{-1}	Degree of Conversion (B/A)*100
Cellulose	**90.8**	**0**	**0**
MW Pyrolysis Cellulose	**90.8**	**4.64**	**5.11%**
MW Wax-Cellulose	**90.8**	**4.05**	**4.5%**

4.6.6 CHN Analysis

CHN analysis was performed on the Scots pine bark large-diameter original sample along with the bio-oil and char that was produced from method A and B. Ash content data was taken from an earlier report of Stanley E. Corder.[549] Oxygen content was calculated as (100-(CHN+ash)). The data is presented in Table 3.

Table 16 CHN data of Scots bark, bio-oil and char.

Sample	C	H	N
Scots bark	50.32	5.76	0.14
FR-01	57.30	6.76	
FR-02	76.09	11.16	0.15
FR-03	56.97	8.27	0.05
Bio-oil-A	60.43	7.86	0.16
Bio-oil-B	51.44	6.73	
Char A	58.03	4.97	0.18
Char B	60.53	4.65	0.18
Cellulose A	45.04	5.78	
cellulose B	46.55	5.75	
Wax A	45.49	5.93	
Wax-B	45.63	5.98	

It can be seen from the table that the carbon content of char obtained from the waxed cellulose is substantially lower than for char obtained from the original cellulose.

All of this evidence supports the initial hypothesis that lipid presence interferes with the MW pyrolysis process of biomass and its major component cellulose.

4.7 Conclusion and Future Work

4.7.1 Conclusion

At the initial stage of the project, fast and inexpensive methods of impurity analysis were designed and developed. The first method was based on NIR spectroscopy and could be used for efficient identification of water and various extractive components within mixed biomass feedstocks. The second approach was based on an innovative modification of TGA methodology, by applying an observed finding that the extractive components significantly influence dTG curves of lignocellulose biomass.

It was established that wax and wax-esters substantially reduced bio-oil yield and proved that the valuable extractives should be removed before MW pyrolysis of lignocellulose biomass. The FT-ATIR of MW pyrolysed cellulose bio-char showed that the presence of a wax coating reduces the production of carbonyl functional group-containing aromatic products of cellulose pyrolysis. It was also shown that wax reduces the bio-oil yield by inhibiting the rate of the pyrolysis process.

The mass balance calculation of MW pyrolysis of cellulose also confirms that the production of gases was reduced by 50% when cellulose was coated with a wheat straw wax.

4.7.2 Future Work

A further calibrated partial least-square (PLS) NIR method needs to be developed for commercially implementing an inexpensive and fast NIR detection method of biomass components, including extractives and water content of forest waste for improving the functionality of a potential biorefinery. The influence of extractives and wax fractions on MW pyrolysis of hemicellulose and lignin also need to be tested in the future.

5 INFLUENCE OF ADDITIVES PHYSICO-CHEMICAL PROPERTIES ON MW PYROLYSIS OF CELLULOSE

As it was shown in Chapter 2, waxes and waxes esters significantly influence on the MW behaviour of the cellulose. It was hypothesised that various physicochemical factors of an added chemical species (i.e. additive) may influence both the initiation and yield of MW pyrolysis and should, therefore, be considered for further study. At the initial stage, a list of parameters which could explain the influence of organic additives on cellulose pyrolysis was proposed. It was presumed that this list has to cover dielectric properties of the compounds (to explain MW interaction with additives), their thermodynamic properties (to explain the additives heating mechanism during pyrolysis), the macroscopic molecular-relaxation time (τ) of the additives and some chemical characteristics such as polarity, acidity and molecular weight.

5.1.1 Influence of Additive-Cellulose Mass Proportion on Bio-oil Yield

To find out the optimum amount of additive which should be used in the investigation of the cellulose-additive experiments, α-pinene and glycerol were initially used to coat with cellulose at 10 wt%, 30 wt% and 60 wt% loading. 10% of additive-coated cellulose was found to produce the maximum amount of bio-oil after MW pyrolysis (*Figure 101*). The reason for choosing those compounds was discussed in the relevant literature review.

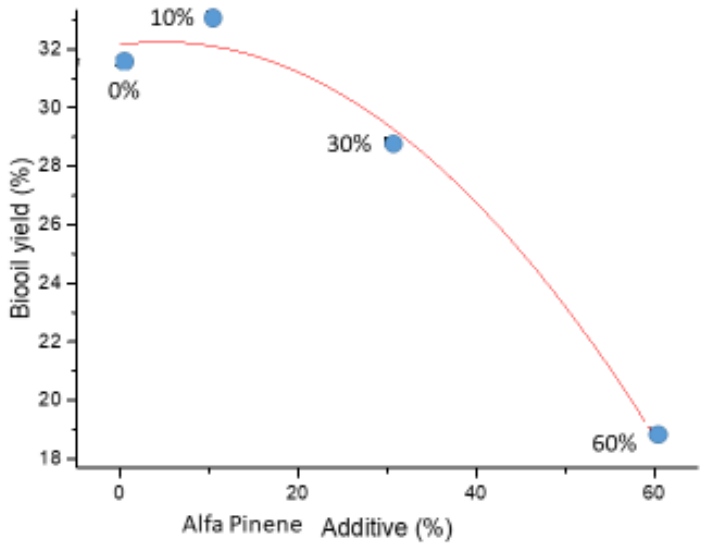

Figure 101 Influence of α-pinene addition on bio-oil yield

5.1.2 MW Pyrolysis of Cellulose under the Influence of Selected Additives

The amount of bio-oil and solid char resulting from MW pyrolysis of cellulose coated with various additives, in addition to the pyrolysis yield are shown in Table 17.

Table 17 Pyrolysis yield of cellulose under the influence of additive

10% additive	Water free biooil %	Yield	
		Solid residue %	Biooil %
Abietic acids	24.03	68.02	31.98
Tetradecane	28.66	61.86	38.14
Water	29.02	61.39	38.61
Linolieic acid	31.02	58.72	41.28
Isoprene	31.24	58.43	41.57
Wheat straw wax	31.49	58.11	41.89
No additive	31.56	58.00	42.00
Docosane	31.75	57.76	42.24
Pinene	33.17	55.86	44.14
Hentriacontane	33.75	55.09	44.91
Glycerol	34.08	54.65	45.35
1,3-propanediol	39.42	47.54	52.46

The biooil of additive-free cellulose sample (no additive sample, Table 17) was tested for water content. Water content test was determined by Karl-Fisher method. It was found 10% of water was contained in the obtained biooil. The production of gas was calculated by subtracting the pyrolysed sample weight from the prepared sample before MW pyrolysis. The residue was calculated after removing extractives with hot EtOH and then oven-dried during an overnight at 105°C. The yield of pyrolysis was determined by subtracting the yield of solid residue from the sample before MW-pyrolysis. The errors in the calculation of the amount of solid residue and bio-oil were around 1% and 1.5% (all experiments were conducted in triplicate). The yield of pyrolysed solid residue calculation was more reliable than the bio-oil calculation.

From the right-hand column of Table 17, it is understood that the yield of pyrolysis could be increased or decreased depending on the identity of the specific extractive additive used. The amplitude of these changes was found around 24%. GC-FID and GCMS analysis were performed to investigate the composition of the bio-oils. From the GC-FID analysis (*Figure 102* and *Figure 103*), it was found (based on comparison with the retention time of the standard compounds) that the major products are 5-hydroxymethyl dihydrofuranone and Levoglucosan. The production of 5-hydroxymethyl dihydrofuranone was determined to be more than 30%

from cellulose-glycerol sample compared to cellulose-abietic acid, for example. However, in the case of cellulose-glycerol, the product levoglucosan was converted into levoglucosenone.

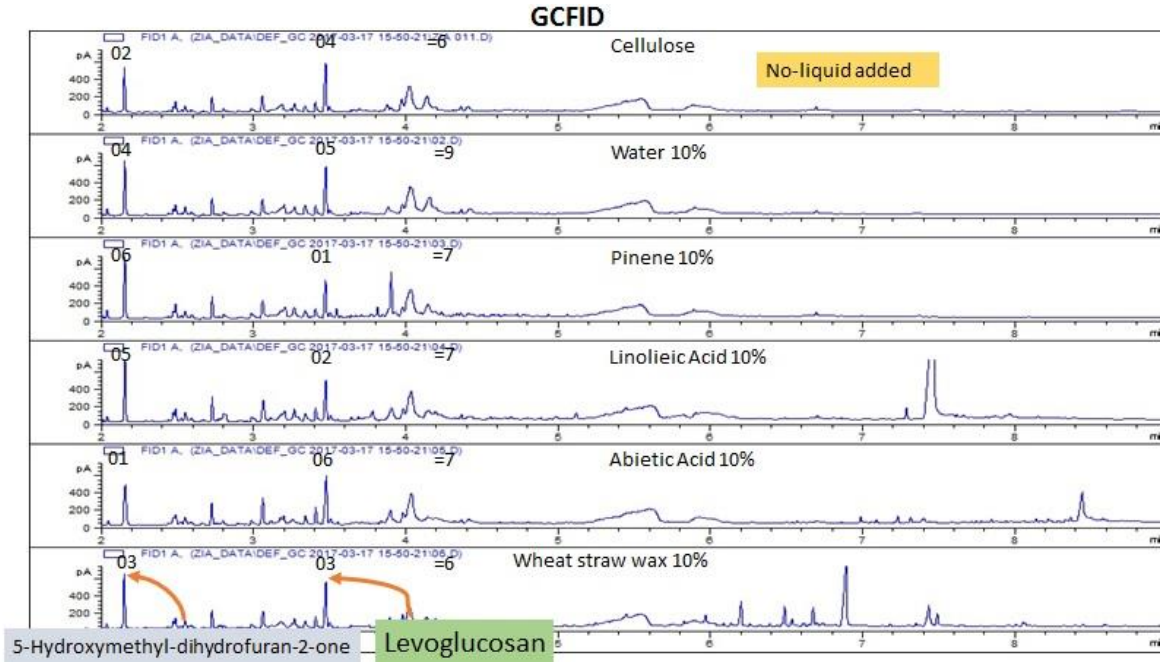

Figure 102 GCFID of some cellulose-additives including water

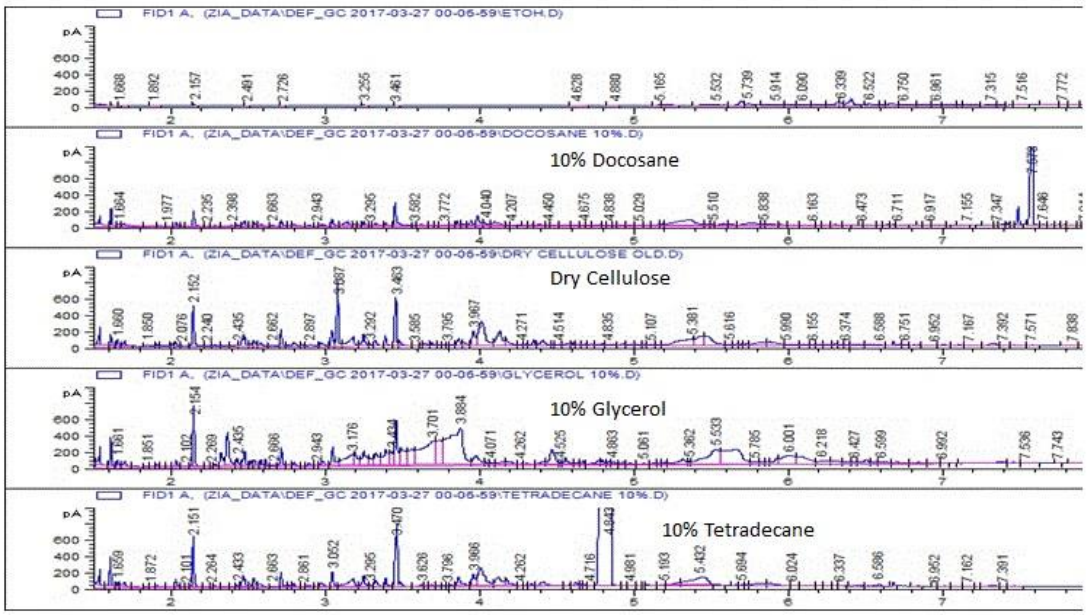

Figure 103 GC-FID of some higher alkane and Glycerine

A conclusion may be drawn from this investigation that additives of organic liquids play an essential role in the MW-assisted pyrolysis of cellulose and significantly change yield and composition of obtained bio-oil. The effect of additives is not apparent: some of them improve the bio-oil yield, while some other additives reduce the bio-oil yield. A balanced proportion of liquid additive or solvent is needed to produce targeted high-value chemicals from cellulose.

5.1.3 Influence of Additives on Conventional Pyrolysis

The MW-assisted pyrolysis of cellulose in the presence of organic additives was compared with the conventional pyrolysis. For this purpose, 10% additive coated cellulose samples were thermogravimetrically analysed with an STA-625 at the temperature range of (20°C to 600°C). The obtained results were compared with TGA of original microcrystalline cellulose. The dTG curves of 1,3 Propanediol coated cellulose, microcrystalline cellulose and abietic acid-coated cellulose are shown in *Figure 104*.

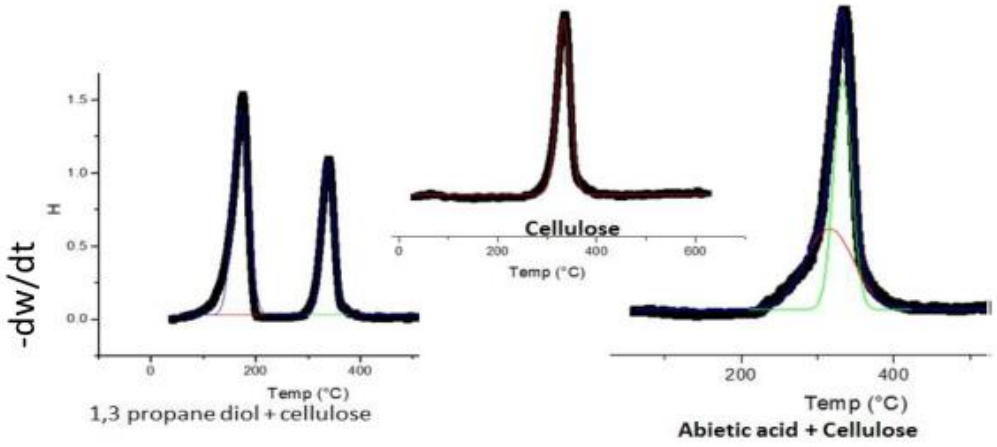

Figure 104 STA analysis of 1,3 Propanediol covered cellulose (left), Cellulose microcrystal (middle) and Abietic acid-coated cellulose

In all of the cases, cellulose decomposed at approximately 333°C independently from the additives nature. Moreover, the additives also do not change the degree of cellulose pyrolysis. This finding suggests that, although a significant impact of additive on MW pyrolysis of cellulose was established, such influence was not observed in conventional cellulose-additive pyrolysis experiments. It stresses the fact that organic liquids/solvents interact with cellulose only during MW-assisted pyrolysis.

A systematic investigation was performed with multivariate chemometric analysis on the organic liquids variance (physicochemical properties) to gain a further understanding of the influence of organic liquids on MW pyrolysis of cellulose.

5.2 Chemometric Select of Additive Parameters which on MW Pyrolysis

5.2.1 Chemometric Analysis

The advantage of various multivariate chemometric data analyses was already demonstrated in section 2.4.2. The theory of one chemometric method, PCA, was explained particularly in section 2.4.2.2. PCA is one of the main ways to reduce the dimension of data by losing the least amount of information. Here another multivariate analysis, principal component regression

(PCR) and some related terminology will be addressed in brief before discussing the extent to which the aforementioned physicochemical factors influence cellulose MW pyrolysis.

5.2.2 Influence of Molecular Weight

A list of organic solvent, liquids and some wood extractive components were selected for evaluating any existing interrelation among molecular weight, specific density and dielectric constant with multivariate PCA data analysis. The aforementioned physical parameters values were collected from various sources and are shown in *Table 18*. The dielectric values and densities displayed in *Table 18* were calculated at room temperature. All other physical parameters mentioned in this section are added in a separate table in the appendix-A (Section 10.2). The database used for collecting relevant data are from ACD labs, NIST physical parameter depository. Dtherm, ChemSpider and ChemAxion through CDS National Chemical Database Service. Some data were collected from wave sites listed in the references.

Table 18 The molecular weight, specific density, dielectric constants of various solvents, organic liquids and wood extractives (*) at room temperature.

Name	Molecular Weight (g/mol)	Specific density gcm^{-3}	Dielectric Constant (Fm^{-1})
Cyclohexanol	100.16	0.96	15
1,2-Propanediol	76.1	1.033	32
Ethylene glycol	62.068	1.1	37.7
Ethylene glycol	62.07	1.111	37
3-Methylphenol	108.14	1.03	11.8
Benzyl alcohol	108.14	1.041	13.1
2-Methylpropyl alcohol	74.12	0.797	17.7
Aniline	93.13	1.018	6.89
Formamide	45.04	1.129	84
2-Butanol	74.12	0.805	15.8
1-Butanol	74.12	0.806	17.1
Propyl alcohol	60.095	0.8	21.8
2-Propanol	60.1	0.783	18.3
Morpholine	87.12	0.997	7.33
Cyclohexanone	98.14	0.942	18.3
1-Propanol	60.1	0.802	20.1
Acetophenone	120.15	1.024	17.39
Methanoic acid	46.03	1.214	58
Benzaldehyde	106.12	1.04	17

1,2-Dichlorobenzene	147	1.301	9.93
Benzonitrile	103.12	1.001	26
1,4-Dioxane	88.11	1.029	2.209
Ethanol	46.07	0.787	24.3
Acetic acid	60.05	1.043	6.15
Decane	142.3	0.7	2
Tetrachloromethane	153.82	1.583	2.2
Cyclohexane	84.16	0.773	2.015
Pyridine	79.1	0.979	12.3
1,1,1-Trichloroethane	133.4	1.33	3.4
1,2-Dichloroethane	98.96	1.246	10.36
o-Xylene	106.17	0.876	2.568
Styrene	104.15	0.9	2.43
Butyl acetate	116.16	0.876	5.01
2-Methyl propyl	116.16	0.869	5.6
Nitromethane	61.04	1.129	39.4
Ethylbenzene	106.17	0.865	2.412
Benzene	78.11	0.873	2.274
p-Xylene	106.17	0.861	2.27
Toluene	92.14	0.865	2.379
Trichloroethylene	131.39	1.458	3.4
Trichloromethane	119.38	1.48	4.806
Propyl acetate	102.13	0.883	6.3
Methanol	32.04	0.787	32.63
Ethyl acetate	88.11	0.894	6.02
Dichloromethane	84.93	1.318	9.08
2-Butanone	72.11	0.799	18.5
n-Heptane	100.2	0.682	2.05
Acetonitrile	41.05	0.779	37.5
Methyl acetate	74.08	0.927	6.68
Acetone	58.08	0.786	20.7
Diethyl ether	74.12	0.708	4.335
**Isoprene	68.117	0.7	2.1
*Alfa Pinene	136.24	0.9	2.7
*Tetradecane	198.39	0.8	2
*Docosane	310.61	0.8	2
*Hentriacontane	436.84	0.8	2

*1, 3 propane diol	76.094	1	32
*Glycerol	92.09	1.3	42.5
*Linoleic Acid	280.45	0.9	2.9
*Abietic Acid	302.46	1.1	2.5

To explain the operational procedure and advantage of PCA the spatial position of the compounds listed in *Table 18* could be shown in three-dimensional space by taking the molecular weight, specific density and dielectric constant as the X, Y and Z axes. The absolute values of molecular weight, specific density and dielectric data are preprocessed and then normalised with mean centred and standard deviation scaling (SVD) before being projected into the three-dimensional coordinate of *Figure 105*. In *Figure 105*, the blue points are the position of the solvent in the generated three-dimensional space. However, as the data points were mean centred, the coordinate X, Y, Z (0,0,0) is moved from the initial coordinate position of *Figure 105*A (orange coloured) to the centre of the *Figure 105*B data cloud.

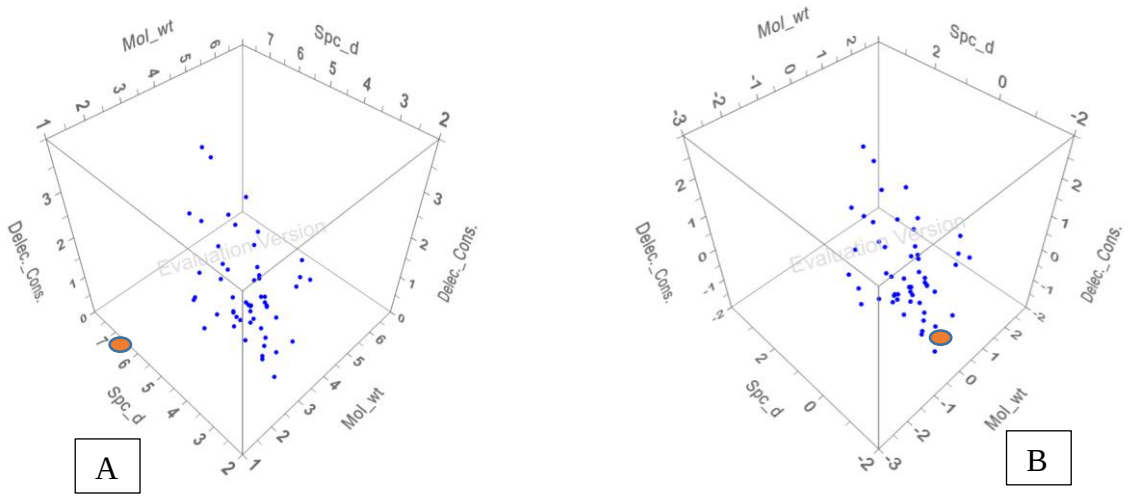

Figure 105 Spreading molecular weight, specific density and dielectric constant data into three-dimensional space. The orange point represents X, Y, Z (0,0,0) coordinates at left-hand side (A) before data centring. After mean-centring of the data, it is moved into the centre of the data cloud (B).

It is possible to draw an imaginary plane (the light golden plane of *Figure 106*) through all of the blue data points in such a way that the plane maintains a minimum distance from all of the blue data points in the least square fashion. The plane describes what happens in the bulk of the data by capturing the main variation of those data and can be described as the Score plot.

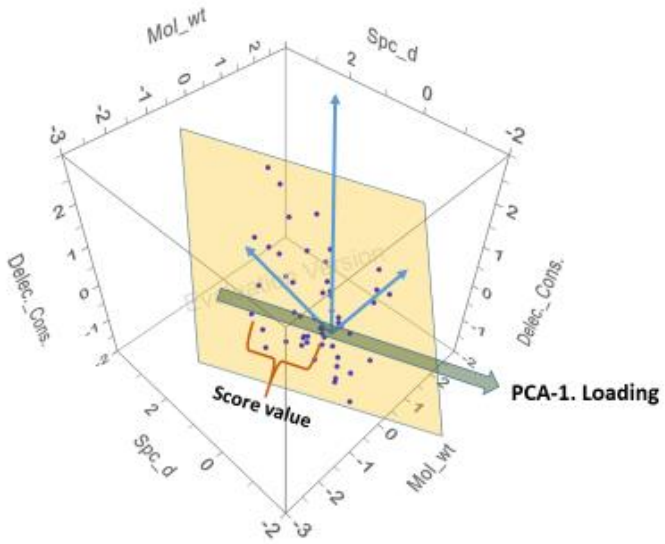

Figure 106 PCA score plot is represented with the light golden plane

The blue lines on *Figure 106* represent the new X, Y and Z axes in the centre of the data cloud. The first loading (PCA-1) of the coloured plane of *Figure 106* runs in the direction with the highest sample variance within the three-dimensional space. The score values are the projection of a particular sample's values on to the loading. If the data projects further out on to the loading, the higher the score value. Depending on the direction, the score can be positive or negative. As the golden plane of *Figure 106* was drawn from only three variables, it can also be represented in two-dimensional space – as shown in *Figure 107*. The biplot of the compounds listed in *Table 18* was constructed in *Figure 107* using the Unscrambler X 10.5.1 software. *Figure 107* is referred to as a biplot because it represents both the samples and variables in the same plane without losing any information concerning the original sample. If the two samples in this plane are very close to each other, it means they have a very similar property with respect to what the plane is describing. If the plane represents most of the variation in the data, then the two samples are indeed very similar. If two samples are oppositely placed in the plane, then those samples are very dissimilar. When one sample is high in a particular variable, then the other one is low and vice versa. In the same way, if the two variables (in this case, molecular weight and specific densities are variables) are very close together and it means they contain more or less same information. If a sample is close to a particular variable, then it means the sample has a high value of that specific variable. In *Figure 107* biplot of dielectric constant, Specific density and molecular weight, the first loading (PC-1) explained 48% of data variation and 34% of the data is explained by PC-2 concerning the orthogonal loading on PC-1 (the table of assigned physicochemical value of the of selected samples are shown in at section 11.2.3 of Appendix-A).

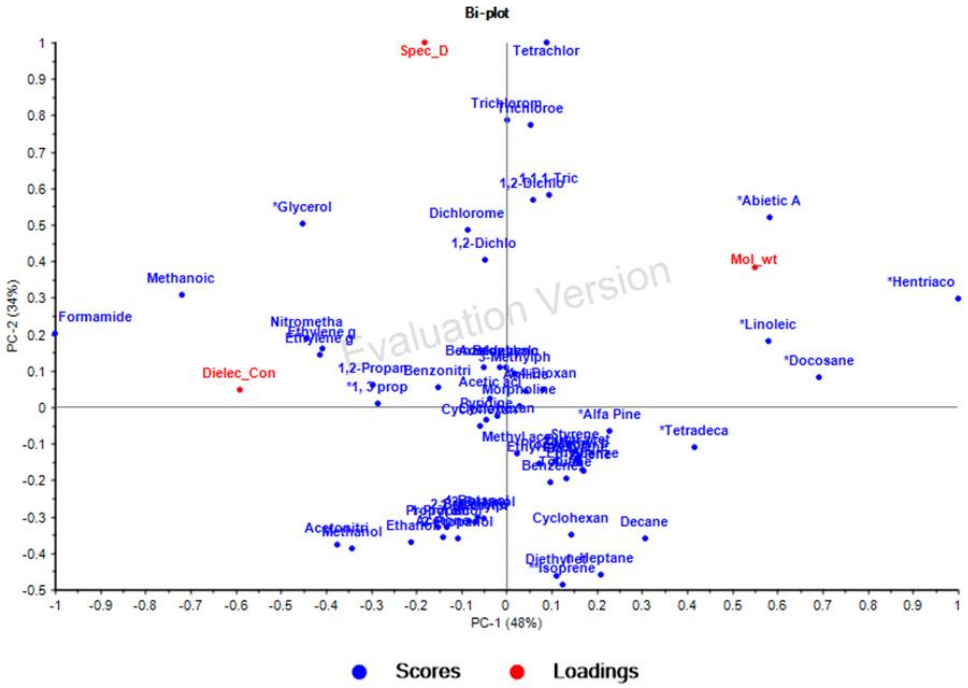

Figure 107 Biplot of molecular weight, specific density and dielectric constant. The score of PC-1 is 48 % and PC-2 is 34 %. Both PC explains 82% of data variation and hence satisfy a correlation among the variables molecular weight, dielectric constant and specific density.

Both PCs together have covered 82% of the variation within the data. Therefore, the biplot of *Figure 107* is satisfactory to examine the correlation among the variable of the data. Since the main purpose of PCA is to the dimensional reduction of multiple variables into a few components of large data set where data points are significantly higher than variables itself, the above-mentioned example (*Figure 105* and *Figure 106*) may not be ideal for PCA operation. In two dimensional space of this paper, it is difficult to show multidimensional space where multiple variables locate mathematically. The description of *Figure 107* was for the simplistic purpose of demonstration how variable and scores location and defines each other's interrelation. If more than three variables molecular weight, polarizability, specific density, dipole moment, relative polarity, dipole moment and dielectric constant is interpreted into two PCs then it would be as *Figure 108* (the table of assigned physicochemical value of the of selected samples are shown in at section 11.2.3 of Appendix-A). Interestingly, both PCA biplot in *Figure 107* and *Figure 108* retains the same interrelation among dielectric constant, specific density and molecular weight. It is noted to mention here that it may not be the case always. Personal understanding and experience of variables of a data matrix are critical in the relation of data interpretation for a specific purpose of such reduction of variables.

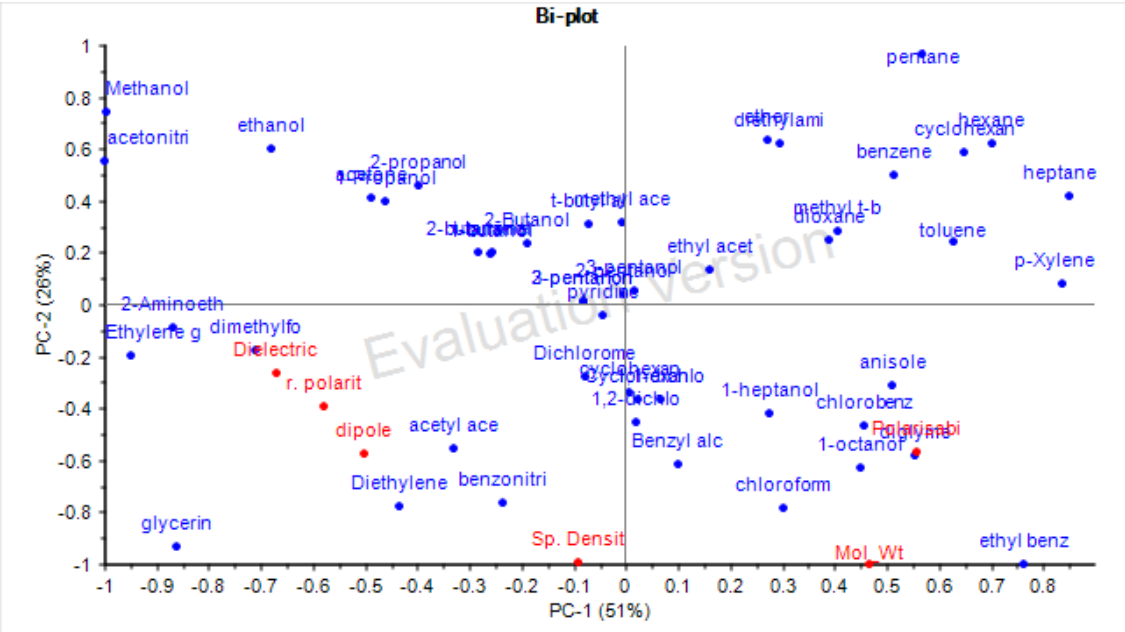

Figure 108 PCA biplot of molecular weight, polarizability, specific density, dipole moment, relative polarity, dipole moment and dielectric constant. Both PC explains 77% of data variation which satisfy more than two-third of data variation, demonstrating, an existing correlation at least among some of the variables.

If each variable is displayed within two-dimensional X-matrix PCA loadings, the position of variables can be seen more clearly in the data structure. The relation of variables in the PCA, as shown in *Figure 109* and is called correlation loadings (X). To indicate how much variance is taken into account in correlation Loadings, two ellipses are drawn on the plot. If the variance falls inside the outer ellipse, then 100% variance is explained in the plot. If the variance position is within the inner ellipse, then this indicates a failure of the PCA plot to explain more than 50% variance. So, the correlation loadings (x) of dielectric constant, molecular weight and specific density in *Figure 109* explain that the PCA biplot of *Figure 107* holds all variances in as such that all three variances are significant enough to explain the sample position in the PC-1 and PC-2 biplot.

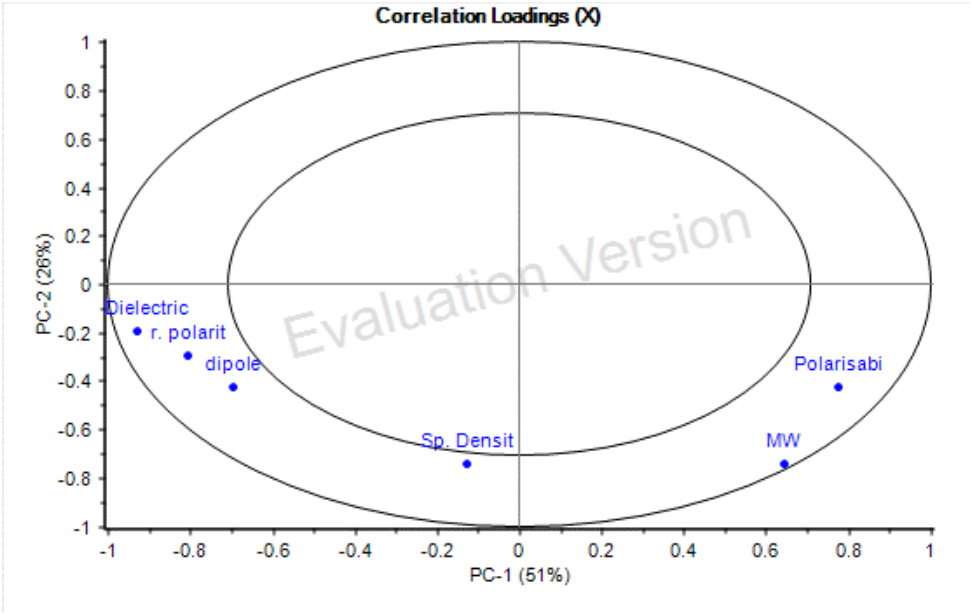

Figure 109 Correlation loadings of molecular weight in respect to dielectric constant and other variables. Since all loadings in between, inner and outer circles, the variables are not random. Depending on the relevant position the PCs, as in the case of dielectric constant, dipole moment and relative polarity explains that they have an inherent strong relation.

Now, it can be noticed in the biplot presented in *Figure 107* that the variance in molecular weight (red coloured-MW) was strongly influenced by higher molecular weight extractives such as hentriacontane and abietic acid (*Figure 110*) (the table of assigned physicochemical value of the of selected samples are shown in at section 11.2.11 of Appendix-A).. Compounds with higher dielectric constant such as glycerol stay more closely to dielectric loadings than molecular weight loadings (*Figure 110*). Compounds with similar molecular weights relative to glycerol but with lower dielectric constants would shift in position within biplot and move closer to molecular weight loadings. Highly dense compounds such as tetrachloromethane stay very close to the loadings of specific density *Figure 110*. All of the denser chloro-molecules are on the orthogonal position of the dielectric loadings, showing indifference to the dielectric property.

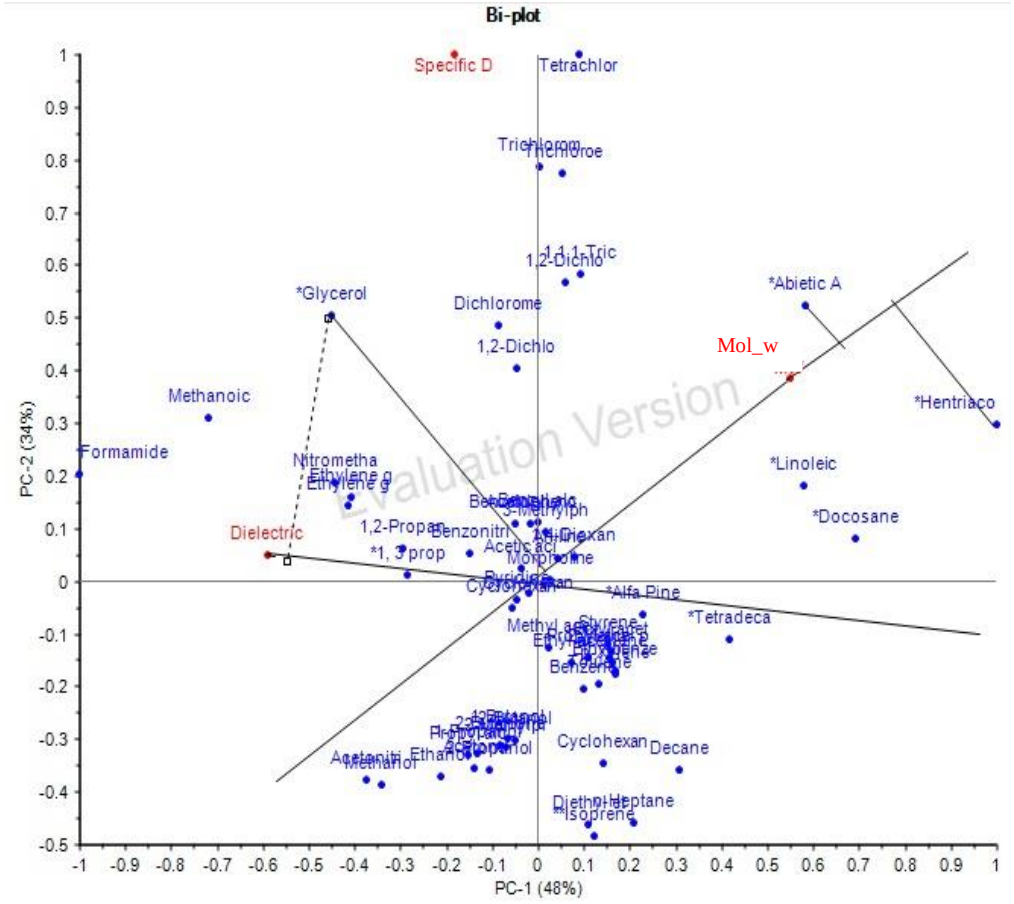

Figure 110 Biplot of molecular weight, specific density and dielectric property with Scores projection into correlation loadings (X) The position of glycerol is closer to dielectric loadings than molecular weight loadings while compounds of high molecular weight such as abietic acid are close by to the Molecular weight loading.

It is already established from the literature that the dielectric property of the solvent is the key factor in the initiation of the microwave pyrolysis of cellulose[247, 252, 599, 601, 602] and the experimental cellulose-additive pyrolysis data also support the same idea as can be seen in the case of glycerol in *Figure 110*. It can now be concluded from the above PCA biplot analysis that the molecular weight of additive cannot alone influence the score plot of the three variables mentioned above. Specific density neither holds any key in the interrelation as it was sketched in *Figure 110*. Therefore, it can also infer that neither specific density nor the molecular weight is an influential factor in the microwave pyrolysis of cellulose or biomass.

5.2.3 Influence of Boiling Point

Some extractive compounds which were coated (10%) on microcrystalline cellulose and subsequently MW-pyrolysed are shown in *Figure 111*. The boiling point and dielectric constant of the compounds (11.2.11 of Appendix-A) along with the bio-oil yield percentage obtained from the MW-pyrolysis products (Table 17) were taken as variables in the biplot of those compounds (*Figure 111*).

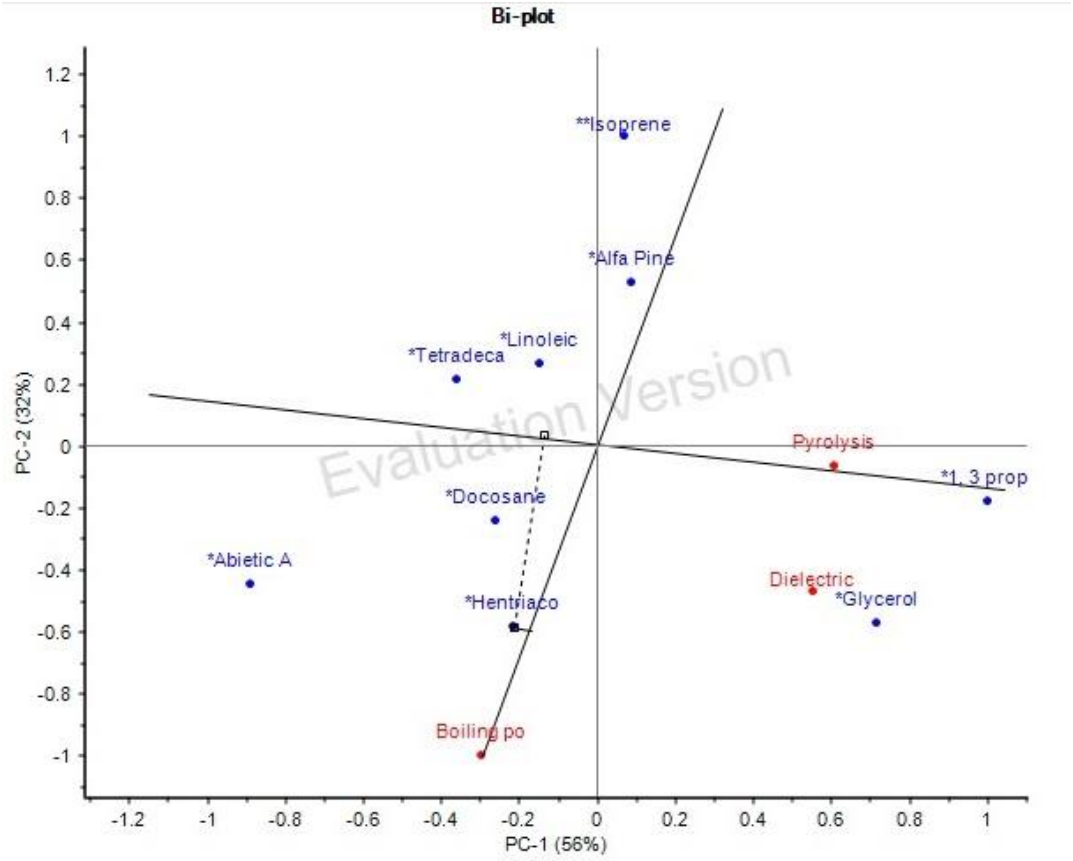

Figure 111 Boiling point, dielectric constant and subsequent biooil yield of various compounds coated microcrystalline cellulose pyrolysis. Considering the position of the organic liquid nearer to specific variable loading, it is demonstrated that higher dielectric property containing compounds are also nearer to the pyrolysis loadings, meaning a correlation of yield of biooil and liquids dielectric property.

From the analysis of biplot of *Figure 111*, it is shown that the boiling point of the samples loading is orthogonal to the yield of pyrolysis loadings. Above information suggests that the boiling points of the extractives do not have any influence on bio-oil production yield from cellulose or from biomass.

5.2.4 Influence of Enthalpy of Vaporisation

In the same way that the boiling point of the additive/solvent appeared not to influence MW pyrolysis. It is shown in *Figure 112* PCA biplot that there is also no direct relation between the enthalpy of vaporisation and dielectric constant (values are at 11.2.19 of Appendix-A). Additionally, neither had any relationship with the yield of cellulose pyrolysis (Figure 113) (values are at section 11.2.9 & Table 17).

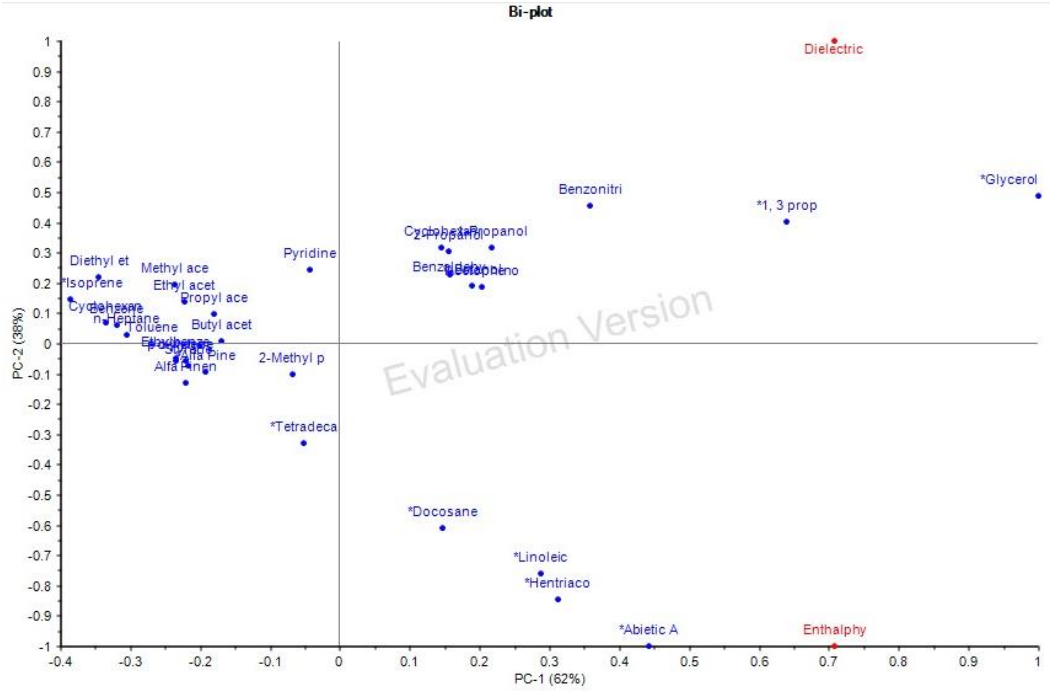

Figure 112 Enthalpy of vaporisation and dielectric constants of selected solvents/additives. The position of scores and loading shows there is no direct relationship between the enthalpy of vaporisation and dielectric constant.

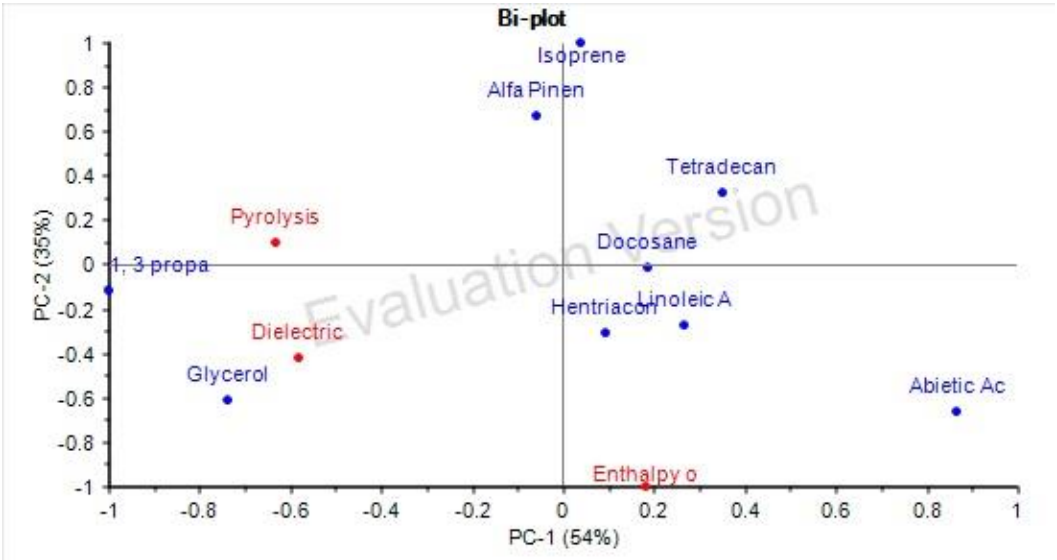

Figure 113 PCA biplot of dielectric constant, pyrolysis and enthalpy of evaporation. Here although Dielectric constant and value of cellulose pyrolysis yield are nearby in the same PC-2, enthalpy is orthogonally situated in the biplot, meaning no direct relation with the other two variables.

5.2.5 Influence of Vapour Pressure

A PCA biplot PC-1(45%) and PC-2 (30%) of vapour pressure, specific density, molecular weight, enthalpy of vaporisation, dielectric constant and viscosity of some additive/solvent are plotted in *Figure 114* (combined table of 11.2.1 & 11.2.10 at Appendix-A). In the correlation loadings of *Figure 115*, it is clearly shown that vapour pressure is placed in the opposite

direction of dielectric constant. The Hotelling T^2 influential plot of the variables and solvents/additives is also seen to be free of outliers or highly influential compounds on the PCs *Figure 116*. In the list of additives that were analysed in *Figure 114* PCA biplot, the boiling point of isoprene is the highest, resulting in its position at the very high end of the vapour pressure loadings.

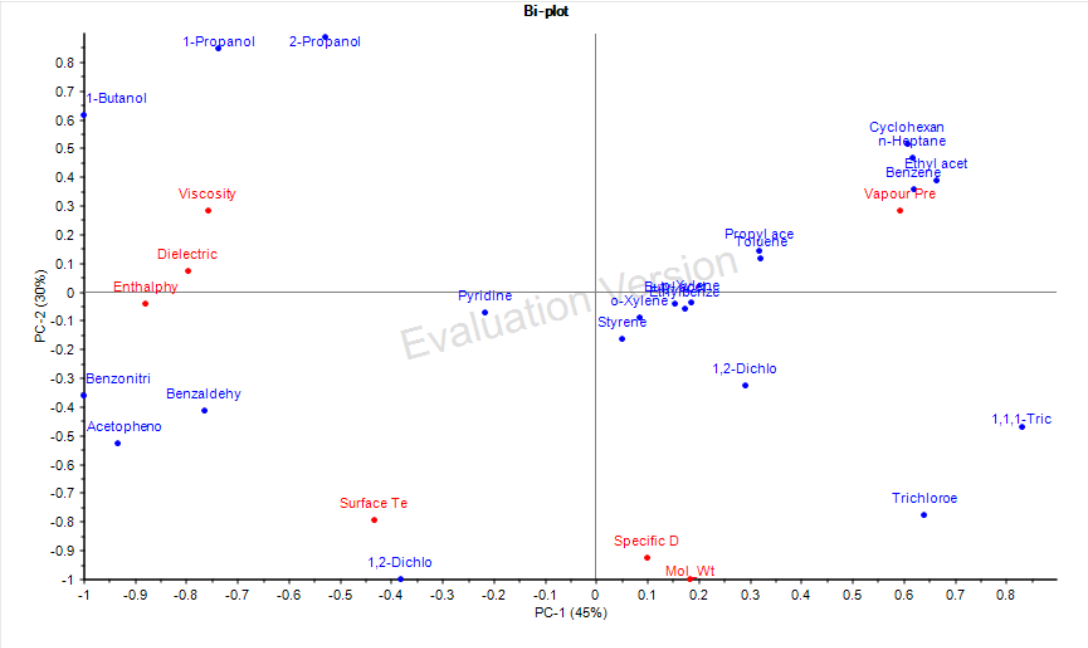

Figure 114 Comparison of vapour pressure variable with specific density, molecular weight, enthalpy of vaporisation, dielectric constant and viscosity in PC-1 and PC-2 biplot. Vapour pressure is placed in the opposite direction of dielectric constant establishing the fact that vapour pressure is showing dissimilar character like all other physicochemical properties in the biplot.

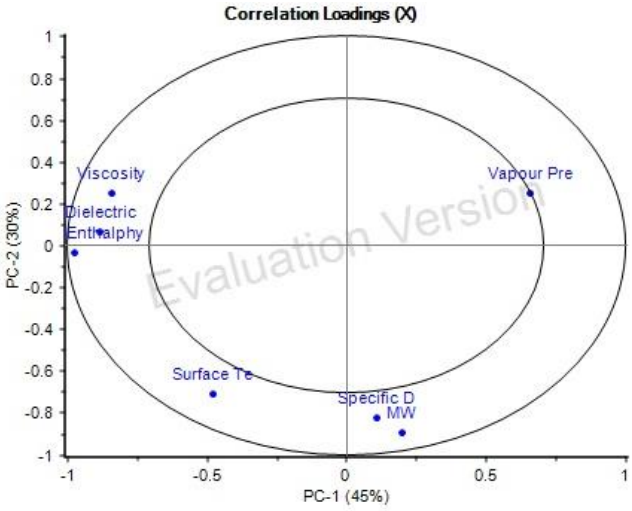

Figure 115 Correlation loadings of vapour pressure, viscosity, molecular weight, specific density, surface tension and dielectric constant at room temperature. Again, like PC biplot, vapour pressure inditates it is not showing more than 50 % satisfactory criteria to fit between inner and outercircle.

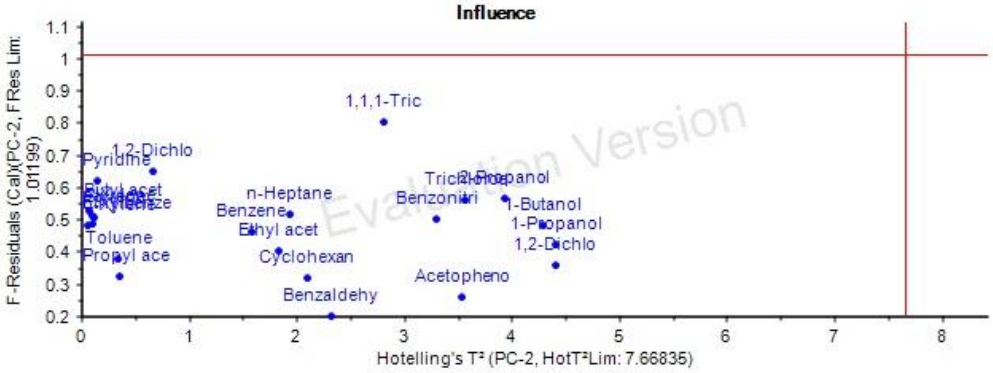

Figure 116 Influence plot of vapour pressure, viscosity, molecular weight, specific density, surface tension and dielectric constant of some organic liquids at room temperature. Since all compounds sit inside the box, there are no compounds in the list which has any extreme property than all other compounds.

The pyrolysis data of Table 17 in Section 3.2.2 already demonstrated that high boiling point isoprene-coated cellulose MW- pyrolysis yield was almost the same as dry cellulose pyrolysis yield. The score and loading position of isoprene in the PCA biplot of *Figure 114*, *Figure 111* and *Figure 113* indicate that isoprene is not correlated with the yield of pyrolysis and dielectric loadings. So it can be strongly express that by increasing or decreasing vapour pressure, the MW-pyrolysis of cellulose or biomass could not be controlled.

5.2.6 Thermal Conductivity and Specific Heat

The biplot of thermal conductivity and specific heat of solvent/additive is somewhat unusual (*Figure 117*) as both the loadings describe a similar correlation in the samples (combined table of 11.2.1&11.2.7 in Appendix-A).

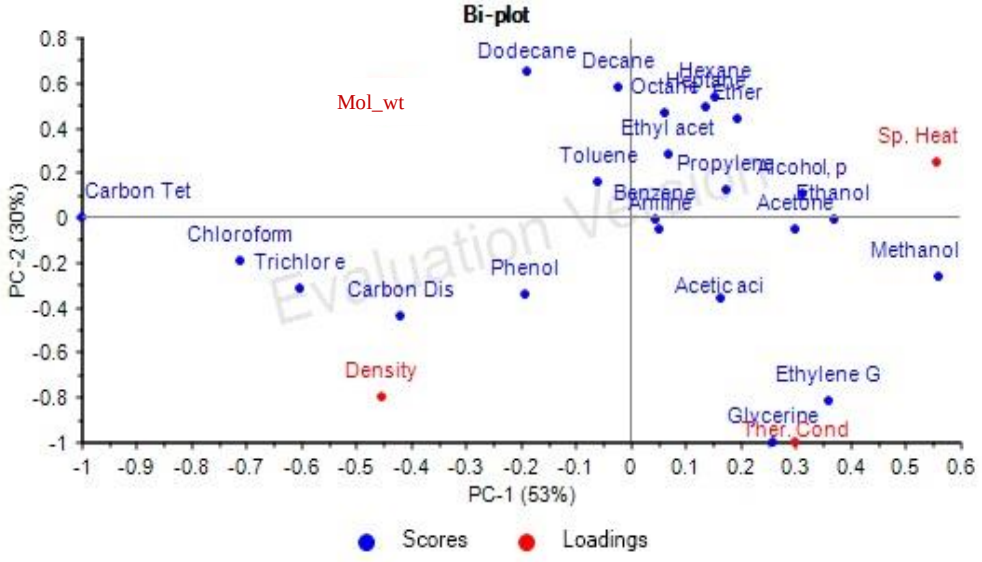

Figure 117 Biplot of thermal conductivity, specific heat, density and molecular weight. In the biplot, thermal conductivity and specific heat do not have strong relationships directly correlate.

It is also worth noting that the density and specific heat loadings are in opposite directions, which mean that having a dense compound does not guarantee to hold high specific heat inside a sample.

5.2.7 Relation of Viscosity, Surface Tension and Density

As was described in the introduction of section 3.1 (*Figure 118*), the relationship between surface tension and viscosity appears to be somewhat unclear. The only equation that was used to explain the link between surface tension and viscosity (*Equation 4*) cannot well explain a complex liquid system such as the mixed extractive system contained within the wood. A linear equation of natural log of surface tension and the inverse of the viscosity of 50 randomly chosen solvent data point after excluding outlier is shown in Figure 118 (from the table of 11.2.6 of Appendix-A). The regression of this equation gave a very poor result and it was not possible to satisfy any relation between either of the variables mentioned above. The fact of this failure is that the solvents used here contain various functional groups, unlike only the alkane liquids that were used to construct *Equation 4*.

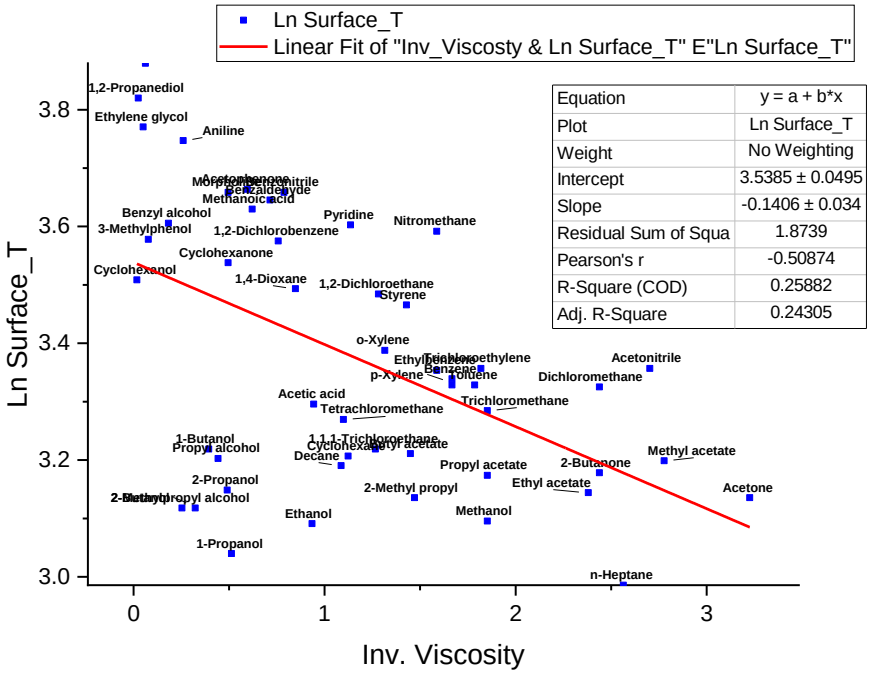

Figure 118 Plot of Ln of surface tension vs. the inverse of viscosity (m2/s). The R-squared value indicates the simple relation of viscosity and surface tension is not applicable to a diverse range of molecules.

However, if the density is related to the equation of surface tension and viscosity, the problem of poor relation of viscosity and surface tension could be better handled. A PCA of viscosity, surface tension and density is depicted in *Figure 119* (11.2.6 of Appendix-A). The biplot of PC-1 and PC-2 (*Figure 119*) explains 93% of the variation within the data matrix. All of the three

correlation loadings were found to be on the same side of the PC-1, which explains 68% of variations of the data matrix. The correlation loadings of density, surface tension and viscosity also support the fact that all of the variables contain the intrinsic information required to explain the data variation in the PCA plot of *Figure 119*.

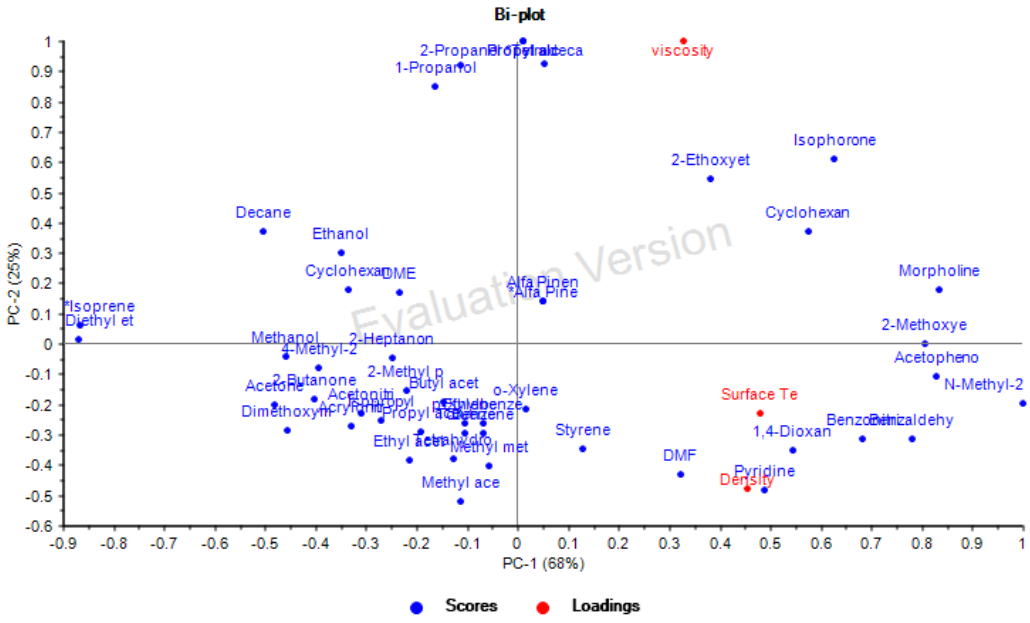

Figure 119 PCA biplot of viscosity, surface tension and density. The biplot of PC-1 and PC-2 (Figure 119) explains 93% of the variation within the data matrix. The correlation loadings of density, surface tension and viscosity indicates a strong intrinsic relation.

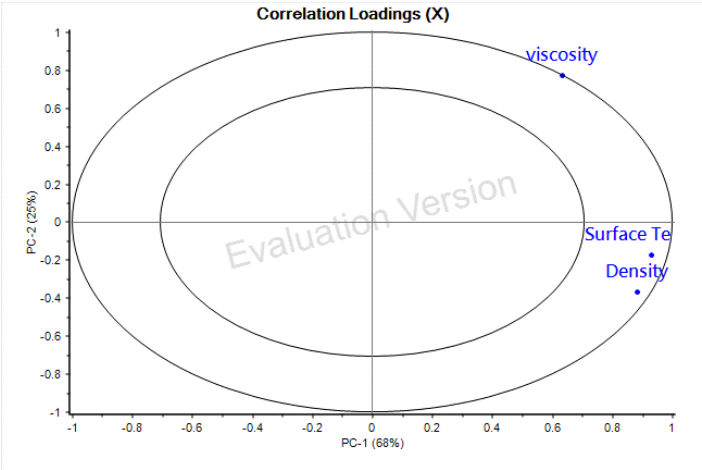

Figure 120 Correlation loadings of viscosity, surface tension and density. The position of viscosity is on the edge of 100%, which means the data set had the best correlation with viscosity.

The position of viscosity is on the edge of 100%, which means the data set had the best correlation with viscosity. A PCR of the three variables (density, surface tension and viscosity) is drawn in *Figure 121* and *Figure 122* shows an unexplained residual after the second principal component is taken into account. *Figure 121* and *Figure 122* highlight the fact that both the calibrated data (blue line) and validated data are representative of the variance and the data

matrix. While the PC3 explains 100% of the data variation, PC-2 can satisfy up to 93% of the variations in the data.

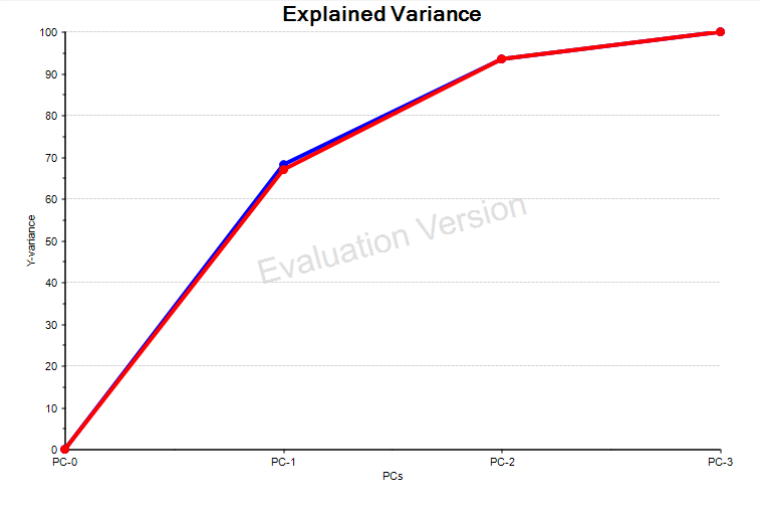

Figure 121 Explained variance of viscosity, surface tension and density. The calibrated data (blue line) and validate data within PC3 explain 100% of the data variation, PC-2 can satisfy up to 93% of the variation. The result indicates there is no random behaviour of all variable for any data they contain..

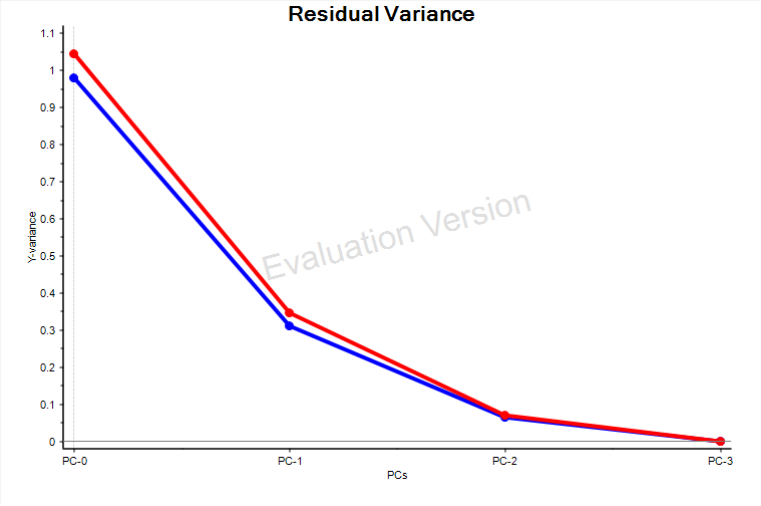

Figure 122 Unexplained residual variance of viscosity, surface tension and density. After PC-3, there is almost no residual value remains explaining a significant agreement among the variables.

The calibration versus validation of viscosity PCR data shown in *Figure 123* suggests that the quality of the regression model is a perfect fit. The slope of the regression is above 0.995 by cross-validation. The predictive information of viscosity through surface tension and density is a completely new insight to the best knowledge of this author. However, to further validate this new idea, a broader data set is needed. This newly established relationship could be beneficial in any future research in this subject matter and beyond.

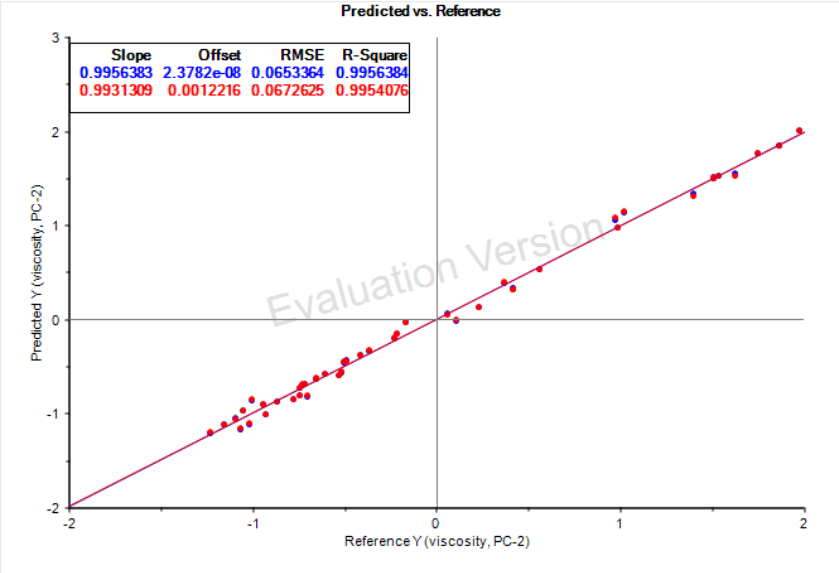

Figure 123 PCR of viscosity at PC-2. The calibration versus validation of viscosity of PCR data suggests that the quality of the regression model is a perfect fit.

5.2.8 Influence of Viscosity, Surface Tension and Density

It may be fruitful to identify the influence of one variable over others which are interrelated like in this case of surface tension, viscosity and specific density PCA, and the best way to achieve such a goal is via an influence plot that is based on Hotelling T^2 statistics. *Figure 124* shows a PCA plot of; surface tension, viscosity, specific density and dielectric constant in which some samples can be considered as being either outliers or influential (11.2.10).

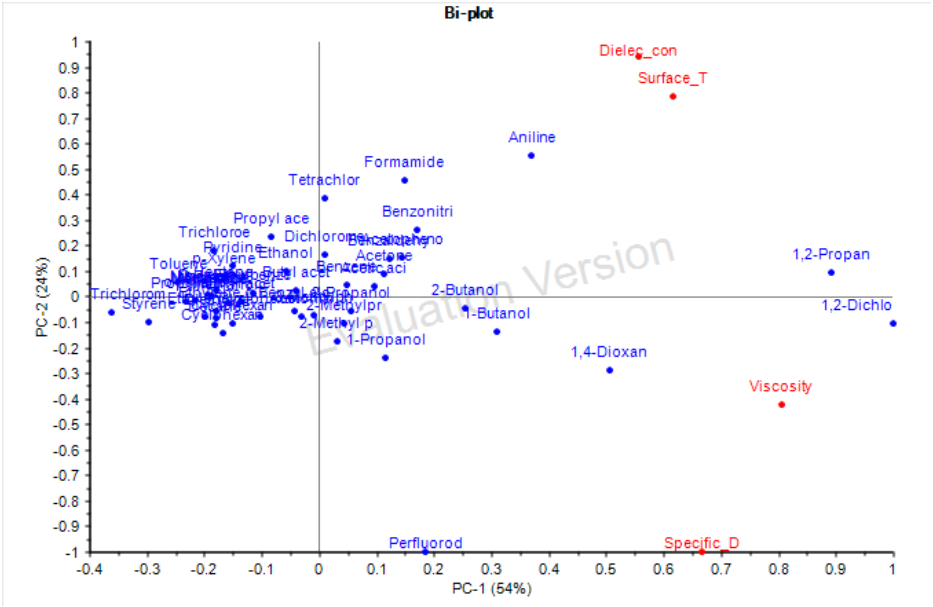

Figure 124 PCA plot of surface tension, viscosity, density and dielectric constant of some organic liquid. Compounds like 1,2 propanediol dominate the PC plot means some characteristic of those compounds has a strong influence on the variables shown in the plot.

An influence plot of Hotelling T^2 statistics is also shown in *Figure 125*. Except for the bottom left quarter of the data in *Figure 125*, the rest of the samples could not be explained after PC-3

operation. The F-residual value, which is higher than 0.5 in *Figure 125*, is the unexplained residual value of subsequent PC-3 operation on the data set. The right-hand quarter of *Figure 125* is the Hotelling T^2 influence contributing samples. The top right-hand samples of *Figure 125* is both highly influential with an unexplained variation on the PCA model. Perfluorodecalin, an unusually high specific dense compound (1.940 g/mL), is strongly influenced by density but has little correlation with other variables, including dielectric constant. As such, it is an ideal candidate to test the influence of density on the microwave pyrolysis process. However, when the cellulose sample was coated with 10% of Perfluorodecalin and MW-pyrolysed, the yield of pyrolysis (43%) was not improved relative to the dry cellulose pyrolysis yield (42%). This result indicates that density of a solvent or extractive component cannot itself improve the MW pyrolysis of cellulose or biomass. Unfortunately, in the present experimental data set, no compound was found to be ideal for testing the influence of surface tension by eliminating the contribution from the dielectric property. For viscosity influence testing without the contribution of other variables, no sample was found to be ideal either in terms of relevance and/or safety within the experiments considered in the present study.

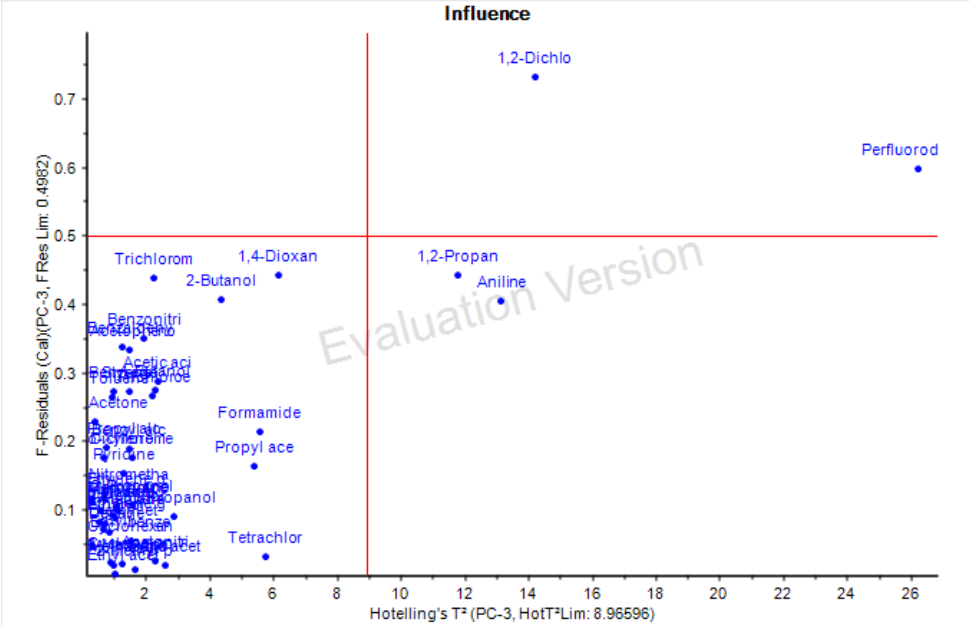

Figure 125 An influence plot of Hotelling T^2 statistics of surface tension, viscosity, density and dielectric constant. The compound on the top right corner like 1,2 dichloromethane dominates the characteristics of the PCs.

5.2.9 Dipole Moment and Polarisability

Although the dipole and polarisability are related to dielectric constant, any simple relation between these two physicochemical properties does not exist as *Figure 126* indicates (values are at section 11.2.3).

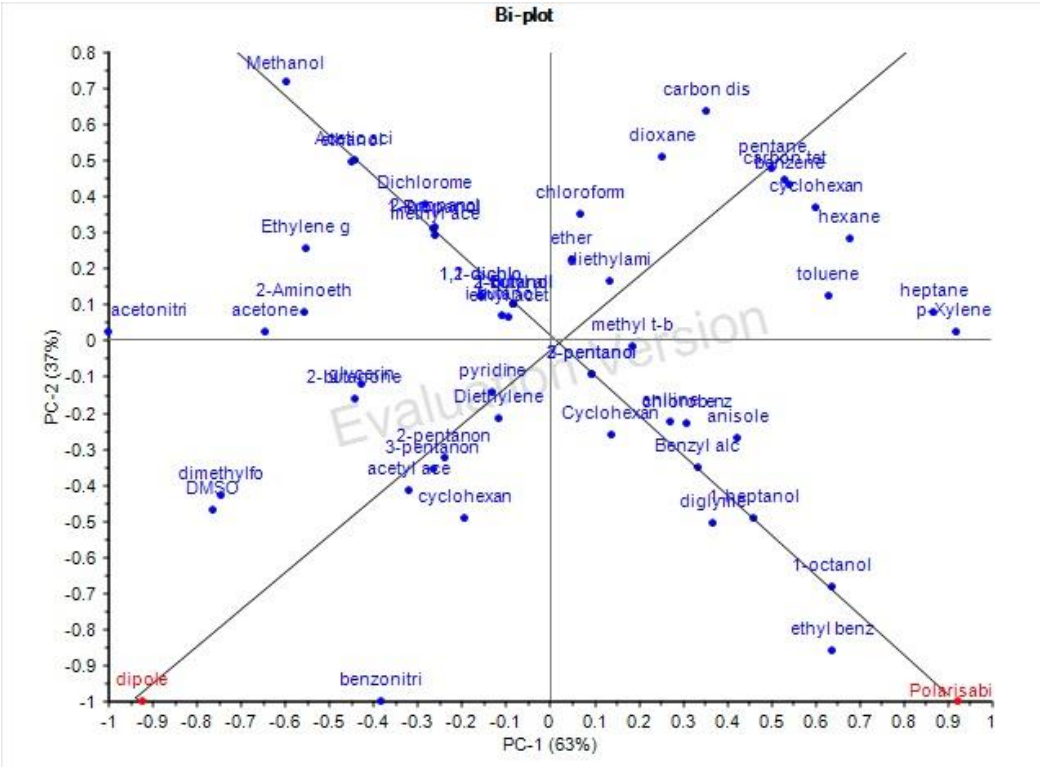

Figure 126 PCA Dipole and polarizability. Although the dipole and polarisability are related to dielectric constant, any simple relation between these two physicochemical properties does not indicate concerning their position in the biplot.

With two extreme values on the polarisation loadings in the biplot of *Figure 126*, ethyl benzoate and benzonitrile could be used as cellulose additives in order to better understand which of the two has the most influence on MW interaction. In the same way, p-xylene and acetonitrile should be tested for the verification of dipole moment. As those samples were not part of the initial experimental design, unfortunately, the output result could not be verified as part of the discussion of this chapter.

5.2.10 Relation of Polarity and pK_a

Although there are some substantial similarities between pK_a and polarity, there do not appear to be any known equation that can link the two variables together. The PCA of pK_a and polarity sits at the opposite angle of PC-2 *Figure 127* (values are at 11.2.5).

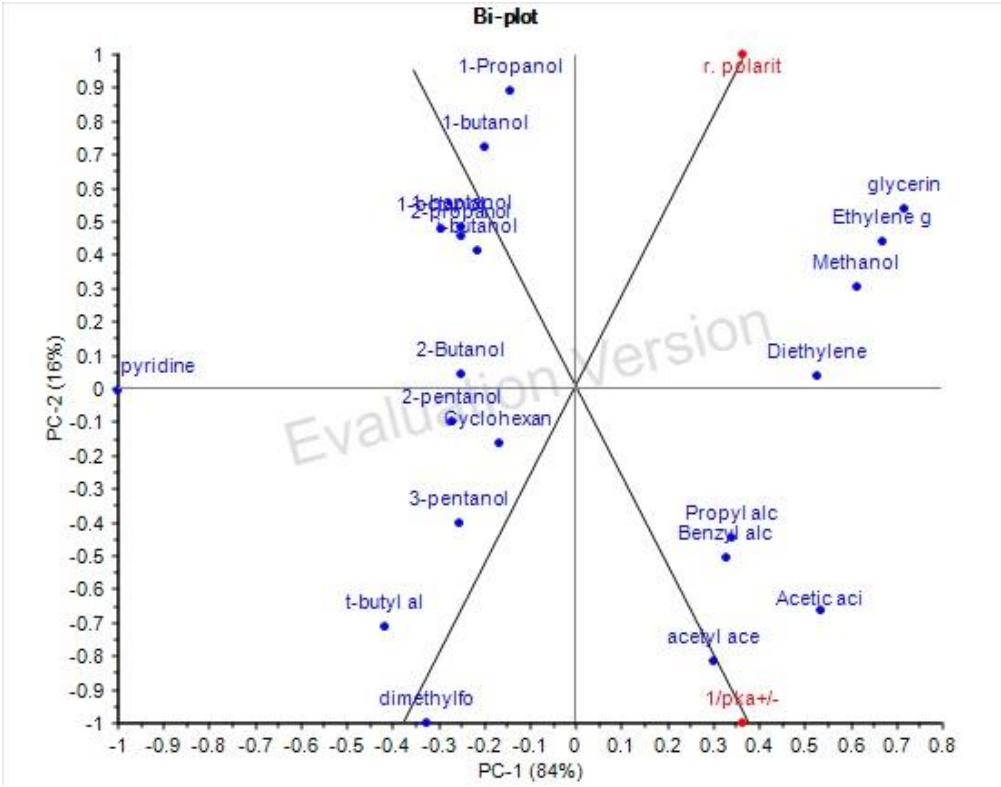

Figure 127 PCA of 1/pKa and relative polarity. pK_a and polarity sit at the opposite angle of each other in the PC biplot of PC-1 and PC-2. Although the strong 100% explanation of this tow variable relation between two yet to establish.

But by using PCA analysis with the combination of pK_a, polarity and dielectric constant, a new relation among these parameters could be established (*Figure 128*) (values are at section 11.2.5). The PCA indicates that the dielectric constant is more relevant to the polarity than to pK_a parameter. Given the position in the relevant plot, acetyl acetate and n-propanol were chosen as a cellulose coating solvent using the same method to investigate the comparative contribution of the aforementioned variables in the MW –pyrolysis of cellulose.

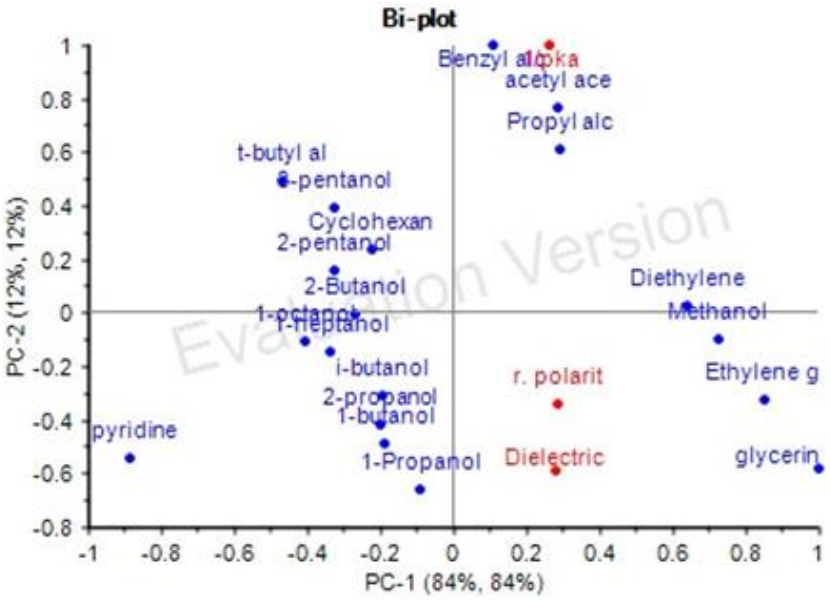

Figure 128 PC biplot of Polarity, dielectric constant and 1/pk$_a$. The score plot indicates there is strong relationships exist among the variables.

5.2.11 Relation of Dielectric Constant, Dipole Moment, Polarity and Polarisability and Their Influence on MW Pyrolysis

The combination of these four variables was found to be very satisfactory as expected by the Debye-Langevin equation. Polarity is the only new variable to be included in the PCA (Figure 31). The dielectric constant and relative polarity were found to be very similar but differ from polarizsability. Ethyl benzoate has strong polarisability contributing property. By increasing the number of additives in the current data set that is presented in Figure 31, an outlier or highly influential compound could be found for testing the effect of relative polarity or dipole moment when being used to coated cellulose during the MW-pyrolysis process (values of the properties are at11.2.3).

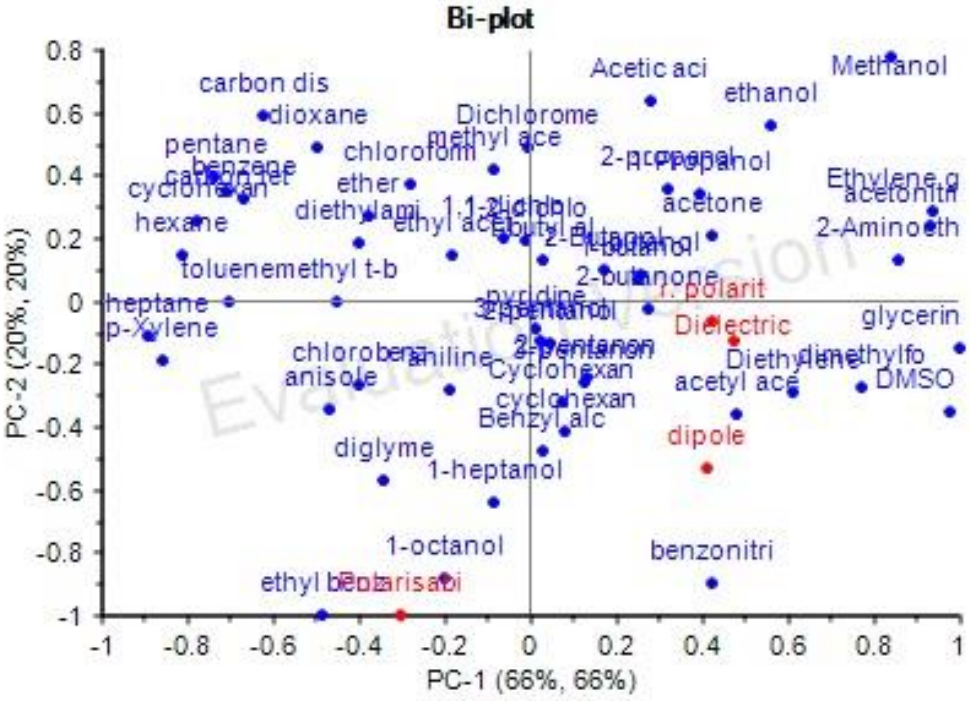

Figure 129 PCA of polarisability

5.3 Conclusion and Future experiment

The influence of additive on the MW-assisted pyrolysis of cellulose was investigated through careful experimental design. The yield of pyrolysis of cellulose was shown to vary by as much as 20%. From the GC-FID data analysis, it was also shown that the yield of MW pyrolysis could influence the acceleration of secondary reactions and hence, that the choice of additive could manipulate the amount of specific value-added chemicals produced. It can also change the route of the secondary reaction, whereby the path of the reaction could be modified to produce expected value-added chemicals by changing the extractive component. Further study needs to be performed to study such phenomena at a greater level of detail.

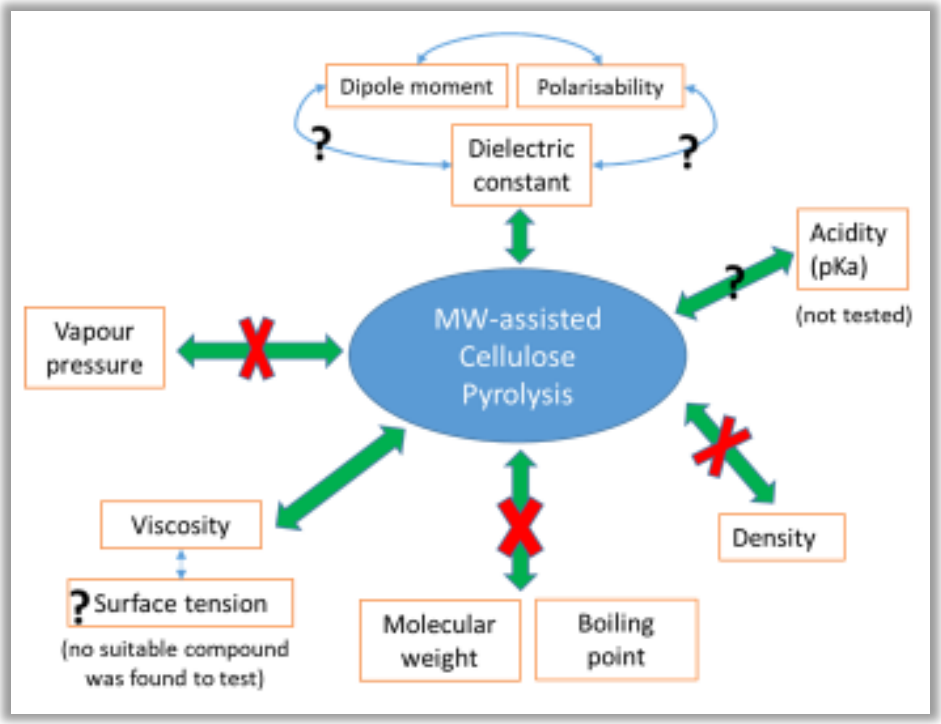

Figure 130 *Interactive nature of chemical parameters based on PCA.*

The MW pyrolysis study by chemometric analysis gave satisfactory explanations of the influence of various physical/chemicals parameters on the MW pyrolysis process (Figure 130). The most important outcome of this experimental design is a significant minimisation of the number of solvent parameters which could influence on MW-assisted pyrolysis process. First of all, it was shown that MW pyrolysis is almost complete independence from the boiling point and vapour pressure of additives. Secondary, molecular weight or density was found to be not interfering with solvent-MW interaction. Therefore, the wide range of physical-chemical properties of additives potentially important for the MW-cellulose interaction has been limited to solvent dielectric properties and viscosity. Both of these parameters are responsible for the efficiency of MW heating. Therefore, it could be proposed that organic additive play the role of an internal heater by stimulating cellulose activation. The hypothesis that the dielectric properties of additives are crucial for the cellulose activation could be proved with observation, that STA analysis shows that they do not influence on yield of conventional pyrolysis.

However, the results demonstrate that, besides the MW-activator role, additives could influence on the cellulose pyrolysis both as acid-based as a medium for primary product stabilisation and as catalysts for their further transformation. This observation is strong evidence that the MW-assisted pyrolysis is determined not only by individual properties of additives but also by their ability to interact with biomass and products of pyrolysis. Therefore,

it was decided that for the proper description of MW-cellulose interaction, it is necessary to include parameters which describe not only bulk behaviour of solvents but also solvent-solute and solvent-cellulose interactions. Solvent solute interactions can be classed as Vander Waals, the ion/dipole forces, hydrogen-bond donor/acceptor, electron-pair donor/electron-pair acceptor and solvophobic interactions.[102] By choosing a particular solvent to quantify multiparameter, the concept of linear solvation energy relationships (LSER) was introduced and will be described in the next chapter.[103]

6 INVESTIGATION OF ORGANIC LIQUID'S INTERACTION WITH CELLULOSE DURING MICROWAVE PYROLYSIS BY CHEMOMETRIC METHOD

6.1 Determination of Solvent-cellulose Interacting Criteria

Ten ml of solvent was added to one gram of microcrystalline cellulose in 40 ml of vials. After allowing for swell, the difference of the height is then converted into the volume as it occupied in the space of the vial. Then the expanded volume was compared with the molar volume of the solvent at room temperature. The calculated fraction of molar-volume was then converted into a molar fraction of solvent. The molar number of anhydroglycopyranose unit (AGU) of microcrystalline cellulose that was present in the vial is also calculated. The degree of expansion was then calculated as follows:

$$nSw = \frac{number\ of\ moles\ of\ solvent}{umber\ of\ mole\ of\ AGU}$$

The advantage of the modified system of cellulose swelling measurement is that weakly bounded solvent-cellulose frame would not destroy and risk of losing weakly bounded solvent if gravimetric filtration or evaporation step would have taken to remove excess solvent. The degree of swelling of all of the cellulose samples in the experiment and the solvents Abraham solvation parameters (calculated by ACD/I-Lab) are compared in *Table 19*.

Table 19 Solvents degree of swelling nSw and Abraham solvation descriptors value.

ID	sample name	volume	nSW	H bond Acidity A	H bond Basicity B	Polarizability /polarity S	Excess molar refraction E	McGowan Volume V
1A	Triethylamine	1.15	1.3855	0	0.53	0.37	0.17	1.0538
2A	Benzylamine	1.4	2.0784	0.21	0.66	0.95	0.78	0.9571
2B	N,N-Dimethylacrylamide	1.025	1.5065	0	0.7	1.12	0.45	0.8856
2C	diethylenetriamine	5.15	7.5557	0.59	1.55	1.02	0.51	0.9716
2D	2,6-dimethylaniline	1.025	1.3393	0.08	0.43	0.97	0.91	1.098
2E	n-Heptylamine	1.025	1.1263	0.21	0.59	0.52	0.2	1.1947
3A	Butyl benzoate	1.025	0.9416	0	0.46	1.05	0.64	1.4953
3B	Diethyl succinate	1.025	0.9933	0	0.7	0.99	0.12	1.3846
3C	Cinnamyl acetate	1.025	0.9974	0	0.52	1.15	0.79	1.4523
3D	Cinnamaldehyde	1.025	1.3036	0	0.47	1.29	0.97	1.1118
3E	Tetraethylene glycol dimethyl ether	1.025	0.7386	0	1.12	0.98	0.19	1.8111
4A	dimethyl sulfoxide	3.65	8.3375	0	0.71	1.37	0.52	0.6126
4B	Sulfolane	1.525	2.5989	0	0.55	1.18	0.31	0.8445
4C	propylene carbonate	0.9	1.6743	0	0.52	0.72	0.26	0.6967
5A	Cyclohexane	1.025	1.5631	0	0.02	0.28	0.21	0.8454
5B	Tetradecane	1.15	0.7195	0	0.07	0.23	-0.01	2.0812
6A	Fluorobenzene	0.9	1.5616	0	0.12	0.66	0.47	0.734
7A	Cyclooctanol	1.275	1.4908	0.31	0.33	0.54	0.42	1.1859
7C	1-phenylethanol	0.65	0.8761	0.31	0.56	0.83	0.81	1.0569
7D	1-Decanol	0.775	0.6586	0.31	0.33	0.48	0.19	1.5763
7E	Geraniol	0.775	0.7075	0.31	0.49	0.56	0.46	1.4903
8A	1,4=Butanediol	1.025	1.8579	0.63	0.59	0.73	0.41	0.7896
8B	1,3-Propanediol	0.9	1.9996	0.63	0.59	0.72	0.41	0.6487
9A	2-tert-Butylphenol	1.15	1.2081	0.5	0.43	0.79	0.79	1.3387
9B	m-cresol	1.15	1.7942	0.5	0.39	0.85	0.81	0.916
9C	2-Hexyldecanoic acid	0.9	0.5082	0.57	0.43	0.66	0.16	2.4374
9D	Oleic acid	1.15	0.595	0.57	0.47	0.78	0.3	2.6762
10A	acetic acid	0.9	2.6009	0.57	0.36	0.61	0.17	0.4648
10C	ethylene glycol	1.4	4.0172	0.54	0.58	0.71	0.41	0.5078
10D	Lactic acid	2.15	4.9459	0.74	0.66	0.66	0.31	0.6644

The relation of cellulose swelling was compared with the Abraham solvation parameter for the solvents by using multilinear regression (MLR). Before discussing the result of this analysis, it would be worth mentioning that Omar A. El Seoud's group have previously attempted to establish a relation of solvent swelling with solvation properties using aprotic and protic solvents.[500-502] Using multilinear regression, they have shown an overall correlation of swelling with dipolarity/polarizability and solvent molar volume by excluding some solvents that do not fit properly into multilinear regression. Also a recent review of Zhanying Zhang et al. mentioned that different molecular structured liquids may not follow the same level of correlation-coefficient with similar, or combinations of, solvatochromic or other parameters.[123, 500]

Here, in this work for the first time, a full spectrum of functional groups with more samples were tested to validate multilinear regression fitting, by considering Abraham solvation descriptors as a predictor and swelling nSw as the response.

6.1.1 Solvent-Cellulose Interaction Determination with MLR

The MLR cellulose swelling response (nSw) was computed against the Abraham solvation parameters of the solvents, listed in *Table 19*, using the Unscrambler-X 10.5.1software. The global overview of the MLR model for solvent-cellulose interaction is shown in Table 20. If the global model's p-value is smaller than 0.05, then it is said that the data are not random or significant at the 5% level. Here in this model, the p-value is 0.000978. So, using the model is worth investigating further. But to check whether the nonlinear part of the model is significant, or not, the interactions need to pass the validation test. Here in this model except for McGowan Volume (0.0019), the rest of the four predictors, hydrogen bond acidity (A), hydrogen bond basicity (B), polarity/polarizability (S) and excess molar refraction (E) do not qualify 5% significant limit.

Table 20 MLR ANOVA table of Abraham solvation parameter vs nSw

Anova Table			
Multiple Correlation: 0.7358934 (cal) 0.4013774 (val)			
R-Square: 0.5415391 (cal) 0.04746062 (val)			
Variables	p value	B-coefficients	STDerr
Model	0.000978289		
Variables	p value	B-coefficients	STDerr
Intercept	0.9999995	-7.75738E-08	0.1332174
A _H bond Acidity	0.1563359	0.2289174	0.1566322
B_H bond Basicity B	0.09848081	0.3072629	0.1790295
S_Polarity/Polarizability S	0.1869643	0.31358	0.2311139
E_Excess molar refraction E	0.1817302	-0.2633921	0.19174
V_McGowan Volume	0.001864035	-0.4845597	0.1393082

If the regression t- distribution value (characterised by the degree of freedom parameter of samples) is close to zero, then the model is likely to be non-significant. The t-value in *Figure 131* of this model shows nSw is zero at four figures (T_0 =0.000).

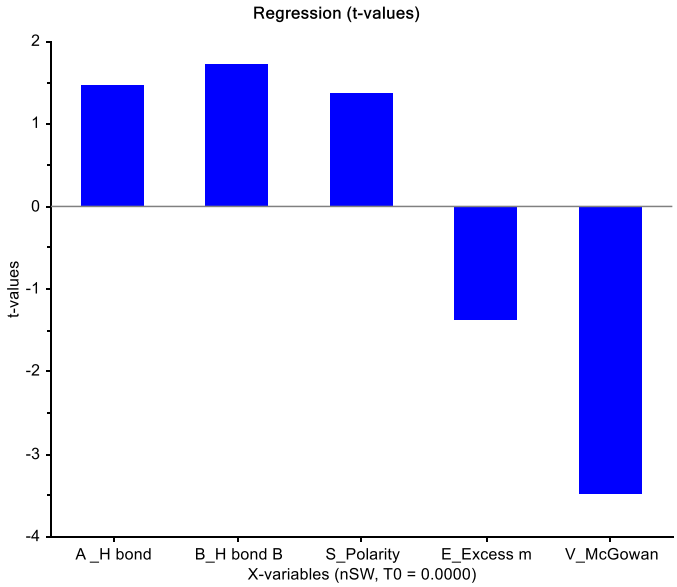

Figure 131 Regression t-value

Moreover, if there is a significant difference between calibration and validation regressions R-Square, then the model cannot be trusted. The value of calibrated R-Square and validated R-square and differences between them are also too high in this case, as shown in *Figure 132* (blue line is calibration and red is validation).

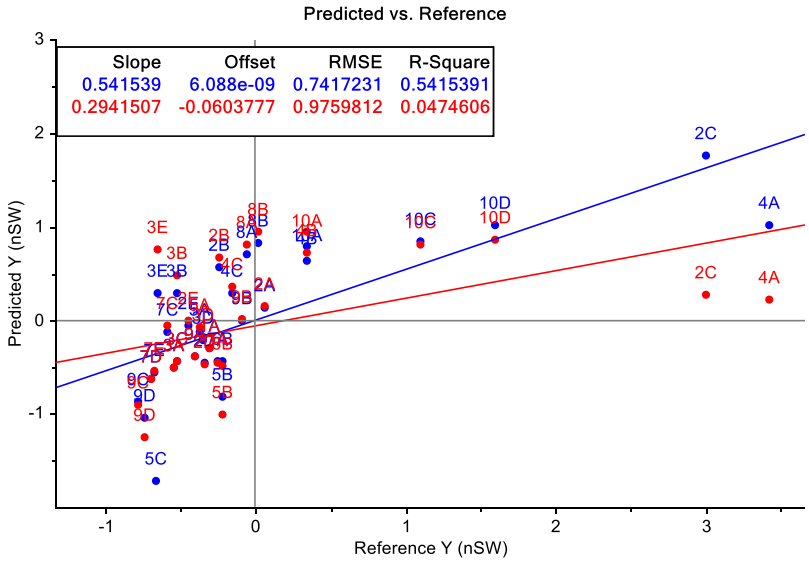

Figure 132 Predicted vs References of swelling MLR

Also, to verify any simple linear relation with nSw and any Abraham descriptor, the best related McGowan volume is shown in *Figure 133*, but yet the relationship is too poor to draw any significant association.

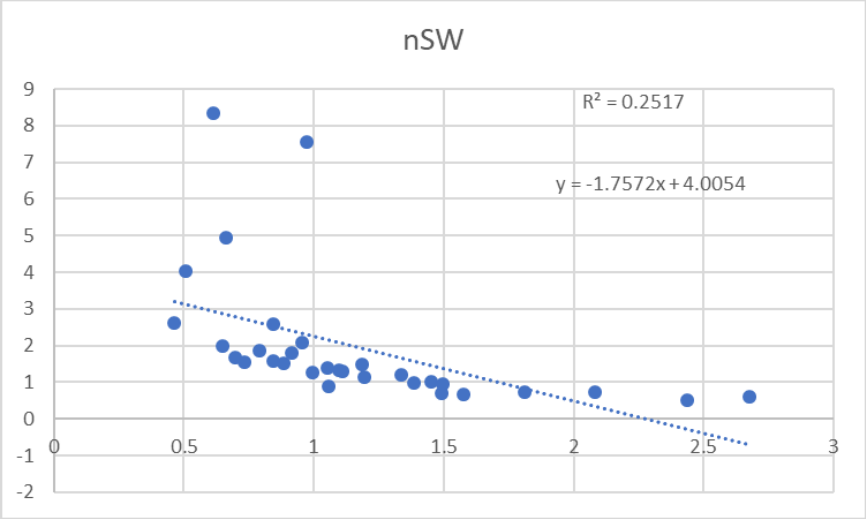

Figure 133 Linear regression of McGowan Volume vs nSw

From the overall MLR analysis, it is for the first time shown that the swelling effect does not have any underlying correlation with solvation property of organic liquids as far as diversity of the functional group is concerned. So, considering the swelling as individual property separated from solvation property to understand the interaction of those organic liquids with cellulose is justified.

6.2 Determination Solvent-product Interaction Criteria

6.2.1 Mass balance of Microwave-assisted Pyrolysis Residue

The initial screening of solvent selection was conducted by taking one gram of cellulose and 3 ml of solvents in a 10-ml reaction vessel. The MW pyrolysis was performed with CEM Discovery with 250 psi pressure in a closed vessel with fixed power of 275W. After pyrolysis, the biooil was removed with acetone, and the remaining residue was dried overnight at an oven set at 85 °C. The mass balance of all of the residue is presented in *Table 21*.

Table 21 The residue of MW pyrolysed products of all cellulose-solvent at 1:3 ratio and 250psi

Sample ID	Solvent	Residue %
1A	Triethylamine	88.18
2A	Benzylamine	89.59
2C	diethylenetriamine	93.43
2D	2,6-dimethylaniline	91.44
2E	n-Helptylamine	89.21
3A	Butyl benzoate	37.36
3B	Diethyl succinate	35.46
3C	Cinnamyl acetate	60.64
3D	Cinnamaldehyde	29.56
3E	Tetraethylene glycol dimethyl ehter	60.44
4A	dimethyl sulfoxide	70.00
4B	Sulfolane	5.47
4C	propylene carbonate	85.79
5A	Cyclohexane	94.70
5B	Tertradecane	61.48
6A	Fluorobenzene	97.58
7A	Cyclooctanol	79.00
7B	PEG 400	34.04
7C	1-phenylethanol	93.41
7D	1-Decanol	74.63
7E	Geraniol	60.02
8A	1,4 Butane diol	51.42
8B	1,3-Propanediol	90.68
9A	2-tert-Butylphenol	69.90
9B	m-cresol	83.47
9C	2-Hexyldecanoic acid	36.01
9D	Oleic acid	30.65
10A	acetic acid	85.89
10B	water	96.40
10C	ethylene glycol	89.38
10D	Lactic acid	10.27

6.2.2 Interpreting Solvent-product Interaction with MLR and PCA

To establish whether any underlying solvent effect on MW pyrolysis of cellulose, a multilinear regression analysis was performed on the Abraham solvation parameters and percentage of produced char through MW pyrolysis. The Abraham solvation parameters of solvents (*Table 19*) used a predictor and the residue (*Table 21*) as the response in MLR analysis. Several MLR operations are initially performed to remove any outlier value from MW pyrolysis residue value to find any inherent correlation with solvent and the rate of MW pyrolysis. But the relation between predictor and response was not satisfying according to the condition as it was discussed in section 4.3.1. The correlation of the predictor excess molar refraction (E) and McGowan Volume (V) with the response MW pyrolysed char was less related among all five Abraham solvation parameter. After taking out the excess molar refraction (E) and McGowan Volume (V) as the outlier, again another MLR was performed with the rest of three Abraham

solvation parameters and MW char residue. The MLR model of the rest of the Abraham solvation parameter with the response is shown in *Table 22*.

Table 22 The MLR overview of residue-solvent interaction

Anova Table
Multiple Correlation: 0.1829345 (cal) -0.5894409 (val)
R-Square: 0.03346497 (cal) -0.4272777 (val)

	p value	B-coefficients
Summary		
Model	0.836628 3	0.278876

Again, the model global P value (0.836) is far higher than 0.05. So, the model is outside the limit of 5% significance, and the response cannot have an underlying correlation with predictor solvation parameters. Moreover, the response residue's calibrated regression and validated regression is not correlated at all (*Figure 134*).

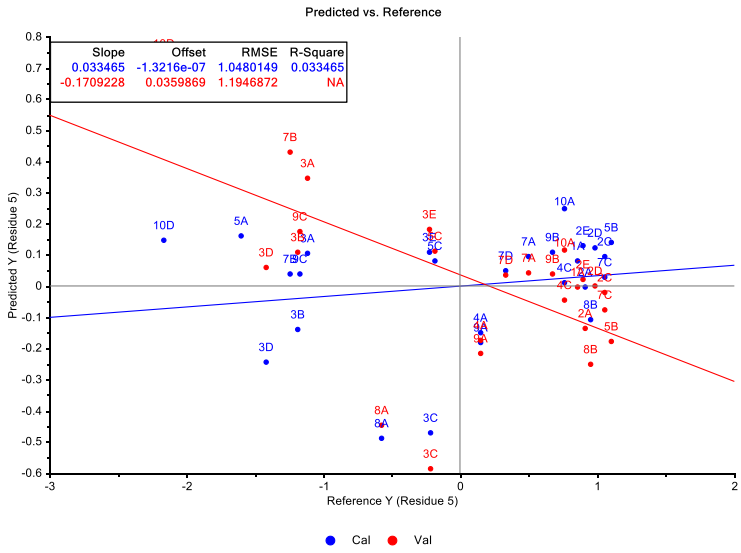

Figure 134 The regression plot of response residue Prediction vs reference

Finally, a PCA plot of three selected Abraham solvation parameter (hydrogen bond acidity, hydrogen bond basicity and solvent polarity) with MW pyrolysed residue is shown in *Figure 135*.

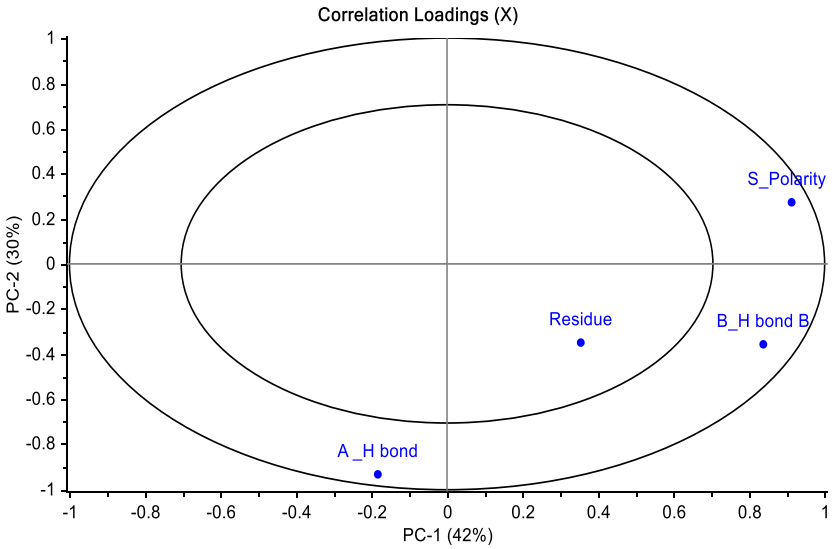

Figure 135 PCA loadings plot of solvent-residue

It can be seen in *Figure 135* that the MW pyrolysed residue was fallen inside the inner circle of PCA while the predictor parameters were positioned meaningfully at the edge of the outer circle. The interpretation of the loadings in *Figure 135* means that the three-solvent parameters (hydrogen bond solubility, hydrogen-bond basicity and polarity) are themselves satisfying about 90%, but MW pyrolysis residue failed to incorporate into the PCA model even at 50% level.

It can be seen that there is no significant linear correlation between all tested Abraham solvation parameters and the solid residue yields using MLR and PCA. The Abraham solvation parameters and the solid residue dependencies were then further investigated with cluster analysis (Figure 136). It was found that there is a special molecular volume (c.a. 1.25 ml/mol) which separates two types of the mechanism that controls the influence of solvent on MW pyrolysis of cellulose. The area above the specific McGowan corresponds to the solvents organised in cluster-3. The yield of the MW-assisted pyrolysis of cellulose in the presence of these solvents is independent of a particular chemical functionality of the molecules and is strongly correlated with their molecular volume. Below the unique volume, the first and second clusters are situated. Within these two clusters influence of other physical-chemical parameters dominant over the McGowan volume. The first cluster contains the compound which completely blocks MW activation reducing bio-oil yield about to four percent, and their influences are nearly independent of molecular volume. The MW-pyrolysis yield of the second group of solvents is higher than the products of MW-pyrolysis of original cellulose, independently from their molecular volume.

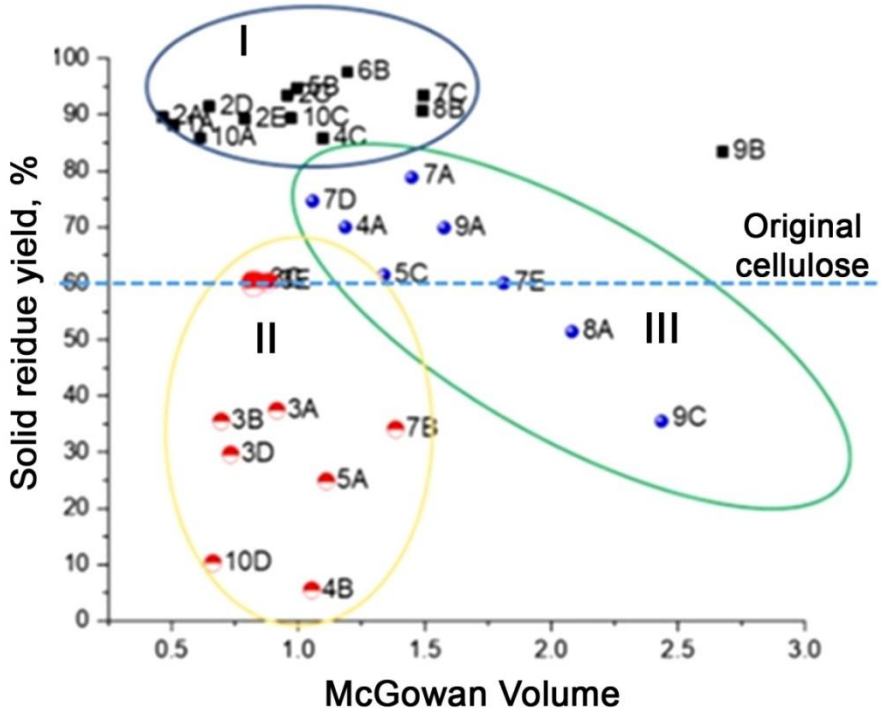

Figure 136 Relation of cellulose pyrolysis residue with McGowan Volume.

It could be proposed here that the molecules with high volume have limited ability to penetrate inside of the amorphous region of the cellulose. However, the high boiling point solvent may help to retain the generated MW dielectric heat and to prevent primary pyrolysis products from undergoing secondary reactions. On the other hand, a small molecule can penetrate inside of the amorphous cellulose region and be able to influence cellulose decomposition with their functional group.

6.2.3 Microwave-assisted Pyrolysis of Cellulose with Some Selected Organic Liquids

To further understand the role of solvent on MW liquefaction of cellulose, five solvents were chosen from *Table 21*, under which presence the cellulose was MW pyrolysed into liquid in a higher amount than other solvents of that table. The solvents that represent for this next step of experiments are 4B (sulfolane), 10D (lactic acid), 3D (cinnamaldehyde), 9D (oleic acid) and 3B (diethyl succinate). The ratio of cellulose and solvent for this experimental setup was taken as 1:10 (300mg: 3ml) to ensure the maximal effect of solvent on cellulose if there is any. The MW pyrolysis condition is set to the milder condition than the first experiment to distinguish the smaller differences of pyrolysis rate. The pyrolysis condition used a constant power of 200W at 255°C and a 'hold time' at a maximum power of only for 30 seconds. The comparison of the solvent-cellulose mixer during stirring and swelling is shown in *Figure 137*.

Figure 137 Short-listed organic liquid was mixed with microcrystalline cellulose at 10:1 ratio during magnetic stirring before MW pyrolysis.

During stirring, the cinnamaldehyde, lactic acid and oleic acid (9D) form such a thick gel-like liquid with cellulose that the magnetic stirrer could not move after a while of mixing. The phenomena mentioned above indicate that interaction of one solvent with cellulose differs from others, but that interaction may not reflect on the MW pyrolysis process. The solvents were also exposed to the same MW condition to compare the interaction of the solvent with MW without adding cellulose into it. The solvents, MW irradiated solvents, and the cellulose-solvent MW pyrolysed liquids (right to the left) are presented on the top of *Figure 138* and *Figure 139* while the remaining solid residue after drying is shown at the bottom of the figures respectively.

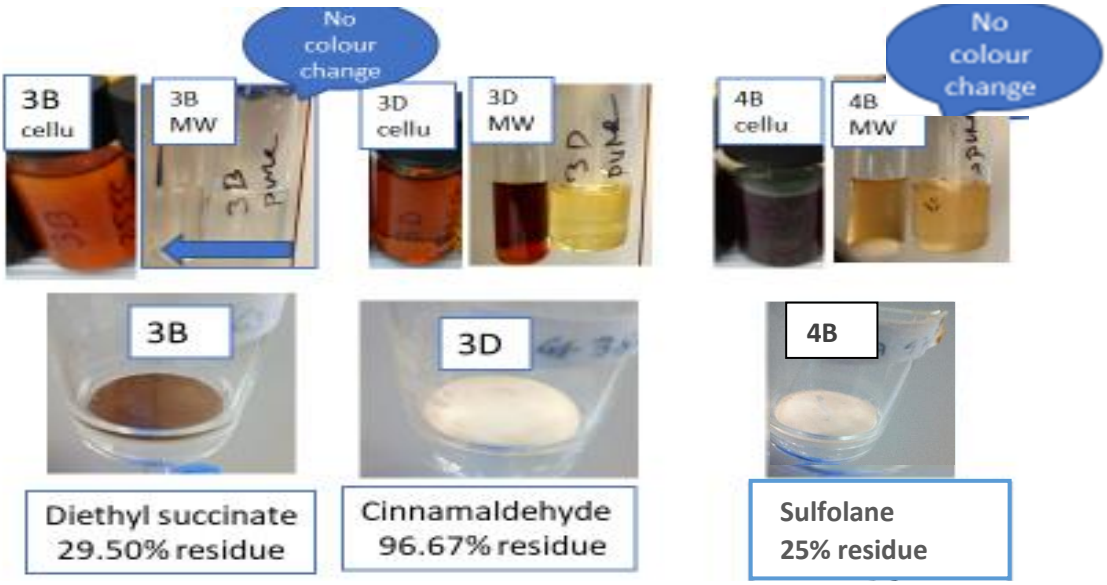

Figure 138 On top: The solvents, MW irradiated solvents only, and the cellulose-solvent MW pyrolysed liquids (right to the left) At the bottom: solid residue of MW pyrolysed cellulose after drying

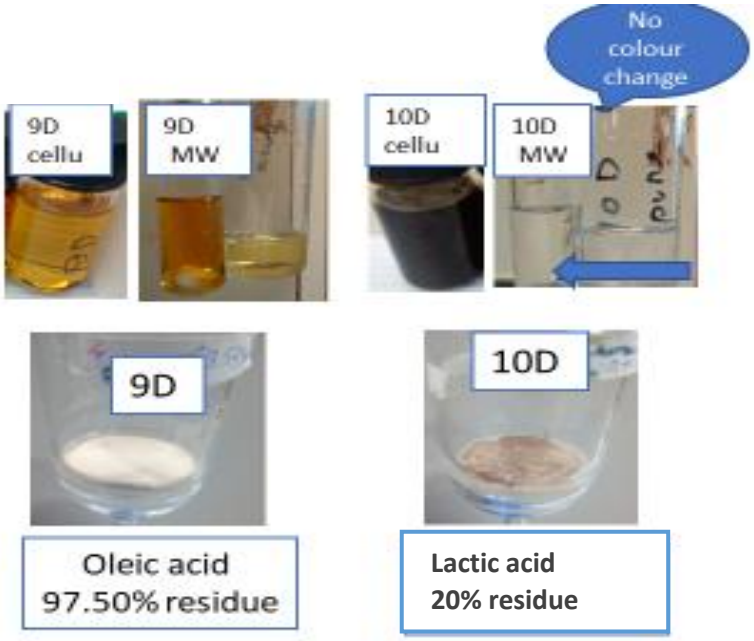

Figure 139 On top: The solvents, MW irradiated solvents only, and the cellulose-solvent MW pyrolysed liquids (right to the left) At the bottom: solid residue of MW pyrolysed cellulose after drying.

The experiment was replicated. The mass balance of the percentage of the residue of selected solvents is presented in *Table 23*. Except for cinnamaldehyde and oleic acid, the other samples have shown a certain degree of MW conversion into liquids. Sulfolane seems to produce the least pyrolysed residue than others. One point to note here that the pyrolysis residue of lactic-cellulose was in very fine particulate form compared to the rest of other char residues.

Table 23 percentage of MW pyrolysis residue of selected samples

Sample ID	Solvent	MW pyrolysed residue %
3B	Diethyl succinate	**29.5**
3D	Cinnamaldehyde	**96.5**
4B	Sulfolane	**25.0**
9D	Oleic acid	**97.5**
10 D	Lactic acid	**30.0**

From the above investigation, it was revealed that Lactic acid, Sulfolane and diethyl succinate are the potential candidate to further investigate for product characterisation and thermo-kinetic analysis.

6.2.4 Separation of Lactic Acid from Products

The technically tricky part of this investigation was to remove MW pyrolysed products from the highly volatile organic liquids. Here only a brief scheme of lactic Acid separation procedure is shown systematically in *Figure 140*. As in *Figure 140*, lactic acid and MW pyrolysed liquid mixture was mixed with water to solubilise the lactic acid. After centrifugation, the liquid and solid is fractionated via decanting. Both the liquid (A) and solid (B) fractions were treated with DCM separately in a separation funnel. The DCM fraction was collected in both cases and then mixed The combined DCM fractions (A1+B1) is then rota-evaporated to collect DCM soluble biooil fraction. The water-insoluble fraction was then treated with toluene in a separation funnel. The toluene fraction (A2) was collected. In the same way, the DCM insoluble fraction was also treated with toluene in a separation funnel and then the toluene soluble fraction was collected (B2). Both parts of toluene fractions (A2+B2) were then mixed and rota-evaporated to collect concentrated toluene soluble biooil fraction.

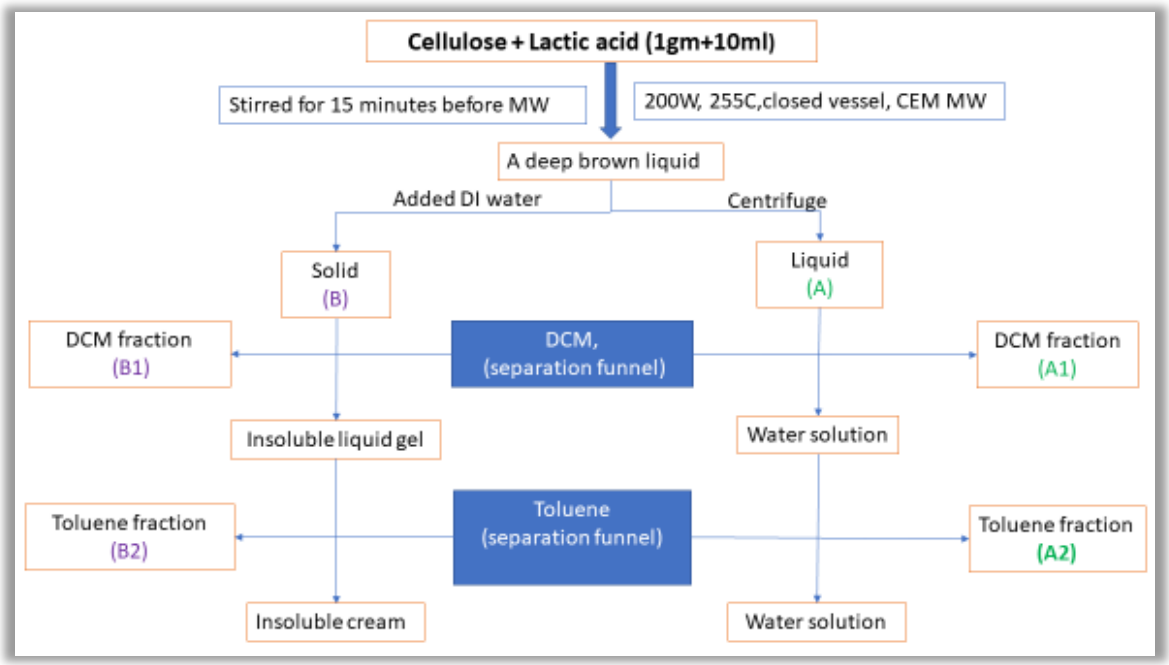

Figure 140 Scheme of separation of Lactic acid

The collected DCM fraction and toluene fractions were then analysed with GC-FID, as shown in *Figure 141*. A lactic acid only sample was also MW pyrolysed as in the condition of cellulose-solvent. A drop of this pyrolysed lactic acid sample was dissolved in DCM and then treated

using the same method as DCM fraction and toluene fraction method for comparison and identification of solvent assisted MW pyrolysed cellulose product. It was demonstrated, by GC-FID spectra, that in DCM fraction no solvent trace remained. In the toluene fraction, there is only a trace amount of lactic acid and biooil collected. In DCM fraction Levoglucosan was positively identified compared with standard.

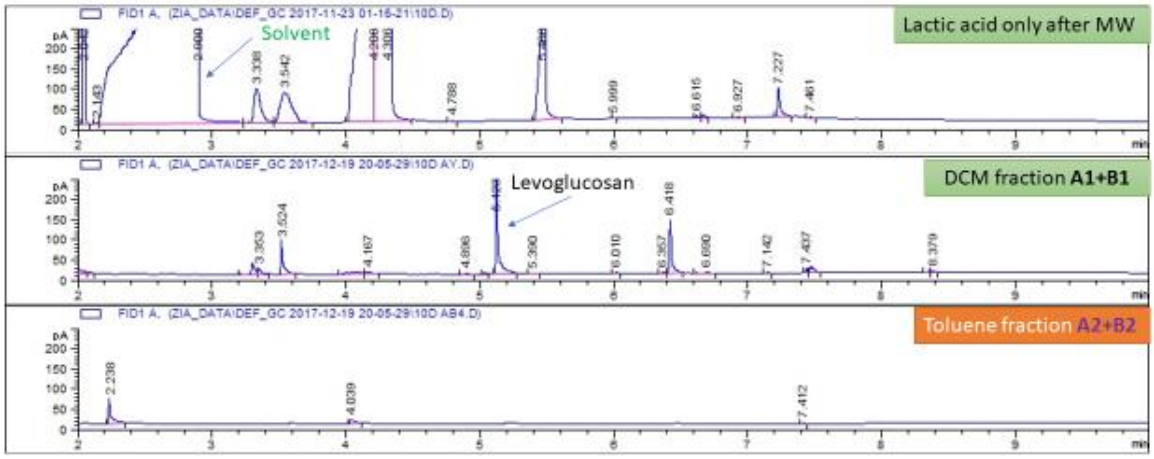

Figure 141 The success of fractionation as shown by GC-FID

From the above discussion, it is shown that the highly volatile solvent removal is possible using various separation methods. It is also understandable that for a different solvent, a different approach is needed. There is still room to improve the above mentioned lactic acid separation method for optimal collection of biooil.

6.3 Determination of solvent-MW interaction

To maximise the product selectivity, stability and yield in the chemical conversion, biomass activation and many more physicochemical processes, the use of microwave (MW) technology are accepted as a green and efficient energy source. However, there is a lack of information about temperature dependence of the dielectric properties of organic solvents, which make it challenging to design, control and optimise MW reactions. Here in this PhD work, the dielectric property (dielectric constant, dielectric loss factor and loss tangent) of some organic solvents mentioned in (Table 19) were analysed using a custom made resonant cavity perturbation (RCP) instrument. Along with those COSMO-RS based solvents of Table 19; some other valuable biomass pyrolysed products such as levoglucosenone, HMF were also characterised by the RCP device at up to the cellulose activation (180°C) temperature.

The details of the instrument development, measurement of dielectric property of solvents at elevated temperature and the outcome result of solvent-MW interaction, are discussed in the next chapter.

6.4 Conclusion

A systematic study of MW-assisted pyrolysis of cellulose in the presence of organic additives was conducted. This systematic investigation includes a detailed analysis of MW-solvent, solvent-cellulose, and solvent-products interactions.

The solvent-cellulose and solvent-products interactions have never been systematically investigated before, therefore new methodologies to study these interactions were designed and applied. The solvent-cellulose interaction was measured by the degree of swelling using the ratio of moles of solvent to the number of anhydroglycopyranose units (AGU). It has been shown that the swelling effect is an individual property separated from solvation property and could be used as an independent parameter.

To explain solvent-products interaction, the correlation between Abraham solvation parameters of solvent and pyrolysis yield were analysed, (focusing on the preservation of cellulose degraded products with organic additives/solvents). The applications of MLR and PCA methods together with cluster analysis demonstrated a complex correlation between Abraham solvation parameters and the solid residue yields. It was found out that there is a particular McGowan volume (c.a. 1.25 mol/g) which separates two different types of mechanisms that control the influence of solvent on MW pyrolysis of cellulose. Above this volume the degree of MW pyrolysis significantly relies on McGowan volume, however, it is independent of other parameters. Alternatively, below the critical value, the McGowan volume does not influence the pyrolysis, while other physical-chemical parameters play a significant role.

It was concluded that the molecules with high volume have limited ability to penetrate inside of the amorphous region of the cellulose. However, a high boiling point solvent helps to retain the generated MW dielectric heat and prevents primary pyrolysis of products from undergoing secondary reactions. On the other hand, a small molecule can penetrate inside of the amorphous cellulose region and be able to influence cellulose decomposition with their functional group.

7 INSTRUMENTAL DEVELOPMENT TO DETERMINE DIELECTRIC LOSS FACTOR AND SOLVENT-MW INTERACTION DURING MW ACTIVATION PROCESS

7.1 The Development of Resonant Cavity Perturbation (RCP) Device

A details discussion of the RCP method is discussed in the literature review. The RCP cavity was built in-house using the resonant cavity principle as shown in the (*Figure 142*).

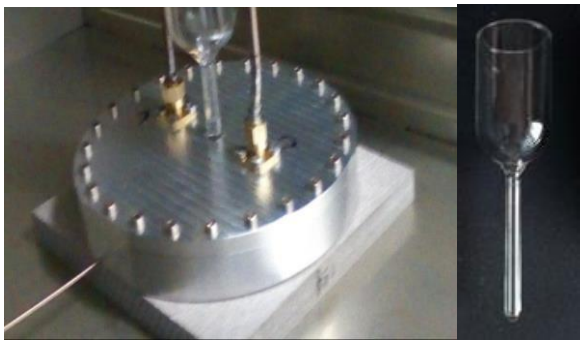

Figure 142 RCP cavity and sample holder tube

A temperature probe is attached at the base plate of the metallic cavity. The dimension of the cavity is 12.5 cm in diameter, 1 cm in height and the thickness of the wall on both top and bottom is 0.5 cm. In the middle of the cavity, there is a hole of 0.5 cm diameter on both the top and the bottom of the plates. The device is placed on a high-temperature resistant pyrolytic graphite plate, as seen in *Figure 142*. The two-coaxial connectors on the VNA are joined with two high-temperature resistant coaxial cables respectively and then attached at the top of the cavity, as shown in (*Figure 142*). Two short monopole antennas extended from the SMA connectors into the cavity to excite and detect the cavity resonance. A Pyrex glass tube of funnel shape is used as a liquid sample holder. There is also about a one-centimetre hole dug inside the thermal resistive material for holding the glass tube when it is placed upright through the hole of the metal cavity. The cavity with the empty pyrex glass tube is calibrated every time at room temperature before placing the sample inside the tube. The sample is then filled inside the glass tube so that about one cm of liquid is kept outside of both ends of the glass tube when inserted inside the metal cavity. The RCP cavity is placed inside of an oven that can be operated between room temperature to 225 ℃. As all parts of the device inside the oven are temperature resistant at up to 225 ℃, all part of the RCP system remains safe from thermal damage. The whole setting is organised in the way, as shown in *Figure 143* (not scaled up with proportional size).

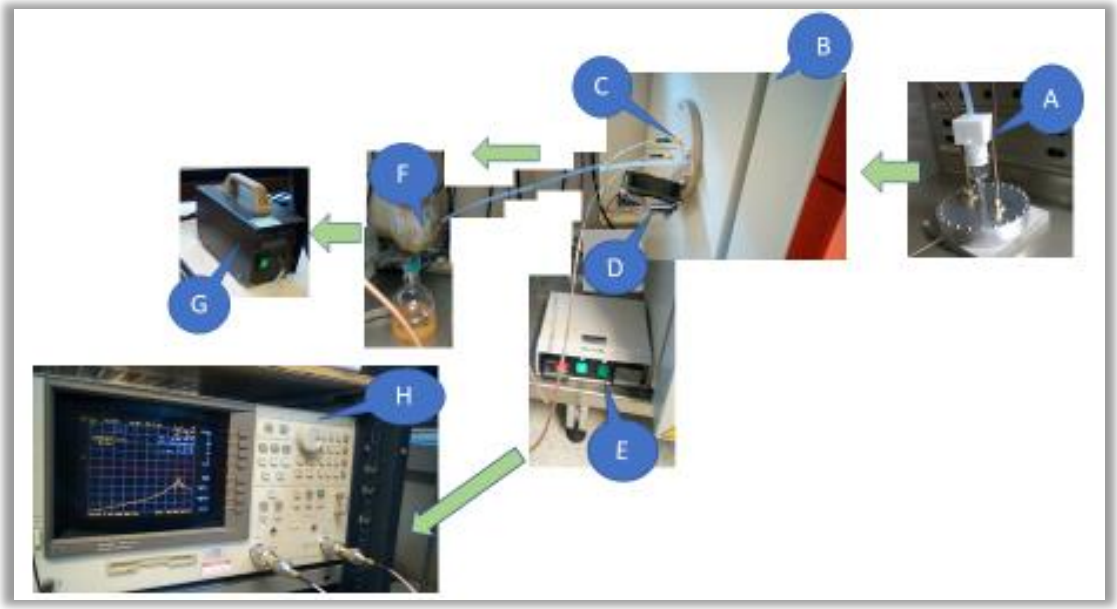

Figure 143 Instrumental setup to measure the dielectric loss of liquids at high temperature

As shown in *Figure 143*, a PTFE mould is placed on the top of the pyrex sample holder consisting of a hole through the top to bottom with an air passage at one side. A flexible PTFE tube is connected to the top of the PTFE mould (*Figure 143A*). All the connecting cables and tubes are then passed through some specific holes of a pyrolytic graphite plate (*Figure 143C*). The pyrolytic graphite plate is placed on the right-hand side of the oven (*Figure 143B*). A small fan (*Figure 143D*) is attached on the top of the plate to cool down the pyrolytic plate and cables during the heating period. The PTFE tube which is connected with the pyrex tube through PTFE mould is passed through a condensation trap (*Figure 143F*). The condensation trap remains filled with fresh ice before every sample measurement as the temperature of the condenser increases up to 10 ℃ at the end of each experimental period. The end of the trap is connected to a vacuum pump (*Figure 143G*). Both the condensation trap temperature sensor and MW cavity temperature sensors are linked to a temperature monitoring device (*Figure 143E*). The VNA is shown at (*Figure 143H*), and it was operated at 2.45 GHz frequency. When the VNA instrument is tuned on and measurement starts, the VNA automatically calculates the maximum frequency f and Q factor of a resonant peak of the frequency response graph, from which the complex permittivity is manually calculated by *Equation 35*. In *Figure 144*, a complex frequency shift of 1,3-propanediol is shown as an example.

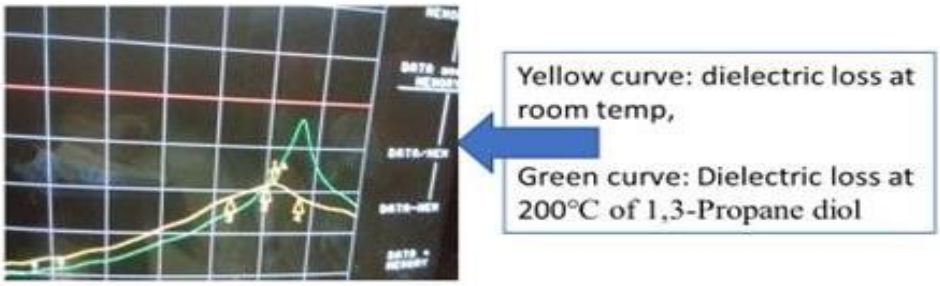

Figure 144 VNA screen with the sample signal

7.1.1 Calibration of The RCP device with standards in Room temperature

The instrument is calibrated at room temperature with standards as listed in the left-hand column of Table 24.

Table 24 Calibration of the cavity with standard solvent

NPL Standards at 24 °C	Ɛ* (complex) Calculated	Ɛ* (complex) Literature	Difference of Ɛ* (complex)	RMSE of Ɛ* (complex)
Ethylene Glycol	13.3713 -15.0534i	14.8400 -14.5500i	-1.4687 - 0.5034i	1.7175
Saline	73.8931 -14.6021i	75.7500 -14.5500i	-1.8569 - 0.0521i	
MeOH	20.7496 -16.0675i	22.5100 -13.1700i	-1.7604 - 2.8975i	
Water	78.5786 - 6.7851i	77.2400 - 8.8700i	1.3386 + 2.0849i	
EtOH	7.0666 - 6.4124i	7.2000 - 6.9700i	-0.1334 + 0.5576i	
Propan-1-ol	4.8239 - 3.6837i	4.3800 - 3.3500i	0.4439 - 0.3337i	
Butan-1-ol	4.1133 - 2.3099i	3.6500 - 1.9900i	0.4633 - 0.3199i	
Acetone	22.1336 - 0.7668i	20.7000 - 0.9500i	1.4336 + 0.1832i	
Cyclohexane	2.1177 - 0.0010i	2.0160 + 0.0000i	0.1017 - 0.0010i	

The calculated complex dielectric constant (ε*) is then compared with the literature value. The literature values are taken from the National Physical Laboratory (NPL) report CETM33, and other sources.[521, 603] The root mean squared error (RMSE) of the calibrated value and this instrumental setup value is reasonably small (1.72) and reliable for this purpose (right-hand column *Table 24*). The relatively small error between standard and calibrated data-set gives confidence in the experimental result of this new RCP device.

7.1.2 Calibration of the New RCP Device with a Standard of Wide-temperature Range

The resonant frequency (f) and the quality factor (Q) of the RCP cavity are measured at the full operating temperature range (25 °C to 225 °C). In the mentioned temperature range, the frequency shifts were from 2402 MHz (at room temperature) to 2386 MHz (at 225 °C). The

difference of the frequency shift was 46 Hz downwards, and the average frequency shift was 0.23 Hz/°C (*Figure 145*). The frequency shift is due to thermal expansion of the cavity.

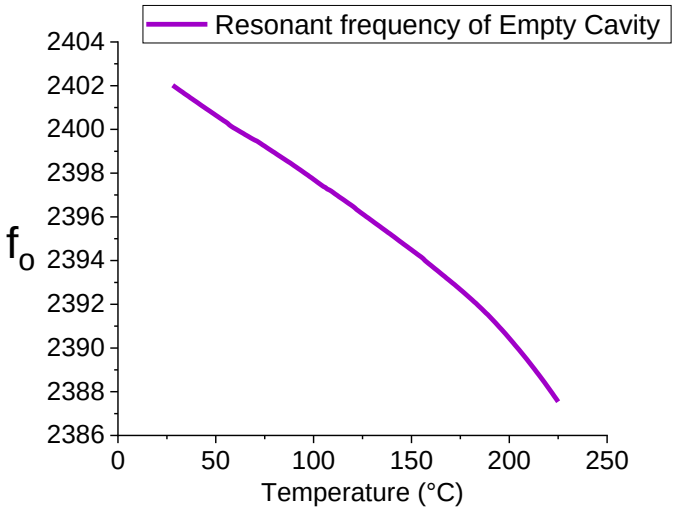

Figure 145 Resonant frequency of the empty RCP cavity

The quality factor change of the empty cavity within the same temperature range was 198 to 168, and through which was 0.15 per degree centigrade (*Figure 146*). It is noted here that the Q factor changes in a wave pattern as temperature changes. When the sample is measured for complex permittivity, the frequency shift and quality factor of the sample were recalculated by subtracting the f_0 and Q_0 of the empty cavity of the relevant temperature.

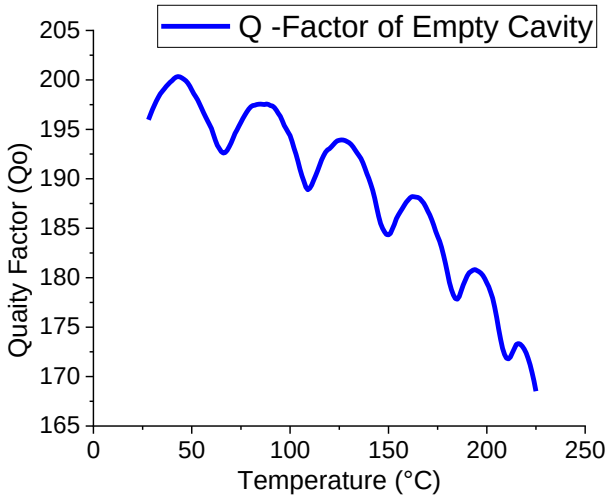

Figure 146 Q factor of the empty RCP cavity

In a scientific report, the NPL has presented ten solvents at a temperature range of 10°C to 50 °C in a systematic analytical procedure using reflection cell, 14-mm transmission cell and 40-mm transmission cell at a range of frequencies (0.01-5GHz). But the solvents used by NPL were common volatile organic solvents which were not suitable to compare for the current

purpose. The only common solvent that was examined in both NPL and this experiment was DMSO. The NPL measurement uncertainty was less than 0.5% for (20°C to 50 °C) the testing temperature range. Among all of three measuring techniques, NPL has found that the dielectric data of DMSO best fit with single Debye equation (*Equation 39*) in the measured temperature range.

$$\varepsilon^* = \varepsilon_\infty + \frac{\varepsilon_s - \varepsilon_\infty}{1 + jf/f_r}$$

Equation 39

In *Equation 39*, ε_s is the static permittivity, ε_∞ is the high-frequency permittivity, and f_r is the relaxation frequency. In the NPL procedure, the temperature incremental and recording steps were 5 ºC steps, which was also followed in this experiment for the calibration purpose. To test the performance of the cavity for nonpolar dielectric transparent liquid, in NPL experiment, cyclohexane was used. The testing frequency shift (Δf) and Q-factor change of NPL operational temperature range were from 20°C to 50 °C. Since in this RCP experimental procedure, the operational temperature range was much higher, a more suitable solvent tetradecane was used for serving the same purpose. The comparison of frequency shift during temperature change is shown in *Figure 147*. The average difference of frequency shift between the empty cavity and tetradecane was about 5 MHz between two methods, while the Q factor change difference was about 3.5 units on average (*Figure 148*).

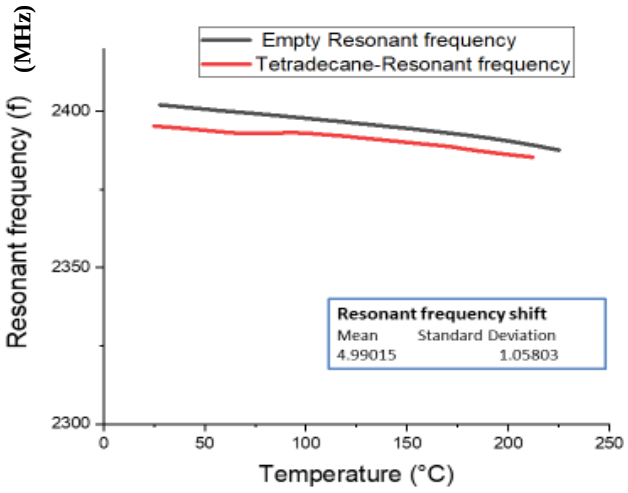

Figure 147 Comparison of frequency shift change of tetradecane compared with the empty cavity as temperature change.

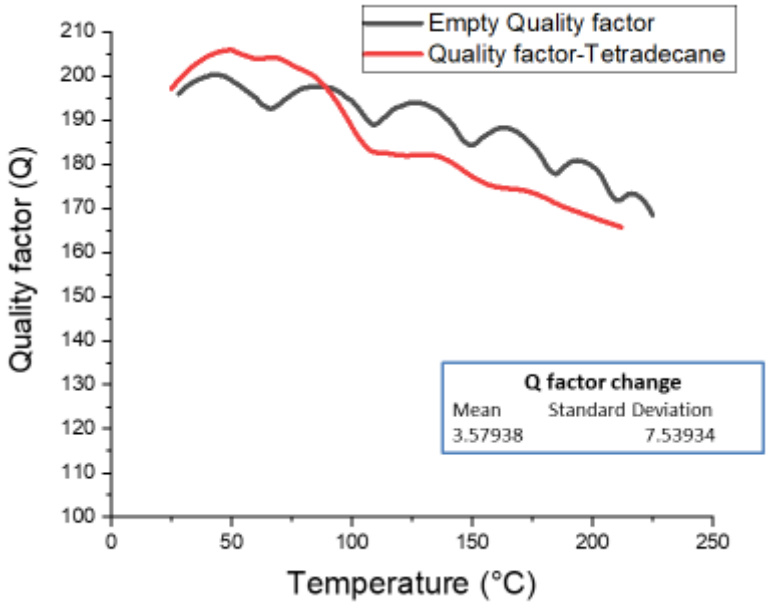

Figure 148 Comparision of Q-factor shift change of tetradecane compared with the empty cavity as temperature change

The single Debye equation fit data of DMSO in NPL measurement and DMSO data of this experiment are presented below. The comparison of the real part of the complex dielectric property is presented in *Figure 149*, while the imaginary part comparison is shown in *Figure 150*.

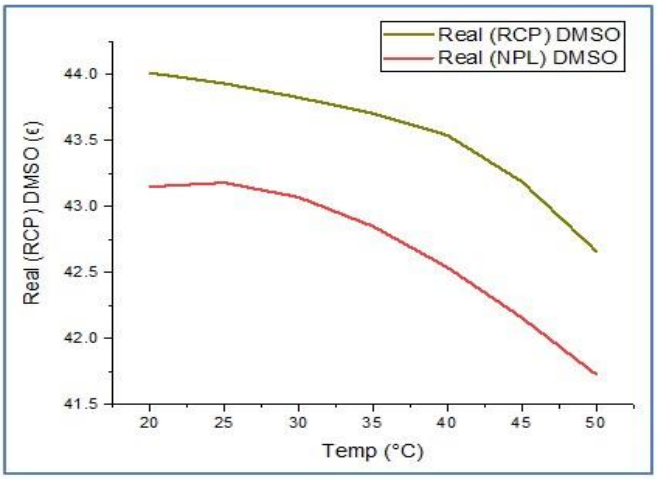

Figure 149 Comparision of standard NPL and experimentally measured real part of DMSO

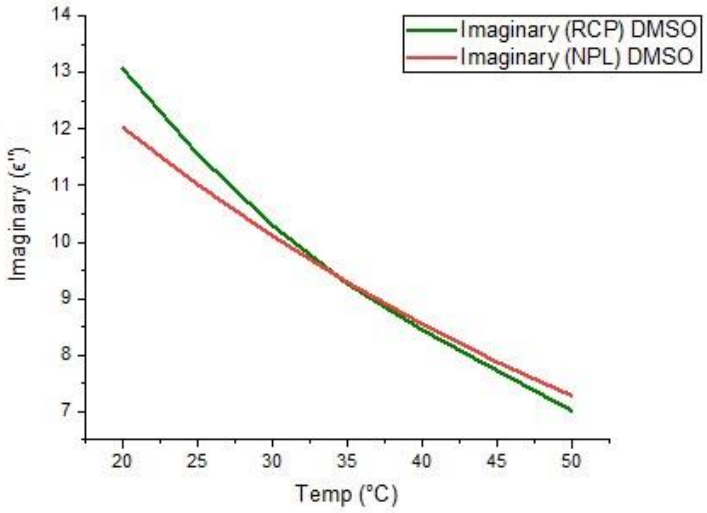

Figure 150 Comparision of standard NPL and experimentally measured imaginary part of DMSO

The percentage of error of the real part of the complex dielectric constant of DMSO is shown in *Figure 151*. All those values are negative, and between 1.5% to 2.5 % deviated from NPL measurement.

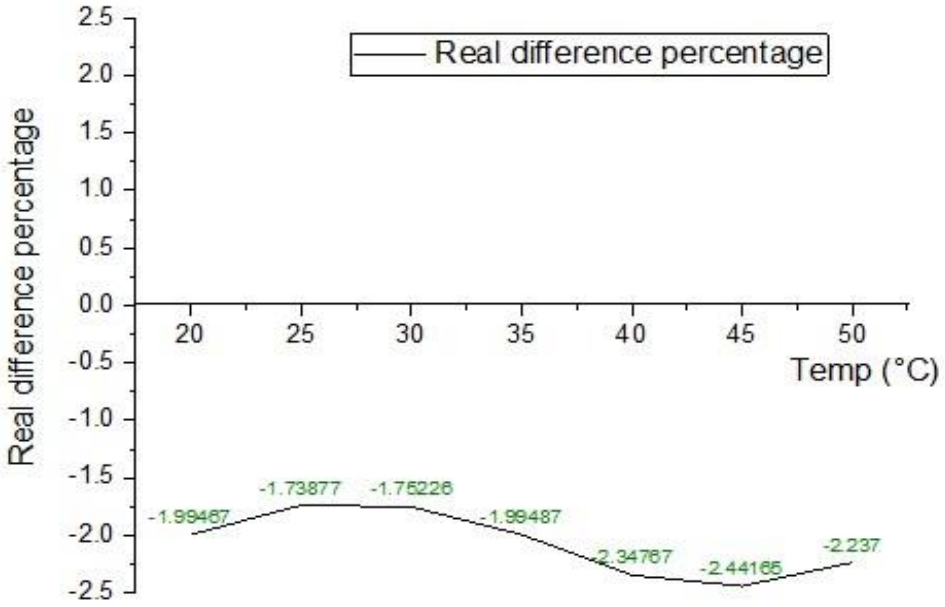

Figure 151 The percentage of error of the real part of the complex dielectric constant of DMSO

The imaginary part difference with NPL data was about -8% to 4% from lower to higher temperature direction, and both methods show the minimum gap of imaginary value at 35 ºC (*Figure 152*).

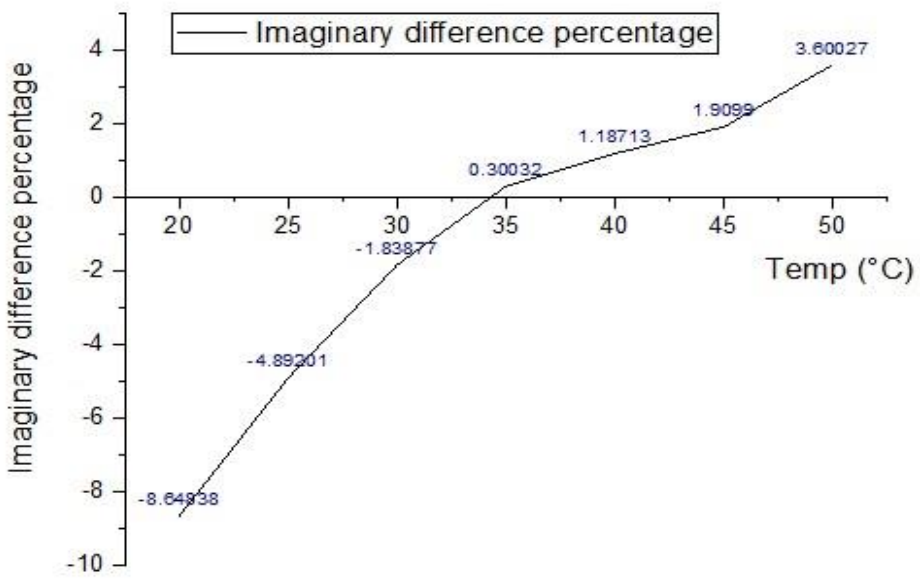

Figure 152 The percentage of error of the imaginary part of the complex dielectric constant of DMSO

7.1.3 Solvent selection

The selection of organic solvent to measure complex dielectric property at a wider temperature range was based on ten subclasses of COSMO-RS, as discussed in section 4.2.4 of chapter 4 (*Table 25*).[31]

Table 25 Organic solvents to measure complex dielectric property at a wider temperature range

Cluster	COSMO_RS type cluster	Compound
2	Weak electron pair donor base	Diethylenetraimine
3	Aprotic dipolar	Butyl benzoate
		Cinnamaldehyde
		Ethyl benzoyl acetate
4	Aprotic highly dipolar	DMSO
		Sulfolane
		Propylene carbonate
		Cyrene
		Levogluocosenone
		γ-valerolactone
5	Apolar	alfa-pinene
		Tetradecane
		p-cymene
7	Amphiprotic	Cyclooctanol
		Olieic Acid
		2-Hexadecanoic acid
		Furfuryl alcohol
8	Polar protic	1, 4-Butanediol
		1,3 propane diol
		2,3-butanediol
		Glycerol
		Triethylene glycol
9	Organic acdic compounds	m-cresol
		Lactic acid
10	Polar structured	Ethylene Glycol

During the selection of specific solvent in every class of COSMO-RS, it was chosen from biobased such as glycerol, ethylene glycol, 1, 3-propanediol, decyl alcohol, lactic acid, oleic acid, geraniol, cyrene, levoglucosenone and furfuryl alcohol or green solvents used in pharmaceutical and cosmetics such as DMSO or at least less health hazard where possible. It was also intended to include high volatile solvents in the specific COSMO-RS class if available. There was no COSMO-RS class-I (strong electron-pair donor base) and class-V1 solvent (asymmetric halogenated hydrocarbon) were found which can satisfy the set criteria. As described in the experimental section, the measurement set was designed to reach a temperature of 225 °C. The measured temperature range was started at room temperature and reached 200 °C or near the boiling point of the solvent. Some solvents were kept in the above

list of solvent which does not fall in high boiling point category but helps to keep the list of solvents to cover a broader range of dielectric constant (one to 30).

7.1.4 Method of Data Recording and Analysis

The measurement of the complex frequency shift ΔΩ and the quality factor, Q, was manually recorded from VNA in a temperature interval. The incremental change of the temperature was set up for 10 °C interval using the temperature setting of the oven and waited for stabilising the temperature of the oven and RCP device before further incremental step. The recording of complex frequency shift was done in every 5 °C temperature interval. When the temperature was reached over 100 °C, the temperature increment was set for every 20 °C, and it was recorded at every 10 °C interval. The low volatile samples temperature incremental was adjusted more frequently. In all cases, the temperature increase was stopped well before the boiling point was reached. The recorded quality factor, Q, and the shift of frequency Δf in the full temperature range was then converted into the complex dielectric loss factor and subsequently the real and imaginary part by applying the *Equation 35* and *Equation 36* using Matlab R2017a and specially written coding for the purpose. The obtained real and imaginary part of the complex dielectric loss data was then processed with Origin lab 2018b for the calculation of loss tangent, data analysis and for curve fitting.

7.1.5 Classification of Solvent-based on Dielectric Thermal Behaviour

From the analysis of real, imaginary and loss tangent data, it was realised that both the real and imaginary parts of the complex dielectric property initially increases as the temperature increase and reached a maximum point. But the maxima position of the real and imaginary parts of the complex dielectric property of a solvent do not arise at the same temperature.

All the solvents that were listed in *Table 25* can be discussed in the following four categories.

- In the first category, all the organic solvents have a peak maximum of imaginary and the real part of dielectric constant with sufficient data point on both sides of the peak maxima in the measured temperature range.
- In the second category, either the real or the imaginary part or both parts do not have enough data point on at one side of the peak maxima in the measured temperature range.
- In the third category, either the real or the imaginary part or both parts have very few data point at one side of the peak maxima in the measured temperature range.

- In the last category, the peak maxima of either the real or the imaginary or both parts were not found in the measured temperature range.

All of those four mentioned categories with their sub-category, the COSMO-RS listed samples are reorganised accordingly in *Table 26*.

Table 26 Reorganised COSMO-RS category solvent according to temperature-dependent dielectric behaviour

Category	Availability of peak maxima between 20 °C to 200 °C		Sub category	Solvent
1	Both the real and imaginary part peak maxima have Sufficient data on both sides of the curve		1	1, 3-Propanediol
				1, 4-Butanediol
				2, 3-Butanediol
2	Insufficient data around peak maxima	Imaginary part peak maxima has insufficient data	2a	Ethylbenzoyl acetate
				Glycerol
				Levoglucosenone
				Triethylene glycol
				m-Cresol
		Real part peak maxima has insufficient data	2b	Cycooctanol
		Both part peak maxima has insufficient data	2c	Cynnamaldehyde
3	Very little data at one side of the peak maxima	Imaginary part peak maxima has little data	3a	Cyrene
				Propylene Carbonate
		Real part peak maxima has little data	3b	
		Both part peak maxima has little data	3c	
4	Peak maxima is not in the range of measured temperature	Imaginary part maxima is missing	4a	γ-valerolactone
				Furfuryl alcohol
				DMSO
				Diethylenetriamine
				Sulfolene
				Ethylene glycol
				Butyl benzoate
		Real part maxima is missing	4b	Lactic acid
		Both part maxima is missing	4c	

An example of a solvent with the real and imaginary part of the complex dielectric constant is presented below from *Table 26*, where appropriate solvents were examined in this experiment:

1. Real and imaginary peak maxima have sufficient data on both sides of the curve (1,3-propanediol *Figure 153*)

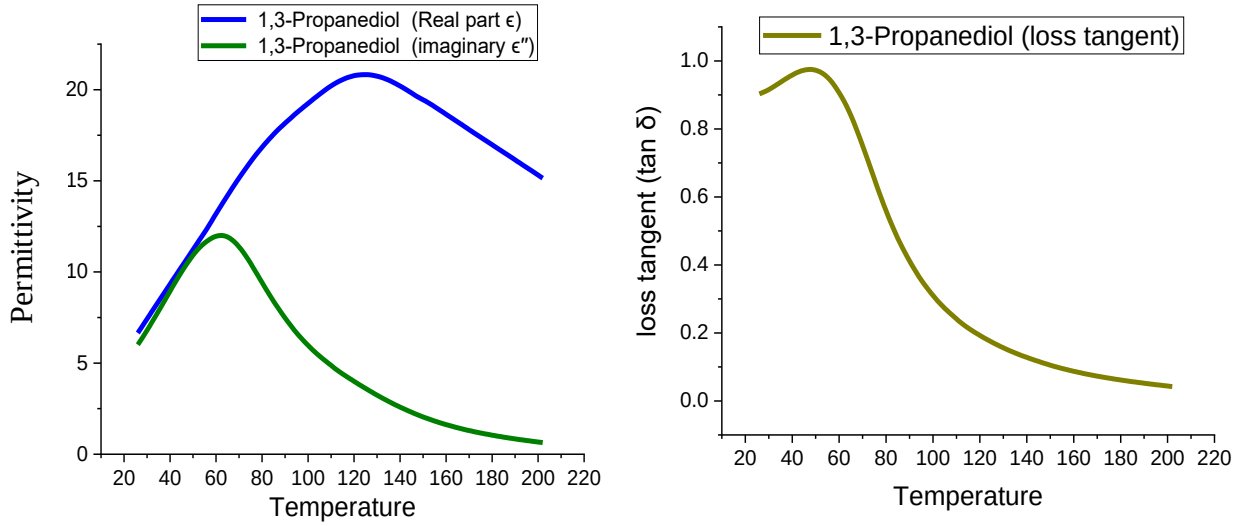

Figure 153 Real, imaginary and loss tangent of 1,3-propanediol

2a. Insufficient data around the imaginary part peak maxima (Levoglucosenone *Figure 154*)

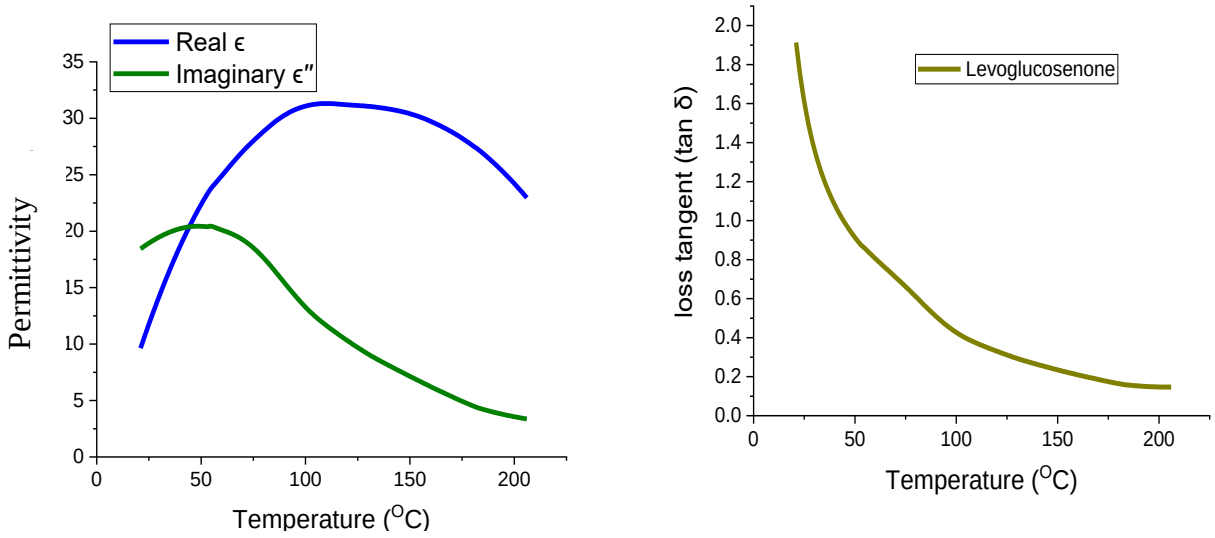

Figure 154 Real, imaginary and loss tangent of Levoglucosenone

2b: Insufficient data around the real part peak maxima (Cyclooctanol, *Figure 155*)

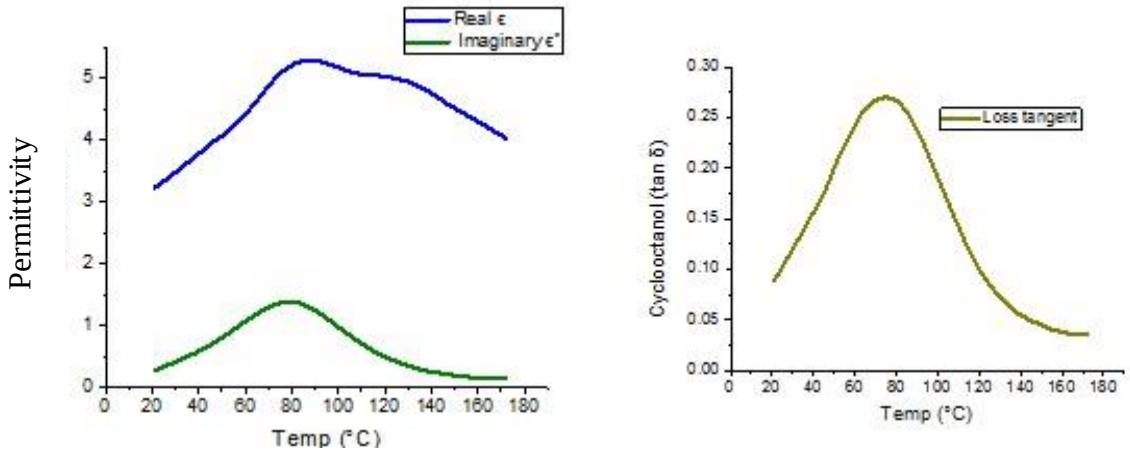

Figure 155 Real, imaginary and loss tangent of Cyclooctanol

2C: Insufficient data around both real part peak maxima (Cinnamaldehyde *Figure 156*)

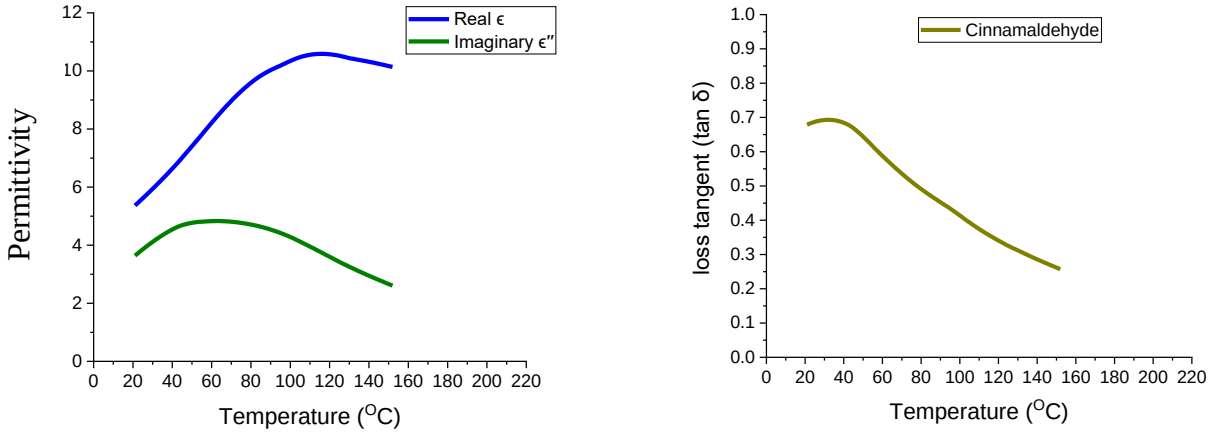

Figure 156 Real, imaginary and loss tangent of Cinnamaldehyde

3a: Imaginary peak maxima shows little data around it (Propylene Carbonate, *Figure 157*)

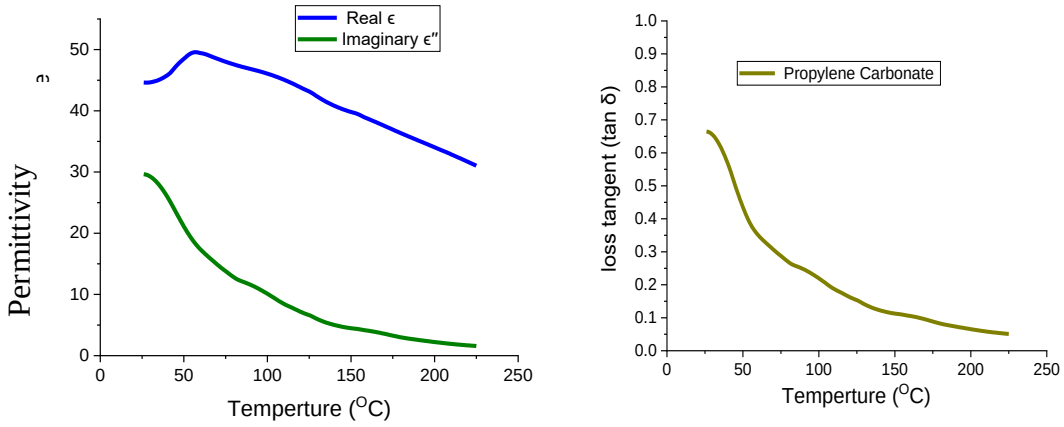

Figure 157 Real, imaginary and loss tangent of propylene carbonate

4a. Imaginary peak maxima are missing (Sulfolane, *Figure 158*)

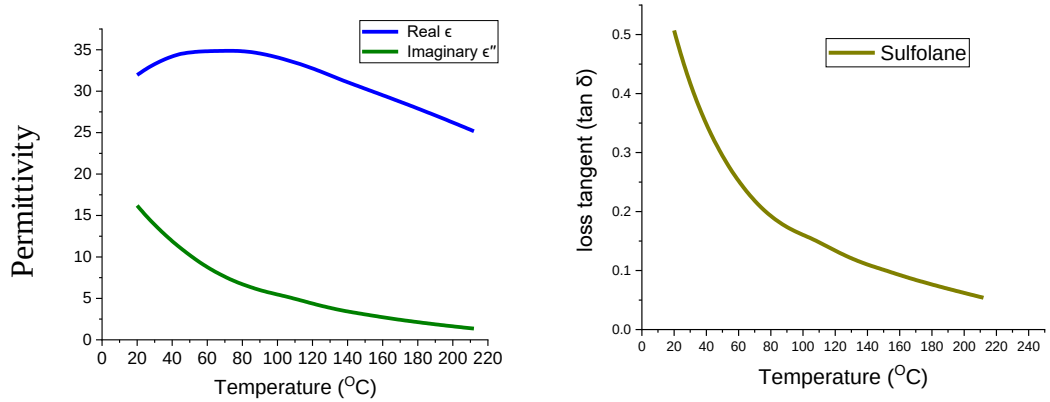

Figure 158 Real, imaginary and loss tangent of Sulfolane

4b. Real and imaginary parts peak (Lactic acid, *Figure 159*)

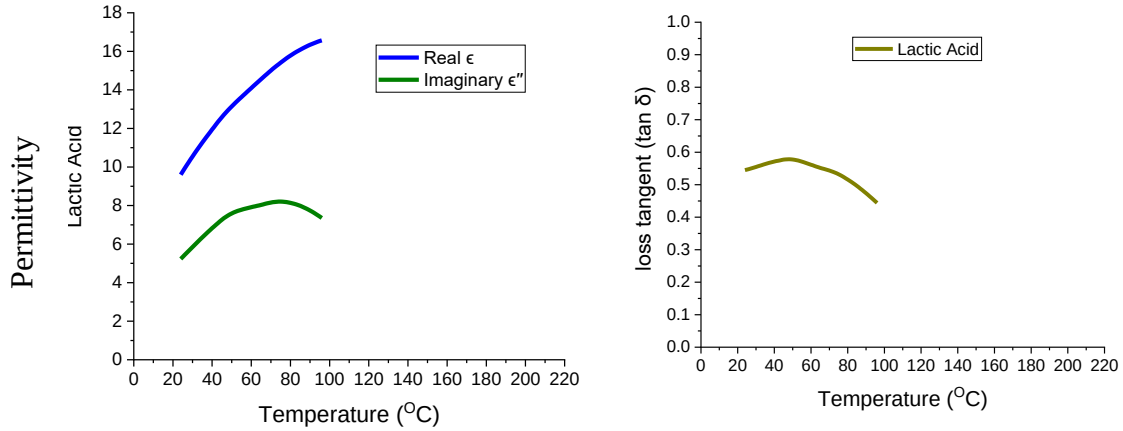

Figure 159 Real, imaginary and loss tangent of Lactic acid

The example of 3b, 3c and 4c are not represented in this work, but it could be predicted based on this work that those types of solvents may exist practically.

Interestingly, the maximum points of the dielectric value of the real and imaginary part of a solvent do not attain at the same temperature. According to our knowledge, this observation has never been published before. This observed phenomenon limits the information which could be gained from the temperatures setup range (22-200°C) of this experiment. Because of the curvature type characteristic behaviour of the real and imaginary part of the complex dielectric property, it was realised that for the full solvent dielectric properties prediction, it is necessary to have the two tails (of left and right-hand sides) of both real and imaginary peak maxima. If either of the real or the imaginary parts do not have enough data point on one side of the peak maxima, the prediction will be limited. Therefore, the first category of the solvent was chosen to analytically describe the organic liquid dielectric properties. In Appendix-A (section 10.3) all of the samples of *Table 26* were analysed with Asym2sig and Pearson curve fitting.

7.2 Analytical Description of Organic liquids Dielectric Behaviour

7.2.1 1, 3-propanediol curve fitting

As category one satisfies both sides of the peak maxima sufficiently for the real and imaginary part, in the first instance an appropriate type of empirical curve fitting will be proposed for this category. In the case of the measured real part of the 1,3-propanediol, asymmetric double sigmoidal function (Asym2sig) satisfies at the statistical tolerance level. The Asm2sig curve fitting with 1,3-propanediol is shown at (Figure 160).

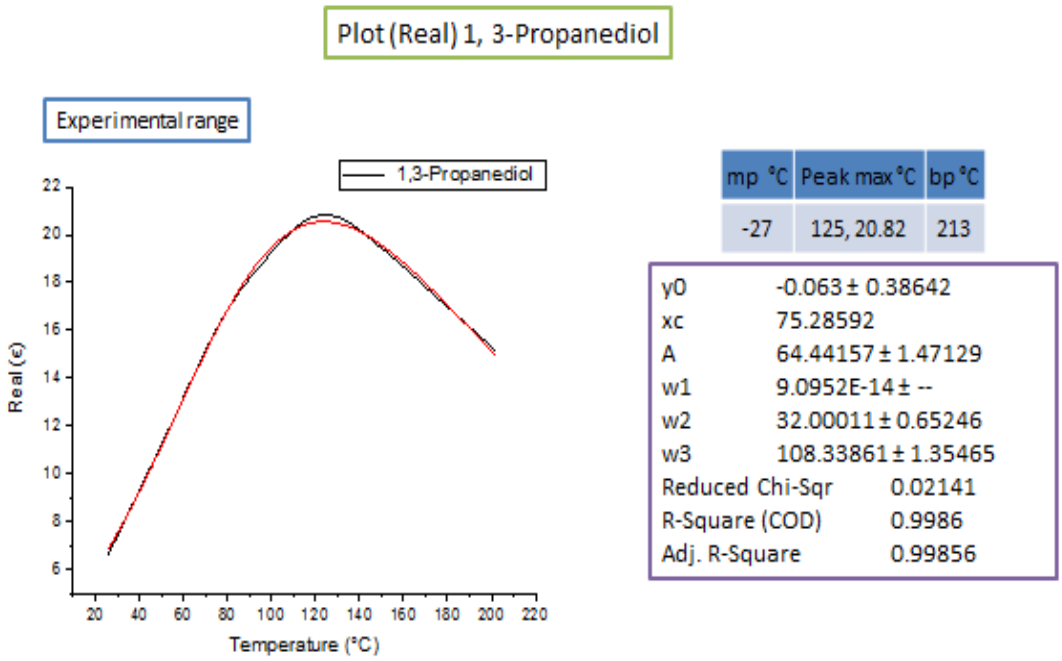

Figure 160 Real part of the complex dielectric data of 1,3-propanediol and Asym2sig curve fitting

The Asym2sig curve-fitting extrapolation (red line), related parameters denotation are presented in *Figure 161*. The Asym2sig curve function equation is shown in *Equation 40*.

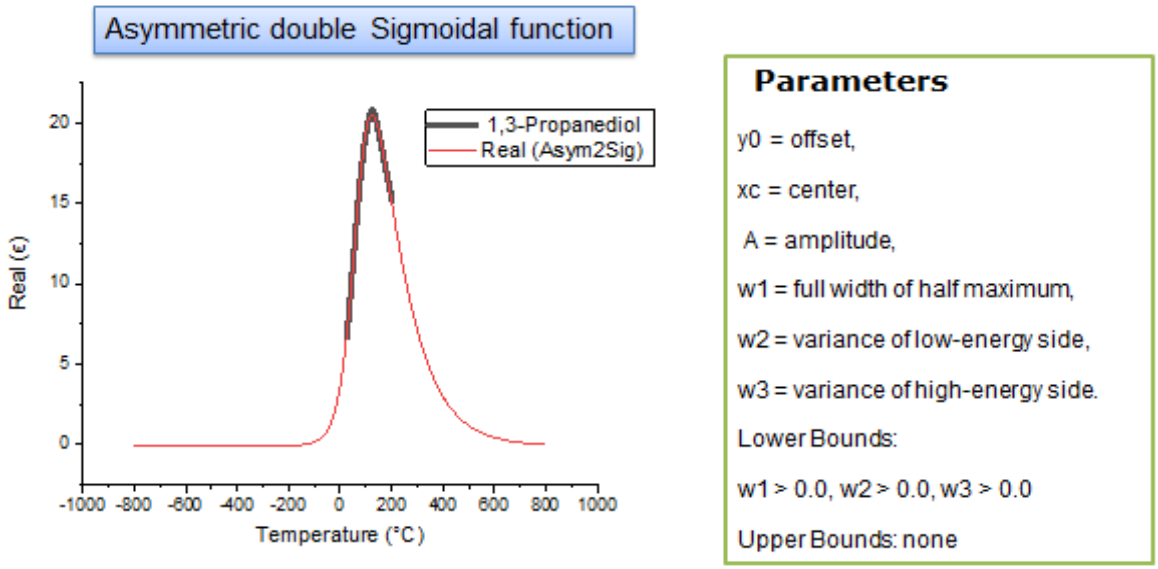

Figure 161 Asym2sig curve fitting extrapolation (red line) and related parameters.

$$y = A \cdot \frac{1}{1+e^{-\frac{x-xc+w_1/2}{w_2}}} \cdot \left[1 - \frac{1}{1+e^{-\frac{x-xc-\frac{w_1}{2}}{w_3}}}\right]$$

Equation 40

Here, in this case, the independent variable x is the temperature. Y_0 is the initial value at X_0; A is the maximum amplitude, X_c is the distance of the centre of the curve from ascending inflection point. W_1 is the width of the curve; w_2 and w_3 are shape parameters of which magnitude indicate peak tailing (distance from the tangent to the curve at 10% peak height) of both side (Figure 162).

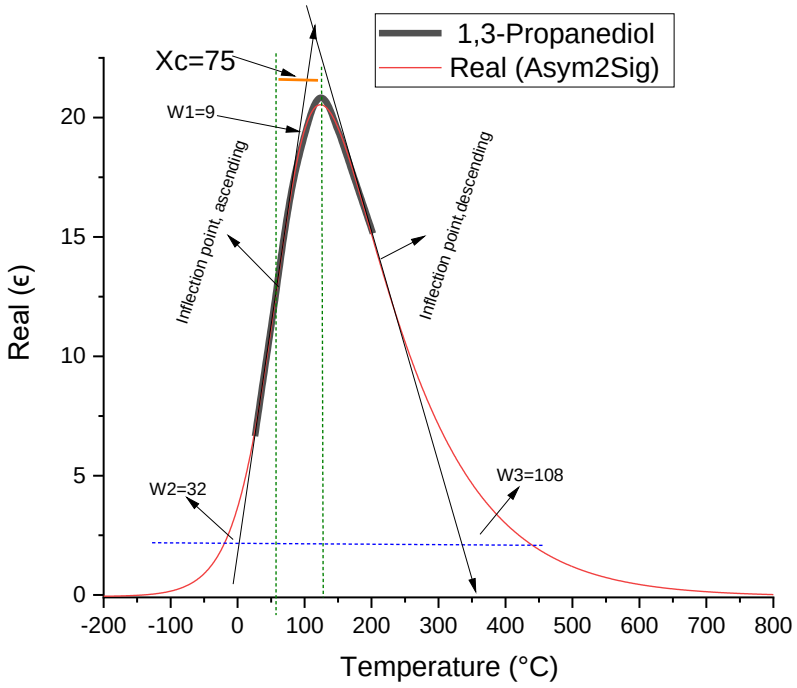

Figure 162 Asym2Sig curve fitting parameters

The imaginary part of the complex dielectric constant of most of the solvent, including 1,3-propanediol satisfies the Pearson V11 curve fitting function (*Figure 163*).

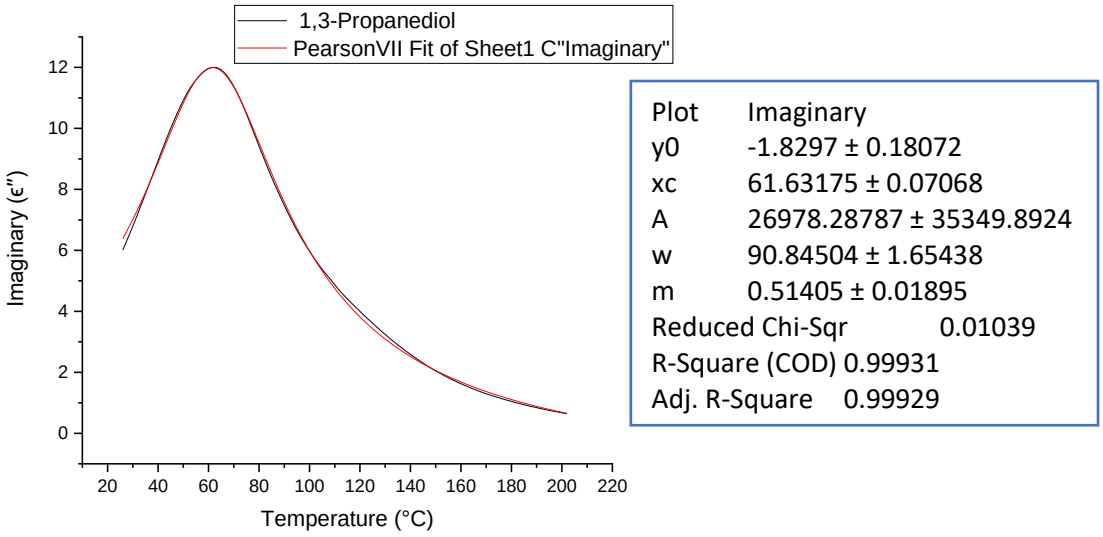

Figure 163 The imaginary part curve fitting of 1,3-propanediol with the Pearson V11 model

The curve fitting empirical formula is written in *Equation 41*

$$y = y_0 + A.\frac{2\Gamma(m).\sqrt{(2^{1/m}-1)}}{\sqrt{\pi}\Gamma\left(m-\frac{1}{2}\right)w}.\left[1+4.\frac{2^{\frac{1}{m}}-1}{w^2}.(x-x_c)^2\right]^{-m}$$

Equation 41

Here, the profile shape factor **m** is the fourth moment of the curve, which indicates the kurtosis or peak tailedness or widthness, in the same way as the third moment describes the peak skewness of a curve. As the fourth moment is free of peak position and magnitude of a curve, two peaks with the same m-value with different peak amplitude and position would still describe the same peak characteristics. In the case of dielectric loss factor, it is thought here that any two solvents with the same **m** factor would indicate an inherent similarity of molecules permanent or induced polarity interaction behaviour in MW influence at changing temperature. The m value of 1,3-propanediol is 0.51405 (*Figure 163*).

As it is shown in *Figure 164* when the denoted m gains the value of one, it becomes a Lorentzian function, and when it approaches infinity, it becomes a Gaussian function. In this operation and for the remaining of the samples, the m-value was limited with the boundary condition of (0.5<m<170).

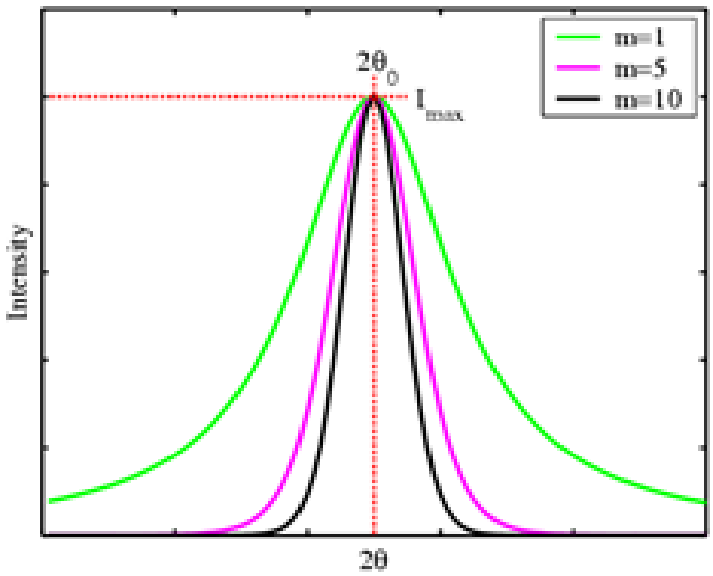

PEARSON FUNCTION V11

A>0, W>0, m> 0

Centre = xc

Area = A

Width = w

Figure 164 (top left): Pearson V11 curve with different m-value, related parameters.

Using the pearson V11 curve fitting model as it was described above, the imaginer part of the dielectric constant of 1,3-propanediol's is extrapolated between -100°C to 400 °C at both sides of the curve (*Figure 165*).

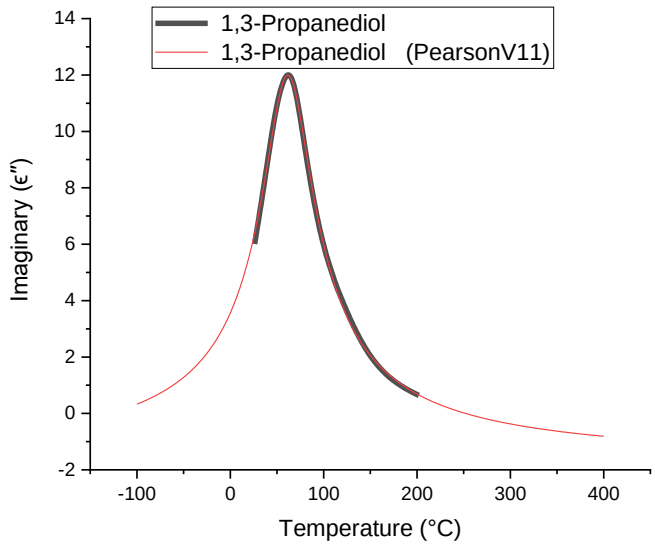

Figure 165 Exploited imaginary curve of 1,3-propanediol. Pearson V11 model is used for extrapolation

The prediction of the real part of the dielectric constant of the 1,3-propanediol between -100°C to 400 °C was already shown in *Figure 161* by using Asy2sig function. The loss tangent of 1,3-propanediol was calculated according to *Equation 29* by using the real value and imaginary value in the experimental temperature range (25°C to 200 °C) (*Figure 166*).

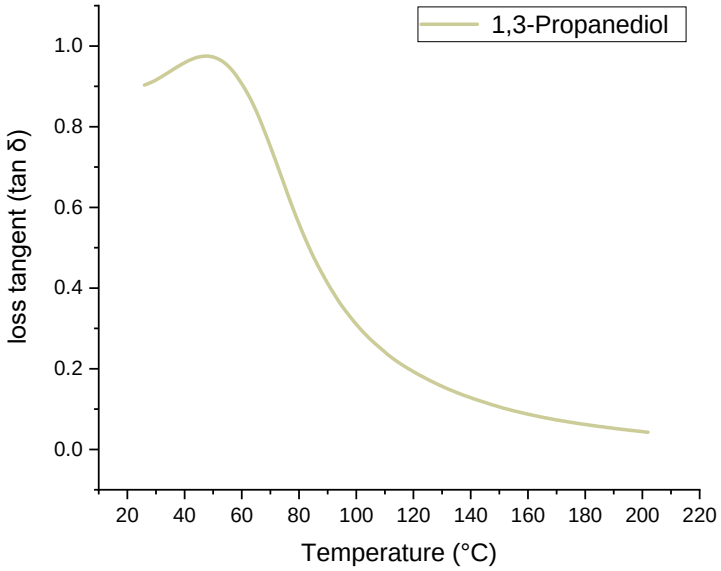

Figure 166 Calculated loss tangent of 1,3-propanediol.

The two-predicted real and imaginary values were then used to further predict the loss tangent (tan δ) of 1,3-propanediol for the temperature range of (-100°C to 400 °C) (*Figure 167*).

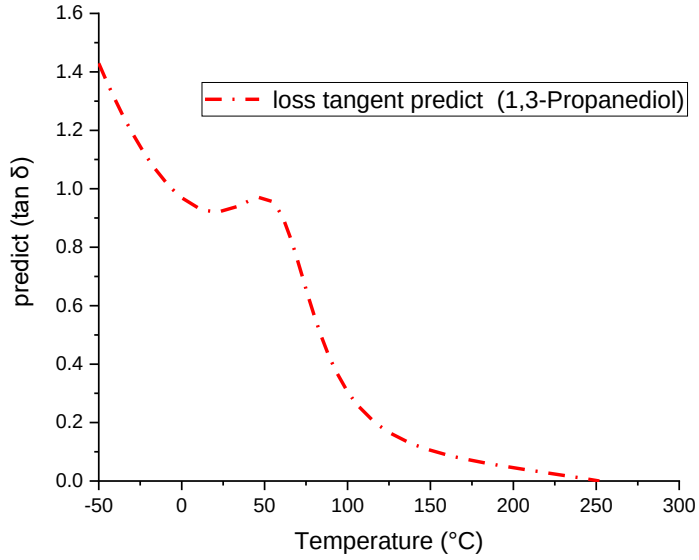

Figure 167 Predicted loss tangent of 1,3-propanediol.

In (*Figure 168*) all predicted values (real, imaginary and tan δ) at the temperature range of -100 °C to 400 °C is presented.

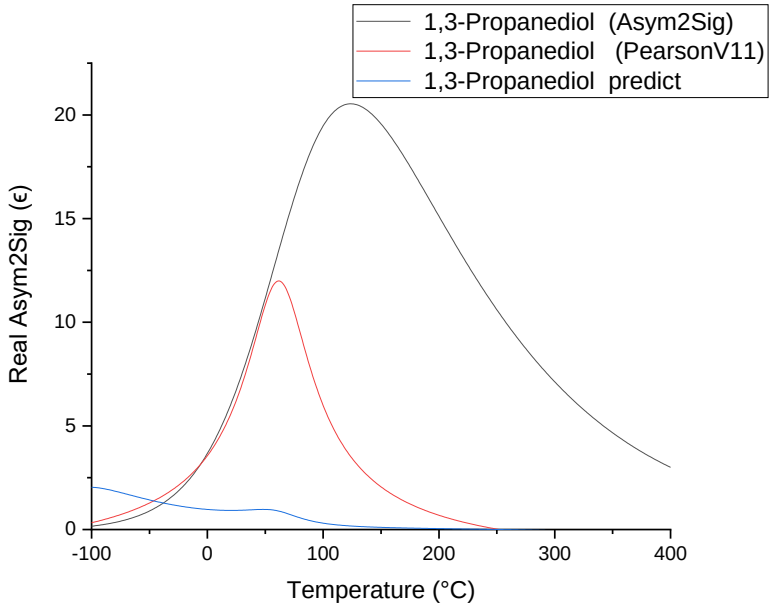

Figure 168 Predicted values real, imaginary and loss tangent of 1,3-propanediol

In (*Figure 169*), the tan δ value, which was gained from dividing the measured imaginary value by measured real value in the experimental temperature range (25°C to 200 °C) (*Figure 166*), is compared with predicted tan δ (*Figure 167*). Both calculated (light ash colour solid line) and predicted tan δ value (short dotted red line) curve almost superimpose each other in the measured temperature range. It is also clear here that the extrapolation of the calculated tan δ would follow and satisfy the predicted tan δ curve. The normalized predicted real and predicted

imaginary curve is also presented on the same scale with real and imaginary value of 1,3-propanediol graph for comparison with both predicted and calculated loss tangent scale (*Figure 169*).

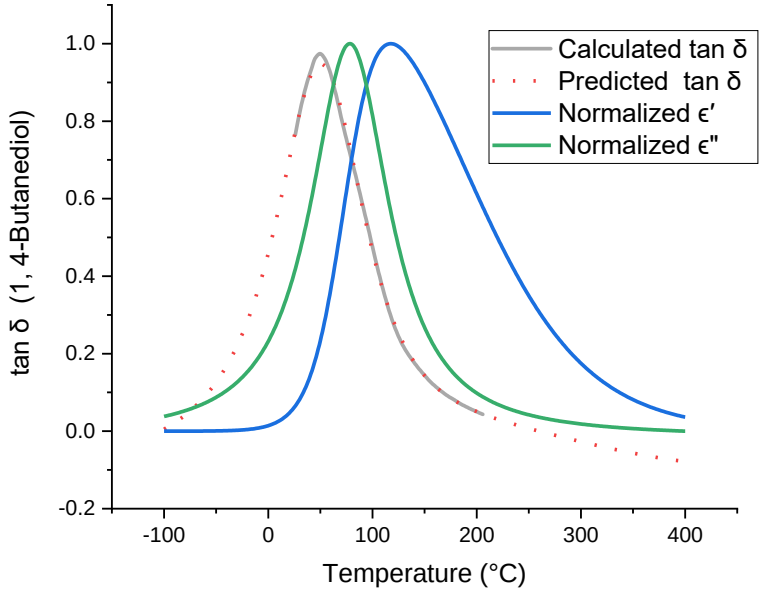

Figure 169 Normalised value of Predicted real, imaginary and loss tangent of 1,3-propanediol(calculated and predicted).

It is assumed that the boiling point and melting point would be the practical cut off point for the empirical curve fitting model as expected from Asym2sig for real and Pearson-V11 curve fitting function for the imaginary part of the complex dielectric constant. According to Debye for a simple spherical molecule of the radius (r), the polar molecular macroscopic rotational relaxation time (τ) could be expressed as (*Equation 42*) of viscosity (η) and temperature (T).[519] Here *k* is Boltzmann's constant and r is the radius of the dipole.

$$\tau = 4\pi r^3 \eta / kT$$

Equation 42

As the viscosity relates to temperature when the solvent cools down to its freezing temperature, the viscosity becomes very high and molecular relaxation time falls off from resonating with MW frequency, and hence its contribution to dielectric permittivity ceases. On the other hand, at the point of boiling point, the solvent becomes gas, and the molecule becomes completely in phase with MW oscillation radiation frequency due to the very small molecular relaxation time of the solvent at this physical state. As the solvent does not lag with the oscillating electric field, there is no generation of thermal energy due to dielectric loss. Practically, in a closed vessel MW reaction the solvent liquid reactant could remain in the liquid phase due to high

vapour pressure. If the liquid molecule at a temperature higher than its boiling point can resonate with applied MW field (2.45 GHz) at around or higher than molecular rotational relaxation rotational time (τ) of 65 picoseconds than the liquid will still be MW active at elevated temperature (*Equation 42*). The phenomenon of molecular resonance with MW depends upon the size of the molecule and intermolecular hydrogen bond.[519] It is suggested here that some liquid organic molecule have a spherical shaped three-dimensional structure such as 2, 3-butanediol which can retain its intramolecular hydrogen bonding or permanent dipole (eg. Levoglucosan) at very high-temperature state. The thermal loss can stay effective at even 1000 picoseconds or higher molecular relaxation time in some cases.[519] The ability of the solvent to resonate with MW at a higher temperature may cause superheat in the system and the boiling point may also raise 10 to 20 °C above than the standard boiling point.[604] Again, for some liquid at even supercooling temperature, the rotational relaxation time could be in the appropriate range of MW frequency to cause dielectric loss through resonance. In all those mentioned circumstances, the prediction of Asym2sig for real and Pearson V11 for the imaginary part of the complex dielectric constant may be applicable beyond boiling and melting point at up to a specific temperature. So, in the case of 1,3-propanediol, the range of the curve fitting prediction would be in the range of -27°C to 213 °C (*Figure 165*) unless it would be proven practically otherwise.

7.2.2 Evaluation of dielectric properties of all of the solvent categories for practical purposes

From the above discussion of all the four categories of solvent-based on complex dielectric behaviour under the influence of varying temperature, the acquired information can be summarized in the following way. The real, imaginary and loss tangent prediction of category one solvent, like 1,3-Propanediol or 1, 4-butanediol, is very reliable considering the other three categories of solvent. The category two and three solvent needed to be carefully considered on a case by case basis for the appropriate purpose of the application. As category four solvents dielectric loss factor (ϵ") data prediction is less reliable at lower temperature range beyond room temperature, hence the dielectric loss tangent (tan δ) prediction is even less reliable, although the data prediction of the real part at lower temperature range may be possible with a degree of confidence. In which case both real and imaginary part peak maxima are missing, as, in the case of lactic acid, the dielectric loss tangent prediction beyond the measured temperature range is not reliable. To calculate the dielectric loss factor (ϵ") curve profile shape factor (m) with confidence, enough data point is needed around the peak head. In some cases, like 2,3-butanediol, a Pearson V11 type curve fitting for the imaginary part may not fully cover both

sides of the curve and hence two curve profile shape factor (m) is needed for left and right-hand side of the peak. Three important parameters, the maximum value of dielectric loss factor (ϵ") and its position in terms of temperature, and the maximum width of the curve at half height (MWHH) are prediction indicators of the range and magnitude of a solvent's dielectric loss factor (ϵ") at a higher temperature. It was noticed that above 200 °C, in almost all cases, the curve profile shape factor (m) or the fourth moment, is enough to predict the dielectric loss factor confidently. In (*Table 27*), all solvents that were tested in this scheme are shown with the melting point (mp), boiling point (bp) and maximum dielectric loss factor (ϵ") value at related temperature with profile shape factor (m). Where it was not possible to assign profile shape factor-m for a specific solvent, then the solvent is assigned with a profile shape factor that best fits with the left-hand side of the curve and another shape factor that best fit with the right-hand side of the curve. Using the unique (m) value of a solvent from *Table 27*, the ability to generate heat with that solvent at higher than 200 °C is possible. The lower the m value, the higher the capacity of a solvent to generate heat under MW interaction. The dielectric loss factor (ϵ") of all solvents from 25°C to 300 °C is presented in (*Table 28*).

Table 27 Maximum value of dielectric loss factor (ϵ") and its curve profile shape factor (m)

Sub category	Solvent	mp	bp	Temp at ϵ" max	ϵ" max	ϵ"at 200 °C	MWHH	m	Left-m	Right-m
1	1, 3-Propanediol	-27	213	61.63	12	0.69	90.84	0.514		
	1, 4-Butanediol	20	235	78.3	9.3	0.6	90.75	1.1008		
	2, 3-Butanediol	19	180.7	75	5.8	0.07			0.506	0.500001
2a	Ethylbenzoyl acetate	0	265	49.5	3.83	0.69	153.37	1.27852		
	Glycerol	-15	230	65	12.41	0.92				1.81483
	Levoglucosenone	0	254.4	47	20.44	3.66	144.89	1.05751		
	Triethylene glycol	-7	285	49	7	0.36	95.69	1.06282		
	m-Cresol	11	202.8	62	2.65	0.2	87.19	0.8661		
2b	Cycloctanol	14.2	97	78.2	1.4		62.62	2.14		
2c	Cynnamaldehyde	-7.5	248	64.8	4.5	1.64			1.17784	1.12228
3a	Cyrene	-20	227	41	15.38	1.89	123.52	1.0538		
	Propylene Carbonate	-48.8	242	26	26.65	2.45	108.72	0.50284		
4a	γ-valerolactone	-31	207	-5	13.28	0.96	120.32	1.0735		
	Furfuryl alcohol	-29	170	22	4.45	0.17	105.67	1.69744		
	DMSO	19	189	19	10.52	1.14	87.89	1.18		
	Diethylenetriamine	-39	204	-3	4.7	0.03	86.9	1.14		
	Sulfolene	27.5	285	27.5	16.2	1.63	140.38	1.03		
	Ethylene glycol	-12.9	197.3	20	13.83	0.7*	95.69	1.06		
	Butyl benzoate	-21	250.4	-21	1.95*	0.178	124.24	1.14		
4b	Lactic acid	17	122	74	8.2					

In *Table 28*, the light grey coloured values are measured value while the light golden and light orange coloured values are predicted values from curve fitting of dielectric loss factor using Pearson V11 model, except the left-hand side curve fitting of glycerol. The left-hand curve fitting of glycerol was performed with Asym2sig curve fitting function as Asym2sig function

assign better prediction on the left-hand side of this solvent than Pearson V11. In terms of the level of confidence to predict the imaginary value, the light golden colour indicates that the probability is higher of these values to be true than light orange colour if it would have been measured practically. It is understandable that the further away from the prediction point from both sides of the curve's measured dielectric loss factor value in terms of temperature, the less probable the assigned value to be true. The prediction of the loss factor at melting point and at the boiling point is also shown in *Table 28*.

Table 28 Dielectric loss factor (ϵ") value (25°C to 300 °C)

Calculation of dielectric loss factor (ϵ") at variour temperature with cofidence limit																	
Category	Solvent	mp °C	at mp	25	50	75	100	125	150	175	200	225	250	275	300	at Bp	bp °C
1	1, 3-Propanediol	-27	2.10	6.20	10.80	10.50	6.00	3.40	2.10	1.20	0.69	0.60	0.55	0.50	0.40	0.65	213
	1, 4-Butanediol	20	3.10	3.60	6.60	9.20	7.50	4.20	2.20	1.20	0.60	0.40	0.30	0.20	0.10	0.40	235
	2, 3-Butanediol	19	3.50	3.60	4.40	5.80	3.70	1.90	1.00	0.40	0.07	0.03	0.02	0.02	0.02	0.60	180.7
2a	Ethyl Benzoylacetate	0	2.70	3.50	3.80	3.40	2.70	1.90	1.40	1.00	0.70	0.50	0.40	0.30	0.20	0.30	265
	Glycerol	-15	2.30	3.30	9.80	11.80	8.80	5.30	2.80	1.40	0.92	0.40	0.20	0.10	0.10	0.30	230
	Levoglucosenone	0	14.60	18.90	20.60	18.00	13.50	9.50	6.80	4.90	3.66	2.80	2.20	1.80	1.50	2.10	254.4
	Triethylene glycol	-7	2.80	5.60	7.00	5.40	3.10	1.80	1.00	0.60	0.36	0.20	0.09	0.02	0.00	0.01	285
	m-Cresol	11	1.10	1.30	2.50	2.40	1.50	0.80	0.50	0.30	0.20	0.10	0.10	0.10	0.00	0.20	202.8
2b	Cycooctanol	14.2	0.20	0.30	0.80	1.40	1.00	0.40	0.20	0.10	0.10	0.10	0.10	0.10	0.10	1.10	97
2c	Cynnamaldehyde	-7.5	2.00	3.90	4.90	4.90	4.40	3.60	2.80	2.10	1.64	1.30	1.00	0.80	0.60	1.00	248
3a	Cyrene	-20	8.00	15.00	14.90	11.50	7.80	5.20	3.60	2.50	1.89	1.40	1.10	0.90	0.70	1.40	227
	Propylene Carbonate	-48.8	9.62	29.70	21.89	13.85	9.19	6.41	4.61	3.36	2.45	1.75	1.21	0.77	0.41	1.37	242
4a	γ-valerolactone	-31	11.13	10.72	7.33	4.76	3.20	2.26	1.66	1.24	0.96	0.77	0.62	0.52	0.43	0.90	207
	Furfuryl alcohol	-29	2.36	4.40	3.47	2.15	1.22	0.70	0.42	0.26	0.17	0.12	0.08	0.06	0.04	0.29	170
	DMSO	19	13.07	11.56	7.02	4.41	3.30	2.53	1.91	1.35	1.14					1.16	189
	Diethylenetriamine	-39	2.76	3.30	1.84	1.06	0.67	0.45	0.32	0.24	0.18	0.15	0.12	0.10	0.08	0.18	204
	Sulfolene	27.5	14.54	15.02	10.18	7.29	5.39	4.04	3.05	2.28	1.63	1.17	0.76	0.42	0.12	0.29	285
	Ethylene glycol	-12.9	9.45	13.60	9.80	5.38	2.99	2.29	1.70	0.93	0.7*					0.70	197.3
	Butyl benzoate	-21	1.95	1.44	1.03	0.70	0.48	0.35	0.26	0.21	0.18	0.16	0.14	0.13	0.12	0.14	250.4
4b	Lactic acid	17	4.60	5.40	7.50	8.20	7.10									6.20	122

Reasonably confidence at prediction
Calculated loss factor (ϵ") data
Less confidence at prediction

In most of the cases, the prediction of dielectric loss factor at or near the melting point is more difficult to predict than to predict at the boiling point with Pearson V11 curve fitting model. The reason for the limitation of the prediction, the curve fitting function is not inherently designed by considering of physical parameters of solvent, let alone incorporating critical physical state changing phenomenon such as liquid to gas or liquid to solid state transforming. The hydrogen bonding, viscosity, physical structure and morphology dramatically change at the point of melting or frozen state. For this reason, to predict the dielectric loss property near the melting point would really be challenging. But if the liquid would possible to be cooled into the supercooling state at a certain temperature below the melting point of the solvent then

the predicting Pearson V11 curve fitting might be true down to the range of supercooled temperature of that liquid. On the other hand, as in most of the circumstances, the MW interaction with solvent is performed under a pressurised closed vessel, the Pearson V11 curve fitting model would hold true above the boiling point.

At (*Table 29*) the dielectric loss tangent is present in a similar way as it was presented the dielectric loss factor in (*Table 28*). The colour code in *Table 29* is also describing the same predictive uncertainty as it was used for *Table 28***.** It is necessary to mention here that to understand a specific solvent-MW interaction, both the dielectric loss factor and loss tangent is needed. So, by using both the *Table 28* and *Table 29*, it will be possible to select the correct solvent for a specific reaction or physicochemical process under MW radiation.

Table 29 Dielectric loss tangent (tan δ) value (25°C to 300 °C)

Calculation of dielectric loss tangent (tan δ) at variour temperature with cofidence limit																	
Category	Solvent	mp °C	at mp	25	50	75	100	125	150	175	200	225	250	275	300	at Bp	bp °C
1	1, 3-Propanediol	-27	1.16	0.92	0.97	0.66	0.31	0.17	0.11	0.07	0.05	0.02	0.00	0.03		0.03	213
	1, 4-Butanediol	20	0.70	0.76	0.95	0.77	0.46	0.25	0.14	0.09	0.05	0.03	0.01			0.02	235
	2, 3-Butanediol	19	0.62	0.61	0.53	0.49	0.27	0.14	0.09	0.05	0.02					0.04	180.7
2a	Ethyl Benzoylacetate	0	0.59	0.60	0.51	0.40	0.29	0.22	0.16	0.12	0.09	0.08	0.06	0.05	0.05	0.06	265
	Glycerol	-15	0.05	0.57	1.02	0.64	0.33	0.20	0.12	0.08	0.05	0.03	0.02	0.01	0.01	0.03	230
	Levoglucosenone	0	2.92	1.55	0.90	0.65	0.42	0.31	0.23	0.17	0.15	0.16	0.20	0.30	0.51	0.21	254.4
	Triethylene glycol	-7	0.61	0.64	0.55	0.36	0.21	0.13	0.08	0.06	0.04	0.02	0.01	0.00			285
	m-Cresol	11		0.35	0.50	0.42	0.24	0.14	0.08	0.06	0.05	0.05					202.8
2b	Cycooctanol	14.2	0.08	0.10	0.20	0.27	0.19	0.09	0.05	0.03	0.03	0.03	0.03	0.03	0.03	0.20	97
2c	Cynnamaldehyde	-7.5	0.44	0.65	0.63	0.51	0.41	0.33	0.26	0.21	0.18	0.15	0.13	0.11	0.10	0.13	248
3a	Cyrene	-20		0.92	0.63	0.43	0.30	0.21	0.15	0.12	0.10	0.08	0.07	0.06	0.06	0.08	227
	Propylene Carbonate	-48.8	0.22	0.66	0.45	0.29	0.20	0.15	0.12	0.09	0.07	0.06	0.04	0.03	0.02	0.05	242
4a	γ-valerolactone	-31	0.60	0.34	0.24	0.16	0.12	0.09	0.07	0.06	0.05	0.04	0.04	0.03	0.03	0.05	207
	Furfuryl alcohol	-29	0.44	0.60	0.35	0.20	0.12	0.08	0.06	0.04	0.03	0.02	0.01	0.01	0.01	0.04	170
	DMSO	19	0.30	0.26	0.16	0.11	0.09	0.07	0.06	0.05							189
	Diethylenetriamine	-39	0.55	0.30	0.17	0.10	0.07	0.05	0.04	0.04	0.03	0.03	0.02	0.02	0.02	0.03	204
	Sulfolene	27.5	0.44	0.46	0.29	0.21	0.16	0.13	0.10	0.08	0.06	0.05	0.03	0.02	0.01	0.01	285
	Ethylene glycol	-12.9		1.21	0.44	0.21	0.11	0.09	0.08	0.05							197.3
	Butyl benzoate	-21	0.75	0.31	0.21	0.15	0.11	0.08	0.07	0.06	0.05	0.05	0.05	0.05	0.05	0.05	250.4
4b	Lactic acid	17	0.54	0.55	0.57	0.53	0.42									0.30	122

Reasonably confidence at prediction
Calculated loss tangent (tan δ) data
Less confidence at prediction

At *Table 30*, an initial suggestion is proposed to select a solvent considering the optimum reaction temperature and level of MW heating energy would be needed. If the reaction temperature is needed to be controlled at or over 175 °C, for example, in the occasion of biomass activation, the solvent of choice would be from the right-hand side column of *Table 30*. The specific solvent will be needed to be chosen based on how much thermal activity is needed at the optimal heating condition and favourable solvent property. If thermal energy

generation is the prime need, then the solvent of choice would be one from (ϵ" =2.5 to 5) as there is no other solvent is on *Table 30*, which can generate higher heat higher than (ϵ" = 5) at right-hand side column. By applying the same logic, a solvent may be chosen for other purposes, taking *Table 30* as a guideline. It is needed to keep in mind that the list of solvent mentioned in *Table 30* is not exhaustive.

Table 30 An approach to select an appropriate solvent for optimum MW heating application

Value of ε"	up to 50 ℃	up to 75 ℃	up to 100 ℃	up to 125 ℃	up to 150 ℃	over 175℃
15 to 30	Propylene Carbonate Levoglucosenone DMSO Cyrene					
12.5 to 15		Levoglucosenone Propylene Carbonate Cyrene Glycerol				
10 to 12.5			Levoglucosenone Propylene Carbonate Glycerol Cyrene 1, 3-Propanediol			
7.5 to 10		EtOH	1, 4-butaneiol	Levoglucosenone Propylene Carbonate Glycerol Cyrene		
5 to 7.5				1, 4-butanediol 1, 3-propanediol Sulfolane	Levoglucosenone Propylene Carbonate Cyrene Glycerol	
2.5 to 5	Water		Lactic acid Cinnamaldehyde Ethyl benzoate acetate	DMSO Ethylene glycol	1, 4-butanediol 1, 3-propanediol	Levoglucosenone Propylene Carbonate Cyrene Sulfolane
1 to 2.5			m-cresol			DMSO Glycerol 1, 4-butanediol 1,3-Propanediol Ethylene glycol Triethylene glycol

It was noticed that cyclic keto functional group-containing solvents are more effective to interact with MW for dielectric heating at high-temperature range than acyclic solvents consisting same carbon chain length and functional group. An explanation of this phenomena may be that most of the hydroxyl group-containing polar solvent start losing their hydrogen bond network as temperature increases while aprotic highly dipolar solvents can maintain their molecular dipoles polar rotation without much interacting with neighbouring molecules. Moreover, if those aprotic dipole molecules were spherical then the molecular rotational relaxation time (τ) would not be increased at the same extent as for straight chain protic dipole molecules with the same chain length when the temperature would have increased. The assumption of less change of spherical molecules rotational relaxation time (τ) from initial resonant with MW energy, is because less frictional energy would be required in a less viscous physical state than it would be required for long-chained acyclic molecule if the temperature is increased. Using the same logic, it can also be shown that why spherical cyclic fused double ring molecule like Cyrene is more effective MW dipolar media than a cyclic flat dipolar liquid such as Furfural. If the cyclic keto group is accompanied with an alternative double bond, then the dielectric loss factor gains even higher magnitude compared to without double-bonded counterpart. For example, the dielectric loss factor of Levoglucosenone is higher than that of Cyrene. The higher dielectric loss factor of Levoglucosenone may be due to the better flexibility of shifting keto groups dipole polarity with the conjugated double bond. All those mentioned features of fused ring cyclic keto functional group give an advantage over other types of solvents when it comes to the MW dielectric interaction and heat dissipation. Since bio-based solvents or molecules like Cyrene or Levoglucosenone represents this class of solvents, this observation would encourage chemist and researcher to use greener solvents by replacing DMSO or Sulfolane for the same purpose of MW heating. Since maximum amplitude of the dielectric loss factor of (S=0) containing groups, like DMSO or Sulfolane is at their melting point according to this experimental observation, those solvent could be used in a circumstance where thermal runaway is a problem at low-temperature heating application but needed higher activation energy at the initial stage of MW heating of materials or chemicals.

7.3 Development of a Climate-controlled Automated RCP Instrument

It was discussed in the section of 5.3 that to have a reliable predictive data of some solvents dielectric loss factor and dielectric constant at the temperature lower than room temperature, the actual measurement of those data is needed. Cyrene, DMSO, Sulfolane are an example of such important solvents. Moreover, the dielectric behaviour of such solvents was never studied with RCP device to have an accurate measurement. It was predicted in the previous experiment that at supercooling temperature, the solvent would follow the Asym2sig and Pearson-V11 for dielectric constant and dielectric loss factor respectively. To have confidence in that prediction, it was crucial that the hypothesis is experimentally proven. Moreover, it will interesting to see how different solvent behave in terms of complex dielectric property at and around freezing or melting point, to see if do all solvents follow the same rule of supercooling and resonate with MW in a similar way or not. Another purpose of this device development was that to measure the complex dielectric property of some solvents which may oxidise in high temperature in the presence of oxygen, an instrumental setting is needed where it can be subjected to an oxygen-free neutral environment. Taking all of those mentioned reasons into account an attempt was taken here to develop an RCP instrument which would be able to automatically measure complex dielectric property parameter in every few seconds time interval, can automatically calibrate temperature correction (ref. section 5.2.2 of this chapter) of (-40°C to 180°C) temperature range and interpret the result within a few clicks. The neutral & moisture free atmospheric environment, minimum RF interference and safest sample handling feature was also a target on the course of this instrumental development.

7.3.1 The Instrumental design

The RCP cavity was used in this instrumental setting was exactly the same one that was used for the previous experiment in section 5.2. The Pyrex sample holder was also the same one as used before. As can be seen in *Figure 170*A, the RCP cavity is placed on a PTFE base. The whole RCP device was then covered with a specially made cylindrical Pyrex tube. The custom made PTFE base, and the pyrex container was covered with a PTFE lid. The top and bottom of PTFE plates can then be airtight with screw fittings as can be seen in *Figure 170*A. Sample can easily be placed after unscrewing the top PTFE plates, and removal of the sample also can be performed using the same way after the measurement is completed. A nitrogen gas inlet and outlet (left-hand side of *Figure 170*A), a temperature probe and the coaxial cables are also passed through the airtight container (right-hand side of *Figure 170*A). All of the parts of the

device are temperature resistant. The glass vessel was then placed inside a cubic shaped temperature resistant radio-frequency (RF) shielding materials (*Figure 170*B) to act as a Faraday cage. The RF shielding material was placed on an aluminium frame for supporting the weight and shape of the RF material, as can be seen in *Figure 170*B. The front and top of the RF shielding material can be removed and put back during sample handling when needed.

Figure 170 The RCP cavity is placed on a PTFE base and covered with round Pyrex glass. An N_2 gas inlet and outlet (left), two temperature probe and two coaxial cables were also passed through the airtight container (left). The glass vessel was then placed inside an RF shielding materials (right).

The glass container with the RF shield was positioned inside a climate control chamber (*Figure 171*).

Figure 171 The RF shielding material is placed on an aluminium frame. The glass container with an RF shield was positioned inside a climate control chamber.

The chamber can be operated in the temperature range of -40 ℃ to 190 ℃ with operating switches and knobs on the top of the climate chamber. The oven temperature can be programmed to a set of oven-temperature ramp for hours, days or weeks (*Figure 172A*). The N_2 gas was passed from an N_2 gas cylinder at a pressure of 1.5 bar. The flow of the gas is restricted to a minimum flow with a gas flow restrictor, as shown in *Figure 172B*. The outlet of the nitrogen is placed out of the lab for safety. The gas line is kept open during the instrumental operation period.

Figure 172 The climate control chamber is programmable with temperature ramp, time and date within the temperature range of -40℃ to 190℃. The flow restrictor controls the pressure and flow of N2 gas inside the glass vessel.

All the cables came out from the climate chamber through a silicone plug (*Figure 174*). A Vector Network Analyser (VNA) is connected with the coaxial cables. (left side) A temperature data logger is also attached (placed on the top of VNA). A sample of complex dielectric constant measurement is shown on the right-hand side of the VNA screen (*Figure 174*) (. A temperature probe is attached at the base plate of the metallic cavity, and another one was placed on the neck of the funnel-shaped Pyrex sample holder (*Figure 173*). During oven program operation setting, it was made sure that enough time is allowed for both the temperature probe shows temperature difference within +/1 ℃. Two L-shaped two-coaxial connectors on the VNA were joined with two high-temperature resistant coaxial cables *Figure 173*.

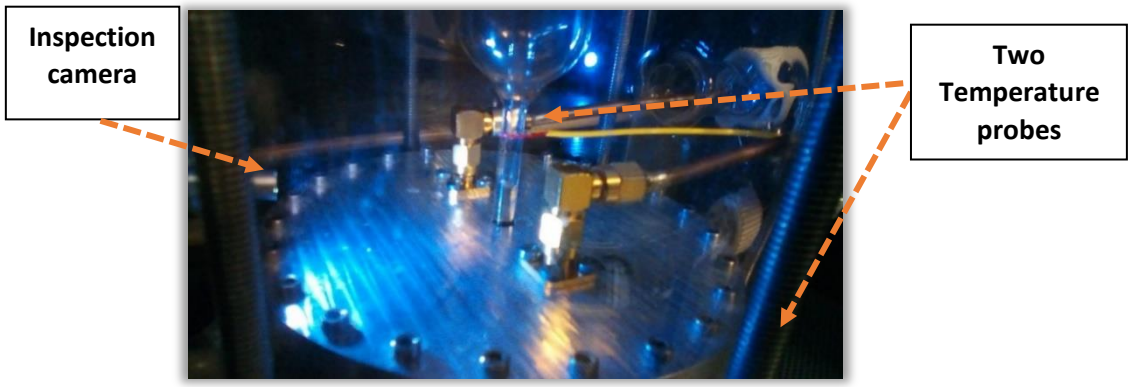

Figure 173 An inspection camera is placed near the sample holder to observe and record the physical state changing of the solvent samples during freezing and melting state of the solvent.

All the cables and tubes then passed through the glass container, Faraday cage and subsequently out of the climate control chamber. The appropriate sealant was maintained via the PTFE seal and ferrule (*Figure 170*A) at the joint of pyrex and via silicone bung on a hole of climate chamber (*Figure 174*, left). A data logger records the temperature inside the pyrex chamber and RCP cavity (*Figure 174*). A VNA display the complex frequency and quality factor shifts during measurement *Figure 174*, right-hand side.

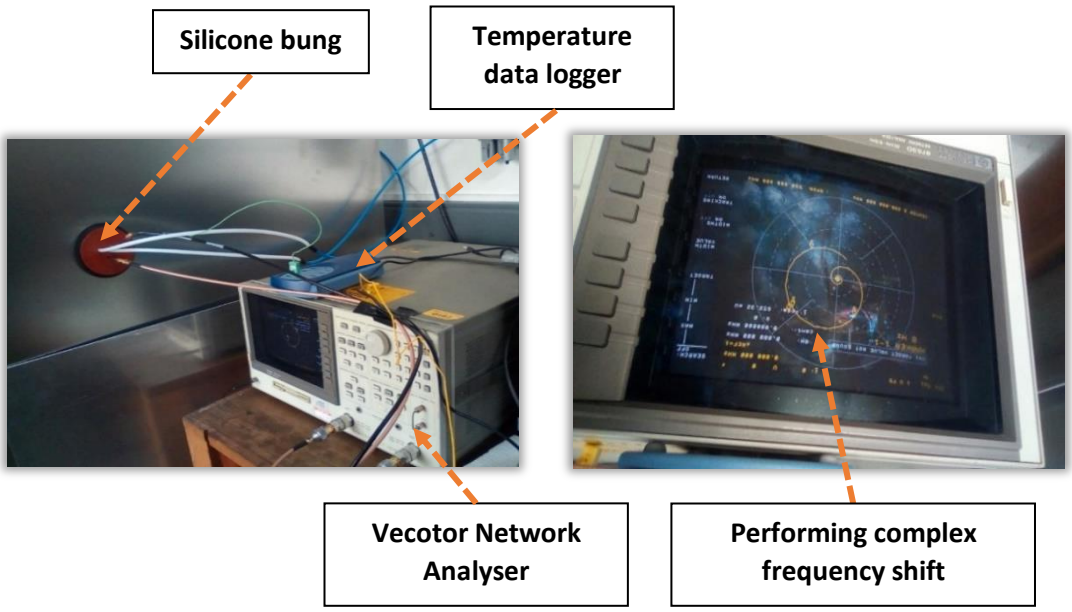

Figure 174 All the cables came out from climate chamber through a silicone plug. A Vector Network Analyser (VNA) is connected with the coaxial cables. (left side) A temperature data logger is also attached (placed on the top of VNA. A samples complex dielectric constant measurement is shown on the VNA screen (right side)

An automated python program was developed to record the complex dielectric data in the form of frequency and Q-factor of every cycle of measurement with temperature stamp in real-time (top left side of *Figure 175*). One cycle of measurement happens in less than three seconds. A user interface of the same python program allows the user to insert the sample details and data recording request (top right of *Figure 175*).

To measure a sample, the following sequences are needed to perform:

A. Set up appropriate climate chamber temperature ramp,
B. Place the sample inside the sample holder,
C. Close the pyrex container with the rod and screw.
D. Cover the RF shields on the aluminium frame,
E. Close the climate chamber,
F. Input the same information for a specific sample with a destination folder,

G. Synchronise the temperature data logger with sample information,
H. Request the time of data recording on the software, and then
I. Press the play button to automatically start recording the data.

The frequency and quality factor shift data is then converted into the form of the real and imaginary part of a complex dielectric signal. The data was then stored in a folder for offline analysis of dielectric shift trend of a sample in terms of temperature changes (bottom right, *Figure 175*). An inspection camera is placed within a distance of a few centimetres for the image capturing and video recording (*Figure 173*). The quality of the image was very good and ten folds in magnitude.

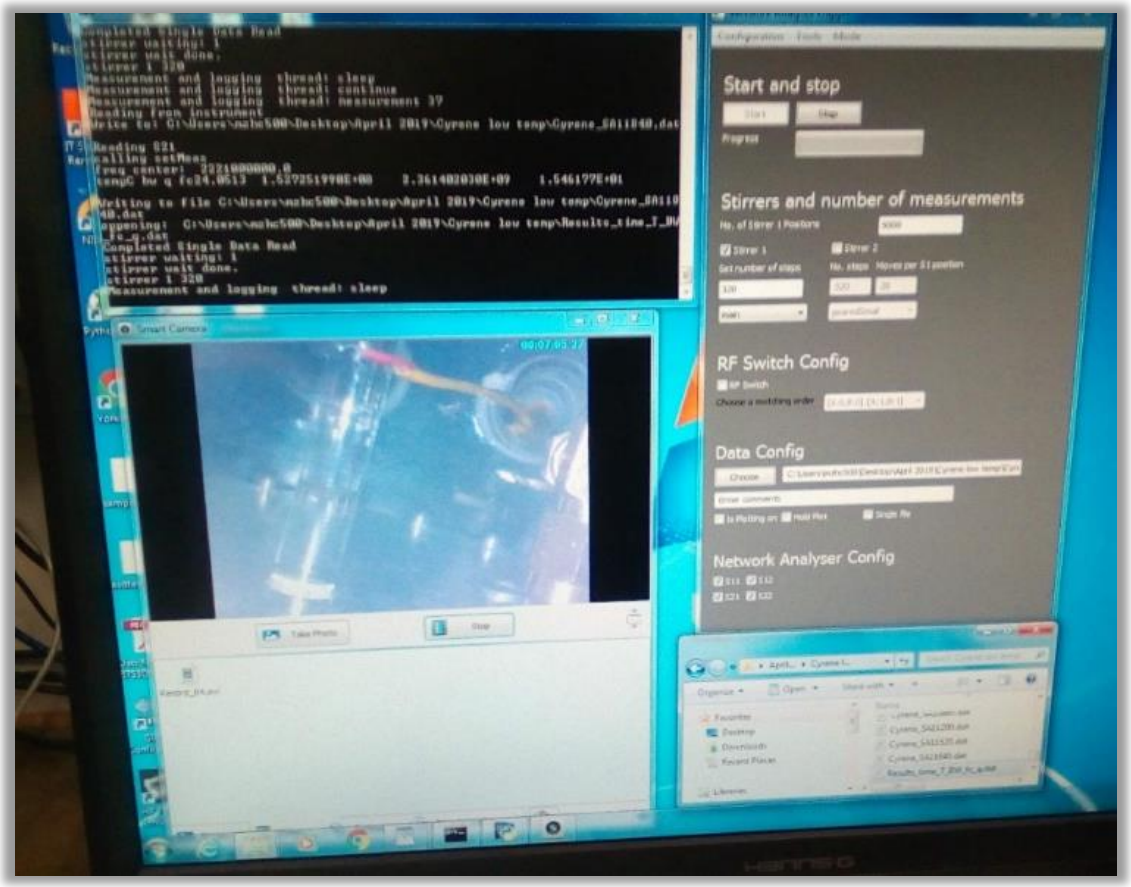

Figure 175 An automated python program was running to record the complex dielectric data (top left). The developed software interface to input sample details and data recording request (top right). The real-time video and photo recording interface (bottom left). The final data is stored (bottom right).

The measurement of dielectric data recording in terms of temperature was performed in two stages. One stage is to ramp the climate control temperature into a U shape pattern as shown in *Figure 176* to observe the dielectric property at lower than room temperature.

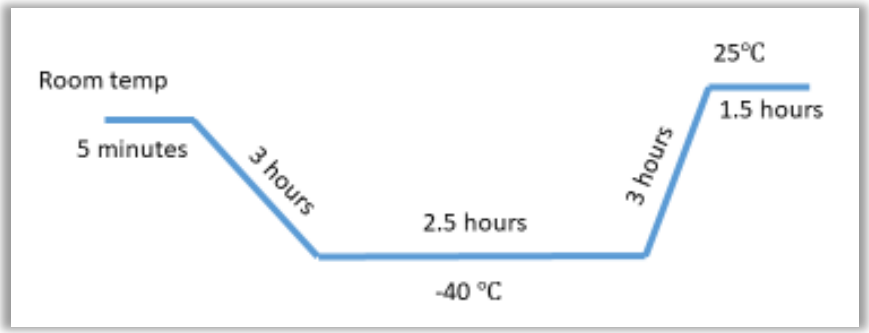

Figure 176 A U shape pattern ramp of the climate control temperature

In this temperature ramp setting the inspection-camera can record the changes of the physical state of the sample from liquid to solid-state and solid to a liquid state if the freezing or melting occurs in the range of temperature ramp setting. On the computer display screen, it can also be seen in real-time if supercooling is happening to the sample or not. It can also be observed how different samples of physical state changes differs from each other. If the transformation from liquid to solid is amorphous and slow or sudden crystal is formed at a particular temperature during freezing that phenomenon can be observed. The purpose of this inspection is to correlate the physical state changes of a sample in a specific temperature change with the change of dielectric loss factor of the sample. Two observations of this purpose are discussed here, taking Sulfolane and Cyrene as examples.

Sulfolane was subjected to dielectric measurement during a U-shaped temperature ramp, as shown in *Figure 176*. The changes in the quality factor (Q) is depicted in *Figure 177*. *Figure 177* represents that while the sample was cooling down, the Q factor was slowly reducing. At -20 ℃ a rapid rise of Q factor happen on a sudden at up to 160, then Q factor gradually further increased at up to 180, which is equivalent to the Q factor of an empty cavity in room temperature. The indication of the Q factor at -40℃ is that the sample becomes completely transparent to microwave frequency at 2.45GHz. But when the sample was once again slowly warmed up the changes of Q factor does not follow the same path. This is an interesting observation which was never reported as of our knowledge.

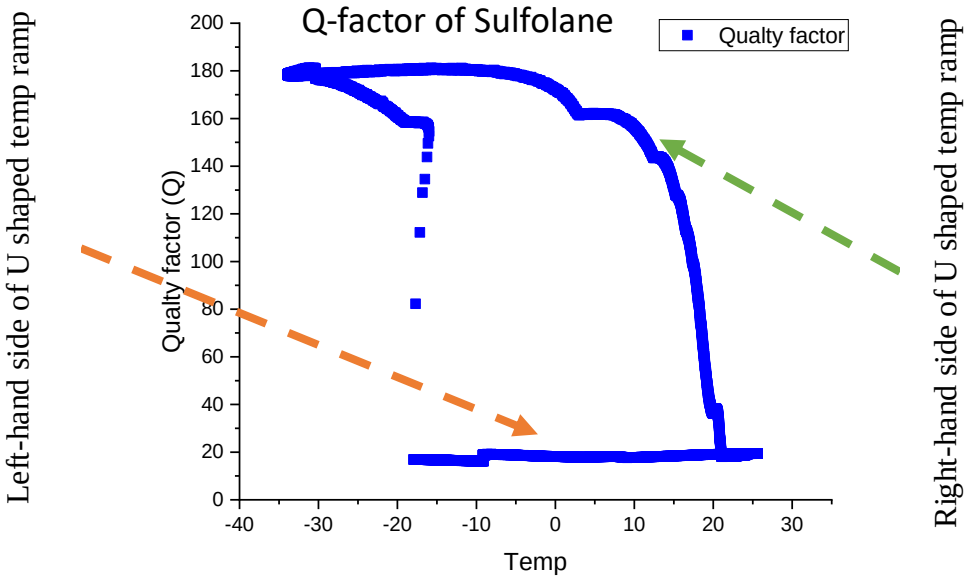

Figure 177 Quality factors of Sulfolane at the low-temperature range.

To further understand the changing behaviour of the Q factor of sulfolane during freezing and colling, the recorded video image was analysed. Some of the video images concerning temperature are presented in *Figure 178* from the left-hand side to the right-hand side as sulfolane cools down. As it can be seen from the pictures, sulfolane slowly forming very light mist at around -0.3℃. The process slowly continues up to -19 ℃ (not shown here), but when the temperature reaches to -20 ℃, Sulfolane freezes suddenly. As temperature further falls downwards, the solid-state of the sample becomes more compact without any drastic changes.

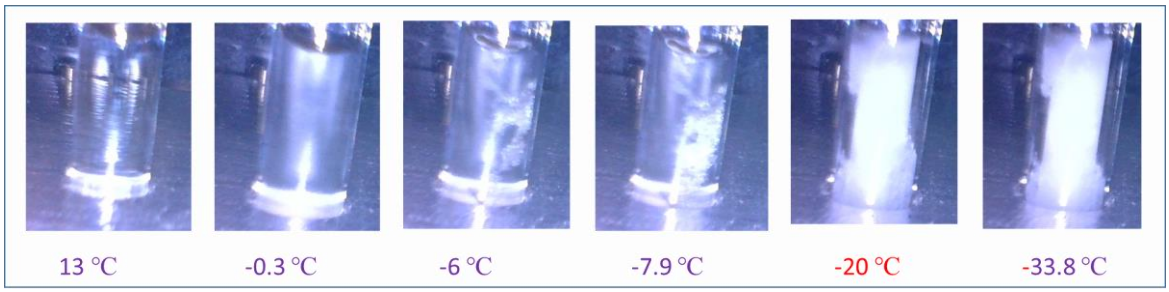

Figure 178 Video Image analysis for Q factor discrepancies during supercooling melting and freezing periods of Sulfolane

Both of the Q factor data and video images support an idea of how Sulfolane interact with microwave at the particular physical state. The analysis of the above data means that when a dielectric liquid completely becomes solid it becomes MW transparent due to the cease of macroscopic molecular relaxation to resonate with MW frequency. But in which pattern the process of becoming a polar molecule into MW transparent or vice versa depends on how the molecules were subjected on a particular temperature in time-dependent route.

7.3.2 Future Prospects

The newly developed, automated RCP device is now fully functional and ready to use. As the instrument was just developed very recently, a comprehensive low-temperature dielectric study of solvent is yet needed to be done. The preliminary data discussed in this section reveals some very interesting feature of polar organic liquids interaction with MW. The more detailed study could open a new door to make clear understanding of Eyring's rate process theory of dielectric relaxation, the macroscopic relaxation time of a liquid near the freezing point. The new information could be used for the theoretical calculation of latent heat and Gibbs free energy when solvent-solute interact without a practical measurement of such.

The developed automated instrument itself is straightforward to use. A depth understanding of theory and operational knowledge of Vector Network Analyser would not be necessary to use this instrument since the complicated measuring, and data interpretation part becomes simple. So, the instrument will be convenient for a chemist to study the dielectric property of liquid. The wider application of MW dielectric property was already discussed in the introduction section

7.4 Conclusion

A dielectric loss factor measuring a technique for liquid at a range of temperature (room temperature to 200 °C) is successfully demonstrated here using some highly volatile solvent. Furthermore, a variety of different COSMO-RS class solvent was categorized into four different types of solvent by identifying appropriate curve fitting function for both real and imaginary part of the complex dielectric constant. Moreover, it was also shown that the Pearson V11 curve profile shape factor (m) could be used as a single parameter to distinguish different solvents ability to generate heat during MW interaction at or above 200 °C. It was also proposed here that these curve fitting functions would work down to supercooling and in a pressurised state over the boiling point.

Two different tables with dielectric loss factor and loss tangent data at 25 °C interval was presented for all the selected solvents at measured temperature range and beyond. It was noticed from the tables that cyclic keto functional group-containing solvents are more effective to interact with MW for dielectric heating at high-temperature range than acyclic solvents consisting same carbon chain length and functional group.

8 Evaluation of Microwave Influence on Solvent Dependent Reaction Kinetics

8.1 Result and Discussion

An equal amount of (10 ml) 0.1N of 1-bromohexane and 0.1N of trihexylamine was dissolved in propylene carbonate solvent, heated up in a heating block until the set temperature was stable. Then both reactants mixed up and stirred. The final volume of the reactant mixture is 20ml, and concentration is 0.05N. The conductance of the reaction mixer was measured using a Jenway 4510 conductivity meter in regular time intervals for a few hours. The slower reactions at low temperature were then followed irregularly until a set pattern of conductivity versus time was found (Figure 179).

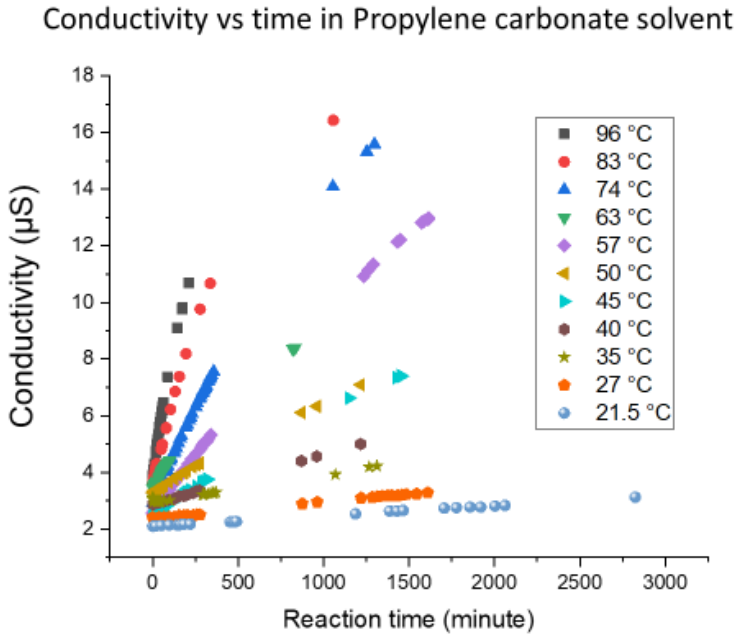

Figure 179 Monitoring Menschutkin reaction progress as Conductivity versus time (minute).

According to the conductance calibration for tetrahexylammonium bromide salt in propylene carbonate solvent, it was found that at 8.5 conductance (μS) the ratio of reactant to the product is 1000. So, it can be assumed that until at this stage of reaction there will be no reverse reaction. After 30 minutes, even at the highest experimental temperature (96°C), the conductance does not exceed this conductivity limit. An initial rate of reaction is measured in the first 30 minutes of reaction at all set temperatures (21.5 °C to 96 °C). The logarithm scale of the rate of reaction and reciprocal of Calvin scale temperature is then plotted to verify an Arrhenius trend for the reaction. However, it was noticed from this data that the progression of the reaction (Figure

180) followed the dielectric constant versus temperature trends which were measured with an in-house developed RCP device (Figure 181).

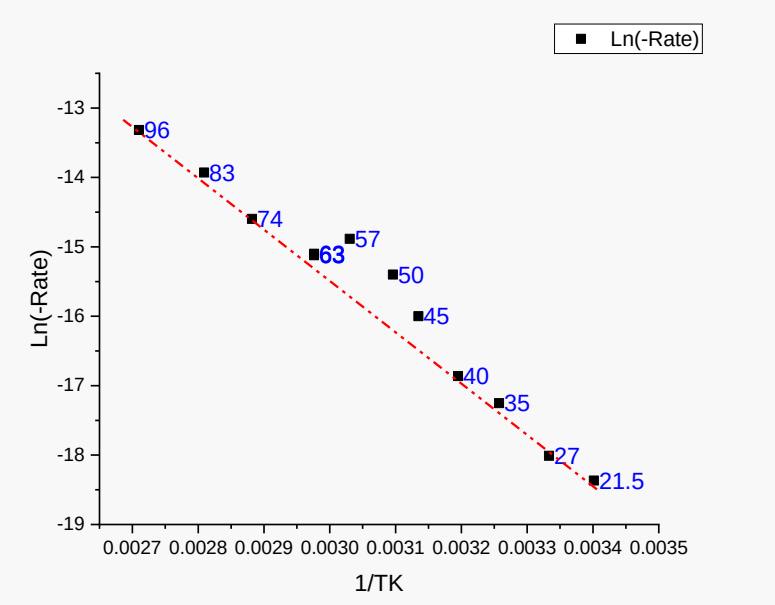

Figure 180 Ln(-Rate) vs 1/T. Blue data points are relevant temperature and dotted red line is the imaginary Arrhenius reaction kinetics trend.

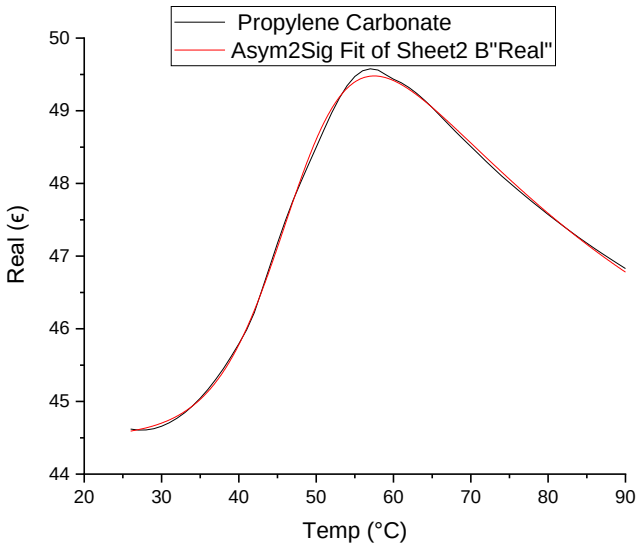

Figure 181 Dielectric constant of propylene carbonate at a range of temperature Peak maximum is at 57.5 °C.

To understand the microwave influence on the solvent dielectric property, and its role on the progression of Menschutkin type reaction, the reaction between 1-bromohexane and trihexylamine reaction in propylene carbonate was then performed for 30 minutes at different temperatures under MW while another reaction at the same temperature was simultaneously performed under conventional conditions. In the case of the MW synthesis, 10 ml of both reactants at the concentration of 0.1N in 35 ml reaction vessel were put together in a closed system using 100 watts of dynamic power, and medium stirring at dynamic method. But no

preheating step is used as the set temperature is achieved within a few seconds in MW condition. During the dynamic MW reaction method, in which a constant temperature condition is applied by adjusting the power, at up to 75°C, a continuously pressurised airflow is also passed on outside of the reaction vessel so that to adjust the temperature, more energy is absorbed. This mentioned method allows at least six times more MW power (40W) penetration inside the reaction system than without cooling (6W) the MW system (Figure 182).

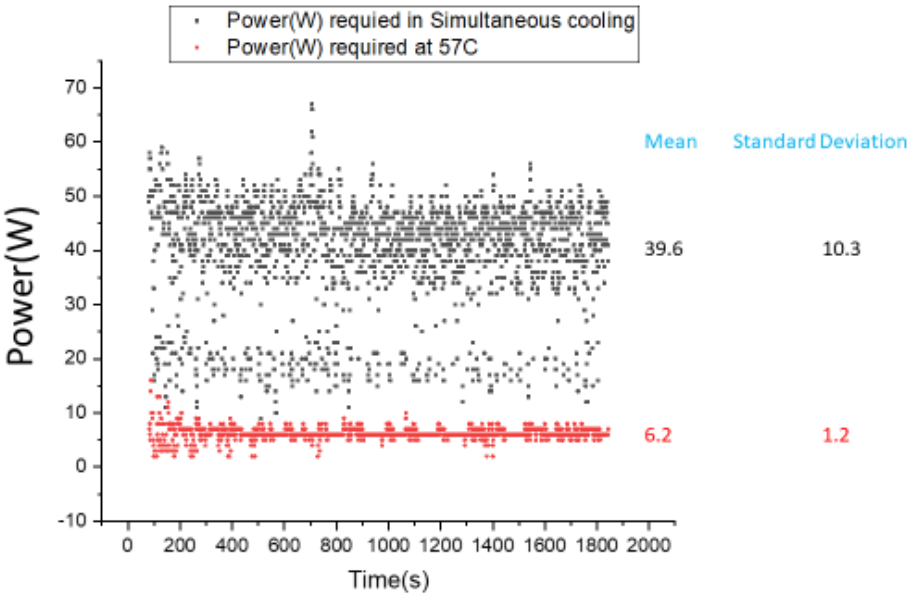

Figure 182 During MW heating with dynamic power. Red dots represent MW power consumed without compressed air cooling of the reaction vessel. Black dots represent MW power consumed during compressed air cooling of the reaction vessel.

When the MW reaction is stopped, both the conventional and MW reaction vial was put into the ice to slow down the reaction as quickly as possible. In ice, the reaction mixtures temperature falls to 5 °C to 6 °C within a minute. When the samples are taken back outside of the ice, again within a few minutes, the sample temperature settles at around 12°C during the conductivity measurement. The comparison of the conductance after 30 minutes of reaction under the conventional method and the MW method is shown in Figure 183.

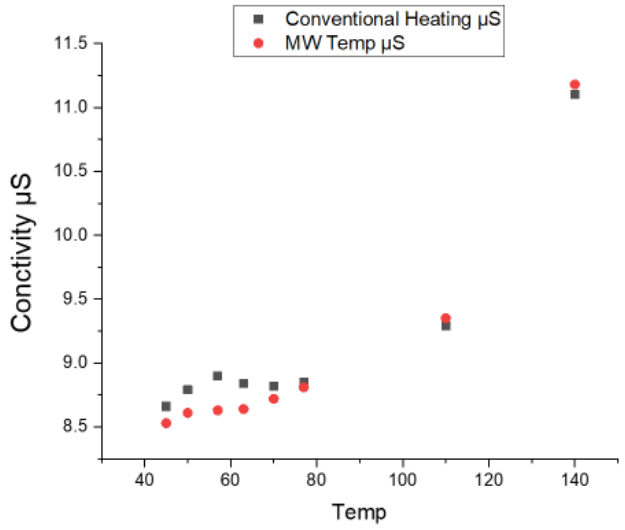

Figure 183 Comparison of traditional and MW method conductivity with temperature.

In Figure 183, the MW and conventional reaction comparison clearly show that the conductivity peak for conventional reaction at around 57°C is absent in MW reactions. When the MW reaction was conducted without compressed air cooling from outside, the gap between traditional and MW heating become narrower, although not wholly diminished.

An explanation of this observed phenomenon might be explained in the following way:

In non-MW reaction condition, the reaction rate increased more than Arrhenius rate and maximised the reaction rate at a certain temperature at which temperature the solvent dielectric constant maximised. At transition state, the maximised dielectric constant of solvent dipole stabilises the activation complex of reactants. This extra stability of activation complex at certain temperature facilitates more population of transition state than it usually should be and hence increases the rate of the overall reaction. In this studied case, the particular temperature at which the reaction maximise is 57.5°C due to the highest dielectric constant of propylene carbonate solvent.

It is established that as MW operational frequency is 2.45 GHz and many orders of magnitude lower in energy than to excite electronic and vibrational transition of a liquid molecule.[605] Therefore MW energy cannot be directly absorbed by any reactant molecule of the solution system to form the excited state of bonded atoms and to free apart the reactants molecular bond to create the new product. Therefore, so-called MW non-thermal effect should not play any role to accelerate or reduce the standard Arrhenius type reaction rate.

Let us assume that both the reactant at neighbouring transition state is surrounded by the solvent molecule in numerous spherical solvent cages (Figure 184).

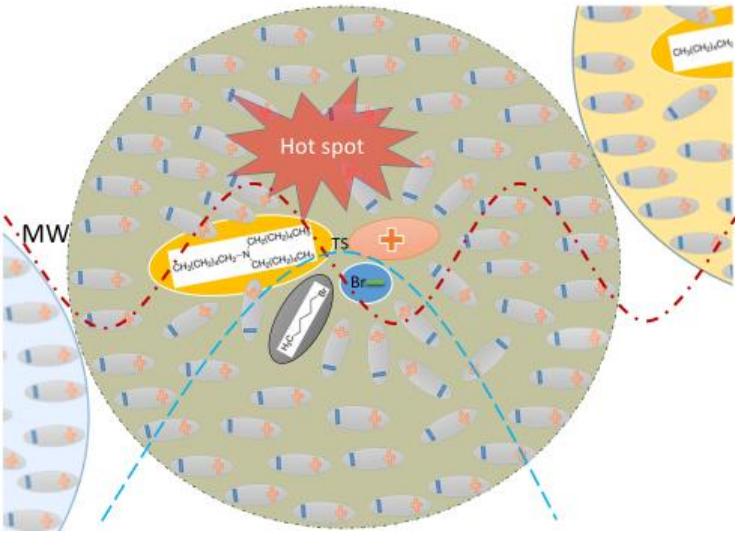

Figure 184 A Solvent cage of transition state (TS) reactant at MW condition.

When this liquid mixture is exposed to MW power, the liquid dielectric molecules try to synchronise with applied MW power.

Gregory B. Dudley et al[605] also suggests that the dielectric relaxation process in the viscous liquid is not homogeneous spatially. In a specific solvent cage, the dielectric solvent of the outer shell will be more synchronised with MW, then the solvent molecules which are tightly aligned with reactant dipoles at TS as shown in *Figure 184*. As the relaxation time of TS will be higher than the outer shell, the reactant solvent complex, the TS complex, may produce more collisional MW heat than the outer edge of the solvent cage. Moreover, in the Menshutkin reaction, although the reactants are not ionic, the product is ionic. This ionic product creates extra dielectric loss phenomena due to ionic conductivity as shown in equation *Equation 43*.[606]

$$\varepsilon''_{obs} = \varepsilon''_{cor} + 2\sigma/f$$

Equation 43

where ε''_{cor} is loss factor due to the orientation of dipole, ε''_{obs} is observed dipole vale, σ is the electrical conductivity and f is the frequency at which conductivity is measured. As in the core of a solvent cage, extra heat is created, and at the same time in the core, the viscosity or free movement of product-ions is less than that of the outer shell, a hot spot is formed in the centre. This assumption is also supported by the empirical equation of viscosity of Doolittle[607] and the theory of relaxation time of the free volume of Cohen and Turnbull[608], according to which the microscopic relaxation time will be as *Equation 44*:

$$\tau` = AT^{-1/2}\exp(B/\upsilon_f) \propto 1/D$$

Equation 44

where A and B are the constant, υf is free volume and D is the notion of diffusion. The created comparative high temperature at or near the TS state species in the microscopic solvent cage is not observed at the bulk temperature of the liquid. But the hot spot at the core and less diffusive ionic product than non-MW condition negatively influence the TS species stability to the product formation and thus reduce the reaction progression. Furthermore, as the Arrhenius plot of reaction rate vs inverse of temperature is plotted with measured bulk temperature, the Arrhenius plot was unable to draw the curvature of deviation of reaction rate vs temperature (hot spot temperature) in MW condition of Menschutkin type reaction.

Since dielectric relaxation is a rate process and it is reciprocal of a mean of rate coefficient, Arrhenius relation for rate coefficient can be written as *Equation 45* or [609]:

$$k = (1/\tau) = A`.\exp(-\Delta H_A*_{\Delta}/RT)$$

Equation 45

or

$$\tau = A.\ \exp(\Delta H_A*/RT)$$

Equation 46

where $A = 1/A`$ and $\Delta H*_E$ = Enthalpy change H (active state)-H(normal state).
Although Arrhenius equation assumes, A as independent of temperature, but different models suggest incorporating a power of temperature in the term A. In general temperature dependence of relaxation time can be expressed as Equation 47:

$$\tau = S.T^n.\exp(\Delta H^*/RT)$$

Equation 47where S is numerical constant. From the above expressions it can also be indicated that as dipolar relaxation time changes with solvent and reactants orientational changes with temperature, an increased temperature due to hot spot will also distort stability of the TS species. For that reason, the overall rate of reaction will be reduced due to the heat generated hot spot at the core of the solvent cage.

8.2 Conclusion

The developed knowledge about dielectric properties of solvents was applied to the explanation of Menschutkin reaction mechanism examining some of the fundamental questions around MW effects on chemical reactions. The experiment also draws attention to the fact that a thoughtful selection of solvent is needed for MW reaction systems. The dielectric constant and

dielectric loss factor do not always affect a reaction process in the same direction. So, the dielectric property knowledge of solvents and reagents is crucial to take advantage of MW power for exploiting a specific reaction process. This experiment also created a new tool to verify an organic reaction mechanism in which a polar molecule believed to play a role but not yet established.

The more detailed study of the dielectric properties of the organic liquids could open a new door to make clear understanding of Eyring's rate process theory of dielectric relaxation, the macroscopic relaxation time of a liquid near the freezing point. The new information could be used for the theoretical calculation of latent heat and Gibbs free energy when solvent-solute interact without a practical measurement of such.

9 Conclusions and Future Work

9.1 Conclusions

At the initial stage of the project, fast and inexpensive methods of biomass analysis were designed and developed. The first method was based on NIR spectroscopy and could be used for efficient identification of water and various extractive components within different biomass feedstocks. The second approach was based on an innovative modification of TGA methodology, by applying an observed finding that the extractive components significantly influence dTG curves of lignocellulose biomass.

It was established that wax and wax-esters substantially reduces bio-oil yield and proved that the valuable extractives should be removed before MW pyrolysis of lignocellulose biomass. The FT-ATIR of MW pyrolysed cellulose bio-char showed that the presence of a wax coating reduces the production of carbonyl functional group-containing aromatic products of cellulose pyrolysis. It was also shown that wax reduces the biooil yield by inhibiting of the rate of the pyrolysis process.

The mass balance calculation of MW pyrolysis of cellulose also confirms that the production of gases was reduced by 50% when cellulose was coated with wheat straw wax.

The influence of additive on the MW-assisted pyrolysis of cellulose was thoroughly investigated. Through a precise experimental design, it was shown that the yield of cellulose pyrolysis varied in the presence of additives by as much as 20%.

The MW pyrolysis study by chemometric analysis gave satisfactory explanations of the influence of various physical/chemicals parameters on the MW pyrolysis process. The most important outcome of this experimental design was a significant minimisation of the number of solvent parameters which could influence MW-assisted pyrolysis. A wide range of physical-chemical properties of additives potentially was crucial for the MW-cellulose interaction and was constricted to only two parameters (solvent dielectric properties and viscosity), which are responsible for the efficiency of MW heating.

Furthermore, it was established that besides the MW-activation role, additives could influence the cellulose pyrolysis both as a medium for primary products stabilisation and as catalysts due to their further transformation. This observation provides strong evidence that the MW-assisted pyrolysis is determined not only by individual properties of additives but also by their ability to interact with biomass and products of pyrolysis.

A systematic study of MW-assisted pyrolysis of cellulose in the presence of organic additives was conducted. This systematic investigation includes a detailed analysis of MW-solvent, solvent-cellulose, and solvent-products interactions.

The solvent-cellulose and solvent-products interactions have never been systematically investigated in the past, therefore, new methodologies to study these interactions were designed and studied. The solvent-cellulose interaction was measured by the degree of swelling using the ratio of moles of solvent to the number of anhydroglycopyranose units (AGU). It has been shown that the swelling effect is an individual property separated from solvation property and could be used as an independent parameter.

To explain solvent-products interaction, a correlation between Abraham solvation parameters of solvent and pyrolysis yield were analysed, focusing on the preservation of cellulose degraded products with organic additives/solvents. Applications of MLR and PCA methods together with cluster analysis demonstrated a complex correlation between Abraham solvation parameters and the solid residue yields. It was found that there is a particular McGowan volume (c.a. 1.25 mol/g) which separates two types of mechanisms that control the influence of solvent on MW pyrolysis of cellulose. Above this volume, the degree of MW pyrolysis significantly relies on McGowan volume. However, it is independent of other parameters. Alternatively, below the critical value, the McGowan volume does not influence the pyrolysis, while other physical-chemical parameters play a significant role.

It was concluded that the molecules with high volume have limited ability to penetrate inside of the amorphous region of the cellulose. However, a higher boiling point solvent helps to retain the generated MW dielectric heat and prevents primary pyrolysis of products from undergoing secondary reactions. On the other hand, a small molecule can penetrate inside of the amorphous cellulose region and be able to influence cellulose decomposition with their functional group.

An instrumental technique to measure the dielectric loss factor and dielectric constant of liquid at a range of temperature (room temperature to 200 °C) was successfully developed.

An optimum list of solvents that represents major COSMO-RS solvent class was chosen, and the influence of nature of solvents on their dielectric properties was studied.

It was established that solvents ability to generate heat during MW interaction at a wide range of temperatures follows the Pearson V11 equation. This discovery opens an opportunity for modelling a microwave behaviour of different organic liquids.

It was also noticed during this work that cyclic keto functional group-containing solvents are the more effective heating agent with MW than acyclic solvents consisting of the same carbon chain length and functional groups. The mechanistic understanding of this phenomenon was proposed.

The study of Menschutkin reaction mechanism also draws attention to the fact that a thoughtful selection of solvent is needed for MW reaction systems. The dielectric constant and dielectric loss factor do not always affect a reaction process in the same direction. So, the dielectric property knowledge of solvents and reagents is crucial to take advantage of MW power for exploiting a specific reaction process. The experiment of Menschutkin reaction also created a new tool to verify an organic reaction mechanism in which a polar molecule believed to play a role but not yet established.

The newly developed dielectric loss factor measuring instrument indicates to the fact that the Asy2sig prediction for dielectric constant and Pearson-V11 for dielectric loss factors was still valid at lower than room temperature. The developed automated instrument itself is straightforward to use. A depth understanding of theory and operational knowledge of Vector Network Analyser would not be necessary to use this instrument since the complicated measuring, and data interpretation part becomes simple. So, the instrument will be convenient for a chemist to study the dielectric property of liquid.

9.2 Future work

For ensuring sustainable use of natural resources, it is understood that a balance of economic, ecological and social impact is needed. For ensuring the circular economy, decoupling of resource consumption from economic growth is vital. By applying the Green Chemistry principle and using renewable biomass resources, the circular economy could be ensured. To develop biorefinery based bioeconomy, knowledge of biomass utilisation is essential. Although there is ongoing research on biomass utilisation through the biochemical and thermochemical way, a fine balance yet needed to find out for ensuring a commercially viable speedy and selective transformation of biomass into chemicals, materials and energy. But a selective and speedy transformation of biomass in a phase-3 biorefinery yet to be established. Microwave-assisted pyrolysis has shown the potential for both selective and speedy process for biomass transformation into the value-added liquid at laboratory scale at very energy effective way. The present challenge is to manage an effective route for quick removal of the primary product of the main biomass components. For example, The main recalcitrant biomass component cellulose could be transformed into levoglucosan or levoglucosenone at low temperature (below 180 °C), but if there is not an effective and quick removal of the primary products from the microwave reaction vessel, the primary product will quickly be converted into less valuable secondary products. It is proposed here that a high volatile organic liquid could potentially interfere with the secondary reaction formation. The initial work in this thesis has shown the prospect of this vision. The work performed in this thesis has shown both the hope and specific barrier which is possible to overcome through planned further research. Some of the main feature, benefit, and barrier and proposed way of overcoming those barriers is discussed below:

1. It is understood that for any successful biorefinery setting, a quick, reliable screening of biomass is needed for selective use biomass feedstock for maximising the productivity of a targeted product. In this work, the potentiality of NIR spectroscopy for this purpose is evaluated. But to take this work forward, a further calibrated partial least-square (PLS) NIR method needs to be developed for commercially implementing an inexpensive and fast NIR detection method of biomass components, including extractives and water content. To make this work forward, the main barrier is the lack of substantial NIR spectroscopic data of woody biomass. The present state of the art application of NIR in the feed meal industry

shows hope that thorough a dedicated integrated approach with relevant industry the implementation NIR for biomass feedstock screening also possible.

2. It is also demonstrated in this work that, a thermogravimetric method is rather simple to identify both quantity and quality of specific woody biomass interns of extractive, lignin, hemicellulose and cellulose component. Further work could potentially implement this information for integration into biorefinery setting to a simple way to identify feedstock component reliably.
3. It was shown in this work that the extractives of woody biomass could play a significant role to determine target product quality and quantity. The extractive component could play a positive or negative role of biomass to transform into a specific product. It is suggested here that the extractive component actively interact with microwave and can either protect or accelerate a biomass transformation into product depending upon extractives dielectric and other physicochemical properties. To exploiting the advantage of extractives role in this aspect, much work is needed to establish the exact mechanism of interaction of specific extractive component with biomass products under the influence of microwave. If it could be established that which part of extractives in which way interact with a specific component of biomass, then by increasing or decreasing the extractive component in microwave biorefinery process the target product could either be protected from decomposing or accelerate the formation of it.
4. Likewise, a specific solvent could also play the same role as extractives under microwave condition. In this work, the COSMO-RS approach was taken to find a specific class of solvents role during microwave-assisted pyrolysis of cellulose. It was proposed that a specific volume of some class of solvent could potentially play a significant role in cellulose pyrolysis. But to have much clear understating, a larger set of solvent is needed to examine both for cellulose pyrolysis and biomass pyrolysis. Biomass is much more complicated than simple cellulose, for biorefinery application, a solvent class which is ideal for cellulose transformation, may not be suitable for whole biomass, may due to due to a different kind of interaction in the presence of microwave irradiation. The solvent could either accelerate the process of biomass activation or decelerate the conversion process depending upon target product and biomass physicochemical state. A systematic investigation of solvent effect on biomass activation in larger-scale microwave experiment is also needed

to investigate once the lab-scale study of any solvent class is proven to be effective in this purpose.

5. Unlike conventional heating for application of microwave-assisted biomass heating, a better understanding of dielectric properties of biomass is essential. Because dielectric heating is volumetric heating and depends on the specific cavity size and electric field, it is essential that the laboratory and pilot-scale microwave heating of biomass needed to design for industrial application of a particular need. A barrier on the progression of microwave application in the field of biomass utilisation is that, lack of expert knowledge of microwave energy application. A combination of electronic engineering, chemical engineering and biochemical knowledge of feedstock is vital for success. The study of the dietetic property of biomass along with solvent at changing temperate up to biomass activation temperature could be a good start for the way forward.
6. The newly developed, automated RCP device is now fully functional and ready to use. As the instrument was just developed very recently, a comprehensive dielectric study of solvent is yet needed to be done. A database of dielectric loss factor of solvents at elevated temperature is needed to make available for overall progressing the research in this field either for application biorefinery purpose or chemical process industry.
7. Here in this work, measurement of dielectric loss factor and dielectric constant of liquid at a range of temperature (room temperature to 200 °C) was successfully performed and significant new knowledge was gained. In the near future, solvent-cellulose, solvent-hemicellulose and solvent-lignin interaction in the presence of MW irradiation could be studied at up to 180 °C. Based on newly gained data and with the help of dielectric loss factor prediction equation, a new method of MW pyrolysis of biomass could be developed for industrial process application.
8. As through the study of Menschutkin reaction mechanism demonstrated that the dielectric constant and dielectric loss factor do not always affect a reaction process in the same direction. So, the dielectric property knowledge of solvents and reagents is crucial to take advantage of MW power for exploiting a specific reaction process. To use this knowledge for practical application in biorefinery, and overall microwave-based process transformation, much more work is needed both in mechanistic understanding and to practical application.

9. The product separation from biooil after biomass pyrolysis both in conventional and microwave setting is challenging. In this work, it was shown that it is possible to separate lactic acid additive from liquid components of pyrolysed cellulose. But significant work is needed to perform in this area of research. A green, cheap and versatile method is necessary to find out for product separation from solvent both at lab scale and large scale and for various biomass types during and after MW pyrolysis of biomass.

10 References

1. G. H. Brundtland, *Environmental Conservation*, 1987, **14**, 291-294.
2. T. Bennich and S. Belyazid, *Sustainability*, 2017, **9**.
3. A. Nayha, *Journal of Cleaner Production*, 2019, **209**, 1294-1306.
4. https://www.ellenmacarthurfoundation.org/assets/downloads/publications/TCE_Ellen-MacArthur-Foundation_26-Nov-, *TOWARDS A CIRCULAR ECONOMY: BUSINESS RATIONALE FOR AN ACCELERATED TRANSITION*, accessd on 16 April 2019.
5. P. Ghisellini, C. Cialani and S. Ulgiati, *Journal of Cleaner Production*, 2016, **114**, 11-32.
6. M. Linder, *Green Chemistry Letters and Reviews*, 2017, **10**, 428-435.
7. J. Korhonen, A. Honkasalo and J. Seppala, *Ecological Economics*, 2018, **143**, 37-46.
8. P. Anastas and N. Eghbali, *Chemical Society Reviews*, 2010, **39**, 301-312.
9. R. A. Sheldon, *Acs Sustainable Chemistry & Engineering*, 2018, **6**, 32-48.
10. R. A. Sheldon, *Green Chemistry*, 2017, **19**, 18-43.
11. T. Keijer, V. Bakker and J. C. Slootweg, *Nature Chemistry*, 2019, **11**, 190-195.
12. W. L. Leffler, *Petroleum refining for the nontechnical person*, PennWell Books, 1985 (2nd ed.).
13. F. Cherubini, *Energy Conversion and Management*, 2010, **51**, 1412-1421.
14. B. Kamm and M. Kamm, *Applied Microbiology and Biotechnology*, 2004, **64**, 137-145.
15. G. De Bhowmick, A. K. Sarmah and R. Sen, *Bioresource Technology*, 2018, **247**, 1144-1154.
16. M. de Besi and K. McCormick, *Sustainability*, 2015, **7**, 10461-10478.
17. B. El-Chichakli, J. von Braun, C. Lang, D. Barben and J. Philp, *Nature*, 2016, **535**, 221-223.
18. S. F. Pfau, J. E. Hagens, B. Dankbaar and A. J. M. Smits, *Sustainability*, 2014, **6**, 1222-1249.
19. B. Urban, J. Krahl, A. Munack, H. Kanning and C. von Haaren, *Landbauforschung Volkenrode*, 2007, **57**, 419-427.
20. D. Viaggi, *Bio-based and Applied Economics*, 2016, **5**, 101-112.
21. R. Bosch, M. van de Pol and J. Philp, *Nature*, 2015, **523**, 526-527.
22. M. Martin, F. Royne, T. Ekvall and A. Moberg, *Sustainability*, 2018, **10**.
23. K. McCormick and N. Kautto, *Sustainability*, 2013, **5**, 2589-2608.
24. S. K. Maity, *Renewable & Sustainable Energy Reviews*, 2015, **43**, 1427-1445.
25. S. J. Liu, *Biotechnology Advances*, 2010, **28**, 563-582.
26. J. H. Clark and F. E. I. Deswarte, *Introduction to chemicals from biomass*, Wiley, Chichester, U.K., 2008.
27. B. Kamm and M. Kamm, *Appl Microbiol Biotechnol*, 2004, **64**, 137-145.
28. E. Thiffault, J. Endres, J. S. N. McCubbins, M. Junginger, M. Lorente, U. Fritsche and L. Iriarte, *Biofuels Bioproducts & Biorefining-Biofpr*, 2015, **9**, 283-292.
29. J. H. Clark, *Current Opinion in Green and Sustainable Chemistry*, 2017, **8**, 10-13.
30. M. Carmona-Cabello, I. L. Garcia, D. Leiva-Candia and M. P. Dorado, *Current Opinion in Green and Sustainable Chemistry*, 2018, **14**, 67-79.
31. R. Ravindran and A. K. Jaiswal, *Trends in Biotechnology*, 2016, **34**, 58-69.
32. J. Esteban and M. Ladero, *International Journal of Food Science and Technology*, 2018, **53**, 1095-1108.
33. N. Sarkar, S. K. Ghosh, S. Bannerjee and K. Aikat, *Renewable Energy*, 2012, **37**, 19-27.
34. K. Karimi, S. Kheradmandinia and M. J. Taherzadeh, *Biomass & Bioenergy*, 2006, **30**, 247-253.

35. F. G. Fermoso, A. Serrano, B. Alonso-Farinas, J. Fernandez-Bolanos, R. Borja and G. Rodriguez-Gutierrez, *Journal of Agricultural and Food Chemistry*, 2018, **66**, 8451-8468.
36. A. Serrano, F. G. Fermoso, B. Alonso-Farinas, G. Rodriguez-Gutierrez, J. Fernandez-Bolanos and R. Borja, *Journal of Cleaner Production*, 2017, **148**, 314-323.
37. *GLOBAL FOREST RESOURCES ASSESSMENT 2015*, FOOD AND AGRICULTURE ORGANIZATION OF THE UNITED NATIONS, Rome, 2015.
38. *Official Statistics of Sweden* Swedish Forest Agency, Sweden, 2010.
39. G. Hogan, *An assessment in the context of Phytophthora ramorum*, Forest Research 2013. The British Bark Industry 2013.
40. I. f. H. u. H. G. SCHULTZE-DEWITZ & G. KOCH, Hamburg-Bergedorf, *Feddes RepertoriumFeddes Repertorium 119 (2008) 7–8, 655–668*, 2008, **119** ,655–668.
41. H. G. Smith and A. Kozak, *Forest Products Journal.*, 1971, **21**, 38-40.
42. G. Melin, *Current use of biomass for energy in Sweden and forecast for the coming years*, President, SVEBIO, Oslo 2009-09-23, 2009.
43. P. Hakkila, *Utilization of Residual Forest Biomass.* , Springer Science & Business Media., 2012.
44. R. Ale'n, *Structure and chemical composition of wood" in forest product chemistry,*, Finish paper engineering association and TaPPI, Helsinki., 2000.
45. J. S. Midgett, B. E. Stevens, A. J. Dassey, J. J. Spivey and C. S. Theegala, *Waste and Biomass Valorization*, 2012, **3**, 259-268.
46. F. E. L. Unit, Madrid, 2015.
47. R. C. Pettersen, *Advances in Chemistry Series*, 1984, 57-126.
48. H.-J. Huang, S. Ramaswamy, U. W. Tschirner and B. V. Ramarao, *Separation and Purification Technology*, 2008, **62**, 1-21.
49. A. Raimo, *Papermaking science and technology, technology, Book 20, Bio-refining of forest resources*, Paperi ja puu, Helsinki, 2011.
50. H. L. Kang, R. G. Liu and Y. Huang, *Polymer International*, 2013, **62**, 338-344.
51. B. Medronho, A. Romano, M. G. Miguel, L. Stigsson and B. Lindman, *Cellulose*, 2012, **19**, 581-587.
52. D. B. Turley, in *Introduction to Chemicals from Biomass*, John Wiley & Sons, Ltd, 2008, p. 24.
53. W. P. Findlay, *Chapter: 5: Chemistry of Wood. Timber properties and uses.*, Granada Publishing limited., London., 1975.
54. B. L. Browning, *The Chemistry of Wood. John Wiley & sons Inc.*, 1963.
55. G. W. Dietrich Fengel, in *Wood Chemistry, Ultrastructure, Reactions*, Walter de Gruyter, 1984, p. 35.
56. G. W. D. Fengel, in *Wood Chemistry, Ultrastructure, Reactions,* , Walter de Gruyter 1984, p. 145.
57. S. Yaman, *Energy Conversion and Management*, 2004, **45**, 651-671.
58. M. A. Stanish, *Wood Science and Technology*, 1986, **20**, 53-70.
59. A. Demirbas and G. Arin, *Energy Sources*, 2002, **24**, 471-482.
60. G. W. D. Fengel, in *Wood Chemistry, Ultrastructure, Reactions,*, Walter de Gruyter, 1984, p. 184.
61. A. L. Horvath, *Journal of Physical and Chemical Reference Data*, 2006, **35**, 77-92.
62. T. J. F. a. M. Mascal, in *Introduction to chemicals from biomass*, eds. J. Clark and F. Deswarte, Wiley, 2015, pp. 89-143.
63. E. Uçkun Kıran, A. P. Trzcinski and Y. Liu, *Journal of Chemical Technology & Biotechnology*, 2015, **90**, 1364-1379.
64. S. Dutta and S. Pal, *Biomass & Bioenergy*, 2014, **62**, 182-197.

65. M. V. Galkin and J. S. M. Samec, *Chemsuschem*, 2016, **9**, 1544-1558.
66. S. M. Kang, X. L. Li, J. Fan and J. Chang, *Renewable & Sustainable Energy Reviews*, 2013, **27**, 546-558.
67. S. N. Khot, J. J. Lascala, E. Can, S. S. Morye, G. I. Williams, G. R. Palmese, S. H. Kusefoglu and R. P. Wool, *Journal of Applied Polymer Science*, 2001, **82**, 703-723.
68. F. S. Guner, Y. Yagci and A. T. Erciyes, *Progress in Polymer Science*, 2006, **31**, 633-670.
69. R. D. Farris, *Journal of the American Oil Chemists Society*, 1979, **56**, A770-A773.
70. K. A. D. Swift, *Topics in Catalysis*, 2004, **27**, 143-155.
71. J. C. a. F. Deswarte, in *Introduction to Chemicals from Biomass, 2nd Edition.*, Wiley, 2015 p. 12.
72. S. Fernando, S. Adhikari, C. Chandrapal and N. Murali, *Energy & Fuels*, 2006, **20**, 1727-1737.
73. M. Wellisch, G. Jungmeier, A. Karbowski, M. K. Patel and M. Rogulska, *Biofuels Bioproducts & Biorefining-Biofpr*, 2010, **4**, 275-286.
74. J. Gravitis, *Journal of Cleaner Production*, 2007, **15**, 1190-1197.
75. B. N. Kuznetsov, I. G. Sudakova, N. V. Garyntseva, V. A. Levdansky, N. M. Ivanchenko, A. V. Pestunov, L. Djakovitch and C. Pinel, *Wood Science and Technology*, 2018, **52**, 1377-1394.
76. A. Corona, M. Ambye-Jensen, G. C. Vega, M. Z. Hauschild and M. Birkved, *Science of the Total Environment*, 2018, **635**, 100-111.
77. A. Morais, A. D. Lopes and R. Bogel-Lukasik, *Abstracts of Papers of the American Chemical Society*, 2016, **252**.
78. J. Ecker, T. Raab and M. Harasek, in *Euromembrane Conference 2012*, ed. N. Marsh, 2012, vol. 44, pp. 1337-1339.
79. J. Ecker, M. Schaffenberger, W. Koschuh, M. Mandl, H. G. Bochzelt, H. Schnitzer, M. Harasek and H. Steinmuller, *Separation and Purification Technology*, 2012, **96**, 237-247.
80. K. Sudhakar, R. Mamat, M. Samykano, W. H. Azmi, W. F. W. Ishak and T. Yusaf, *Renewable & Sustainable Energy Reviews*, 2018, **91**, 165-179.
81. P. Gegg and V. Wells, *Journal of Marine Science and Engineering*, 2017, **5**.
82. N. Wei, J. Quarterman and Y. S. Jin, *Trends in Biotechnology*, 2013, **31**, 70-77.
83. L. Sanchez-Silva, D. Lopez-Gonzalez, J. Villasenor, P. Sanchez and J. L. Valverde, *Bioresour Technol*, 2012, **109**, 163-172.
84. G. Guerriero, J. F. Hausman, J. Strauss, H. Ertan and K. S. Siddiqui, *Engineering in Life Sciences*, 2016, **16**, 1-16.
85. N. Mosier, C. Wyman, B. Dale, R. Elander, Y. Y. Lee, M. Holtzapple and M. Ladisch, *Bioresource Technology*, 2005, **96**, 673-686.
86. H. Y. Chen, J. B. Liu, X. Chang, D. M. Chen, Y. Xue, P. Liu, H. L. Lin and S. Han, *Fuel Processing Technology*, 2017, **160**, 196-206.
87. S. Dahadha, Z. Amin, A. A. B. Lakeh and E. Elbeshbishy, *Energy & Fuels*, 2017, **31**, 10335-10347.
88. H. Q. Li, Y. S. Qu, Y. Q. Yang, S. L. Chang and J. Xu, *Bioresource Technology*, 2016, **199**, 34-41.
89. T. H. K. Wan Chi Lam, Vitaliy L. Budarin, Egid B. Mubofu, jiajun Fan and Carol Sze Ki Lin, in *Introduction to Chemical from Biomass*, Wiley, 2015, pp. 52-83.
90. A. K. Kumar and S. Sharma, *Bioresources and Bioprocessing*, 2017, **4**.
91. M. K. Moro, R. S. S. Teixeira, A. S. da Silva, M. D. Fujimoto, P. A. Melo, A. R. Secchi and E. P. D. Bon, *Industrial Crops and Products*, 2017, **97**, 509-517.
92. R. Ravindran and A. K. Jaiswal, *Bioresource Technology*, 2016, **199**, 92-102.

93. D. Koutsianitis, C. Mitani, K. Giagli, D. Tsalagkas, K. Halasz, O. Kolonics, C. Gallis and L. Csoka, *Ultrasonics Sonochemistry*, 2015, **23**, 148-155.
94. N. A. M. Liyakathali, P. D. Muley, G. Aita and D. Boldor, *Bioresource Technology*, 2016, **200**, 262-271.
95. J. Baruah, B. K. Nath, R. Sharma, S. Kumar, R. C. Deka, D. C. Baruah and E. Kalita, *Frontiers in Energy Research*, 2018, **6**.
96. X. Q. Chen, Y. Li, L. L. Jiang and W. H. Shen, *STUDY ON ENZYMOLYSIS PREPARATION OF NANOCRYSTALLINE CELLULOSE (NCC) FROM CHEMICALLY PRETREATED COTTON FIBERS*, 2010.
97. A. O. Wagner, N. Lackner, M. Mutschlechner, E. M. Prem, R. Markt and P. Illmer, *Energies*, 2018, **11**.
98. H. Z. Chen and Z. H. Liu, *Biotechnology Journal*, 2015, **10**, 866-885.
99. J. Singh, M. Suhag and A. Dhaka, *Carbohydrate Polymers*, 2015, **117**, 624-631.
100. E. Shirkavand, S. Baroutian, D. J. Gapes and B. R. Young, *Renewable & Sustainable Energy Reviews*, 2016, **54**, 217-234.
101. L. Capolupo and V. Faraco, *Applied Microbiology and Biotechnology*, 2016, **100**, 9451-9467.
102. X. S. Zhuang, W. Wang, Q. Yu, W. Qi, Q. Wang, X. S. Tan, G. X. Zhou and Z. H. Yuan, *Bioresource Technology*, 2016, **199**, 68-75.
103. H. Q. Li, W. Jiang, J. X. Jia and J. Xu, *Bioresource Technology*, 2014, **153**, 292-299.
104. R. Biswas, H. Uellendahl and B. K. Ahring, *Bioenergy Research*, 2015, **8**, 1101-1116.
105. A. W. Bhutto, K. Qureshi, K. Harijan, R. Abro, T. Abbas, A. A. Bazmi, S. Karim and G. R. Yu, *Energy*, 2017, **122**, 724-745.
106. A. Sorensen, P. J. Teller, T. Hilstrom and B. K. Ahring, *Bioresource Technology*, 2008, **99**, 6602-6607.
107. J. S. Kim, Y. Y. Lee and T. H. Kim, *Bioresource Technology*, 2016, **199**, 42-48.
108. S. N. Sun, S. L. Sun, X. F. Cao and R. C. Sun, *Bioresource Technology*, 2016, **199**, 49-58.
109. D. P. Maurya, A. Singla and S. Negi, *3 Biotech*, 2015, **5**, 597-609.
110. S. Behera, R. Arora, N. Nandhagopal and S. Kumar, *Renewable & Sustainable Energy Reviews*, 2014, **36**, 91-106.
111. T. A. Lloyd and C. E. Wyman, *Bioresource Technology*, 2005, **96**, 1967-1977.
112. H. S. Du, C. Liu, Y. D. Zhang, G. Yu, C. L. Si and B. Li, *Industrial Crops and Products*, 2016, **94**, 736-745.
113. S. Y. Jeong and J. W. Lee, *Industrial Crops and Products*, 2016, **79**, 1-6.
114. Y. H. Jung, H. M. Park and K. H. Kim, *Bioprocess and Biosystems Engineering*, 2015, **38**, 1639-1644.
115. I. Kim, Y. H. Seo, G. Y. Kim and J. I. Han, *Fuel*, 2015, **143**, 285-289.
116. M. A. Karcher, Y. Iqbal, I. Lewandowski and T. Senn, *Bioresource Technology*, 2015, **180**, 360-364.
117. S. Zu, W. Z. Li, M. J. Zhang, Z. H. Li, Z. Y. Wang, H. Jameel and H. M. Chang, *Bioresource Technology*, 2014, **152**, 364-370.
118. C. G. Yoo, Y. Q. Pu and A. J. Ragauskas, *Current Opinion in Green and Sustainable Chemistry*, 2017, **5**, 5-11.
119. Q. G. Zhang, J. J. Hu and D. J. Lee, *Renewable Energy*, 2017, **111**, 77-84.
120. M. Zdanowicz, K. Wilpiszewska and T. Spychaj, *Carbohydrate Polymers*, 2018, **200**, 361-380.
121. G. C. Xu, J. C. Ding, R. Z. Han, J. J. Dong and Y. Ni, *Bioresource Technology*, 2016, **203**, 364-369.

122. M. N. Borand and F. Karaosmanoglu, *Journal of Renewable and Sustainable Energy*, 2018, **10**.
123. Z. Y. Zhang, M. D. Harrison, D. W. Rackemann, W. O. S. Doherty and I. M. O'Hara, *Green Chemistry*, 2016, **18**, 360-381.
124. K. Zhang, Z. J. Pei and D. H. Wang, *Bioresource Technology*, 2016, **199**, 21-33.
125. D. E. Kim and X. J. Pan, *Industrial & Engineering Chemistry Research*, 2010, **49**, 12156-12163.
126. Z. Y. Zhang, I. M. O'Hara and W. O. S. Doherty, *Cellulose*, 2013, **20**, 3179-3190.
127. L. P. Novo, L. V. A. Gurgel, K. Marabezi and A. A. D. Curvelo, *Bioresource Technology*, 2011, **102**, 10040-10046.
128. C. Martin, J. Puls, B. Saake and A. Schreiber, *Cellulose Chemistry and Technology*, 2011, **45**, 487-494.
129. F. B. Sun and H. Z. Chen, *Bioresource Technology*, 2008, **99**, 6156-6161.
130. M. Gonzalez Alriols, A. Tejado, M. Blanco, I. Mondragon and J. Labidi, *Chemical Engineering Journal*, 2009, **148**, 106-114.
131. S. S. Hassan, G. A. Williams and A. K. Jaiswal, *Bioresource Technology*, 2018, **262**, 310-318.
132. S. H. Hong, J. T. Lee, S. Lee, S. G. Wi, E. J. Cho, S. Singh, S. S. Lee and B. Y. Chung, *Radiation Physics and Chemistry*, 2014, **94**, 231-235.
133. C. Y. Zhang, X. J. Su, X. Y. Xiong, Q. L. Hu, S. Amartey, X. H. Tan and W. S. Qin, *Biomass & Bioenergy*, 2016, **85**, 207-214.
134. F. J. Barba, O. Parniakov, S. A. Pereira, A. Wiktor, N. Grimi, N. Boussetta, J. A. Saraiva, J. Raso, O. Martin-Belloso, D. Witrowa-Rajchert, N. Lebovka and E. Vorobiev, *Food Research International*, 2015, **77**, 773-798.
135. P. Kumar, D. M. Barrett, M. J. Delwiche and P. Stroeve, *Industrial & Engineering Chemistry Research*, 2011, **50**, 10996-11001.
136. C. Cholet, C. Delsart, M. Petrel, E. Gontier, N. Grimi, A. L'Hyvernay, R. Ghidossi, E. Vorobiev, M. Mietton-Peuchot and L. Geny, *Journal of Agricultural and Food Chemistry*, 2014, **62**, 2925-2934.
137. A. Golberg, M. Sack, J. Teissie, G. Pataro, U. Pliquett, G. Saulis, T. Stefan, D. Miklavcic, E. Vorobiev and W. Frey, *Biotechnology for Biofuels*, 2016, **9**.
138. J. Luo, Z. Fang and R. L. Smith, *Progress in Energy and Combustion Science*, 2014, **41**, 56-93.
139. M. Kunaver, E. Jasiukaityte and N. Cuk, *Bioresource Technology*, 2012, **103**, 360-366.
140. R. M. Rodriguez-Jasso, S. I. Mussatto, L. Pastrana, C. N. Aguilar and J. A. Teixeira, *Carbohydrate Polymers*, 2011, **86**, 1137-1144.
141. D. Chiaramonti, M. Prussi, S. Ferrero, L. Oriani, P. Ottonello, P. Torre and F. Cherchi, *Biomass & Bioenergy*, 2012, **46**, 25-35.
142. J. Fan, M. De bruyn, V. L. Budarin, M. J. Gronnow, P. S. Shuttleworth, S. Breeden, D. J. Macquarrie and J. H. Clark, *J Am Chem Soc*, 2013, **135**, 11728-11731.
143. M. Takahashi and H. Takenaka, *Polymer Journal*, 1983, **15**, 625-629.
144. H. Wang, M. L. Maxim, G. Gurau and R. D. Rogers, *Bioresour Technol*, 2013, **136**, 739-742.
145. T. Palav and K. Seetharaman, *Carbohydrate Polymers*, 2007, **67**, 596-604.
146. S. Popescu, T. Misawa, Y. Ohtsu, H. Fujita and S. Sanematsu, *Resources Conservation and Recycling*, 2008, **52**, 671-677.
147. J. A. Liu, R. Takada, S. Karita, T. Watanabe and Y. Honda, *Bioresource Technology*, 2010, **101**, 9355-9360.
148. S. D. Zhu, Y. X. Wu, Z. N. Yu, J. T. Liao and Y. Zhang, *Process Biochemistry*, 2005, **40**, 3082-3086.

149. J. Gabhane, S. William, A. N. Vaidya, K. Mahapatra and T. Chakrabarti, *Biomass & Bioenergy*, 2011, **35**, 96-102.
150. G. F. Gong, D. Y. Liu and Y. D. Huang, *Biosystems Engineering*, 2010, **107**, 67-73.
151. P. Verma, T. Watanabe and Y. Honda, *Bioresource Technology*, 2011, **102**, 3941-3945.
152. J. Shi, Y. Q. Pu, B. Yang, A. Ragauskas and C. E. Wyman, *Bioresource Technology*, 2011, **102**, 5952-5961.
153. F. Pang, S. L. Xue, S. S. Yu, C. Zhang, B. Li and Y. Kang, *Bioresource Technology*, 2012, **118**, 111-119.
154. B. J. Gu, J. W. Wang, M. P. Wolcott and G. M. Ganjyal, *Bioresource Technology*, 2018, **251**, 93-98.
155. B. Lamsal, J. Yoo, K. Brijwani and S. Alavi, *Biomass & Bioenergy*, 2010, **34**, 1703-1710.
156. A. Duque, P. Manzanares and M. Ballesteros, *Renewable Energy*, 2017, **114**, 1427-1441.
157. M. J. Eisenmenger and J. I. Reyes-De-Corcuera, *Enzyme and Microbial Technology*, 2009, **45**, 331-347.
158. S. Murao, Y. Nomura, M. Yoshikawa, T. Shin, H. Oyama and M. Arai, *Bioscience Biotechnology and Biochemistry*, 1992, **56**, 1366-1367.
159. S. G. Jin, G. M. Zhang, P. Y. Zhang, L. Y. Jin, S. Y. Fan and F. Li, *International Biodeterioration & Biodegradation*, 2015, **104**, 477-481.
160. C. L. Duarte, M. A. Ribeiro, H. Oikawa, M. N. Mori, C. M. Napolitano and C. A. Galvao, *Radiation Physics and Chemistry*, 2012, **81**, 1008-1011.
161. A. Janositz, J. Semrau and D. Knorr, *Innovative Food Science & Emerging Technologies*, 2011, **12**, 269-274.
162. M. J. Bussemaker and D. Zhang, *Industrial & Engineering Chemistry Research*, 2013, **52**, 3563-3580.
163. V. Yachmenev, B. Condon, T. Klasson and A. Lambert, *Journal of Biobased Materials and Bioenergy*, 2009, **3**, 25-31.
164. M. Tayyab, A. Noman, W. Islam, S. Waheed, Y. Arafat, F. Ali, M. Zaynab, S. Lin, H. Zhang and W. Lin, *Applied Ecology and Environmental Research*, 2018, **16**, 225-249.
165. E. Ruiz, C. Cara, P. Manzanares, M. Ballesteros and E. Castro, *Enzyme and Microbial Technology*, 2008, **42**, 160-166.
166. V. B. Agbor, N. Cicek, R. Sparling, A. Berlin and D. B. Levin, *Biotechnology Advances*, 2011, **29**, 675-685.
167. F. Teymouri, L. Laureano-Perez, H. Alizadeh and B. E. Dale, *Bioresource Technology*, 2005, **96**, 2014-2018.
168. F. Teymouri, L. Laureano-Perez, H. Alizadeh and B. E. Dale, *Applied Biochemistry and Biotechnology*, 2004, **113**, 951-963.
169. M. Meshartree, B. E. Dale and W. K. Craig, *Applied Microbiology and Biotechnology*, 1988, **29**, 462-468.
170. C. E. Wyman, B. E. Dale, R. T. Elander, M. Holtzapple, M. R. Ladisch and Y. Y. Lee, *Bioresource Technology*, 2005, **96**, 1959-1966.
171. M. W. Lau and B. E. Dale, *Proceedings of the National Academy of Sciences of the United States of America*, 2009, **106**, 1368-1373.
172. Y. E. Brodeur G, Badal K, Collier J, Ramachandran KB, Ramakrishnan S., *Enzyme Research*, 2011, 1- 17
173. J. Y. Park, R. Shiroma, M. I. Al-Haq, Y. Zhang, M. Ike, Y. Arai-Sanoh, A. Ida, M. Kondo and K. Tokuyasu, *Bioresource Technology*, 2010, **101**, 6805-6811.
174. V. Sundaram, K. Muthukumarappan and S. R. Kamireddy, *Industrial Crops and Products*, 2015, **74**, 45-54.

175. X. X. Zhang, S. Heinonen and E. Levanen, *Rsc Advances*, 2014, **4**, 61137-61152.
176. M. J. Diaz, C. Cara, E. Ruiz, M. Perez-Bonilla and E. Castro, *Fuel*, 2011, **90**, 3225-3229.
177. C. Martin, H. B. Klinke and A. B. Thomsen, *Enzyme and Microbial Technology*, 2007, **40**, 426-432.
178. A. S. Schmidt, S. Mallon, A. B. Thomsen, S. Hvilsted and J. M. Lawther, *Journal of Wood Chemistry and Technology*, 2002, **22**, 39-53.
179. G. Lissens, H. Klinke, W. Verstraete, B. Ahring and A. B. Thomsen, *Journal of Chemical Technology and Biotechnology*, 2004, **79**, 889-895.
180. C. Martin, Y. Gonzalez, T. Fernandez and A. B. Thomsen, *Journal of Chemical Technology and Biotechnology*, 2006, **81**, 1669-1677.
181. Y. Sun and J. Y. Cheng, *Bioresource Technology*, 2002, **83**, 1-11.
182. R. Sindhu, M. Kuttiraja, P. Binod, R. K. Sukumaran and A. Pandey, *Industrial Crops and Products*, 2014, **52**, 169-176.
183. M. T. Garcia-Cubero, G. Gonzalez-Benito, I. Indacoechea, M. Coca and S. Bolado, *Bioresource Technology*, 2009, **100**, 1608-1613.
184. R. Travaini, M. D. M. Otero, M. Coca, R. Da-Silva and S. Bolado, *Bioresource Technology*, 2013, **133**, 332-339.
185. S. V. Farahani, Y. W. Kim and C. A. Schall, *Catalysis Today*, 2016, **269**, 2-8.
186. A. Brandt-Talbot, F. J. V. Gschwend, P. S. Fennell, T. M. Lammens, B. Tan, J. Weale and J. P. Hallett, *Green Chemistry*, 2017, **19**, 3078-3102.
187. C. W. Zhang, S. Q. Xia and P. S. Ma, *Bioresource Technology*, 2016, **219**, 1-5.
188. J. Shi, M. S. Chinn and R. R. Sharma-Shivappa, *Bioresource Technology*, 2008, **99**, 6556-6564.
189. R. Sindhu, P. Binod and A. Pandey, *Bioresource Technology*, 2016, **199**, 76-82.
190. C. A. C. Alzate, J. C. S. Toro and A. G. Pena, *Catalysis Today*, 2018, **302**, 61-72.
191. A. Demirbas, *Energy Conversion and Management*, 2009, **50**, 2239-2249.
192. A. Aguilar-Reynosa, A. Romani, R. M. Rodriguez-Jasso, C. N. Aguilar, G. Garrote and H. A. Ruiz, *Energy Conversion and Management*, 2017, **136**, 50-65.
193. A. Richel and N. Jacquet, *Biomass Conversion and Biorefinery*, 2015, **5**, 115-124.
194. T. Song, A. Pranovich, I. Sumerskiy and B. Holmbom, *Holzforschung*, 2008, **62**, 659-666.
195. A. K. Chandel, V. K. Garlapati, A. K. Singh, F. A. F. Antunes and S. S. da Silva, *Bioresource Technology*, 2018, **264**, 370-381.
196. T. K. Morales-Martinez, D. I. Diaz-Blanco, J. A. Rodriguez-de la Garza, J. Morlett-Chavez, A. J. Castro-Montoya, J. Quintero, G. Aroca and L. J. Rios-Gonzalez, *Bioresources*, 2017, **12**, 8093-8105.
197. M. Balat, H. Balat and C. Oz, *Progress in Energy and Combustion Science*, 2008, **34**, 551-573.
198. M. Balat and H. Balat, *Applied Energy*, 2009, **86**, 2273-2282.
199. T. C. Ezeji, N. Qureshi and H. P. Blaschek, *Current Opinion in Biotechnology*, 2007, **18**, 220-227.
200. M. Kumar and K. Gayen, *Applied Energy*, 2011, **88**, 1999-2012.
201. P. Durre, *Current Opinion in Biotechnology*, 2011, **22**, 331-336.
202. R. C. Kuhad, R. Gupta, Y. P. Khasa, A. Singh and Y. H. P. Zhang, *Renewable & Sustainable Energy Reviews*, 2011, **15**, 4950-4962.
203. S. R. Kim, S. J. Ha, N. Wei, E. J. Oh and Y. S. Jin, *Trends in Biotechnology*, 2012, **30**, 274-282.
204. C. H. Zhou, X. Xia, C. X. Lin, D. S. Tong and J. Beltramini, *Chem Soc Rev*, 2011, **40**, 5588-5617.

205. S. K. Maity, *Renewable and Sustainable Energy Reviews*, 2015, **43**, 1427-1445.
206. T. D. Foust, A. Aden, A. Dutta and S. Phillips, *Cellulose*, 2009, **16**, 547-565.
207. H. Kobayashi, T. Komanoya, S. K. Guha, K. Hara and A. Fukuoka, *Applied Catalysis a-General*, 2011, **409**, 13-20.
208. H. J. Huang and X. Z. Yuan, *Progress in Energy and Combustion Science*, 2015, **49**, 59-80.
209. F. Behrendt, Y. Neubauer, M. Oevermann, B. Wilmes and N. Zobel, *Chemical Engineering & Technology*, 2008, **31**, 667-677.
210. A. K. Hossain and P. A. Davies, *Renewable & Sustainable Energy Reviews*, 2013, **21**, 165-189.
211. M. F. R. N. a. M. T. A. Murni M. Ahmad, *American Journal of Applied Sciences* 2010, 7 (6): 746-755.
212. M. Puig-Arnavat, J. C. Bruno and A. Coronas, *Renewable & Sustainable Energy Reviews*, 2010, **14**, 2841-2851.
213. A. Kumar, D. D. Jones and M. A. Hanna, *Energies*, 2009, **2**, 556-581.
214. R. Hoogenboom, T. F. A. Wilms, T. Erdmenger and U. S. Schubert, *Australian Journal of Chemistry*, 2009, **62**, 236-243.
215. C. James, *Handbook of Green Chemistry and Technology*, Blackwell Science, Malden, USA., 2002.
216. M. Letellier and H. Budzinski, *Analusis*, 1999, **27**, 259-271.
217. S. H. Gold and G. S. Nusinovich, *Review of Scientific Instruments*, 1997, **68**, 3945-3974.
218. S. Bhattacharjee, H. Amemiya and Y. Yano, *Journal of Applied Physics*, 2001, **89**, 3573-3579.
219. J. C. Atuonwu and S. A. Tassou, *Journal of Food Engineering*, 2018, **234**, 1-15.
220. T. Y. See, R. Yusoff, C. H. Chan and G. C. Ngoh, *Food and Bioproducts Processing*, 2018, **109**, 98-106.
221. T. C. Edwards, *Introduction to Microwave ELectronics*, Edward Arnold, Baltimore, 1983.
222. R. Meredith, *Engineers' Handbook of Industrial Microwave Heating*, Institution of Electrical Engineers,, London, 1998.
223. T. V. C. T. C. a. H. C. Reader, *Understanding microwave heating cavities,*, Artech House, , Boston, , 2000.
224. CEM, Microwave Chemistry: How it all Works. Chemist, an Electrical engineer, and a Mechanical engineer, http://cem.com/page130.html, (accessed 23rd July, 2014).
225. K. Adlington, G. J. Jones, J. El Harfi, G. Dimitrakis, A. Smith, S. W. Kingman, J. P. Robinson and D. J. Irvine, *Macromolecules*, 2013, **46**, 3922-3930.
226. R. K. Arvela, N. E. Leadbeater, T. L. Mack and C. M. Kormos, *Tetrahedron Letters*, 2006, **47**, 217-220.
227. S. Bag, S. Dasgupta and B. Torok, *Current Organic Synthesis*, 2011, **8**, 237-261.
228. J. M. Bermudez, D. Beneroso, N. Rey-Raap, A. Arenillas and J. A. Menendez, *Chemical Engineering and Processing-Process Intensification*, 2015, **95**, 1-8.
229. V. L. Budarin, P. S. Shuttleworth, M. De Bruyn, T. J. Farmer, M. J. Gronnow, L. Pfaltzgraff, D. J. Macquarrie and J. H. Clark, *Catalysis Today*, 2015, **239**, 80-89.
230. R. Cherbanski, M. Komorowska-Durka, G. D. Stefanidis and A. I. Stankiewicz, *Industrial & Engineering Chemistry Research*, 2011, **50**, 8632-8644.
231. S. J. Choi, J. Kuwabara and T. Kanbara, *Acs Sustainable Chemistry & Engineering*, 2013, **1**, 878-882.
232. A. de la Hoz, A. Diaz-Ortiz and A. Moreno, *Chemical Society Reviews*, 2005, **34**, 164-178.

233. C. Ebner, T. Bodner, F. Stelzer and F. Wiesbrock, *Macromolecular Rapid Communications*, 2011, **32**, 254-288.
234. B. Fidalgo, A. Arenillas and J. A. Menendez, *Fuel Processing Technology*, 2011, **92**, 1531-1536.
235. A. Loupy, L. Perreux, M. Liagre, K. Burle and M. Moneuse, *Pure and Applied Chemistry*, 2001, **73**, 161-166.
236. R. T. McBurney, F. Portela-Cubillo and J. C. Walton, *Rsc Advances*, 2012, **2**, 1264-1274.
237. X. L. Zhang and D. O. Hayward, *Inorganica Chimica Acta*, 2006, **359**, 3421-3433.
238. W. K. Teng, G. C. Ngoh, R. Yusoff and M. K. Aroua, *Chemical Engineering Journal*, 2016, **284**, 469-477.
239. K. Kempe, C. R. Becer and U. S. Schubert, *Macromolecules*, 2011, **44**, 5825-5842.
240. e. A. D. L. H. a. A. Loupy, *Wiley-VCH, Weinheim, 3rd edn,*, 2013.
241. C. O. Kappe and D. Dallinger, *Mol Divers*, 2009, **13**, 71-193.
242. P. Lidstrom, J. Tierney, B. Wathey and J. Westman, *Tetrahedron*, 2001, **57**, 9225-9283.
243. A. De La Hoz, A. Diaz-Ortiz and A. Moreno, *Current Organic Chemistry*, 2004, **8**, 903-918.
244. S. L. Pedersen, A. P. Tofteng, L. Malik and K. J. Jensen, *Chemical Society Reviews*, 2012, **41**, 1826-1844.
245. J. Klinowski, F. A. A. Paz, P. Silva and J. Rocha, *Dalton Transactions*, 2011, **40**, 321-330.
246. K. J. Rao, B. Vaidhyanathan, M. Ganguli and P. A. Ramakrishnan, *Chemistry of Materials*, 1999, **11**, 882-895.
247. D. E. Clark and W. H. Sutton, *Annual Review of Materials Science*, 1996, **26**, 299-331.
248. C. O. Kappe and D. Dallinger, *Nature Reviews Drug Discovery*, 2006, **5**, 51-63.
249. M. Baghbanzadeh, L. Carbone, P. D. Cozzoli and C. O. Kappe, *Angewandte Chemie-International Edition*, 2011, **50**, 11312-11359.
250. J. M. Collins and N. E. Leadbeater, *Organic & Biomolecular Chemistry*, 2007, **5**, 1141-1150.
251. M. Miura, H. Kaga, A. Sakurai, T. Kakuchi and K. Takahashi, *Journal of Analytical and Applied Pyrolysis*, 2004, **71**, 187-199.
252. A. Al Shra'ah and R. Helleur, *Journal of Analytical and Applied Pyrolysis*, 2014, **105**, 91-99.
253. G. Gellerstedt, *Proceedings of International Conference on Pulping, Papermaking and Biotechnology 2008: Icppb '08, Vol I*, 2008, 9-15.
254. C. O. Kappe, *Angewandte Chemie-International Edition*, 2004, **43**, 6250-6284.
255. F. Yu, S. Deng, P. Chen, Y. Liu, Y. Wan, A. Olson, D. Kittelson and R. Ruan, *Applied Biochemistry and Biotechnology*, 2007, **137**, 957-970.
256. M. J. Gronnow, R. J. White, J. H. Clark and D. J. Macquarrie, *Organic Process Research & Development*, 2005, **9**, 516-518.
257. F. Chemat, M. E. Lucchesi, J. Smadja, L. Favretto, G. Colnaghi and F. Visinoni, *Analytica Chimica Acta*, 2006, **555**, 157-160.
258. D. E. Clark and W. H. Sutton, *Annual Review of Materials Science*, 1996, **26**, 299-331.
259. G. Y. Li, C. Y. Hse and T. F. Qin, *Journal of Forestry Research*, 2015, **26**, 1043-1048.
260. J. Yip, M. J. Chen, Y. S. Szeto and S. C. Yan, *Bioresource Technology*, 2009, **100**, 6674-6678.
261. Z. A. Liu and F. S. Zhang, *Energy Conversion and Management*, 2008, **49**, 3498-3504.
262. C. R. T. N. Wang, X. Y. Lin, and J. H. Wang,, *Biomass Chemical Engineering*, 2013, vol. 47, no. 41, pp. 33–38.

263. W. H. Xiao, L. J. Han and Y. Y. Zhao, *Industrial Crops and Products*, 2011, **34**, 1602-1606.
264. X. J. Kong, X. L. Li, S. X. Wu, X. Zhang and J. H. Liu, *Rsc Advances*, 2016, **6**, 28532-28537.
265. A. Krzan and M. Kunaver, *Journal of Applied Polymer Science*, 2006, **101**, 1051-1056.
266. A. Krzan and E. Zagar, *Bioresource Technology*, 2009, **100**, 3143-3146.
267. W. H. Xiao, W. J. Niu, F. Yi, X. Liu and L. J. Han, *Energy & Fuels*, 2013, **27**, 3204-3208.
268. J. H. Liu, Y. B. Zhuang, Y. Li, L. M. Chen, J. X. Guo, D. M. Li and N. H. Ye, *Energy*, 2013, **60**, 69-76.
269. P. Biller, C. Friedman and A. B. Ross, *Bioresource Technology*, 2013, **136**, 188-195.
270. Z. Q. Zheng, Y. Liu, D. Li, L. J. Wang, B. Adhikari and X. D. Chen, *International Journal of Food Engineering*, 2017, **13**.
271. U. A. Amran, S. Zakaria, C. H. Chia, Z. Fang and M. Z. Masli, *Energy & Fuels*, 2017, **31**, 10975-10982.
272. J. X. Guo, Y. B. Zhuang, L. M. Chen, J. H. Liu, D. M. Li and N. H. Ye, *Bioresource Technology*, 2012, **120**, 19-25.
273. S. Y. X. J. Wu, F. R. Meng, J. Zhang, Y. C. Zhang, and D. Wang, *Biomass Chemical Engineering*,, 2018., vol. 52, no. 53, pp. 40–44, .
274. N. Soto-Reyes, A. Lopez-Malo, R. Rojas-Laguna, J. A. Gomez-Salazar and M. E. Sosa-Morales, *Journal of the Science of Food and Agriculture*, 2018, **98**, 3659-3666.
275. X. L. Sun, W. G. Li, J. Li, Y. G. Zu, C. Y. Hse, J. L. Xie and X. H. Zhao, *International Journal of Food Science and Technology*, 2016, **51**, 2663-2673.
276. X. C. Z. G. Y. Li, X. W. Zou, and T. F. Qin, *Chemistry and Industry of Forest Products*, 2015., vol. 35,no. 31, pp. 107–112, .
277. L. Zhou, V. Budarin, J. J. Fan, R. Sloan and D. Macquarrie, *Acs Sustainable Chemistry & Engineering*, 2017, **5**, 3768-3774.
278. X. Z. H. X. P. Ouyang, and X. Q. Qiu, *Journal of Fuel Chemistry and Technology*,, 2014, vol. 42, no. 10, pp. 1212–1217,.
279. W. Zhou, W. X. Fu and Y. C. Zhang, *Journal of Wuhan University of Technology-Materials Science Edition*, 2018, **33**, 1437-1443.
280. A. Sequeiros, L. Serrano, R. Briones and J. Labidi, *Journal of Applied Polymer Science*, 2013, **130**, 3292-3298.
281. J. F. L. Z. D. Liao, J. R. Ruan, and X. D. Li,, *Hubei Agricultural Sciences*, 2013., , vol. 52, no. 57, .
282. W. H. Xiao, X. M. Zhang, X. Wang, W. J. Niu and L. J. Han, *Bioresources*, 2015, **10**, 4038-4047.
283. X. Q. L. X. Y. Li, X. X. Duan, W. Qi, J. Y. Shi, and Y. Z. Lei, *Acta Energiae Solaris Sinica*,, 2017, vol. 38, no. 35, pp. 1453–1458,.
284. J. L. Xie, C. Y. Hse, C. J. Li, T. F. Shupe, T. X. Hu, J. Q. Qi and C. F. De Hoop, *Acs Sustainable Chemistry & Engineering*, 2016, **4**, 3477-3485.
285. Y. B. Zhuang, J. X. Guo, L. M. Chen, D. M. Li, J. H. Liu and N. H. Ye, *Bioresource Technology*, 2012, **116**, 133-139.
286. L. C. Cao, C. Zhang, H. H. Chen, D. C. W. Tsang, G. Luo, S. C. Zhang and J. M. Chen, *Bioresource Technology*, 2017, **245**, 1184-1193.
287. C. Liu, Q. Zhao, Y. C. Lin, Y. H. Hu, H. Y. Wang and G. C. Zhang, *Energy & Fuels*, 2018, **32**, 510-516.
288. J. Remon, L. Zhou, J. J. Fan, D. Macquarrie, V. L. Budarin and J. H. Clark, *Papers of the 25th European Biomass Conference*, 2017, 1412-1416.

289. J. L. Xie, C. Y. Hse, T. F. Shupe and T. X. Hu, *European Journal of Wood and Wood Products*, 2016, **74**, 249-254.
290. J. M. Xu, J. C. Jiang, C. Y. Hse and T. F. Shupe, *Energy & Fuels*, 2013, **27**, 4791-4795.
291. H. J. Shao, H. L. Zhao, J. L. Xie, J. Q. Qi and T. F. Shupe, *International Journal of Polymer Science*, 2019, **2019**.
292. J. M. Xu, J. C. Jiang, C. Y. Hse and T. F. Shupe, *Green Chemistry*, 2012, **14**, 2821-2830.
293. J. L. Xie, C. Y. Hse, T. F. Shupe, J. Q. Qi and H. Pan, *Journal of Applied Polymer Science*, 2014, **131**.
294. J. Xie, J. Qi, C. Hse and T. F. Shupe, *Journal of Forestry Research*, 2015, **26**, 261-265.
295. J. L. Xie, X. L. Zhai, C. Y. Hse, T. F. Shupe and H. Pan, *Materials*, 2015, **8**, 8496-8509.
296. M. Tayier, D. L. Duan, Y. F. Zhao, R. S. Ruan, Y. P. Wang and Y. H. Liu, *Bioresources*, 2018, **13**, 412-424.
297. X. P. Ouyang, G. D. Zhu, X. Z. Huang and X. Q. Qiu, *Journal of Energy Chemistry*, 2015, **24**, 72-76.
298. S. Hassanzadeh, N. Aminlashgari and M. Hakkarainen, *Carbohydrate Polymers*, 2014, **112**, 448-457.
299. E. C. Gaudino, G. Cravotto, M. Manzoli and S. Tabasso, *Green Chemistry*, 2019, **21**, 1202-1235.
300. J. F. Feng, J. C. Jiang, C. Y. Hse, Z. Z. Yang, K. Wang, J. Ye and J. M. Xu, *Sustainable Energy & Fuels*, 2018, **2**, 1035-1047.
301. D. Carnaroglio, S. Tabasso, B. Kwasek, D. Bogdal, E. C. Gaudino and G. Cravotto, *Chemsuschem*, 2015, **8**, 1342-1349.
302. Z. X. Lu, Z. G. Wu, L. W. Fan, H. Zhang, Y. Q. Liao, D. Y. Zheng and S. Q. Wang, *Bioresource Technology*, 2016, **199**, 423-426.
303. S. H. F. da Silva, P. S. B. dos Santos, D. T. da Silva, R. Briones, D. A. Gatto and J. Labidi, *Journal of Wood Chemistry and Technology*, 2017, **37**, 343-358.
304. X. Y. Huang, F. Li, J. L. Xie, C. F. De Hoop, C. Y. Hse, J. Q. Qi and H. Xiao, *Bioresources*, 2017, **12**, 1968-1981.
305. D. L. Duan, Y. F. Zhao, L. L. Fan, L. L. Dai, J. Q. Lv, R. Ruan, Y. P. Wang and Y. H. Liu, *Bioresources*, 2017, **12**, 5308-5320.
306. C. O. Kappe, *Chemical Society Reviews*, 2013, **42**, 4977-4990.
307. M. Gharibeh, G. Tompsett, F. Lu, S. M. Auerbach, K. S. Yngvesson and W. C. Conner, *Journal of Physical Chemistry B*, 2009, **113**, 12506-12520.
308. M. O'Brien, R. Denton and S. V. Ley, *Synthesis-Stuttgart*, 2011, 1157-1192.
309. V. L. Budarin, J. H. Clark, B. A. Lanigan, P. Shuttleworth and D. J. Macquarrie, *Bioresource Technology*, 2010, **101**, 3776-3779.
310. A. Dominguez, J. A. Menendez, M. Inguanzo and J. J. Pis, *Bioresource Technology*, 2006, **97**, 1185-1193.
311. X. Zhao, Z. Song, H. Liu, Z. Li, L. Li and C. Ma, *Journal of Analytical and Applied Pyrolysis*, 2010, **89**, 87-94.
312. A. Domínguez, J. A. Menéndez, Y. Fernández, J. J. Pis, J. M. V. Nabais, P. J. M. Carrott and M. M. L. R. Carrott, *Journal of Analytical and Applied Pyrolysis*, 2007, **79**, 128-135.
313. Y. F. Huang, W. H. Kuan, S. L. Lo and C. F. Lin, *Bioresour Technol*, 2010, **101**, 1968-1973.
314. Y. F. Huang, W. H. Kuan, S. L. Lo and C. F. Lin, *Bioresour Technol*, 2008, **99**, 8252-8258.
315. Y. Wan, P. Chen, B. Zhang, C. Yang, Y. Liu, X. Lin and R. Ruan, *Journal of Analytical and Applied Pyrolysis*, 2009, **86**, 161-167.

316. H. Lei, S. Ren and J. Julson, *Energy & Fuels*, 2009, **23**, 3254-3261.
317. V. L. Budarin, J. H. Clark, B. A. Lanigan, P. Shuttleworth, S. W. Breeden, A. J. Wilson, D. J. Macquarrie, K. Milkowski, J. Jones, T. Bridgeman and A. Ross, *Bioresour Technol*, 2009, **100**, 6064-6068.
318. Z. Du, Y. Li, X. Wang, Y. Wan, Q. Chen, C. Wang, X. Lin, Y. Liu, P. Chen and R. Ruan, *Bioresour Technol*, 2011, **102**, 4890-4896.
319. X. Wang, H. Chen, K. Luo, J. Shao and H. Yang, *Energy & Fuels*, 2007, **22**, 67-74.
320. M.-q. Chen, J. Wang, M.-x. Zhang, M.-g. Chen, X.-f. Zhu, F.-f. Min and Z.-c. Tan, *Journal of Analytical and Applied Pyrolysis*, 2008, **82**, 145-150.
321. Q. Bu, H. Lei, S. Ren, L. Wang, J. Holladay, Q. Zhang, J. Tang and R. Ruan, *Bioresour Technol*, 2011, **102**, 7004-7007.
322. X. Guo, Y. Zheng and B. Zhou, 2008.
323. A. A. Salema and F. N. Ani, *Bioresour Technol*, 2011, **102**, 3388-3395.
324. A. A. Salema and F. N. Ani, *Journal of Analytical and Applied Pyrolysis*, 2012, **96**, 162-172.
325. R. Omar, A. Idris, R. Yunus, K. Khalid and M. A. Isma, *Fuel*, 2011, **90**, 1536-1544.
326. A. A. Salema and F. N. Ani, *Bioresource technology*, 2012, **125**, 102-107.
327. V. L. Budarin, J. H. Clark, B. A. Lanigan, P. Shuttleworth and D. J. Macquarrie, *Bioresour Technol*, 2010, **101**, 3776-3779.
328. J. Robinson, S. Kingman, R. Barranco, C. Snape and H. Al-Sayegh, *Industrial & Engineering Chemistry Research*, 2009, **49**, 459-463.
329. M. Miura, H. Kaga, S. Tanaka, K. Takahashi and K. Ando, *JOURNAL OF CHEMICAL ENGINEERING OF JAPAN*, 2000, **33**, 299-302.
330. Z. Hu, X. Ma and C. Chen, *Bioresour Technol*, 2012, **107**, 487-493.
331. A. A. Salema and F. N. Ani, *APCBEE Procedia*, 2012, **3**, 188-193.
332. J. Menéndez, A. Domínguez, Y. Fernández and J. Pis, *Energy & Fuels*, 2007, **21**, 373-378.
333. J. A. Menéndez, A. Domínguez, M. Inguanzo and J. J. Pis, *Journal of Analytical and Applied Pyrolysis*, 2004, **71**, 657-667.
334. C. G. Yin, *Bioresource Technology*, 2012, **120**, 273-284.
335. K. M. Picker and S. W. Hoag, *Journal of Pharmaceutical Sciences*, 2002, **91**, 342-349.
336. M. Wallace, D. Attwood, R. J. Day and F. Heatley, *Journal of Materials Science*, 2006, **41**, 5862-5869.
337. D. V. Kuznetsov, V. A. Raev, G. L. Kuranov, O. V. Arapov and R. R. Kostikov, *Russian Journal of Organic Chemistry*, 2005, **41**, 1719-1749.
338. X. H. Qi, M. Watanabe, T. M. Aida and R. L. Smith, *Industrial & Engineering Chemistry Research*, 2008, **47**, 9234-9239.
339. T. W. Ching, V. Haritos and A. Tanksale, *Carbohydrate Polymers*, 2017, **157**, 1794-1800.
340. T. Nomura, H. Kawamoto and S. Saka, *Journal of Analytical and Applied Pyrolysis*, 2017, **126**, 209-217.
341. T. Shoji, H. Kawamoto and S. Saka, *Journal of Analytical and Applied Pyrolysis*, 2017, **124**, 638-642.
342. A. P. Gregory, R. N. Clarke and M. G. Cox, *Measurement Science and Technology*, 2009, **20**.
343. S. Jenkins, T. E. Hodgetts, R. N. Clarke and A. W. Preece, *Measurement Science and Technology*, 1990, **1**, 691-702.
344. I. Backlund, L. Karlsson, L. Mattsson and U. Bergsten, *Biomass & Bioenergy*, 2014, **70**, 207-216.

345. A. Kilpelainen, H. Peltola, A. Ryyppo, K. Sauvala, K. Laitinen and S. Kellomaki, *Tree Physiology*, 2003, **23**, 889-897.
346. K. P, Kemiallisten pääkomponenttien jakautuminen puuaineksessa ja puukuidun soluseinässä [Master's thesis].).
347. K. E. Saarela, L. Harju, J. Rajander, J. O. Lill, S. J. Heselius, A. Lindroos and K. Mattsson, *Science of the Total Environment*, 2005, **343**, 231-241.
348. N. J, *Acta Forestalia Fennica*, 1993., 236:230.
349. N. J, *Acta Forestalia Fennica*, 1997, 256:228.
350. L. T. Voipio R, *Folia forestalia*, 1992, 789:722.
351. B. K.-T. L. Valentin, S. Willfor, J. Hemming, A. Hatakka, K. Steffen and M. Tuomela,, *Bioresource Technology*, 2010, 101, 2203-2209.
352. P. S, *Paperi ja Puu*, 1981, 63:593-595.
353. B. D. G. K. Dietrichs HH, Sinner M,, *Holzforschung*, 1978, 32, 60-97.
354. P. T. Vávřová P, Laiho R,, *Forest Ecology and Management*, 2009, **257(2)**, 401-412.
355. C. Celhay, C. E. Mathieu, L. Candy, G. Vilarem and L. Rigal, *Comptes Rendus Chimie*, 2014, **17**, 204-211.
356. S. J. Liu, H. F. Lu, R. F. Hu, A. Shupe, L. Lin and B. Liang, *Biotechnology Advances*, 2012, **30**, 785-810.
357. M. Poletto, A. J. Zattera, M. M. C. Forte and R. M. C. Santana, *Bioresource Technology*, 2012, **109**, 148-153.
358. R. W. Hemingway and W. E. Hillis, *Appita*, 1971, **24**, 439-+.
359. G. Varhegyi, M. G. Gronli and C. Di Blasi, *Industrial & Engineering Chemistry Research*, 2004, **43**, 2356-2367.
360. S. Baroutian, M. Robinson, A. M. Smit, S. Wijeyekoon and D. Gapes, *Bioresource Technology*, 2013, **146**, 294-300.
361. G. G. Wan and C. E. Frazier, *Acs Sustainable Chemistry & Engineering*, 2019, **7**, 17999-18004.
362. H. Horhammer, C. Dou, R. Gustafson, A. Suko and R. Bura, *Biotechnology for Biofuels*, 2018, **11**.
363. Z. M. Li, Y. L. Yu, J. X. Sun, D. M. Li, Y. D. Huang and Y. J. Feng, *Bioresources*, 2016, **11**, 54-70.
364. N. P. K. Nielsen, D. J. Gardner and C. Felby, *Fuel*, 2010, **89**, 94-98.
365. A. Korus, A. Szlek and A. Samson, *Fuel Processing Technology*, 2019, **185**, 106-116.
366. R. Moya and C. Tenorio, *Biomass & Bioenergy*, 2013, **56**, 14-21.
367. S. W. X. Guo, K. Wang, Q. Liu, Z. Luo, *Journal of Fuel Chemistry and Technology*, February 2010, , Volume 38, Issue 31, Pages 42-46.
368. Y. P. Wang, L. B. Wu, C. Wang, J. Y. Yu and Z. Y. Yang, *Bioresource Technology*, 2011, **102**, 7190-7195.
369. M. T. Das, V. Budhraja, M. Mishra and I. S. Thakur, *Bioresource Technology*, 2012, **110**, 71-78.
370. J. M. Leach and A. N. Thakore, *Progress in Water Technology*, 1978, **9**, 787-798.
371. H. Sekido, J. Takezawa, G. Motoki and T. Akatsuka, *Agricultural and Biological Chemistry*, 1990, **54**, 287-290.
372. R. Sierra - Alvarez, *The role of natural wood constituents on the anaerobic treatability of forest industry wastewaters*, Wageningen, Wageningen, The Netherlands, 1990.
373. S. Bianchi, A. N. Gloess, I. Kroslakova, I. Mayer and F. Pichelin, *Industrial Crops and Products*, 2014, **61**, 430-437.
374. S. Wang, K. Wang, Q. Liu, Y. Gu, Z. Luo, K. Cen and T. Fransson, *Biotechnol Adv*, 2009, **27**, 562-567.

375. G. G. Wan and C. E. Frazier, *Acs Sustainable Chemistry & Engineering*, 2017, **5**, 4830-4836.
376. T. Demirbas and C. Demirbas, *Energy Sources Part a-Recovery Utilization and Environmental Effects*, 2009, **31**, 1464-1472.
377. E. Ranzi, A. Cuoci, T. Faravelli, A. Frassoldati, G. Migliavacca, S. Pierucci and S. Sommariva, *Energy & Fuels*, 2008, **22**, 4292-4300.
378. S. Ramasamy and B. Moghtaderi, *Energy & Fuels*, 2010, **24**, 4534-4548.
379. D. M. Alonso, J. Q. Bond and J. A. Dumesic, *Green Chemistry*, 2010, **12**, 1493-1513.
380. S. G. Wettstein, D. M. Alonso, E. I. Gurbuz and J. A. Dumesic, *Current Opinion in Chemical Engineering*, 2012, **1**, 218-224.
381. C. H. Zhou, X. Xia, C. X. Lin, D. S. Tong and J. Beltramini, *Chemical Society Reviews*, 2011, **40**, 5588-5617.
382. M. J. Climent, A. Corma and S. Iborra, *Green Chemistry*, 2014, **16**, 516-547.
383. D. J. Krasznai, R. C. Hartley, H. M. Roy, P. Champagne and M. F. Cunningham, *Critical Reviews in Biotechnology*, 2018, **38**, 199-217.
384. H. J. G. Jung, *Journal of Nutrition*, 1997, **127**, S810-S813.
385. O. Faix and J. H. Bottcher, *Holzforschung*, 1993, **47**, 45-49.
386. S. Tsuchikawa, *Applied Spectroscopy Reviews*, 2007, **42**, 43-71.
387. K. Nkansah, B. Dawson-Andoh and J. Slahor, *Bioresource Technology*, 2010, **101**, 4570-4576.
388. C. A. Sellick, R. Hansen, R. M. Jarvis, A. R. Maqsood, G. M. Stephens, A. J. Dickson and R. Goodacre, *Biotechnology and Bioengineering*, 2010, **106**, 432-442.
389. P. Geladi, B. Sethson, J. Nystrom, T. Lillhonga, T. Lestander and J. Burger, *Spectrochimica Acta Part B-Atomic Spectroscopy*, 2004, **59**, 1347-1357.
390. P. Geladi, *Spectrochimica Acta Part B-Atomic Spectroscopy*, 2003, **58**, 767-782.
391. T. B. L. Eriksson, E. Johansson, J. Trygg and C. Vikström, *Multi- and Megavariate Data Analysis*, Umetrics Academi, Umea, 2006.
392. C. R. Warren and M. A. Adams, *Phytochem Anal*, 2004, **15**, 407-413.
393. C. J. Gómez, E. Mészáros, E. Jakab, E. Velo and L. Puigjaner, *Journal of Analytical and Applied Pyrolysis*, 2007, **80**, 416-426.
394. G. Toscano, A. Rinnan, A. Pizzi and M. Mancini, *Energy & Fuels*, 2017, **31**, 2814-2821.
395. Y. Ozaki, *Analytical Sciences*, 2012, **28**, 545-563.
396. D. Sorak, L. Herberholz, S. Iwascek, S. Altinpinar, F. Pfeifer and H. W. Siesler, *Applied Spectroscopy Reviews*, 2012, **47**, 83-115.
397. Y. O. H. W. Siesler, S. Kawata, H. M. Heise, *Near-Infrared Spectroscopy; Principles, Instruments, Applications*, WILEY-VCH, Weinheimm, 2006.
398. T. Lestander, P. Geladi, S. Larsson and M. Thyrel, *Journal of Near Infrared Spectroscopy*, 2012, **20**, 591-599.
399. C. Pasquini, *Analytica Chimica Acta*, 2018, **1026**, 8-36.
400. L. Q. Wang, Y. M. Li, L. P. Zhang, H. X. Xiao, Q. Zhou and S. Q. Sun, *Guang Pu Xue Yu Guang Pu Fen Xi*, 2006, **26**, 1061-1066.
401. I. Backlund, M. Arshadi, A. J. Hunt, C. R. McElroy, T. M. Attard and U. Bergsten, *Industrial Crops and Products*, 2014, **58**, 220-229.
402. T. M. Attard, M. Arshadi, C. Nilsson, V. L. Budarin, E. Valencia-Reyes, J. H. Clark and A. J. Hunt, *Green Chemistry*, 2016, **18**, 2682-2690.
403. T. M. Attard, N. Bukhanko, D. Eriksson, M. Arshadi, P. Geladi, U. Bergsten, V. L. Budarin, J. H. Clark and A. J. Hunt, *Journal of Cleaner Production*, 2018, **177**, 684-698.
404. M. Arshadi, A. J. Hunt and J. H. Clark, *RSC Advances*, 2012, **2**, 1806-1809.

405. J. Chen, X. Ren, Q. Zhang, X. M. Diao and Q. Shen, *Journal of Cereal Science*, 2013, **58**, 241-247.
406. H. Bailleres, F. Davrieus and F. H. Pichavant, *Annals of Forest Science*, 2002, **59**, 479-490.
407. J. Sandak, A. Sandak and R. Meder, *Journal of near Infrared Spectroscopy*, 2016, **24**, 485-505.
408. G. E. Acquah, B. K. Via, O. O. Fasina and L. G. Eckhardt, *Journal of near Infrared Spectroscopy*, 2015, **23**, 93-102.
409. P. F. Kurt Varmuza, *Introduction to Multivariate Analysis in Chemometrics*, CRC Press, London, 2009.
410. S. Kudo, Z. Zhou, K. Yamasaki, K. Norinaga and J. Hayashi, *Catalysts*, 2013, **3**, 757-773.
411. S. Kudo, Z. W. Zhou, K. Norinaga and J. Hayashi, *Green Chemistry*, 2011, **13**, 3306-3311.
412. Q. Lu, X. N. Ye, Z. B. Zhang, C. Q. Dong and Y. Zhang, *Bioresource Technology*, 2014, **171**, 10-15.
413. M. L. Nieva, M. A. Volpe and E. L. Moyano, *Cellulose*, 2015, **22**, 215-228.
414. A. M. Sarotti, R. A. Spanevello and A. G. Suárez, *Green Chemistry*, 2007, **9**, 1137-1140.
415. R. H. Furneaux and F. Shafizadeh, *Carbohydrate Research*, 1979, **74**, 354-360.
416. X. W. Sui, Z. Wang, B. Liao, Y. Zhang and Q. X. Guo, *Bioresource Technology*, 2012, **103**, 466-469.
417. H. Kawamoto, S. Saito, W. Hatanaka and S. Saka, *Journal of Wood Science*, 2007, **53**, 127-133.
418. F. Cao, T. J. Schwartz, D. J. McClelland, S. H. Krishna, J. A. Dumesic and G. W. Huber, *Energy Environ. Sci.*, 2015, **8**, 1808-1815.
419. M. De Bruyn, J. Fan, V. L. Budarin, D. J. Macquarrie, L. D. Gomez, R. Simister, T. J. Farmer, W. D. Raverty, S. J. McQueen-Mason and J. H. Clark, *Energy & Environmental Science*, 2016, **9**, 2571-2574.
420. G. Dobele, G. Rossinskaja, G. Telysheva, D. Meier and O. Faix, *Journal of Analytical and Applied Pyrolysis*, 1999, **49**, 307-317.
421. Q. Lu, X. M. Zhang, Z. B. Zhang, Y. Zhang, X. F. Zhu and C. Q. Dong, *Bioresources*, 2012, **7**, 2820-2834.
422. Q. Lu, X. C. Yang, C. Q. Dong, Z. F. Zhang, X. M. Zhang and X. F. Zhu, *Journal of Analytical and Applied Pyrolysis*, 2011, **92**, 430-438.
423. M. E. Zakrzewska, E. Bogel-Lukasik and R. Bogel-Lukasik, *Chemical Reviews*, 2011, **111**, 397-417.
424. J. N. Chheda, Y. Roman-Leshkov and J. A. Dumesic, *Green Chemistry*, 2007, **9**, 342-350.
425. R. Weingarten, A. Rodriguez-Beuerman, F. Cao, J. S. Luterbacher, D. M. Alonso, J. A. Dumesic and G. W. Huber, *Chemcatchem*, 2014, **6**, 2229-2234.
426. T. S. Deng, X. J. Cui, Y. Q. Qi, Y. X. Wang, X. L. Hou and Y. L. Zhu, *Chemical Communications*, 2012, **48**, 5494-5496.
427. H. A. Xia, S. Q. Xu, X. P. Yan and S. L. Zuo, *Fuel Processing Technology*, 2016, **152**, 140-146.
428. J. Yang, K. D. Vigier, Y. L. Gu and F. Jerome, *Chemsuschem*, 2015, **8**, 269-274.
429. Y. Roman-Leshkov, J. N. Chheda and J. A. Dumesic, *Science*, 2006, **312**, 1933-1937.
430. L. Atanda, S. Mukundan, A. Shrotri, Q. Ma and J. Beltramini, *Chemcatchem*, 2015, **7**, 781-790.

431. L. Atanda, M. Konarova, Q. Ma, S. Mukundan, A. Shrotri and J. Beltramini, *Catalysis Science & Technology*, 2016, **6**, 6257-6266.
432. R. Rinaldi, R. Palkovits and F. Schuth, *Angewandte Chemie-International Edition*, 2008, **47**, 8047-8050.
433. J. B. Binder and R. T. Raines, *Journal of the American Chemical Society*, 2009, **131**, 1979-1985.
434. H. B. Zhao, J. E. Holladay, H. Brown and Z. C. Zhang, *Science*, 2007, **316**, 1597-1600.
435. J. He, M. Liu, K. Huang, T. W. Walker, C. T. Maravelias, J. A. Dumesic and G. W. Huber, *Green Chem.*, 2017, **19**, 3642-3653.
436. K. D., *Biomass for renewable energy, fuel and chemicals*, Academic press, 1998.
437. H. Kawamoto, W. Hatanaka and S. Saka, *Journal of Analytical and Applied Pyrolysis*, 2003, **70**, 303-313.
438. H. Kawamoto, T. Hosoya, Y. Ueno, T. Shoji and S. Saka, *Journal of Analytical and Applied Pyrolysis*, 2014, **109**, 41-46.
439. H. Kawamoto, *Current Organic Chemistry*, 2016, **20**, 2444-2457.
440. H. Kawamoto, Y. Ueno and S. Saka, *Journal of Analytical and Applied Pyrolysis*, 2013, **103**, 287-292.
441. T. Hosoya, H. Kawamoto and S. Saka, *Carbohydrate Research*, 2006, **341**, 2293-2297.
442. Y. Halpern and S. Patai, *Israel Journal of Chemistry*, 1969, **7**, 673-&.
443. F. Shafizadeh and A. G. W. Bradbury, *Journal of Applied Polymer Science*, 1979, **23**, 1431-1442.
444. A. Broido, Javierso.Ac, A. C. Ouano and E. M. Barrall, *Journal of Applied Polymer Science*, 1973, **17**, 3627-3635.
445. M. L. Nelson and V. W. Tripp, *Journal of Polymer Science*, 1953, **10**, 577-586.
446. Y. Nishiyama, *Journal of Wood Science*, 2009, **55**, 241-249.
447. Y. Nishiyama, U. J. Kim, D. Y. Kim, K. S. Katsumata, R. P. May and P. Langan, *Biomacromolecules*, 2003, **4**, 1013-1017.
448. S. Elazzouzi-Hafraoui, Y. Nishiyama, J. L. Putaux, L. Heux, F. Dubreuil and C. Rochas, *Biomacromolecules*, 2008, **9**, 57-65.
449. D. Y. Kim, Y. Nishiyama, M. Wada, S. Kuga and T. Okano, *Holzforschung*, 2001, **55**, 521-524.
450. H. Kawamoto and S. Saka, *Journal of Analytical and Applied Pyrolysis*, 2006, **76**, 280-284.
451. G. A. Zickler, W. Wagermaier, S. S. Funari, M. Burghammer and O. Paris, *Journal of Analytical and Applied Pyrolysis*, 2007, **80**, 134-140.
452. K. C. Badgujar and B. M. Bhanage, *Bioresource technology*, 2015, **178**, 2-18.
453. T. A. Bioni, E. P. G. Areas, L. G. Couto, G. Favarin and O. A. El Seoud, *Nordic Pulp & Paper Research Journal*, 2015, **30**, 105-111.
454. R. Casarano and O. A. El Seoud, *Macromolecular Bioscience*, 2013, **13**, 191-202.
455. G. Cheng, P. Varanasi, R. Arora, V. Stavila, B. A. Simmons, M. S. Kent and S. Singh, *Journal of Physical Chemistry B*, 2012, **116**, 10049-10054.
456. S. J. Dee and A. T. Bell, *Chemsuschem*, 2011, **4**.
457. F. Ibrahim, M. Moniruzzarnan, S. Yusup and Y. Uemura, *Journal of Molecular Liquids*, 2015, **211**, 370-372.
458. S. Possidonio, L. C. Fidale and O. A. E. Seoud, *Journal of Polymer Science Part a-Polymer Chemistry*, 2010, **48**, 134-143.
459. G. Bao, S. Shiro and H. Wang, *Science in China Series B: Chemistry*, 2008, **51**, 479-486.
460. F. Motasemi and M. T. Afzal, *Renewable & Sustainable Energy Reviews*, 2013, **28**, 317-330.

461. Shaveta, N. Bansal and P. Singh, *Tetrahedron Letters*, 2014, **55**, 2467-2470.
462. B. Kriegerbrockett, *Research on Chemical Intermediates*, 1994, **20**, 39-49.
463. P.-T. C. Yu-Fong Huang, Shang-Lien Lo*, *Sustainable Environment Research*, 2016, 103-106.
464. J. J. Wang, J. X. Xi and Y. Q. Wang, *Green Chemistry*, 2015, **17**, 737-751.
465. V. I. Markin, M. Y. Cheprasova and N. G. Bazarnova, *Russian Journal of Bioorganic Chemistry*, 2015, **41**, 686-699.
466. S. Dutta, S. De and B. Saha, *Biomass & Bioenergy*, 2013, **55**, 355-369.
467. M. Bartoli, L. Rosi, A. Giovannelli, P. Frediani and M. Frediani, *Journal of Analytical and Applied Pyrolysis*, 2016, **120**, 284-296.
468. A. Szabolcs, M. Molnar, G. Dibo and L. T. Mika, *Green Chemistry*, 2013, **15**, 439-445.
469. R. J. Chimentao, E. Lorente, F. Gispert-Guirado, F. Medina and F. Lopez, *Carbohydrate Polymers*, 2014, **111**, 116-124.
470. S. G. Sudrik, S. P. Chavan, K. R. S. Chandrakumar, S. Pal, S. K. Date and H. R. Sonawane, *Journal of Organic Chemistry*, 2002, **67**, 1574-1579.
471. E. Mentese, F. Islamoglu and B. Kahveci, *Revue Roumaine De Chimie*, 2012, **57**, 907-913.
472. A. M. Rodriguez, P. Prieto, A. de la Hoz, A. Diaz-Ortiz, D. R. Martin and J. I. Garcia, *Chemistryopen*, 2015, **4**, 308-317.
473. Y. M. Tang, X. L. Hu, P. Guan, T. Tian and S. J. Wang, *Journal of Chemical and Engineering Data*, 2014, **59**, 2464-2471.
474. Y. J. Alvarado, N. Cubillan, P. H. Labarca, A. Karam, F. Arrieta, O. Castellano and H. Soscun, *Journal of Physical Organic Chemistry*, 2002, **15**, 154-164.
475. S. Hemwimon, P. Pavasant and A. Shotipruk, *Separation and Purification Technology*, 2007, **54**, 44-50.
476. H. Huang, Z. N. Wang, H. Aalim, J. Limwachiranon, L. Li, Z. H. Duan, G. P. Ren and Z. S. Luo, *International Journal of Food Science and Technology*, 2019, **54**, 1363-1371.
477. S. Messieh, *Journal of Molecular Liquids*, 2003, **105**, 37-51.
478. A. J. Queimada, I. M. Marrucho, E. H. Stenby and J. A. P. Coutinho, *Fluid Phase Equilibria*, 2004, **222-223**, 161-168.
479. O. A. Esin, B. R. Gelchinskii, N. A. Vatolin and V. F. Ukhov, *Zhurnal Fizicheskoi Khimii*, 1975, **49**, 2955-2957.
480. A. H. Pelofsky, *Journal of Chemical & Engineering Data*, 1966, **11**, 394-397.
481. A. DelleSite, *Journal of Physical and Chemical Reference Data*, 1997, **26**, 157-193.
482. Levine, 2008.
483. C. Reichardt and T. Welton, *Solvents and Solvent Effects in Organic Chemistry, Fourth Edition*, waley, 1988.
484. J. Robinson, S. Kingman, D. Irvine, P. Licence, A. Smith, G. Dimitrakis, D. Obermayer and C. O. Kappe, *Physical Chemistry Chemical Physics*, 2010, **12**, 4750-4758.
485. V. C. Smith and R. L. Robinson, *Journal of Chemical and Engineering Data*, 1970, **15**, 391-&.
486. Z. D. Nan, Q. Z. Jiao, Z. C. Tan and L. X. Sun, *Thermochimica Acta*, 2003, **406**, 151-159.
487. I. Nagata, *Fluid Phase Equilibria*, 1977, **1**, 93-111.
488. I. Nagata, K. Tamura and K. Gotoh, *Thermochimica Acta*, 1986, **104**, 179-202.
489. T. Sumi, R. Dillert and S. Horikoshi, *Journal of Physical Chemistry B*, 2015, **119**, 14479-14485.
490. L. Onsager, *Journal of the American Chemical Society*, 1936, **58**, 1486-1493.
491. Y. B. Huang and Y. Fu, *Green Chemistry*, 2013, **15**, 1095-1111.

492. Y. S. Qu, Q. Y. Wei, H. Q. Li, P. Oleskowicz-Popiel, C. P. Huang and J. Xu, *Bioresource Technology*, 2014, **162**, 358-364.
493. J. Y. Kim, H. W. Lee, S. M. Lee, J. Jae and Y. K. Park, *Bioresource Technology*, 2019, **279**, 373-384.
494. J. F. Feng, C. Hse, Z. Z. Yang, K. Wang, J. C. Jiang and J. M. Xu, *Bioresource Technology*, 2017, **244**, 496-508.
495. C. G. Lopez and W. Richtering, *Soft Matter*, 2017, **13**, 8271-8280.
496. T. Liebert, *Cellulose Solvents: for Analysis, Shaping and Chemical Modification*, 2009, **1033**, 3-54.
497. M. R. Gomezanton, R. M. Masegosa and A. Horta, *Polymer*, 1987, **28**, 2116-2121.
498. H. Wang, G. Gurau and R. D. Rogers, *Chemical Society Reviews*, 2012, **41**, 1519-1537.
499. B. Medronho and B. Lindman, *Current Opinion in Colloid & Interface Science*, 2014, **19**, 32-40.
500. O. A. El Seoud, *Quimica Nova*, 2010, **33**, 2187-2192.
501. O. A. El Seoud, L. C. Fidale, N. Ruiz, M. L. O. D'Almeida and E. Frollini, *Cellulose*, 2008, **15**, 371-392.
502. L. C. Fidale, N. Ruiz, T. Heinze and O. A. El Seoud, *Macromolecular Chemistry and Physics*, 2008, **209**, 1240-1254.
503. G. S. Jiang, W. F. Huang, B. C. Wang, Y. M. Zhang and H. P. Wang, *Cellulose*, 2012, **19**, 679-685.
504. O. Kuzmina, S. Jankowski, A. Fabiainska, E. Sashina and D. Wawro, *Cellulose Chemistry and Technology*, 2014, **48**, 45-51.
505. L. F. V. Ferreira, A. R. Garcia, M. R. Freixo and S. M. B. Costa, *Journal of the Chemical Society-Faraday Transactions*, 1993, **89**, 1937-1944.
506. R. W. Taft, J. L. M. Abboud, M. J. Kamlet and M. H. Abraham, *Journal of Solution Chemistry*, 1985, **14**, 153-186.
507. M. J. Kamlet and R. W. Taft, *Journal of the American Chemical Society*, 1976, **98**, 377-383.
508. R. W. Taft and M. J. Kamlet, *Journal of the American Chemical Society*, 1976, **98**, 2886-2894.
509. M. H. Abraham, *Chemical Society Reviews*, 1993, **22**, 73-83.
510. A. Klamt and G. Schuurmann, *Journal of the Chemical Society-Perkin Transactions 2*, 1993, 799-805.
511. A. Klamt, *Journal of Physical Chemistry*, 1995, **99**, 2224-2235.
512. A. Klamt, *Abstracts of Papers of the American Chemical Society*, 2003, **226**, U432-U433.
513. M. Durand, V. Molinier, W. Kunz and J. M. Aubry, *Chemistry-a European Journal*, 2011, **17**, 5155-5164.
514. L. Moity, M. Durand, A. Benazzouz, C. Pierlot, V. Molinier and J. M. Aubry, *Green Chemistry*, 2012, **14**, 1132-1145.
515. A. C. M. R. J. Meredith, in *Industrial Microwave heating*, Peter Peregrinus Ltd, Exter. England, 1993, p. 10.
516. Y. X. Hua and C. P. Liu, *Transactions of Nonferrous Metals Society of China*, 1996, **6**, 35-40.
517. H. Mooiweer, *Microwave Techniques*, MacMillan, New York, 1971.
518. A. C. M. R. J. Meredith, in *Industrial Microwave heating*, Peter Peregrinus Ltd, Exter. England, 1993, p. 10.
519. C. Gabriel, S. Gabriel, E. H. Grant, E. H. Grant, B. S. J. Halstead and D. Michael P. Mingos, *Chemical Society Reviews*, 1998, **27**, 213-223.

520. T. V. C. T. Chan and H. C. Reader, *Understanding Microwave heating cavities*, Artech House, London, 2000.
521. A. P. Gregory and R. N. Clarke, *Tables of the complex permittivity of dielectric reference liquids at frequencies up to 5 GHz.*, NPL 2001, NPL Report No: CETM 33.
522. M. P. Robinson, I. D. Flintoft, L. Dawson, J. Clegg, J. G. Truscott and X. Zhu, *Measurement Science and Technology*, 2010, **21**.
523. J. Barthel and R. Buchner, *Chemical Society Reviews*, 1992, **21**, 263-270.
524. Y. Marcus, *Chemical Society Reviews*, 1993, **22**, 409-416.
525. H. Tjong and H. X. Zhou, *Journal of Chemical Physics*, 2006, **125**.
526. A. P. Abbott and J. F. Rusling, *Journal of Physical Chemistry*, 1990, **94**, 8910-8912.
527. J. Kim, D. S. Clark and J. S. Dordick, *Biotechnology and Bioengineering*, 2000, **67**, 112-116.
528. J. L. Rivail and D. Rinaldi, *Chemical Physics*, 1976, **18**, 233-242.
529. U. Maran, T. A. Pakkanen and M. Karelson, *Journal of the Chemical Society-Perkin Transactions 2*, 1994, 2445-2452.
530. A. Melo, A. J. I. Alfaia, J. C. R. Reis and A. R. T. Calado, *Journal of Physical Chemistry B*, 2006, **110**, 1877-1888.
531. L. Z. Jiang, Y. Orimoto and Y. Aoki, *Journal of Chemical Theory and Computation*, 2013, **9**, 4035-4045.
532. M. D. Halls and H. B. Schlegel, *Journal of Physical Chemistry B*, 2002, **106**, 1921-1925.
533. A. Chaudhari, H. Chaudhari and S. Mehrotra, *Journal of the Chinese Chemical Society*, 2002, **49**, 489-494.
534. G. K. Johri, R. Sharma, A. Tiwari, M. Johri, S. Saxena and J. A. Roberts, *Physics and Chemistry of Liquids*, 2001, **39**, 711-722.
535. U. Westhaus, T. Droge and R. Sass, *Fluid Phase Equilibria*, 1999, **158**, 429-435.
536. M. Petrowsky, D. T. Glatzhofer and R. Frech, *Journal of Physical Chemistry B*, 2013, **117**, 14432-14437.
537. D. D. Campos, J. C. A. dos Santos and L. E. P. Borges, *Revista Virtual De Quimica*, 2017, **9**, 2593-2624.
538. J. F. Lou, T. A. Hatton and P. E. Laibinis, *Journal of Physical Chemistry A*, 1997, **101**, 5262-5268.
539. A. A. M. Bahar, Z. Zakaria, S. R. Ab Rashid, A. A. M. Isa and R. A. Alahnomi, *Microwave and Optical Technology Letters*, 2017, **59**, 367-371.
540. M. A. Herrero, J. M. Kremsner and C. O. Kappe, *Journal of Organic Chemistry*, 2008, **73**, 36-47.
541. O. Chokichiro Shibata and Tomohiro Kashima and Kimihiro, *Japanese Journal of Applied Physics*, 1996, **35**, 316.
542. C. O. Kappe, *Angew Chem Int Ed Engl*, 2004, **43**, 6250-6284.
543. N. F. K. Kaiser, U. Bremberg, M. Larhed, C. Moberg and A. Hallberg, *Angewandte Chemie-International Edition*, 2000, **39**, 3596-3598.
544. A. M. Fleshman, M. Petrowsky, J. D. Jernigen, R. S. P. Bokalawela, M. B. Johnson and R. Frech, *Electrochimica Acta*, 2011, **57**, 147-152.
545. C. O. Kappe, B. Pieber and D. Dallinger, *Angewandte Chemie-International Edition*, 2013, **52**, 1088-1094.
546. T. Razzaq and C. O. Kappe, *Chemsuschem*, 2008, **1**, 123-132.
547. O. Yemiş and G. Mazza, *Bioresource Technology*, 2012, **109**, 215-223.
548. E. H. K. Sin, *The extraction and fractionation of waxes from biomass,*, PhD thesis.University of York., 2012.

549. A. P. o. F. P. Stanley E. Corder, *XVI IUFRO World Congress,Oslo, Norway,June 20-July 2*, 1976.
550. *A5TM D 2974-87*, American Society of Testing and Materials, 1916.
551. S. Ajith, S. Pramod, C. P. Kumari and V. P. Potty, *Journal of Food Science and Technology-Mysore*, 2015, **52**, 4631-4636.
552. F. R. Amin, Y. Huang, Y. F. He, R. H. Zhang, G. Q. Liu and C. Chen, *Clean Technologies and Environmental Policy*, 2016, **18**, 1457-1473.
553. Y. B. Tao, S. J. Li, P. Li and Q. L. Wu, *Holzforschung*, 2016, **70**, 1175-1182.
554. P. O. Biney, M. Gyamerah, J. Shen and B. Menezes, *Bioresour Technol*, 2015, **179**, 113-122.
555. F. Nsaful, F.-X. Collard, M. Carrier, J. F. Görgens and J. H. Knoetze, *Journal of Analytical and Applied Pyrolysis*, 2015, **116**, 86-95.
556. Y.-M. Kim, S. Kim, T. U. Han, Y.-K. Park and C. Watanabe, *Journal of Analytical and Applied Pyrolysis*, 2014, **110**, 435-441.
557. D. Lopez-Gonzalez, M. Fernandez-Lopez, J. L. Valverde and L. Sanchez-Silva, *Bioresour Technol*, 2013, **143**, 562-574.
558. C. Tenorio and R. Moya, *Thermochimica Acta*, 2013, **563**, 12-21.
559. L. Sanchez-Silva, D. Lopez-Gonzalez, J. Villasenor, P. Sanchez and J. L. Valverde, *Bioresource Technology*, 2012, **109**, 163-172.
560. T. Sebio-Puñal, S. Naya, J. López-Beceiro, J. Tarrío-Saavedra and R. Artiaga, *Journal of Thermal Analysis and Calorimetry*, 2012, **109**, 1163-1167.
561. S. Y. Yorulmaz and A. T. Atimtay, *Fuel Processing Technology*, 2009, **90**, 939-946.
562. Q. Liu, S. Wang, Y. Zheng, Z. Luo and K. Cen, *Journal of Analytical and Applied Pyrolysis*, 2008, **82**, 170-177.
563. A. Kännaste, T. Zhao, A. Lindström, E. Stattin, B. Långström and A. K. Borg-Karlson, *Trees - Structure and Function*, 2013, **27**, 149-159.
564. G. Uçar, M. Balaban and M. Usta, *Flavour and Fragrance Journal*, 2003, **18**, 368-375.
565. P. Costa, C. Pionneau, G. Bauw, C. Dubos, N. Bahrmann, A. Kremer, J. M. Frigerio and C. Plomion, *Electrophoresis*, 1999, **20**, 1098-1108.
566. B. K. Via, C. F. Zhou, G. Acquah, W. Jiang and L. Eckhardt, *Sensors*, 2014, **14**, 13532-13547.
567. D. Cozzolino, *Planta Med*, 2009, **75**, 746-756.
568. M. Schwanninger, J. Rodrigues and K. Fackler, *Journal of Near Infrared Spectroscopy*, 2011, **19**, 287-308.
569. B. Leblon, O. Adedipe, G. Hans, A. Haddadi, S. Tsuchikawa, J. Burger, R. Stirling, Z. Pirouz, K. Groves, J. Nader and A. LaRocque, *The Forestry Chronicle*, 2013, **89**, 595-606.
570. S. Tsuchikawa and H. Kobori, *Journal of Wood Science*, 2015, **61**, 213-220.
571. S. Tsuchikawa and M. Schwanninger, *Applied Spectroscopy Reviews*, 2013, **48**, 560-587.
572. O. D. Sparkman, *Journal*.
573. V. V. Klára Urbanová, * Irena Valterová, * Martina Háková, * ,† and Josef Cvačka, *Journal of Lipid Research*, 2012, 53, 2012.
574. L. X. Zhang, Y. F. Yun, Y. Z. Liang and D. S. Cao, *J Chromatogr A*, 2010, **1217**, 3695-3701.
575. A. H. M. a. M. R. Islam, *Modern Mass Spectrometry.*, Bangla Academi, Dhaka, 1993.
576. R. Gedye, F. Smith, K. Westaway, H. Ali, L. Baldisera, L. Laberge and J. Rousell, *Tetrahedron Letters*, 1986, **27**, 279-282.
577. K. Crombie, O. Masek, S. P. Sohi, P. Brownsort and A. Cross, *Global Change Biology Bioenergy*, 2013, **5**, 122-131.

578. N. Hao, H. X. Ben, C. G. Yoo, S. Adhikari and A. J. Ragauskas, *Energy & Fuels*, 2016, **30**, 6863-6880.
579. T. Burgi and A. Baiker, *Advances in Catalysis, Vol 50*, 2006, **50**, 227-283.
580. F. Kusumattaqiin and W. Chonkaew, *Macromolecular Symposia*, 2015, **354**, 35-41.
581. L. Zhang, J. Ye, S. Y. Wang and P. Chem Ind, *Proceedings of the 2007 International Conference on Advanced Fibers and Polymer Materials Vols 1 and 2*, 2007, 180-183.
582. X. H. Wang, H. P. Chen, X. J. Ding, H. P. Yang, S. H. Zhang and Y. Q. Shen, *Bioresources*, 2009, **4**, 946-959.
583. D. Ciolacu, F. Ciolacu and V. I. Popa, *Cellulose Chemistry and Technology*, 2011, **45**, 13-21.
584. I. Pastorova, R. E. Botto, P. W. Arisz and J. J. Boon, *Carbohydrate Research*, 1994, **262**, 27-47.
585. H. P. Yang, R. Yan, H. P. Chen, C. G. Zheng, D. H. Lee and D. T. Liang, *Energy & Fuels*, 2006, **20**, 388-393.
586. A. J. Z. a. V. P. Matheus Poletto1, in *Cellulose-Fundamental Aspects*, INTECH open science, 2013.
587. H. P. Yang, R. Yan, H. P. Chen, D. H. Lee and C. G. Zheng, *Fuel*, 2007, **86**, 1781-1788.
588. F. C. a. V. P. P. P. Diana Clolacu, *Cellulose Chemistry and Technology.*, 2011, 45 (41-42),13-21.
589. X.-H. Wang, H.-P. Chen, X.-J. Ding, H.-P. Yang, S.-H. Zhang and Y.-Q. Shen, *Bioresources*, 2009, **4**, 946-959.
590. S. Xin, H. Yang, Y. Chen, M. Yang, L. Chen, X. Wang and H. Chen, *Journal of Analytical and Applied Pyrolysis*, 2015, **116**, 263-271.
591. b. Shanzhi Xina, Haiping Yanga,∗, Yingquan Chena, Mingfa Yanga, Lei Chena, Xianhua Wanga, Hanping Chena, *Journal of Analytical and Applied Pyrolysis 116 (2015) 263–271*, 2015, 116; 263–271.
592. F. J. Ramirez, P. Luque, A. Heredia and M. J. Bukovac, *Biopolymers*, 1992, **32**, 1425-1429.
593. S. Merk, A. Blume and M. Riederer, *Planta*, 1998, **204**, 44-53.
594. H. Schulz and M. Baranska, *Vibrational Spectroscopy*, 2007, **43**, 13-25.
595. Y. Ozaki, R. Cho, K. Ikegaya, S. Muraishi and K. Kawauchi, *Applied Spectroscopy*, 1992, **46**, 1503-1507.
596. E. H. K. Sin, *The extraction and fractionation of waxes from biomass*, , PhD thesis.University of York., 2012.
597. A. F. M. R.G. Sinclair, G.S. Myers and R.N. Jones, *J. Am. Chem. Soc.*, , 1952, 74, 2578-2585.
598. M. D. G. a. N. Cabo, *J. Am. Oil Chem. Soc.*, 1997, 74, 1281-1286.
599. V. P. A. R. S. VARMA, in *Aqueous Microwave Assisted Chemistry : Synthesis and Catalysis*, Royal Society of Chemistry, 2010, p. 6.
600. James H. Clark*, Jiajun Fan, † Mario De bruyn,† Vitaliy L. Budarin,† Mark J. Gronnow,† Peter S. Shuttleworth,‡Simon Breeden,† Duncan J. Macquarrie,†, *Journal of the American Chemical Society, JACS*, 2013, 135, 11728−11731.
601. R. W.-C. Chan and B. B. Krieger, *Journal of Applied Polymer Science*, 1981, **26**, 1533-1553.
602. G. G. Allan, B. B. Krieger and D. W. Work, *Journal of Applied Polymer Science*, 1980, **25**, 1839-1859.
603. A. P. Gregory and R. N. Clarke, *Ieee Transactions on Dielectrics and Electrical Insulation*, 2006, **13**, 727-743.

604. D. R. Baghurst and D. M. P. Mingos, *Journal of the Chemical Society, Chemical Communications*, 1992, 674-677.
605. G. B. Dudley, R. Richert and A. E. Stiegman, *Chemical Science*, 2015, **6**, 2144-2152.
606. Y. Y. Akhadov, *Dielectric Properties of Binary Solutions*, Pergamon Press, OXford, 1980.
607. A. K. Doolittle, *Journal of Applied Physics*, 1951, **22**, 1471-1475.
608. M. H. Cohen and D. Turnbull, *Journal of Chemical Physics*, 1959, **31**, 1164-1169.
609. N. E. Hill, *Dielectric properties and molecular behaviour*, Van Nostrand Reinhold, London, 1969.

11 Appendix-A

11.1 DTG/Temp peaks deconvolution of all pine assortments

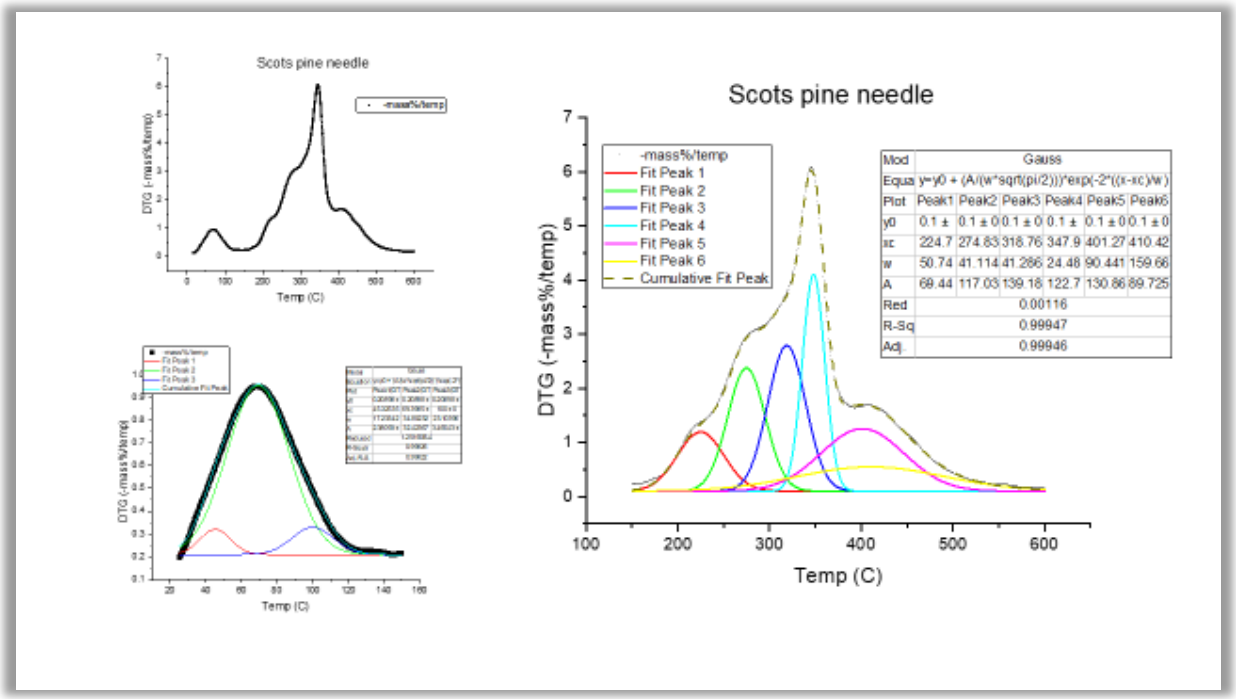

Figure 185 11.1 DTG/Temp peaks deconvolution of Scots pine needle pine

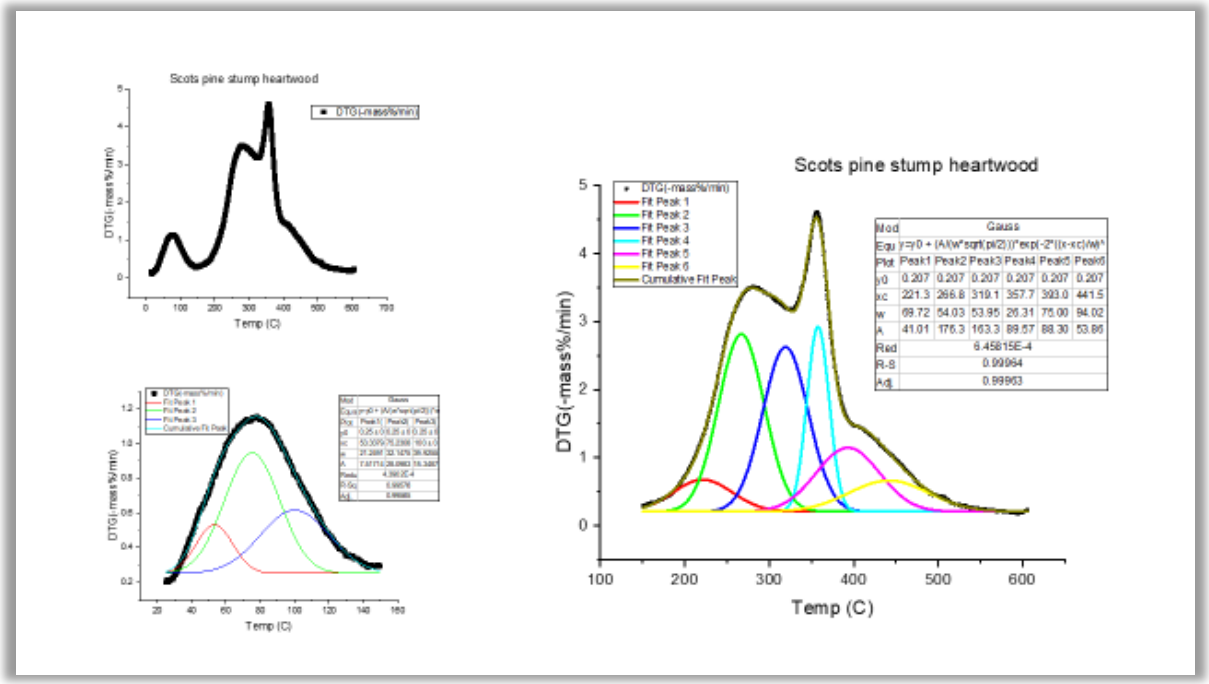

Figure 186 DTG/Temp peaks deconvolution of Scots pine stump heartwood

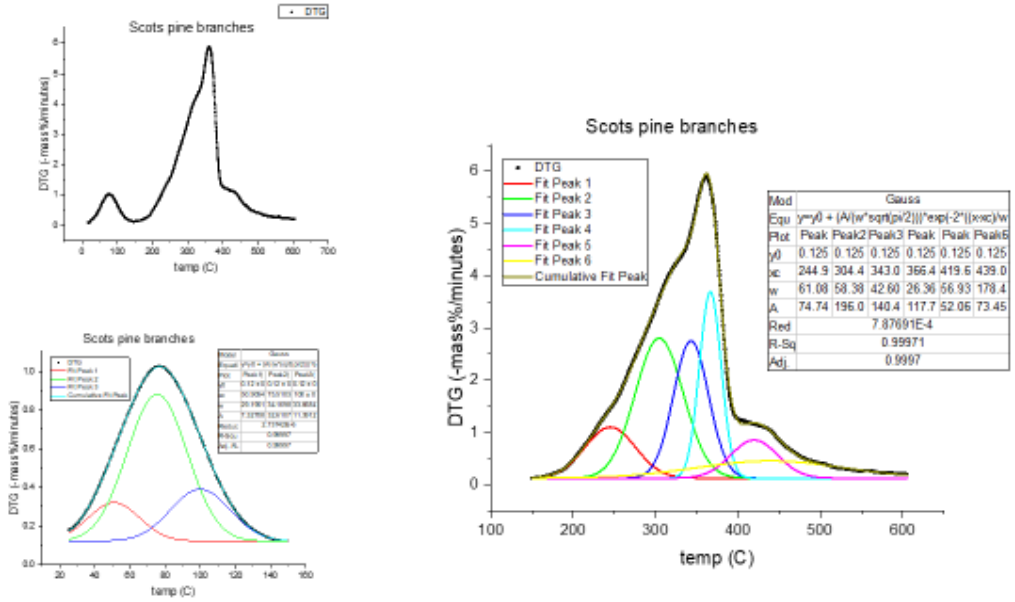

Figure 187 DTG/Temp peaks deconvolution of Scots pine branches

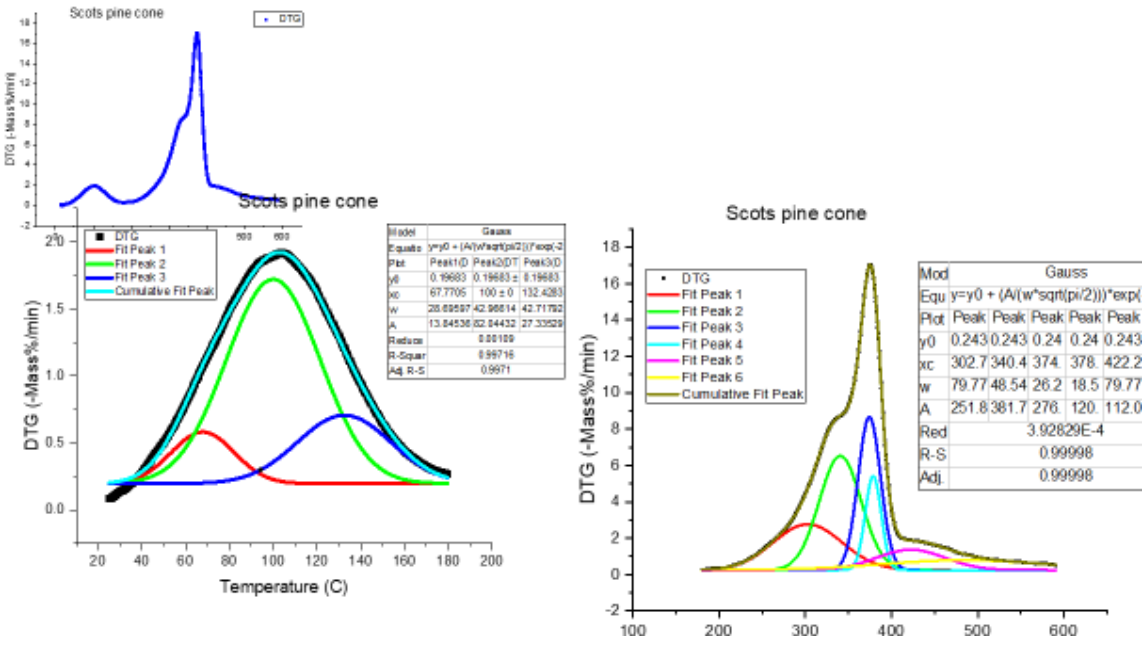

Figure 188 DTG/Temp peaks deconvolution of Scots pine cone

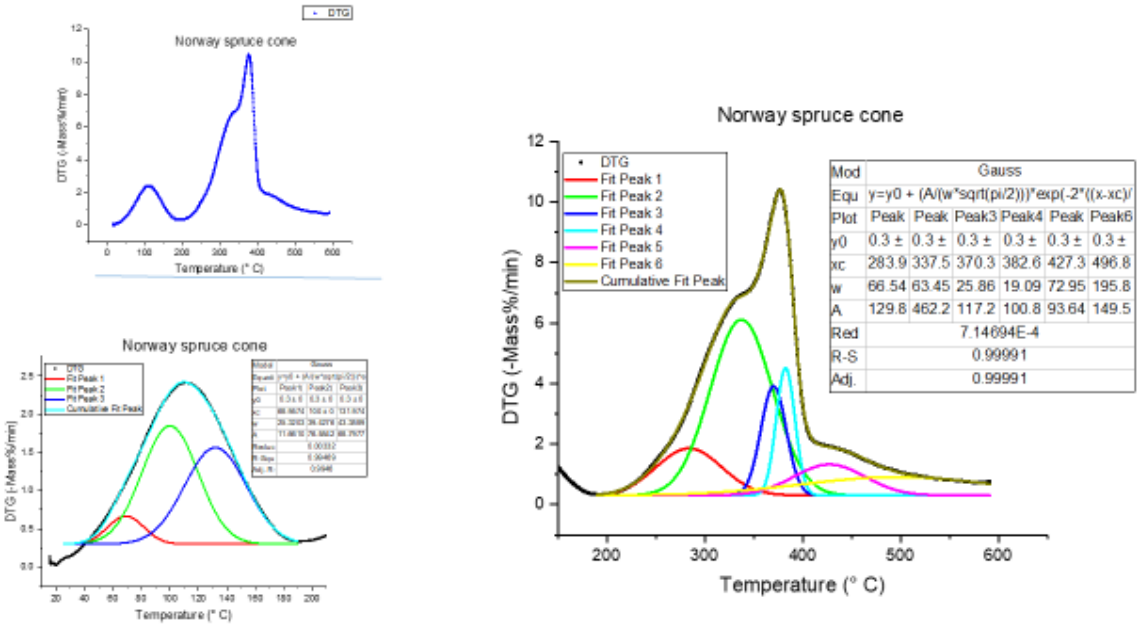

Figure 189 DTG/Temp peaks deconvolution of Norway spruce cone

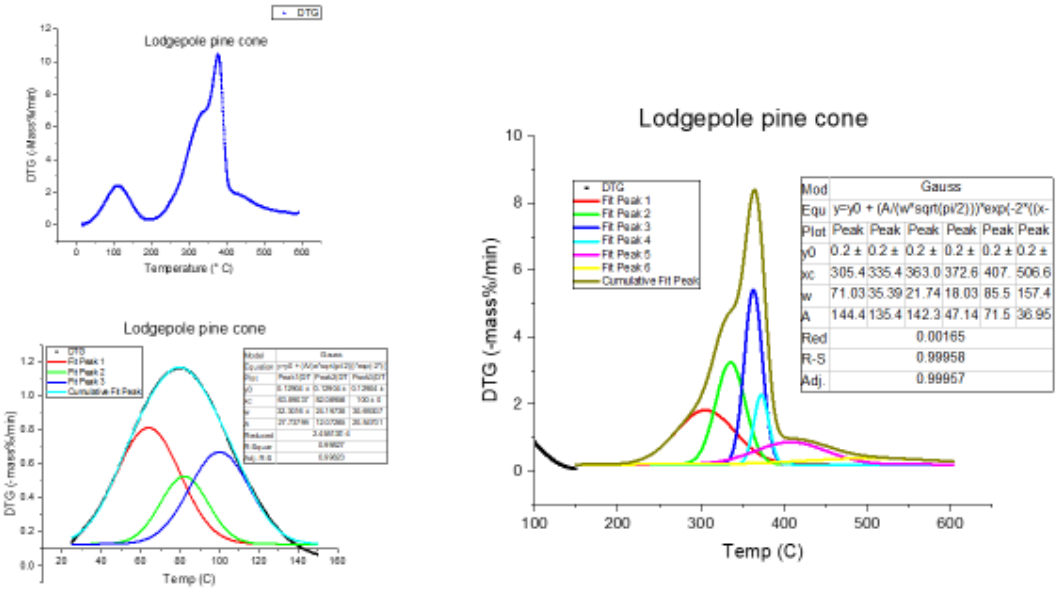

Figure 190 DTG/Temp peaks deconvolution of Lodgepole pine cone

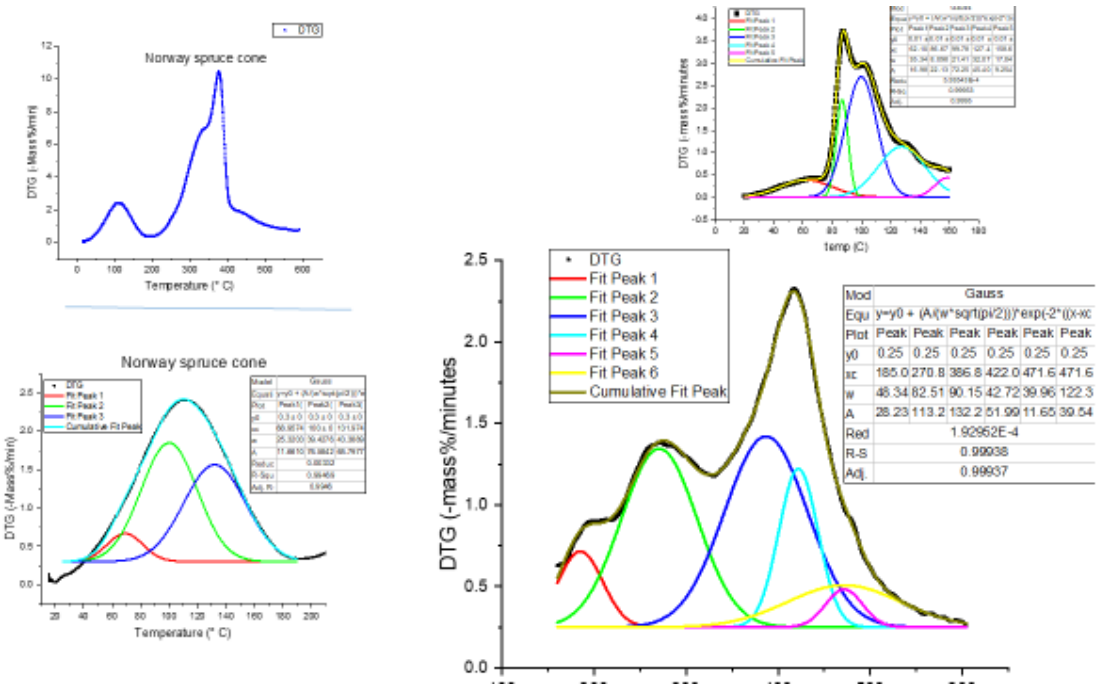

Figure 191 DTG/Temp peaks deconvolution of Norway spruce cone

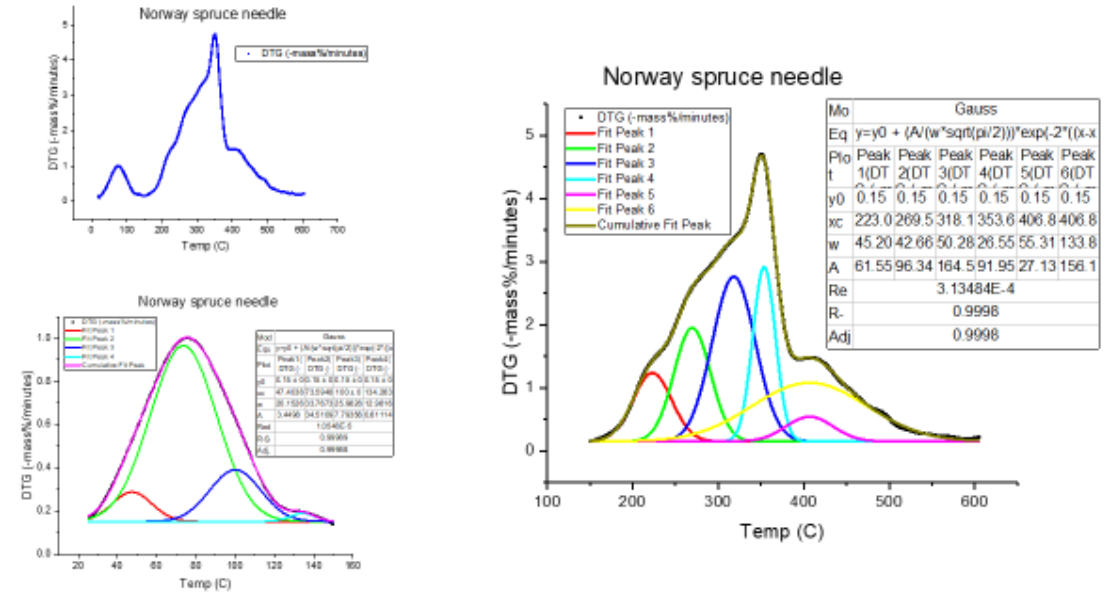

Figure 192 DTG/Temp peaks deconvolution of Norway spruce needle

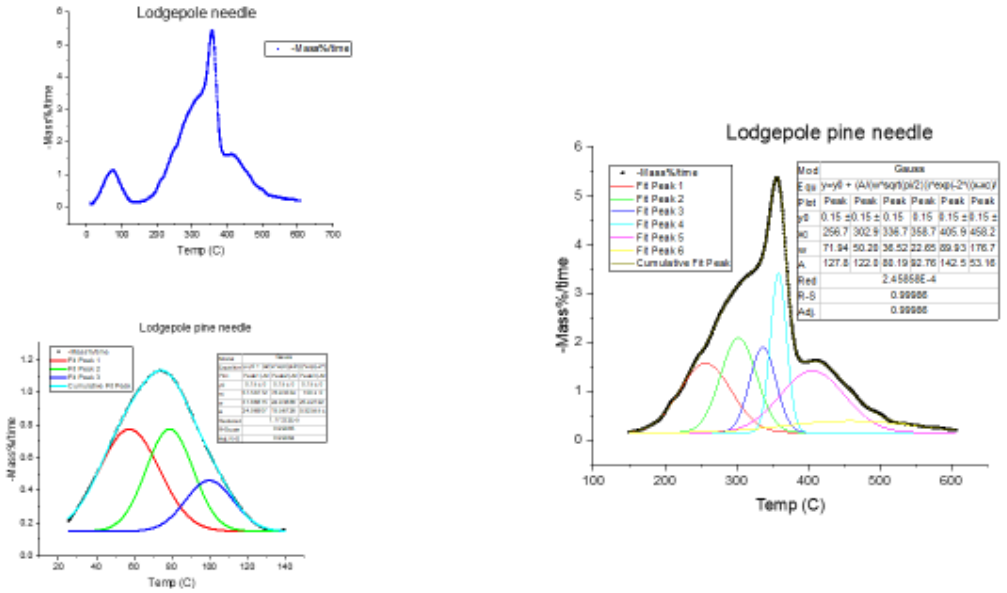

Figure 193 DTG/Temp peaks deconvolution of Lodgepole pine needle

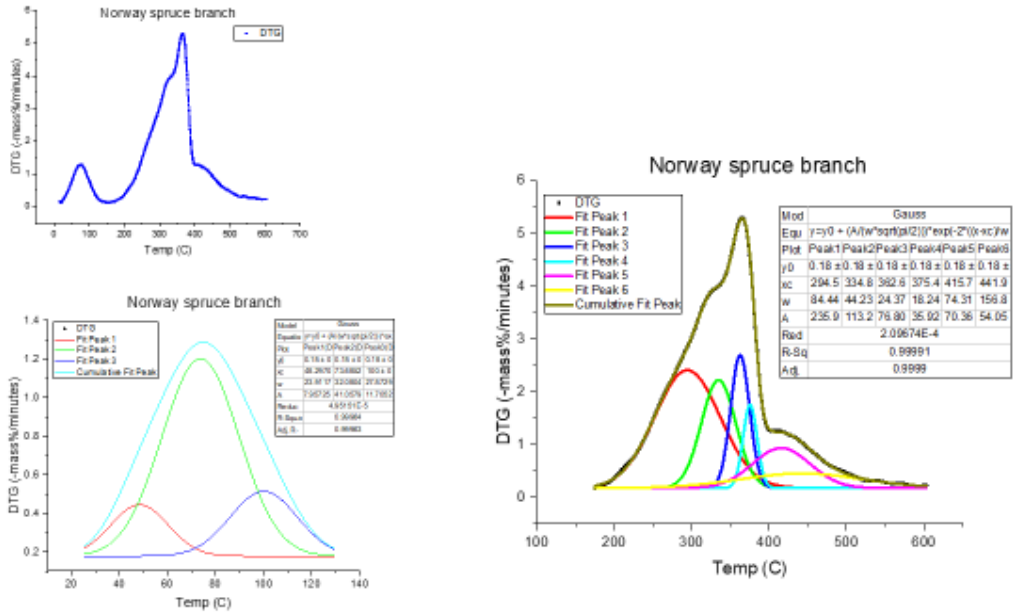

Figure 194 DTG/Temp peaks deconvolution of Norway spruce branches

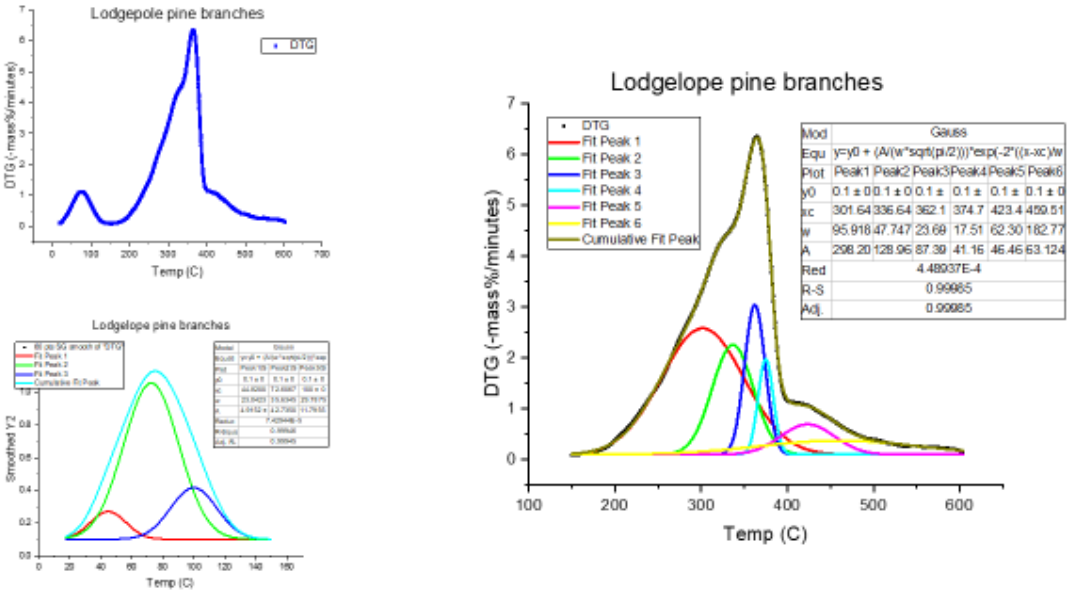

Figure 195 DTG/Temp peaks deconvolution of Lodgepole pine branches

11.2 Solvent Physical properties applied for chemometric analysis

11.2.1 Molecular W., Density, BP and VP and Enthalpy of Vaporisation of Some Organic Liquids

Cellulose Additive	Mol. Wt	Density	Boiling Point	Vapour Pres.	Enthalpy of Vap.
(-)-β-caryophyllene	204.36	0.9	268.4	0	48.6
Tetradecane	198.39	0.8	253.9	0	47.1
Docosane	310.61	0.8	368.3	0	59.1
Hentriacontane	436.84	0.8	458.4	0	69.1
1, 3 propane diol	76.094	1	214.4	0	52.4
Docosanol	326.60	0.8	375.9	0	72.1
Tetracosanol	354.65	0.8	394.5	0	74.5
p-hydroxy bezaldehyde	122.12	1.2	246.6	0	50.3
Vanillin	152.15	1.2	282.6	0	54.2
Coniferylaldehyde	178.19	1.2	338.8	0	60.5
Cholesterol	386.654	1	480.6	0	85.9
Stigmasterol	412.70	1	501.1	0	88.7
γ-Sitosterol	414.71	1	501.9	0	88.8
Linoleic Acid	280.45	0.9	360.6	0	66.6
Abietic Acid	302.46	1.1	439.5	0	76.4
Docosanoic acid	340.58	0.9	391.8	0	67.7
Tetracosanoic acid, methyl ester	382.66	0.9	419.5	0	67.3
Campesterol acetate	442.72	1	502.2	0	77.1

11.2.2 Value of Specific Density, VP and Enthalpy of Vapour Pressure of Some Organic Liquid

Name	Specific Density	Vapour Pressure	Enthalpy of vap.
Acetophenone	1.024	0.3	43.8
Benzonitrile	1.001	0.5	42.7
Benzaldehyde	1.04	1	41.5
Cyclohexanone	0.942	3	39.2
Alfa Pinene	0.9	3.5	37.8
Styrene	0.9	6.2	36.6
Butyl acetate	0.876	11.5	36.3
o-Xylene	0.876	6	36.2
p-Xylene	0.861	7.9	35.7
Ethylbenzene	0.865	9.2	35.6
Ethyl acetate	0.894	111.7	31.9
2-Butanone	0.799	114.5	31.3
Benzene	0.873	100.9	30.7
Cyclohexane	0.773	93.7	30

11.2.3 Molecular Weight, Specific Density, Dielectric Constant, Polarizability, Relative polarity and Dipole Moment of Some Organic Liquid

Solvent	MW	Sp. Density	Dielectric	Polarisability	polarity	dipole
carbon tetrachloride	153.823	1.700	2.300	10.300	0.052	0.000
chloroform	119.380	1.480	4.806	8.400	0.259	1.000
Dichloromethane	84.930	1.318	9.080	6.500	0.309	1.600
glycerin	92.094	1.300	42.500	8.100	0.812	2.700
carbon disulfide	76.141	1.300	2.600	8.500	0.065	0.000
1,2-dichloroethane	98.960	1.246	10.400	8.300	0.327	1.800
1,1-dichloroethane	98.959	1.200	10.000	8.300	0.269	1.800
Diethylene glycol	106.120	1.114	31.800	10.100	0.713	2.300
Ethylene glycol	62.070	1.111	37.000	5.700	0.790	2.300
DMSO	78.133	1.100	46.700	8.000	0.444	3.900

chlorobenzene	112.557	1.100	5.700	12.300	0.188	1.540
Acetic acid	60.050	1.043	6.150	5.100	0.648	1.680
Benzyl alcohol	108.140	1.041	13.100	13.000	0.608	1.700
2-Aminoethanol	61.080	1.014	37.700	6.500	0.651	2.600
benzonitrile	103.120	1.001	26.000	12.400	0.333	4.100
acetyl acetone	100.116	1.000	23.000	10.000	0.571	3.000
aniline	93.127	1.000	6.800	12.100	0.420	1.600
ethyl benzoate	150.174	1.000	6.000	16.900	0.228	2.000
anisole	108.138	1.000	4.300	13.100	0.198	1.400
dioxane	88.105	1.000	2.000	8.600	0.164	0.400
pyridine	79.100	0.979	13.000	9.700	0.302	2.200
Cyclohexanol	100.160	0.960	15.000	11.600	0.509	1.900
cyclohexanone	98.140	0.942	15.000	11.000	0.281	2.900
methyl acetate	74.080	0.927	6.680	7.000	0.253	1.700
dimethylformamide	73.094	0.900	37.000	7.900	0.386	3.800
diglyme	134.174	0.900	7.230	13.900	0.244	1.900
ethyl acetate	88.110	0.894	6.000	8.900	0.228	1.780
benzene	78.110	0.873	2.300	10.400	0.111	0.000
toluene	92.140	0.865	2.400	12.300	0.099	0.360
p-Xylene	106.170	0.861	2.270	14.200	0.074	0.000
1-butanol	74.120	0.806	17.500	8.800	0.586	1.700
2-Butanol	74.120	0.805	15.800	8.800	0.506	1.700
1-Propanol	60.100	0.802	20.100	6.900	0.617	1.680
i-butanol	74.122	0.800	17.900	8.800	0.552	1.800
1-heptanol	116.201	0.800	12.000	14.300	0.549	1.700
1-octanol	130.228	0.800	10.300	16.100	0.537	1.700
2-pentanol	88.148	0.800	13.700	10.600	0.488	1.700
3-pentanol	88.148	0.800	13.300	10.600	0.463	1.700
t-butyl alcohol	74.122	0.800	12.400	8.800	0.389	1.700
2-pentanone	86.132	0.800	15.400	10.000	0.321	2.700
Solvent	MW	Sp. Density	Dielectric	Polarisability	polarity	dipole
3-pentanone	86.132	0.800	17.000	10.000	0.265	2.800
methyl t-butyl ether	88.148	0.800	2.600	10.700	0.124	1.400
2-butanone	72.110	0.799	18.600	8.200	0.327	2.800

Methanol	32.040	0.787	32.630	3.300	0.762	1.600
ethanol	46.070	0.787	24.000	5.100	0.654	1.700
acetone	58.080	0.786	21.000	6.300	0.355	2.850
2-propanol	60.100	0.783	19.000	6.900	0.546	1.660
cyclohexane	84.160	0.773	2.000	11.000	0.006	0.000
ether	74.120	0.708	4.300	8.900	0.117	1.250
acetonitrile	41.052	0.700	37.500	4.500	0.460	3.500
diethylamine	73.137	0.700	3.800	9.600	0.145	1.200
hexane	86.175	0.700	1.900	11.800	0.009	0.000
heptane	100.200	0.682	1.900	13.700	0.012	0.000
pentane	72.149	0.600	1.840	10.000	0.009	0.000

11.2.4 Relative Polarity and Dielectric Constant of Some Organic Liquid

Solvent	Dielectric Constant	**r .polarity**
glycerin	42.5	0.812
Ethylene glycol	37.0	0.790
Methanol	32.6	0.762
Diethylene glycol	31.8	0.713
ethanol	24.0	0.654
2-Aminoethanol	37.7	0.651
Acetic acid (ethanoicacid)	6.150	0.648
1-Propanol	20.1	0.617
Benzyl alcohol	13.1	0.608
1-butanol	17.5	0.586
acetyl acetone	23.0	0.571
i-butanol	17.9	0.552
1-heptanol	12.0	0.549
2-propanol	19.0	0.546
1-octanol	10.3	0.537
Cyclohexanol	15.0	0.509

2-Butanol	15.8	0.506
2-pentanol	13.7	0.488
3-pentanol	13.3	0.463
acetonitrile	37.5	0.460
DMSO	46.7	0.444
aniline	6.800	0.420
t-butyl alcohol	12.4	0.389
dimethylformamide (DMF)	37.0	0.386
acetone	21.0	0.355
benzonitrile	26.0	0.333
2-butanone	18.6	0.327
1,2-dichloroethane	10.4	0.327
2-pentanone	15.4	0.321
Dichloromethane	9.080	0.309
pyridine	13.0	0.302
cyclohexanone	15.0	0.281
1,1-dichloroethane	10.0	0.269
3-pentanone	17.0	0.265
chloroform	**4.806**	0.259
methyl acetate	6.680	0.253
diglyme	7.230	0.244
ethyl benzoate	6.000	0.228
ethyl acetate	6.000	0.228

11.2.5 Dielectric Constant, Polarity and pka of Some Organic Liquid

Solvent	Dielectric	1/pka	relative polarity
Acetyl acetone	23	0.116414	0.571
Glycerin	42.5	0.073475	0.812
Diethylene glycol	31.8	0.067476	0.713
Ethylene glycol	37	0.067431	0.79
Methanol	32.63	0.063371	0.762
Propyl alcohol	21.8	0.062893	0.617
Cyclohexanol	15	-0.29078	0.509
3-pentanol	13.3	-0.29078	0.463
t-butyl alcohol	12.4	-0.31973	0.389
2-pentanol	13.7	-0.36306	0.488
2-Butanol	15.8	-0.38272	0.506
i-butanol	17.9	-0.4382	0.552
2-propanol	19	-0.46809	0.546
1-heptanol	12	-0.47368	0.549
1-butanol	17.5	-0.49495	0.586
1-Propanol	20.1	-0.49749	0.617
1-octanol	10.3	-0.49749	0.537

11.2.6 Density, Surface Tension and Viscosity of Some Organic Liquids

Additive	Density	Surface Tension	Viscosity
Formamide (methanomide)	1.129	57	3.34
2-Butanol (sec-butanol)	0.805	22.6	3.1
1-Butanol (n-butyl alcohol)	0.806	25	2.54
Propylene carbonate	1.2	40.9	2.5
Isophorone	0.92	35.5	2.33
Propyl alcohol	0.8	24.6	2.26
Tetradecane	0.8	26.5	2.18
2-Ethoxyethanol	0.925	28.8	2.1
2-Propanol (isopropyl alcohol)	0.783	23.3	2.04
Morpholine	0.997	38.8	2.02
Cyclohexanone	0.942	34.4	2.02
Dimethyl sulfoxide (DMSO)	1.095	42.9	1.99
1-Propanol	0.802	20.9	1.95
2-Methoxyethanol	0.96	42.8	1.7
Acetophenone (1-phenylethanone)	1.024	39	1.68
N-Methyl-2-pyrrolidine	1.025	44.6	1.67
Methanoic acid (formic acid)	1.214	37.7	1.61
Benzaldehyde	1.04	38.3	1.4
1,2-Dichlorobenzene	1.301	35.7	1.32
Alfa Pinene	0.9	25.3	1.30
Benzonitrile	1.001	38.8	1.27
1,4-Dioxane	1.029	32.9	1.18
1,2-Dimethoxyethane (DME)	0.865	20	1.1
Epichlorohydrin	1.174	36.3	1.07
Ethanol (ethyl alcohol)	0.787	22	1.07
Acetic acid (ethanoic acid)	1.043	27	1.06
Decane	0.7	24.3	0.92
Tetrachloromethane	1.583	26.3	0.91
Cyclohexane	0.773	24.7	0.89
Pyridine	0.979	36.7	0.88
1,1,1-Trichloroethane	1.33	25	0.79

N,N-Dimethylformamide (DMF)	0.945	34.4	0.79
1,2-Dichloroethane	1.246	32.6	0.78
o-Xylene	0.876	29.6	0.76
2-Heptanone (methyl n-amyl ketone)	0.811	26.1	0.71
Styrene (phenylethene)	0.9	32	0.7
Butyl acetate	0.876	24.8	0.69
2-Methyl propyl ethanoate	0.869	23	0.68
Nitromethane	1.129	36.3	0.63
Ethylbenzene	0.865	28.6	0.63
Benzene	0.873	28.2	0.6
p-Xylene	0.861	27.9	0.6
Methyl methacrylate	0.937	24.2	0.57
Toluene	0.865	27.9	0.56
Trichloroethylene (TCE)	1.458	28.7	0.55
4-Methyl-2-pentanone	0.796	23.5	0.55
Trichloromethane (chloroform)	1.48	26.7	0.54
Propyl acetate (propyl ethanoate)	0.883	23.9	0.54
Methanol (methyl alcohol)	0.787	22.1	0.54
Isopropyl acetate	0.871	22.3	0.52
Tetrahydrofuran	0.88	26.7	0.46
Ethyl acetate (ethyl ethanoate)	0.894	23.2	0.42
Dichloromethane (DCM)	1.318	27.8	0.41
2-Butanone (methyl ethyl ketone)	0.799	24	0.41
n-Heptane	0.682	19.8	0.39
Acetonitrile (ethane nitrile)	0.779	28.7	0.37
Methyl acetate	0.927	24.5	0.36
Acrylonitrile (ethenylnitrile)	0.801	26.7	0.34
Dimethoxymethane (methylal)	0.854	18.8	0.33
Acetone (propanone)	0.786	23	0.31
Diethyl ether (ethoxyethane)	0.708	16.7	0.22

11.2.7 Thermal conductivity, Sp. heat, Density and Dielectric constant of Some Organic Liquid

Compound	Thermal Cond.	Sp. Heat	Density	Dielectric
Ethylene Glycol	0.258	2.36	1.111	37.7
Methanol	0.204	2.51	0.787	32.63
Propylene glycol	0.147	2.5	1	32.00
Ethanol	0.171	2.3	0.787	24.30
Alcohol, propyl	0.161	2.37	0.802	21.8
Acetone	0.18	2.15	0.786	20.70
Aniline	0.172	2.18	1.018	6.89
Acetic acid	0.193	2.043	1.043	**6.15**
Ethyl acetate	0.137	2.22	0.894	6.02
Ether	0.13	2.21	0.7	4.34
Benzene	0.167	1.8	0.873	2.27
Heptane	0.14	2.24	0.682	2.05
Decane	0.147	2.21	0.7	2

11.2.8 Molecular weight, Density, Enthalpy of Vap. and Sp. Heat of Some Organic Liquid

Compound	MW	Specific Density	Enthalphy of vapour pressure	Specific heat
methanol	32.04	0.80	35.20	2.51
1, 3 propane diol	76.09	1.00	52.40	2.50
Propyl acetate	102.13	0.88	34.10	2.37
Ethylene Glycol	62.07	1.10	50.50	2.36
Ethanol	46.07	0.79	38.60	2.30
Hexane	86.18	0.70	28.90	2.26
n-Heptane	100.20	0.68	31.80	2.24
Ethyl acetate	88.11	0.89	31.90	2.22
Diethyl ether	74.12	0.71	26.50	2.21
Decane	142.28	0.70	38.80	2.21
Aniline	93.13	1.00	42.40	2.18
Acetone	58.08	0.79	29.10	2.15
n-Octane	114.23	0.70	34.40	2.15
Acetic acid	60.05	1.10	23.70	2.04
Benzene	78.11	0.87	30.70	1.80
Toluene	92.14	0.87	33.50	1.72
1,1,1-Trichloroethane	133.40	1.33	29.90	1.30
Carbon Disulfide	76.14	1.30	26.70	0.99

11.2.9 Molecular weight, Density, Enthalpy of Vaporisation, Specific Heat and Dielectric constant of Some Organic Liquid

Compound	MW	Specific Density	Enthalphy of vap	Specific heat	Dielectric
Glycerine	92.09	1.30	61.40	2.43	42.50
1, 3 propane diol	76.09	1.00	52.40	2.50	40.40
Ethylene Glycol	62.07	1.10	50.50	2.36	37.00
methanol	32.04	0.80	35.20	2.51	32.63
Ethanol	46.07	0.79	38.60	2.30	24.30
Acetone	58.08	0.79	29.10	2.15	20.70
Propyl acetate	102.13	0.88	34.10	2.37	6.30
Ethyl acetate	88.11	0.89	31.90	2.22	6.02
Trichloromethane	119.38	1.48	29.20	1.05	4.81
Diethyl ether	74.12	0.71	26.50	2.21	4.34
1,1,1-Trichloroethane	133.40	1.33	29.90	1.30	3.40
Carbon Disulfide	76.14	1.30	26.70	0.99	2.60
Toluene	92.14	0.87	33.50	1.72	2.38
Carbon Tetrachloride	153.82	1.70	29.80	0.87	2.30
Benzene	78.11	0.87	30.70	1.80	2.27
n-Heptane	100.20	0.68	31.80	2.24	2.05
Hexane	86.18	0.70	28.90	2.26	1.90
Aniline	93.13	1.00	42.40	2.18	1.90

11.2.10 Molecular Weight, Density, Surface Tension, Viscosity and Dielectric Constant of Some Organic Liquid

Name	MW	Density	Surface Tension	Viscosity	Dielectric
Trichloromethane	**119.38**	**1.48**	**26.7**	**0.54**	**4.81**
Trichloroethylene	**131.39**	**1.458**	**28.7**	**0.55**	**3.40**
1,1,1-Trichloroethane	133.4	1.33	25	0.79	3.40
Dichloromethane	**84.93**	**1.318**	**27.8**	**0.41**	**9.08**
1,2-Dichlorobenzene	147	1.301	35.7	1.32	9.93
1,2-Dichloroethane	98.96	1.246	32.6	0.78	10.36
Benzaldehyde	106.12	1.04	38.3	1.4	17.00
Acetophenone	120.15	1.024	39	1.68	17.39
Benzonitrile	103.12	1.001	38.8	1.27	26.00
Pyridine	79.1	0.979	36.7	0.88	12.30
Cyclohexanone	98.14	0.942	34.4	2.02	18.30
Methyl acetate	74.08	0.927	24.5	0.36	6.68
Styrene	104.15	0.9	32	0.7	2.43
Ethyl acetate	88.11	0.894	23.2	0.42	6.02
Propyl acetate	102.13	0.883	23.9	0.54	6.30
o-Xylene	106.17	0.876	29.6	0.76	2.57
Butyl acetate	116.16	0.876	24.8	0.69	5.01
Benzene	78.11	0.873	28.2	0.6	2.27
2-Methyl propyl	116.16	0.869	23	0.68	5.60
Ethylbenzene	106.17	0.865	28.6	0.63	2.41
Toluene	92.14	0.865	27.9	0.56	2.38
p-Xylene	106.17	0.861	27.9	0.6	2.27
1-Butanol	74.12	0.806	25	2.54	17.10
1-Propanol	60.1	0.802	20.9	1.95	20.10

2-Butanone	72.11	0.799	24	0.41	18.50
Ethanol	46.07	0.787	22	1.07	24.30
Acetone	58.08	0.786	23	0.31	20.70
2-Propanol	60.1	0.783	23.3	2.04	18.30
Cyclohexane	84.16	0.773	24.7	0.89	2.02
Diethyl ether	74.12	0.708	16.7	0.22	4.34
n-Heptane	100.2	0.682	19.8	0.39	2.05

Name	MW	Specific Density	Surface Tension	Viscosity	Dielectric
Cyclohexanol	**100.16**	**0.96**	**33.4**	**57.5**	15.00
1,2-Propanediol	76.1	1.033	45.6	40.4	32.00
Ethylene glycol	62.07	1.1	43.4	19.90	37.7
Ethylene glycol	62.07	1.111	48.4	16.1	37.00
3-Methylphenol	108.14	1.03	35.8	12.9	11.80
Benzyl alcohol	108.14	1.041	36.8	5.47	13.10
2-Methylpropyl alcohol	74.12	0.797	22.6	3.95	17.70
Aniline	93.13	1.018	42.4	3.85	6.89
Formamide	**45.04**	**1.129**	**57**	**3.34**	**84.00**
2-Butanol	74.12	0.805	22.6	3.1	15.80
1-Butanol	74.12	0.806	25	2.54	17.10
Propyl alcohol	60.10	0.8	24.6	2.26	21.8
2-Propanol	60.1	0.783	23.3	2.04	18.30
Morpholine	87.12	0.997	38.8	2.02	7.33
Cyclohexanone	98.14	0.942	34.4	2.02	18.30
1-Propanol	60.1	0.802	20.9	1.95	20.10
Acetophenone	120.15	1.024	39	1.68	17.39
Methanoic acid	46.03	1.214	37.7	1.61	58.00

Benzaldehyde	106.12	1.04	38.3	1.4	17.00
1,2-Dichlorobenzene	147	1.301	35.7	1.32	9.93
Benzonitrile	103.12	1.001	38.8	1.27	26.00
1,4-Dioxane	88.11	1.029	32.9	1.18	2.21
Ethanol	46.07	0.787	22	1.07	24.30
Acetic acid	60.05	1.043	27	1.06	6.15
Decane	142.30	0.7	24.3	0.92	2
Tetrachloromethane	153.82	1.583	26.3	0.91	2.20
Cyclohexane	84.16	0.773	24.7	0.89	2.02
Pyridine	79.1	0.979	36.7	0.88	12.30
1,1,1-Trichloroethane	133.4	1.33	25	0.79	3.40
1,2-Dichloroethane	98.96	1.246	32.6	0.78	10.36
o-Xylene	106.17	0.876	29.6	0.76	2.57
Styrene	104.15	0.9	32	0.7	2.43
Butyl acetate	116.16	0.876	24.8	0.69	5.01
2-Methyl propyl	116.16	0.869	23	0.68	5.60
Nitromethane	61.04	1.129	36.3	0.63	39.40
Ethylbenzene	106.17	0.865	28.6	0.63	2.41
Benzene	78.11	0.873	28.2	0.6	2.27
p-Xylene	106.17	0.861	27.9	0.6	2.27
Toluene	92.14	0.865	27.9	0.56	2.38
Trichloroethylene	131.39	1.458	28.7	0.55	3.40
Trichloromethane	119.38	1.48	26.7	0.54	4.81
Propyl acetate	102.13	0.883	23.9	0.54	6.30
Methanol	32.04	0.787	22.1	0.54	32.63
Ethyl acetate	88.11	0.894	23.2	0.42	6.02
Dichloromethane	84.93	1.318	27.8	0.41	9.08
2-Butanone	72.11	0.799	24	0.41	18.50

n-Heptane	100.2	0.682	19.8	0.39	2.05
Acetonitrile	41.05	0.779	28.7	0.37	37.50
Methyl acetate	74.08	0.927	24.5	0.36	6.68
Acetone	58.08	0.786	23	0.31	20.70
Diethyl ether	74.12	0.708	16.7	0.22	4.34

11.2.11 Molecular Weight, Specific Density, Dielectric Constant of Some Organic Liquid

Name	**MW**	**Specific Density**	**Dielectric**
Cyclohexanol	100.16	0.96	15
1,2-Propanediol	76.1	1.033	32
Ethylene glycol	62.068	1.1	37.7
Ethylene glycol	62.07	1.111	37
3-Methylphenol	108.14	1.03	11.8
Benzyl alcohol	108.14	1.041	13.1
2-Methylpropyl alcohol	74.12	0.797	17.7
Aniline	93.13	1.018	6.89
Formamide	45.04	1.129	84
2-Butanol	74.12	0.805	15.8
1-Butanol	74.12	0.806	17.1
Propyl alcohol	60.095	0.8	21.8
2-Propanol	60.1	0.783	18.3
Morpholine	87.12	0.997	7.33
Cyclohexanone	98.14	0.942	18.3
1-Propanol	60.1	0.802	20.1
Acetophenone	120.15	1.024	17.39
Methanoic acid	46.03	1.214	58
Benzaldehyde	106.12	1.04	17

1,2-Dichlorobenzene	147	1.301	9.93
Benzonitrile	103.12	1.001	26
1,4-Dioxane	88.11	1.029	2.209
Ethanol	46.07	0.787	24.3
Acetic acid	60.05	1.043	6.15
Decane	142.3	0.7	2
Tetrachloromethane	153.82	1.583	2.2
Cyclohexane	84.16	0.773	2.015
Pyridine	79.1	0.979	12.3
1,1,1-Trichloroethane	133.4	1.33	3.4
1,2-Dichloroethane	98.96	1.246	10.36
o-Xylene	106.17	0.876	2.568
Styrene	104.15	0.9	2.43
Butyl acetate	116.16	0.876	5.01
2-Methyl propyl	116.16	0.869	5.6
Nitromethane	61.04	1.129	39.4
Ethylbenzene	106.17	0.865	2.412
Benzene	78.11	0.873	2.274
p-Xylene	106.17	0.861	2.27
Toluene	92.14	0.865	2.379
Trichloroethylene	131.39	1.458	3.4
Trichloromethane	119.38	1.48	4.806
Propyl acetate	102.13	0.883	6.3
Methanol	32.04	0.787	32.63
Ethyl acetate	88.11	0.894	6.02
Dichloromethane	84.93	1.318	9.08
2-Butanone	72.11	0.799	18.5
n-Heptane	100.2	0.682	2.05

Acetonitrile	41.05	0.779	37.5
Methyl acetate	74.08	0.927	6.68
Acetone	58.08	0.786	20.7
Diethyl ether	74.12	0.708	4.335
**Isoprene	68.117	0.7	2.1
*Alfa Pinene	136.24	0.9	2.7
*Tetradecane	198.39	0.8	2
*Docosane	310.61	0.8	2
*Hentriacontane	436.84	0.8	2
*1, 3 propane diol	76.094	1	32
*Glycerol	92.09	1.3	42.5
*Linoleic Acid	280.45	0.9	2.9
*Abietic Acid	302.46	1.1	2.5

11.3 Asym2sig and Pearson V11 Curve Fitting of Dielectric Constant and Loss Factor of Some Organic Liquids

11.3.1 I-4 Butanediol

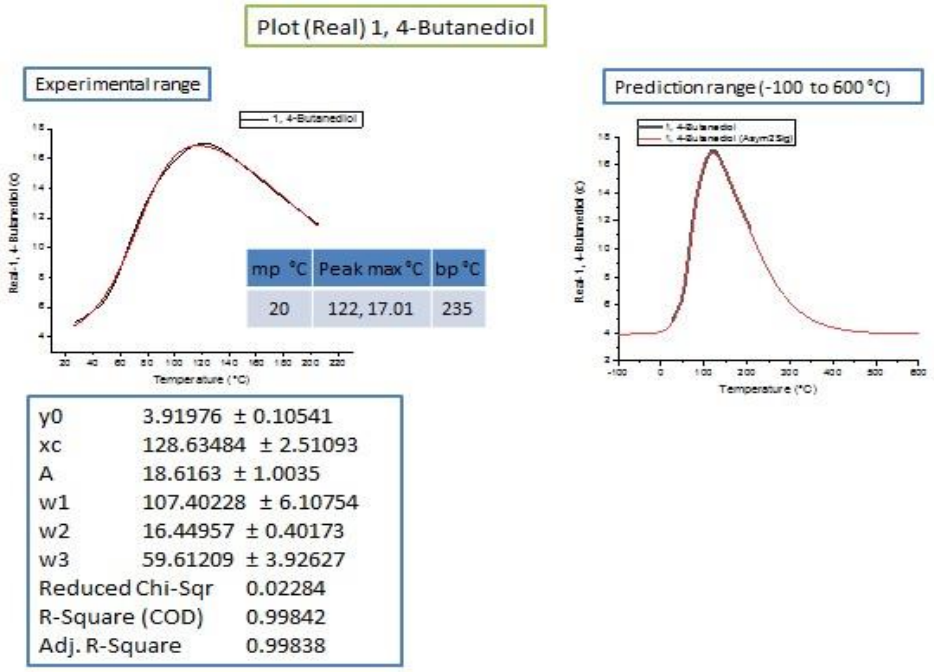

Figure 196 Dielectric real value curve fitting of 1,4-butanediol

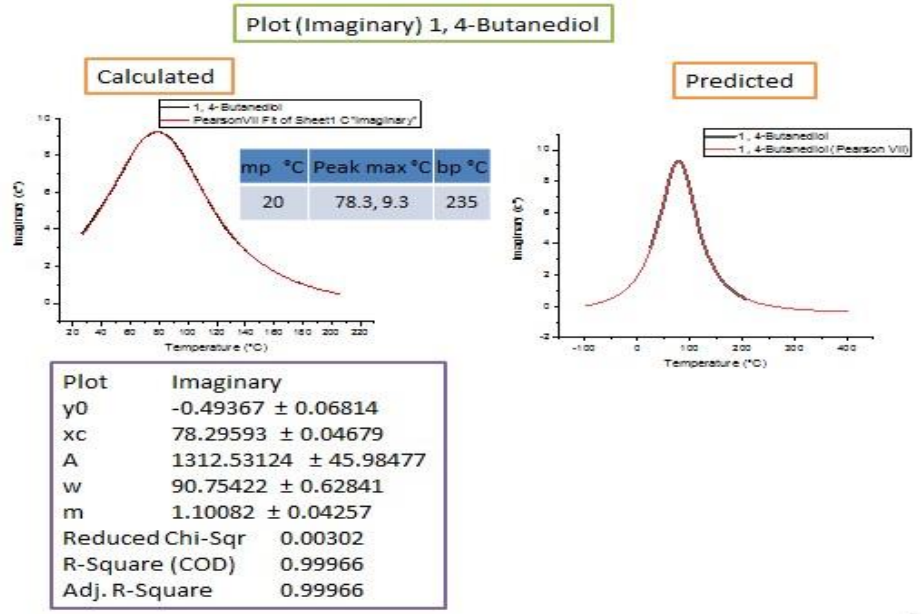

Figure 197 Dielectric imaginary value curve fitting of 1,4-butanediol

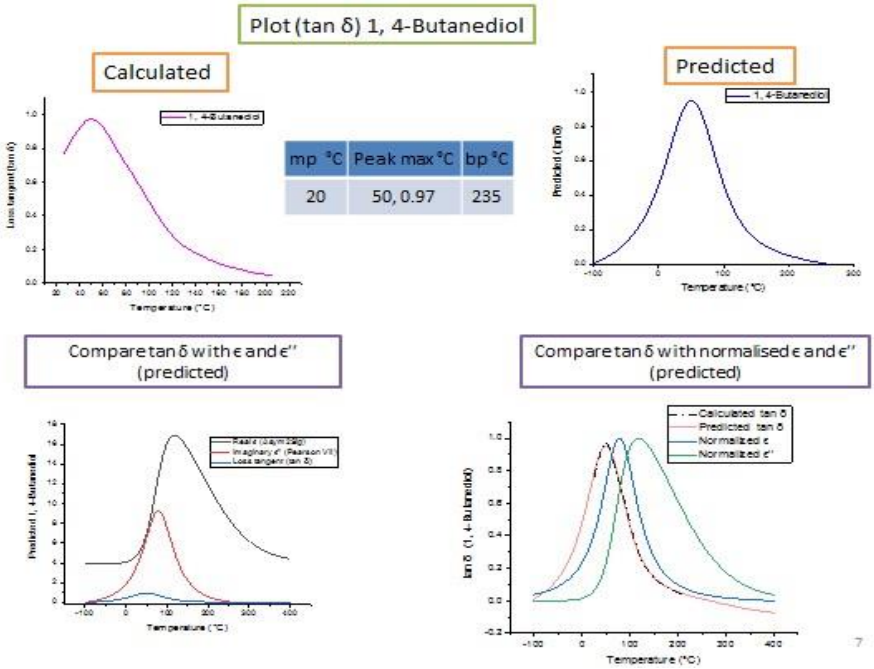

Figure 198 Dielectric loss tangent value curve fitting of 1,4-butanediol

11.3.2 2, 3 butanediol

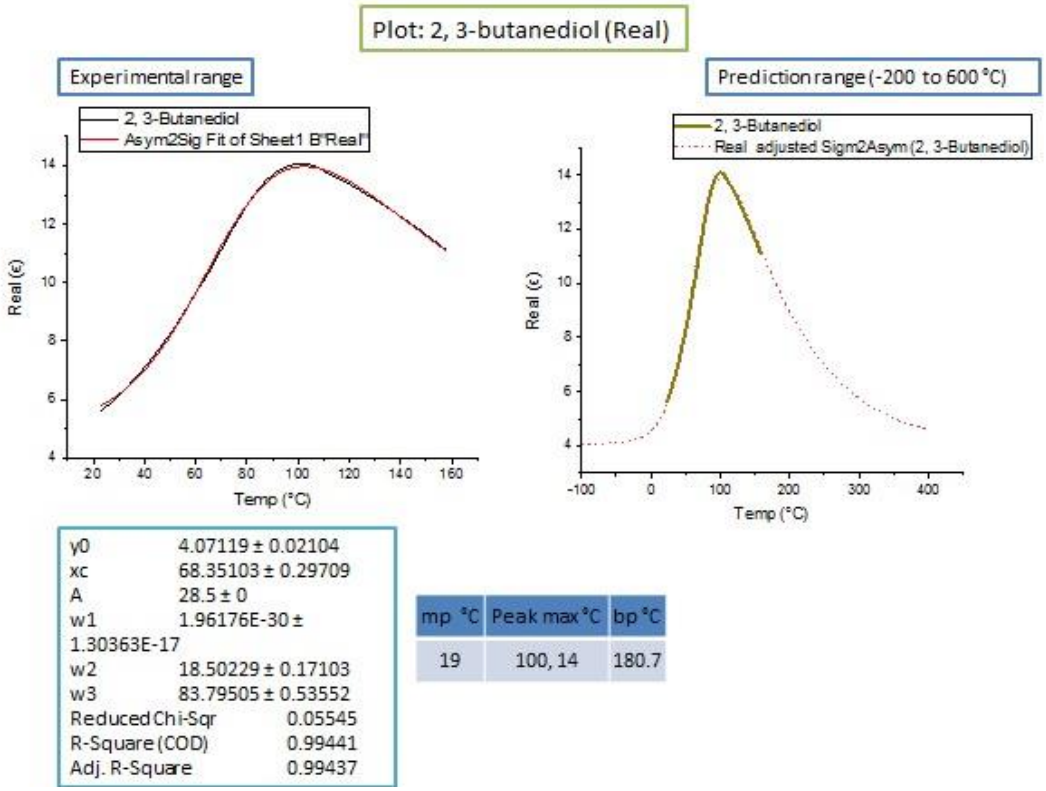

Figure 199 Dielectric real value curve fitting of 2, 3-butanediol

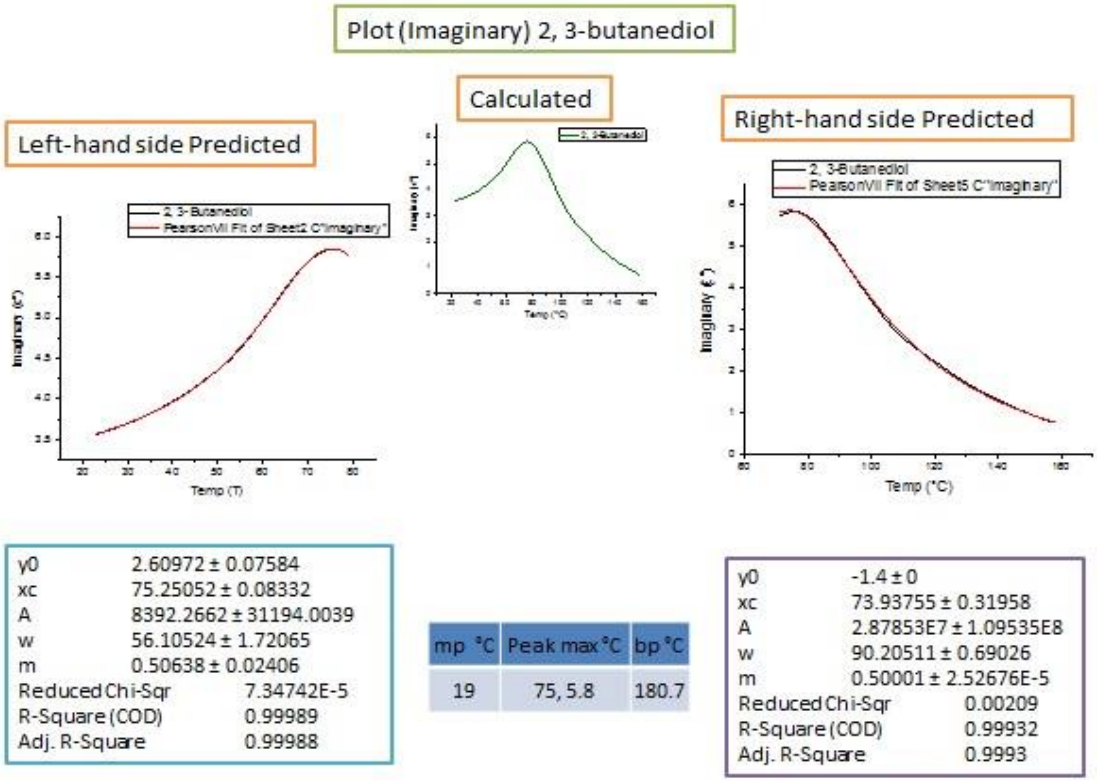

Figure 200 Dielectric imaginary value curve fitting of 2, 3-butanediol

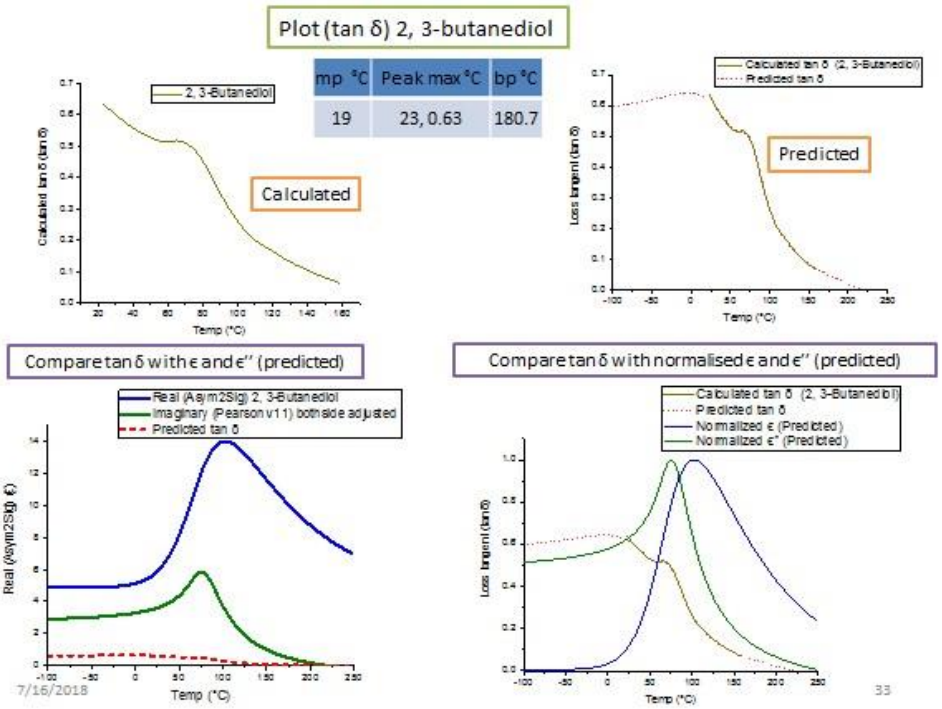

Figure 201 Dielectric loss tangent value curve fitting of 2,3-butanediol

11.3.2.1 Levoglucosenone

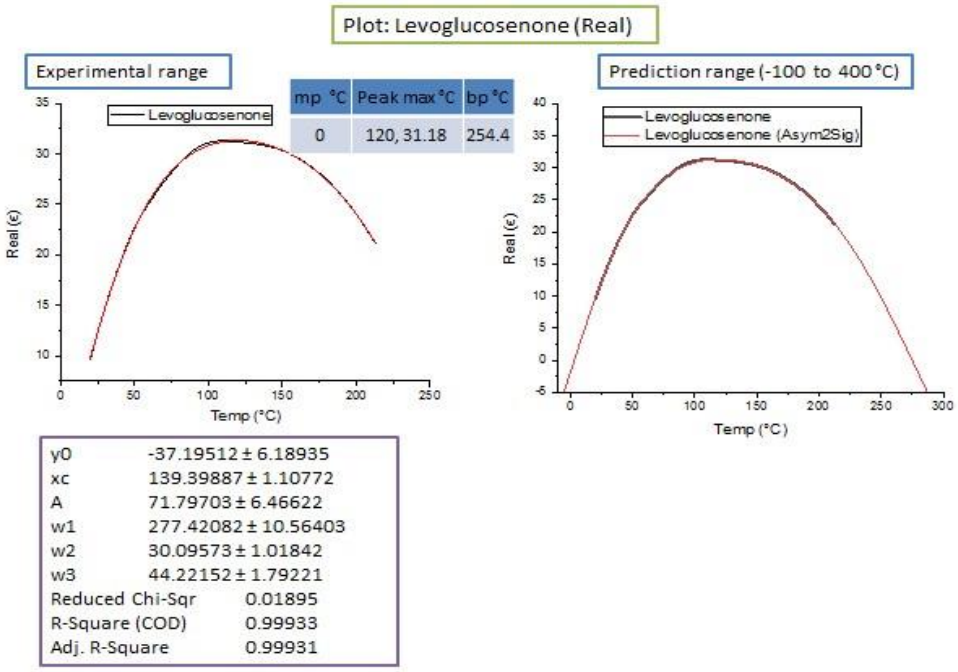

Figure 202 Dielectric real value curve fitting of Levoglucosenone

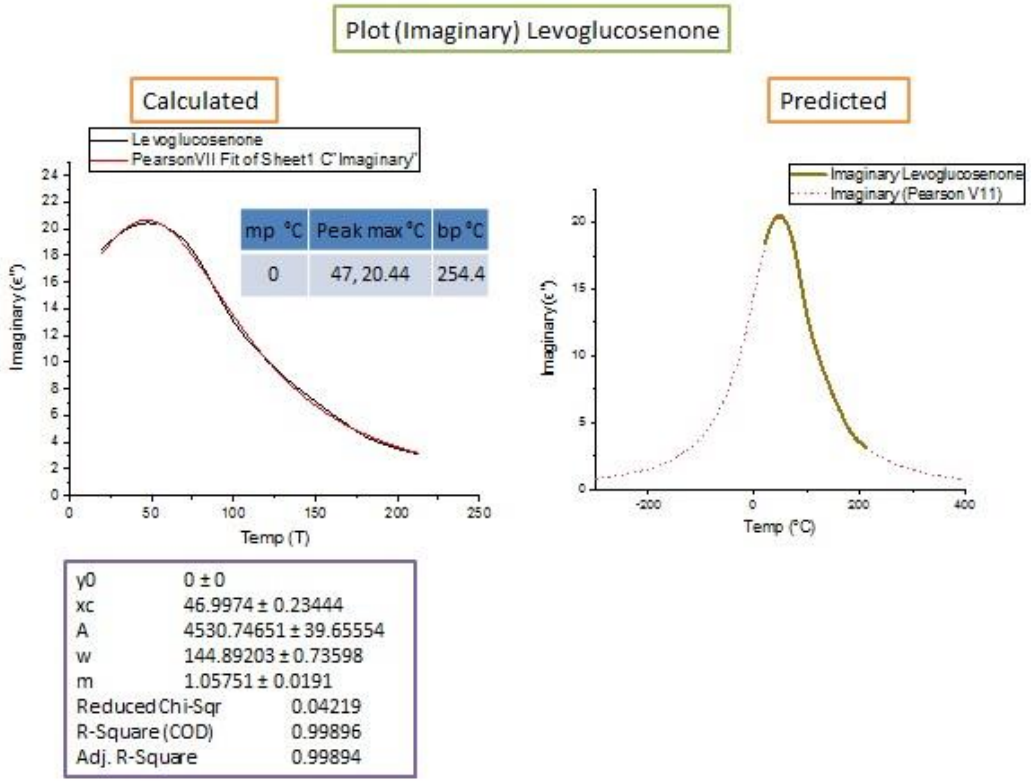

Figure 203 Dielectric imaginary value curve fitting of levoglucosenone

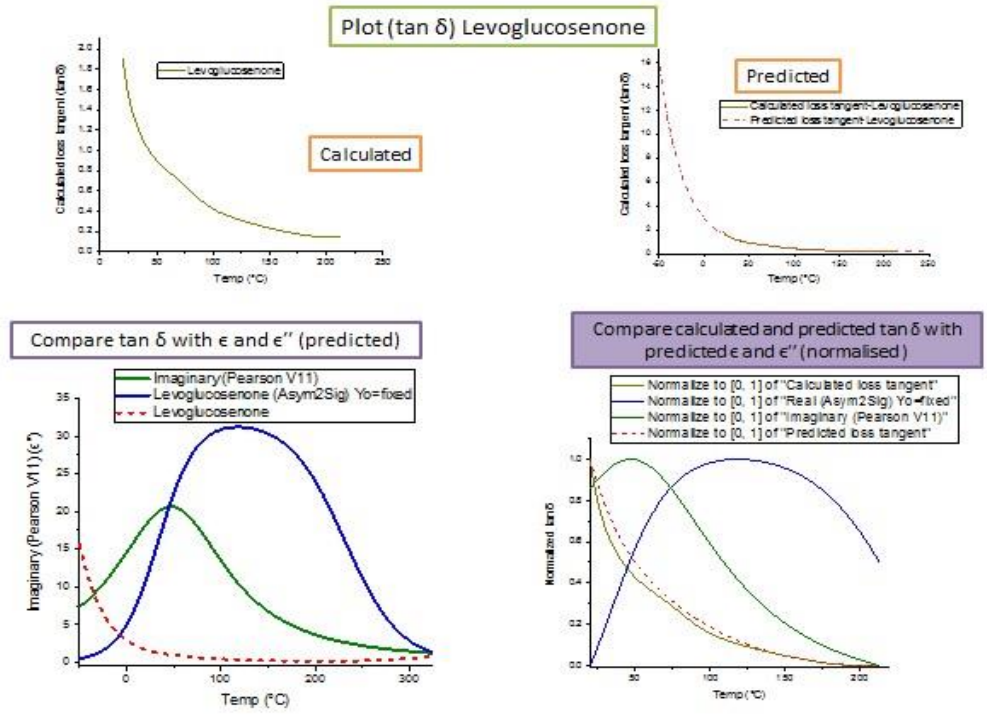

Figure 204 Dielectric loss tangent value curve fitting of Levoglucosenone

11.3.2.2 Triethylene glycol

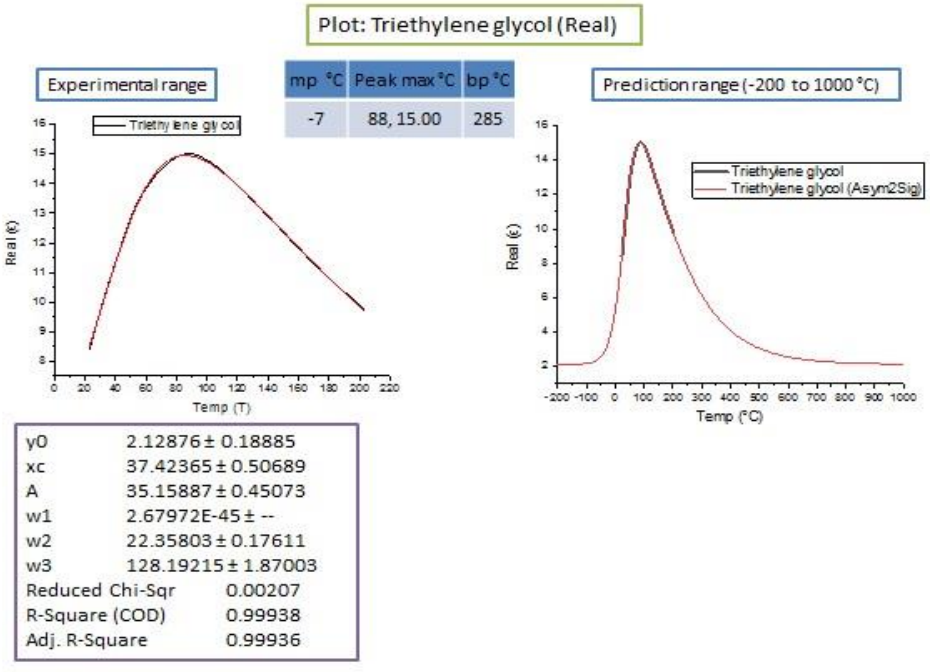

Figure 205 Dielectric real value curve fitting of Triethylene glycol

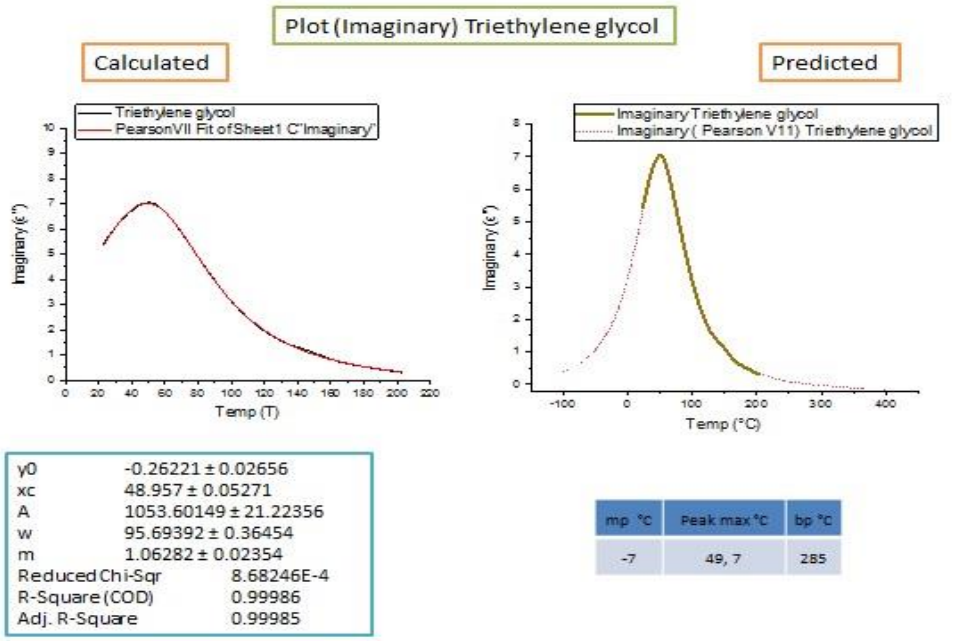

Figure 206 Dielectric imaginary value curve fitting of Triethylene glycol

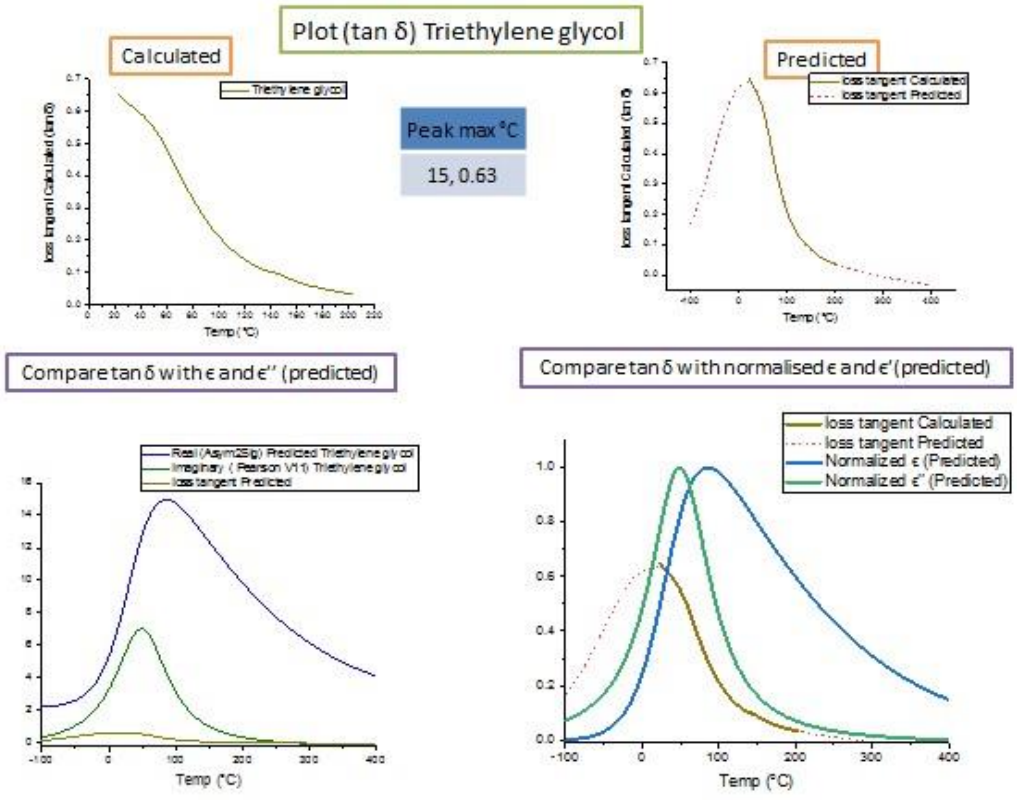

Figure 207 Dielectric loss tangent value curve fitting of Triethylene glycol

11.3.2.3 Glycerol

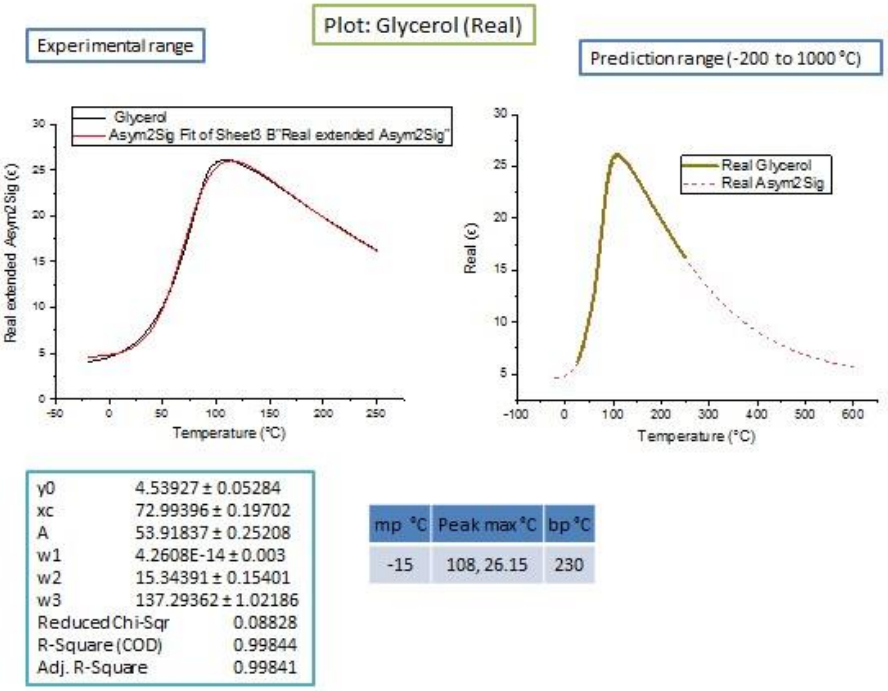

Figure 208 Dielectric real value curve fitting of Glycerol

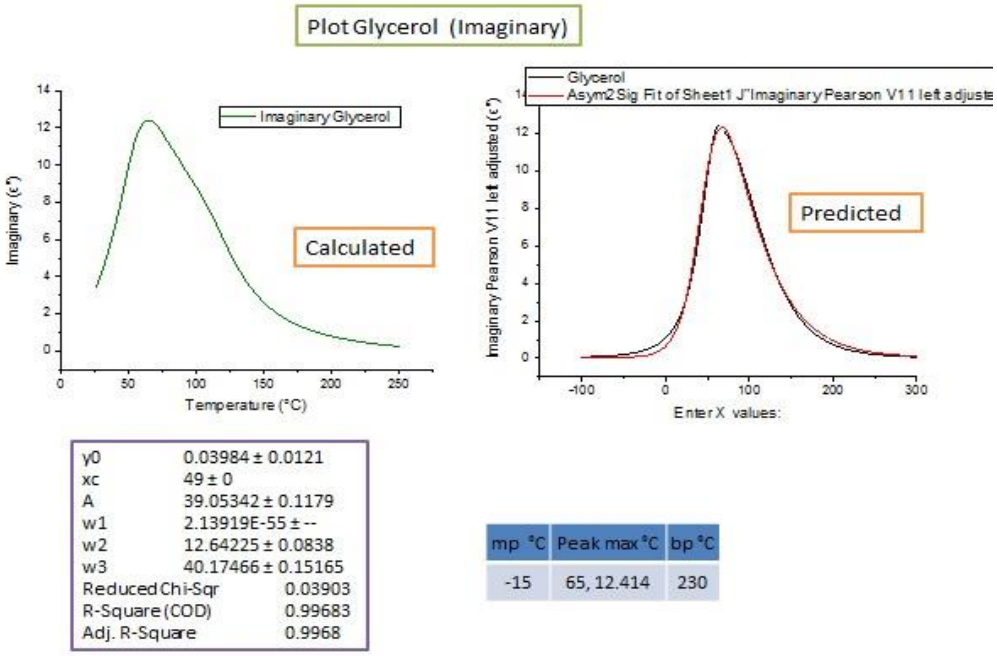

Figure 209 Dielectric imaginary value curve fitting of Glycerol

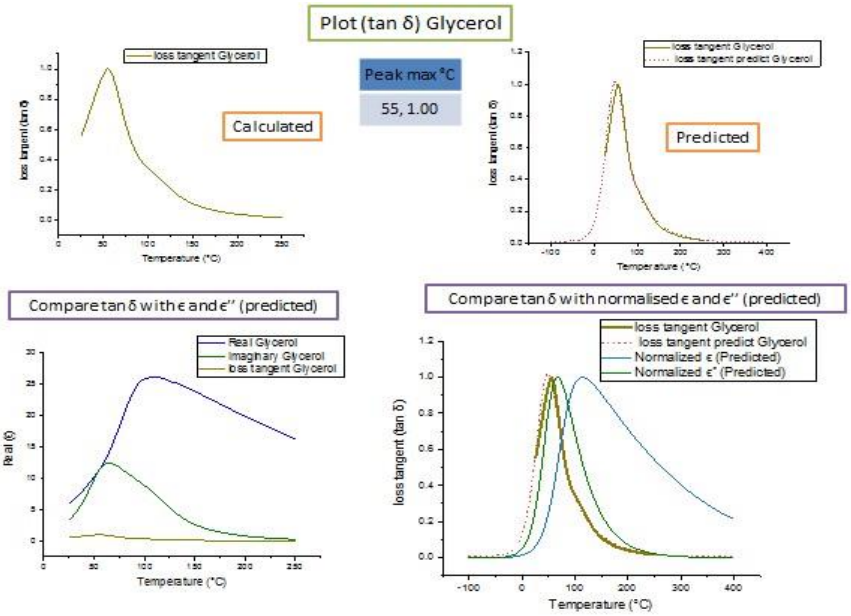

Figure 210 Dielectric loss tangent value curve fitting of Glycerol

11.3.2.4 m-cresol

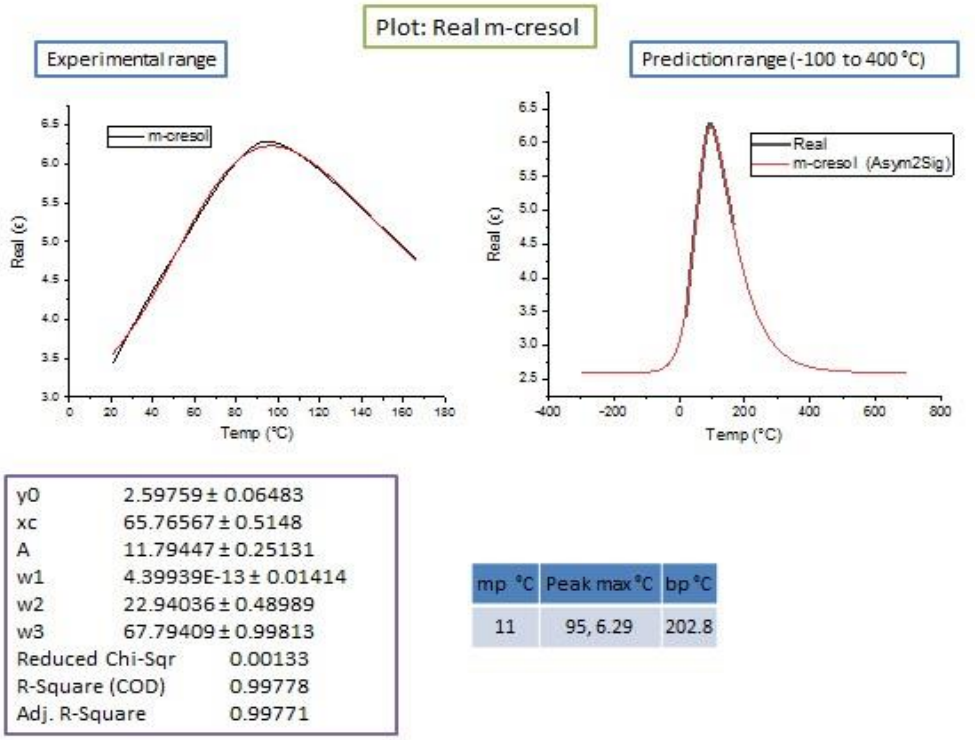

y0	2.59759 ± 0.06483
xc	65.76567 ± 0.5148
A	11.79447 ± 0.25131
w1	4.39939E-13 ± 0.01414
w2	22.94036 ± 0.48989
w3	67.79409 ± 0.99813
Reduced Chi-Sqr	0.00133
R-Square (COD)	0.99778
Adj. R-Square	0.99771

mp °C	Peak max °C	bp °C
11	95, 6.29	202.8

Figure 211 Dielectric real value curve fitting of m-cresol

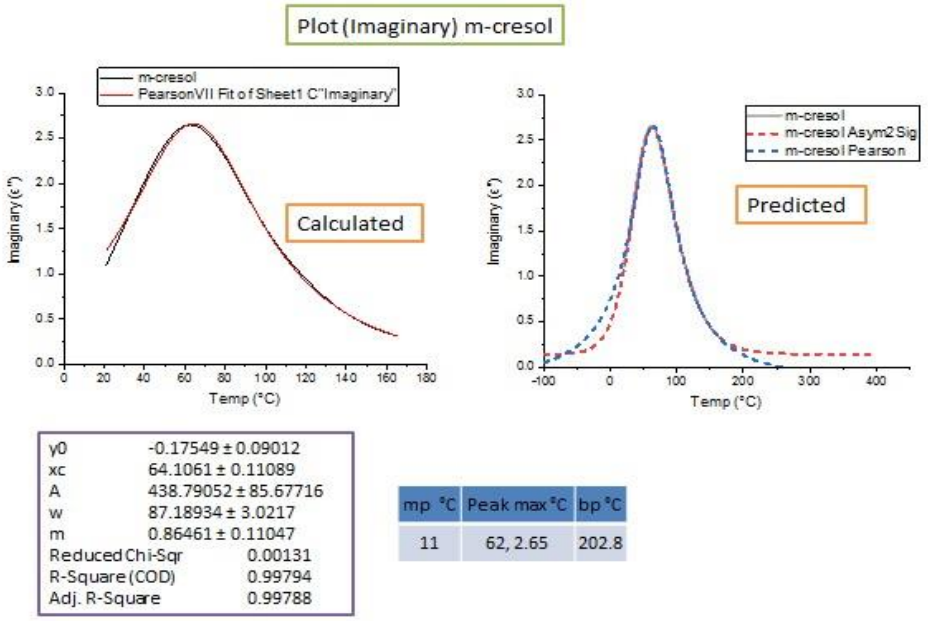

Figure 212 Dielectric imaginary value curve fitting of 2, 4 m-cresol

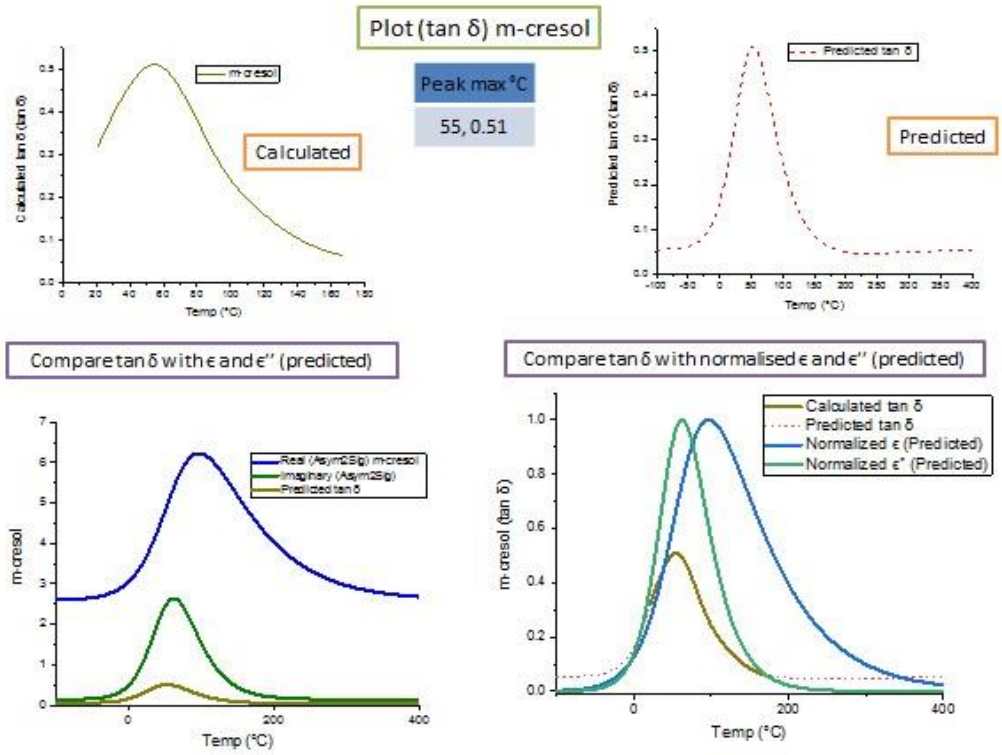

Figure 213 Dielectric loss langent value curve fitting of 2, 4 m-cresol

11.3.2.5 Cyclooctanol

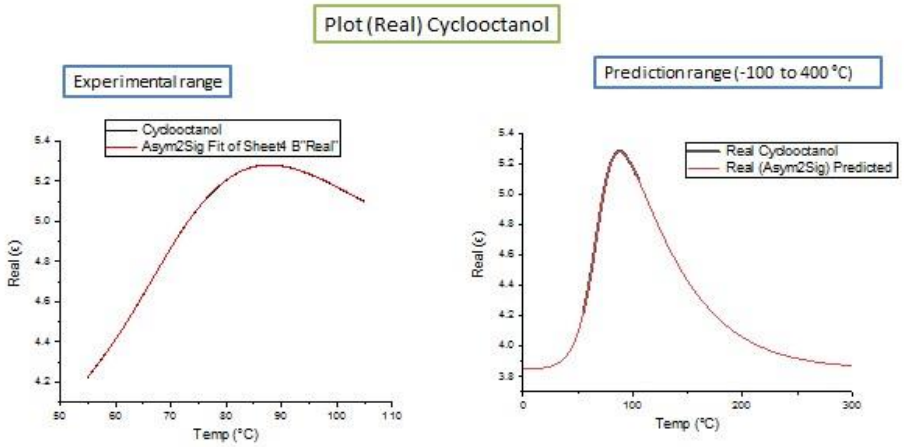

y0	3.8478 ± 0.00794
xc	69.85667 ± 0.07804
A	4.05301 ± 0.03581
w1	3.99401E-11 ± 0.12997
w2	9.00902 ± 0.07038
w3	44.90854 ± 0.30465
Reduced Chi-Sqr	3.85044E-6
R-Square (COD)	0.99997
Adj. R-Square	0.99997

mp °C	Peak max °C	bp °C
14.2	88, 5.28	97

Figure 214 Dielectric real value curve fitting of Cyclooctanol

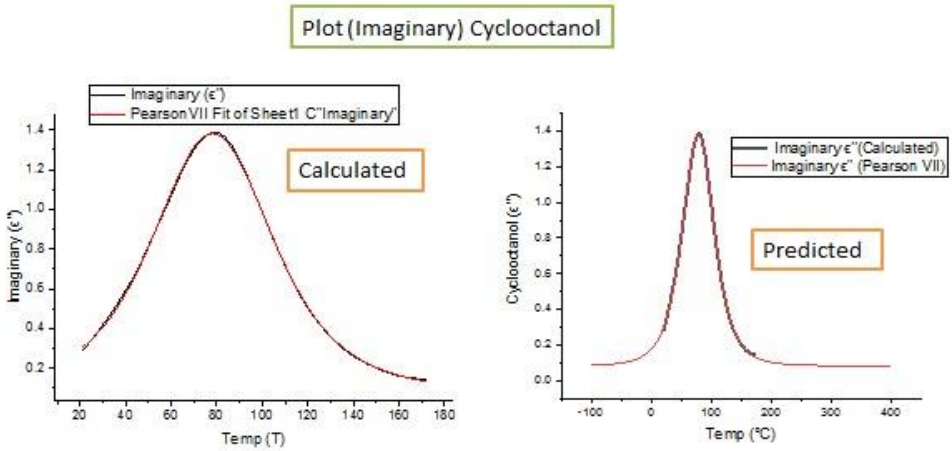

Plot	Imaginary
y0	0.0812 ± 0.00575
xc	78.22514 ± 0.03651
A	98.26101 ± 1.51133
w	62.61925 ± 0.23265
m	2.13815 ± 0.10206
Reduced Chi-Sqr	6.22574E-5
R-Square (COD)	0.99965
Adj. R-Square	0.99964

mp °C	Peak max °C	bp °C
14.2	78.2, 1.4	97

Figure 215 Dielectric imaginary value curve fitting of Cyclooctanol

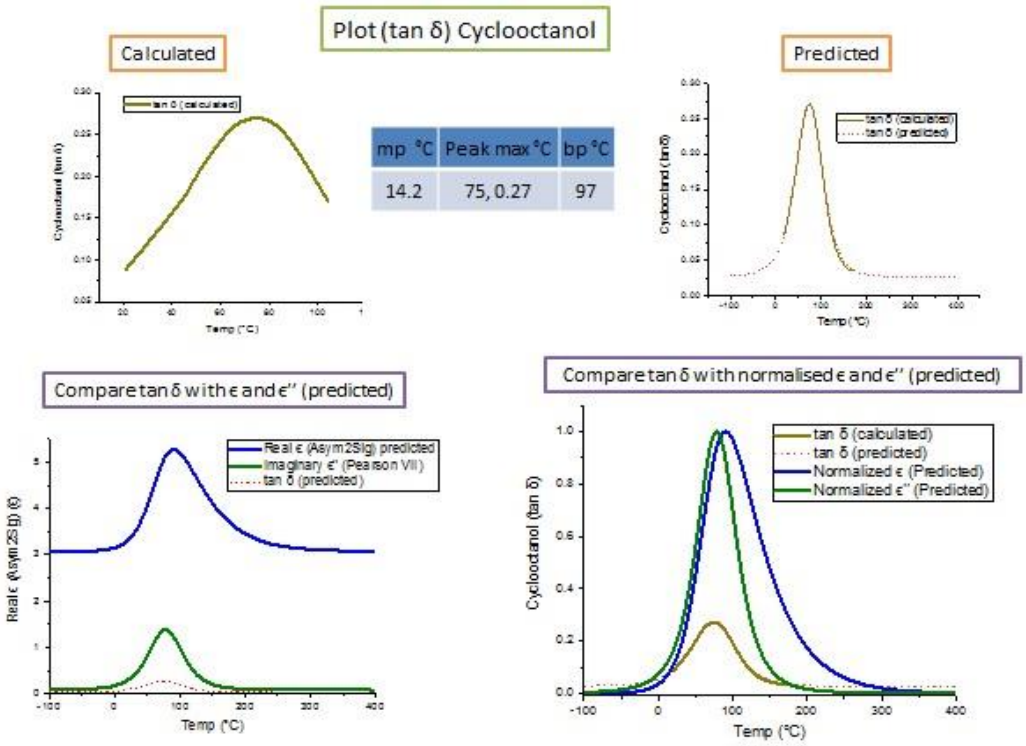

Figure 216 Dielectric loss tangent value curve fitting of Cyclooctanol

11.3.2.6 Propylene Carbonate

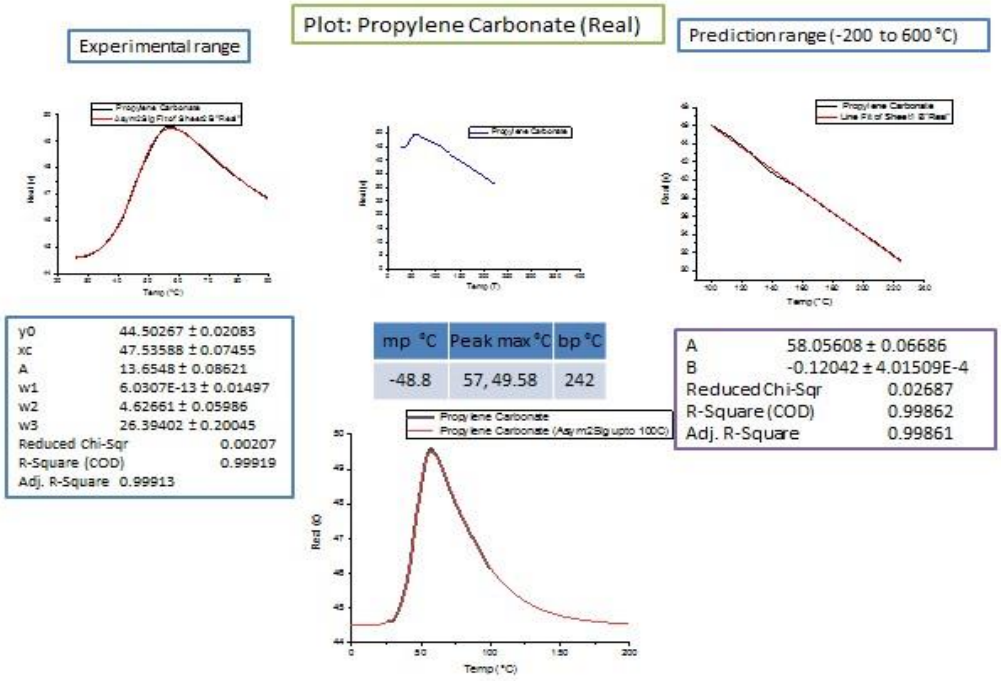

Figure 217 Dielectric real value curve fitting of Propylene Carbonate

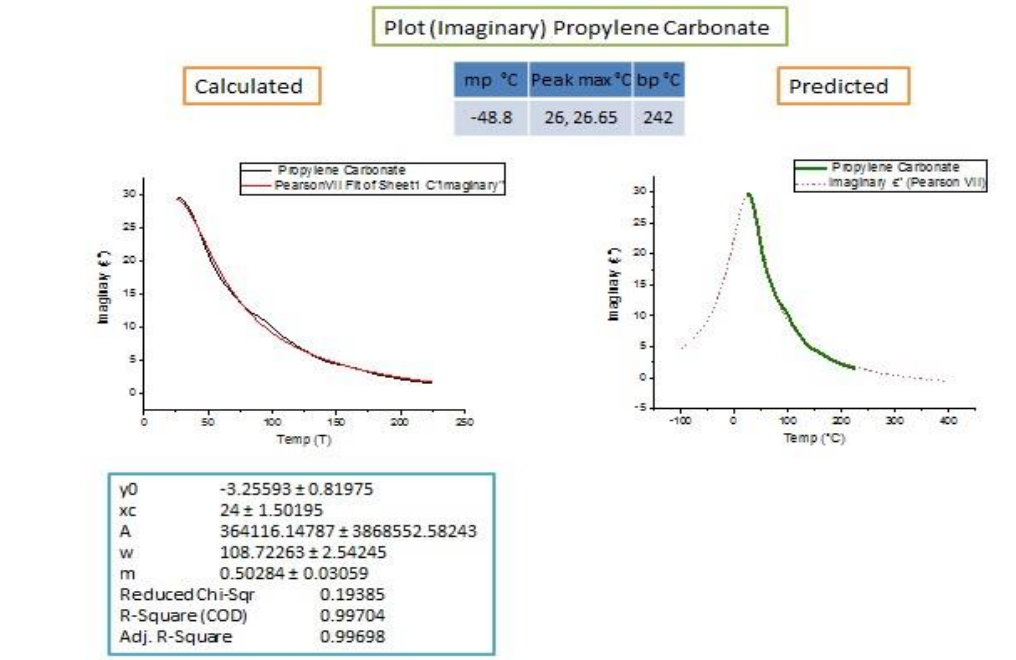

Figure 218 Dielectric imaginary value curve fitting of Propylene Carbonate

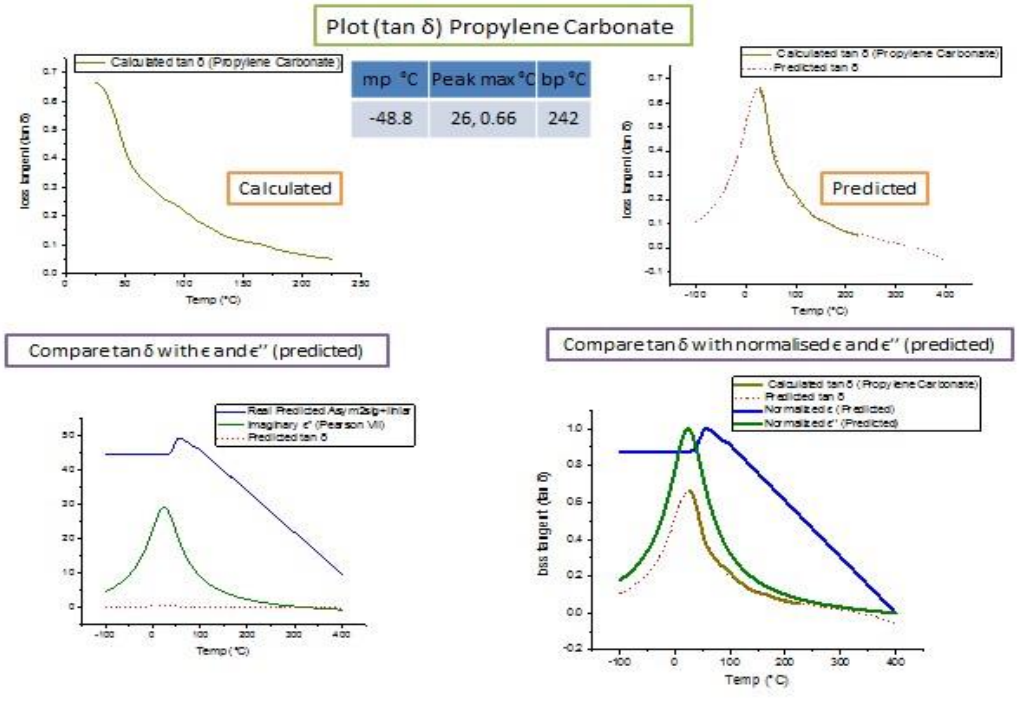

Figure 219 Dielectric loss tangent value curve fitting of Propylene Carbonate

11.3.2.7 Butyl Benzoate

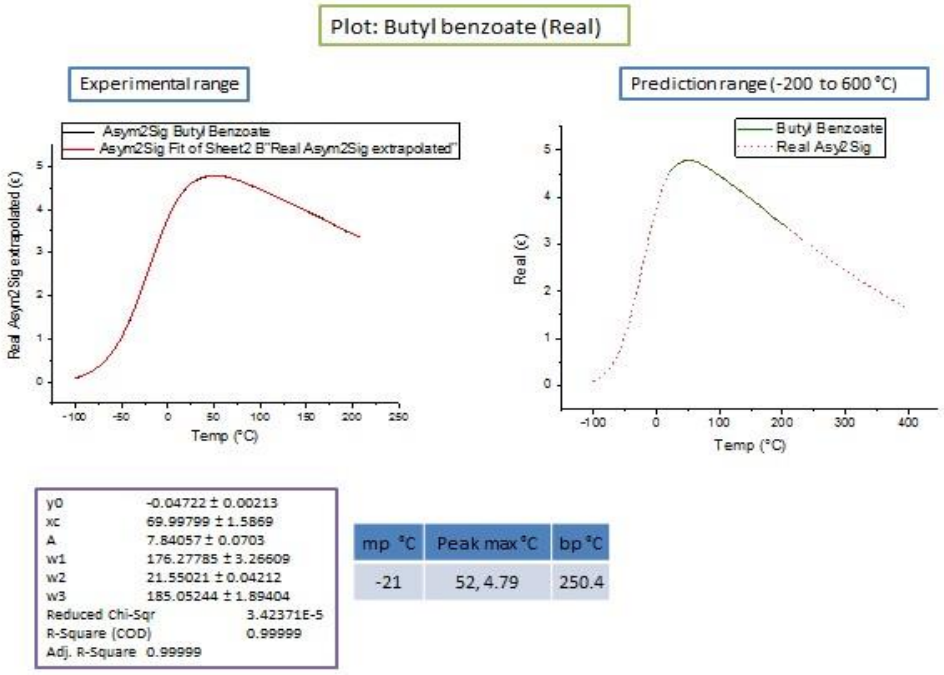

Figure 220 Dielectric real value curve fitting of Butyl Benzoate

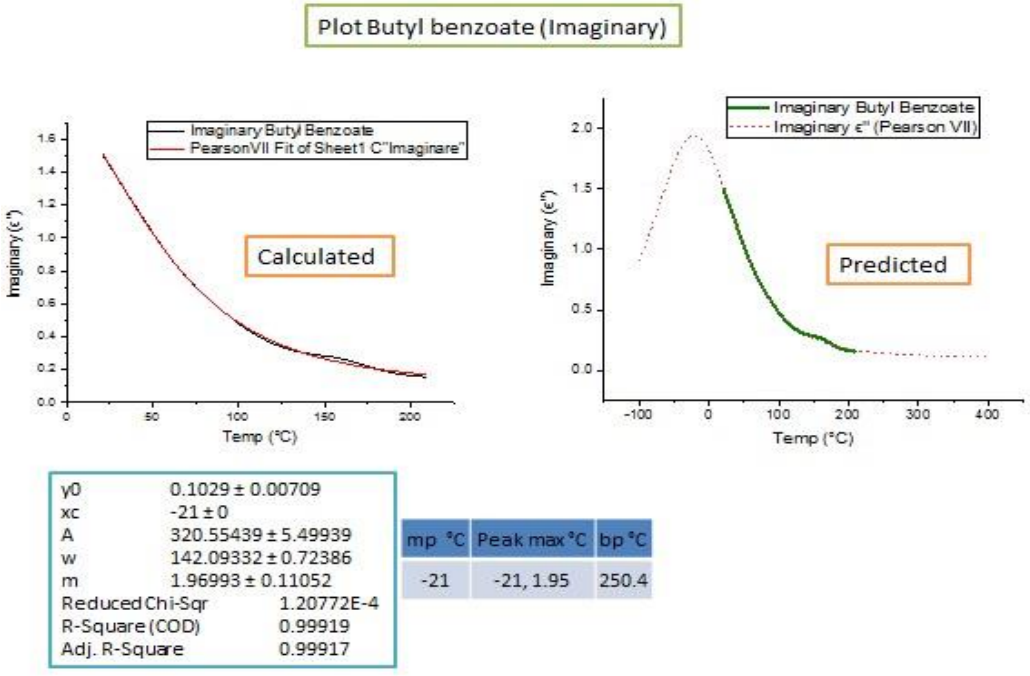

Figure 221 Dielectric imaginary value curve fitting of Butyl benzoate

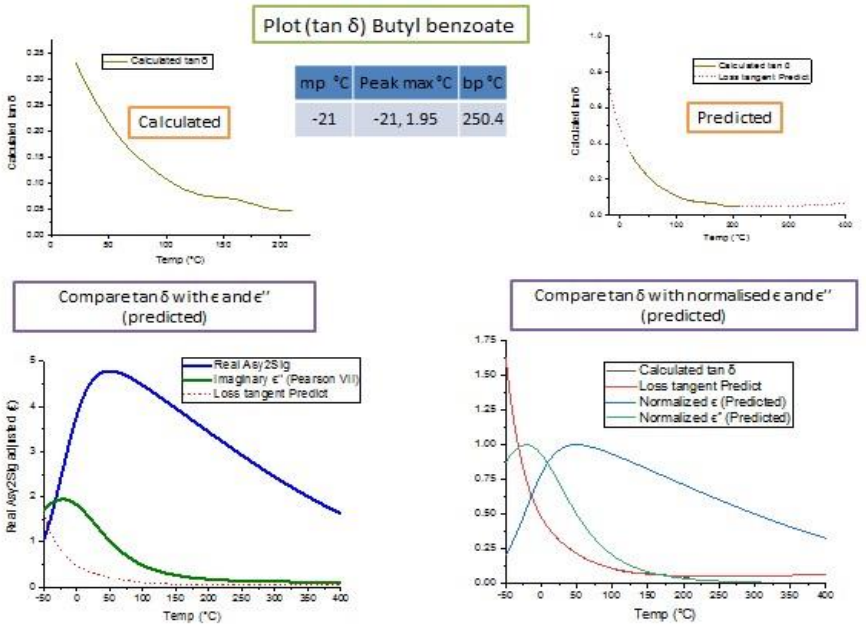

Figure 222 Dielectric loss tangent value curve fitting of butyl benzoate

11.3.2.8 γ-valerolactone

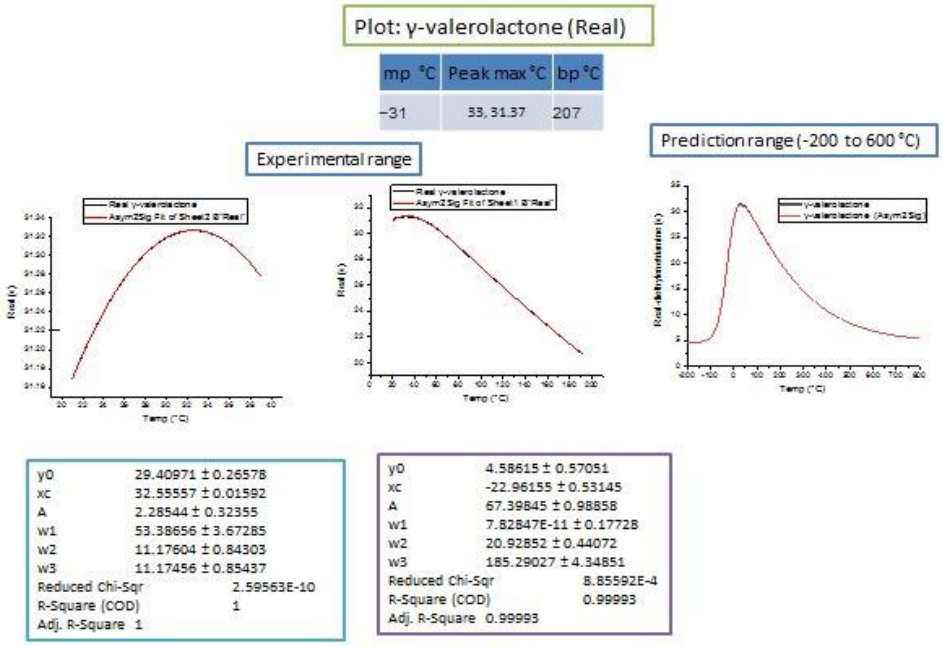

Figure 223 Dielectric real value curve fitting of γ-valerolactone

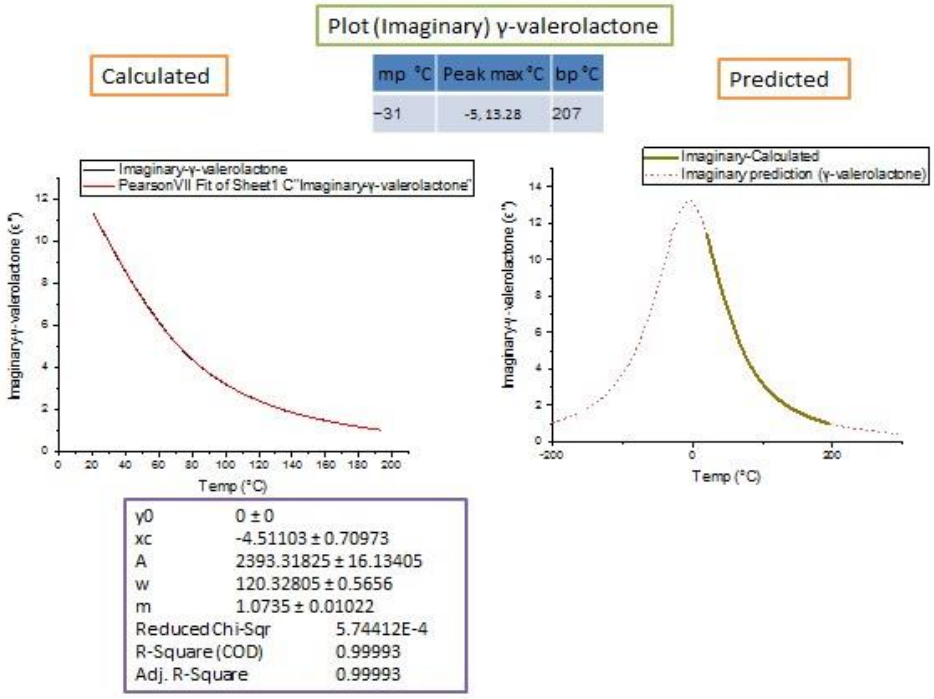

Figure 224 Dielectric imaginary value curve fitting of γ-valerolactone

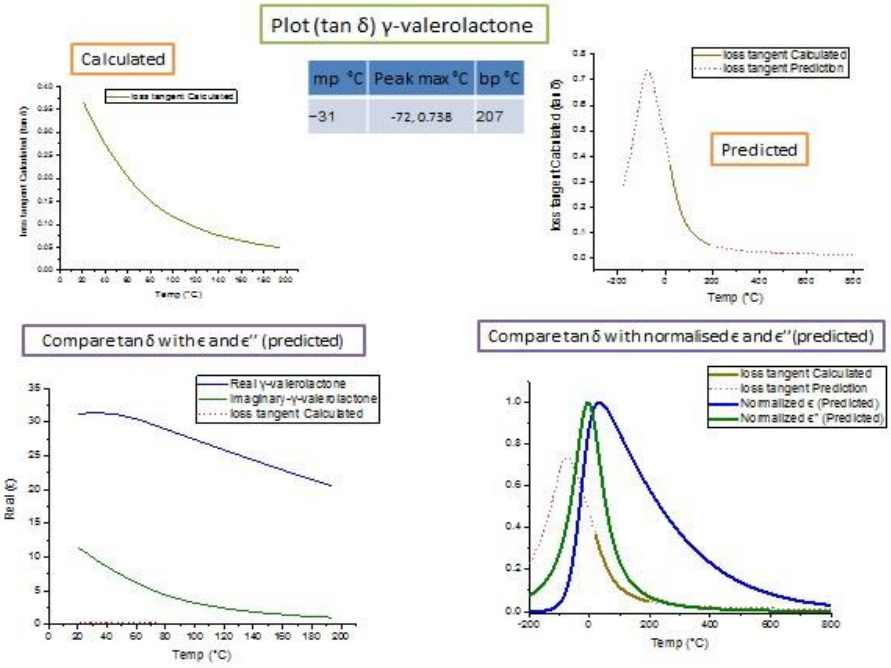

Figure 225 Dielectric loss tangent value curve fitting of γ-valerolactone

11.3.2.9 DMSO

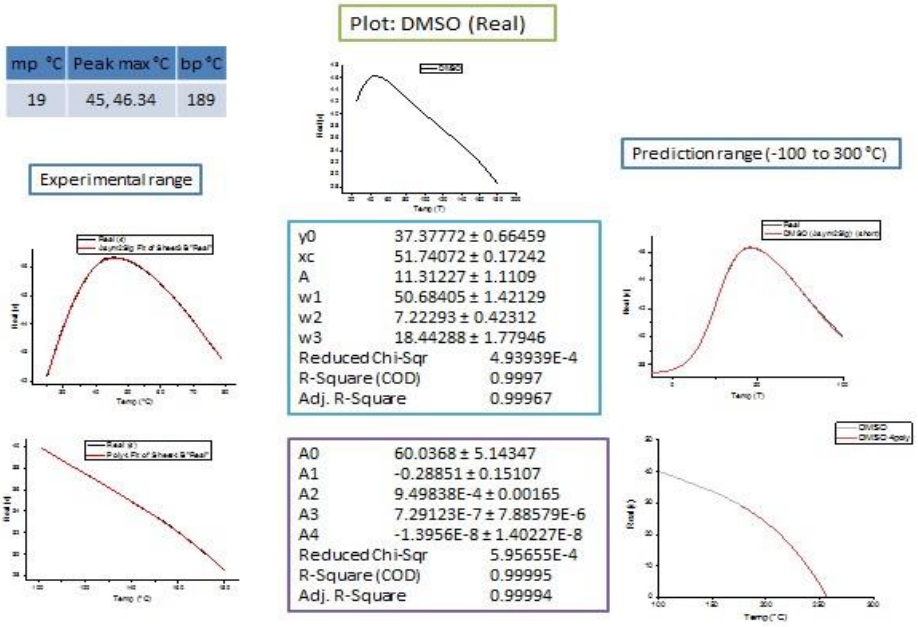

Figure 226 Dielectric real value curve fitting of DMSO

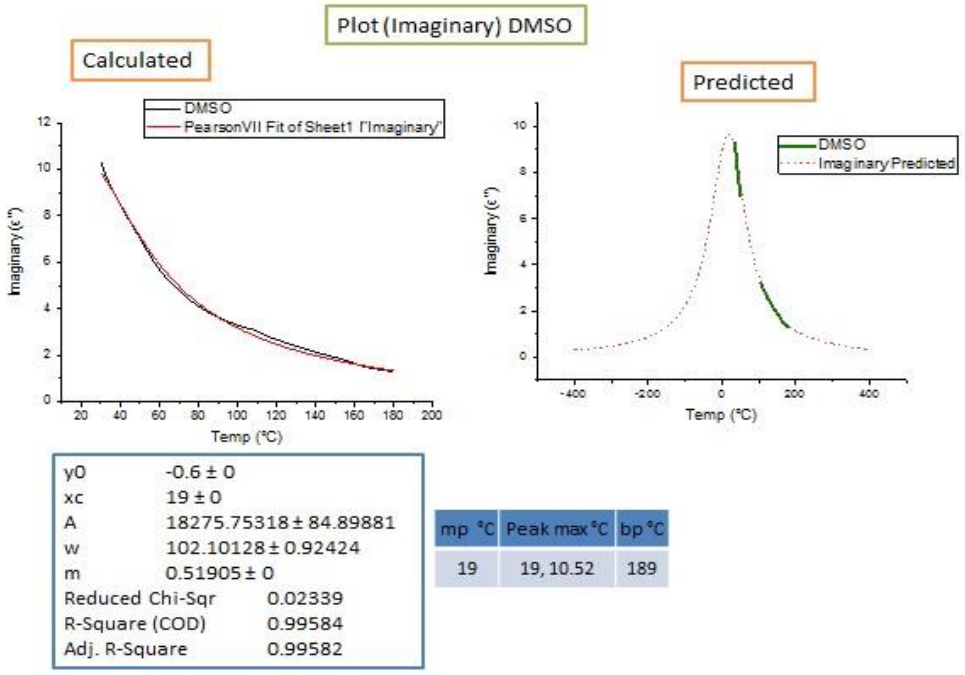

Figure 227 Dielectric imaginary value curve fitting of DMSO

11.3.2.10 Diethylenetriamine

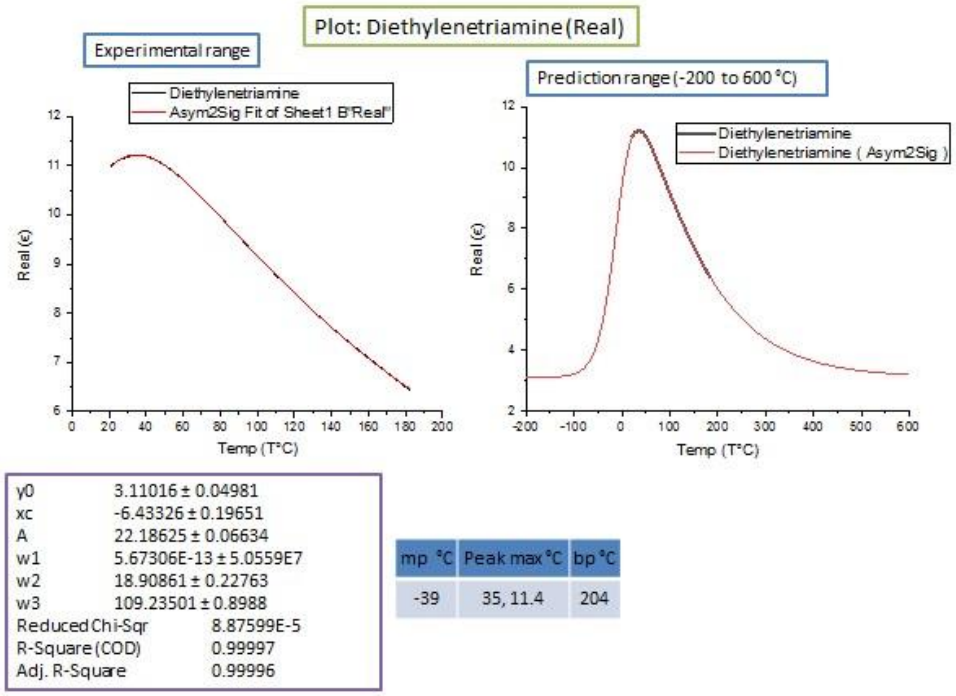

Figure 228 Dielectric real value curve fitting of Diethylenetriamine

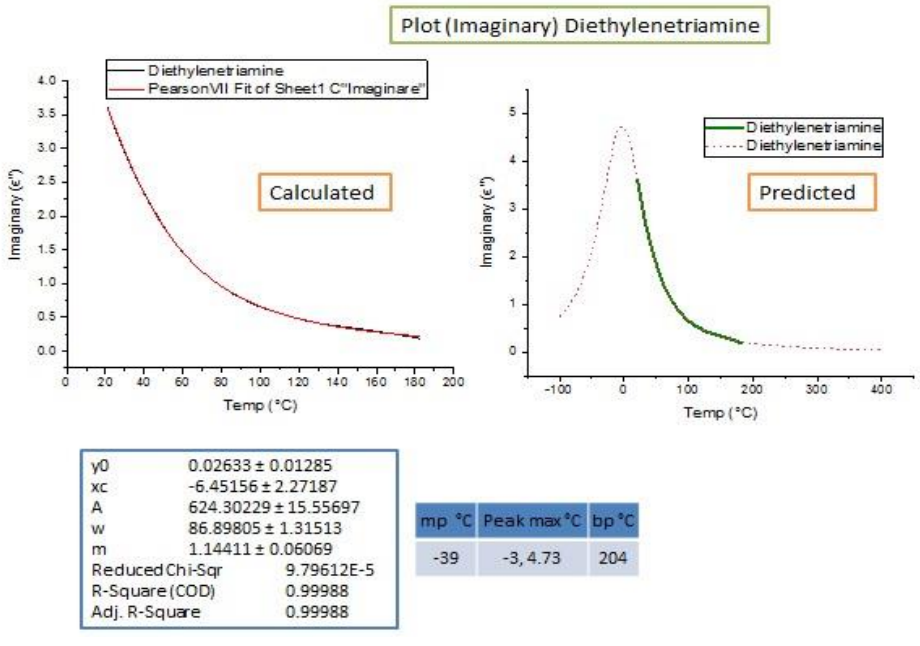

Figure 229 Dielectric imaginary value curve fitting of Diethylenetriamine

11.3.2.11 Sulfolane

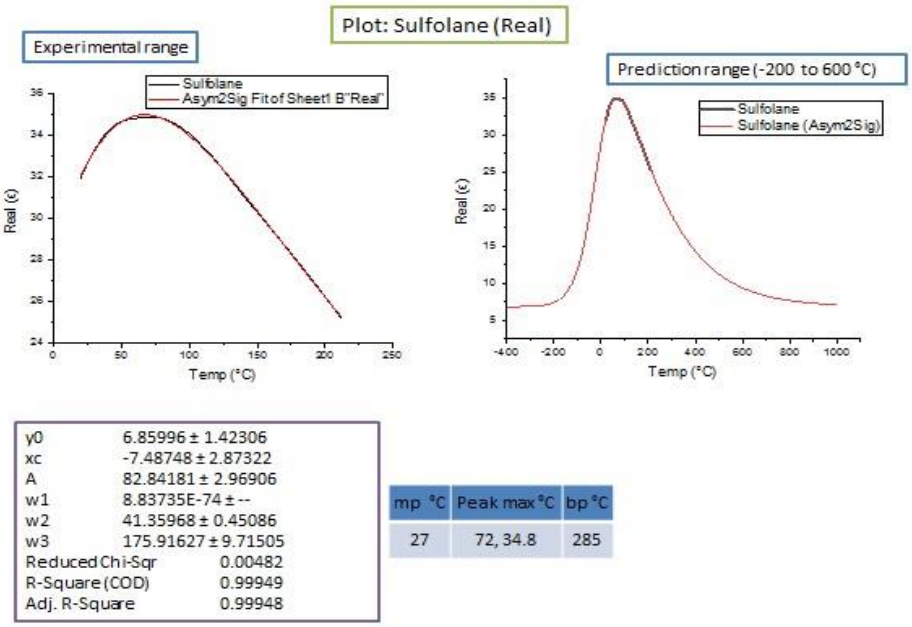

y0	6.85996 ± 1.42306
xc	-7.48748 ± 2.87322
A	82.84181 ± 2.96906
w1	8.83735E-74 ± --
w2	41.35968 ± 0.45086
w3	175.91627 ± 9.71505
Reduced Chi-Sqr	0.00482
R-Square (COD)	0.99949
Adj. R-Square	0.99948

mp °C	Peak max °C	bp °C
27	72, 34.8	285

Figure 230 Dielectric real value curve fitting of Sulfolane

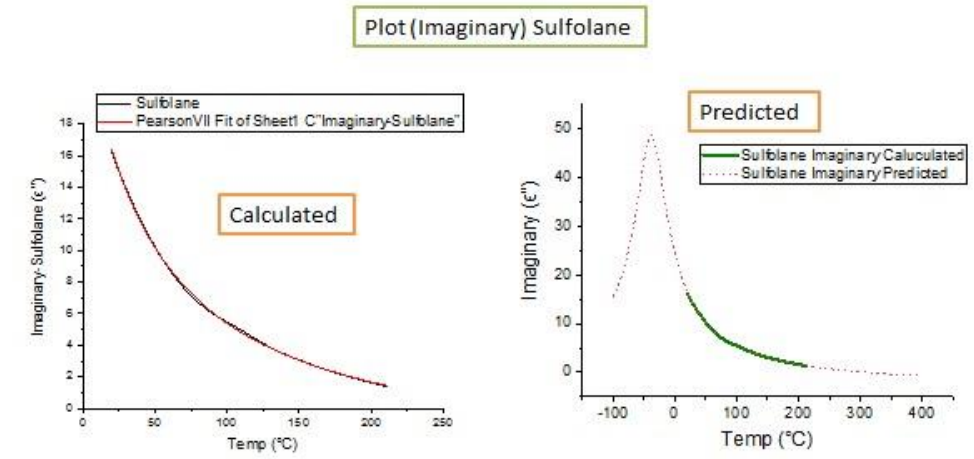

y0	-3.60043 ± 1.20609
xc	-38.35824 ± 34.13317
A	1.04795E16 ± 7.04782E17
w	83.76388 ± 73.99475
m	0.5 ± 8.21287E-12
Reduced Chi-Sqr	0.00686
R-Square (COD)	0.99956
Adj. R-Square	0.99955

mp °C	Peak max °C	bp °C
27.5	27.5, 16.2	285

Figure 231 Dielectric imaginary value curve fitting of Sulfolane

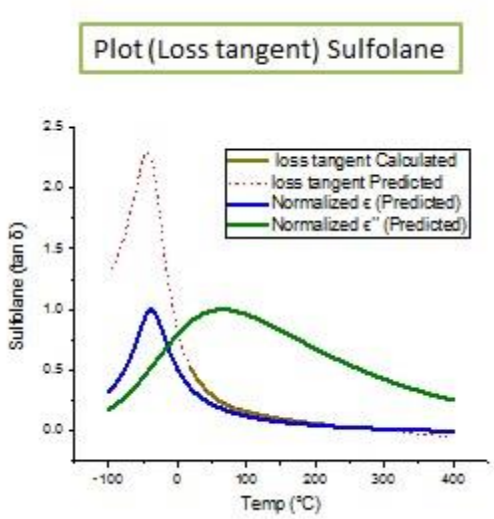

Figure 232 Dielectric loss tangent value curve fitting of Sulfolane

11.3.2.12 Ethylene Glycol

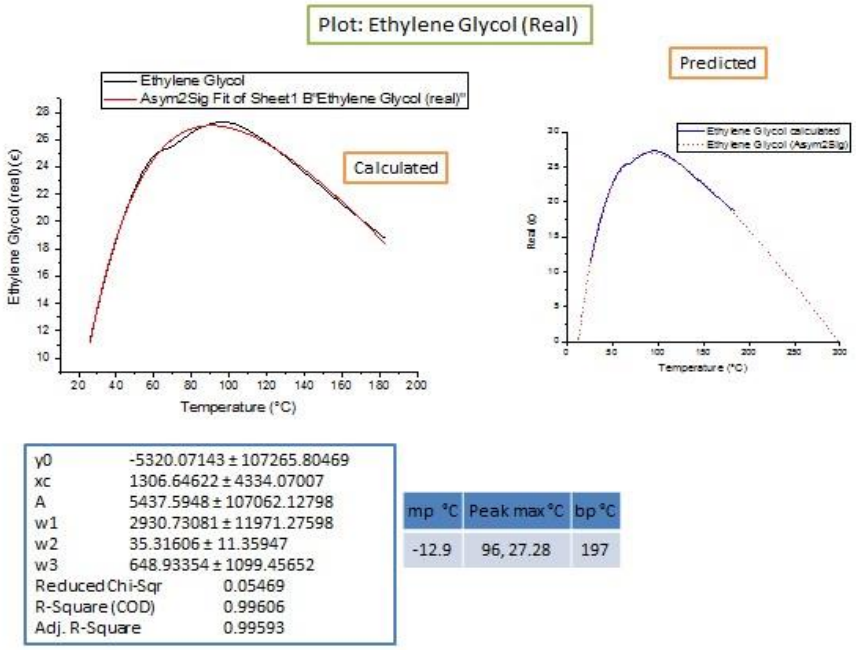

y0	-5320.07143 ± 107265.80469
xc	1306.64622 ± 4334.07007
A	5437.5948 ± 107062.12798
w1	2930.73081 ± 11971.27598
w2	35.31606 ± 11.35947
w3	648.93354 ± 1099.45652
Reduced Chi-Sqr	0.05469
R-Square (COD)	0.99606
Adj. R-Square	0.99593

mp °C	Peak max °C	bp °C
-12.9	96, 27.28	197

Figure 233 Dielectric real value curve fitting of Ethylene Glycol

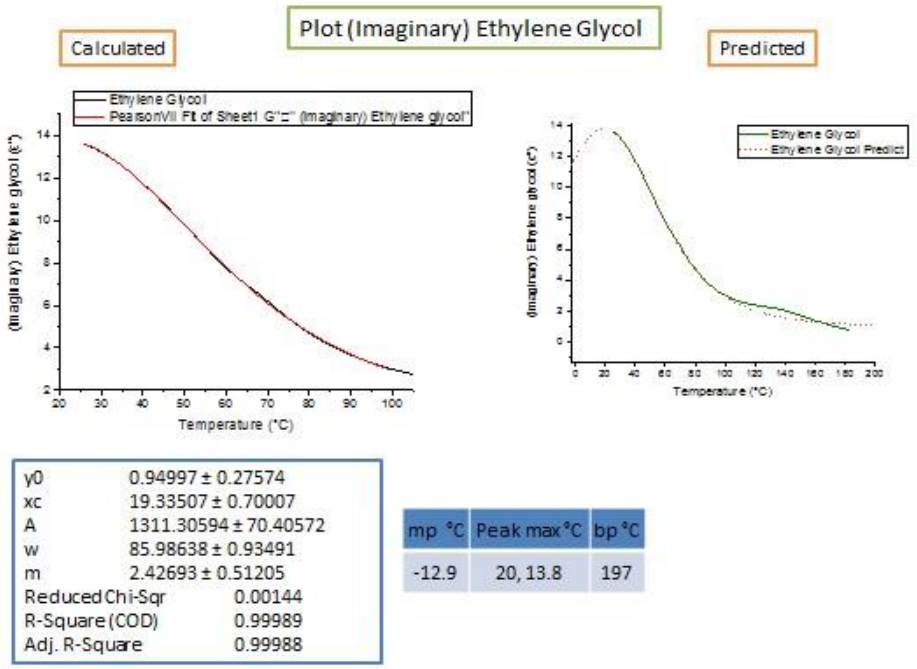

Figure 234 Dielectric imaginary value curve fitting of Ethylene Glycol

11.3.2.13 Furfuryl alcohol

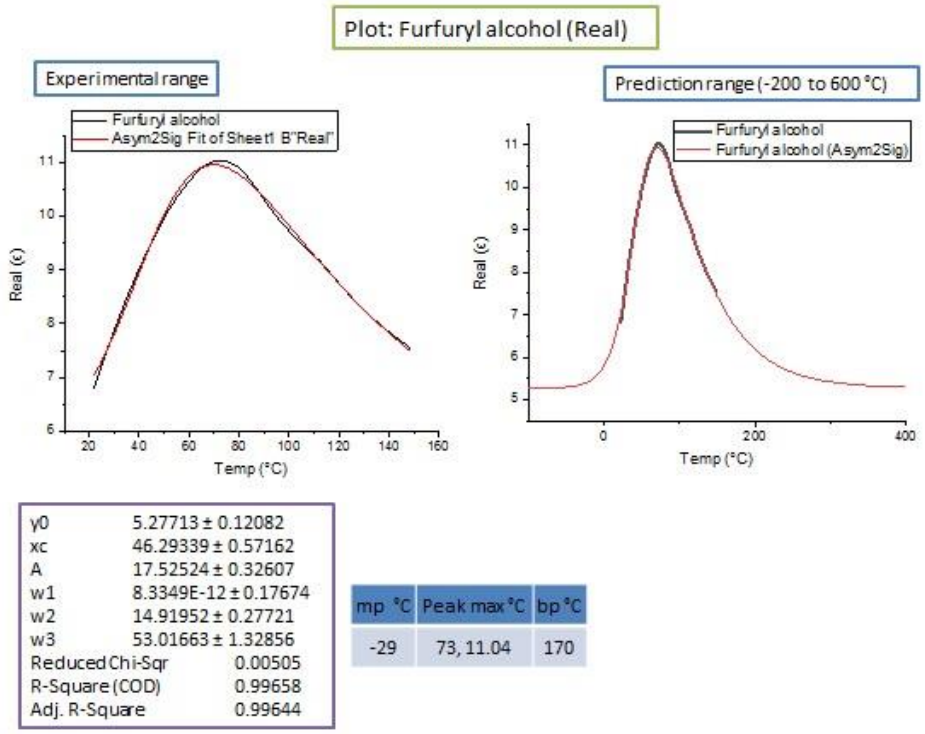

Figure 235 Dielectric real value curve fitting of γ-valerolactone

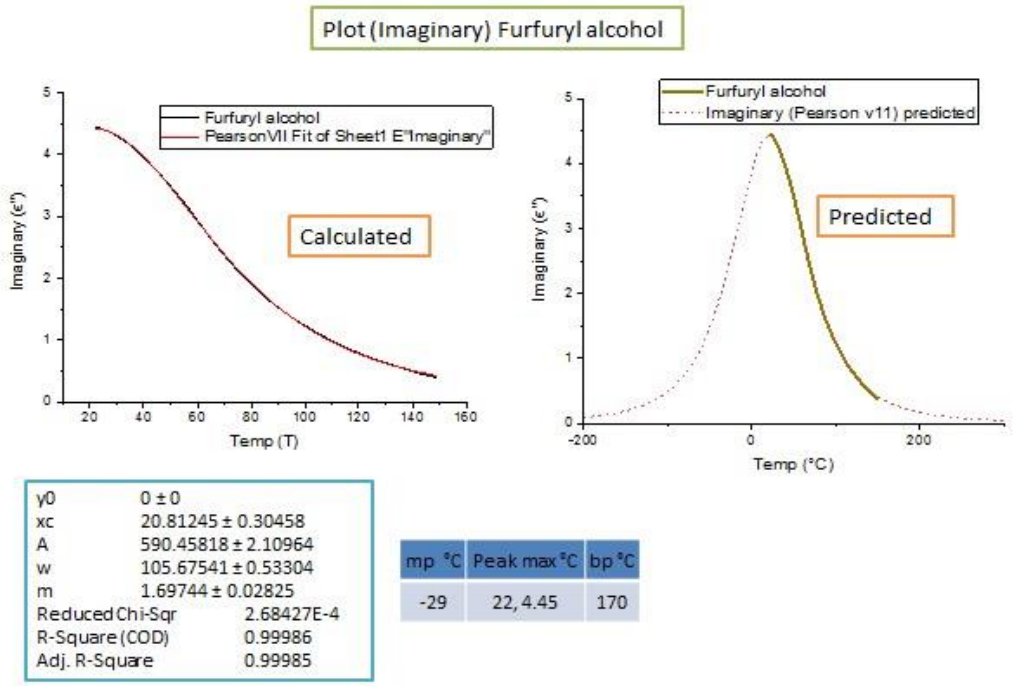

Figure 236 Dielectric imaginary value curve fitting of Furfuryl alcohol

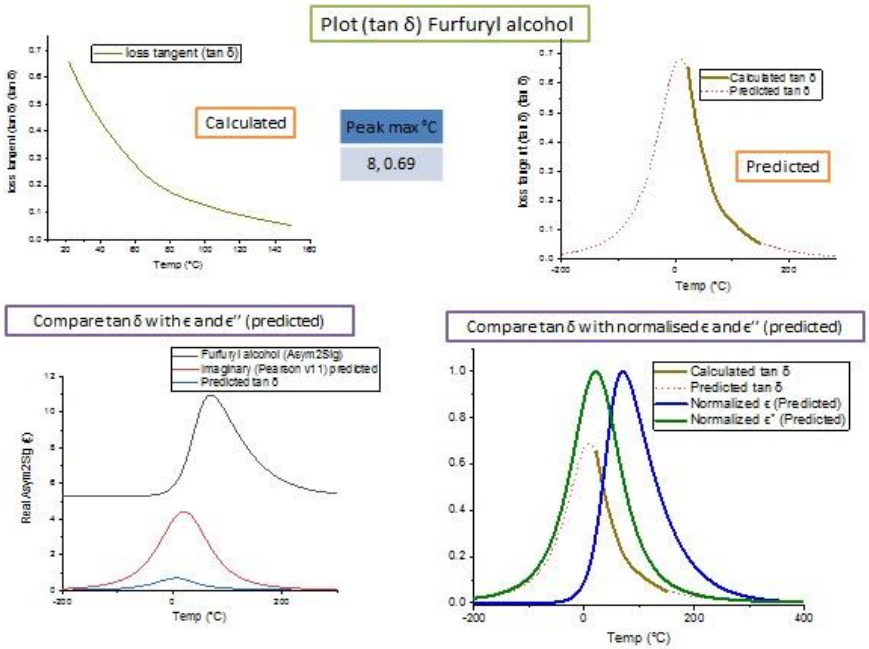

Figure 237 Dielectric loss tangent value curve fitting of Furfuryl alcohol